AGARD-CP-566

AGARD

ADVISORY GROUP FOR AEROSPACE RESEARCH & DEVELOPMENT
7 RUE ANCELLE, 92200 NEUILLY-SUR-SEINE, FRANCE

AGARD CONFERENCE PROCEEDINGS 566

Advanced Aeroservoelastic Testing and Data Analysis

(les Essais aéroservoélastiques et l'analyse des données)

This publication was prepared at the request of the Structures and Materials Panel (SMP) of AGARD. Papers presented at the 80th Meeting of the AGARD Structures and Materials Panel, held in Rotterdam, The Netherlands, 8-10 May 1995.

NORTH ATLANTIC TREATY ORGANIZATION

Published November 1995

Distribution and Availability on Back Cover

DISCLAIMER NOTICE

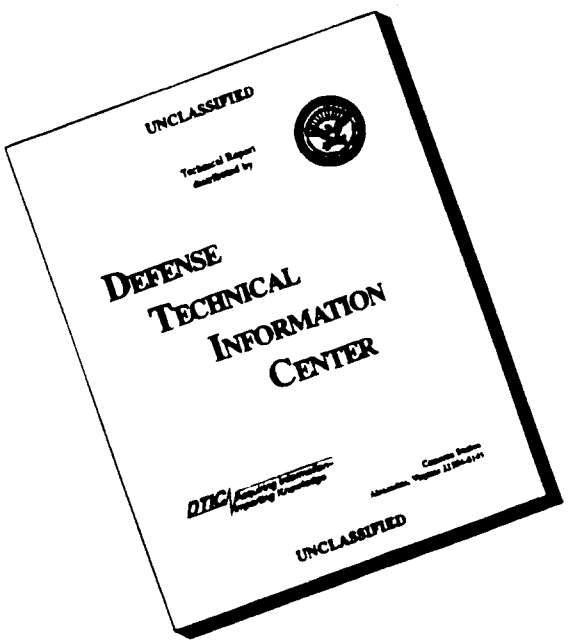

THIS DOCUMENT IS BEST QUALITY AVAILABLE. THE COPY FURNISHED TO DTIC CONTAINED A SIGNIFICANT NUMBER OF PAGES WHICH DO NOT REPRODUCE LEGIBLY.

AGARD-CP-566

AGARD

ADVISORY GROUP FOR AEROSPACE RESEARCH & DEVELOPMENT
7 RUE ANCELLE, 92200 NEUILLY-SUR-SEINE, FRANCE

AGARD CONFERENCE PROCEEDINGS 566

Advanced Aeroservoelastic Testing and Data Analysis

(les Essais aéroservoélastiques et l'analyse des données)

This publication was prepared at the request of the Structures and Materials Panel (SMP) of AGARD. Papers presented at the 80th Meeting of the AGARD Structures and Materials Panel, held in Rotterdam, The Netherlands, 8-10 May 1995.

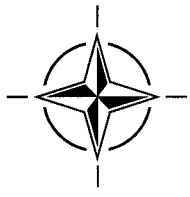

North Atlantic Treaty Organization
Organisation du Traité de l'Atlantique Nord

The Mission of AGARD

According to its Charter, the mission of AGARD is to bring together the leading personalities of the NATO nations in the fields of science and technology relating to aerospace for the following purposes:

- Recommending effective ways for the member nations to use their research and development capabilities for the common benefit of the NATO community;
- Providing scientific and technical advice and assistance to the Military Committee in the field of aerospace research and development (with particular regard to its military application);
- Continuously stimulating advances in the aerospace sciences relevant to strengthening the common defence posture;
- Improving the co-operation among member nations in aerospace research and development;
- Exchange of scientific and technical information;
- Providing assistance to member nations for the purpose of increasing their scientific and technical potential;
- Rendering scientific and technical assistance, as requested, to other NATO bodies and to member nations in connection with research and development problems in the aerospace field.

The highest authority within AGARD is the National Delegates Board consisting of officially appointed senior representatives from each member nation. The mission of AGARD is carried out through the Panels which are composed of experts appointed by the National Delegates, the Consultant and Exchange Programme and the Aerospace Applications Studies Programme. The results of AGARD work are reported to the member nations and the NATO Authorities through the AGARD series of publications of which this is one.

Participation in AGARD activities is by invitation only and is normally limited to citizens of the NATO nations.

Published November 1995

ISBN 92-836-0017-7

Printed by Canada Communication Group
45 Sacré-Cœur Blvd., Hull (Québec), Canada K1A 0S7

Advanced Aeroservoelastic Testing and Data Analysis

(AGARD CP-566)

Executive Summary

The new generation of high performance fighter aircraft rely upon digital controls, which improve their handling and manoeuvring capabilities, and allow unstable aeroplanes to fly. The development of these advanced digital flight control systems for a modern military aircraft is strongly influenced by aeroservoelastic effects (ASE), which, therefore, play a very important role in the qualification of aircraft with digital controls.

The recognition of ASE as a serious design issue evolved as a result of advancements within independent technical disciplines, all aimed at improving the performance of flight vehicles. For example in the technical disciplines of structures and materials, structural efficiency and weight minimization resulted in very flexible structures which satisfied aeroelastic and strength requirements. There were also advancements in fly-by-wire and digital flight control system technologies that further increased their performance and capability. As a result of these advancements, large magnitude adverse aeroservoelastic responses and instabilities had the potential to, and at times did, couple to produce the phenomenon known as flutter.

Flight flutter testing should be viewed as involving an inherent element of danger. The flight test procedures must be first and foremost concerned with flight safety. During the initial stages of flight flutter testing a new type of aircraft, the flight envelope is opened progressively in terms of Mach number and airspeed. Most of the tests could be improved.

The conclusions of the AGARD Specialists' Meeting on "Aeroservoelastic Testing and Data Analysis" are that most of the tests need improvements, some tests should be better exploited and at least one test — the in-flight measurement of unsteady airloads — should become standard practice to close a gap in the logic of flutter certification. The need for an accurate aeroservoelastic model, in order to limit the testing activity to a reduced number of external store configurations selected on the basis of structural coupling criticalities, has been pointed out.

Contents

SESSION III: AEROSERVOELASTIC TESTING

Preface

Flutter is a potentially catastrophic aeroelastic dynamic instability. Flight flutter tests are conducted to demonstrate freedom from flutter for critical aircraft conditions and to collect data to validate the flutter analysis. Active control systems add to the scope and complexity of these tests in that control system instability due to aeroservoelastic interactions must also be considered.

Reliable flight test procedures are therefore required to minimize the hazard of these tests. This in turn requires that effective methods be used for exciting the aircraft and that reliable data analysis methods be applied for estimating the level of flutter stability from the measured structural and control system responses. Impediments to achieving reliable estimates for the flutter stability parameters are the short test time, the high noise levels in the collected data and nonlinearities in the system characteristics. The situation described above extends also to wind tunnel tests with flutter models.

The objective of this Specialists' Meeting was to evaluate current methods for aeroservoelastic testing and data analysis. The meeting comprised three sessions: 1) Flutter testing, 2) Flutter signal processing, 3) Aeroservoelastic testing, and was concluded by a Round table discussion.

R.J. Zwaan
Chairman Specialists' Meeting

Préface

Le flottement est un phénomène d'instabilité dynamique aéroélastique qui est potentiellement catastrophique. Des essais en vol du flottement sont effectués afin de démontrer l'absence de flottement dans des conditions de vol critiques et de collecter des données permettant de valider l'analyse du flottement. L'arrivée des systèmes de contrôle actifs a eu pour effet d'élargir le champ couvert par ces essais et de les rendre plus complexes, puisque il faut désormais tenir compte de l'éventuelle instabilité des systèmes de contrôle, due aux interactions aéroservoélastiques.

Des procédures fiables d'essais en vol sont donc recherchées afin de réduire au minimum les risques associés à de tels essais. En conséquence, des méthodes efficaces doivent être appliquées en ce qui concerne l'excitation de l'aéronef et des méthodes d'analyse de données fiables doivent être mises en œuvre pour l'estimation du niveau de stabilité vis-à-vis du flottement à partir des réponses obtenues des systèmes structuraux et de contrôle. Les facteurs qui gênent l'obtention d'estimations fiables pour les paramètres de stabilité au flottement sont: la durée réduite des essais, les niveaux de bruit élevés dans les données collectées et les non-linéarités des caractéristiques des systèmes. Ces commentaires s'appliquent également aux essais en soufflerie de maquettes instables.

Cette réunion de spécialistes a eu pour objet d'évaluer les méthodes courantes d'essais aéroservoélastiques et d'analyse de données. La réunion a été organisée en trois sessions: 1. Les essais de flottement. 2. Le traitement des signaux de flottement. 3. Les essais aéroservoélastiques. La séance a été clôturée par une table ronde.

Structures and Materials Panel

SUB-COMMITTEE MEMBERS

PANEL EXECUTIVE

TECHNICAL EVALUATION REPORT ON THE 1995 SPECIALISTS' MEETING ON ADVANCED AEROSERVOELASTIC TESTING AND DATA ANALYSIS

by

Dr. Jonathan E. Cooper
University of Manchester
School of Engineering
Oxford Road
Manchester M13 9PL
United Kingdom

Dr. Thomas E. Noll
NASA Langley Research Center
Structures Division
Hampton, VA 23681-0001
United States

SUMMARY

This paper presents a technical overview of the Specialists' Meeting on "Advanced Aeroservoelastic Testing and Data Analysis" held at the 80th meeting of the AGARD Structures and Materials Panel on 8-12 May 1995, in Rotterdam, The Netherlands.

1. INTRODUCTION

This Specialists' Meeting was the third meeting devoted specifically to Flight Flutter Testing. The previous meetings were:

- 1958 - Flight Flutter Testing Symposium, Washington DC, NASA SP-385
- 1975 - Flutter Testing Techniques, Dryden Flight Research Center, NASA SP-415

The 1958 Symposium consisted of 27 contributions divided into sessions on "Theory", "Methods and Techniques", and "Flight Flutter Testing - Past and Future". Although the overall test procedure is comparable roughly to that used today, the analysis methods can be considered to be somewhat archaic, with estimates of frequency and damping being found generally from the amplitude of the response. The final session was a Panel Discussion on "The Future of Flight Flutter Testing." The conclusion drawn by the speakers was that a great deal of work was required in all aspects of Flight Flutter Testing, but especially in the area of data analysis.

The 20 papers that made up the 1975 Meeting demonstrated the advances that had been made in the intervening 17 years, particularly in the extraction of frequencies and dampings through the developments of the Fast Fourier Transform and the Digital Computer. There were four sessions: "Theory, Methodology & Techniques", "Wind Tunnel Techniques & Applications", "Flight Test Techniques &Applications", and "Flight Test Techniques & Applications - Rotary Wing". Also included was a Panel Discussion on "Theoretical Analysis Versus Testing - A Trade-Off". The extremely interesting debate that ensued expressed a number of differing viewpoints as to how great an impact the increasingly available computing power would make on the design and testing procedures.

This Specialists' Meeting had originally been proposed in the Spring of 1989 with the aim of examining some of the new developments in Flight Flutter Testing, in particular those relating to improved parameter estimation techniques. However, a number of new trends in the technology used for Flight Flutter Testing were emerging at that time, namely: strap-on flutter vanes, improved parameter estimation methods, and an increased awareness of the problems caused by non-linearities in closed-loop flight control systems. It was felt that some time was needed to consider these advances before a meeting should be held. Two pilot papers [1, 2] were presented during 1990 describing some of the recent developments relevant to Flight Flutter Testing.

The terms of reference for this Specialists' Meeting were eventually defined in the Fall of 1991, aiming to discuss the success of the state-of-the-art on-line and off-line aeroelastic and aeroservoelastic testing techniques, as well as the

parameter estimation methods used for both linear and non-linear applications. Specific emphasis was placed upon the examination of:

- excitation systems
- force and response measurement
- real time and off-line stability analysis
- testing of aircraft with MIMO control concepts
- test procedures with emphasis on safety measures

2. OVERVIEW OF PAPERS

The Meeting was divided into three technical sessions consisting of: "Flutter Testing", "Flutter Signal Processing" and "Aeroservoelastic Testing". The 21 papers that were presented included all aspects of Flight Flutter Testing. The distribution of the topics covered by the papers is shown in Table 1.

	Papers	*Overview*
Excitation Devices	3	
Flutter Clearance	12	1
Data Analysis	13	1
Aeroservoelasticity	8	1
Non-linear / LCO	6	
Related Topics	3	

Table 1. Topics covered in the meeting.

Each of the sessions was preceded by an invited Overview paper that reviewed the state-of-the-art of: Flight Flutter Test Procedures [Paper 1] , the Analysis of Flight Flutter Test Data [Paper 10] and Aeroservoelasticity [Paper 14]. Papers [2-6] describe current Flight Flutter Test clearance procedures. The use and relative advantages and disadvantages of the DEI Flutter Vane, the most significant advance in excitation techniques for many years, are discussed in papers [2-4]. Current modal parameter estimation techniques with particular relevance to Flight Flutter Testing are detailed in papers [11-13]; these contributions show how flight flutter data analysis has developed considerably since the last Flutter Testing Meeting in 1975.

Procedures for Aeroservoelastic Testing are described in papers [15-18] and [21-23] including a number of examples from actual flight tests. It was apparent from the content of many of the contributions that the problems being encountered due to Aeroservoelastic phenomena and non-linearities, including Limit Cycle Oscillations, are going to provide significant challenges to the Flight Flutter Test engineer for many years to come. Also presented at the meeting were three papers covering areas related to those described above, namely: the design of aeroelastically scaled models [Paper 7], the transonic and supersonic testing of shingles [Paper 9], and applications of system identification to flight mechanics [Paper 19].

3. CONTENT OF PAPERS AND PRESENTATIONS

This section of the report provides a brief description of each of the papers presented.

Session I - Flutter Testing

1. M.W. Kehoe: A Historical Overview of Flight Flutter Testing

An overview of the flight flutter test techniques and procedures that have evolved over the last several decades in the United States is presented in this paper. Included in the review are descriptions of the structural excitation systems, the instrumentation systems, the digital data preprocessing, and the parameter identification algorithms (for frequency and damping estimates from the response data) employed by the test centers. Practical experiences and examples from general aviation, commercial, and military flight flutter test programs are also reviewed to illustrate the combined integrated effectiveness of the various approaches described in the paper. The paper concludes by summarizing present requirements to increase flight flutter testing efficiency, accuracy, and safety and by providing recommendations regarding the direction of future developments. Areas mentioned which need further development included on-line real-time monitoring of

aeroelastic stability, broad-band excitation systems, and methods that provide a reliable determination of flutter speed at conditions well below the actual flutter speed.

2. F. Weiss, J.Schweiger and H Hoenlinger: Flutter Flight Test of the RANGER 2000 Aircraft

This paper describes the flight flutter test activities for the RANGER 2000 training aircraft, a vehicle which was jointly developed by DASA and Rockwell International between 1991 and 1994 as a competitor for the next generation U.S. Air Force and Navy "Joint Primary Advanced Training System" (JPATS). After a brief description of the program and the main aircraft features, an overview of the aeroelastic analysis and the ground vibration tests performed during the design process are provided. The report of the flight test activities is divided into a description of the test equipment, aircraft instrumentation, flight envelope, test procedures, real–time telemetry parameter monitoring, and post–flight data reduction. For the efficient performance of the flutter flight test program, the use of an external system to excite the structural dynamic eigenfrequencies of this small aircraft in the range of 10 to 40 Hz is also described. The selected system, manufactured by Dynamics Engineering Inc., consists of small vanes mounted to the tips of the wings and on top of the vertical tail. The unsteady aerodynamic excitation forces are produced by rotating cylinders with slots at the trailing edge of these vanes. Typical time histories of response, frequency response functions, power spectra, and typical plots of the frequencies and damping versus dynamic pressure are provided in the paper. The flight test results in combination with the aeroelastic analysis and the experiences with the excitation system are also discussed.

3. P. Schippers and A. J. Persoon: Flight Flutter Testing of a Turbo–Prop Aircraft by Using External Excitation Devices

A summary of the flight flutter test performed on a twin-turbo prop aircraft (Fokker 50 Mk2S) with external mounted stores is provided in this paper. Because the accurate detection of damping factors of critical aeroelastic modes often fails when using methods like stick raps or turbulence as input, an external excitation system was determined to be required for this program. The paper describes the excitation system purchased from Dynamics Engineering Inc. To evaluate the exciter system, the paper summarizes preliminary flight flutter tests conducted on the F-50 prototype. For these tests a single exciter was mounted on an external store and microphones, installed near the exciter, were used to measure the unsteady pressures generated when the exciter was operating. Further objectives of this preliminary test were to familiarize the flight crew with the test procedures and to evaluate and select the type of excitation and data reduction methods to be used for the Fokker 50 Mk2S test. The paper then describes the preparations for and execution of the Fokker 50 Mk2S flight flutter tests and presents some of the flight test results. In addition, experiences gained and the difficulties encountered using the DEI external excitation systems are also highlighted.

4. B. M. Shirley and E. L. Anderson: U.S. Air Force/DEI Flutter Exciter Test Program

This paper describes a recent F-16 flight flutter test investigation performed by the United States Air Force to evaluate an external excitation system purchased from Dynamic Engineering Inc. (DEI) as a low–cost, easily–installed, alternative to using the existing aircraft flight control integrated systems. The paper describes flight flutter tests using the external excitation devices and, separately, using the existing onboard integrated Flutter Exciter System (FES). The existing F–16 FES provides excitation via the flaperons and is capable of symmetric and antisymmetric sweeps and bursts of up to about 20 Hz for selectable time durations. For the external excitation system, two exciters were installed

on the outboard side of two weapons pylons (one on each side of the aircraft). Testing of the DEI flutter exciter system was limited to matching FES time/frequency capabilities, although frequency response and time duration capabilities of the DEI exciter were greater than the FES. The paper presents a one–for–one comparison of excitation levels, frequency content, and damping values at various Mach/airspeed/altitude combinations for three different aircraft/weapon configurations. Conclusions are also presented regarding the use of the DEI exciter in a high dynamic pressure environment and its application as an alternative excitation method.

5. F. Kiessling, H. Rippel, and H. Hoenlinger: Flight Flutter Testing of the High Altitude Research Aircraft STRATOS 2C (presentation only; no published paper)

The presentation described the characteristics of the STRATOS 2C aircraft, a manned vehicle designed for high altitude, long duration missions. The vehicle is completely composite and has a wing span of about 50 meters. The vehicle, being very large, has elastic mode frequencies beginning below 2 Hz. As a result of being a large flexible vehicle, unstable aeroelastic phenomena associated with the wing, the T-tail, the control surfaces, and the propellers were of significant concern. The presentation described the flutter prevention criteria applied during the design of the vehicle, the full-scale propeller tests conducted in the Russian T-101 tunnel to evaluate whirl flutter, and the flight test investigation.

6. B. H. K. Lee, M. J. Plosenski, P. E. Barrington, A. B. Markov, and C. G. Coffey: Aeroelastic Testing of an Unmanned Air Vehicle

Full-scale HATT–X flutter tests performed in an Open Jet Wind-Tunnel Facility and in flight are reviewed in this paper. The HATT-X (High-Speed Aeronautical Technologies Test Bed - Experimental) is an agile, high subsonic speed platform configured for conducting a variety of research missions. It is a highly instrumented test vehicle with equally sophisticated ground support subsystems. The paper discusses the occurrence of a destructive 57 Hz canard flutter mode that occurred in the wind-tunnel at a Mach number of about 0.75. A mass balanced and stiffer canard was then manufactured and installed on the HATT–X for flight testing. During the flight tests, large vertical oscillations of the canard were detected, followed by the structural failure of the canard linkage system in the forward fuselage. At the failure point the vehicle was decelerating after the rocket motor burn and the Mach number was approximately 0.75. The paper provides test data measured in the wind tunnel and in flight, and presents comparisons of the observed aeroelastic behavior for the two canards which were structurally different.

7. M. French and F. E. Eastep: Design and Testing of an Aeroelastically Scaled Model Structure

The development of an optimization method useful in automating the design of wind-tunnel flutter models and unique ground testing techniques are described in this paper. The design algorithm uses physical parameters of a finite element discretization of the scaled model as design variables. The design process is then broken down into two distinct steps. In the first step, the size of the elements in the model finite element representation are varied so that the stiffness of the scaled model matches desired values. The second step varies point masses so that desired natural frequencies and mode shapes are also correctly matched. The paper provides an example problem (a generic low aspect ratio wing) to demonstrate the application of the proposed method and describes unique ground testing techniques used to identify the static and dynamic characteristics of the model to verify the design procedure. The ground test methods described in the paper make use of state-of-the-art laser holographic techniques. The authors summarize that these optical test methods are well suited to testing subscale models and can show either static or

dynamic out of plane deflections for the entire model using a single image. In addition, these methods are shown to reduce the time required to characterize the test specimen and more accurate than conventional ground test methods.

8. Paper 8 was not presented.

9. A. J. Persoon: Wind Tunnel Flutter Testing on Shingles in the Transonic and Supersonic Speed Regime

This paper describes wind-tunnel tests conducted to investigate the flutter characteristics of various types of shingles used as part of the heat protection system for re–entry vehicles. These tests were performed in the transonic and supersonic speed regime using NLR's High-Speed (HST) and Supersonic (SST) wind tunnels. A review is given of the wind-tunnel experiments with emphasis on the generation and control of noise levels of the boundary layer in which the shingles were placed during the tests. The use of a spoiler or suction of the flow, both affecting the flutter characteristics of a shingle, are discussed in the paper. The behavior of unsteady pressures close to the shingle (upstream and downstream) is also highlighted in the paper as these pressures might act as a monitoring device to define the onset of flutter or limit cycle oscillations of a panel.

Session II - Flutter Signal Processing

10. J. E. Cooper: Parameter Estimation Methods for Flight Flutter Testing

A review and assessment of the various techniques that have been used to estimate modal parameters from wind-tunnel and flight flutter test data is presented in this overview paper. The relative advantages and disadvantages of the methods are examined, with particular emphasis being given to their suitability for analyzing flutter test data. The problems associated with analyzing non–linear and aeroservoelastic test data are highlighted. Recent advances in modal parameter identification are considered in terms of their relevance to flutter testing. Emphasis is placed upon determining the methods that have been used by the aerospace industry and to what extend the use of the methods has been successful. Consideration is also made of the theoretical limitations of the various methods. Finally, conclusions are drawn as to whether the state-of-the-art in parameter estimation techniques for flutter testing is satisfactory and whether future work is required in this area, particularly in dealing with non-linear aeroservoelastic systems. The paper also provides a very extensive list of references on the subject.

11. M. Dickinson: CF–18 Flight Flutter Test (FFT) Techniques

The paper describes Canadair's role in the flight flutter testing of the CF–18 aircraft with the 480 gallon external fuel tank installed. The flight test program was conducted at the Canadian Aerospace Engineering Test Establishment (AETE) located in Cold Lake, Alberta. The paper emphasizes the flight flutter test techniques employed, and the difficulties encountered due to non–linear modal behavior and a transonic external fuel tank buffet condition. The test program marked the first flight flutter test application of AETE's Leuven Measurement Systems (LMS) frequency analysis system. The paper also describes the user programs, written in the LMS User Programming and Acquisition language, that were developed to tailor and automate the frequency analysis system for the CF–18 flight flutter tests. In addition, the paper discusses the two frequency analysis techniques used during the program. Results of the two methods, dwell–decay Power Spectral Density method and Frequency Response Function/Maximum Likelihood Estimator curve fitting method, are directly compared with each other and with pre–flight finite element model predictions. Differences between the two sets of flight flutter test results are explained in the paper through the use of data from a simple

logarithmic decrement analysis of a response decay.

12. H. Van der Auweraer and P. Guillaume: A Maximum Likelihood Parameter Estimation Technique to Analyze Multiple Input/Multiple Output Flutter Test Data

The formulation, development, and checkout of Maximum Likelihood Estimators (MLE) for use during flight flutter tests requiring artificial excitation is discussed in this paper. Approaches for both single-input/single-output and multi-input/multi-output applications were developed and applied. The behavior of the MLEs developed are compared in the paper for examples involving both real data and synthetic data. Conclusions on their applicability and shortcomings are also discussed.

13. J. E. Cooper, M. J. Desforges, P. R. Emmett, and J. R. Wright: Advances in the Analysis of Flight Flutter Test Data

This paper describes a number of methods developed with the aim of improving the analysis and interpretation of flight flutter test data. Discussions relative to the following approaches are included: 1) the envelope function, a method used to determine an overall measure of system stability without actually performing any curve fitting; 2) advanced system identification techniques; and 3) the analysis of stick jerks using Eigensystem Realization Algorithms (ERA) and ERA with Data Correlation methods. The paper separates the discussion of the various approaches into improved curve fitting techniques and methods for enabling increased confidence in the flutter clearance procedure. Real flight flutter data are used to illustrate the various approaches. In addition, using simulated data the comparative performance of the various methods is examined, and the most effective approaches for performing flight flutter testing are identified.

Session III - Aeroservoelastic Testing

14. T. E. Noll, B. Perry III, and M. W. Kehoe: A Quarter Century of NASA Wind-Tunnel and Flight Experiments Involving Aeroservoelasticity

Some of the more interesting aeroservoelastic investigations conducted in the NASA Langley Research Center's Transonic Dynamics Tunnel and in flight at the NASA Dryden Flight Research Center are described in this overview paper. Four wind-tunnel and four flight test projects are reviewed in the paper. These projects include: the B-52, the YF-17, the F-16, and the Active Flexible Wing active control programs; and the DAST (Drones for Aerodynamic and Structural Testing), the X-29A, the F-16 AFTI (Advanced Fighter Technology Integration), and the F-18 HARV (High Angle of Attack Vehicle) programs. Each wind-tunnel test project presented in the paper discusses demonstrations of advanced active control concepts aimed at interacting with and/or exploiting the aeroelastic characteristics of flexible structures. Each flight test program presented in the paper discusses the identification and prevention of adverse aeroservoelastic interactions that allowed unique flight test demonstrations or flight envelope clearance programs to be successfully completed. These test projects were selected because of their contributions to the state-of-the-art in active controls technology (ACT) or because of the knowledge gained in further understanding the complex mechanisms that cause adverse aeroservoelastic interactions.

15. M. Ch. Zitchenkov, V. I. Dovbishchuk, and V. N. Popovsky: System of Aeroservoelastic Experimental and Numerical Investigations for Aircraft Design and Certification

The resources (databases, analytical methods, and experimental procedures) used by the aircraft industry in Russia in performing research in the technical areas of structural dynamics, aeroelasticity, and aeroservo-

elasticity (ASE) and in certifying that aircraft are free from vibrations of various types is described in the paper. Emphasis is placed on the vibrations resulting from the interaction between the airframe and the flight control systems as well as from systems that are actively controlling aeroelastic/dynamic deformations of the aircraft. The resources are used to provide a qualitative determination and analysis of ASE characteristics during all aircraft development stages. Some actual results obtained in ASE research programs on wide body civil and aerospace aircraft are presented in the paper as an illustration.

16. M. Lacabanne: Flight Flutter Tests of Transport Civil Aircraft with an Electronic Flight Control System

The strategy used at Aerospatiale when performing flight clearance tests of modern civil aircraft equipped with electronic flight control systems (EFCS), particularly if the aircraft is prone to adverse interactions between the structural modes of the aircraft and the flight control system, is presented in the paper. Because of the potential for adverse interactions it is shown that, in addition to the classical flutter tests, it is necessary to check the inflight dynamic behavior of the aircraft with EFCS operating at various flight conditions. The following topics are discussed in the paper: the choice of excitation devices; the description of recorded parameters; the importance of pre-flight analyses; the choice of flight conditions and configurations to be tested; and the correlation between the analytical model and the flight test modal analysis results. The paper also provides examples of aeroservoelastic flight test results.

17. K. Koenig: Pretension and Reality of Flutter—Relevant Tests

The paper gives a short review of all flutter relevant activities and tests required for large modern flexible aircraft, and discusses the differences between the desired and the achieved reliability and accuracy of the measured data. These activities and tests include weight measurements, stiffness tests, actuator impedance tests, tests of the electronic flight control systems, ground vibration tests, flight vibration tests, inflight measurements of unsteady airloads, and safety tests for active control systems. The conclusions provided in the paper are that: 1) most of the tests used today need some improvements; 2) some tests should be better exploited; and 3) the inflight measurement of unsteady airloads should become standard practice. These recommend-ations will provide higher confidence to the aircraft manufacturer, the certifying agency, and the user that the aircraft is free from flutter and adverse aeroservoelastic instabilities throughout its intended flight envelope.

18. R. B. Ramsay: Flight Flutter Testing of Combat Aircraft

A system for exciting the modes of vibration, performing analyses to extract flutter data, and displaying flutter parameters during flight flutter testing of an unstable digitally controlled fly–by–wire combat aircraft is presented in the paper. The paper indicates that applying such a system of tools increases aircraft safety during flight testing since critical parameters involved in the flutter mechanisms can be identified more quickly and more visibly displayed to the test engineer. The system, which is part of the flight test ground station, is fully integrated with the telemetry facility and is capable of analyzing and displaying test data for comparison with prediction in near–real time. This facility, which includes parallel processing transputers combined with high performance digital signal processing devices, will enable the engineer to assess analyzed data quickly and efficiently in order to decide whether or not the aircraft can safely progress the envelope expansion test. In addition, the paper discusses aircraft excitation systems under development. These systems will permit, under cockpit control, predefined waveforms to be generated within the Flight Control Computers and summed into the Flight Control System actuation loops. The overall clearance

philosophy for identifying critical flutter parameters through calculations, ground testing, and flight testing is also presented in the paper.

19. P. G. Hamel and R. V. Jategaonkar: The Evolution of Flight Vehicle System Identification

After providing a brief account of historical background, the paper traces chronologically the evolution of flight vehicle system identification starting from determination of aircraft frequency and damping ratio from flight data in the early twenties to the present day advanced applications such as estimation of high fidelity aerodynamic data bases for flight simulators or evaluation of highly augmented unstable flight vehicles of unconventional configurations. Through selected examples, the paper demonstrates that system identification methods have reached a maturity level that makes them a powerful and useful tool to support not only research but also industry activity in model validation, handling qualities evaluation, control law design, and flight vehicle design, and thus contribute significantly to risk and cost reduction in the optimal deployment of the existing aircraft and in the development of new generation aircraft. Although the paper focuses mainly on applications in the area of flight mechanics, some aspects of interdisciplinary flight vehicle modeling, for applications such as aeroservo-elasticity or high bandwidth rotorcraft modeling, are addressed as well.

20. Paper 20 was not presented.

21. R. T. Britt and B. Winther: Elements of the B-2 Flight Flutter Test Program (presentation only; no published paper)

This presentation described the basic test techniques and analysis methodology utilized during the execution of the flutter flight test program on the USAF/Northrop B-2 Stealth Bomber aircraft. Key elements of the program that were presented included: excitation systems that used control surfaces and turbulence (with comments on actuator capabilities, bandwidth and rates, and digital system effects); the use of an on-board test panel to provide excitation inputs (sine sweep, dwells, and random inputs with full control over frequency, magnitude, rate, and spectrum shape); the simultaneous recording of all instrumentation signals (distributed accelero-meters, strain gauges, and control surface deflections); methodologies used to provide modal frequency and damping estimates; and real-time data acquisition/analysis procedures with point-to-point clearance.

22. J. Becker, O. Sensburg, and V. Vaccaro: Aeroservoelastic Design, Test Verification and Clearance of an Advanced Flight Control System

This paper discusses the design of notch filters using a model of the aircraft that includes information that accurately describes the coupled flight dynamics, flight control dynamics, and structural dynamics behavior experienced on the ground and during inflight structural coupling tests. The paper also discusses design procedures, design and clearance requirements, correlation between model predictions and structural coupling tests, and model updates based on ground and in-flight measurements.

23. V. Vaccaro and J. Becker: Ground Structural Coupling Testing and Model Updating in the Aeroservoelastic Qualification of a Combat Aircraft

The role played by the ground Structural Coupling Test and the update of the aeroservoelastic model in the qualification process of a modern combat aircraft is the emphasis of this paper. Most modern combat aircraft are equipped with fly–by–wire and electronic flight control systems. The problem of the interaction between the dynamic response of the airframe and the flight control system is usually solved through an appropriate set of notch filters, designed to attenuate the level of structural vibrations picked up by the flight

control system sensors. A fundamental part of the qualification of the notch filter set is the ground testing activity, generally known as ground Structural Coupling Test. The main subject of this paper is the description of the test procedure followed for a modern fly–by–wire fighter aircraft that carries external stores. The latter part of the paper deals with the utilization of test results in updating the aeroservoelastic model. Emphasis is placed upon the necessity of developing and validating an adequate model to reduce the test activity to a limited set of additional external store configurations.

4. ROUND TABLE DISCUSSION

Following the technical presentations, a Round Table discussion was held. The discussion was led by a panel chaired by Dr. Jim Olsen along with the two technical evaluators, Dr. Jonathan Cooper and Dr. Thomas Noll.

Dr. Jim Olson started the proceedings by highlighting a number of issues that had arisen during the course of the meeting. He considered that the physics of the problem, the relationship between flutter testing and flight mechanics, aeroelastic modeling, excitation signal and devices, instrumentation, and data processing were all areas that required a great deal of further investigation.

Dr. Jonathan Cooper gave a brief overview of the papers that had been presented. He concluded that the meeting had shown that future work was required in each of the three basic elements that are used for Flight Flutter Testing, namely:

- Excitation: optimal signals and devices
- Data Analysis: which method is best ? non-linear identification
- Flutter Clearance: stability estimation between test points, flutter speed prediction

Dr. Thomas Noll then defined the topics to be considered by the Round Table:

- what are the issues ?
- where are the gaps in flutter testing ?
- who will close the gaps ?
- what is next for the SMP ?

Contributions were made by the following attendees: Dr. Ing J. Becker, Mr. R. T. Britt, Mr. B. D. Caldwell, Mr. J. Cochran, Mr. M. Curbillon, Mr. J. Ellis, Dr. R.M. French, Mr. J. J. Glaser, Mr. F. Goerung, Mr. M. W. Kehoe, Dr. Ing H. Hoenlinger, Prof. Ing O. Sensburg, Mr. B. Shirley, Mr. C. W. Skingle and Dr. J. R. Wright.

The main points raised during the discussion were as follows:

Excitation

The same type of excitation signals had been used, essentially, since the 1930s. Better signals were required in order to give better excitation levels in the frequency ranges of interest. Although the DEI vane was good for sine sweeps, it was felt that an improved device was required in order to give a random input with reduced crest factors and therefore a better power distribution. It was also noted that different input signals for the same test case generally gave different results, and this effect should be investigated to see whether it was due to different excitation levels from the various devices or was due to non-linearities.

Data Analysis

It was still not clear whether there was a best method to obtaining frequency and damping estimates. Probably there is no superior technique, but a wide range of methods should be used as a "tool-box" and implemented when appropriate. Further effort should be devoted to obtaining confidence bands on the damping values. It was also queried as to whether frequency and damping were the best parameters to consider during a Flight Flutter Test.

Clearance Procedure

It had become apparent during the course of the meeting that there were still a significant number of difficulties in performing a successful Flight Flutter Test programme and every aspect could lead to errors. The requirement for monitoring stability between flight points was apparent, as

was the need for new improved methods to deal with aeroservoelastic (ASE) systems. At some point in the near future the best practice for Flight Flutter Testing should be defined.

Other Problems
Major difficulties in the foreseeable future included the issues of non-linearities and Limit Cycle Oscillations (LCO). It was felt that the amount of non-linearity could be limited somewhat at the design stage and also through better quality manufacturing. The repeatability of Flutter Test results was of great concern - how well do the tests of one aircraft represent the entire fleet ? How much do the flutter characteristics change as aircraft age ? These questions will become even more important as the design of future aircraft becomes closer to optimal.

The determination of the parameters most sensitive to defining flutter and LCO behaviour would aid the design process. Also, the determination of the critical tests in the clearance procedure is important as the number of possible test cases will increase greatly with the use Flight Control Systems (FCS).

Other Comments
The test procedure has changed little since the 1970s except for the increase in computing power. However, the next generation of aircraft will require an improvement in the process due to the increase of FCS and also the size of proposed aircraft will cause other problems. It was observed that the number of people worldwide with Flight Flutter Test experience is getting smaller and that aeroservoelasticians were getting older. In order to start to counteract this loss of experience, it was suggested that benchmark flight test data should be generated, including systems with controls, that could be used to train engineers as well as providing a data base to compare the various analysis methods. The concept of a "Flutter Simulator" was raised that would involve the simulation of an actual test for training purposes.

It was felt that 20 years was far too long a gap between meetings on such an important topic. The question as to whether the SMP was the best place to hold such meetings was also raised, due to the bias away from Dynamics in the SMP and also the increasing importance of Flight Control Systems in Flight Flutter Testing.

Dr. Jim Olson closed the meeting by thanking the organizers and all of the speakers and attendees. He concluded that the meeting had been excellent, with a high quality of papers and presentations that had stimulated a lot of thoughts and discussion.

5. RECOMMENDATIONS

It is recommended that AGARD stimulate future developments in Flight Flutter Testing through the following:

- Establish a database of simulated and real flight test data including that from aircraft with Flight Control Systems.
- Coordinate a Round-Robin exercise comparing a number of modal parameter estimation methods.
- Hold a further meeting on Aeroservoelastic Testing within the next 10 years.

Significant further work is required in the following areas:

- Aeroservoelastic testing
- Behaviour and identification of non-linear aeroelastic systems
- Repeatability of flutter test results on aging aircraft and also across aircraft fleets
- Improved excitation signals and devices

6. REFERENCES

1. K. Koenig, "Flight Flutter Parameter Identification". Presented at the 70th AGARD SMP Meeting April 1990.
2. J. E. Cooper," Modal Parameter Identification for Flight Flutter Testing". Presented at the 71st AGARD SMP Meeting October 1990.

A HISTORICAL OVERVIEW OF FLIGHT FLUTTER TESTING

Michael W. Kehoe
NASA Dryden Flight Research Center
P.O. Box 273, MS 4840D
Edwards, California 93523-0273
USA

1. SUMMARY

This paper reviews the test techniques developed over the last several decades for flight flutter testing of aircraft. Structural excitation systems, instrumentation systems, digital data preprocessing, and parameter identification algorithms (for frequency and damping estimates from the response data) are described. Practical experiences and example test programs illustrate the combined, integrated effectiveness of the various approaches used. Finally, comments regarding the direction of future developments and needs are presented.

2. INTRODUCTION

Aeroelastic flutter involves the unfavorable interaction of aerodynamic, elastic, and inertia forces on structures to produce an unstable oscillation that often results in structural failure. High-speed aircraft are most susceptible to flutter, although flutter has occurred at speeds of 55 mph on home-built aircraft. In fact, no speed regime is truly immune from flutter.

Aeroelasticity plays a significant role in the design of aircraft. The introduction of thinner wings, all-movable horizontal and vertical stabilizers, and T-tail configurations increases the likelihood of flutter occurring within the desired flight envelope. Today's aircraft designs undergo sophisticated aeroelastic analyses to ensure that the design is free of flutter within the flight envelope. These analytical results are often verified by wind-tunnel flutter models and ground vibration tests. Flight flutter testing provides the final verification of the analytical predictions throughout the flight envelope.

In the early years of aviation, no formal flutter testing of full-scale aircraft was carried out. The aircraft was simply flown to its maximum speed to demonstrate the aeroelastic stability of the vehicle. The first formal flutter test was carried out by Von Schlippe in 1935 in Germany (Ref 1). His approach was to vibrate the aircraft at resonant frequencies at progressively higher speeds and plot amplitude as a function of airspeed. A rise in amplitude would suggest reduced damping with flutter occurring at the asymptote of theoretically infinite amplitude as shown in Fig 1. This idea was applied successfully to several German aircraft until a Junkers JU90 fluttered and crashed during flight tests in 1938.

Early test engineers were faced with inadequate instrumentation, excitation methods, and stability determination techniques. Since then, considerable improvements have been made in flight flutter test technique, instrumentation, and response data analysis. Flutter testing, however, is still a hazardous test for several reasons. First, one still must fly close to actual flutter speeds before imminent instabilities can be detected. Second, subcritical damping trends cannot be accurately extrapolated to predict stability at higher airspeeds. Third, the aeroelastic stability may change abruptly from a stable condition to one that is unstable with only a few knots' change in airspeed.

This paper presents a historical overview of the development of flight flutter testing, including a history of aircraft flutter incidents. The development of excitation systems, instrumentation systems, and stability determination methods is reviewed as it pertains to flight flutter testing.

3. FLUTTER HISTORY

The first recorded flutter incident was on a Handley Page O/400 twin engine biplane bomber in 1916. The flutter mechanism consisted of a coupling of the fuselage torsion mode with an antisymmetric elevator rotation mode. The elevators on this airplane were independently actuated. The solution to the problem was to interconnect the elevators with a torque tube (Ref 2).

Control surface flutter began to appear during World War I. Wing-aileron flutter was widely encountered during this time

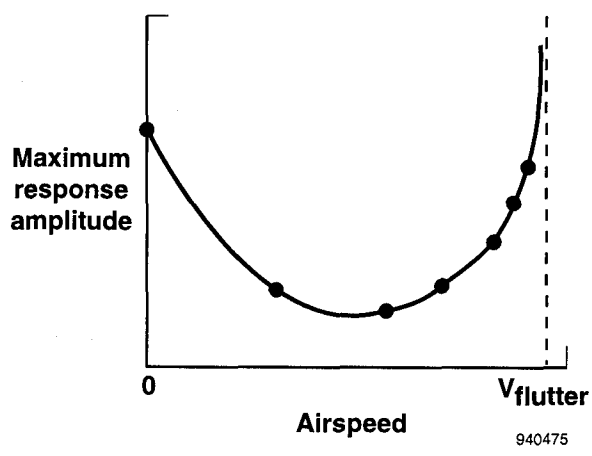

Fig 1 Von Schlippe's flight flutter test method.

Paper presented at the Structures and Materials Panel Specialists' Meeting on "Advanced Aeroservoelastic Testing and Data Analysis", held in Rotterdam, The Netherlands, from 8-10 May 1995, and published in CP-566.

(Ref 3). Von Baumhauer and Koning suggested the use of a mass balance about the control surface hinge line as a means of avoiding this type of flutter. Although some mild instances of control surface flutter were encountered afterwards, these were usually eliminated by increasing the mass balance of the control surface.

After World War I, higher airspeeds and a shift from external wire-braced biplanes to aircraft with cantilevered wings resulted in more wing flutter incidents. Primary surface flutter began to appear around 1925 (Ref 4). Air racers experienced many incidents of flutter from the mid-1920's until the mid-1930's as attempts were made to break speed records. References 3, 4, and 5 give many examples of these incidents.

Another form of flutter dealt with in the 1930's was servo tab flutter. Collar (Ref 3) predicted that this type of flutter would be around for many years. This prediction was correct, for between 1947 and 1956, 11 cases of tab flutter incidences were reported for military aircraft alone (Ref 6). Even today servo tab flutter is still a problem. In 1986, the T-46A trainer experienced aileron flutter during a test flight that was being flown to find the proper amount of mass balance. These ailerons were free floating and driven by tabs at the trailing edge of the aileron (Ref 7).

New aeroelastic problems emerged as aircraft could fly at transonic speeds. In 1944, while flight testing the new P-80 airplane, NACA pilots reported an incident of aileron buzz (Ref 5). From 1947 to 1956, there were 21 incidences of flutter involving transonic control surface buzz. Prototypes of both the F-100 and F-14 fighters had incidences of rudder buzz. Today, the transonic flight regime is still considered the most critical from a flutter standpoint.

Chuck Yeager first achieved supersonic speeds in level flight in 1947. Supersonic flutter then began to be studied more seriously as these speeds became routinely flown. Supersonic speeds also produced a new type of flutter known as panel flutter. Panel flutter involves constant amplitude standing or traveling waves in aircraft skin coverings. This type of instability could lead to abrupt fatigue failure, so the avoidance of panel flutter is important. In the 1950's a fighter airplane was lost because of a failed hydraulic line that was attached to a panel that had experienced such panel flutter (Ref 5).

The carriage of external stores affects the aeroelastic stability of an aircraft. Seven incidents of flutter from 1947 to 1956 involved the carriage of external stores, as well as pylon-mounted engines (Ref 5). The stores carriage problem is still significant today, particularly with the many store configurations that an airplane can carry. Certain combinations of external stores carried by the F-16, F-18, and F-111 aircraft produce an aeroelastic instability known as a limit cycle oscillation (LCO) (Refs 8 and 9). Although these oscillations are mostly characterized by sinusoidal oscillations of limited amplitude, flight testing has shown that the amplitudes may either decrease or increase as a function of load factor (angle of attack) and airspeed.

Much has been learned about the prevention of flutter through proper aircraft design. Flight flutter incidences still occur, however, on primary lifting surfaces as for the F-117 stealth fighter (Ref 10) and the E-6 Tacamo (Ref 11) aircraft, both of which experienced vertical fin flutter.

4. DEVELOPMENT OF FLIGHT FLUTTER TEST TECHNIQUES

Von Schlippe conducted the first formal flight flutter test in Germany in 1935. The objective of his test method was to lessen the risk associated with flutter testing. The usual practice at this time was to fly the airplane to the maximum speed and then to observe the stability of the structure.

Von Schlippe's technique consisted of exciting the structure using a rotating unbalance weight, measuring the response amplitude, and then recording the response amplitude as a function of airspeed. The forced response amplitude would rapidly increase as the aircraft approached its flutter speed. Therefore, the flutter speed could be estimated from data obtained at subcritical airspeeds.

The Germans successfully used this technique until 1938 when a Junkers JU90 aircraft fluttered in flight and crashed. Inadequate structural excitation equipment and unsatisfactory response measurement and recording equipment were identified as probable causes for this accident (Ref 4).

The United States attempted this technique in the 1940's with flutter tests of a Martin XPBM-1 flying boat and a Cessna AT-8 airplane (Ref 4). Figure 2, taken from Ref 4, shows the response amplitude data as a function of airspeed. The graph shows that destructive flutter for this airplane was averted by the narrowest of margins during this flight test.

In the late 1950's, excitation systems consisted of inertia shakers, manual control surface pulses, and thrusters (bonkers). Instrumentation had improved and response signals were then being telemetered to the ground for display and analysis. Some programs still displayed response signals on oscillographs in the airplane. Many experimenters realized the importance of adequate structural excitation for obtaining a high signal-to-noise ratio

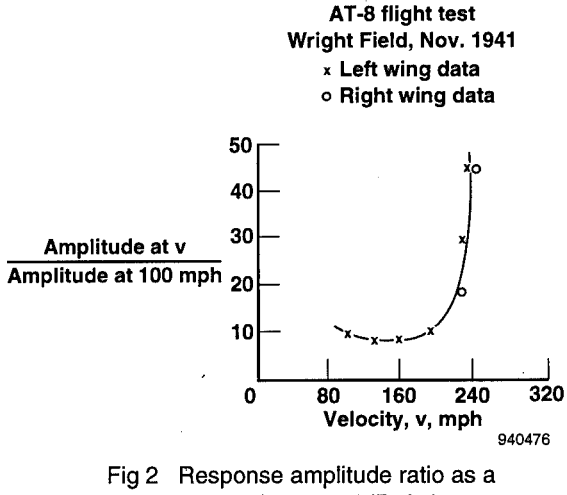

Fig 2 Response amplitude ratio as a function of airspeed (Ref 4).

(Ref 12). The use of oscillating vanes to excite the structure was being considered during this time.

From the 1950's until the 1970's, many aircraft were equipped with excitation systems. Frequency sweeps were made to identify resonances. These sweeps were often followed by a frequency dwell–quick stop at each resonant frequency. In-flight analysis was usually limited to log decrement analysis of accelerometer decay traces on strip charts to determine damping.

The F-111 program is an example of this procedure. Fig 3 shows a schematic of the process, taken from Ref 13. Filtered and unfiltered accelerometer response data were displayed on strip charts and on X-Y frequency sweep plotters. Damping was manually determined from the frequency dwell–quick stop decay traces. Computers were not used for analysis of the data.

The P6M aircraft program took a departure from this methodology (Ref 14). This flight flutter program used random atmospheric turbulence to excite the structure and spectral analysis to analyze the response data for stability. The objective of this technique was to use every minute of flight time for dynamics data and to eliminate special test points for flutter.

Since the 1970's, digital computers have significantly affected flight flutter testing techniques. The computer has allowed for the rapid calculation of the fast Fourier transform (FFT). Computers have fostered the development of more sophisticated data processing algorithms that are useful for analysis of response data from either steady-state or transient excitation. Frequency and damping are now estimated with parameter identification techniques. Such analysis is done online in a near-real-time manner. Frequency and damping trends are established as a function of airspeed or Mach number. These trends are extrapolated to determine the stability at the next higher airspeed test point. As computer speeds have increased, the time required to conduct flight flutter testing per test point has decreased. The ability to analyze more data at each test point and the increased number of flight test points resulting from more sophisticated aircraft designs, however, have increased the total time to clear the flight flutter envelope.

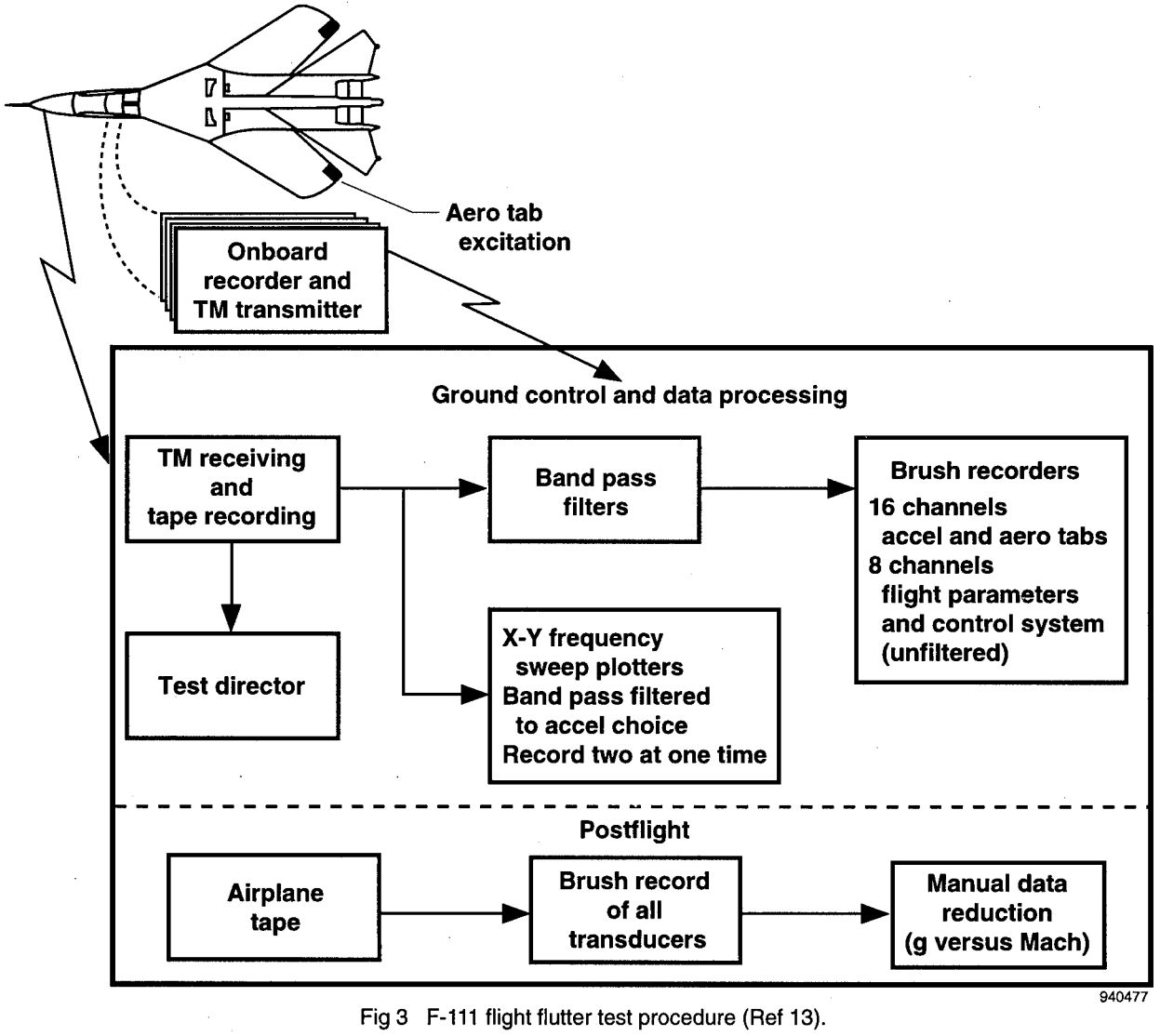

Fig 3 F-111 flight flutter test procedure (Ref 13).

The test technique typically used is to monitor the telemetered response signals with real-time frequency analyzers and strip charts. These data are also acquired by digital computers that process the data using parameter identification techniques for estimating frequency and damping (Ref 15). Fig 4 shows this process. In this figure, data are telemetered from the airplane and simultaneously displayed on strip charts, and real-time frequency analyzers. A computer acquires the data for analysis to determine frequency and damping estimates. The test director, who communicates with the test aircraft, has access to all of this information to make decisions on continuing the flutter envelope expansion.

Although flight flutter test techniques have advanced, today's techniques are still based upon the same three components as Von Schlippe's method: structural excitation, response measurement, and data analysis for stability. Technology development associated with each component will be reviewed and a discussion of the impact on the safety of flight flutter testing will follow.

5. EXCITATION SYSTEMS

Structural excitation is a necessary part of the flight flutter testing methodology. Detection of impending aeroelastic instabilities cannot be made without adequate excitation. Adequate excitation provides energy to excite all of the selected vibration modes with sufficient magnitudes to accurately assess stability from the response data.

The Transavia PL12/T-400 airplane (Ref 16) clearly demonstrated the importance of adequate excitation levels in 1986. This airplane was excited on the initial flight tests by control surface pulses and random atmospheric turbulence. Flutter did not occur during the flight test. In a subsequent flight, the airplane experienced violent oscillations of the rudder and tail boom when it was flown in rough weather conditions. These weather conditions provided higher levels of excitation than the levels induced during the flight flutter test.

In the 1930's, the Germans decided that improper exciter location resulted in poor responses that prevented the determination of the onset of flutter and sometimes resulted in flutter occurring unexpectedly (Ref 4). In the 1950's, the United States learned that low excitation levels tend to give a large scatter in the damping values estimated from the response data. In addition, the estimated values suggested lower aerodynamic damping than actually existed. During flutter testing of the B-58 airplane (Ref 17), it was found that a structural excitation level at least three to four

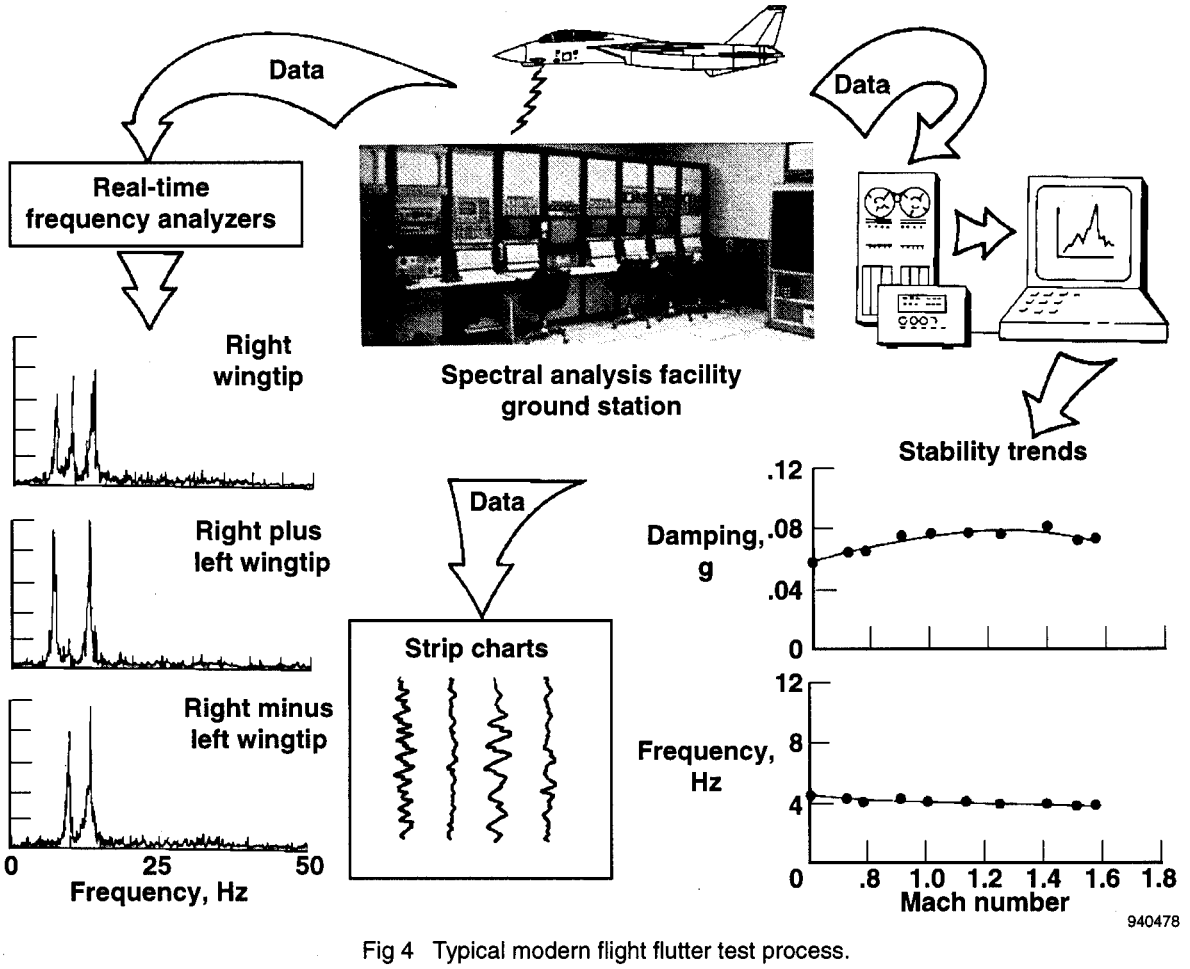

Fig 4 Typical modern flight flutter test process.

times higher than was obtained by random atmospheric turbulence was necessary to provide an acceptable level of excitation.

The excitation system must not only provide adequate force levels but must also (1) provide adequate excitation over the desired frequency range of interest, (2) be lightweight so as not to affect the modal characteristics of the airplane, and (3) have power requirements (electric or hydraulic) that the airplane can meet. It is difficult for any one system to meet these requirements simultaneously. Over the years, many types of excitation have been tried with varying degrees of success. Some more common means include control surface pulses, oscillating control surfaces, thrusters, inertial exciters, aerodynamic vanes, and random atmospheric turbulence.

5.1 Control Surface Pulses

Manual control surface pulses were the first means of excitation. This provided sudden control surface movements. Depending on the type of control system, modes up to about 10 Hz can be excited this way. Such pulses approximate a delta function that theoretically has a high frequency content. Two benefits of this type of excitation are that no special excitation equipment is required and that the transient response signature of the structure is easy to analyze for stability. Test duration for each pulse is short, so many can be applied at each test point.

There are several drawbacks, however. First, it is difficult to get repeatable pulses, and thus the degree of excitation is inconsistent. Second, either the pilot cannot provide a sharp enough input or the control system is unable to provide a sharp enough disturbance to excite any critical flutter modes above 10 Hz. Third, such pulses often do not provide an adequate level of excitation to determine the onset of flutter. The fact that flight was possible beyond the flutter speed without exciting flutter with pulses was demonstrated during a flight flutter test in the 1950's (Ref 18). The purpose of this particular flight was to investigate the stability of a vertical stabilizer. The structure was excited using rudder pulses and by thrusters (impulse generator). The thrusters excited flutter at a speed 5 knots below that where the structure was previously excited by rudder pulses without incident.

In spite of their limitations, control surface pulses have continued in use to excite the structures of many airplanes since 1950. The F-101 (mid-1950's), the early testing of the F-4 aircraft (late 1950's), the A-7A (1965), some of the early Boeing 747 flutter testing (1969), and low-speed testing of the DC-10 airplane (1970) all used control surface pulses for structural excitation.

Flight control surface pulses are still used today as excitation for flight testing. Most modern fly-by-wire flight control systems (analog and digital), however, have low-pass filters in the stick input path that filter out high-frequency signal content. For example, the F-16XL airplane flight control system has a 1.6-Hz low-pass filter (single pole) in the stick input path that would washout any sharp stick motion commands to the control surface actuators. Manual control surface pulses are still used today on most small aircraft and sailplanes because this is usually the only affordable type of excitation for these aircraft.

5.2 Oscillating Control Surfaces

Commanded oscillations of the control surfaces were also used in the 1950's. The XF3H-1 airplane used an oscillating rudder for excitation to investigate a rudder buzz instability (Ref 19). The rudder was oscillated by supplying a variable frequency command signal into the rudder servo of the autopilot system. This system could excite over a frequency range of 5 to 35 Hz and with the frequency stepped every 3 sec by an automatic rotary switch located in the cockpit.

In the mid-1960's, electronic function generators were developed to provide signals to control surface servos in the autopilot system. These function generators provided signals to oscillate the horizontal stabilator and the ailerons of the F-4 airplane (Ref 19). The stabilator could sweep from 8 to 30 Hz and the ailerons from 2 to 16 Hz. The actuators for each surface were modified to provide the required gain and frequency response. A cockpit controller provided the capability to adjust the excitation amplitude, mode selection (sweep or dwell), start and stop sweep frequency, and dwell frequency. Further advances in electronics during the 1970's and 1980's resulted in the ability to send excitation signals to the control surface actuators that were not sinusoidal. The F-18 aircraft excitation system can generate sinusoidal and bandpass-filtered pseudo-random commands to the flight control surfaces (Ref 19).

This method of excitation has been successfully used for the X-31 and YF-22 airplanes and for the stores clearance work on the F-16, F-15, and F-18 airplanes. The X-31 airplane could sweep frequencies from 0.1 to 100 Hz. Although significant actuator roll-off occurred above 20 Hz, the combination of aerodynamic force at low frequencies and control surface inertia forces at higher frequencies provided adequate excitation for this airplane (Ref 20).

The primary advantage of this type of system is that no additional hardware is required except for an excitation control box located in the cockpit. As a result, the flutter speed of the airplane is not affected as it might be with other types of excitation systems.

A disadvantage of this type of system is the frequency response limitations of the control surface actuators. Often, special actuators are required to excite critical high-frequency modes, as was the case for the F-4 flutter testing (Ref 19).

5.3 Thrusters

Thrusters, sometimes known as bonkers, ballistic exciters or impulse generators, are an early device circa (1940) used for structural excitation. These small, single-shot, solid-propellant rockets have burn times of 18–26 msec and maximum thrust levels of 400–4,000 lbs (Ref 21).

Thrusters are simple, lightweight devices that generally do not affect the modal characteristics of the airplane. These devices produce transient responses of short duration, which is important when the airplane has to dive to attain a test condition.

The disadvantages for these devices include single-shot operation, difficulty in firing two or more either in phase or out of phase with respect to each other, and their inability to provide a wide frequency band of excitation. Usually required are thrusters with three different burn times to excite modes in a frequency range that covers 5 to 50 Hz.

Thrusters were used for part of the flutter clearance of the F-101 airplane in the mid 1950's. Six thrusters were mounted on each wingtip, three on top and three on the bottom. Use of these devices was partially successful for this program (Ref 18).

Thrusters were also used by Douglas Aircraft Company in the 1950's (Ref 19) on several airplanes to investigate flutter characteristics. Thrusters were also used for portions of the F-4 flutter testing in the early 1960's. Since then, thrusters have not been used in the United States for any major flight flutter test program.

5.4 Inertial Exciters

A large variety of rotating eccentric weight and oscillating weight inertia exciters have also been tried. The rotating unbalance exciter was widely used for flight flutter testing in the 1940's and 1950's. These systems derive their forces from mass reactions. The inertia force is proportional to the exciter weight multiplied by the square of the rotating speed. As a result, the excitation capability may be limited at lower frequencies and excessive at higher frequencies.

The Martin XPBM-1 flying boat flight flutter test program used such a system. The precise control of frequency was difficult with the equipment available; thus the exciter would not stay tuned on the resonant frequency. One method of tuning the exciter frequency, as done by a Convair F-92 pilot in 1950, was by observing a meter in the cockpit that measured the response of selected vibration pickups during flutter tests (Ref 4).

The magnitude of the forces required to adequately excite an airplane is usually very large. As a result, the hardware required to produce the unbalance forces often could not be contained within the wing contour. In addition, these systems often are very heavy and raise concerns about the effect on the modal characteristics of the airplane that they are installed on. For example, the rotating unbalance equipment designed for (but never installed on) the XB-36 had a maximum force output of 1000 lb, and installation in each wing weighed between 400 and 500 lb (Ref 12).

Inertia shakers were used for the B-58 flutter testing in the early 1950's. These shakers were hydraulically powered and electrically controlled and were used to excite a frequency range of 5 to 40 Hz. The overall dimensions were 4.5 by 4.5 by 8.5 in., and each unit weighed 25 lb. The force output was 40 lb at 7.5 Hz and 150 lb at 40 Hz; the force level increased linearly between these two frequency values (Ref 17). This type of shaker worked well, particularly in exciting the higher frequency modes of the airplane.

The Convair F-102A, which was flutter tested in the late 1950's, also used inertial shakers. In the frequency range between 5 and 50 Hz, the force varied from approximately 20 to 300 lb. This shaker was sufficiently compact to be installed inside the wingtip, which has a depth of 4.5 in. The weight of the shaker was 8.5 lb (Ref 22).

After the 1950's, inertia exciters were not used extensively. However, there has been limited use of such systems to provide partial structural excitation for the F-14 horizontal stabilizer, the F-111 horizontal and vertical stabilizer, and the X-29 flaperon. The B-1A airplane also used an inertia shaker system (Fig 5) for flight flutter testing. The system consisted of five hydraulically driven, electronically controlled, oscillating mass exciters. One exciter was placed at each wingtip, one at each horizontal stabilizer tip, and one at the tip of the vertical stabilizer. Each wingtip and horizontal stabilizer tip could be operated in and out of phase with respect to each other. This system was capable of producing a maximum force of about 550 lb of force with an exciter weighing approximately 40 lb (Ref 23). This system adequately excited the modes of interest and was essential for safely expanding the flight envelope.

5.5 Aerodynamic Vanes

An aerodynamic vane consists of a small airfoil that is usually mounted to the tip of a wing or stabilizer. The vane is generally mounted on a shaft, driven either electrically or hydraulically, and oscillates about some mean angle. Oscillation of the vane will result in a varying aerodynamic force acting on the airplane. The amount of force depends on the size of the vane, dynamic pressure, and angle of rotation.

Aerodynamic vanes were first used in the 1950's. The YB-52 airplane used a wingtip oscillating airfoil shaker for flight flutter testing (Ref 24). This wingtip unit weighed 150 lb and was mounted on the right wingtip only. A similar amount of weight was installed on the opposite wingtip. Typical sweep times were approximately 7 min. The excitation frequency could be varied from 1.4 to 10 Hz.

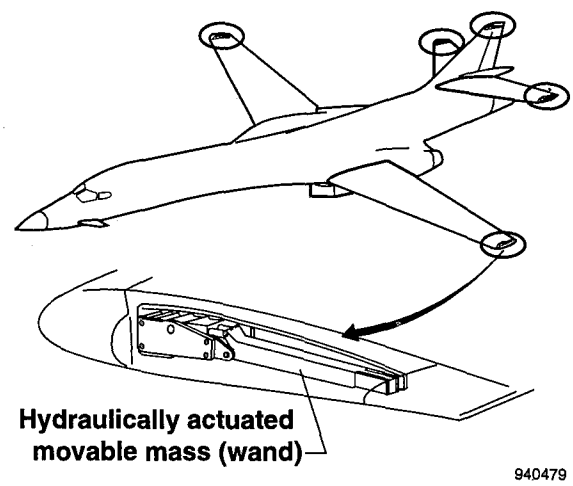

Fig 5 Inertial excitation system (Ref 23).

Since then, many flight flutter test programs have used the aerodynamic vane as a means of excitation. These programs include the DC-10, L-1011, Boeing 747, Boeing 757, S-3A, F-14, F-111, A-10, C-17, and T-46A. Tables 1 and 2 which were taken from Ref 13, show the characteristics of some of these excitation systems.

The advantage of this type of system is that it can excite low frequencies well; the amplitude at high frequencies is limited only by the response characteristics of the vane drive mechanism. The excitation frequency and amplitude at a given airspeed can be controlled, and the force time history produced is repeatable.

The main disadvantage is that the maximum force produced varies with the square of the equivalent airspeed. Other disadvantages include the addition of mass, the disturbance of the normal airflow around the wingtip or stabilizer tip with the vane present, and the large power requirements usually needed to operate this system.

There are two notable variations of the oscillating aerodynamic vane concept: a rotating vane and a fixed vane with a rotating slotted cylinder attached to the vane trailing edge.

The C-5A airplane excitation system consisted of a rotating vane mounted on top of the wing at each tip and on top of each horizontal stabilizer at each tip (Ref 13). The vanes were continuously rotated through 360 degrees, and both sets of vanes were synchronized to provide either symmetric or antisymmetric excitation. This system produced periodic excitation to the structure and was successfully used for flight flutter testing.

The fixed vane with a slotted rotating cylinder attached to the trailing edge (Fig 6) was developed by W. Reed (Ref 25). The vane/cylinder assembly weighs approximately 10 lb. The device generates periodic lifting forces by alternately deflecting the airflow upward and downward through the slot. This system was used for the flutter clearance of a F-16XL airplane with a modified laminar flow glove (Ref 26). Frequency sweeps were

Table 1. Summary of aerodynamic excitation systems used in U.S.

Airplane	Surface	Location	Frequency range	Time to sweep, sec	Sweep law
747	Wings	External vanes at wingtips	1.5–7.0 Hz	90	Exponential
DC-10	Wings horizontal Vertical tail	External vanes at tips of main surfaces	1–20 Hz and 1–10 Hz	90 90	Exponential
L-1011	Wing stabilizer	External vanes	1–18 Hz 3–25 Hz	90 30	Linear period
S-3A	Side of fuselage under stabilizer	External vanes	1.5–18 Hz 3–25 Hz	90	Linear period
C-5A	Wing stabilizer	External vanes on top of surfaces near tips	.5–25 Hz	60 normal 30 dive only	Exponential
F-14	Wing fin	Aero-tab External vane	5–50 Hz	15	Exponential
F-15	Normal control Ailerons Stabilator		2–16 Hz 5–10 Hz	100–200 45	Linear frequency
F-111	Wing	Aero-tab	35–2 Hz	45	Exponential

Table 2. Summary of inertial excitation systems used in U.S.

Airplane	Surface	Location	Frequency range	Time to sweep, sec	Sweep law
F-14	Horizontal tail	Right side stabilizer only	5–50 Hz	15	Exponential
F-111	Horizontal, vertical tail surfaces	Inboard on stabilizer near side of fuselage, top of fin	35–2 Hz	45	Exponential

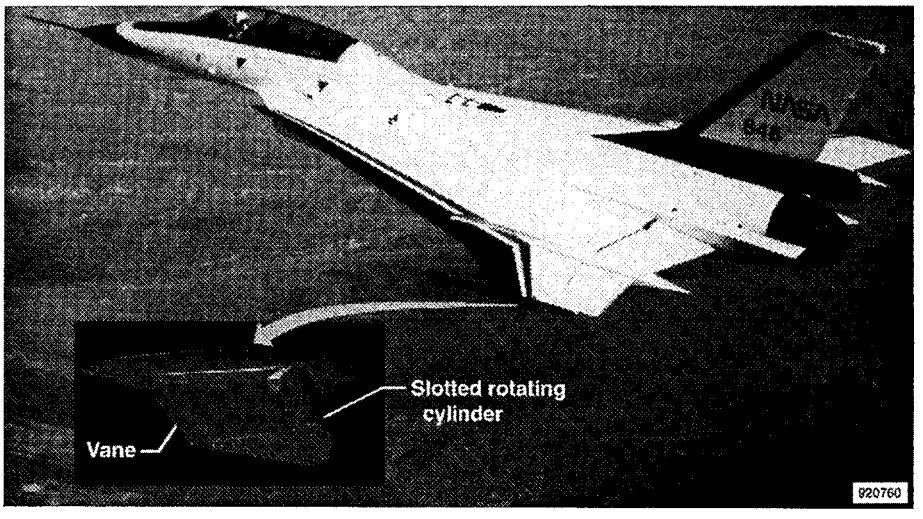

Fig 6 F-16XL with vane and rotating slotted cylinder excitation system (Ref 26).

conducted from 5 to 35 Hz for this program. The system uses exceptionally little electric power and is easy to install.

5.6 Random Atmospheric Turbulence

Atmospheric turbulence has been used for structural excitation in many flight flutter test programs (Ref 15). The greatest attraction to this type of excitation is that no special onboard exciter hardware is required. Turbulence excites all of the surfaces simultaneously, which causes both symmetric and antisymmetric modes to be excited at the same time. This method eliminates the need to perform symmetric or antisymmetric sweeps.

Natural turbulence is the random variation in wind speed and direction. Turbulence is generally produced by weather-front winds and thermal activities; the extent of turbulence within an air mass can vary widely. Reference 27 provides an excellent description of turbulence and its use for excitation in flight flutter testing.

This approach was tried in the late 1950's. The P6M *Seamaster* flight flutter program (Ref 14) used random atmospheric turbulence to excite the structure and spectral analysis to analyze the response data for stability. Objectives of this technique were to use every minute of flight time for dynamics data and to eliminate special test flights for flutter. The YF-16 also used random atmospheric turbulence along with the random decrement technique for data analysis to clear the flutter envelope of the basic airplane (Ref 28).

Although this method has been used with some success over the years, there are several disadvantages. The turbulence that is found is often not intense enough to produce sufficient excitation compared with that obtained with onboard exciters. Turbulence usually excites only the lower frequency modes for most airplanes. Long data records are required to obtain results with a sufficiently high statistical confidence level. The signal-to-noise ratio of the response data is often low, which makes data analysis very difficult. Flight time is lost looking for sufficient turbulence, and turbulence often interferes with other engineering disciplines data.

Fig 7 compares the power spectrum plots obtained from the F-16XL airplane excited by random atmospheric turbulence and by a vane with a slotted rotating cylinder attached to the trailing edge. The turbulence was reported to be light-to-moderate for this flight condition. All of the structural modes were excited by the vane, while only the 8-Hz mode was well excited by turbulence. This data comparison clearly indicates the poor data quality that is typically obtained with random atmospheric turbulence.

This flight test program also illustrates the lessons learned during the B-58 flutter test program. Inadequate excitation levels usually give a large scatter of the estimated damping values, and the estimated damping values often indicate lower damping than actually exists. A comparison of response data damping values from random atmospheric turbulence and vane excitation (Fig 8) shows that the turbulence response data, which have a lower excitation level, consistently have lower estimated damping values.

Although the flutter envelopes of many modern aircraft (i.e., X-29A, advanced fighter technology integration (AFTI) F-111 mission adaptive wing, AFTI F-16, Schweizer SA 2-37A motor glider, and F-15 short takeoff and landing/maneuver technology demonstrator) have been cleared using atmospheric turbulence, caution should be used when using this form of excitation to ensure that the critical flutter mode has been excited throughout the flight envelope.

6. INSTRUMENTATION

The instrumentation used to record the structural responses of an airplane to excitation is another critical component of flight flutter testing methodology. The response data must be measured at enough locations and be of high enough quality that the flight can be conducted safely. Included in the instrumentation system is

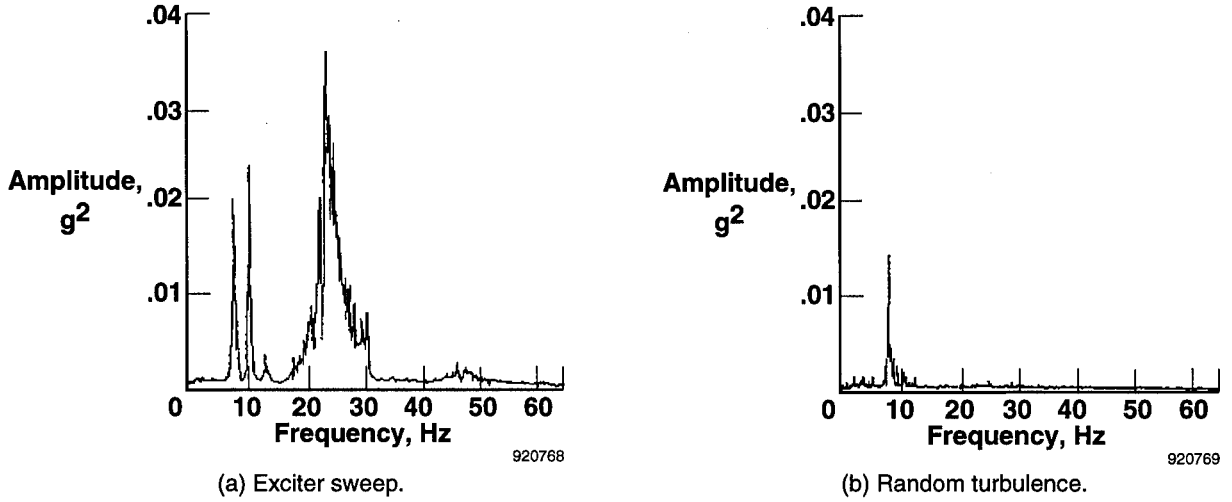

Fig 7 Comparison of excitation of the left-wing aft accelerometer at Mach 0.9 and 30,000 ft (Ref 26).

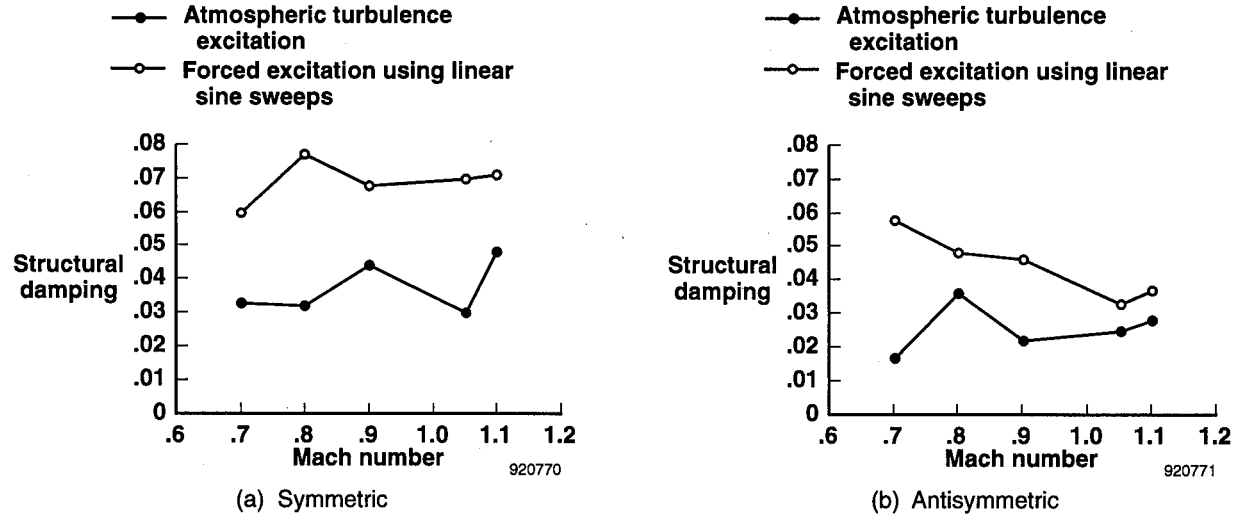

Fig 8 Structural damping values for wing bending modes (Ref 26).

the measurement, telemetry, recording, and displaying of the flight data.

6.1 Measurement

The most commonly used transducers to measure the excited response of a structure have been the accelerometer and strain-gage bridge. The selection of the device to use often depends on the ease with which installation can be accomplished, although today the more commonly used device is the accelerometer.

Accelerometers used in the early 1940's were large and heavy. As an example, the accelerometers were about 3 in. high, 2 in. wide, and weighed about 1 lb. Subminiature accelerometers were developed later and these were lighter but still were large (1/2-in. high, and 1-in. wide). The calibration of these devices drifted during operation mainly because of the electronics in use then.

The accelerometers used for the B-58 flutter testing in the 1950's were of the strain-gage type. These were fluid damped devices. To minimize the effects of the outside air temperature on the damping, these units had built-in electric heaters to maintain a constant temperature of 165 °F (Ref 17).

Piezoelectric accelerometers have been developed such that miniature units today weigh less than one-tenth of an ounce, operate in a temperature range of –65 to 200 °F, have high sensitivity, have a linear frequency range of 1 to 10,000 Hz, and have amplitude linearity from 1 to 500 *g*. Typically the dimensions are as small as 0.25 in. wide and 0.15 in. high. Today's accelerometers accurately measure the structural response in almost any kind of environment.

Subminiature instrumentation has also been developed as self-contained peel and stick devices (Ref 29). Each unit contains a

battery, sensor, antenna, processor, and transmitter. These devices do not require any wiring and the signals may be transmitted either to a receiver located on board the airplane or directly to a receiver located on the ground within a small flight radius of the transmitter. Advances such as this will significantly reduce the cost associated with flutter testing.

6.2 Telemetry and Recording

Recording equipment was not adequate during the 1930's and was cited as a possible reason that the Germans lost several airplanes during flutter testing (Ref 4) in that decade. In the 1930's, a Junker JU86 airplane underwent flight flutter testing to identify the effects of balance weights on rudder stability. The recording system used was a thin wire attached to the rudder, which mechanically actuated a recorder installed in the observer's seat of the airplane (Ref 4).

During the 1940's, the accelerometer responses were recorded on photographic oscillographs mounted in the cockpit or airplane cabin. These devices required a developing time for the paper; the time history responses could not be viewed immediately as a result.

In the 1950's, data were commonly FM/FM telemetered to the ground, recorded on magnetic tape, and then displayed on strip chart recorders. The telemetry systems during this period were small and typically only 8 to 12 channels of data could be telemetered to the ground (Refs 30, 31, and 32). As a result, onboard tape recorders captured all of the flight data while the recorders on the ground captured only the data that could be sent down from the airplane. The ground tapes were typically noisier than the onboard tapes mainly because of data-transmission problems.

Pulse code modulation (PCM) or digital telemetry was initiated in the 1960's, although FM/FM telemetry was still widely used for flutter testing because of the frequency bandwidth required. The PCM telemetry significantly increases the number of parameters that can be transmitted to the ground but requires a filter to prevent frequency aliasing of the analog response signal during digital sampling on board the airplane.

The frequency bandwidth of PCM systems had increased significantly by the 1980's. A frequency bandwidth of 200 Hz is easily attainable and sufficient for most flutter applications. As a result, PCM telemetry is now usually preferred for most flight flutter testing.

Today the available portable digital recorders are compact and can acquire data from flight instrumentation for storage within the unit's computer memory. Direct storage of the data eliminates the need for expensive equipment associated with PCM systems. Although these units can acquire a limited amount of data, they have been used for low-cost flutter testing (for example, the Pond Racer airplane). The data from the unit's computer memory are downloaded after each flight into a digital computer for analysis.

6.3 Displays

Computers were used to manipulate and display data to some extent during the 1950's. Analog computers were sometimes used to add, subtract, multiply, integrate, and filter the data signals telemetered (Ref 30) and then to display these signals on strip charts for the flutter engineer.

Sometimes the pilot had a small cathode ray tube oscilloscope in the cockpit to display the decay trace of a single, selected accelerometer (Ref 33). The pilot was briefed before each flight by the flutter engineer on the anticipated response amplitudes and safe operating limits.

In the 1950's, data were primarily displayed on strip charts in the control room for analysis by the flutter engineer. Strip chart capabilities have greatly increased, and today strip charts continue to be the primary device to display real-time accelerometer and strain-gage response time histories.

In the 1970's, computer technology had advanced to the point that it became feasible to use a computer to perform online stability analysis of the flight flutter test data. Computers were also used to provide discretes and alphanumerics in the control room. Many basic airplane parameters, such as Mach number, airspeed, angles of attack and sideslip, and fuel quantities, could now be displayed on cathode-ray tubes. This display provided the flutter engineer with the ability to more closely monitor the flight test conditions of the airplane.

In the 1980's, it became possible to provide the pilot a real-time guidance system for maintaining flight conditions. With this system the pilot flies the airplane to minimize the computed differences between the desired and actual flight condition (Mach number and altitude). The computed differences are telemetered to the airplane from a ground-based computer. The pilot then uses a cockpit display as an aid to reach and hold desired test conditions; this has resulted in exceptionally accurate stabilized flight test conditions (Ref 34).

As computer technology has advanced, so have the capabilities in the control room. Figure 9 shows a graphic representation of the control-room capabilities and the flight program requirements from 1946 to 1989 for NASA Dryden Flight Research Center (Ref 35). The general trend is that instrumentation on the airplane, the number of displays required in the control room, and the number of flights per year have steadily increased from 1946. Ref 36 describes the instrumentation and data-acquisition system for the X-29A flight test program. To meet the objectives of the program, PCM data acquisition system with five remote units operating asynchronously and one constant-bandwidth frequency modulation (FM) data-acquisition system were required to telemeter the 503 parameters of data to the control rooms on the ground.

7. DATA REDUCTION METHODS

The next component of flight flutter testing methodology is the analysis of the response signal. The response signal can consist

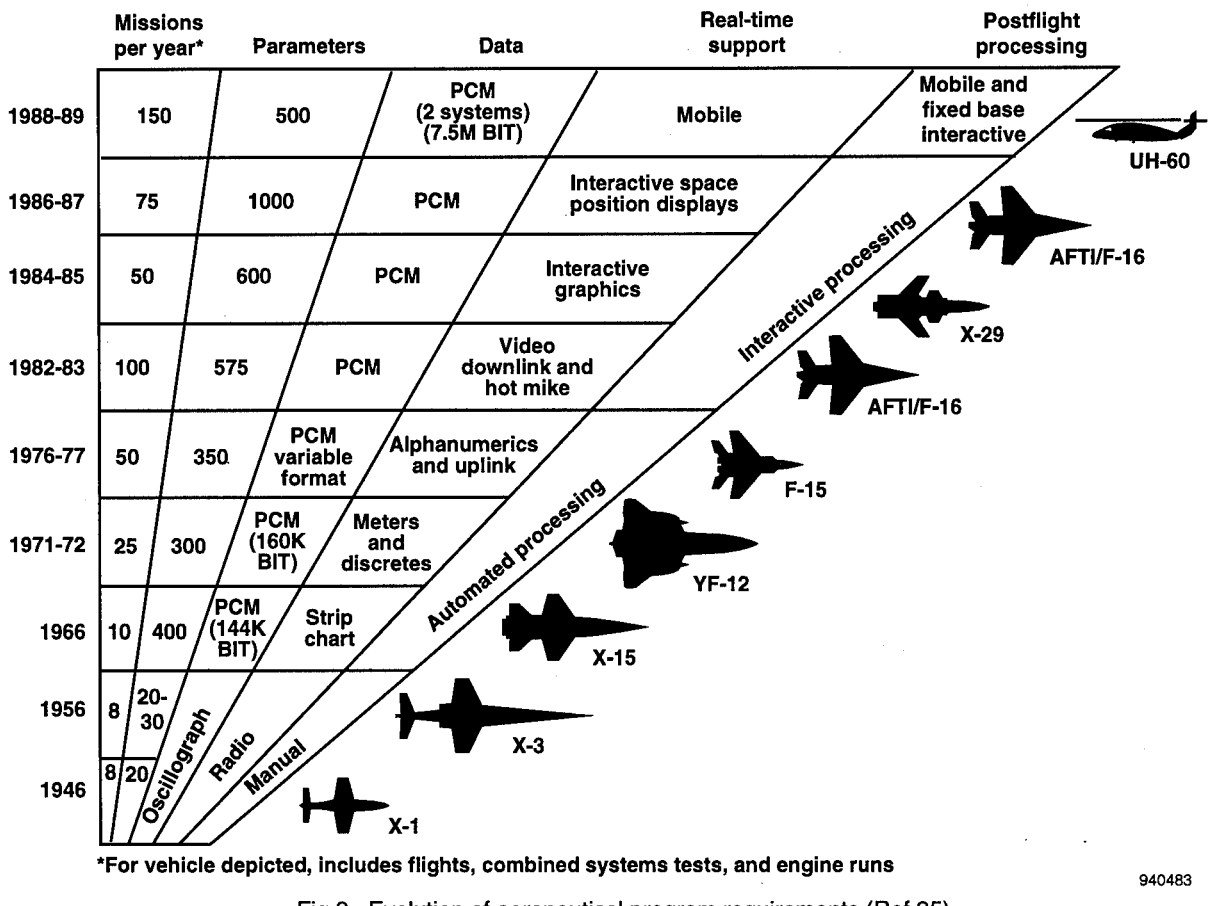

Fig 9 Evolution of aeronautical program requirements (Ref 35).

of random response caused by atmospheric turbulence or exciter input, transient responses caused by either impulse input or exciter frequency dwell–quick stops, or steady-state responses caused by exciter frequency sweeps. The accurate and timely evaluation of this data to determine stability is critical to the overall safety of the flight flutter test program.

In the 1930's and 1940's, the methods used consisted of measuring the response amplitude caused by a frequency sweep or determining the damping from a response caused by a control surface pulse. These data were recorded on an oscillograph recorder. All of this analysis was usually done by hand between flights, because no computers with sophisticated identification algorithms were available. The damping estimation consisted of using the log decrement method on the decay portion of a time history response. Occasionally, in lieu of telemetry, the flutter engineer was on board the airplane to do these analyses (Ref 4).

As telemetry became more available in the 1950's, the data analysis methods just described were still used, but the analysis was generally conducted on the ground. It became more common to excite the airplane at stabilized test points, analyze the response for stability, and then clear the airplane to the next higher airspeed (Refs 17, 22, and 24).

Data transmission problems usually added noise to the telemetered data. Filtering of the response data was common to reduce the scatter in the damping estimates. Data were often passed through a filter to reduce the data to a single-degree-of-freedom response. Closely spaced modes, however, proved to be difficult to separate for damping estimation using these analysis techniques.

Another method for enhancing the data analysis was to add and subtract time history signals. The symmetric and antisymmetric modes could then be separated, reducing the modal density of the response signal (Ref 32).

In the 1950's, vector plotting (Ref 31) and spectral analysis (Ref 14) were also used to determine stability. Modal damping was not estimated from the spectral analysis technique. This analysis only provided the frequencies and amplitudes of the response signal being analyzed.

These manual or analog analysis techniques continued to be used until the 1970's. Using tracking filters during an exciter frequency sweep improved the data quality obtained. Such a technique was used in the 1960's (Ref 19) to filter data provided to an analyzer to produce a real-time plot of frequency and amplitude.

Even so, no phase or damping information was available from this approach.

By 1970, digital computer systems could be used for interactive analysis of flight data. During the early 1970's, the fast Fourier transform was implemented on the computer, providing the capability to obtain frequency content of acquired signals in less that a second. The speed of computers then allowed parameter identification algorithms to be programmed for estimation of damping from the response signals.

The F-14 and F-15 aircraft programs were among the first to take advantage of this advance in technology. For the F-14, an equation error identification technique was used to estimate frequency and damping information (Ref 37). The F-15 program used an analysis technique to predict the flutter boundary based on frequency and damping data acquired at subcritical speeds (Ref 38). Other programs, that used the random decrement technique, such as the YF-16 (Ref 28), also took advantage of the increased capabilities of the digital computer to increase the efficiency and safety of flight flutter testing.

Since the 1970's, many identification algorithms have been developed to estimate frequency and damping from flight flutter data. Refs 39 and 40 are excellent reports on modal parameter estimation and provide numerous references for the many different approaches taken.

8. CONCLUDING REMARKS

8.1 Current State-of-the-Art

Today, the typical approach to flight flutter testing is to fly the aircraft at several stabilized test points arranged in increasing order of dynamic pressure and Mach number. Data are analyzed at these points only. The number of stabilized test points required to clear the flutter envelope of an airplane is typically high and consequently requires many flights to accomplish them. For example, the F-14 required 489 shaker sweeps to clear the basic airplane flight envelope; 177 shaker sweeps were required for the Gulfstream III; and 264 shaker sweeps were required for the Gulfstream II ER airplane (Ref 37). The F-15 required 132 shaker sweeps and 156 frequency dwells to clear the basic airplane flight envelope (Ref 41).

The data obtained at each stabilized test point establish a damping trend as a function of airspeed. Information is then extrapolated to predict the stability of the next planned test point. This practice is questionable because actual damping trends can be nonlinear. The most critical part of expanding the flutter envelope is the acceleration from one test point to the next. During this phase, response data are not being quantitatively analyzed. Instead, engineers, relying on intuition and experience, are limited to real-time monitoring of sensor responses on strip charts.

An examination of several flight flutter test programs shows the effectiveness of the techniques used today to warn of the onset of flutter. Fig 10 shows the frequency and damping trend information obtained, in near-real-time, during the flutter testing of the KC-135 airplane configured with winglets (Ref 42). The aircraft structure was excited by pilot-induced control surface pulses and damping was estimated using an FFT algorithm (Ref 15). The subcritical damping trend for a 2.6-Hz and 3.0-Hz mode indicated that as airspeed was increased, these two modes coupled and caused a decrease in the damping level. The damping level decreased with increasing airspeed until it was no longer safe to continue the test. In this instance, the techniques used provided a sufficient and adequate warning of the onset of flutter mainly because the decrease in damping was gradual.

Figure 11 shows the damping trend obtained in near-real time for an F-16 airplane configured with AIM-9J missiles, GBU-8 stores, and 370-gal external fuel tanks (Ref 15). Flight of the airplane with this store configuration is characterized by an LCO. Decay traces were obtained by using the flaperons to excite the structure with frequency dwells–quick stops. The damping was estimated using FFT algorithms. This set of data provided a unique opportunity to validate the accuracy of this algorithm because this configuration could be safely flown to a condition of zero damping. A linear extrapolation of the data trend provided an instability airspeed prediction that agreed closely with the actual instability onset airspeed encountered.

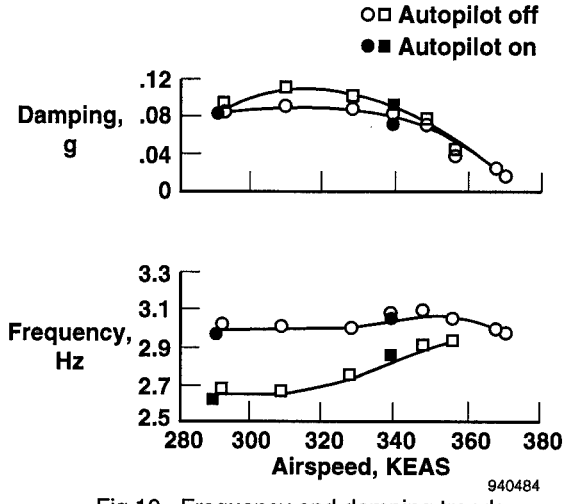

Fig 10 Frequency and damping trends established from flight data.

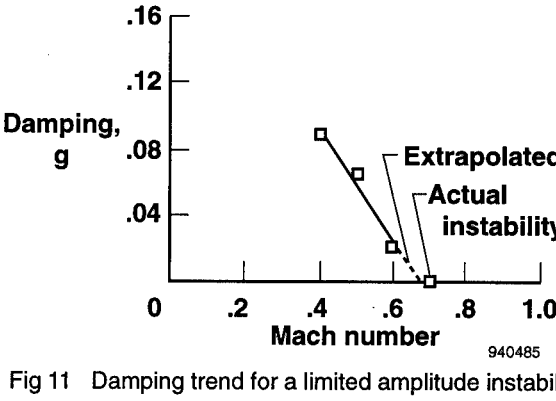

Fig 11 Damping trend for a limited amplitude instability.

Although today's techniques appear adequate to warn of the onset of flutter for gradual decreases in damping, it is doubtful that sudden changes in damping, which may occur between flutter test points, can be predicted with the accuracy and timeliness required to avoid flutter.

8.2 Future of Flight Flutter Testing

The future of flight flutter testing has been defined at several times. The flutter testing symposia held in 1958 and 1975 identified future directions and needs (Refs 43 and 44). These symposia proceedings will be reviewed to confirm the progress made toward those needs. Our future needs will then be presented.

8.2.1 1958 Flight Flutter Test Symposium

The final sentence in Ref 4, which was presented at the 1958 flight flutter test symposium, was, "It is hoped that improvements in test techniques will eventually result in flight flutter tests that will give all the information wanted and will be considerably less hazardous than they are today." Ref 17 stated that improvements needed were to shorten the time required to obtain data and to provide complete and higher quality data. The way to fulfill this need was to automate the data-reduction equipment. Ref 22 stated the need for completely automatic excitation, data-recording and data-reduction systems.

8.2.2 1975 Flutter Testing Techniques Symposium

The 1975 symposium contained several papers describing the application of techniques that used computers to estimate frequency and damping from flight flutter test data. Two future needs identified from the papers presented at the symposium were (1) to further develop parameter estimation algorithms that would provide better estimates from noisy data and closely spaced modes (Ref 28), and (2) to develop effective noise reduction and transfer function enhancement (Ref 45). The high-speed computer was identified as the tool for developing advanced data analysis methods that would more fully satisfy the desired objectives of flight flutter testing (Ref 46). Most agreed that the current (i.e., 1975) techniques were faster and, more accurate, increased safety, and reduced flight test time when compared with previous methods of flight flutter testing.

The future needs expressed in the 1958 symposium were partially met at the time of the 1975 symposium. Flight flutter testing was, more automated, and the data were complete and of higher quality. The time required to acquire the data was not significantly less because most of the flight test organizations were conducting sine sweeps at stabilized test points. Testing was less hazardous in 1975 than in the 1950's, although Ref 47 warned that the current techniques may still not predict flutter for explosive flutter cases. Ref 48 recommended that frequency and damping estimates for clearance to the next flutter test point be made between flights.

8.2.3 Recommendations for Future Research and Development

Online, real-time monitoring of aeroelastic stability during flight testing needs to be developed and implemented. Techniques such as modal filtering (Refs 49 and 50) can uncouple response measurements to produce simplified, single-degree-of-freedom responses. These responses could then be accurately analyzed with less sophisticated algorithms that are more able to run in real time. The ideal display would show predicted frequency and damping values being compared with flight test values in real time.

Real-time monitoring of stability eliminates the most hazardous part of flight flutter testing, which is the acceleration from one test point to the next. Such monitoring also eliminates the need for stabilized test points, which is extremely time consuming.

Broad-band excitation techniques also need to be developed so that a response signal of sufficient amplitude over the entire frequency range of interest is continually provided for real-time analysis.

New methods should be researched to permit a reliable determination of flutter speed at a speed that is well below the actual one. The technique proposed by Nissim (Ref 51), which is based on identifying the coefficients of the equations of motion followed by solving of these equations to determine the flutter speed, may be one approach. The whole process of flight flutter testing needs to be fully automated so flight flutter testing can be done much faster but more safely.

REFERENCES

1. Von Schlippe, B., "The Question of Spontaneous Wing Oscillations (Determination of Critical Velocity Through Flight-Oscillation Tests)," NACA TM-806, October 1936 (translation).

2. Lancaster, F. W., "Torsional Vibrations of the Tail of an Aeroplane," Reports and Memoranda, no. 276, July 1916, *in* "AIAA Selected Reprint Series, Volume V, Aerodynamic Flutter," I. E. Garrick, ed., March 1969, pp. 12–15.

3. Collar, A. R., "The First Fifty Years of Aeroelasticity," *Aerospace*, vol. 5, no. 2, (Royal Aeronautical Society), February 1978, pp. 12–20.

4. Tolve, L. A., "History of Flight Flutter Testing," *in* "Proceedings of the 1958 Flight Flutter Testing Symposium," NASA SP-385, 1958, pp. 159–166.

5. Garrick, I. E., and Reed, W. H., III, "Historical Development of Aircraft Flutter," AIAA 81-0491, J. Aircraft, vol. 18, no. 11, November 1981, pp. 897–912.

6. NACA Subcommittee on Vibration and Flutter, "A Survey and Evaluation of Flutter Research and Engineering," NACA RM-56I12, October 1956.

7. French, M., Noll, T., Cooley, D., Moore, R., and Zapata, F., "Flutter Investigations Involving a Free Floating Aileron," AIAA Paper no. 87-0909, April 1987.

8. Champion, L. S., and Cabrera, E. A., "F-16C/D Block 40 With Advanced Medium-Range Air-to-Air Missile (AMRAAM) Flutter Flight Test Evaluation," AFFTC TR-92-19, December 1992.

9. Norton, W. J., "Limit Cycle Oscillation and Flight Flutter Testing," *in* "Proceedings, Society of Flight Test Engineers, 21st Annual Symposium," August 1990, pp. 3.4-1–3.4-12.

10. Farley, H. C., Jr., and Abrams, R., "F-117A Flight Test Program," *in* "Proceedings of the 34th Society of Experimental Test Pilots Symposium," September 1990, pp. 141–167.

11. Borst, R. G., and Strome, R. W., "E-6 Flutter Investigation and Experience," AIAA-92-4601-CP, AIAA Guidance, Navigation, and Control Conference, Hilton Head, South Carolina, August 1992.

12. Schwartz, M. D., and Wrisley, D. L., "Final Report on the Investigation of Flight Flutter Testing Techniques for the Bureau of Aeronautics, U. S. Navy," Aeroelastic and Structures Research Laboratory, Massachusetts Institute of Technology, December 1950.

13. Rosenbaum, R., "Survey of Aircraft Subcritical Flight Flutter Testing Methods," NASA CR-132479, August 1974.

14. Kachadourian, G., Goldman, R. L., and Roha, D. M., "Flight Flutter Testing of the P6M," *in* "Proceedings of the 1958 Flight Flutter Testing Symposium," NASA SP-385, 1958, pp. 91–96.

15. Kehoe, M. W., "Aircraft Flight Flutter Testing at the NASA Ames-Dryden Flight Research Facility," NASA TM-100417, May 1988.

16. Goldman, A., Rider, C. D., and Piperias, P., "Flutter Investigations on a Transavia PL12/T-400 Aircraft," Aeronautical Research Laboratories, Melbourne, Australia, Aircraft Structures Technical Memorandum 515, July 1989.

17. Mahaffey, P. T., "Flight Flutter Testing the B-58 Airplane," *in* "Proceedings of the 1958 Flight Flutter Testing Symposium," NASA SP-385, 1958, pp. 121–125.

18. Stringham, R. H., Jr., and Lenk, E. J., "Flight Flutter Testing Using Pulse Techniques," *in* "Proceedings of the 1958 Flight Flutter Testing Symposium," NASA SP-385, 1958, pp. 69–72.

19. Meany, J. J., "The Evolution of Flutter Excitation at McDonnell Aircraft," *in* "14th Annual Symposium Proceedings," Society of Flight Test Engineers, August 1983, pp. 4.6-1–4.6-11.

20. Hodson, C. H., Dobbs, S. K., Brosnan, M. J., and Chen, J. B., "X-31A Flight Flutter Test Excitation by Control Surfaces," AIAA-93-1538-CP, 34th AIAA Structures, Structural Dynamics and Materials Conference, La Jolla, California, April 1993.

21. Laure, P., Millet, M., and Piazzoli, G., "Pyrotechnic Bonkers for Structural Tests in Flight," ONERA TP no. 1389 E, 1974.

22. Dublin, M., and Peller, R., "Flight Flutter Testing of Supersonic Interceptors," *in* "Proceedings of the 1958 Flight Flutter Testing Symposium," NASA SP-385, 1958, pp. 111–120.

23. Dobbs, S. K., and Hodson, C. H., "Determination of Subcritical Frequency and Damping From B-1 Flight Flutter Test Data," NASA CR-3152, June 1979.

24. Bartley, J., "Flight Flutter Testing of Multi-Jet Aircraft," *in* "Proceedings of the 1958 Flight Flutter Testing Symposium," NASA SP-385, 1958, pp. 103–110.

25. Reed, W. H., III, "A New Flight Flutter Excitation System," *in* "19th Annual Symposium Proceedings," Society of Flight Test Engineers, Arlington, Texas, August 14–18, 1988, pp. V-1.1–V-1.7.

26. Vernon, L., "In-Flight Investigation of a Rotating Cylinder-Based Structural Excitation System for Flutter Testing," NASA TM-4512, 1993.

27. Norton, W. J., "Random Air Turbulence as a Flutter Test Excitation Source," *in* "Proceedings, Society of Flight Test Engineers, 20th Annual Symposium," Reno, Nevada, September 18–21, 1989.

28. Brignac, W. J., Ness, H. B., Johnson, M. K., and Smith, L. M., "YF-16 Flight Flutter Test Procedures," *in* "Flutter Testing Techniques: A conference held at Dryden Flight Research Center, October 9–10, 1975," NASA SP-415, 1976, pp. 433–456.

29. Nordwall, B. D., "Mobile Communications to Capture Consumer Market," Aviation Week & Space Technology, May 31, 1993, pp. 41–42.

30. Baird, E. F., Sinder, R. B., and Wittman, R. B., "Stabilizer Flutter Investigated by Flight Test," *in* "Proceedings of the 1958 Flight Flutter Testing Symposium," NASA SP-385, 1958, pp. 73–81.

31. Reed, W. H., III, "A Flight Investigation of Oscillating Air Forces: Equipment and Technique," *in* "Proceedings of the 1958 Flight Flutter Testing Symposium," NASA SP-385, 1958, pp. 41–50.

32. Philbrick, J., "Douglas Experience in Flight Flutter Testing," *in* "Proceedings of the 1958 Flight Flutter Testing Symposium," NASA SP-385, 1958, pp. 127–132.

33. Laidlaw, W. R., and Beals, V. L., "The Application of Pulse Excitation to Ground and Flight Vibration Tests," *in* "Proceedings of the 1958 Flight Flutter Testing Symposium," NASA SP-385, 1958, pp. 133–142.

34. Meyer, R. R., Jr., and Schneider, E. T., "Real-Time Pilot Guidance System for Improved Flight Test Maneuvers," AIAA-83-2747, November 1983.

35. Rhea, D. C., and Moore, A. L., "Development of a Mobile Research Flight Test Support Capability," *in* "Proceedings of the 4th AIAA Flight Test Conference," San Diego, California 1988.

36. Sefic, W. J., and Maxwell, C. M., "X-29A Technology Demonstrator Flight Test Program Overview," NASA TM-86809, May 1986.

37. Perangelo, H. J., and Waisanen, P. R., "Flight Flutter Test Methodology at Grumman," *in* "Flight Testing Technology: A State-of-the-Art Review," Society of Flight Test Engineers, 13th Annual Symposium, New York, September 19–22, 1982, pp. 91–ff.

38. Katz, H., Foppe, F. G., and Grossman, D. T., "F-15 Flight Flutter Test Program," *in* "Flutter Testing Techniques: A conference held at Dryden Flight Research Center," NASA SP-415, 1976, pp. 413–431.

39. Allemang, R. J., and Brown, D. L., "Experimental Modal Analysis and Dynamic Component Synthesis," AFWAL-TR-87-3069, vol. I, Flight Dynamics Laboratory, Wright-Patterson Air Force Base, Ohio, December 1987.

40. Cooper, J. E., "Modal Parameter Identification Techniques for Flight Flutter Testing," *in* Aeronautical Engineering Group, Aeronautical Report no. 9105, University of Manchester, Manchester U.K., 1991.

41. Nash, D. E., Katz, H., and Moody, W. C., "F-15 Flight Flutter Testing: Aircraft Systems and Test Operations," AIAA Paper no. 75-1031, AIAA 1975 Aircraft Systems and Technology Meeting, Los Angeles, California, 1975.

42. Kehoe, M. W., "KC-135 Winglet Flight Flutter Test Program," AFFTC TR-81-4, Air Force Flight Test Center, Edwards Air Force Base, California, June 1981.

43. NASA Langley Research Center, *Proceedings of the 1958 Flight Flutter Testing Symposium,* NASA SP-385, May 1958.

44. National Aeronautics and Space Administration, *Flutter Testing Techniques*, NASA SP-415, October 1975.

45. Lenz, R. W., and McKeever, B., "Time Series Analysis in Flight Flutter Testing at the Air Force Flight Test Center: Concepts and Results," *in* "Flutter Testing Techniques: A conference held at Dryden Flight Research Center," NASA SP-415, 1976, pp. 287–317.

46. Hurley, S. R., "The Application of Digital Computers to Near-Real-Time Processing of Flutter Test Data," *in* "Flutter Testing Techniques: A conference held at Dryden Flight Research Center," NASA SP-415, 1976, pp. 377–394.

47. Foughner, J. T., Jr., "Some Experience Using Subcritical Response Methods in Wind-Tunnel Flutter Model Studies," *in* "Flutter Testing Techniques: A conference held at Dryden Flight Research Center," NASA SP-415, 1976, pp. 181–191.

48. Wright, J. R., "Introduction to Flutter of Winged Aircraft," von Karman Institute for Fluid Dynamics, Lecture Series 1992-01, December 1991.

49. Shelley, S. J., Freudinger, L. C., and Allemang, R. J., "Development of an On-line Parameter Estimation System Using the Discrete Modal Filter," *in* "Proceedings of the 10th International Modal Analysis Conference," San Diego, California, February 3–7, 1992, pp. 173–183.

50. Shelley, S. J., Freudinger, L. C., and Allemang, R. J., "Development of an On-line Modal State Monitor," *in* "Proceedings of the 11th International Modal Analysis Conference," Kissimmee, Florida, February 1–4, 1993.

51. Nissim, E., and Gilyard, G. B., "Method for Experimental Determination of Flutter Speed by Parameter Identification," NASA TP-2923, 1989.

Flutter Flight Test of the RANGER 2000 Aircraft

F. Weiss
J. Schweiger
Structural Dynamics Group
Daimler Benz Aerospace AG
Military Aircraft, Abt. LME24
Postfach 80 11 60
81663 Munich, GERMANY

Dr. H. Hönlinger
DLR, Institute for Aeroelasticity
DLR, Bunsenstrasse 10
37073 Göttingen
GERMANY

ABSTRACT

This paper describes the flight flutter test activities for the RANGER 2000 training aircraft, which was jointly developed by DASA and Rockwell International between 1991 and 1994 as a competitor for the next generation U.S. Air Force and Navy "Joint Primary Advanced Training System" (JPATS). After a brief description of the program and the main aircraft features, an overview of the aeroelastic analysis and the ground vibration tests during the design process are given. The report of the flight test activities is divided into the description of the test equipment, aircraft instrumentation, flight envelope, test procedures, real-time telemetry parameter monitoring and post-flight data reduction. Typical time histories of response, frequency response functions, power spectra and typical plots of the frequencies and damping versus dynamic pressure are given. The flight test results in combination with the aeroelastic analysis are discussed at the end.

BACKGROUND

The design of the RANGER 2000 training aircraft was based on the German FANTRAINER aircraft from Rhein Fugzeugbau which has an unusual power concept. The propeller, located behind the piston engine in the rear fuselage is ducted to give a jet-like power characteristic.

For the RANGER 2000, depicted in Fig. 1, a turbofan engine was chosen. Table 1 presents the main features of the aircraft. Main characteristics are a T-tail and a keel beam fuselage wing structure. Fuselage, wing and all control surfaces are graphite or glass fiber composite structures while the tail is an aluminium design. The aircraft has a manual flight control system. Fig. 2 shows the design flight envelope.

The two prototype aircraft were certified according to FAR 23 regulations with the German "Luftfahrtbundesamt" authorities.

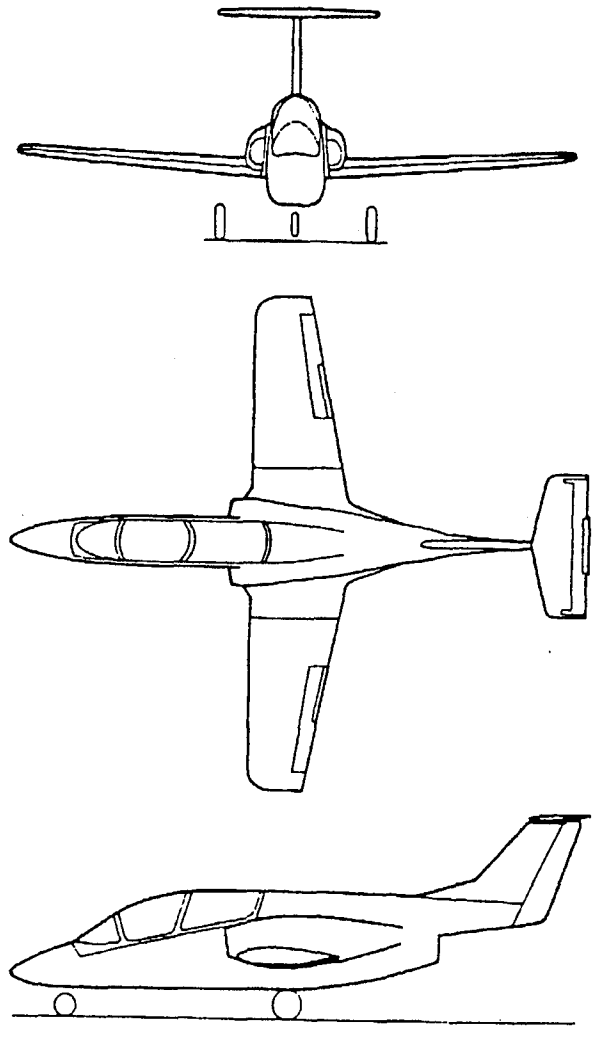

Fig. 1 RANGER 2000

INTRODUCTION

Design for flutter prevention must be considered for all aircraft. It is especially important for jet-aircraft, because flutter failures at high speeds can occur suddenly and cause catastrophic results. Extensive flutter analy-

Paper presented at the Structures and Materials Panel Specialists' Meeting on "Advanced Aeroservoelastic Testing and Data Analysis", held in Rotterdam, The Netherlands, from 8-10 May 1995, and published in CP-566.

sis, ground tests, and flight tests are usually required to provide evidence of a 20 percent minimum margin of safety in flutter speed above the maximum operating speeds. During the design phase the major attention was placed on developing an appropriate finite element model to perform flutter analysis for all the important flutter characteristics as well as to predict the influence of structural modifications. In addition to the major ground vibration test prior to first flight several check tests for all important design improvements were carried out.

Wing Span:	34 ft 4 in.
Total Length	34 ft 4 in.
Height	12 ft 10 in.
Wing Area	167 sq.ft
Gross Weight	7800 lb
Maximum Cruise Speed (KEAS) at SL	330 kts
Maximum Dive Speed	390 kts
Approach Speed in Landing Configuration	105/120 kts
Range (with Maximum Internal Fuel, 45 min Reserve)	800 nm
Operational Ceiling	31,000 ft
Load Factor at Maximum Take-Off Weight Exceeding	+6/-3 g
Static Thrust at Take-Off Power. Standard Day (uninstalled)	3190 lb-f

Table 1: Technical Data

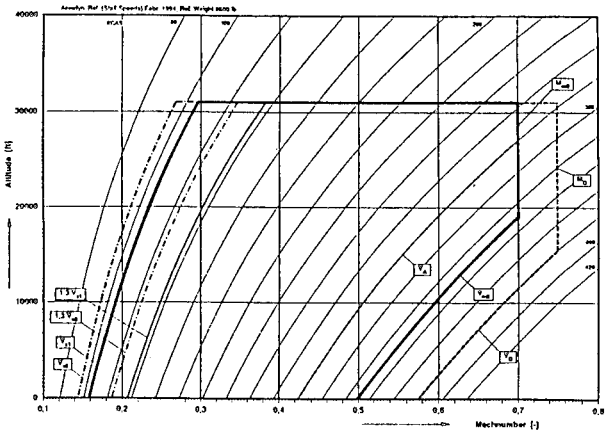

Fig. 2 Flight Envelope

ROUTE TO AIRWORTHINESS WITH RESPECT TO AEROELASTICITY

FAR § 23.629 provides several options to demonstrate that the airplane is free from flutter, control reversal and divergence for any operating conditions within the limit V-n envelope.

Besides the mandatory ground vibration test, it is possible to demonstrate freedom from aeroelastic instabilities

- by a rational analysis,
- by flight flutter tests,
- by compliance with the rigidity and mass balance criteria from the FAA Airframe and Equipment Engineering Report No. 45. The last option is ruled out for the RANGER 2000 because
  - — it has a T-tail
  - — there is fuel in the outboard wing section
  - — and the maximum speed is above 260 knots.

To reduce development risks, it was decided to start with flutter analysis early during the design and to verify the results by an efficient flight test program.

AEROELASTIC ANALYSIS

The aeroelastic analysis is based on the Finite Element Model depicted in Fig. 3. This model includes the complete flight control system. The flutter analysis was performed with the DASA structural analysis and optimization program LAGRANGE /1/. The unsteady aerodynamic forces were calculated by means of a doublet lattice method developed by W. Rodden /2/. Before and during the analysis for the complete model, component analysis were performed for the wing and tail separately to identify the critical flutter mechanisms. All critical flutter cases involve the main control surfaces. This behaviour is typical for airplanes with a manual flight control system.

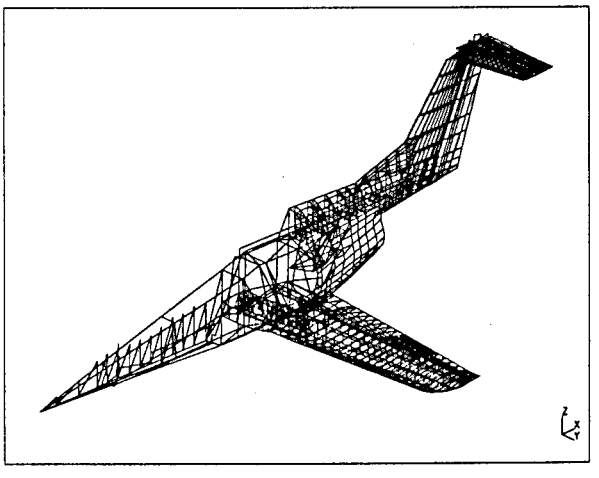

Fig. 3 Finite Element Model

To obtain subcritical flutter cases with sufficient margins of safety, the proper amount and location of mass balance was determined by means of structral optimization. Mass balance on the control surfaces was more efficient than masses on the main surfaces or structural reinforcements.

An important parameter for flutter sensitivities was given by the adjustable gearing ratios between main control surfaces and tabs (Flettner factor).

Because it is known from other projects that a reduction of the aerodynamic effectiveness of control surfaces can cause a reduction in flutter stability, the aerodynamic forces on control surfaces were also treated as parameters.

The LAGRANGE program and the same structural and aerodynamic models were used for aeroelastic divergence, control surface reversal and steady aeroelastic control surface effectiveness investigations. In addition, flutter results were verified by NASTRAN for some check cases.

GROUND VIBRATION TESTS

The main ground vibration test was performed in Nov. 1992 prior to first flight. Approximately 150 accelerometer and multiple shakers wer used for this test to identify all important vibration modes. During the test, the aircraft was supported by low frequency air springs (Fig. 4) to simulate free-free boundary conditions.

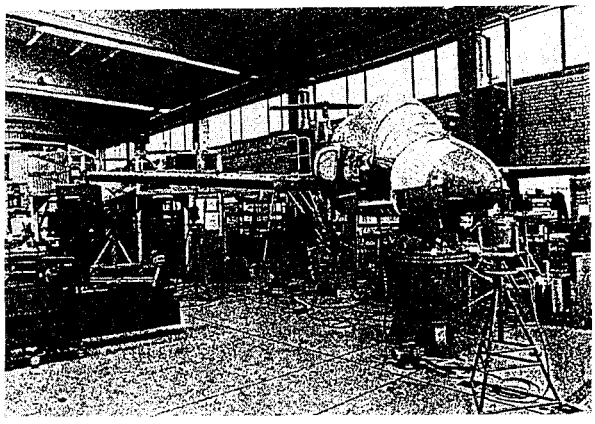

Fig. 4 Ground Vibration Test Set-Up

The test was performed for two basic conditions, empty and approximately 85% fuel. In addition, the stick and pedals were either blocked by stick clamping structures to simulate a fixed condition or suspended by soft spring bungee chords to simulate free control surfaces.

Additional tests were performed to identify changes of the dynamic characteristics after all major design upgrades. These changes were:

- installation of an aileron booster system
- modifications of the aileron and rudder hinge line location
- changes of the control surfaces' mass balance
- modifications of the main structure.

EXCITATION SYSTEM

The safe approach to demonstration of flutter stability requires that the structural modes which are important for flutter can be excited in flight.

Various methods can be used for flight flutter test excitation, among others control surface pulses by stick raps or rudder kicks, explosive charges, oscillating vanes or control surfaces, oscillating masses and slatted rotating cylinders. Oscillatory methods require a frequency sweep to excite all modes in the frequency range of interest. The optimum choice for a particular aircraft depends on the characteristics of an aircraft such as its control surface, control system, the number and types of modes which must be excited, whether or not wind tunnel flutter modul tests were performed, the flight envelope to be expanded and the flutter margins of safety predicted by flutter analysis. Ideally, the installation of the flutter excitation system should not change the flutter characteristics of the aircraft. For the RANGER 2000, stick raps are insufficient, because almost all major eigenfrequencies are above 10 Hz. Control surface sweeps through the flight control system are excluded because of the manual flight control system.

For this reason an excitation system with slotted rotation cylinders was chosen. It was developed by Wilmer H. Reed and is distributed by DYNAMIC ENGINEERING INC. (DEI) /3/. The exciters, Fig. 5, mounted at locations which are able to excite natural modes of interest, produce sinusoidal aerodynamic forces of controllable frequency and amplitude.

The basic flutter exciter unit is a pair of rotatable concentric cylinders mounted on either a fixed vane or an aircraft wing or tail surface. Each cylinder has a slot which allows the air to pass through, Fig. 6. As the cylinder rotates about its axis the airstream is alternately deflected upward and downward at a frequency twice that of the cylinder's rotation frequency.

The amplitude of the excitation force depends upon the dynamic pressure and the degree of slot opening.

Because the cylinder rotates at a constant or slowly varying frequency the torsional force which is neccessary to surmount the inertia forces is not present. The

drive motor therefore only needs to overcome mechanical and aerodynamic friction forces which are relatively small.

The power required to rotate the slotted cylinders is minimal, thus allowing the use of a low wattage electric motor which can be mounted together with the rotating cylinders and the fixed airfoil to a simple compact flutter exciter system.

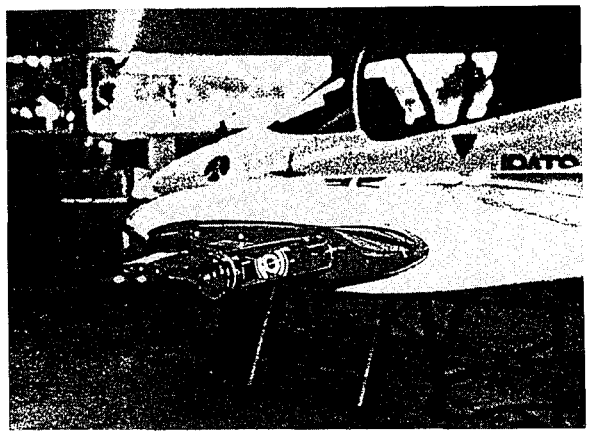

Fig. 5 Flutter Exciter Mounted on Wing Tip

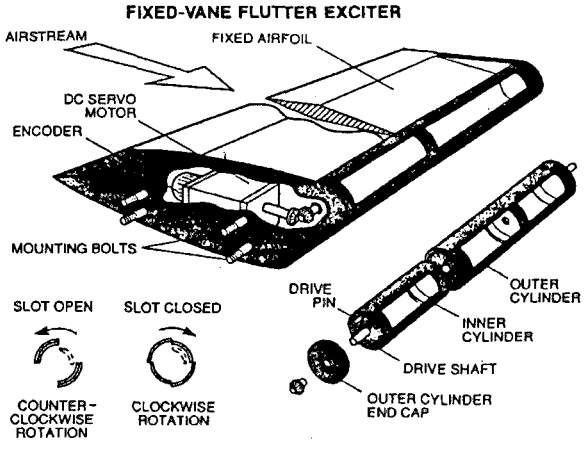

Fig. 6 Flutter Exciter Components

The DEI flutter exciter uses a digital control system to maintain the proper cylinder speed under varying loads. The control system is packaged in two separate units. One unit, the Cockpit Control Interface is a small cockpit mounted box housing all the interface switches and controls for the pilot's operation of the system. The second unit is the Avionics Box and contains the principal control system components and motor amplifier neccessary to drive the brushless motors used in the exciter assembly.

The system allows three principal modes of operation: sine dwell where the pilot selects a dwell frequency and a dwell or run duration time, linear sweeps where the pilot chooses both the start and stop frequencies and the sweeps or run time, and logarithmic sweeps with the same inputs as the linear sweep mode, but the sweep rate is varying logarithmically instead of linearly.

Another possibility is the choice of two forces outputs, either high or low. These levels correspond to the opening and closing of the outboard cylinder. Closing the outboard cylinder results in a 50% reduction in force. An additional blockage plug is included which allows the inboard slot to be half closed for an additional 25% reduction in force. This inboard plug is attached on the ground prior to flight and thus cannot be modified while in flight, see Fig. 7. The control system also maintains phase control over the two exciters. The pilot can choose to operate the units either in-phase or 180° out-of-phase, thus allowing symmetric or antisymmetric excitation, respectively.

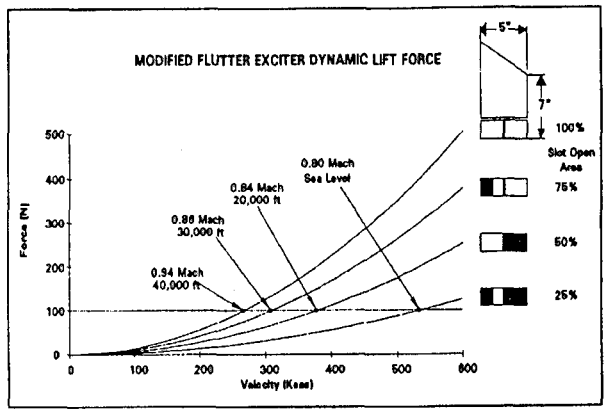

Fig. 7 Optional Force Levels

The induced sinusoidal forces or respectively bending moments are measured by strain gauges mounted at the root of the exciter vane. The amplitude and frequency of excitation are displayed on the operator's control panel and are also available as analogue voltage inputs for data recording systems, as are the control panel switch positions. A typical Autopowerspectrum of an antisymmetrical excitation is shown in Fig. 8.

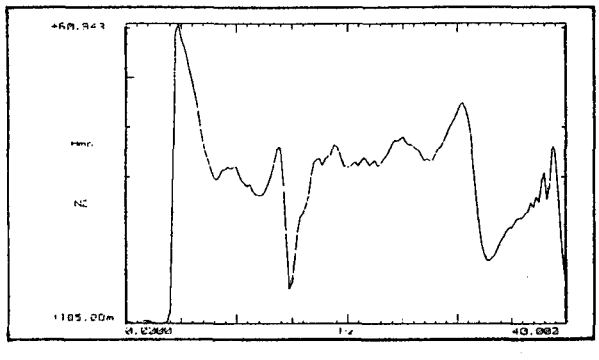

Fig. 8 Power Spectrum of Excitaion Force

On the RANGER 2000 prototype RP01 two flutter exciters were mounted at the wing-tips. During early pretests a third exciter on top of the fin was used, but it was demonstrated that the two wing tip mounted exciters were adequate for exciting the important tail symmetric and antisymmetric modes. The only problem that occured with these flutter exciters was during test flights in the winter period. At high altitudes there was formation of ice between the cylinders and the motor was too weak to start the cylinder rotation. This could be avoided by running the system during climbs and flying at high altitudes.

FLUTTER FLIGHT TEST INSTRUMENTATION

The essential parameters for flutter tests are the accelerometers distributed over the aircraft for the determination of structural vibrations, and the induced forces of the flutter exciters. Important are also the general parameters for the determination of speed, Mach number, altitude and fuel condition. All these signals were recorded on an on-board PCM tape recorder and in addition they were sent via telemetry to the ground station for real time quick-look monitoring on stripcharts and for a quasi on-line analysis of frequency and damping values for dominant modes.

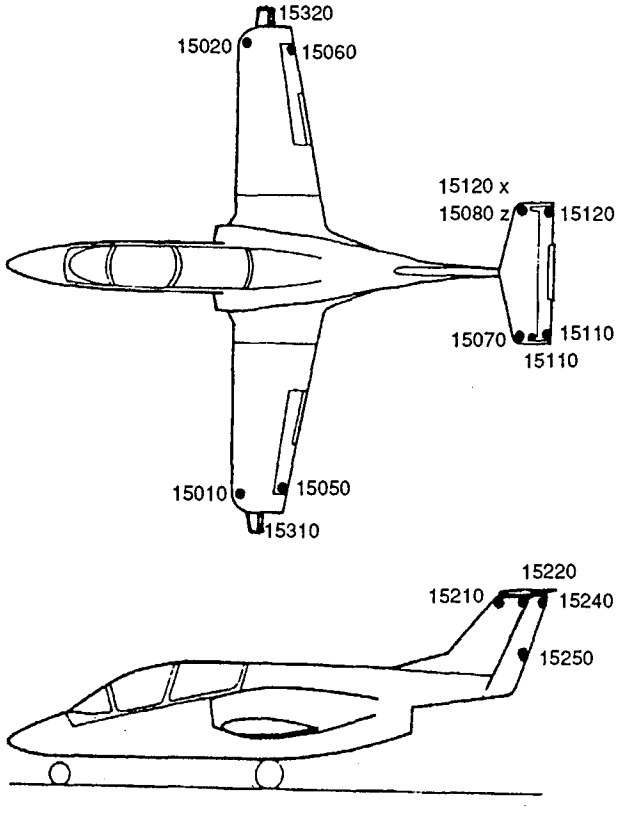

Fig. 9 Accelerometer Locations

The accelerometer positions are shown in Fig. 9. Two accelerometers in z-direction were placed on each wing; additional sensors were fitted on the right wing in x-direction and one on each aileron in z-direction. The vertical tail was equipped with two lateral acceleromers at the fin and two on the rudder. The horizontal tail had two sensors in z-direction and one in x-direction on the fixed surface, and three sensors on the elevator, one of them on the horn. The instrumentation was changed a few times during the proceeding test phases.

FLIGHT VIBRATION ANALYSIS METHODS

General Remarks

For analyzing the measured vibration signals, several methods were available. Different test aims however may require different methods of analyzing or even combinations or sequences of different methods. But for all methods it is assumed that the flying aircraft can be represented by a linear system. The evaluation of the model data of this linear system could be done in the time damain, or more common, in the frequency domain. If the analysis is done in the time domain it is possible to use the free response of the aircraft structure, for example the decay curve after a stick-rap or rudder kick (see Fig. 10).

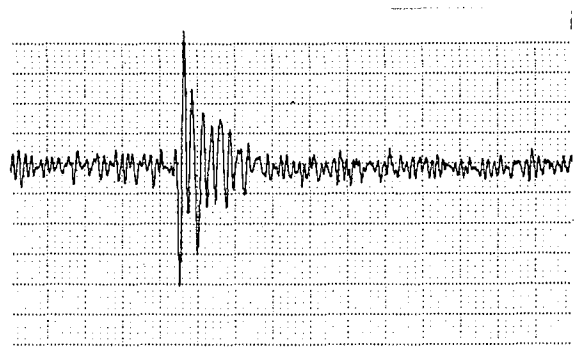

Fig. 10 Decay of a Stick-Rap

In most cases the free response is of short duration and therefore the accuracy of the measurement may be reduced. But for a first guess one could include a brief analysis. Usually the analysis is done in the frequency domain. In this case transfer functions between excitation and responses are calculated, or if no excitation signal is available, auto power spectra are collected. Normally they are acquired by computation of power spectra of subsequent data blocks and averaging the single spectra. Because of short test duration and short data block length, problems with insufficient noise reduction and effects of truncation can arise /4/. The block overlapping is a useful procedure to reduce trun-

cation and noise effects. The amplitudes in the low and high frequency boundary are diminished by the averaging procedure of the overlapped data blocks, but this has no influence on the transfer function if stable averaging is used.

From the averaged input and cross power spectrum the transfer function $H_{i\omega}$ is computed. This represents the available complete composed system parameter description. For this task a Hewlett Packard workstation with an installed Fourier System of Leuven Measurements & Systems (LMS), Ref. /5/, was used.

For the system identification and parameter estimation several methods were used. During the test flights an automated half-band width method and a maximum likelihood estimation method were used as a quasi online evaluation. Therefore the evaluation was done only for the critical modes. For the estimation of the modal data with maximum likelihood, only three minutes were required for the evaluaton. After flutter test flights an more detailed evaluation of all parameter was done with MLE and Least Square Complex Estimation techniques.

Maximum Likelihood Method

Maximum likelihood is a standard statistical method for estimating unknown parameters in a probability distribution. This procedure, shown in Fig. 11, has been programmed at Daimler Benz Aerospace AG and implemented by "User Programming" in the LMS Fourier System. A very detailed description of this method is given in Ref. /6/ and Ref. /7/. The principle of maximal likelihood for use in parameter estimation was introduced by R.A. Fisher in 1912, and was also further expanded by him. The idea behind this technique is the assumption that the outcome y of an experiment depends on unknown parameters Θ. The maximum likelihood estimates of the unknown parameters are those values for which the observed value y would be "most likely" to occur. Here we have a set of observation vectors y which constitute the flight flutter data, and a mathematical model dependent upon a set of unknown parameters Θ.

The likelihood function is defined as the conditioned probability density function of the observation y given the parameters Θ. To get the searched parameters the problem of maximum likelihood estimation can be indicated as

$$\hat{\Theta} = \max p\left(y \mid \Theta\right)$$

Where $\hat{\Theta}$ is the maximum likelihood estimator of Θ and p (y ! Θ) is the joint conditional probability density function of the data given the parameters.

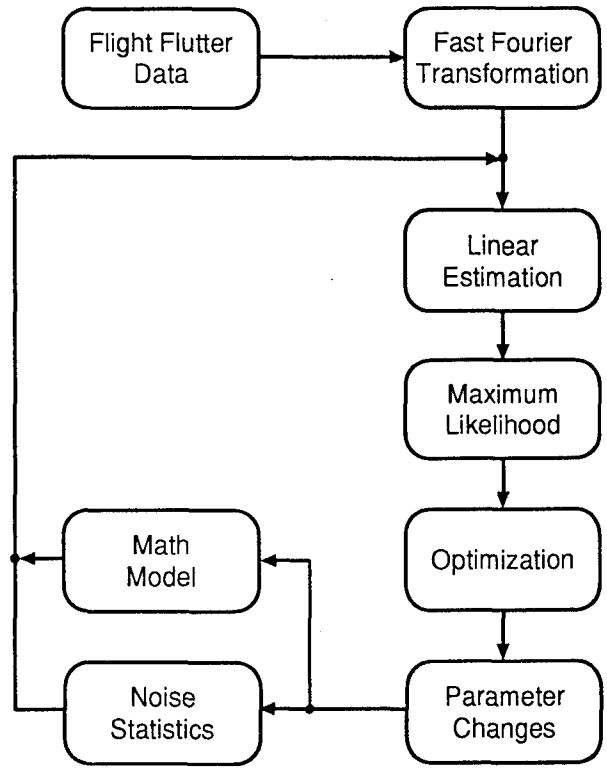

Fig. 11 Float Chart of MLE for Flutter Test Data

This method can solve the most general estimation problems which involves the extraction of airplane parameters also for a nonlinear model from flight data containing the process and measurement noise. Shown in several flutter flight test evaluations the maximum likelihood method is firmly established as the optional method for parameter estimation.

Least Squares Complex Exponential Method

The least square complex exponential method (LSCE) allows to estimate values of modal frequency and damping for several modes simulataneously by operating on single-input multiple-output autospectra or frequency response functions.

This parameter estimation technique which is implemented in the LMS Modal package is described in /7/. The aim of this method is to define a model in terms of modal parameters of a set of measured data - most commonly frequency response functions (FRF), or the time domain equivalent, impulse responses (IP). For IPs the relationship between modal parameters and the measurements is

$$h_{ij}(t) = \sum_{k=1}^{N} \left(r_{ijk}\, e^{\lambda_k t} + r^{*}_{ijk}\, e^{\lambda^{*}_k t} \right)$$

The corresponding relation for FRFs is

$$h_{ij}(j\omega) = \sum_{k=1}^{N}\left(\frac{r_{ijk}}{j\omega-\lambda_k} + \frac{r^*_{ijk}}{j\omega-\lambda^*_k}\right)$$

where:

- $h_{ij}(t)$ = IR between the response degree of freedom i and the reference DOF j
- $h_{ij}(j\omega)$ = FRF between the response degree of freedom i and the reference DOF j
- N = number of modes that contribute to the structure's dynamic response within the frequency range of interest
- r_{ijk} = residue value for mode k
- λ_k = pole value for mode k
- * designates complex conjugate.

The pole values λ_k in the first equation are not a function of a particular response or reference DOF. They are characteristics of the system and should be found in any function measured on the structure.

In the upper equation there is a problem to work with because it contains the residues r_{ijk}, which depend on the response and reference DOF.

When working with the least squares complex exponential method it is essential to define another parametric model for the data h_{ij} in which the coefficients are independent of response and reference, and which can be used to identify estimates for λ_k. It can be proved that such model is in the form of a linear differential equation with constant real coefficients, when the whole set of equations is expanded in its dimension from N to $2N$.

In the practical application of the Least Square Complex Exponential as implemented in the LMS CADA-X Modal package /9/ the following steps are summarized:

- specify response DOFs and reference DOF for which data is to be analysed
- specify frequency band of analysis
- select number of time points to be used
- build covariance matrix
- determine optimal number of modes using error diagram, singular value diagram and stabilization diagram.

To determine the optimal number of modes one could attempt to compare frequency and damping estimates that are calculated from the model with various number of modes. Intuition would lead you to expect that estimates of frequency and damping corresponding to true structural modes, should recur as the number of modes is increased. Computational modes will not reappear with identical frequency and damping.

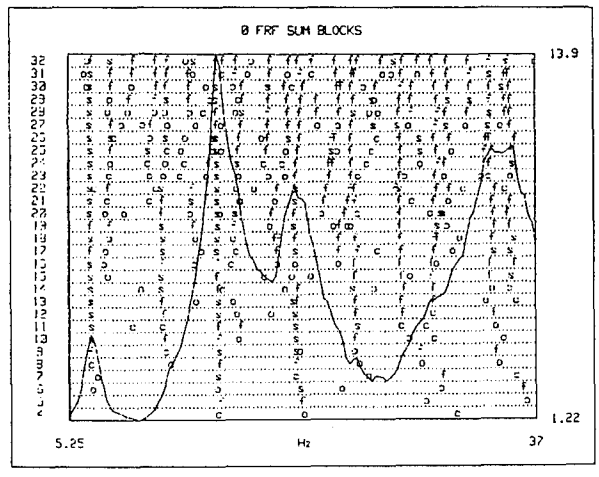

Fig. 12 Stabilization Diagram

A diagram that shows the evolution of frequency and damping as the number of modes is increased is called a stabilization diagram. An example is given in Fig. 12. The minimum number of modes that can be calculated for use can be seen as those modes for which the frequency and damping values do not change significantly.

FLIGHT TEST PROCEDURE

Basis for the tests was the availability of a comprehensive flutter analysis for the aircraft in all possible configurations. Starting from an initial flight envelope, cleared from a flutter point of view by analysis, the flight envelope expansion was made in progressive steps. At each extension step the determination of in-flight damping and frequency of all important structural modes of the aircraft and its control surfaces was made. The general philosophy of testing was that such test points were scheduled for each flight, which allowed expansion of the flown envelope to higher speed only after extrapolation of the damping trends. If the analysis of the flight records at lower speeds showed no evidence of the onset of flutter, a claerance for the next airspeed increment was given. Maximum use was made of real-time analysis techniques to reduce as much as possible the number of flight trials required.

A typical flutter manoeuvre consisted of stabilization of airspeed, Mach no., altitude and A/C attitudes for the duration of the excitation. The only exceptions were the high speed flutter points at V_{Dive}, where one tried to keep constant Mach no. or constant airspeed respectively. A test point consisted of a symmetrical and anti-

symmetrical frequency sweep, each required approximately 60 seconds.

The main flutter test points are indicated in Fig. 13. Some of these test points were repeated with different fuel content to cover the sensitivity of fuel mass with respect to eigenfrequencies and damping values.

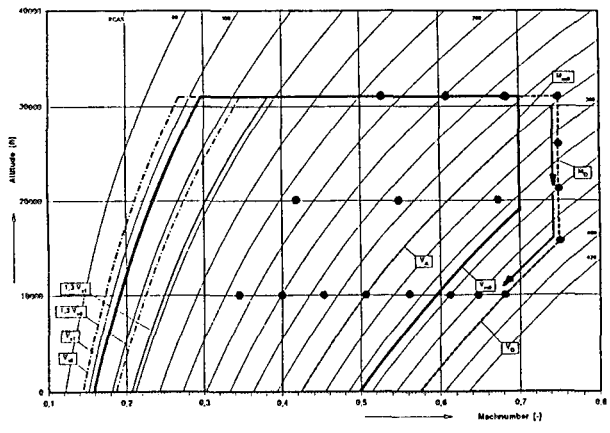

Fig. 13 Flutter Test Points

FLUTTER FLIGHT TEST RESULTS

After on-line analysis during the test flights with telemetry data, data from the on-board tape recorder was used for past-flight analysis. The time histories of accelerometer and reference excitation signals were first plotted to determine the position of the sweep and the parameters which contained the modes of interest. A typical example is given in Fig. 14.

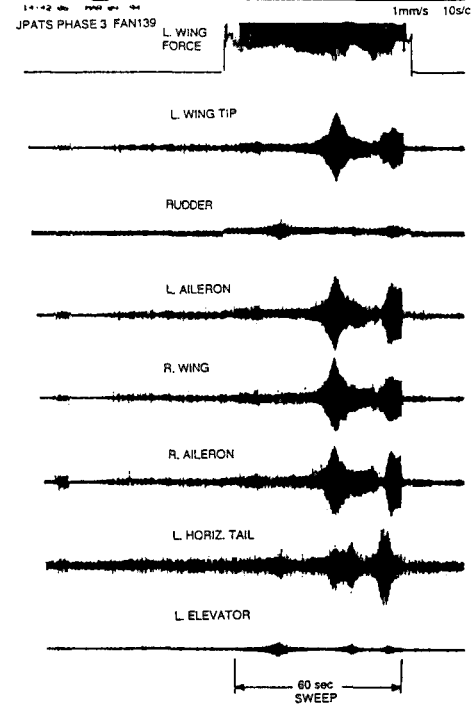

Fig. 14 Typical Flutter Excitation Time Histories

For all parameters FRFs and curve fits - described previously - were performed with a minimum of two different procedures. Fig. 15, 16 and 17 show some characteristic FRFs and the corresponding curve fits for a symmetrical and an antisymmetrical excitation. After the frequencies and damping values had been determined, the v-g-plots were supplemented under consideration of the A/C attitudes. Therefore the fuel condition had a big influence on the frequencies and damping, especially for wing modes. Also other aspects like changes of the Flettner factors or different angles of incidence for the horizontal tail had to be considered. The aileron tab gearing ratio was taken from -0.6 to -0.8 and finally to a value of -1.0 during the flutter testing period to optimize the control forces. This variation showed smaller effects in the flight test damping data compared to the analytical predictions.

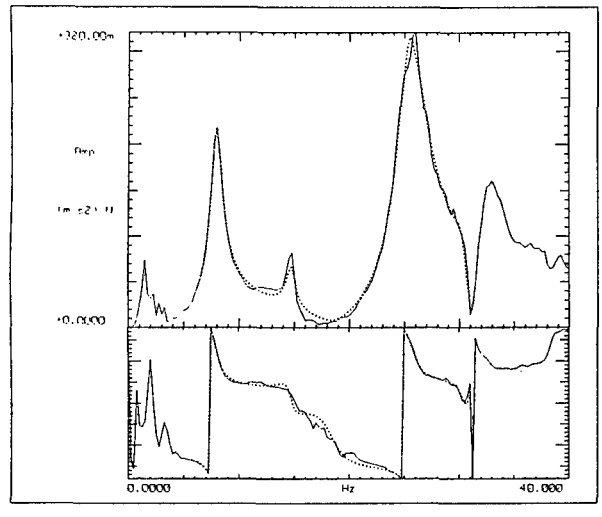

Fig. 15 FRF of a Wing Sensor with Sym. Excition

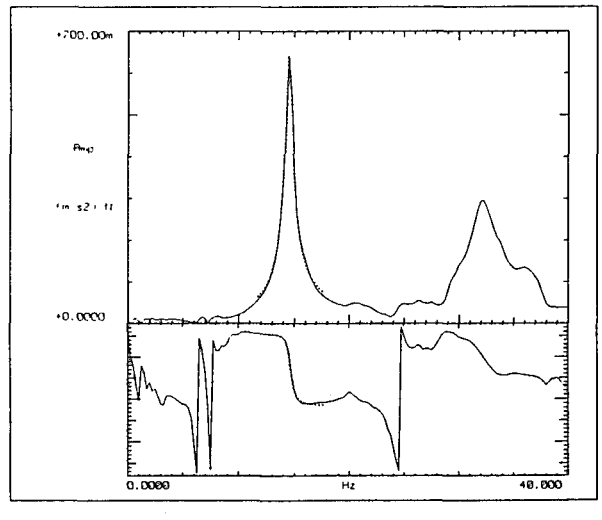

Fig. 16 FRF of a Wing Sensor with A/S Excitation

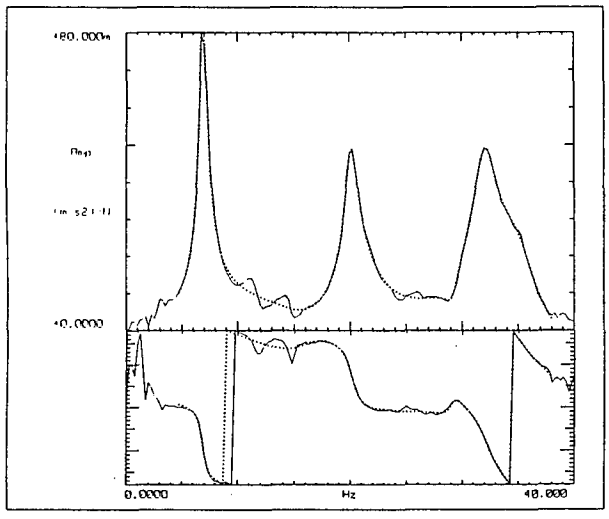

Fig. 17 FRF of a Tail Sensor with A/S Excitation

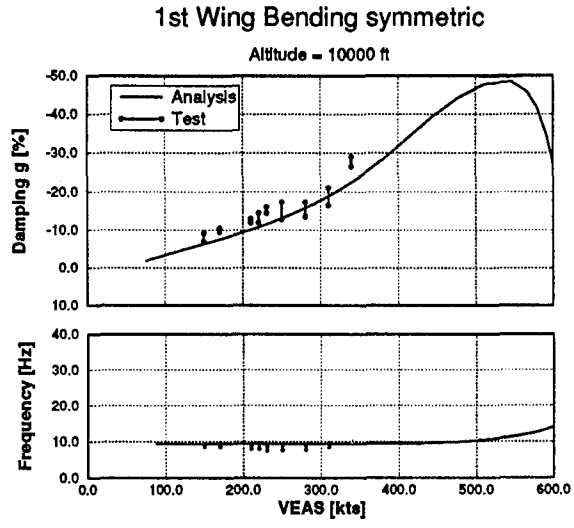

Fig. 18 Flight Results for Sym. Wing Bending Mode

A small analysis problem arose at the beginning of the flutter flight test in the calculation of the frequency response functions. At the low speed test points the high force mode of the flutter exciters was used. This led to local flow separation at the flutter exciter wing during the excitation of the antisymmetrical wing bending mode which resulted in a break-down of the excitation signal. This effect, shown in a reduced form in Fig. 8 at about 16 Hz, was enhanced by an insufficient modulation percentage of the ADC (analog digital converter). The mode separation technique increased the signal level and the generated results became acceptable. During further flutter flights the excitation force was reduced and it was shown that it would be sufficient enough to excite modes at higher frequencies, for example the 2nd wing bending mode.

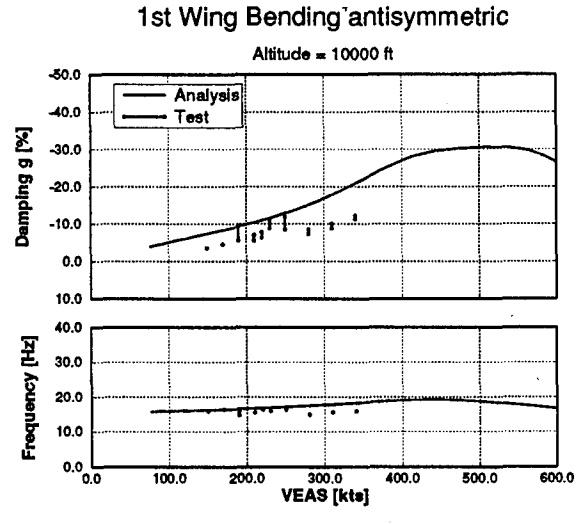

Fig. 19 Flight Results for A/S Wing Bending Mode

The flight flutter test points shown in Fig. 13 consist of increasing speed at three constant altitudes (10000 ft, 20000 ft and 31000 ft) for speeds up to V_{mo} and Ma_{mo}. Testing at speeds above V_{mo} and Ma_{mo} up to V_{Dive} and M_{Dive} required diving the aircraft at constant Mach number (0.75) for altitudes from 31000 ft to 15800 ft, and at constant equivalent air speed (up to 380 KEAS) for altitudes below 15800 ft. Before the final configuration was frozen flutter tests were also conducted during the development phase, in the stage of the control surfaces' hinge lines, mass balances, and final aileron booster configuration being finally determined. These tests also demonstrated freedom from flutter and indicated a robust flutter design relative to variations in the control system design.

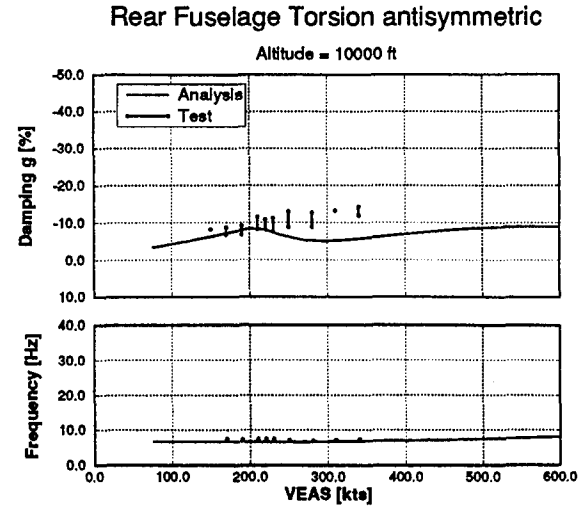

Fig. 20 Flight Results for Rear Fuselage Torsion Mode

Fig 18 through 20 show some results of the symmetric and antisymmetric wing first bending mode and of the torsion mode of the rear fuselage. Some damping values at the same test point are different, because different calculation methods were used. In general, the least

squares complex exponential technique leads to slightly higher damping values compared to the maximum likelihood method.

The plots of the measured frequency and damping trends versus speed at all altitudes show, that the RANGER 2000 prototype aircraft is free from flutter up to V_{Dive} and Ma_{Dive}, and that damping values for all modes exceed g=0.03 under test conditions. The damping trends also show that there is no large and rapid reduction in damping near V_{Dive}. Therefore the aircraft meets or exceeds the requirements of FAR § 23.629.

In general, the predicted trends for frequency and damping versus airspeed, altitude and Mach number showed good compliance with test results. Damping values from test data are never below the predicted values, and the extrapolation of test data to higher speeds do not show trends for inadequate flutter stability within the $1.2 \times V_{Dive}$ range.

CONCLUSIONS

An efficient flight flutter test program for the RANGER 2000 training aircraft was possible because of the following reasons:

- reliability of analytical predictions
- verification of the dynamic characteristics by a state-of-the-art ground resonance test
- an efficient and reliable excitation system
- on-line and post-flight test data analysis
- good correlation between predicted values and test data.

Especially for a considerable amount of design improvements during the flight test program it was important to repeat some flutter test points with a minimum effort to re-install the exciters and set-up the test data acquisition and data processing equipment.

REFERENCES

/1/ MBB-LAGRANGE Benutzerhandbuch
Version LAG 09

/2/ Giesing, J.P.; Kalmann, T.P.; Rodden, W.P.:
Subsonic Steady and Oscillatory Aerodynamics for Multiple Interfering Wings and Bodies.
Journal af Aircraft, Vol. 9, No. 10

/3/ Wilmer H. Reed (DEI)
Design News, 27th March 1989

/4/ G. Haidl; M. Steininger
Excitation and Analysis Technique for Flight Flutter Tests
AGARD Report No. 672

/5/ LMS CADA-X
Fourier Monitor Manual 3.2

/6/ M.L. Russo, P.T. Richards and H.J. Perangelo
Identification of Linear Flutter Models
AIAA-83-1696

/7/ V. Klein
Identification Evaluation Methods
AGARD Lecture Series No. 104

/8/ LMS CADA-X
Modal Analysis Manual 3.2

Flight Flutter Testing of a Turbo-prop Aircraft by using External Excitation Devices

P. Schippers
Afd. ETFA/AE
Fokker Aircraft B.V.
Postbus 7600
1117 ZJ Schiphol
the NETHERLANDS

A.J. Persoon
National Aerospace Laboratory
P.O. Box 90502
1059 CM Amsterdam
the NETHERLANDS

Summary

In modern flutter testing of aircraft artificial excitation is applied. A recently developed aerodynamic vane has been tested in a preliminary flight test to become familiar with installation and use. Two of these vanes have been applied at flutter testing of an configuration of the Fokker 50 Mk2S. Some results of the flight tests and properties of the aerodynamic vane are highlighted.

1. Introduction

An important element in flutter testing an aircraft is the use of controllable aerodynamic vanes to generate a well defined shaking force. The force has to be high enough to excite the aircraft structure beyond its normal flight vibration level. The responses of the aircraft structure due to the shaking have to be analyzed to determine the vibrational stability parameters. The flutter test is carried out for a series of test points starting from a safe initial condition with small speed increments up to the ultimate speed/Mach condition. In the present paper a brief overview is presented of the conventional in flight excitation methods. The application of the new vane on the Fokker 50 and some test results are highlighted.

2. Aspects of flutter testing

The following aspects about excitation and analysis of the responses are of great interest.

Excitation.
The locations for excitation have to be chosen so that both the symmetric and the anti-symmetric bending and torsion modes of the lifting surface can be excited beyond its normal flight vibration level. Sine-sweep and sine-dwell excitation types yield higher structural response levels compared with random/impulse/step excitation and therefore make analysis less complicated. Next a brief resumé of various conventional excitation methods is given:

- Stick raps and servo-control input can be used to shake the aircraft by its own control surfaces (figure 1a) and avoid thereby the installation of special devices. However, the frequency range is usually limited to low frequencies and the quantification of the excitation force(s) generated by the control surface deflection(s) is not well possible.
- The low quality impulse excitation with pyro-technics is considered for application for supersonic flight flutter testing and control surface testing, where the installation of vanes or inertia shakers is not allowed.
- The excitation by air turbulence is still in use too. The quantification of the vibrational stability of the aircraft for the entire flight envelope using airturbulence is not possible accurately, and requires that certain assumptions are made about the spectral contents of this natural source. This (cheap) excitation source is not always present where and when needed and is therefore limited in practical application.
- With controllable aerodynamic vanes the upper frequency range of the excitation can be enlarged and besides accurate measurement of the excitation force is possible. At present three types of aerodynamic vane are applied:
  a) rotating vane with adjustable width (Lockheed application reference 1, figure 1b),
  b) pitching vane (figure 1c), and
  c) fixed vane with rotating slotted cylinder along trailing edge (figure 1d) references 2 and 3.

Paper presented at the Structures and Materials Panel Specialists' Meeting on "Advanced Aeroservoelastic Testing and Data Analysis", held in Rotterdam, The Netherlands, from 8-10 May 1995, and published in CP-566.

Vibrational stability parameters.
In the frequency range of interest, the vibrational stability parameters of the aircraft are:
1) the resonance frequencies,
and for each resonance frequency
2) the accompanying damping value, and
3) the accompanying value representing the ratio of the responding motion of the vibration mode and the excitation force (the complex transmission factor).
For each test point, the vibrational stability parameters have to be determined from the excitation forces and the responses.

Instrumentation.
The vane forces and the responses have to be measured. For that purpose the aircraft has to be instrumented at locations where the aircraft responses the best to the excitation. In general, this will be the extremities of the lifting surfaces of the aircraft: the tips of the wing, the stabilizer and the fin and, if applicable, the front and rear ends of stores are good locations too.

Analysis.
The courses of the resonance frequencies, the damping values and the transmission as a function of the speed, give, in combination with the theoretical prediction, an estimation of the critical speed beyond which vibrational instability will occur.
For the quick and safe continuation of a flutter test, especially the damping value of the least damped vibration mode has to become available almost instantly for each test point. This requires quick look analysis of a number of transmitted response and excitation signals at each test point.

Two ways of quick look analysis are applied at Fokker.
Firstly, the most important and direct way to make the decision to continue flutter testing at a next test point was made on the basis of real time monitoring of the time traces of a limited number of response signals. The level of vibration and the shape of the response due to sweep excitation contain important information about the vibrational damping, especially in relation to previous test points. If a low damped mode is present, comparing the shape of the measured sweep response with pre-calculated sweep responses of a single-degree-of-freedom system for a series of damping values, gives a good indication of the amount of damping remaining in that low damped mode.
Secondly, for the least damped mode on-line damping estimation was applied with a dedicated software package. The methods of analysis are based on curve-fitting one or a limited number of resonance peaks in either the power spectrum or the frequency response function (FRF) or its complex plane representation.

Post-flight analysis was performed by an accurate, multiple-degree-of-freedom curve-fitting technique on all relevant power spectra or FRF's on all on-board registered signals.

Flight test procedure.
Test points have to be taken starting from a safe initial condition and then with small speed increments up to the ultimate speed/Mach condition V_D/M_D.
To reduce the complexity of the analysis the symmetrical and the anti-symmetrical behaviour were treated separately. At each test point the sweep excitation was performed for symmetric and anti-symmetric excitation by which the vanes act in phase respectively in counter phase after one another. The length and the number of repetitions of the sweep excitation can be regarded as an acceptable compromise to the non-steady flight test conditions at the high speed descending flight path.
The progress of a flight flutter test depends strongly on the test procedure, on previous experience with similar aircraft configurations, and on the results of reliable flutter calculations.

3. Two test cases.

Case a) A familiarization test to try out one 60 sq. inches fixed vane with rotating slotted cylinder along its trailing edge (manufacturer DEI) on the Fokker 50 prototype 1, and case b) a flutter certification test with two of these vanes on the Fokker 50 Mk2S.

3.1 Fokker 50 preliminary test.

The preliminary test comprised of two flights, each with a series of tests at level flight.
In the first flight the DEI vane was mounted in an front position on a pylon mounted store; in the second flight the vane was moved to a rear position on the store (see photographs 1a & 1b).
The aim of this preliminary test was
i) to find the best way of

installation, ii) to become familiar with the control of the vane and the test procedure (pilots and ground crew), and iii) to select the best location of a vane on the store and a type of excitation and analysis. With seven accelerometers the responses of the store were measured. The signals of the excitation force and the acceleration responses were recorded on board and transmitted to the ground station as well.
In this preliminary test several kinds of sweeps and sine dwell/free decays were tested and stick raps (aileron) and air turbulence were applied as well.
From the results of this preliminary test it was decided as a compromise between short test time and high response level to use only one sweep setting for flight flutter certification test of the Fokker 50 Mk2S. The selected sweep was linear from 2 Hz to 25 Hz in 16 seconds, repeated four times (up-down-up-down), resulting in a measurement time of 64 seconds. An advantage of the linear sweep is that it has a flat spectrum, making the interpretation of the spectrum of the response easier.
The repetition of the sweep excitation makes spectral averaging possible, resulting in a 'cleaner' spectrum.

The preparation of the aircraft for this test took about one week (including a limited ground vibration test).

3.2 Fokker 50 Mk2S certification test.

Four pylon/store combinations were symmetrically attached to the wing at about semi span.
For symmetric and anti-symmetric excitation two DEI vanes were mounted to the fronts of the outer pair of the four stores (figure 2). These positions for the vanes were chosen to excite the wing in its bending modes as well as in its torsion modes.
With a total of 24 accelerometers the responses were measured at the wing tips, the fronts of the four stores, the gear boxes of both propellers and of the vanes themselves (figure 3). Both wing tips were instrumented with two accelerometers: one at the front spar and one at the rear spar to measure the vertical acceleration. From these four wing tip accelerations the symmetric and the anti-symmetric vertical & rotational acceleration were derived via analog weighing and summation/subtraction. By this way of separation of the motions of the wing tips, the quick look observation and analysis was easier.
The signals of the excitation forces and the acceleration responses were recorded on board and a selection of signals was transmitted to the ground station for real time analysis (figure 4).

The time needed for this flutter test, including a limited ground vibration test was pretty short: vane & other instrumentation on and off in two days!

Sample of flight test data
From the flutter test on the Fokker 50 Enforcer at about 180 knots, time traces of the excitation and the vertical acceleration responses at the wing tip and the front of the store of the left wing only are presented in figure 5. Excitation was anti-symmetrical and the time window presented covers more than a full up sweep of 16 seconds. Obviously, the responses are strongly contaminated with excitation by the number of revolutions of the propellers (20 Hz) and some aerodynamic flow separation. The power spectra (2 Hz to 25 Hz) of both responses are inserted in figure 5. The peaks of the wing bending modes both symmetric and anti-symmetric can be recognized in the power spectrum of the wing tip response at 3 Hz, 5 Hz and 7 Hz. The power spectrum of the response of the store front has a dominant peak at 13 Hz of the outer wing torsion mode.

Similar time traces from sweep excitation from the ground test with external shakers are presented in figure 6. The shape of the bursts in the responses are typical for low damped resonant modes; quite distinctive are the responses of the wing tip the front of the store at 11 Hz and 13 Hz of the anti-symmetric wing bending mode respectively of the outer wing torsion mode.

Test points
The actually flown test points took approximately 140 seconds: ≈64 seconds for symmetric sweep excitation plus ≈64 seconds for anti-symmetric sweep excitation. Except for the test points near V_D/M_D where only anti-symmetric excitation could be applied due to substantial loss of altitude and there was no valid argument to repeat the test point with symmetric excitation.The entire flutter test of the Fokker 50 Mk2S up to V_D/M_D was performed in one flight.

4. Overall assessment

A maximum excitation force of 220 Newton (dependent on the dynamic pressure) was generated by one 60 sq-inch vane. For low damped modes this excitation force is sufficient; for higher damped modes the response level will remain low as a matter of course, but in that case there is no vibrational stability problem.
A relative high frequency component (20 Hz) originating from the propeller revolutions contaminated the response due to vane excitation. With response analysis in the frequency domain the frequency components not related with the excitation can be distinguished from the intended excitation.

Quality of the generated dynamic forces.
The generated dynamic force is strongly distorted by harmonics. Figures 7a and 7b show the onset of the excitation forces of the two vanes at counter phase and in phase setting at about 2 Hz. The generated forces of the two vanes as measured with the strain gauges, are saw-tooth like. Although the resonance behaviour of the lifting surface structure will filter out the symmetric and the anti-symmetric components in the excitation, the non-sinusoidal shape of the vanes makes the symmetric/anti-symmetric excitation with two vanes not well separated. This will result in an anti-symmetric response contribution at symmetric excitation and its pendant, a symmetric response contribution at anti-symmetric excitation. This makes analysis of responses to separate the symmetric and the anti-symmetric flutter behaviour somewhat more complicated. The excitation forces contain also a frequency component at about 67 Hz originating from the low damped bending mode of the vanes. This bending mode is easily excited by the non-smooth aerodynamics around the slotted cylinder.
At higher excitation frequencies the distortion of the measured forces seems to decrease (see figure 8).

Another thing that can be remarked is, that the generated dynamic force is non-symmetric about the mean steady force. This may be caused by the non-zero mean steady force of the vanes, both vanes had a small negative effective incidence resulting in a downwards mean steady force.

Finally, the electrically operated DEI vane was relatively easy to install and has no impact on the aircraft's hydraulic systems. Its presence does not affect the aircraft's control and this independent means of excitation is easy to use (start & forget). Another technical advantage is that, compared with moving vanes, the force measured on the fixed surface cannot contain inertia forces due to its own motion. Only a minor inertia contribution in the force signal appears as the lifting surface at the vane position responses. If necessary this inertia contribution in the force signal can be cancelled out easily by subtracting the vertical acceleration part.

5. Conclusions

With the DEI vane as an easy to operate means of in-flight excitation, flight flutter testing of an aircraft can be accomplished in a quick, accurate and above all in a safe way.

With the vane excitation higher excitation frequencies were reached than were possible with stick raps: The wing torsion mode at ≈12 Hz could never have been excited and found when excitation with control surface from stick raps was applied.

References

1. Rosenbaum R. Survey of subcritical flight flutter testing methods. A.R.A.P. report no. 218, 1972.

2. Reed III W.H. A new flight flutter excitation system. Dynamic Engineering Incorporated, 1988.

3. Reed III W.H., Kehoe M.W., Nilsson B., Schippers P. An excitation system for aircraft flutter testing: Some highlights of flight test applications.
24-th Annual symposium of the Society for Flight Test Engineers, 1993.

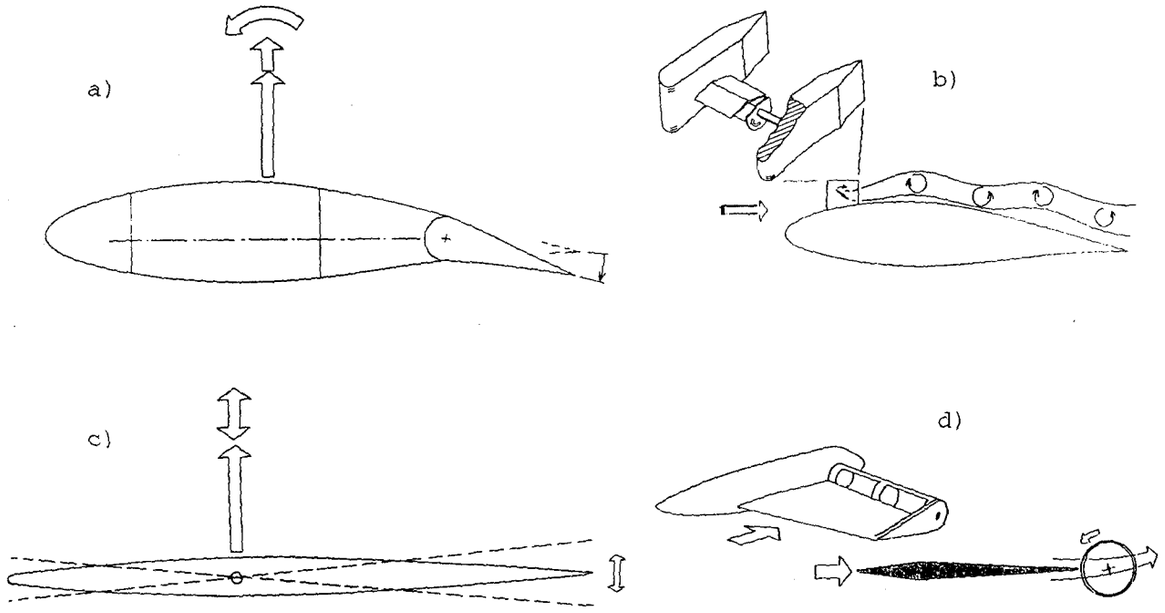

Figure 1 Various excitation methods: a) control surface deflection by stick raps, b) rotating vane with adjustable width, c) pitching vane, and d) fixed vane with rotating slotted cylinder.

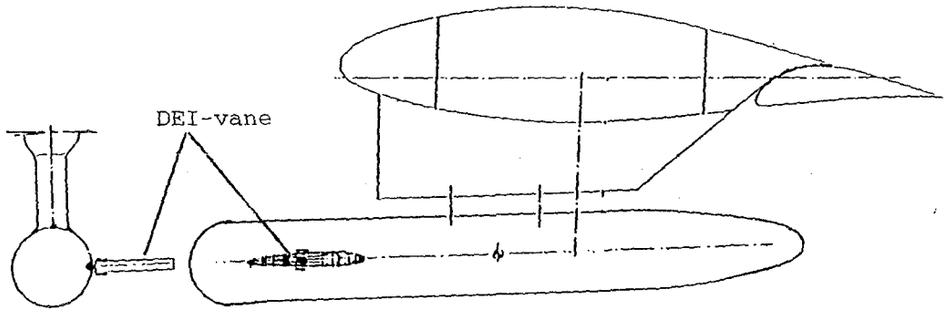

Figure 2 Vane installation on the front of the store at semi wing span (inboard side only).

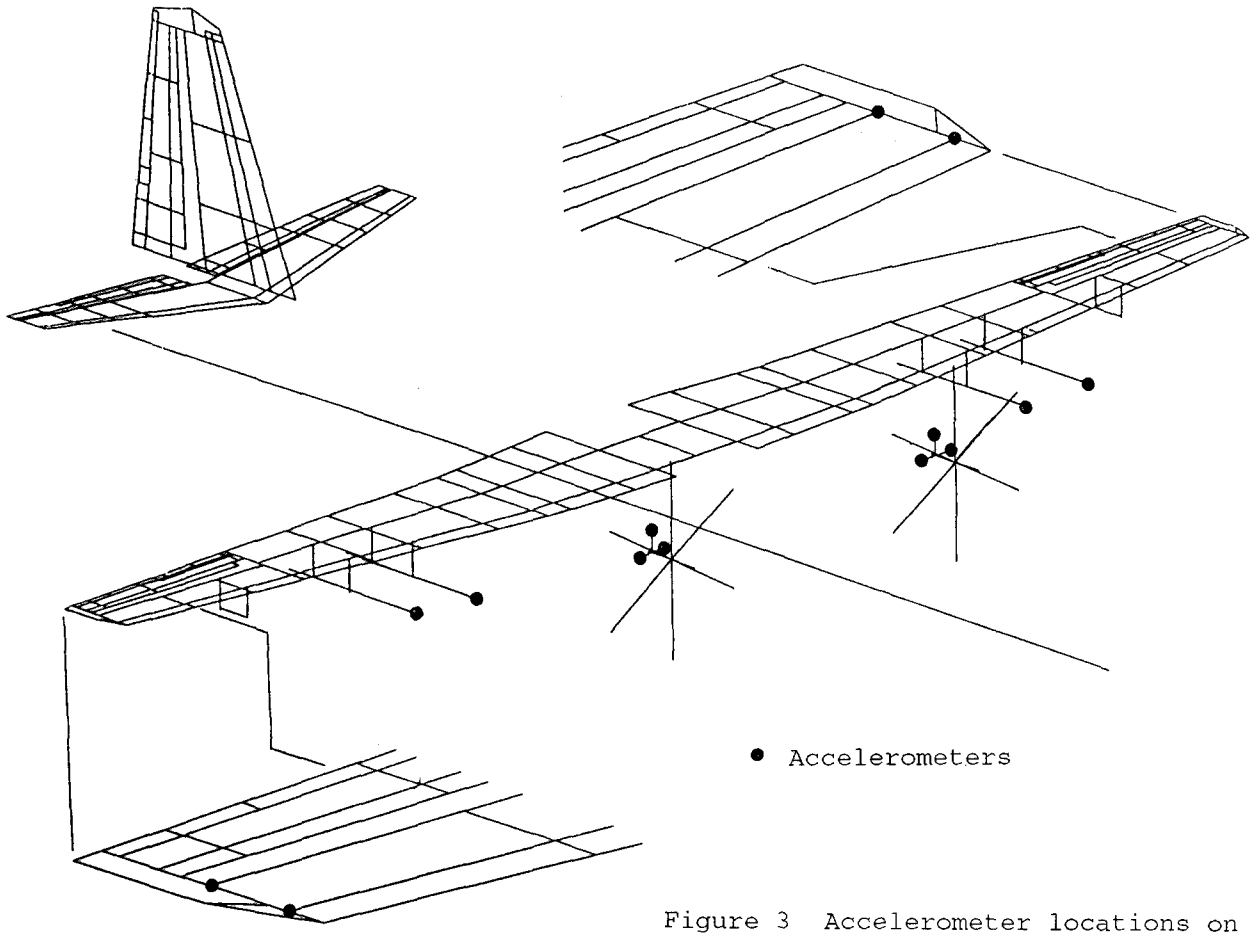

Figure 3 Accelerometer locations on Fokker 50 Mk2S aircraft.

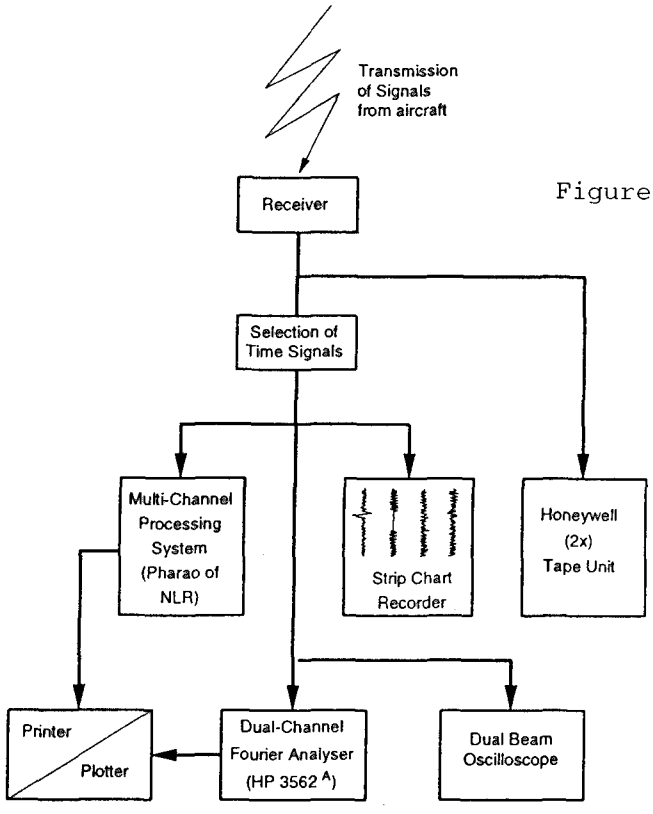

Figure 4 Ground station equipment.

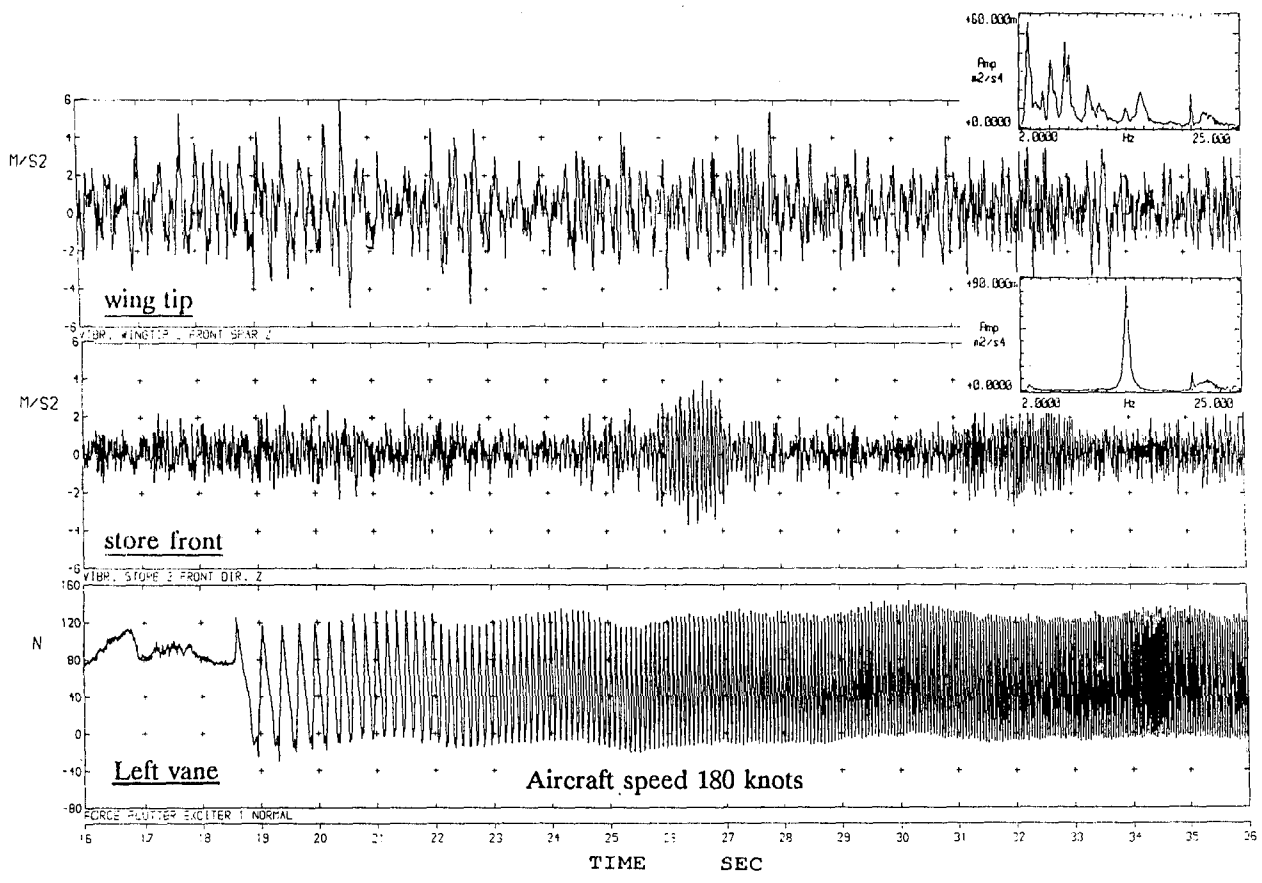

Figure 5 Responses and power spectra of the wing tip and the store front at in-flight anti-symmetrical sweep excitation (2 Hz to 25 Hz in about 16 seconds).

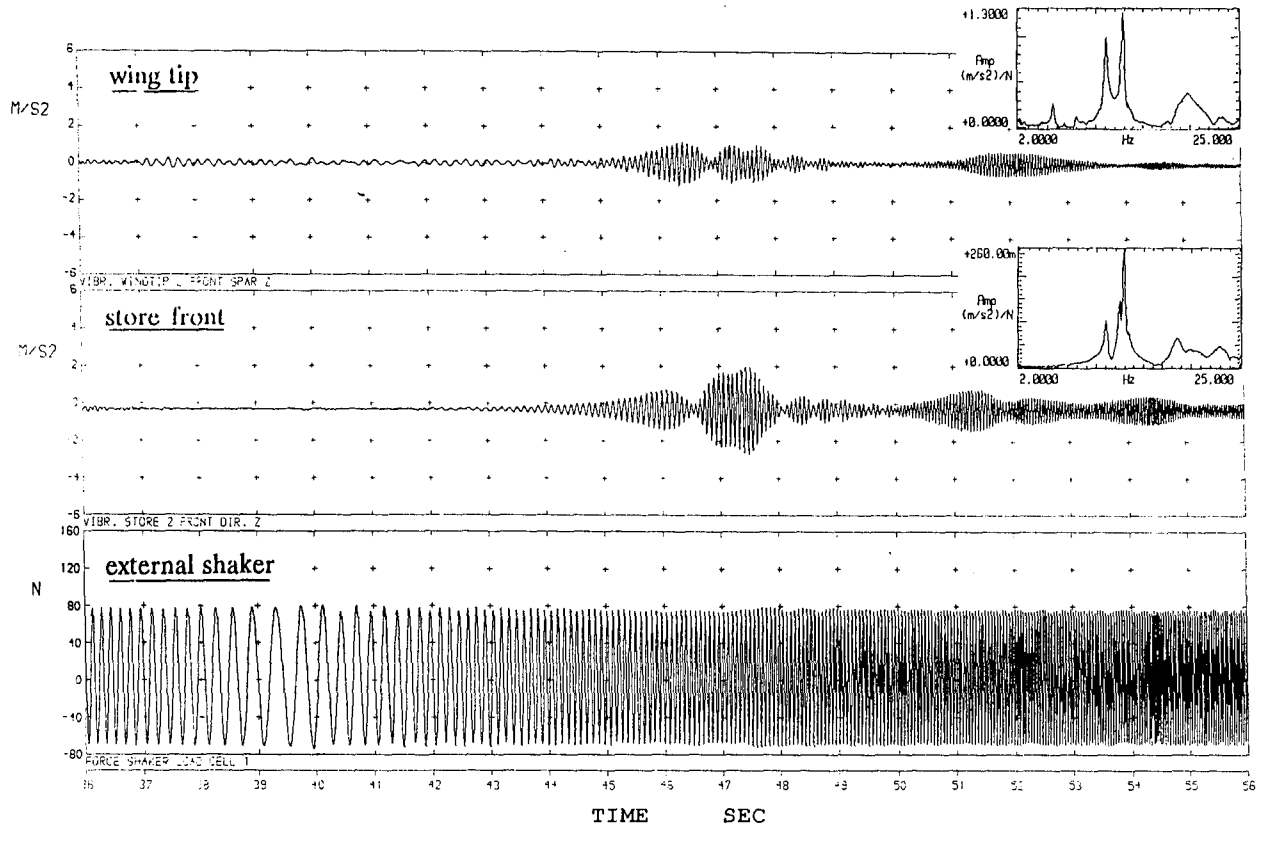

Figure 6 Responses and power spectra of the wing tip and the store front at **ground test** anti-symmetrical sweep excitation (2 Hz to 25 Hz in about 16 seconds).

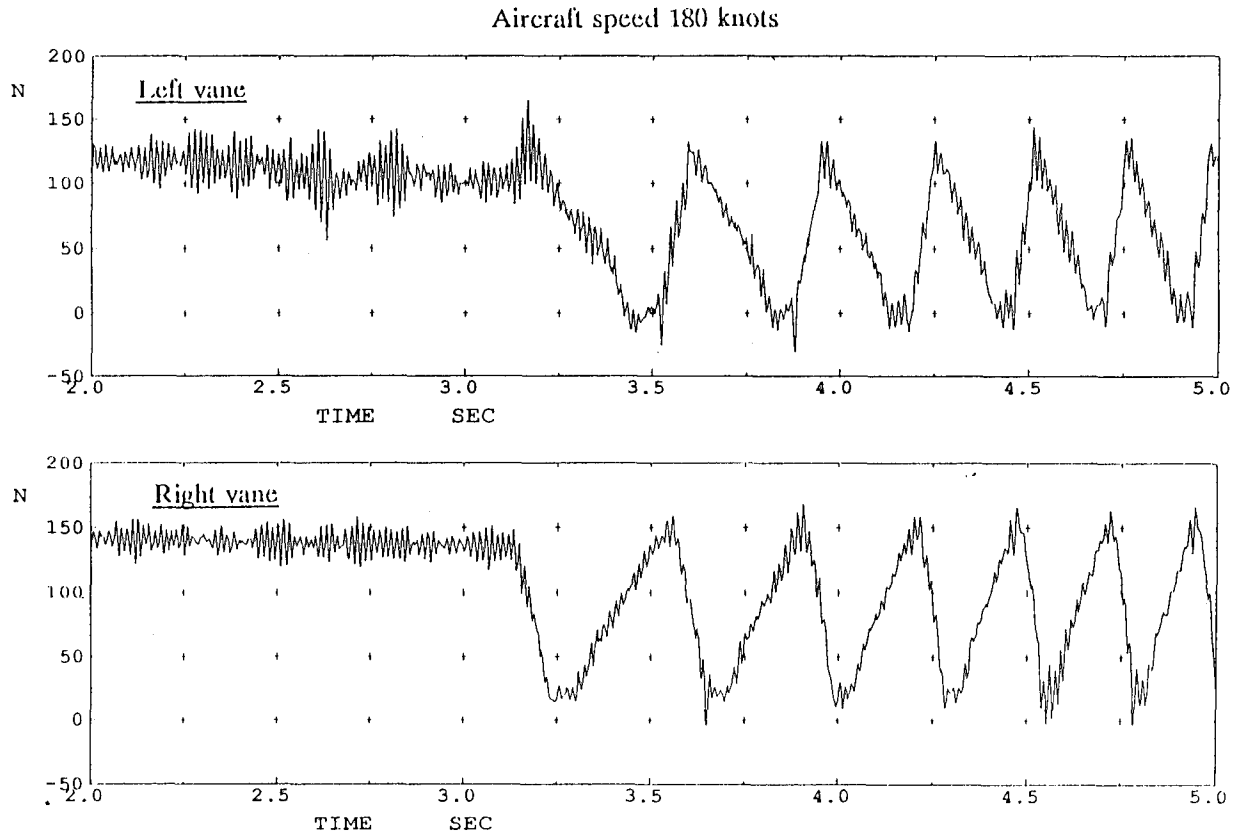

Figure 7a Onset of counter phase excitation, frequency approximately 2 Hz.

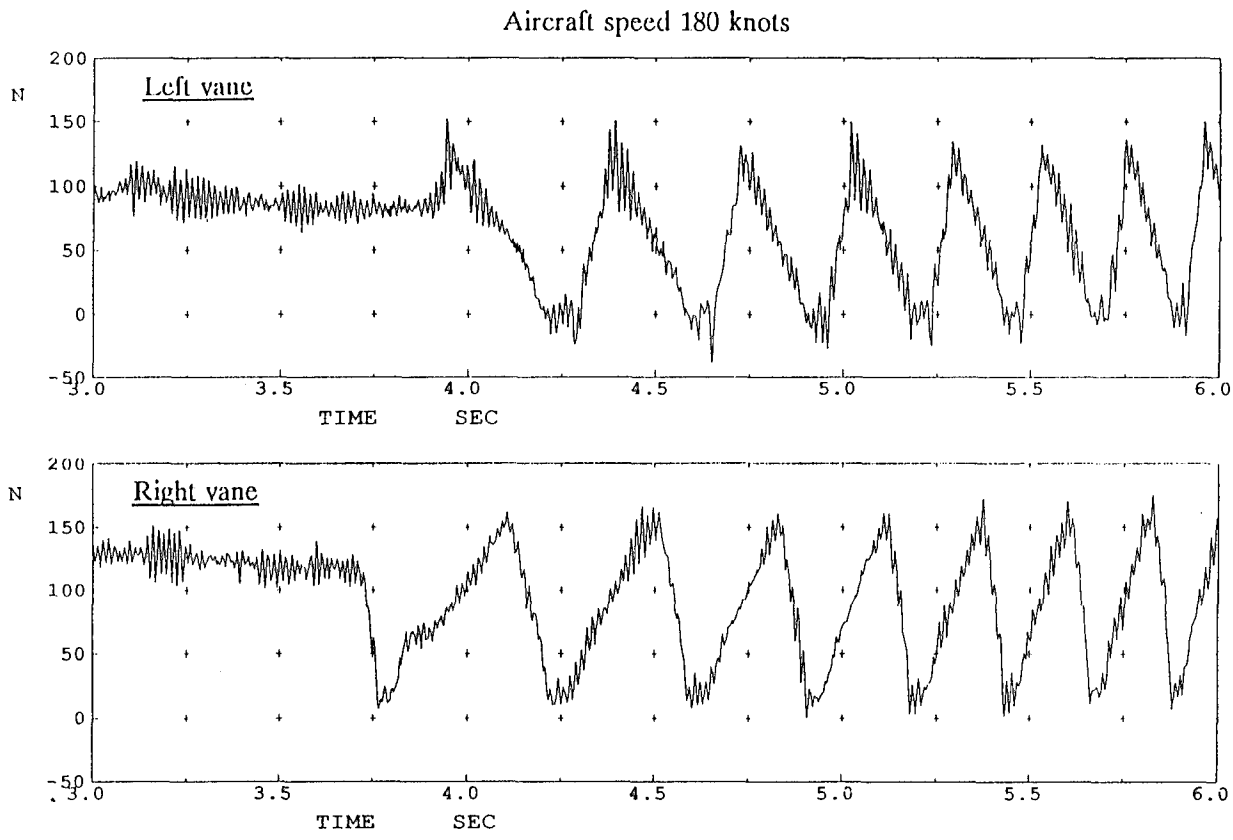

Figure 7b Onset of in phase excitation, frequency approximately 2 Hz.

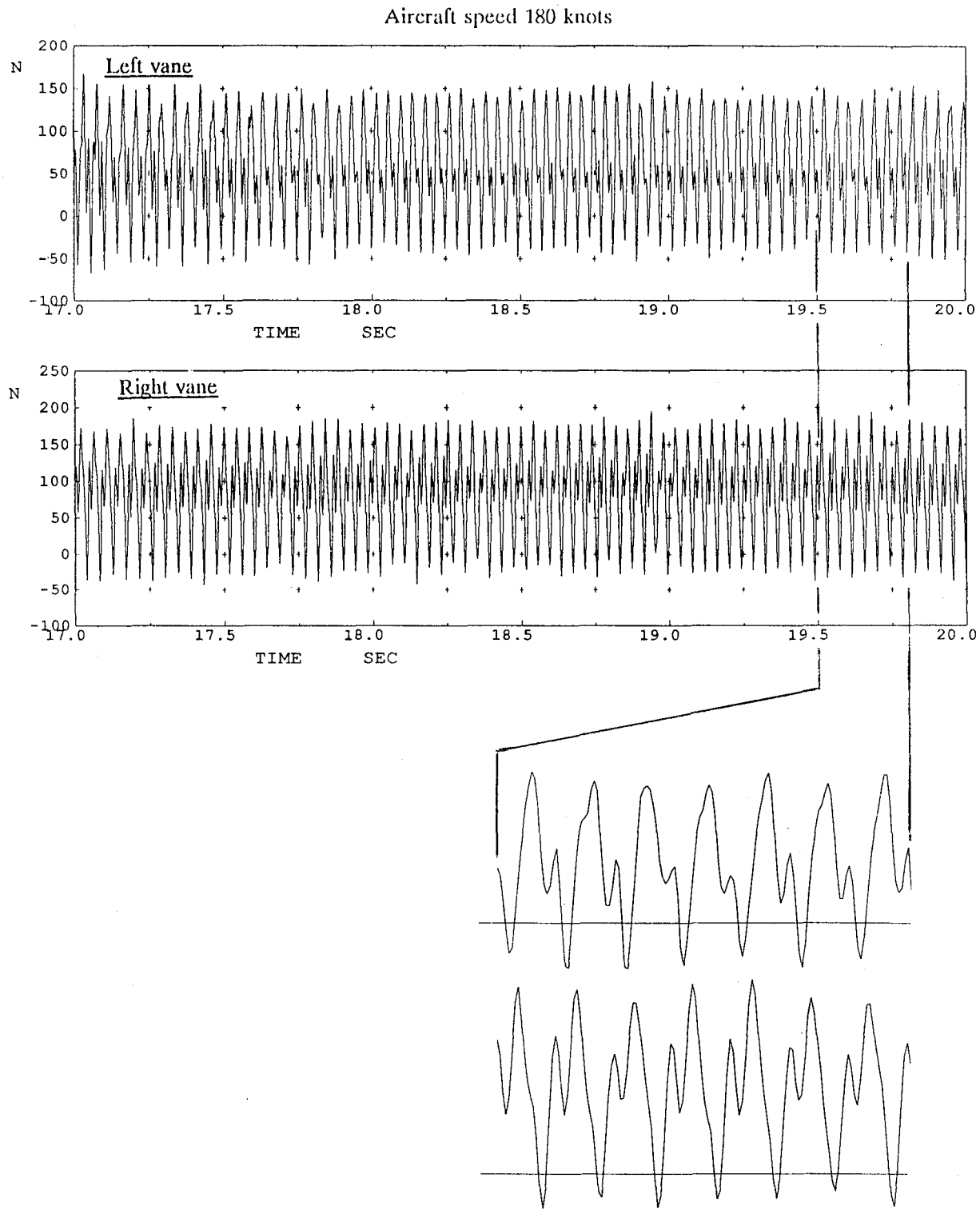

Figure 8 Counter phase excitation, frequency approximately 25 Hz.

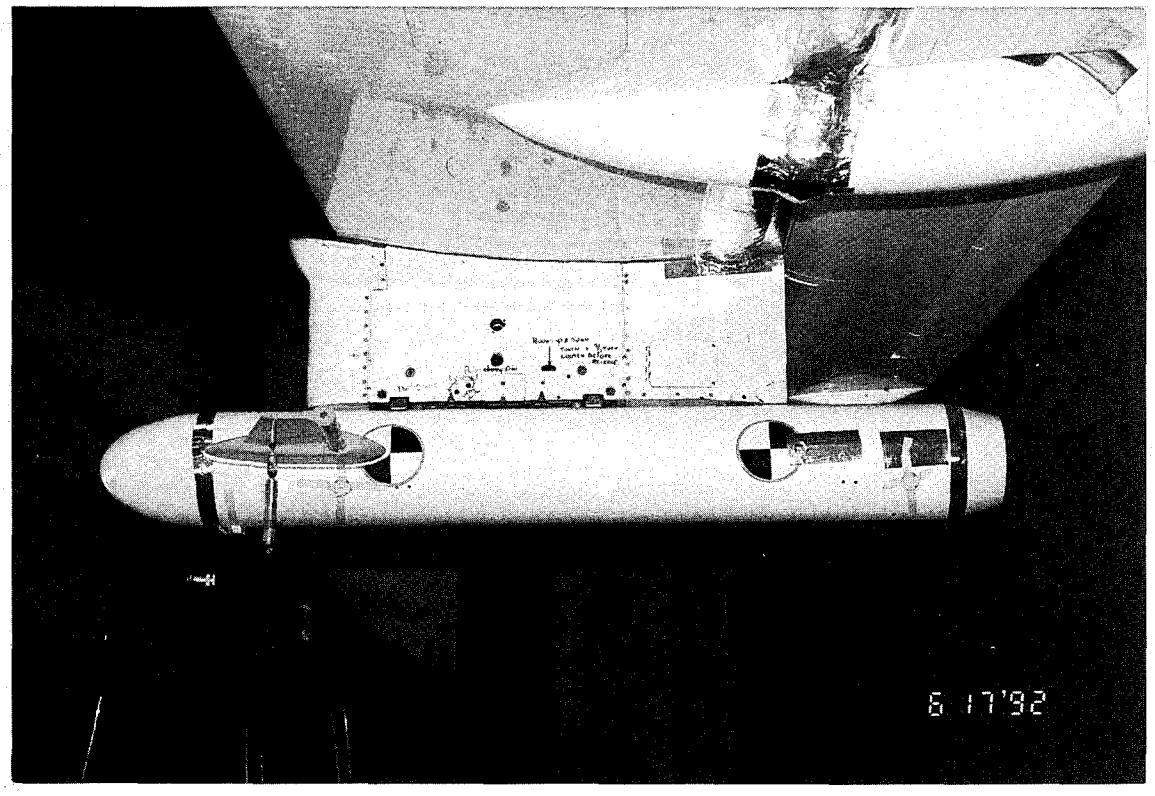

Photograph 1a Vane in front position on store of preliminary flight test Fokker 50 prototype 1.

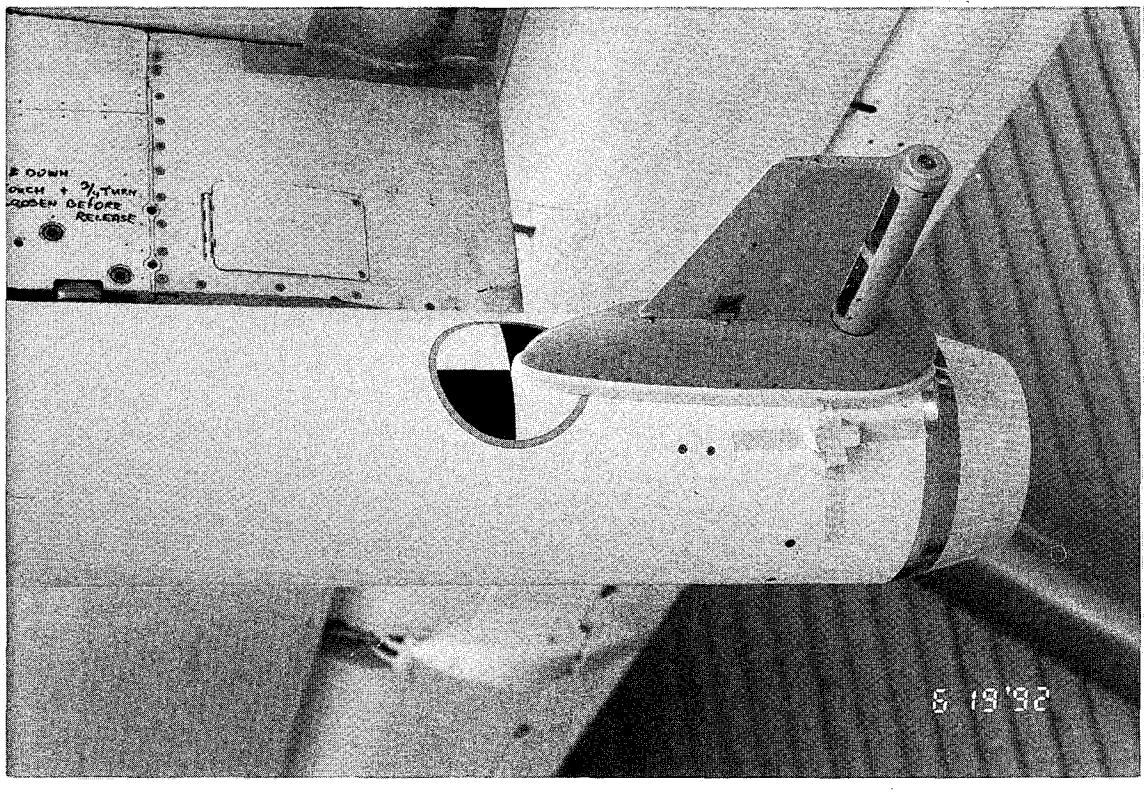

Photograph 1b Vane in rear position on store of preliminary flight test Fokker 50 prototype 1.

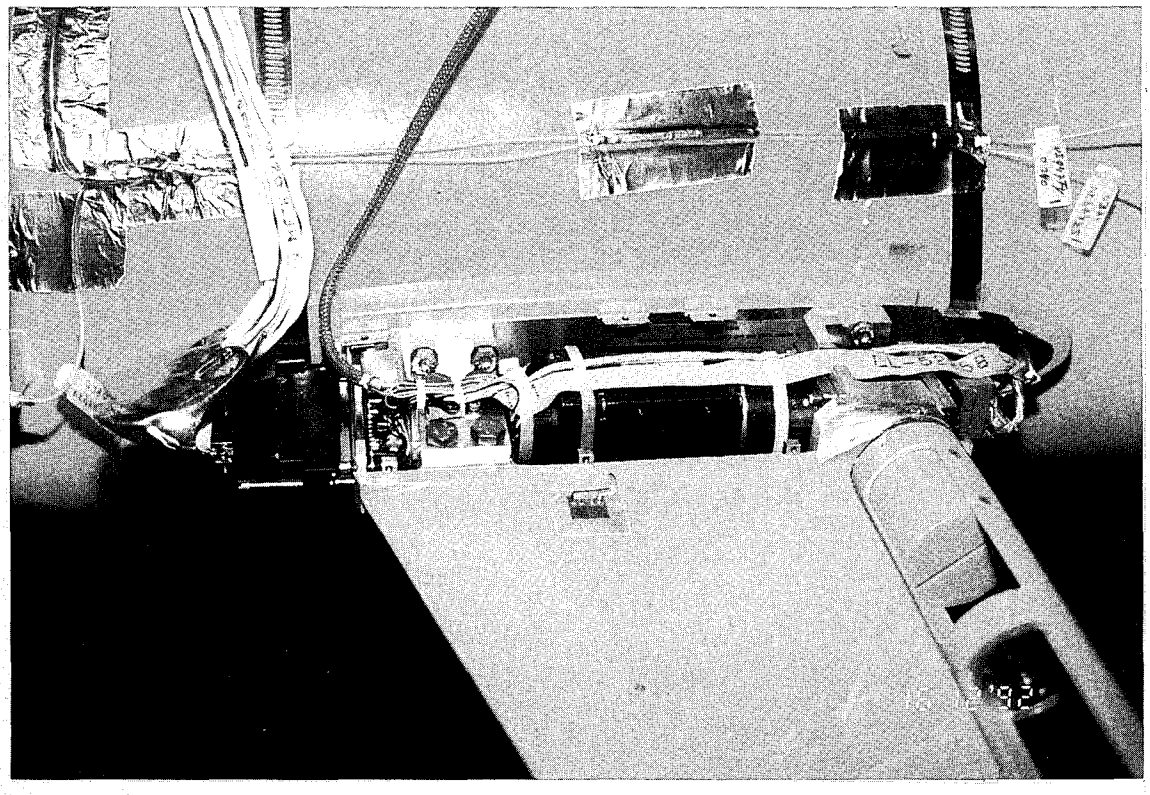

Photograph 2 Vane at front of store of Fokker 50 Mk2S.

US Air Force/DEI Flutter Exciter Test Program

B.M. Shirley
Compatibility Engineering Flight Munitions Test Division (46 OG/OGME)
205 West D Avenue, Suite 241
Eglin Air Force Base, Florida 32542-6866, USA

E.L. Anderson
TYBRIN Corporation
745D Beal Parkway NW, Unit 10
Ft. Walton Beach, Florida 32547, USA

1. SUMMARY

United States Air Force (USAF) testing of the Dynamic Engineering Incorporated (DEI) flutter exciter was conducted from July to September, 1993, using pylon-mounted exciters on an existing F-16A flutter test aircraft (see Figure 1). The intent was to evaluate the system as a low-cost, easily-installed alternative to the existing aircraft flight control integrated systems.

A dual exciter system with an exciter mounted on the outboard side of each weapons pylon (aircraft weapons stations 3 and 7) was flight tested in conjunction with the existing integrated Flutter Exciter System (FES). The existing F-16 system provides excitation via the flaperons; it is capable of symmetric and antisymmetric sweeps and bursts of up to 20 Hertz (Hz) for selectable time durations.

Testing of the DEI flutter exciter system was limited to matching FES time/frequency capabilities, although it has greater frequency response and time duration capabilities. A one-for-one comparison of excitation levels, frequency content and damping values was made at various Mach/airspeed/altitude combinations for five different aircraft/weapon configurations (see Table 1), three of which are presented herein. Conclusions are drawn regarding 1) the use of the DEI exciter in a high-q environment, and 2) its application as an alternative excitation method.

2. LIST OF SYMBOLS

AFDTC	Air Force Development Test Center
ft	feet
g	structural damping
Hz	Hertz (frequency)
KCAS	Knots Calibrated Air Speed
lbf	pounds force
M	Mach number
psf	pounds per square foot
q	dynamic pressure (psf)

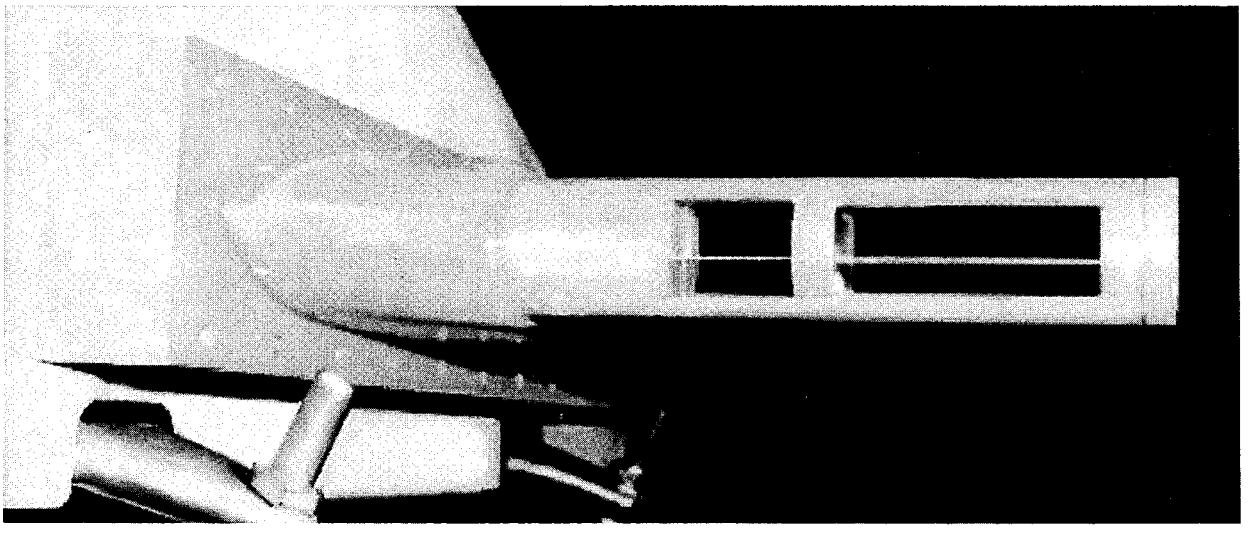

Figure 1. DEI Exciter Installation

Paper presented at the Structures and Materials Panel Specialists' Meeting on "Advanced Aeroservoelastic Testing and Data Analysis", held in Rotterdam, The Netherlands, from 8-10 May 1995, and published in CP-566.

CONFIGURATION	MODE	UFAP	FES	DEI	DESCRIPTION
1 (Flutter)	1	9.2	9.6	9.8	Wing 1st Bending
	2	12.3	12.3	12.7	Wing 1st Torsion
4 (LCO)	1	8.2	7.6	7.6	Wing 1st Bending
	2	9.6	9.4	9.4	Wing 1st Torsion
	3	10.7	10.0	10.0	Tip Missile Pitch
5 (LCO)	1	5.1	5.1	5.1	Outer Wing Torsion
	2	5.5	5.9	5.9	Tip Missile Pitch
	8	9.8	9.8	10.0	Outer Wing Bending
	9	10.9	10.9	10.7	Outboard Store Pitch

Table 1. Frequency (Hz) Comparison

3. INTRODUCTION

In 1991, the Compatibility Engineering Section of the 46 Operations Group at Eglin Air Force Base, FL, received Test Technology Development and Demonstration funding from the Office of the Secretary of Defense to evaluate the DEI flutter exciter. The program basis was evaluating the effectiveness of the DEI flutter exciter for use in support of USAF SEEK EAGLE weapons certification.

Recent problems with the F-16 FES and F-111 Spoiler Excitation System – involving structural cracking and fatigue failures – prompted the search for other means of providing a controlled excitation into the airframe. The intent was to identify an alternative method of aircraft excitation for flight flutter testing that was easily installable and low-cost, relative to aircraft modification and initial procurement costs. Aircraft modification costs associated with the installation of the DEI system were approximately $52,000 U.S. dollars. Installation time was less than three weeks.

An analysis of the F-16 airframe was conducted using the Lockheed Fort Worth dynamic response model, which was modified to include the DEI exciter. Various exciter locations were evaluated for five candidate flight configurations. While installation on the wingtip was the most desirable choice and had been demonstrated successfully (reference 1), USAF testing of flutter-critical configurations varied extensively between wingtip missile on/wingtip missile off. The outboard side of the weapons pylon was selected for the installation of the DEI exciter, based on: 1) response characteristics of the

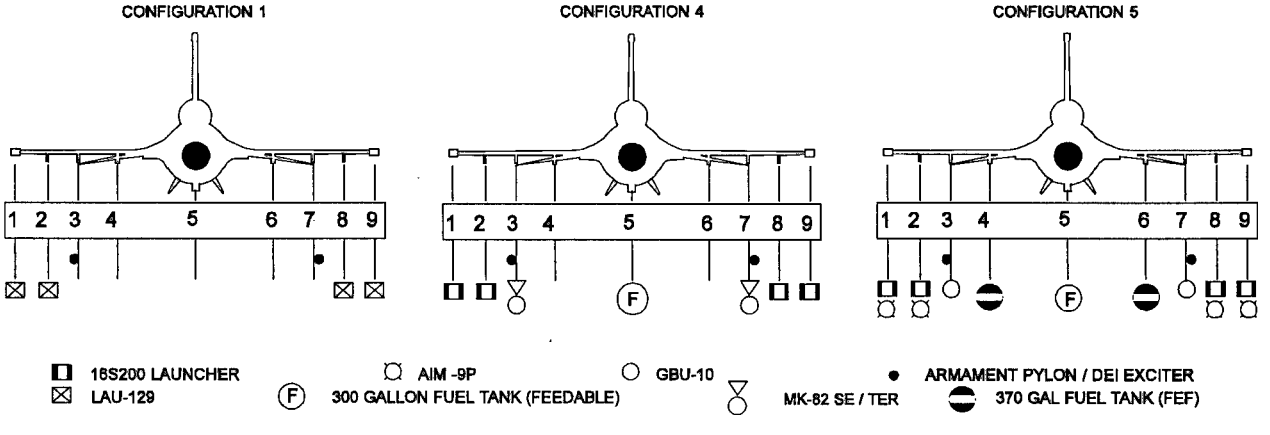

Figure 2. Flight Test Configurations

wingtip, 2) relative ease of installation, 3) flow fields considerations (especially the flow fields involving LCO), and 4) exciter mass effects altering the very dynamic characteristics that were being investigated.

Flight testing of the DEI exciter was conducted on an F-16A aircraft that was previously modified with instrumentation to support flight flutter testing. This test program was called the Strap-On Flutter Exciter (SOFE) program, and complete test results will be contained in an AFDTC Technical Report to be published in 1995. The DEI excitation system consisted of 1) two exciter vanes – each of which is a fixed, flow-field vane that is faired into a slotted, rotating cylinder – 2) an avionics box, and 3) a cockpit control panel. Each vane was cantilevered on the forward, outboard sides of the stations 3 and 7 pylons. The excitation frequency was modulated by controlling the rotational speed of the slotted cylinder. Prior to flight, the force level could be adjusted by installing a cylindrical plug, blocking one-quarter of the slotted opening. Figure 1 shows the force level plug as it was installed for testing at three-quarters of maximum force. The system was designed to generate both symmetric and antisymmetric excitation by phasing the (pylon stations 3 and 7) rotating cylinders at either 0 or 90 degrees, respectively.

4. DISCUSSION

F-16 flutter and LCO tests were conducted for five aircraft configurations. Representative results for three of the five configurations tested (one flutter configuration and two LCO configurations) are presented. Data acquisition and analysis included: 1) time histories, 2) power spectral density (PSD) plots, and 3) transfer function plots. Supporting flutter analyses were performed using the USAF Universal Flutter Analysis Program (UFAP) aeroelastic program and the Block 25 F-16 structural influence coefficient model. Frequency comparisons between analysis and flight test results are presented in Table 1.

4.1 Configuration 1 Results

4.1.1 *General Results*

This configuration (Figure 2) demonstrates a classical flutter bending/torsion mechanism with acceptable correlation to analysis. The minimum, predicted antisymmetric flutter speed is 1043 KCAS/9.5 Hz/g=0.00 (flutter speed/flutter frequency/damping level). The predicted mechanism is primarily a coupling of mode 1 (9.2 Hz - wing first bending)

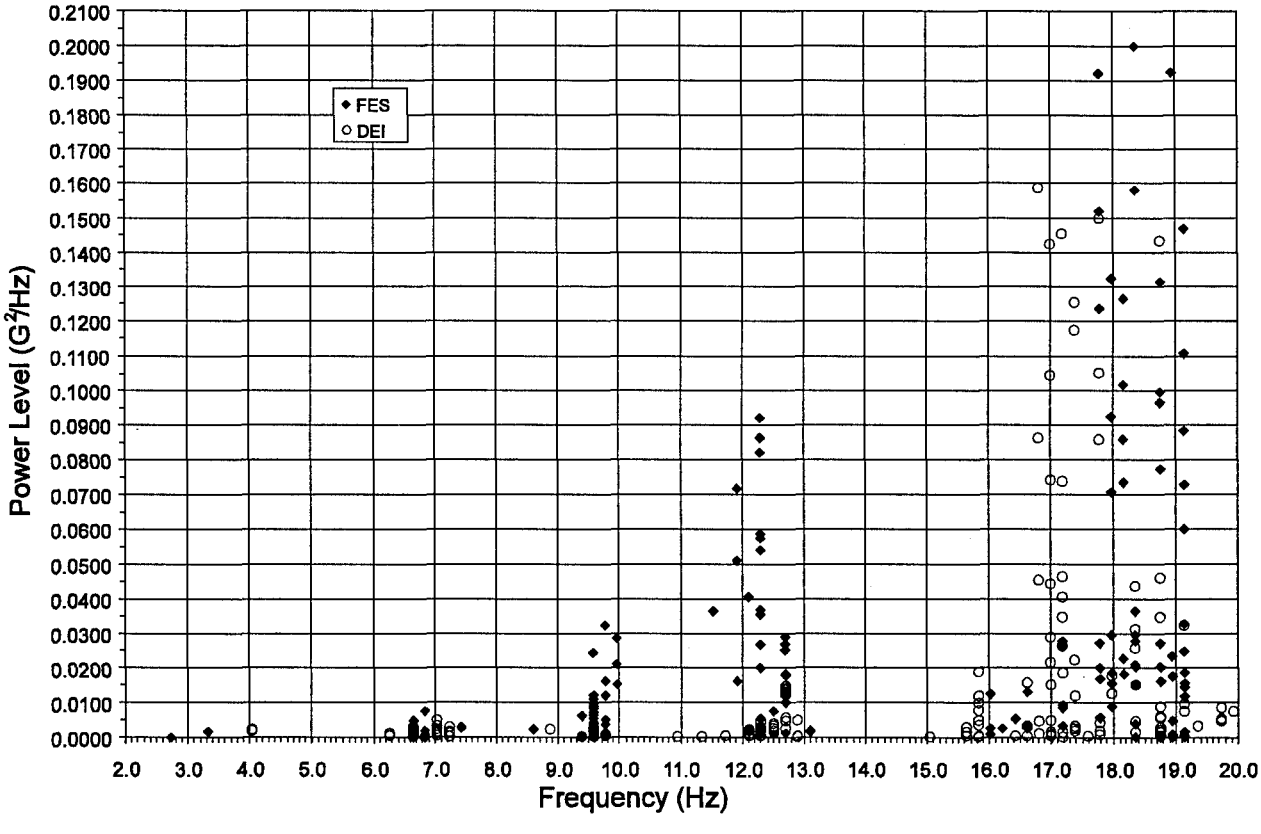

Figure 3. Configuration 1 Sweep Response – Vertical Accelerometers

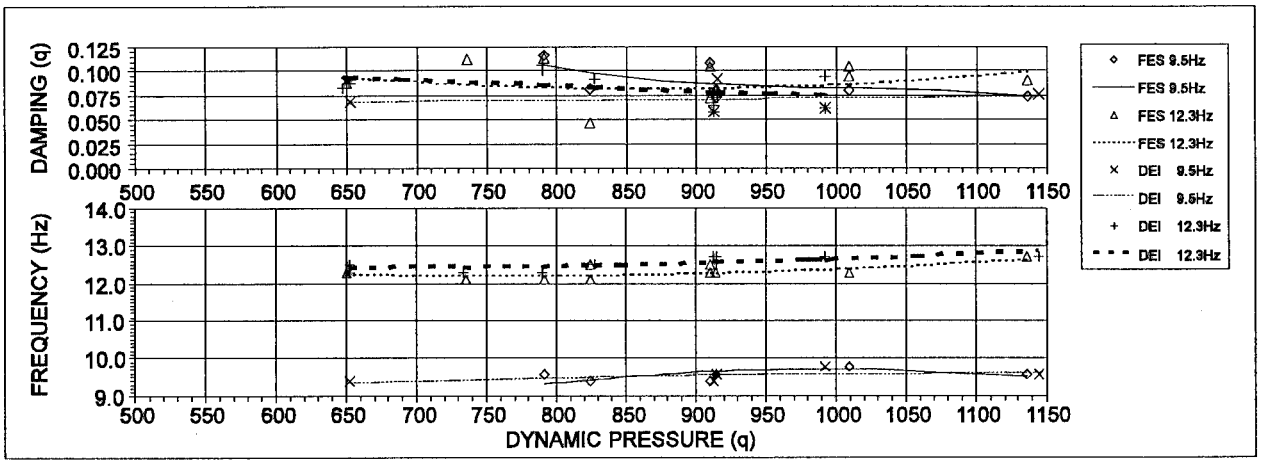

Figure 4. Flutter Frequency/Damping Trends

and mode 2 (12.3 Hz - wing first torsion). Linear rate antisymmetric sweep results were evaluated for both excitation systems at various flight conditions. Accelerometers on wing stations 1 and 9 were not functional for this configuration. Reliance on the underwing stations 2 and 8 accelerometers was sufficient to describe aircraft motion and primary modes involved in the predicted flutter mechanism.

4.1.2 *FES Results*

A scatter plot of the response power level versus frequency (obtained from the PSD analyses) is provided for the vertical accelerometer data set in Figure 3. Frequency and damping trends obtained from PSDs are presented in Figure 4. The FES PSD analysis plots clearly depicted the critical mode 1 / mode 2 coupling.

Additional modes – although not directly involved in the critical flutter mechanism – were identified, based on the PSDs. A large frequency scatter is found within the 17-20 Hz range. The 19.3 Hz wing second bending mode is prominent in this range. A response at 18.4 Hz was also noted and is the local pylon pitch mode.

4.1.3 *DEI Exciter Results*

The DEI excitation level was consistently lower than the FES. Analysis of the transfer functions shows an increasing, nonlinear phase shift with increasing q. Figures 5 and 6 are indicative of this q effect. Acceptable phasing and magnitude are found for the 0.80 M, 10000 ft (q = 737 psf) test condition; nonlinear phase shifts and magnitude responses are indicated for the 0.90 M, 5000 ft (q = 992 psf) test condition. (NOTE: All altitudes contained within this report are to be considered pressure altitudes.)

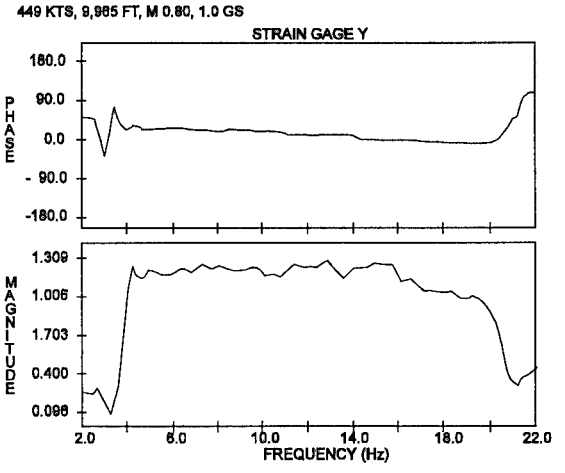

Figure 5. DEI Transfer Function (Config. 1 / 10,000 ft)

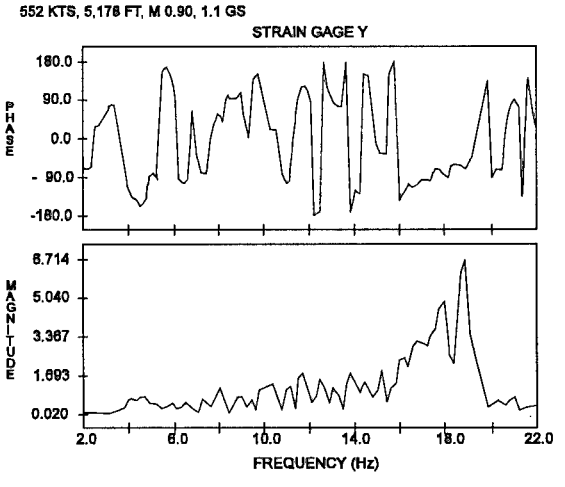

Figure 6. DEI Transfer Function (Config. 1 / 5,000 ft)

Response power level versus frequency data for the vertical accelerometer set is superimposed against the FES data in Figure 3. The modes associated with the critical flutter mechanism (mode 1 / mode 2) are defined by the PSD response as 9.8 Hz and 12.7 Hz. Figure 3 shows scatter within the frequency data due to the phase and magnitude nonlinearity.

The low exciter energy level and erratic phasing at higher dynamic pressures resulted in decreased modal definition. The primary wing first bending mode, in particular, is difficult to distinguish due to: 1) the lack of functional station 1 and 9 accelerometers, 2) low excitation energy and nonlinear phasing, and 3) DEI exciter location. The wing first bending modeshape involves primarily outer wing bending, which could have been best detected by the stations 1 and 9 accelerometers. Additionally, the DEI exciter location on stations 3 and 7 are in a low response location for this mode. Finally, mode 2 (wing first torsion) and mode 6 (wing second bending) dominate the PSD response, masking mode 1.

As found during the FES excitation, considerable frequency scatter exists within 17-20 Hz. The 17.4 Hz mode (pylon pitch) appears more strongly using the DEI exciter. The response of this mode demonstrates 1) the criticality of the exciter installation location, and 2) the ability to excite higher frequency modes.

4.1.4 *FES and DEI Comparison*

The FES was able to more clearly identify the mode 1 (wing first bending) / mode 2 (wing first torsion) critical antisymmetric flutter mechanism. The DEI system's nonlinear phase and gain behavior at higher q resulted in decreased modal definition.

The results demonstrate the criticality of DEI exciter placement; positioning near the node lines for critical modes results in a diminished input excitation level. Nonlinear gain and phase behavior also degraded the quality of input excitation to critical modes. The FES excitation provides a better distribution of energy for these critical modes. Placing the DEI exciter further outboard – or on the wingtip launchers – would improve excitation input levels for this clean wing configuration.

In general, the DEI exciter provides between 0.1 and 0.5 times lower response levels than the FES. The DEI system does excite modes greater than 16 Hz more effectively than it does the low frequency modes, and its placement did provide better excitation for the 17.4 Hz pylon pitch mode. The PSD analyses results (summarized in Figure 4) show the general frequency trends to be consistent, with both systems tracking critical modes adequately. Figure 4 also shows that additional scatter is found in the DEI damping data, although the trends are similar.

4.2 Configuration 4 Results

4.2.1 *General Results*

This configuration (Figure 2) exhibits a 9.4 Hz LCO response that dominates the spectral data. The minimum predicted antisymmetric flutter speed is 410 KCAS/10.6 Hz/g=0.00 and 586 KCAS/10.5 Hz/g=0.01. The flutter mechanism involves a coupling of mode 2 (9.6 Hz - wing first torsion) and mode 3 (10.7 Hz - tip missile pitch). Mode 3 contains a minimal amount of wing bending motion, which assists in the analytical coupling. Flight test results indicate that mode 1 is directly involved in the LCO response.

4.2.2 *FES Results*

Scatter plots of the response power level versus frequency show distinct mechanism frequencies, as well as the LCO response. Figure 7 shows the dominance of the 9.4 Hz LCO response in the PSD plot. Frequency and damping levels were obtained from the PSDs for primary modes where possible. The FES measured modes (see Table 1) associated with the critical flutter mechanism are mode 2 (9.4 Hz) and mode 3 (10.0 Hz), and to a lesser degree, mode 1 (7.6 Hz).

A Mach effect (historically seen with aircraft encountering LCO) is evidenced by a distinct difference in the response of the aircraft at 0.80M, compared to 0.90 M conditions (regardless of altitude). At 0.80 M, the FES excitation shows more clarity with regard to the fundamental modes. At 0.90M, these modes shift and are obscured by 9.4 Hz LCO response (see Figure 7).

4.2.3 *DEI Exciter Results*

The DEI excitation level was lower than the FES and showed phase and gain fluctuations with increasing q, similar to that found for Configuration 1. The excitation phase and gain nonlinearity contributed to the frequency and damping data scatter. Fundamental frequencies obtained from the DEI excitation are identified as previously shown in Table 1. The modes associated with the analytically predicted critical flutter mechanism (mode 2 / mode 3) are defined by DEI as 9.4 Hz and 10.0 Hz (with mode 1 at 7.6 Hz).

Scatter plots of the response power level versus frequency showed trends similar to those found for the flutter configuration, except near the LCO frequency. At conditions where strong LCO exists (i.e. 0.90 M), much of the modal response excitation was due more to the self-excited LCO

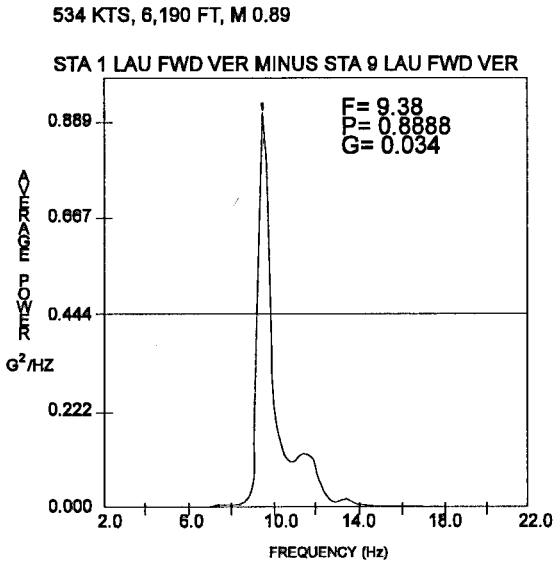

Figure 7. Configuration 4 FES PSD

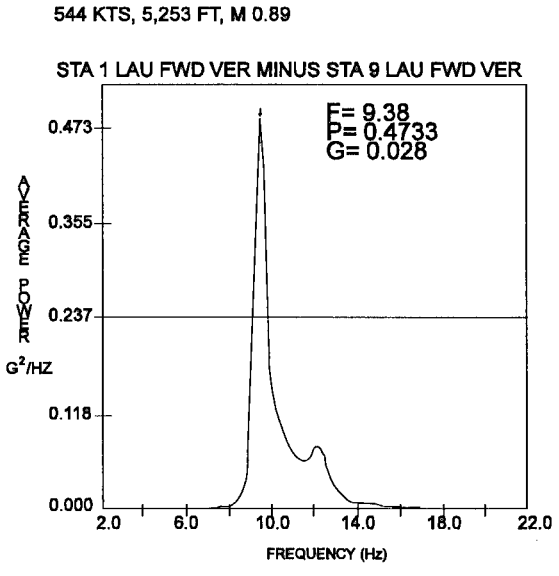

Figure 8. Configuration 4 DEI PSD

aircraft response than the DEI excitation. This can be seen by examining Figure 8, which shows the PSD response level and frequency clarity at 0.90 M. The 9.4 Hz LCO response dominates the spectral data, while the overall power level of the PSD remains relatively low.

A significant side effect of the testing was noted for Configuration 4; it is discussed further in section 4.3. The DEI exciter dampens the LCO response for some conditions when phased opposite to the LCO response.

4.2.4 *FES and DEI Comparison*

The DEI system excitation level is approximately 0.1 to 0.5 times lower than that provided by the FES (except near strong LCO conditions). As a consequence, modes are less distinguished in the PSDs. Frequency and damping level scatter – while more pronounced for the DEI system – were evident for both systems. Both systems were able to identify fundamental modes; degraded DEI gain levels and phasing resulted in a lower modal definition than that provided by the FES.

The DEI phase nonlinearity found for this configuration is due to a high loading flight environment that causes frictional binding, which results in a variable rotation frequency for the slotted cylinder. Variable cylinder loading is due to: 1) a steady-state pre-load, caused primarily by a high q loading, and 2) a combination of a turbulent underwing flow field and the dynamics of the cantilevered vane. Apparently the existing drive controller and/or drive motors are not able to respond rapidly enough to counter the combined steady-state and nonlinear dynamic airloads and overcome the binding forces.

4.3 Configuration 5 Results

4.3.1 *General Results*

Flight test Configuration 5 (Figure 2) exhibits a 5.1 Hz LCO response that dominates the spectral data. The minimum predicted antisymmetric flutter speed is 276 KCAS/5.4 Hz/g=0.00 and 357 KCAS/5.3 Hz/g=0.01. The critical antisymmetric flutter mechanism (please refer to Table 1) is primarily a coupling of mode 1 (5.1 Hz - outer-wing torsion) and mode 2 (5.5 Hz - wing-bending/tip missile pitch). A secondary antisymmetric flutter mechanism is predicted at 887 KCAS/10.7 Hz/g=0.00. This mechanism primarily involves mode 8 (9.8 Hz outer-wing bending/empennage rotation) coupling with mode 9 (10.9 Hz outboard store pitch/empennage rotation.

4.3.2 *FES Results*

The closely spaced modes and the dominance of the 5.1 Hz LCO response allow only the most lowly damped modes to be shown with sufficient clarity within the PSDs. The FES identifies the critical flutter mechanism as a coupling of mode 1 (5.1 Hz - outer wing torsion) and mode 2 (5.9 Hz - tip missile pitch/wing bending).

The secondary mechanism involves a coupling of mode 8 (10 Hz - outer wing bending) and mode 9 (10.9 Hz - outboard store pitch). The identification of critical modes involved in the first two flutter mechanisms – plus the additional modal frequencies identified – demonstrate that marginal excitation levels are provided by the FES. The dominance of the LCO response could be minimized by increasing the FES sweep amplitude and duration. However, a practical level of additional excitation force (within the limits of the FES) may

not be sufficient to separate the closely spaced modes near the 5.1 Hz LCO. Acceptable correlation was obtained from the flight test FES excitation system when compared to the analytical results, although FES excitation levels are marginal during strong LCO conditions.

4.3.3 *DEI Exciter Results*

The DEI excitation level was again consistently lower than the FES. The DEI transfer functions (Figures 9 and 10) show 1) a slight magnitude roll-off and phase drift for low q (Figure 9), and 2) erratic exciter behavior for both phase and gain at higher q (Figure 10). Figure 10 shows the stepped phasing that occurs when the exciters begin to bind, due to higher q loads causing friction in the drive mechanism and concentric cylinders. The binding continues to worsen with increasing q, resulting in erratic phasing and force levels. This erratic phase and force level input is responsible for the additional frequency and damping data scatter.

The 5.1 Hz LCO response dominates the spectral data. With the modes so closely spaced and the erratic DEI excitation, more scatter than is present within the data would be expected. However, the PSD response at flight conditions where LCO exists gives the appearance of a stronger DEI excitation than is actually present. The higher level response is due to the self-excited LCO response, rather than DEI excitation. A PSD comparison of Figures 11 and 12 illustrates that (during strong LCO) random turbulence excitation actually provides responses similar to the DEI system.

Although the DEI excitation energy level is quite low, the critical modal frequencies – as predicted by analysis – can be identified. The modes associated with the critical flutter mechanism (mode 1 / mode 2) are defined by DEI as 5.1 Hz and 5.9 Hz. The modes associated with the secondary mechanism cannot be clearly identified at the lower q test points. The highest q test points show these modes to be at 10 Hz and 10.7 Hz.

While the critical modes involved in the first flutter mechanism modes were identified (primarily due to the additional energy provided during LCO), the lack of clear definition of the second mechanism, the low number of additional modes identified, and the poor phase and gain relationship to increasing q indicate that the DEI excitation is marginal.

A significant side effect of the testing was noted. The DEI exciter dampens the LCO response for some conditions (see Figure 14). This occurs when 1) the sweep or burst frequency is close to the LCO response frequency, and 2) when the excitation phasing drifts either symmetrically or nearly 180 degrees opposite of the LCO response. While this is a natural result of applying opposite-phased excitation, the ability of the DEI exciter to dampen the LCO response with such a low excitation level and a nonlinear phase drift is of significant interest.

4.3.4 *FES and DEI Comparison*

The DEI system excitation level remains 0.1 to 0.5 times lower than that provided by the FES. As with Configuration 4, the DEI phase nonlinearity is due to a high q, high dynamic-load flight environment that induces binding in the drive linkage and concentric cylinders. This binding effect is best illustrated by a comparison of DEI transfer functions presented in Figures 9 and 10.

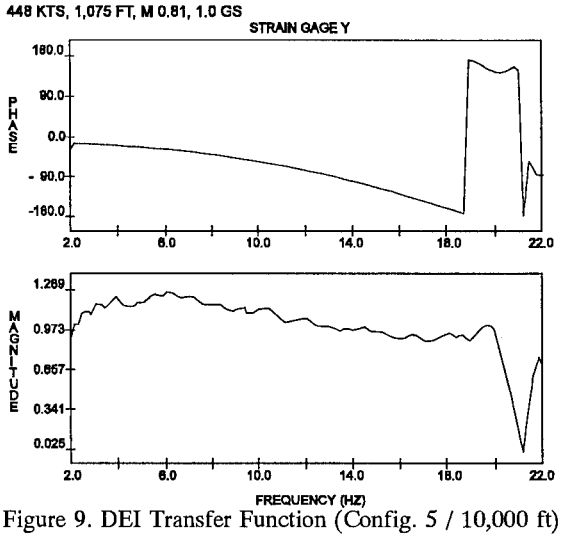

Figure 9. DEI Transfer Function (Config. 5 / 10,000 ft)

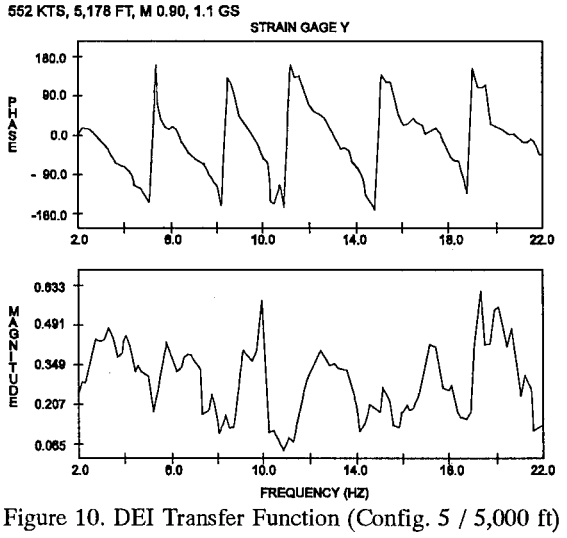

Figure 10. DEI Transfer Function (Config. 5 / 5,000 ft)

The 5.1 Hz LCO affected the response clarity for both the FES and, to a greater degree, the DEI system. The aircraft

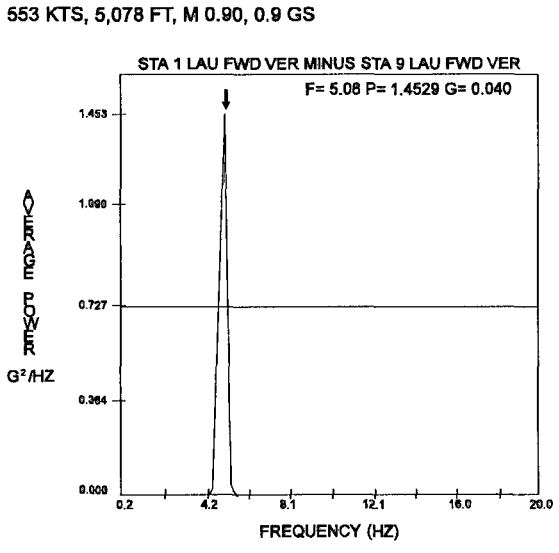

Figure 11. Configuration 5 Turbulence PSD

self-excited LCO response gives the appearance that the DEI exciters are imparting more energy into the structure that they actually are. This is explicitly shown by the PSD response comparison of random turbulence excitation (Figure 11) to both the DEI (Figure 12) and FES (Figure 13) system responses. The FES excitation provides approximately 25 to 30 percent higher response power levels than either DEI or random turbulence excitation. Overall, due to the closely space modes and dominance of the LCO, both the FES and DEI systems provided marginal excitation energy.

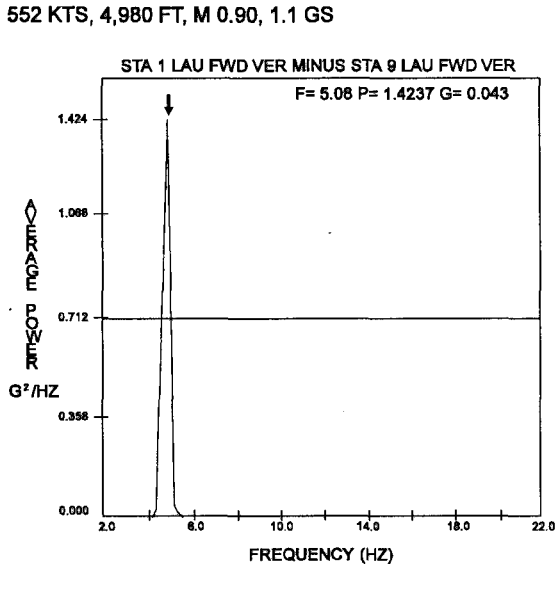

Figure 12. Configuration 5 DEI PSD

5. CONCLUSIONS

The DEI Flutter Exciter system concept is valid, but the present design is inadequate for high subsonic/transonic flutter testing. The existing DEI system provided marginal excitation force levels and phasing. A modified system that delivers increased excitation force levels and accurate phasing seems feasible.

Test results show that the FES provides a higher level of excitation into the aircraft structure than does the DEI system. The FES PSDs show more clearly defined modes in general, but the DEI system is able to generate higher response levels for frequencies greater than 16 Hz. Where LCO dominates the response of the aircraft, the FES produces response levels between 30 to 100 percent higher than either DEI or random turbulence excitation.

The DEI system – as presently manufactured – is not an acceptable flutter flight test excitation system for high q test conditions. Results indicate that a *modified* DEI system could be a low-cost alternative to existing flight control-integrated excitation systems. The DEI system generates degraded excitation energy levels and a non-linear phase drift. Until these issues are resolved, the present DEI design would only be applicable to low subsonic dynamic pressure testing regimes.

The DEI exciter force level is adjustable from the maximum to one-quarter of maximum by installing cylindrical plugs that block the slotted opening. Removing the concentric plug will not provide the required additional force input (DEI excitation

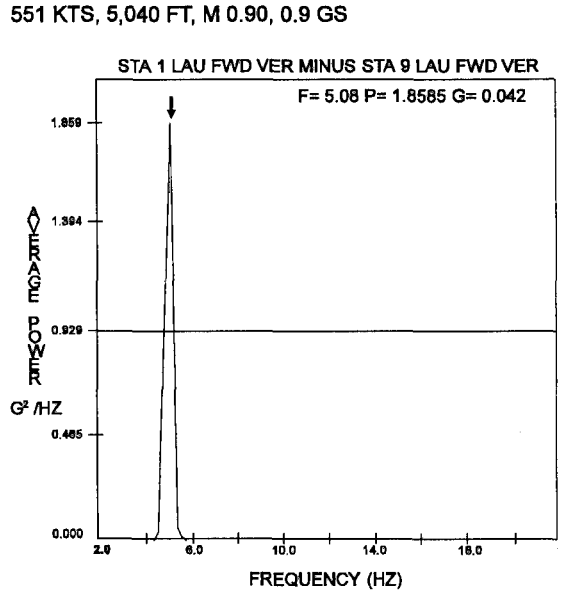

Figure 13. Configuration 5 FES PSD

response was from 0.5 to 0.1 times lower than that provided by the FES). Increased vane size and/or cylinder slot width would increase the available forcing energy, but either plug removal or increased size would increase the load on the rotational actuator and worsen the phasing characteristics.

Moving the DEI exciters to more outboard positions on the aircraft would result in increased response levels without worsening the already erratic phase behavior. However, DEI exciter attachment locations were evaluated at length prior to this testing. The inboard location was chosen with the understanding that this was less than optimum for ultimate exciter performance.

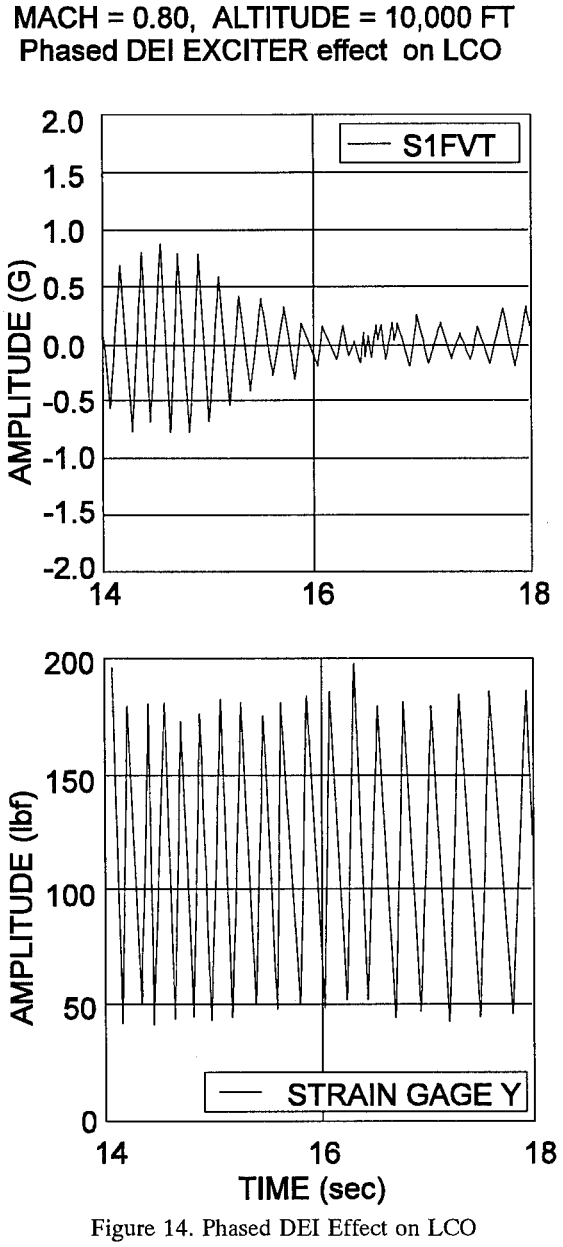

Figure 14. Phased DEI Effect on LCO

The existing DEI non-linear phase shift is likely due to: 1) cylinder binding under load, and 2) the rotational actuators' inability to overcome these binding forces. Overcoming the frictional binding seems feasible, but could involve modifications to hardware such as the motor, controller cards, gearbox/drive assembly linkage and rotating cylinder.

Any modification to the DEI exciter requires considering the effect (on the baseline aircraft) of increasing the mass properties and aerodynamic interference. Flutter clearance efforts that use the DEI exciter should include aeroelastic analysis of the system installed on the aircraft. Installation location needs to be determined on a case-by-case basis, considering the impact of modeshapes, nodelines and aerodynamics (such as shock or vortex flow effects on LCO), mass properties, structural modification requirements, etc.

The use of a suitably modified DEI system must be carefully considered. The DEI system might not be as practical for envelope clearance during pre-production envelope expansion as it would be for follow-on stores clearance testing. Envelope expansion requires excitation using multiple surfaces to add sufficient energy to the structure. This includes flaperon, aileron, horizontal tail and rudder excitation. Excitation by these surfaces is required 1) for flutter critical clearance of the basic aircraft and surfaces, and 2) to determine empennage interaction. Attaching DEI vanes to either vertical or horizontal lifting surfaces would involve significant flutter, loads and stability analyses and testing (due to changes in mass properties, stiffness and aerodynamics required for installation). A flight control system-integrated flutter excitation system is recommended during pre-production envelope expansion.

Of significant interest, the DEI excitation system showed some ability to dampen the LCO response of the aircraft during testing. While this was not the intent of testing, the dampening effect was demonstrated when 1) the sweep or burst frequency was close to the antisymmetric LCO response frequency, and 2) when the excitation phasing drifts either symmetrically or nearly 180 degrees opposite of the LCO response. This dampening effect is a natural response to applying opposite phased excitation during LCO. Of tremendous significance is that the LCO dampening effect was accomplished by the DEI exciters with marginal force level input and erratic phase behavior. The results of the DEI testing – when the phase inadvertently drifted from antisymmetric excitation – demonstrated that *controlling LCO is possible on the F-16* by means other than flight control system modifications.

6. ACKNOWLEDGEMENTS

The authors wish to express their sincere appreciation to Mr. D.M. Latta, Ms. M.A. Marshall and Mr. W. Yuen for their support of the DEI exciter flight test progarm. Post-flight data reduction, analyses and final data formatting contributions made by Mr. S.D. Courtney and Mr. K.S. Dawson are also gratefully appreciated. The significant efforts made by Ms. M.V. Braun through her editing skills and by Mr. D.W. Thompson applying his computerized graphics abilities resulted in this paper being published.

7. REFERENCES

Conference Proceedings

1. "In-flight Investigation of a Rotating Cylinder-Based Structural Excitation System for Flutter Testing," AIAA 34th Structures, Structural Dynamics and Materials Conference, Preprint No. AIAA-93-1537, April 1993, Vernon, Lura E.

STATUS ON STRATO 2C FLIGHT FLUTTER TESTING ACTIVITIES

F. Kießling, M. Rippl, H. Hönlinger
DLR, Institute of Aeroelasticity
Bunsenstr. 10
D-37073 Göttingen, Germany

SUMMARY

The STRATO 2C aircraft is currently being developed for manned stratospheric research missions up to 80,000 ft. It is powered by two 330 kW turbocharged piston engines. The requirements for flight endurance, altitude, payload, and operating range can only be met if high aerodynamic quality, high propulsion effiency, and low empty weight are achieved simultaneously. The large wing span (56.5 m) and aspect ratio (21.3) result from aerodynamic optimization. Carbon fibre composites are applied to reduce weight and deflections. Possible aeroelastic problems are dealt with during aircraft development. This paper gives an overview on these activitities.

When considering its flutter proneness, STRATO 2C may be compared with modern high-performance sailplanes. However, this analogy fails when taking into account its size, operating altitude, and large wing mounted nacelles with pusher propellers.

In the early stages, a modal survey test on the stabilizer spar box similar to that of the wing was performed to check finite-element modelling assumptions.The idealization of the complete aircraft leads to a verified model which is used for aeroelastic predictions for various configurations without excessive test efforts. A ground vibration test on the proof-of-concept aircraft serves as the main experimental data base. The flutter analysis includes the design of control surface mass balance and attachment flexibility.

The five-bladed wood/composite propellers with a size of 6 m in diameter are constrained to minimum weight. Two types of aeroelastic vibrations were observed in the first windtunnel test and were identified as blade flutter and forced response at yawed flow conditions, respectively. An improved design was checked by analytical comparison based on modal test data. Whirl flutter is possible with large elastically mounted propellers operating at high advance ratios. This subject is briefly adressed in this paper.

BACKGROUND

STRATO 2C is a manned vehicle for high-altitude and long-endurance in-situ and remote sensing measurement campaigns (Ref. 1):

- the dynamics and chemistry of the atmosphere
- clouds and their influence on climate processes
- exchange processes between biosphere and atmosphere
- pollution by air traffic and its influence on trace gases and the radiation field
- observation of land/ocean/polar icecaps from a high altitude
- test and calibration of Earth observation sensors and facilities to be flown on satellites.

The STRATO 2C crew consists of two pilots and two experimenters. Mission goals are defined as follows:

- high altitude mission, 8 hours at an altitude of 24 km with a payload of 800 kg, and a range of 7000 km
- long-duration mission, 48 hours at an altitude of 18 km with a payload of 1000 kg, and a range of 18000 km.

The aircraft manufacturer Burkhart Grob Luft- und Raumfahrt, experienced in the development of the high-altitude aircraft EGRETT, is the main contractor for the STRATO 2C. IABG is responsible for the power plant system. DLR is involved in project management and technical development support and is designated as the operator of the completed aircraft.

The development of STRATO 2C involves two steps: a proof-of-concept aircraft (POC) and a mission aircraft (MAC). The costs of the POC amount to 72.0 million DM, financed by German government, and 21.4 million DM, financed by GROB.

Some major milestones of the project are highlighted in Table 1. The POC on its first flight dated March 31, 1995 from 8:52 to 9:53 GMT can be seen on Figure 1. Important technical data of the STRATO 2C are given in Table 2.

Paper presented at the Structures and Materials Panel Specialists' Meeting on "Advanced Aeroservoelastic Testing and Data Analysis", held in Rotterdam, The Netherlands, from 8-10 May 1995, and published in CP-566.

Table 1. STRATO 2C Time Table

contract signatures	April/May 1992
molds finished	Oktober 1993
engine test 23 km altitude	June 1994
POC airframe completed	September 1994
propeller ground test	October 1994
limit load tests	Oktober 1994
POC ground vibration test	Dezember 1994
first flight	March 1995

Table 2. STRATO 2C Technical Data

Dimensions		
span	56.5	m
wing area	150	m^2
aspect ratio	21.3	
length	24	m
height	7.8	m
Masses		
empty mass	7,500	kg
maximum take-off mass	13,500	kg

The compound propulsion system incorporates two liquid-cooled 300 kW piston engines (POC) and a 3-stage turbocharger (pressure ratio 1:39). The engine rotational speed is reduced by a gearbox to drive a 5-bladed pusher propeller with 6 m in diameter.

The construction of the aircraft is based on a full carbon fibre design including the pressure cabin and the wing structure with a box spar.

STRATO 2C is operated with a preliminary airworthiness certification based on FAR 23 with special conditions. The design maximum air speeds are V_D = 151 knots (EAS) and M_D = 0.55 above an altitude of 41,440 ft, respectively. The stalling speed is predicted to be 57 knots (maximum take-off weight).

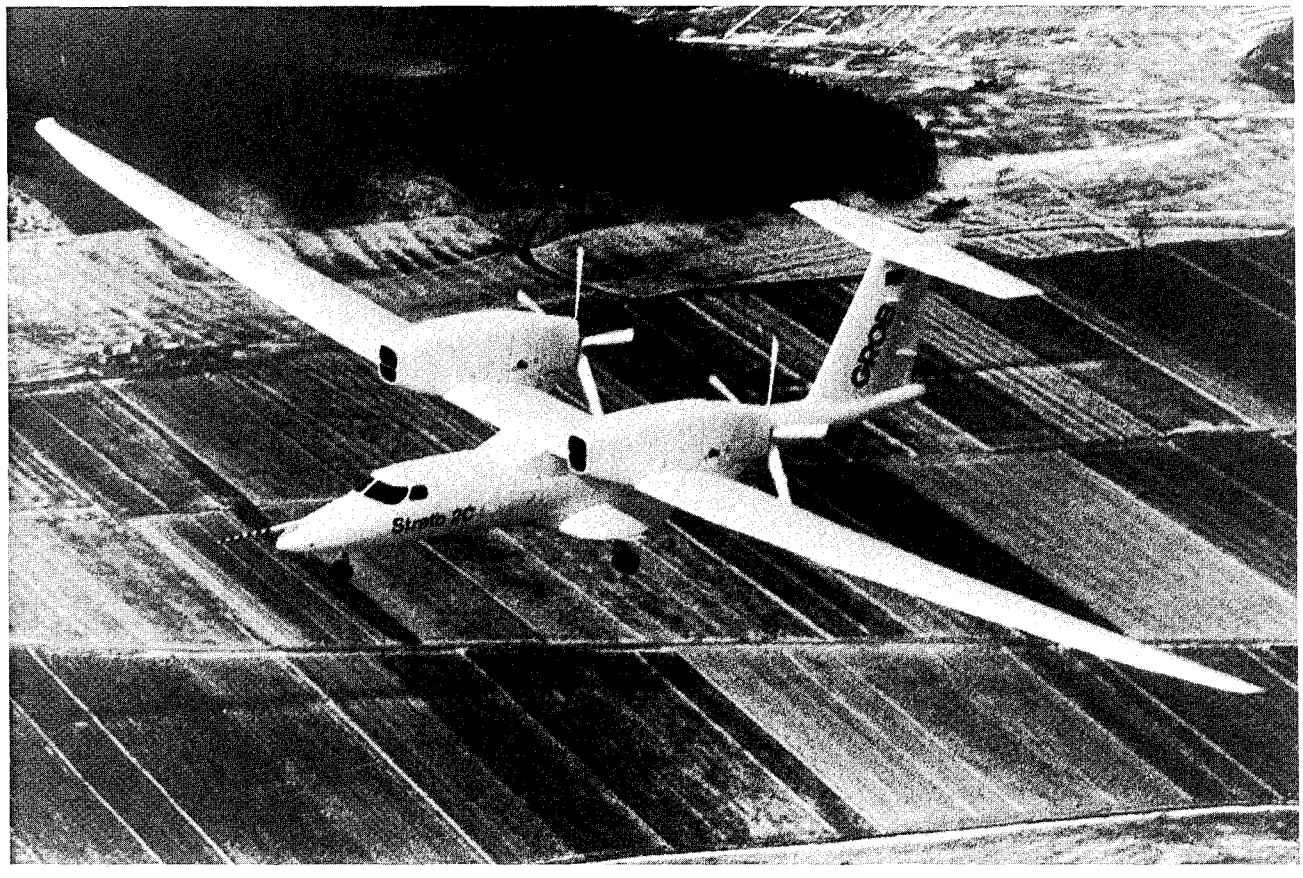

Figure 1. STRATO 2C POC Maiden Flight

AEROELASTIC PROBLEM AREAS

The air speed range (EAS) as well as wing and T-tail design of the STRATO 2C are similar to those of modern high-performance gliders. Thus, it may be argued that flutter can be treated simply by applying acquired experience in this field. This approach is obviously limited, considering the pusher configuration with large power plants. External payloads on the MAC wing are requested by the scientific users of the aircraft.

All control surfaces are operated manually by cable systems. Servo tabs are used to alleviate the pilot's actuating forces.

The propeller features flexible light-weight blades with a large diameter. At high advance ratio is achieved at high altitudes.

For general flutter prevention of the airframe it is recommended to design

- a torsional stiff wing,
- light control surfaces, especially tabs,
- a stiff control system,
- a partial mass balance of the primary control surfaces,
- a stiff servo tab linkage with minimum backlash.

The propeller design should provide

- torsional stiff and mass-balanced blades
- sufficient mount stiffness.

As far as the performance of dynamic aeroelastic analyses are concerned, the manufacturer has limited capabilities. Thus, the DLR Institute of Aeroelasticity was asked to provide support in the design, to conduct ground vibration test and flutter investigation, and to assist in flight flutter tests.

For computational aeroelastic analyses, data had to be provided by GROB's design office and stress department. The modeling efforts for the complete aircraft are still continuing, combining beam data for the wing and horizontal tail and a large finite element model for the fuselage and vertical tail. Mass data has to be updated to describe the actual configurations. The usefulness of a valid mathematical model will become evident when modifications towards the mission aircraft must be treated.

The data of the last modification of the wing box spar with increased stiffness and mass was not available prior to the GVT. Detailed math modeling was postponed after test evaluation.

The main data sources for current aeroelastic analyses are various vibration tests, especially the POC ground vibration test.

AEROELASTIC INVESTIGATIONS FOR DESIGN SUPPORT

Based on available data, a vibration analysis of a wing beam model was performed. It results in the lowest eigenfrequency of less than 2 Hz. A bending/torsion flutter analysis based on calculated normal modes showed flutter boundaries at air speeds higher than 1.2 V_D. The conclusion that bending/torsion is not likely to present a real problem was confirmed later by the results based on ground vibration test.

Because of the uncertainties, especially in the elastic material properties used in the structural design, the analysis approach was validated by testing a representative structure.

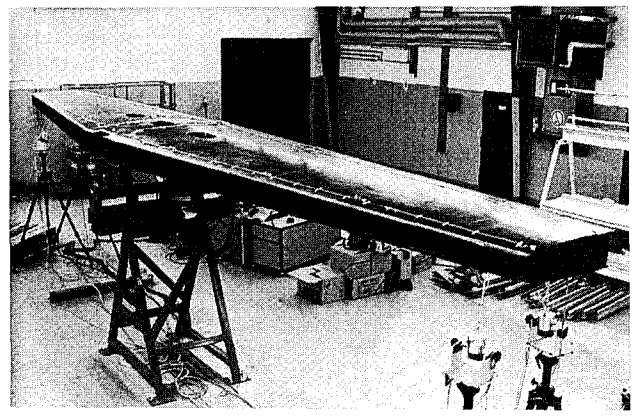

Figure 2. Vibration Test of Stabilizer Box Spar

The structural design features of wing and horizontal tail are quite similar. A test specimen of the stabilizer box spar was constructed at an early stage of development for the performance of a static load test. Before this test, a vibration test was performed to check and improve the modeling of the corresponding finite element model with simple beams. The test setup is shown in Figure 2. The structure was supported by a rotational hinge in the symmetry plane. The test and analysis frequencies obtained are presented in Table 3.

Table 3. Results of Stabilizer Box Spar Test

Mode	Test Hz	Analysis Hz
1. sym. bending	19.9	20.2
1. anti. bending	50.5	57.7
2. sym. bending	68.0	84.8
2. anti. bending	114.3	164.5
1. sym. torsion	85.5	114.2
1. anti. torsion	90.9	114.2
1. sym. inplane bending	63.8	63.8
1. anti. inplane bending	125.9	183.7

Whirl flutter investigations were performed using the 6x6 flexibility matrix of the hub of a rigid propeller and with regard to the isolated nacelle fixed at the wing interface points.

PROPELLER FLUTTER

The STRATO 2C propeller developed by the manufacturer mt-Propeller operates at a maximum rotational speed of 636 rpm. The structural design is based on composite material using highly-compressed multilayer beechwood at the root and a fiber-reinforced skin.

Full-scale propeller tests were conducted in the T-101 windtunnel (TSAGI, Russia) with a 24 m times 14 m elliptic test section. In the first test, high-frequency blade flutter near maximum rotational speed was encountered, causing a failure in the pitch control mechanism. High dynamic blade bending response in crosswind flow conditions were also observed.

An improved blade with a mass reduction in the rear blade part and with an increase of torsional stiffness by larger root section areas was designed and constructed.

A vibration test of the different propeller blade versions was performed. The blades were fixed on a seismic table and equipped with 21 accelerometers to measure flap and lag bending and torsion at 7 radial stations. The test setup is shown in Figure 3.

The test results were used for comparative flutter analyses of the different propeller blades which in shown in Figure 4. It was concluded that the observed flutter is a classical type and the new blade design (right hand side of the figure) offers a 44 percent increase in flutter speed.

POC GROUND VIBRATION TEST

The DLR Mobile Ground Vibration Test Facility was used for the STRATO 2C POC test. The test method followed the lines of the classical phase resonance procedure supported by a computer for on-line calculation and display. A total of 315 accelerometers was used to obtain the normal modes in the frequency range up to at least 20 Hz. An air spring supension system was used to simulate as closely as possible the free-flying condition. The largest suspension frequency was 0.86 Hz (plunge). The ground vibration test arrangement is shown in Figure 5.

Considering the test condition of the control system, the prefered procedure was to not apply constraints, e.g. to obtain all the modes with control surface deflections. The effect of additional mass on the control wheel was investigated. For the control system modes, extensive tests with varying amplitude levels were performed to portray the nonlinear behaviour.

The different weight conditions of the aircraft are covered by testing the configurations with

- minimum take-off weight (without fuel)
- maximum take-off weight (with fuel).

Unfortunately, not all components of the aircraft were actually available and installed at the scheduled time of the POC ground vibration test. Thus, some missing parts had to be simulated or replaced by dummies featuring proper mass and stiffness. The most significant parts were the complete nacelles which were substituted by dummy structures. The propellers were attached to the gear box mass which, in turn, was supported by the designated shock mounts. Each propeller blade was equipped with two accelerometers at the tip to obtain in-plane and out-of-plane deflections. The typical propeller pitch and yaw modes were checked later with the actual nacelle in a briefer test.

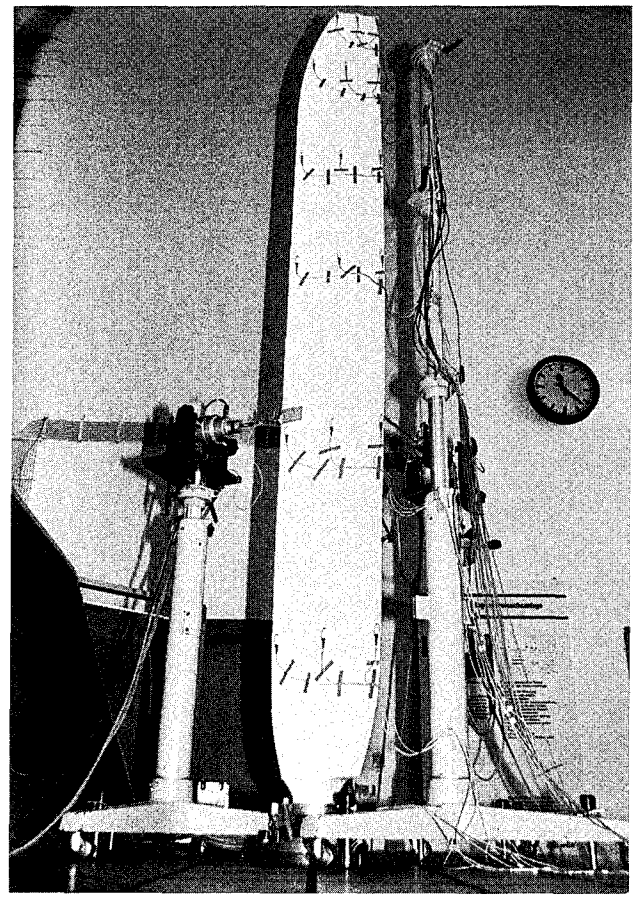

Figure 3. Vibration Test of Propeller Blade

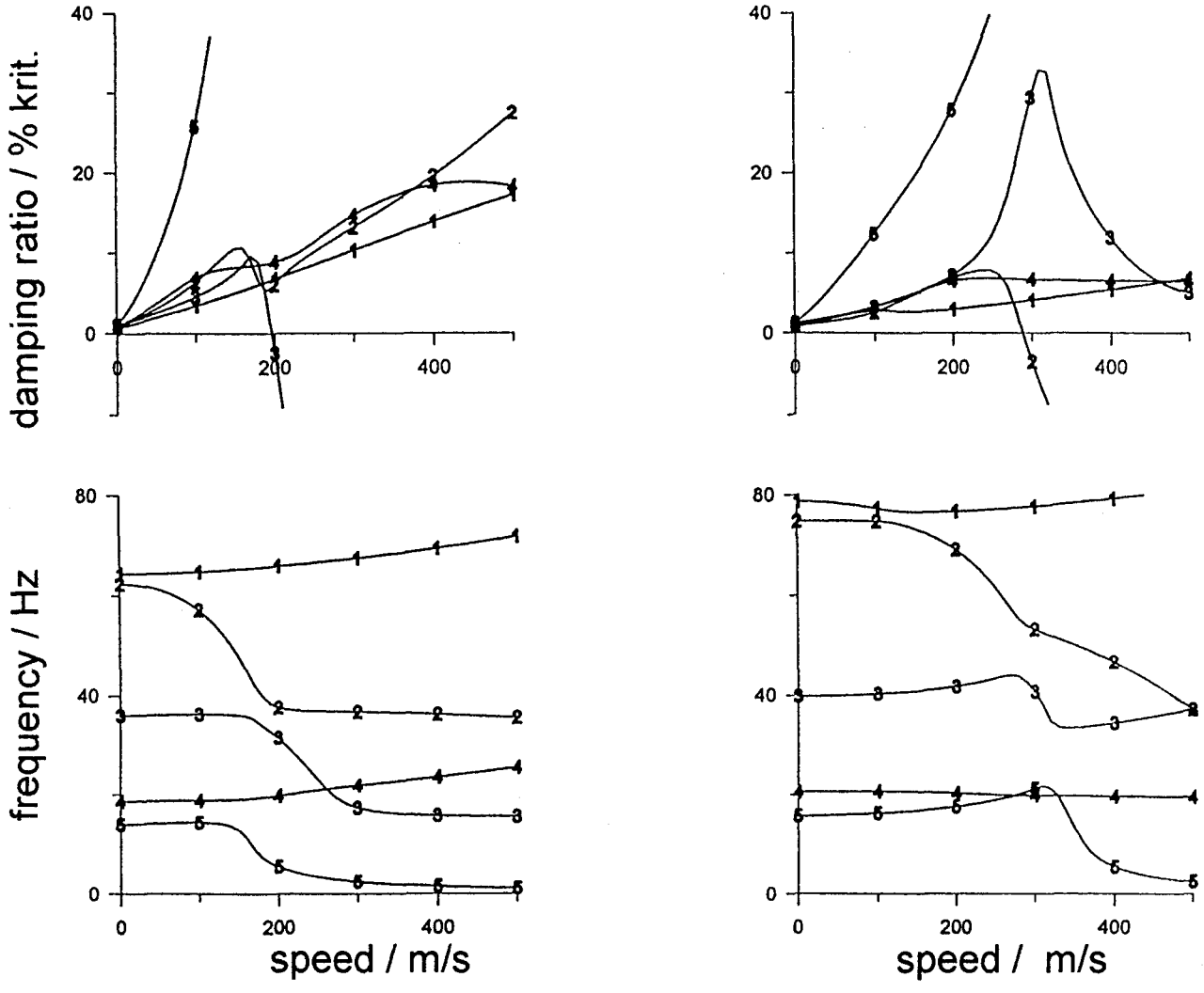

Figure 4. Comparative Flutter Analysis of Different Propeller Blades

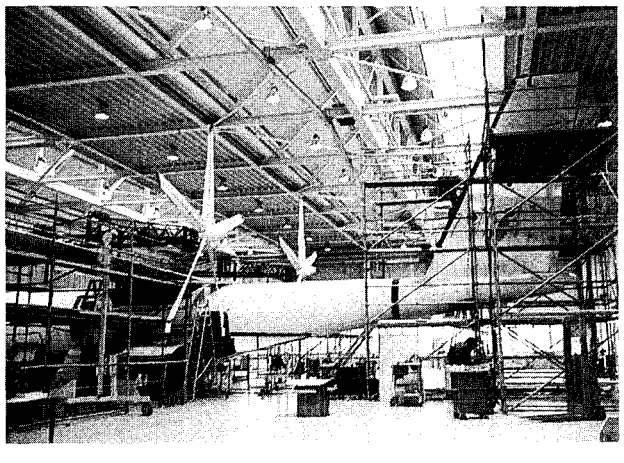

Figure 5. Ground Vibration Test

Out of 177 measurements including different excitation levels, 101 modes were identified and recorded. A pin plot of the antisymmetric wing torsion mode at 15.3 Hz is shown in Figure 6. This kind of picture is displayed on-line during the test. The deformation plot of symmetric fuselage bending at 9.3 Hz is given in Figure 7. This kind of presentation can be animated off-line to look at the details of the normal mode. 61 modes were considered relevant for the aeroelastic calculations.

FLUTTER ANALYSIS

The normal mode data from the ground vibration test were smoothed and interpolated along the span of each lifting surface. Distributions of heave, pitch, relative control surface rotation, and lead-lag were calculated and evaluated at aerodynamic span stations. The measured mode shapes were used directly without symmetrization to calculate the generalized forces. Sets of 18 and 21 modes were formed which represent the symmetrical and antisymmetrical case.

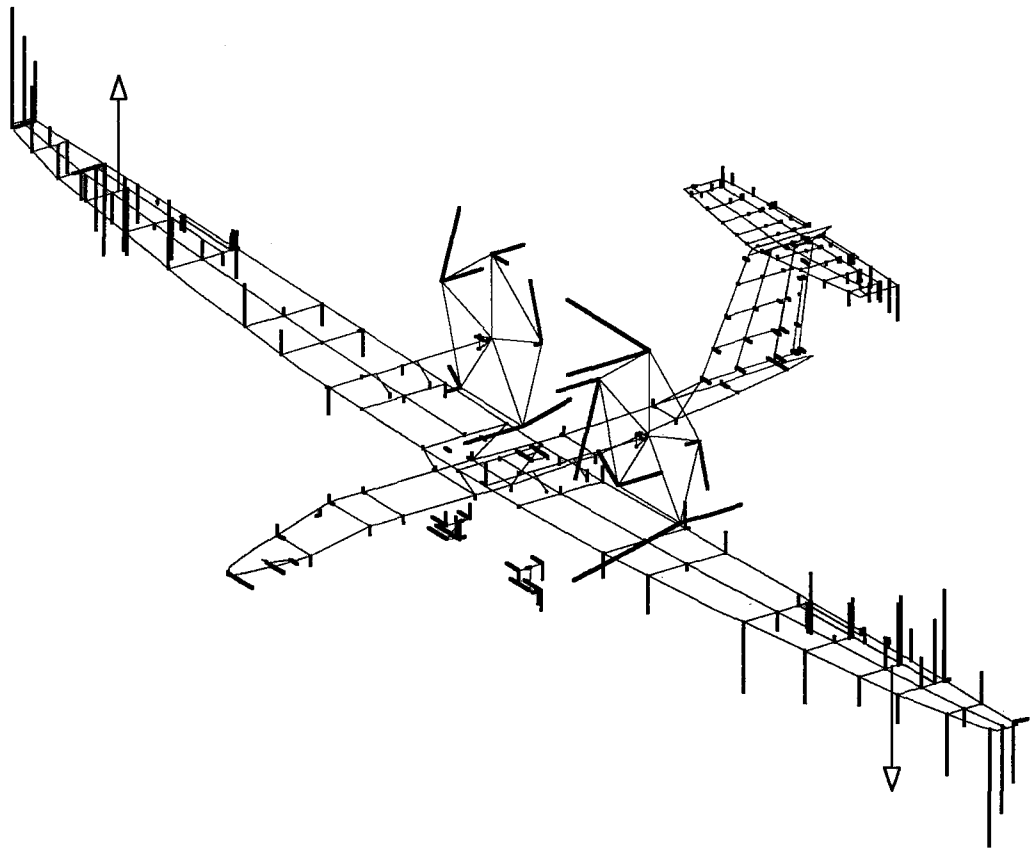

Figure 6. Pin Plot, Antisymmetric Wing Torsion AT at 15.3 Hz

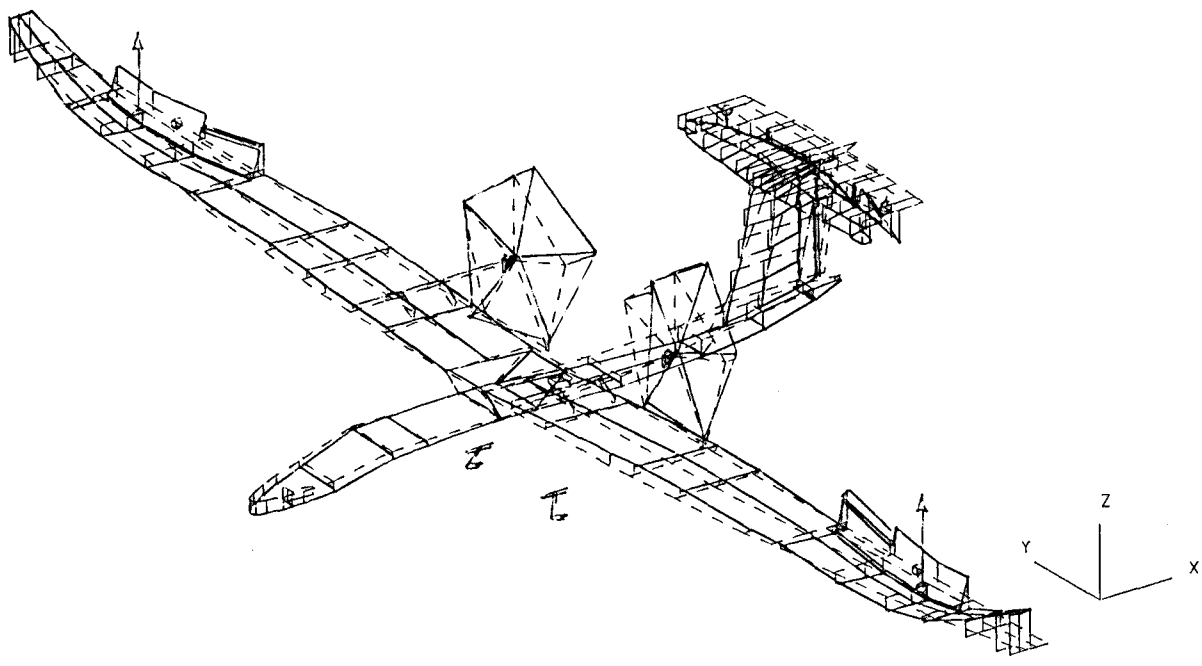

Figure 7. Deformation Plot, Symmetric Fuselage Bending SR3 at 9.3 Hz

The flutter calculation is based on a p,k-type method. The two-dimensional unsteady aerodynamic theory was applied due to the high aspect ratio. Correction factors were used to investigate hinge moment variations.

Modal correction terms can be calculated for modifications of mass balance and control system stiffness as well as for taking ballast and suspension into account. Coupling terms can be calculated using control surface data if the input modes are not orthogonal with respect to mass.

The STRATO 2C flight envelope and typical flutter boundaries are shown in Figure 8. At high altitude, a narrow range between stall and maximum speed can be recognized. The indicated flutter boundaries represent the situation found after the ground vibration test.

Aileron Flutter In the ground vibration test, the aileron control system was recognized to be too flexible. In a first step, the diameter of the cables was increased but this measure alone did not improve the flutter stability. Sufficient stiffness was attained by partially replacing the cables with carbon fibre rods.

The effect of increasing wing control system stiffness is shown in Figure 9. The critical speed is first reduced but, at the same time, the severity of the flutter mode ceases. As the frequency of the wing/fuselage mode SR3 is reached and exceeded, the flutter instability vanishes.

Rudder Flutter A typical example of this flutter coupling is shown in Figure 10. With increasing altitude (12, 14, ... 24 km), a hump is observed in the damping curves, which becomes increasingly negative in a certain air speed range. The damping minimum is nearly at constant EAS. It should be mentioned in passing that the occurence of control surface flutter regions above a certain altitude was already found with gliders.

Whirl Flutter It is well-known that large elastically mounted propellers operating at high advance ratios are prone to whirl flutter. An example using the rigid propeller assumption is shown in Figure 11. The gyroscopic effect causes coupling of pitch and yaw modes, resulting in backward and forward whirl modes. With increasing rotational speed, the frequencies are separated.With increasing air speed, the frequencies of both modes increase slightly due to the pusher arrangement.

The damping of the backward whirl mode continuously decreases. The whirl flutter boundary is observed at nearly constant true air speed. Out-of-plane bending flexibility of the blades increases damping significantly and the critical speed is shifted beyond V_D/M_D.

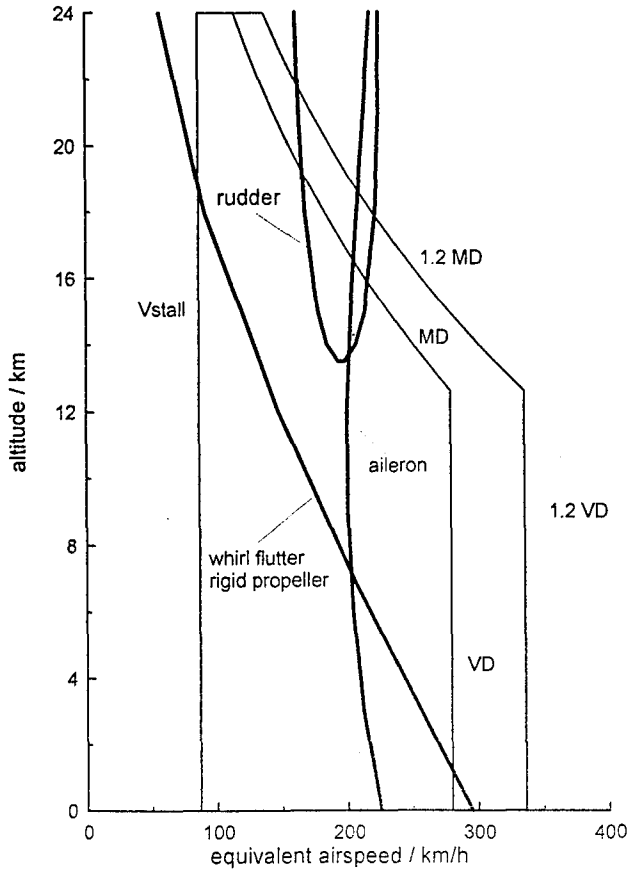

Figure 8. Flight Envelope and Typical Flutter Boundaries

FLIGHT FLUTTER TESTS

STRATO 2C flutter tests are prepared to measure the dynamic responses to manual and artificial excitation.

A total of 24 accelerometers (calibrated for environments at high altitude) are provided. Five transducers are used for control surface rotations. Three accelerometers located near the aircraft C.G. can be used, too. Gearbox motions relative to the nacelle frames are measured by four displacement transducers. These signals indicate propeller whirl. Blade and propeller shaft strain gauge signals can also be obtained from rotating systems. The amplified signals are filtered by a 100 Hz low-pass filter and are digitized at a sample rate of 200 Hz per channel.

During flight tests, PCM data are recorded on tape and are telemetered to the ground station for monitoring. A total of 18 channel analog outputs is available for quick look and on-line processing.

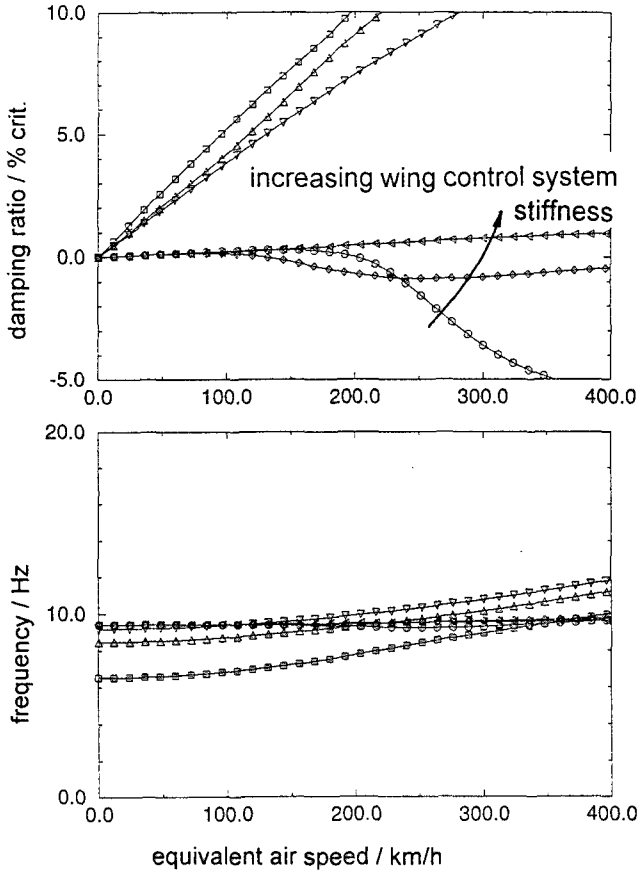

Figure 9. Aileron Flutter

Excitation is performed manually (may work in a frequency range < 5 Hz) and artificially for the high-frequency range. A hydraulically-driven inertia device with a control unit was kindly provided by DASA Dornier for this purpose. The exciters are installed at both wing tips and can be operated in-phase and out-of-phase. The in-plane force component also permits the excitation of tail modes.

CONCLUSIONS AND OUTLOOK

Five flight tests have been performed up to now (< 90 knots IAS, <22000 ft) with emphasis on handling qualities, airspeed calibration, and propeller vibrations. Aileron rap and cyclic input were tried out. The POC test plan continues for the demonstration of high-altitude performance.The ability for a fast and safe emergency descent is a main consideration for expanding the cleared envelope.

Aeroelastic work continues on flight test support and on the establishment of a complete analytical aeroelastic aircraft model validated by test data. An elastic propeller model based on test data is being developed.

The MAC development will include flight control and stabiliy augmentation systems. Improvements by means of mass/stiffness reductions while observing acroelastic constraints are planned.

REFERENCES

1. Schumann U. et al.: Wissenschaftlich-technisches Konzept für die Nutzung des Höhenforschungsflugzeugs STRATO 2C. Bericht des wissenschaftlichen Beirats für STRATO 2C, Februar 1993.

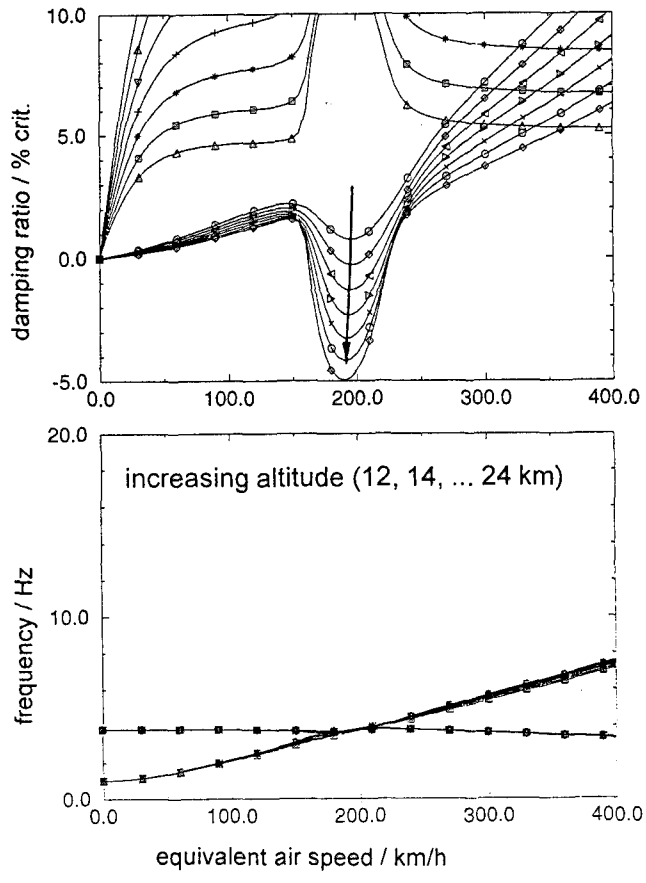

Figure 10. Rudder Flutter

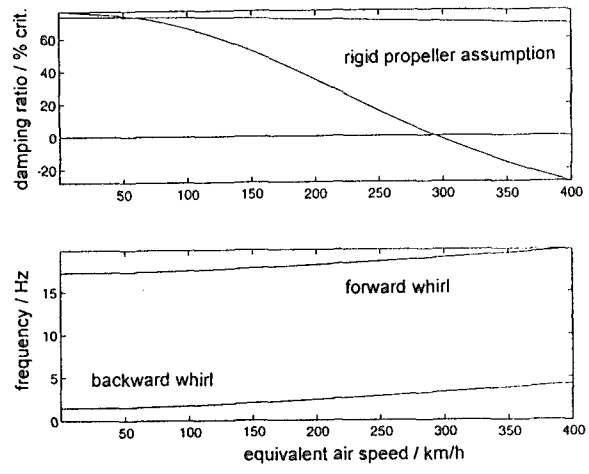

Figure 11. Whirl Flutter

AEROELASTIC TESTING OF AN UNMANNED AIR VEHICLE

B.H.K. Lee, M.J. Plosenski
Institute for Aerospace Research
National Research Council
Ottawa, Ontario, Canada K1A 0R6

P.E. Barrington
Department of Mechanical and Aerospace Engineering
Carleton University
Ottawa, Ontario, Canada K1S 5B6

A.B. Markov[1], C.G. Coffey
Defence Research Establishment Suffield
Medicine Hat, Alberta, Canada T1A 8K6

SUMMARY

A full scale unmanned air vehicle (HATT-X) was tested in an Open Jet Wind Tunnel Facility. Strain gauges were installed on the canard shafts to measure the unsteady aerodynamic loads. The data was recorded on a high speed data acquisition system for off-line analysis. High speed photography was also used to study the canard motion. A destructive 57 Hz canard flutter was observed at a Mach number of approximately 0.75 and dynamic pressure of 5.95 psi for a canard incidence angle of approximately 4°. A mass balanced and stiffer canard was manufactured and installed on the HATT-X. A flight test on the modified HATT-X was conducted. Approximately 2 seconds after initiation of the stage 7 motor burn, large vertical oscillations of the port side canard were detected, followed by the structural failure of the canard linkage system in the forward fuselage. At the failure point the vehicle was decelerating after the rocket motor burn and the Mach number was approximately 0.75. Failure of the canard system was investigated and where possible comparisons were made of the aeroelastic behaviour in the wind tunnel and flight tests of the two canards that are structurally different

1. INTRODUCTION

The HATT-X (High-Speed Aeronautical Technologies Test Bed - Experimental) was developed by the Canadian Department of National Defence as an agile, high subsonic speed platform configured for conducting a variety of research missions. HATT-X is an extensively instrumented flight vehicle with associated ground support sub-systems. The airframe and its sub-systems are based on a rocket-boosted aerial target named ROBOT-X.

During a number of proof of concept and engineering development flight tests, canard failures were encountered. This problem has limited the reliable sea level performance envelope of the vehicle to speeds below Mach number of 0.7, and the maximum manoeuvre g's to below 5. The cause of the canard flutter could not be readily identified from the telemetry data.

A test program was initiated to investigate the cause of the canard system aeroelastic failure. A full scale HATT-X was tested in the Defence Research Establishment Valcartier Open Jet Wind Tunnel Facility. The choice of this facility was largely based on the consideration that damage to the wind tunnel due to test model failure was not likely to occur. Only strain gauges were installed on the canard shafts to measure the aerodynamic loads. The data was recorded on a high speed data

[1]Now with Amtech Aeronautical Limited, Medicine Hat, Alberta, Canada

Paper presented at the Structures and Materials Panel Specialists' Meeting on "Advanced Aeroservoelastic Testing and Data Analysis", held in Rotterdam, The Netherlands, from 8-10 May 1995, and published in CP-566.

acquisition system for off-line analysis. High speed photography was also used to investigate the canard motion.

A destructive 57 Hz canard flutter was observed at a Mach number of approximately 0.75 and dynamic pressure of 5.95 psi for a canard incidence angle of approximately 4°. Based on the results of this series of wind tunnel tests, mass balanced and stiffer canards were manufactured and installed on the HATT-X.

Flight test of the modified HATT-X was conducted at the Defence Research Establishment Suffield Experimental Proofing Ground in Medicine Hat. The canards were instrumented with accelerometers and strain gauges to provide information on the structural and aerodynamic characteristics of the air vehicle during the test. The flight proceeded normally to stage 7 rocket motor burn, climbing to and maintaining 1400 metres above ground level. Approximately 2 seconds after initiation of the stage 7 motor burn, the forward looking video camera showed large vertical oscillations in the port side canard, followed by the structural failure of the canard linkage system. At the failure point the vehicle Mach number was approximately 0.75 and decelerating after the rocket motor burn.

This paper presents results for both the wind tunnel and flight tests. Though the canards were structurally different in the two tests, failure of the canard system was analysed and where possible some comparisons are made of the aeroelastic behaviour of the two canards.

2. DESCRIPTION OF HATT-X

The HATT-X airframe is shown in Figure 1. It is made up of a forward fuselage, propulsion module, and wings with vertical stabilizers. The forward fuselage consists of a crushable nose cone (the vehicle recovers in a nose down attitude), canards that are utilized for vehicle pitch control, a recovery bay for a two stage parachute system, and auxiliary and primary avionics bays.

The wings, complete with ailerons for roll control, are attached to the propulsion module. They have a sweepback angle of 40° and 0° dihedral. The wingspan is 2.4m and the planform area is 1.25m^2.

The propulsion system of the rocket-boosted configuration that was flight tested and reported in this paper consists of 19 standard 70mm CRV-7 rocket motors that are fired in stages. Surface launch is from a modular rail launcher shown in Figure 2.

A two-stage parachute recovery system is used to recover the vehicle throughout its flight envelope. Recovery by parachute is normally achieved through the flight control and guidance system (FCGS) at the completion of the mission profile. The recovery system also acts as a flight termination system and may be deployed by radio command or when imminent failure is sensed by a multi-processor digital autopilot. Failure mode detection is provided for additional range safety and as a means of maximizing the probability of recovering the flight vehicle after a flight failure.

A HATT-X mission may be executed autonomously based on a defined profile and loaded into the vehicle's flight control computer prior to flight. Alternatively, semi-autonomous profiles may be selected with commands sent from a ground control station. The mission profile is defined by waypoints and what is to occur at the waypoints, for example, heading change, altitude change, the execution of discrete high-g manoeuvres, and track/position navigation based on global positioning system or other sources of position data.

The ground control station communicates with the FCGS computer prior to launch and performs preflight checks of the HATT-X. In-flight monitoring is performed through multi-channel PCM telemetry that is configured for up to 250K bits of data per second. In the flying laboratory role the flight vehicle is heavily instrumented with data sources from inboard sensors and transducers. The air vehicle is designed to fly at high subsonic speed up to Mach 0.85 at altitudes from 25 metres to above 9,150 metres. It can carry up to 59 kilograms of supplementary payloads including active and/or passive radar augmentation, X-band or C-band radar transponders, and PCM telemetry. Additional background information on the HATT-X is given in References 1-3.

2.1 The Canard and Drive System

The canards of the HATT-X tested in the Open Jet

Facility (OJF) Wind Tunnel has a span of 1.1m with a leading-edge sweepback angle of 45° and a maximum thickness of 32 mm. The canard structure is made of fibreglass laminate.

The canards can be pitched about an axis located along the quarter chord line up to a maximum incidence angle of ±25°. The attachment of the drive shaft to the canard and the drive mechanism is shown in Figure 3. The system controls the position of the two forward canards, with the canards operating in unison to control vehicle pitch. The servo drive which controls the canard pitch angle is a Simmonds Precision DR2148M44-3 actuator. It is a small, high torque rotary actuator sealed against the outside environment. It includes a feedback potentiometer, a gear train, a motor with a fail-safe brake, and an integral position loop servo-controller. The controller uses pulse width modulation type circuitry for high efficiency.

In the OJF tests, normally the canards were commanded to ramp from 0° to 16° at a rate of 2°/second. In some tests, a constant amplitude swept sinusoidal input with frequency varying from 1 Hz to 6 Hz was used. The canard position normally followed the commanded position quite closely. However, there were many cases where the canard position departed from the command function.

In an attempt to eliminate the canard flutter problem in the flight test, a design modification was made. The canards in the OJF were not adequately stiff and were not mass balanced for the entire span. The elastic axis was quite far aft of the aerodynamic centre which was located on the quarter chord line. The modified canard was constructed of graphite laminate in lieu of fibreglass to stiffen the canard structure. The elastic axis was moved forward and the canard was mass balanced over the entire span.

3. GROUND TESTING IN THE OPEN JET FACILITY

3.1 Open Jet Facility

The Open Jet Facility shown in Figure 4 is located at the Defence Research Establishment Valcartier. It is a blowdown wind tunnel with a test section open to the atmosphere. It consists of a 123m long, 3.05m diameter reservoir with a volume of 900m^3 which is pressurized to a maximum of 514 kPa. A thermal matrix consisting of 8400 steel tubes is stacked near the downstream end of the reservoir to minimize the temperature drop during a test run. The flow exits through a circular nozzle producing a jet of short duration. Two nozzles of diameter 0.915m and 1.22m are available. The Mach number can vary from 0.3 to 0.9. The run time varies from 30 seconds or more at Mach 0.3 to 10 seconds at Mach 0.9 using the 0.915m diameter nozzle at the maximum tank pressure. Run time with the 1.22m jet is approximately 50% shorter. Within the potential core of the jet where the test section is located, the flow is uniform and smooth. The length of the core is approximately 4.2 jet diameters. During a run, the Mach number variation is approximately 0.01 and the maximum temperature drop is 10°C . In this investigation, the larger diameter nozzle was used.

A 1.22m diameter butterfly valve is motor driven to isolate the pressure tank from the control valve and test section for safety purposes. A second 1.22m diameter or a 0.91m diameter Butterfly control valve is hydraulically operated to control the flow through the settling chamber and exit nozzle. The movable settling chamber contains honeycomb, screens and perforated baffles to provide good flow quality at the test section.

3.2 Wind Tunnel Model

The model tested in the wind tunnel was a full scale rocket boosted HATT-X vehicle. The only modification required prior to the wind tunnel tests was to rotate the strongback 180° on the vehicle. The strongback is an aluminum mount used to hold the air vehicle to an aircraft for air launch capability. In the OJF tests, it was used to mount the vehicle to the test stand.

The instrumentation used consisted of strain gages mounted on both canard shafts to measure the lift, torque and drag; pressure transducers located at various positions on the HATT-X; vertical accelerometers located at approximately the vehicle CG; drive mechanism servo commanded and actual canard positions; and the servo voltage and current. The sampling rate was 5120 Hz for data acquisition.

For photographic measurements, four different camera systems were used. These systems were a video camera onboard the vehicle, tripod mounted camcorders, EktaPro 1000 high speed video system, and LOCAM high speed photography. An armour plated camera hut situated behind the vehicle on the port side houses the cameras for the EktaPro and LOCAM systems.

The onboard video camera was mounted on top of the ogive section of the HATT-X vehicle. During the flight, video was transmitted to the ground in real time. For the OJF tests, the video was hard-wired into the control room for monitoring and recording. Cameras for low speed filming were used to photograph the port side of the entire vehicle including the test stand. A camcorder was used to provide coverage of the starboard side of the vehicle.

Figure 5 shows a schematic of the HATT-X installation and gives the location of key vehicle components relative to the nozzle exit plane.

After a few preliminary test runs the wings were removed from the HATT-X and empty rocket casings were installed. The reason for using the casings was that they took some of the loading in the propulsion module. The stand was modified and tie rods connected the forward wing attachment lugs to the test stand. This modification stiffened the vehicle and test stand. By applying the tie rods and deflecting the HATT-X towards the ground, the moment arm from the canard to the vehicle test stand attachment point was reduced. This procedure eliminated the large deflections of the HATT-X detected during the preliminary tests.

4. FLIGHT TEST

The flight vehicle was propelled with 19 CRV-7 (C14) rocket motors. The canards used were the modified version. They were instrumented with strain gages for load measurements. Accelerometers were installed on the port side canard root and tip (Figure 1) to detect the dynamic response of the HATT-X during different stages of the rocket firing.

Fifty two channels of PCM telemetry data were collected at various sampling rates. The accelerometer data was collected at 2500 Hz, the strain gages data at 625 Hz and the rest of the data such as dynamic pressure, Mach number, canard position and so forth were collected at 78 Hz. Real time telemetry was available throughout the flight with the aid of an S-band telemetry link. A forward looking video camera was mounted on the port wing tip with a clear view of the canard. Tracking radar was provided throughout the flight together with video tracking from a number of ground bases.

The vehicle was recovered by radio command from the ground with drogue parachute deployment.

5. RESULTS AND DISCUSSION

5.1 Open Jet Facility Results

A total of 18 runs were performed in the OJF. Initial runs included shake down tests to verify the operation of the Open Jet Wind Tunnel, vehicle test stand rigidity, instrumentation and data acquisition system. The primary objective of the tests was to obtain a better understanding of the mechanisms that caused canard failure. Secondary objectives were to calibrate and determine a more suitable location for the pitot-static pressure tube presently located at the tip of the current nose cone, and to collect pressure data for flow over the nose cone at various angles of attack data in order to add correction algorithms to the autopilot software.

Two wind tunnel runs where canard failure was encountered were analysed in detail and some of the more relevant results related to aeroelastic failure are reported in this paper. In the first run the wind tunnel test time was 6.5 seconds and a fairly uniform Mach number of 0.75 was achieved for approximately four seconds of the test. The canards were commanded to move from 0° to 6° at a rate of 2°/sec as shown in Figure 6. The actual canard position did not follow the commanded signal. The deflections showed large fluctuations which were also observed in the servo current and voltage outputs. In the analysis of the data, the time series for the aerodynamic loads were segmented into smaller intervals of 1 second starting from 1.5 seconds when the run was initiated. A total of 4 time segments were obtained with the last segment ending at 5.5 seconds when the canard failed. For each time segment, the data was assumed to be statistically stationary; this is an approximation

based on the assumption that the variation of the mean value of the canard deflection is sufficiently small so that the aerodynamic forces and canard motion do not vary significantly during the 1 second time interval.

After the fourth time segment, the canard servo failed. The 5/16" bolt (P/N AN5-20A in Figure 3) on the port side connecting the servo linkage to the canard shaft failed at the thread relief. Also, three teeth were stripped on the main drive gear. It was also observed that the canards had interfered with the fuselage at the canard root. There was heavy abrasion with paint missing from the fuselage in this area. The mean canard deflection was approximately 4° and the dynamic pressure was 5.95 psi.

The wind tunnel run was repeated with the profile command identical to the previous run. The Mach number during the run was not as steady as in the previous run and the average value was slightly higher at 0.76. The canard deflection fluctuations were found to be slightly less severe. Failure occurred after 5.5 seconds from initiation of wind tunnel run when the mean canard deflection angle was approximately 5°.

The results presented in this paper are mainly for the first wind tunnel flutter test. The results from the second run are almost identical.

5.1.1 *Power Spectral Density*
Power spectral density (PSD) analyses were performed for the starboard and port side strain gages which measured the lift, torque and drag. The acceleration of the vehicle CG and other data were analysed but the results are not presented herein.

All Fast Fourier Transforms (FFT) were performed using a block size of 1024, window length of 512 and approximately 18 averages were carried out.

A representative series of port lift PSD are shown in Figure 7 for three time segments. The first time segment contains large transients and the results are not included in the figure. The mean canard deflection varied quite gradually in the second, third and fourth segments and the results presented in this paper can be taken as the average over the one second interval where data was collected. In general, the results show that a dominant peak occurs at 57 Hz. A second harmonic at 114 Hz is detected, whose magnitude is smaller by nearly three orders of magnitude. A third peak at 175 Hz is also noted, but the magnitude is very small. A number of higher frequency peaks are also observed, but their amplitudes are so small that they can be neglected. The PSD for the three time segments are quite similar indicating the small change in canard angle of attack has little effect on the spectral shape of the lift.

In Figure 8 the PSD for the port lift, torque and drag for the fourth time segment are shown and the shape of the spectral curves are similar. The second peak in the drag PSD has the same frequency as the lift and is about two orders of magnitude smaller than the fundamental. This peak is more pronounced than that for the lift and torque. The torque channel shows the same fundamental frequency of 57 Hz. The second harmonic is very weak and difficult to detect. The 175 Hz peak (third harmonic) is observed and similar to the drag, it is about two orders of magnitude smaller than the fundamental.

The PSD curves for the starboard strain gauges are similar to those for the port side signals. On the starboard side, the lift shows a stronger second harmonic. This is also true for the drag. The second peak for the torque signal is also very weak and difficult to detect, and the ratio of the fundamental to third harmonic is approximately the same as that for the port side strain gauge.

5.1.2 *Correlation Ananlysis*
Auto-correlation plots show a characteristic damped cosine curve for all the strain gauge signals. Since the first peak observed from the PSD results is the dominant one with magnitude much larger than the other peaks, the curves do not show any noticeable distortion due to the higher harmonics. The frequency measured from the period of oscillation agrees with that of the peak fundamental frequency determined from the PSD plots.

Cross-correlation shows at the 4th time segment, on the starboard canard, the lift lags the torque by approximately 75° and lags the drag by 163°; on the port canard, the lift leads the torque by 99° and leads the drag by 168°. The torque lags the drag by 88° on the starboard canard and leads the drag

by 77° on the port canard.

The lift-torque phase difference is approximately constant for the three time segments while the lift-drag and torque-drag phase differences vary slightly between the 3rd and 4th segments and larger discrepancies are observed between the 2nd and 4th segments. A sample of the cross-correlation between these three aerodynamic quantities on the port side canard is shown in Figure 9.

Cross-correlation between starboard and port canard lift, torque and drag signals shows that the lift on the starboard canard leads by 168°. The torque is approximately in phase, with the starboard side leading slightly by 4°. The drag on the starboard canard leads by 160°. A typical plot of the cross-correlation between starboard and port canard lift, torque and drag signals is shown in Figure 10 for the 4th time segment.

5.1.3 *Probability density functions*
Spectral and correlation analyses are valuable tools to show the frequency contents and the phase relations between signals. Some useful characteristics of the time series can also be obtained from the probability distribution functions (PDF).

In general, it is found that the probability density functions for the lift, torque and drag at different time segments are quite similar except for the first time segment. This is to be expected since there are large transients and fluctuations in those signals. The shape of the PDF for the three aerodynamic loads are not quite the same but they all show the presence of a dominant frequency component. The signals possess the characteristics of a sine wave contaminated with noise. Figure 11 shows the lift and drag PDF for the 4th time segment. The PDF curves are not symmetrical but are biased either for positive or negative sigma, where sigma is the rms value of the signal. It is interesting to observe that the time series for the same aerodynamic quantity have different statistical properties on the two canards.

5.1.4 *Phase plots*
The phase space reconstruction procedure of Packard et al[4] is a convenient first step in analyzing experimental data obtained from a nonlinear dynamical system. This method has been used successfully in nonlinear mechanics and appears to be an attractive tool for analyzing nonlinear flutter of aircraft structures where only single quantity time series such as accelerometer response or aerodynamic forces are available. Nonlinear flutter normally arises in the presence of a structural nonlinearity or at high amplitude vibration situations where the aerodynamic forces cease to be linear [5].

Given a time series of a single quantity, F(t), a reconstruction of the phase space can be obtained by using a time delay technique so that

$$\mathbf{X}(t) = \{F(t), F(t+\tau),.....F(t+(m-1)\tau)\} \quad (1)$$

where τ is the time delay and m is the embedding dimension. There are a number of procedures[6] for choosing the time delay, but the simplest one which is used in this paper is the time determined from the auto-correlation function at the first zero crossing.

Figure 12 shows the phase space plots for the canard port side torque signal for m = 3. Techniques to determine m are discussed in Reference 6. Since the aerodynamic forces are dominated by the first harmonic, choosing m = 3 is sufficient to illustrate the limit cycle oscillation behaviour of the aerodynamic forces. The three-dimensional figures are rotated at different angles in two planes to show the shape of the curves.

5.1.5 *Photographic studies of canard motion*
A test was conducted with a broken servo locked at 0° deflection angle to investigate the canard motion when flutter was approached. This was carried out with the HATT-X set at an angle of attack of 2°. Flutter occurred at a lower Mach number and dynamic pressure. It was found that at M=0.6 and q=3.1 psi, the vibration was so intense that the internal canard attachment structure was separated from the vehicle fuselage. The starboard canard also split at the bonding seam. A graph of the canard bending and torsion deflections determined from the high speed video photography at M=0.58 is shown in Figure 13. The bending deflection δ is the vertical displacement of the canard tip measured in inches relative to a reference line at WL 00 (see

inset in Figure 13). The torsion is given by η in degrees where η is the chord axis angle at the canard tip. The deflection time histories are very close to those for sinusoidal motion with the torsion motion leading the bending motion by approximately 90°. A few frames from the high speed video photography are shown in Figure 14 for canard positions at different times in an oscillation cycle corresponding to the points marked by the filled circle symbol on the torsion deflection curve in Figure 13.

It is expected that some freeplay is present in the canard linkage system but the exact amount is not known until further testing is carried out. By locking the servo, the canard system becomes less flexible since the additional structural damping from the freeplay is eliminated. This decrease in structural damping from the previous flutter test results in more intense vibration of the canard as flutter is approached.

The frequency computed from the period of oscillation in Figure 13 is approximately 45 Hz which is lower than that for the unlocked canard at 57 Hz. No test was performed at M=0.58 in the OJF with the unlocked servo to measure the frequency of the canard motion. Such a test would be useful since a comparison of the frequencies will give an indication of the amount of freeplay in the canard linkage system.

Aerodynamic loads were measured for only a very short time duration in this test and the signal quality was so poor that no statistical analysis was attempted.

5.2 Flight Test Results

The HATT-X was accelerated during each rocket burn and times for successive rocket firings were programmed when the Mach number decelerated to below a certain value. At the seventh stage, the peak Mach number reached was 0.8 and the canard was destroyed when the Mach number was decelerated to 0.75. Due to the nature of the vehicle propulsive system, the HATT-X can be imagined to be given an impulse at specific times during its flight path.

Figure 15 shows the Mach number and canard deflection angle versus time. There is large unsteadiness in the canard position during the first two rocket firings. At the later stages, the average canard angle of attack increases with decreasing Mach number and larger fluctuations are observed. The results presented in this paper are obtained for the 6th stage prior to canard failure. At the 7th stage where flutter occurred, no useful data was available for analysis.

Different segment lengths of the time series for the strain gauges and accelerometers were used for analysis. For the 6th time segment, 6 seconds of the time series were analysed. It should be emphasised that the results from the statistical studies must be interpreted to be a representation of the overall characteristics of the measurements averaged over the length of the time segment. For this time duration, the Mach number decreased from 0.69 to 0.56.

5.2.1 *Power Spectral Density*

Figure 16 shows the power spectral densities of the port side strain gauge results for the lift, torque and drag. The results are similar to those given in Figure 8 for the Open Jet Facility tests. The spectra show the first harmonic at 41.4 Hz to be the dominant mode with a magnitude which is much larger than those of the higher harmonics. The starboard PSD show very similar results except for the torque whose second and third harmonics are smaller by an order of magnitude. There are a number of frequency components which are not harmonics, but their magnitudes are too small to be of any significance.

The spectra of the accelerometer response at the canard root and tip are shown in Figure 17. The first three harmonics at 41.4 Hz, 82.8 Hz and 124.2 Hz are distinctly visible. Spectral plots covering larger frequency range show the presence of higher frequencies. The more important ones are at 336Hz, 450Hz, 816Hz, 948Hz and 1020Hz. These modes have smaller magnitudes than the three harmonics shown in Figure 17 by a factor of 5 to 10 and the spectral shapes are typical of those for broadband noise.

Ground vibration tests were performed on a canard support system identical to that used on the HATT-X flight test. The structure was excited by a rubber mallet. The spectra of the port canard lift, torque,

drag, canard tip and root accelerometers all showed a sharp peak at approximately 38 Hz. This frequency is close to the value observed in flight test. It should be mentioned that the frequencies measured from the PSD plots from flight tests can vary up to a maximum value of ±2 Hz. The frequency resolution in computing the spectra for the aerodynamic forces is at best 1.22 Hz and 4.9 Hz for the accelerometer signals.

5.2.2 *Correlation analysis*

The accelerometer and the port torque strain gauge signals were sampled at 2500 Hz while the rest of the strain gauge signals were sampled at 625 Hz. In performing cross-correlation analysis between a high and low sampling rate time series, a new time series of the higher sampling frequency signal was reconstructed using the lower sampling rate. Cross-correlation was then carried out at 625 Hz.

Auto-correlation curves show a characteristic damped cosine curve for all the strain gauge signals. The accelerometer auto-correlation functions show the presence of high frequency components in the signals. Distortion of the damped cosine waveform due to the higher frequencies are more noticeable at the tip than at the root accelerometer. The frequency measured from the period of oscillation agrees with that determined from the PSD curve for the fundamental frequency.

Cross-correlation shows the lift and torque at the 6th time segment to be approximately 68° and 66° out of phase on the starboard and port canards. The lift lags the torque on the starboard canard and leads the torque on the port canard. The torque leads the drag by 155° at the starboard side and lags behind by 18° at the port side. The lift leads the drag by 85° and 28° on the starboard and port canards respectively. A sample of the cross-correlation plots between these three aerodynamic quantities on the port side canard is shown in Figure 18. Comparison with Figure 9 shows that correlation values are smaller and the phase lead or lag relations are different.

Cross-correlation between the lift, torque and drag signals on the starboard and port canards shows that the lift and drag are approximately in phase, with an observed phase shift of 17° and 13°respectively. The torque signals on the two canards are 154° out of phase. On comparing the cross-correlation plots shown in Figure 19 with those from Figure 10, it is seen that the phase relation between the torque and drag on the canards reverses for the ground and flight tests.

Correlation between the aerodynamic forces and the accelerometers is given in Figures 20 and 21. The placement of the accelerometers shown in Figure 1 indicates that the root gauge should have larger response to the torque while the tip gauge should respond more to the bending or lifting force. This is demonstrated in Figure 20 which shows that the cross-correlation values are largest for the torque and root accelerometer signals. The lift has smaller correlation than the drag. The phase lead between the lift and drag forces and the root accelerometer are 64° and 15° respectively, while the torque and the accelerometer signal are practically in phase. The corresponding correlations between the three aerodynamic forces with the tip accelerometer are shown in Figure 21. The correlation values between the torque and acceleration are less than those for the root gauge. The correlation between the lift and tip acceleration is also smaller than that for the other two aerodynamic forces and has approximately the same values as those shown in Figure 20. The drag-acceleration correlation signals are weaker at the tip than at the root, but they are still stronger than that for the lift-acceleration correlation. The tip accelerometer signal has large high frequency components and noticeable distortions in the correlation curves are observed. Approximate phase angles for the three aerodynamic forces and tip acceleration correlations are 144°, 70° and 100° respectively, with the acceleration lagging the forces.

A plot of the correlation between the root and tip accelerometers is shown in Figure 22. The sampling rate is 2500Hz and the higher frequency components are more visible. The root accelerometer signal leads the tip signal by approximately 70°.

5.2.3 *Phase plots*

Phase plots of the aerodynamic forces for the 6 seconds time segment show that structured toroidal-shaped curves given in Figure 12 were not observed. This is probably due to statistical nonstationary behaviour of the time series. The Mach number varied from 0.69 to 0.56 and resulted

in large mean aerodynamic force variations within the time segment. The centre of each orbit of the lift, torque or drag moves in the phase plane and the results resemble those for a chaotic dynamical system. The aerodynamic forces may not be chaotic and the standard technique of time reconstruction needs further investigation before being used to study signals with time varying means.

The accelerometer signals contain high frequency components that are not harmonic components of the fundamental mode. In the wake flow of an airfoil, Williams-Stuber and Gharib[7] have demonstrated that nonlinear interaction of three incommensurate frequencies can generate a chaotic state. Figures 23 and 24 show the phase plots for the tip and root accelerometers. Because the sampling rate was 2500 Hz, a 2 seconds time segment was chosen since this would give sufficient points for the phase plots. The Mach number varied from 0.58 to 0.56 during the 2 second time interval. Examination of the time series did not reveal any large changes in the mean acceleration level. However, the phase plots show a chaotic behaviour. It is not certain whether this is due to small movement of the centre of the orbits as suggested earlier, or whether the response is chaotic. Larger values of the embedding dimension m have been used. With values up to 8, similar phase plots as Figures 23 and 24 were generated. Tests in the Open Jet Facility for constant Mach number and canard deflection angle runs should be able to shed more light on the behaviour of the accelerometer signals.

5.3 Comparisons Between Ground and Flight Tests

The fact that the canard structural properties are different for the HATT-X vehicles used in the ground and flight tests makes meaningful comparisons between the test results difficult. In the OJF studies, the Mach number was held constant and the variation in the canard angle of attack was small during the 1 second period where analysis was carried out. Relatively longer signals were used in the flight tests during which time the Mach number varied significantly and the canard deflection angles also changed by a substantial amount.

In both tests, the aerodynamic forces exhibit similar spectral characteristics but the frequencies of the first few harmonics are different. This is to be expected since the canards fitted to the HATT-X were different. Ground vibration tests performed for the modified HATT-X canards used in the flight tests show that the fundamental frequencies are close. Similar tests were not carried out for the canards used in the OJF experiments.

There are differences in the phase relations between the aerodynamic forces in the two tests. For the OJF test, cross-correlation of the torque shows that it is approximately in phase between the starboard and port canards. However, the lift on the two canards has a phase difference of 168° and the drag has a phase difference of 160° with the starboard side leading in both cases. For the flight tests, the lift and the drag on the two canards are approximately in phase, but the torque on the starboard side leads the port side by 154°. This suggests that some mechanism, different in the two tests, is responsible for altering the phase relationship. A possible explanation is the constraint placed on the HATT-X in the OJF tests.

The canard flutter mechanism may involve more than two degrees of freedom. Since the modified canards on the HATT-X used in the flight tests were mass balanced, it would be correct to assume that bending-torsion flutter may not be the primary flutter mechanism. The observation that the correlation between torque and drag with acceleration is large suggests that a possible flutter mechanism may be the coupling between the canard torsion and lead-lag modes in addition to the bending mode. In the OJF tests, it was observed that canard angle of attack plays a role in determining the intensity of the canard vibration. Usually flutter will not occur when the deflection angle is high and exceeds the stall angle. This suggests that a large increase in steady state drag may add an appreciable preload to the canard linkage equivalent lead-lag spring and the resulting change in phase relation with the torsion may have an effect on the onset of flutter. An attempt was made to carry out a sensitivity analysis using a simple theoretical flutter model. No meaningful conclusions can be obtained without information from a ground vibration test on the mode shapes, equivalent spring constants and other structural properties of the canard system.

The accelerometer signals from the flight test show

that the phase space reconstruction produces plots resembling chaotic behaviour. Higher order phase plots did not reveal any pattern. This may be an indication that the response signals have very large embedding dimensions and existing techniques from nonlinear dynamical system studies may not be too useful for flight flutter tests on the HATT-X unless some modifications to these techniques are devised. Analysis performed in the OJF under more controlled conditions will be required to explore the feasibility of this technique for future HATT-X flight tests.

6. CONCLUSIONS

The limited amount of ground and flight tests carried out on two structurally different canards made it difficult to identify the flutter mechanism with confidence. Useful information such as the magnitudes of the aerodynamic forces, acceleration data from the OJF tests, and mode shapes from ground vibration tests are not available even though there are plans to obtain these data in future tests.

In the OJF tests, it was found that flutter does not normally occur at large canard deflection angles. This may be due to the increase in steady state drag force resulting in a large preload on the canard linkage equivalent lead-lag spring. Also, the phase relation between the drag and the other two aerodynamic forces is altered and this will have an effect on the flutter mechanism.

The stiffer and mass balanced canard used in the flight tests did not suppress flutter as first expected. Since the flutter phenomenon was similar to that encountered by the unbalanced canard in the OJF studies, it is likely that the coupling of the torsion and lead-lag degrees of freedom plays an important role in the HATT-X canard flutter. Correlation between aerodynamic forces and canard acceleration shows that the drag has correlation values larger than the lift, with the torque correlation being the largest.

In ground and flight tests, the phase relations between the aerodynamic forces on the two canards show a phase change of nearly 180° for the drag and torque. This is probably due to the different constraints placed on the HATT-X.

ACKNOWLEDGEMENTS

The authors would like to thank the Institute for Aerospace Research, the Defence Research Establishment Suffield and Carleton University for their support.

REFERENCES

1. Markov, A.B., Coffey, C.G., and Herring, R.W., "Autonomous Unmanned Aircraft R&D with a High Performance Flying Laboratory", First IFAC International Workshop on Intelligent Autonomous Vehicles, U.K. 18-21 April, 1993.

2. Markov, A.B. and Herring, R.W., "A High Performance Flying Laboratory for Autonomous Unmanned Aircraft R&D", Third Conference on Military Robotic Applications (MRV91), Defence Research Establishment Suffield/Alberta Research Council, Suffield, Alberta, Canada, 9-12 September, 1991.

3. Markov, A.B. and Herring, R.W., "Guidance and Control Considerations for a Maneuvering Aerial Target System"' Advances in Techniques and Technologies for Air Vehicle Navigation and Guidance, AGARD Conference Proceedings 455, Lisbon, May 1989.

4. Packard , N.H., Crutchfield, J.P., Farmer, J.D., and Shaw, R.S., "Geometry from a Time Series", Physics Review Letters, Vol. 45, No. 9, September 1980, pp. 712-716.

5. Lee, B.H.K. and Tron, A., "Effects of Structural Nonlinearities on Flutter Characteristics of the CF-18 Aircraft", Journal of Aircraft, Vol. 26, No. 8, August 1989, pp. 781-786.

6. Abarbanel, H. D.I., Brown, R., Sidorowich, J.J. and Tsimring, L.S., "The Analysis of Observed Chaotic Data in Physical Systems", Reviews of Modern Physics, Vol. 65, No. 4, October 1993, pp. 1331-1392.

7. Williams-Stuber, K. and Gharib, M., "Transition from Order to Chaos in the Wake of an Airfoil", J. Fluid Mechanics,Vol. 213, 1990, pp. 29-57.

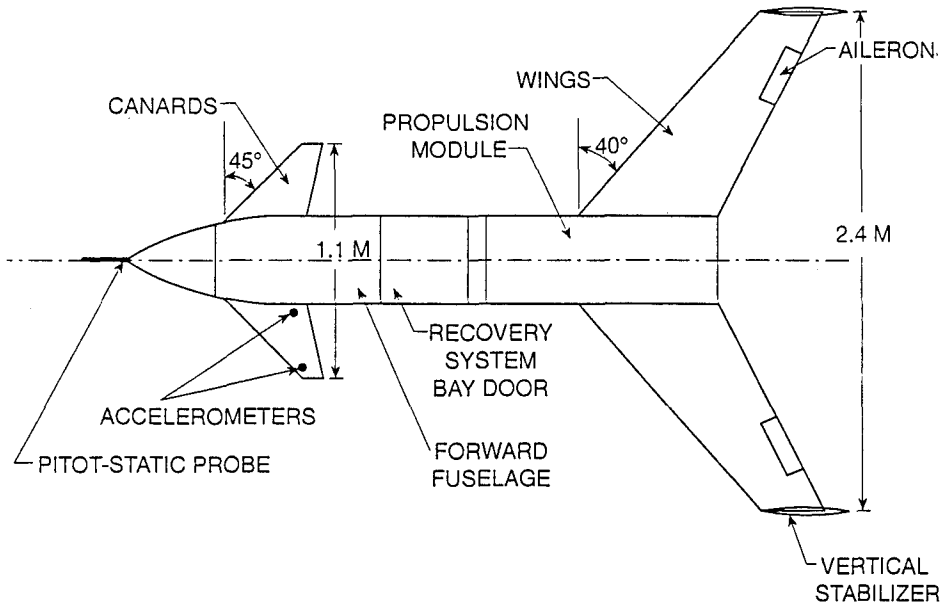

Figure 1 Schematic of HATT-X

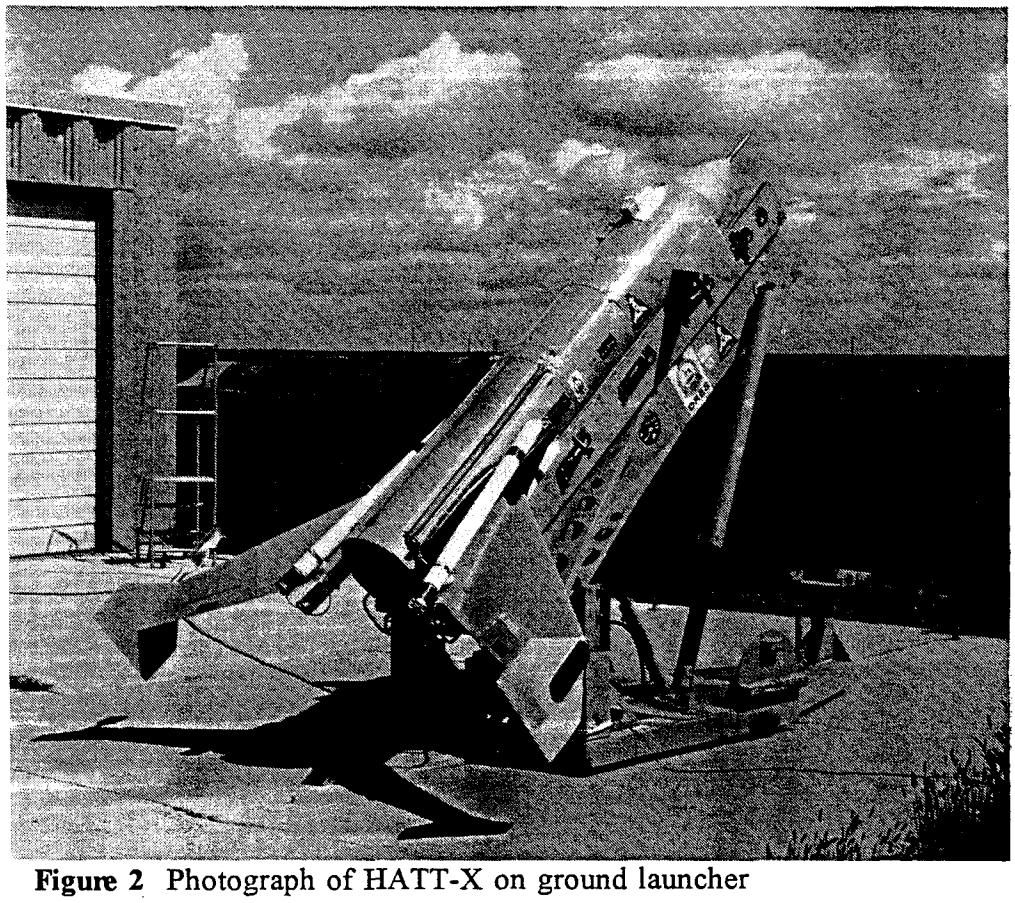

Figure 2 Photograph of HATT-X on ground launcher

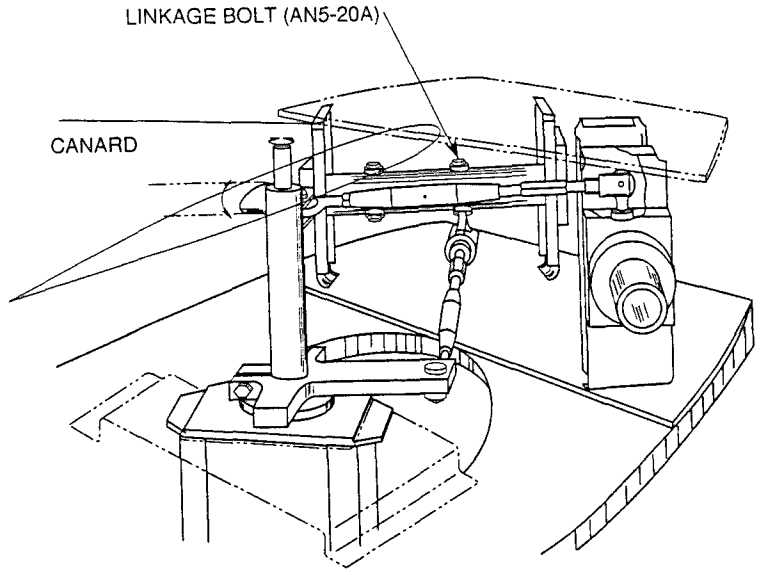

Figure 3 Schematic of canard drive mechanism

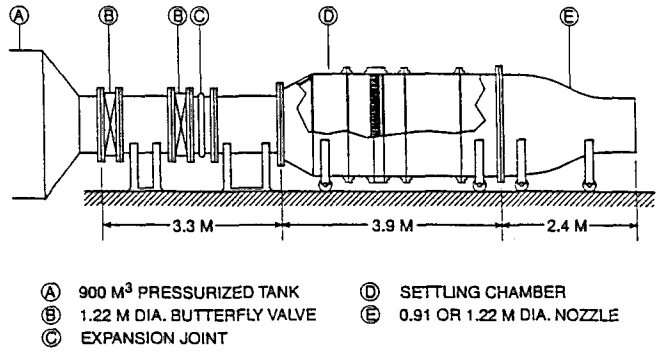

Figure 4 Schematic of Open Jet Facility

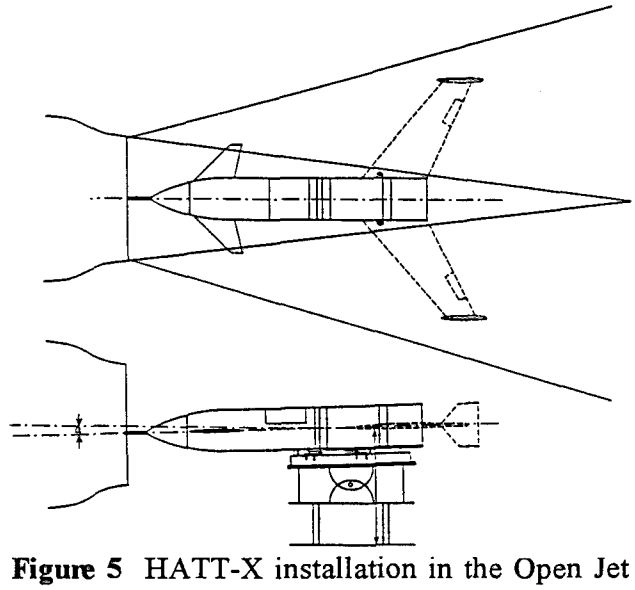

Figure 5 HATT-X installation in the Open Jet Facility

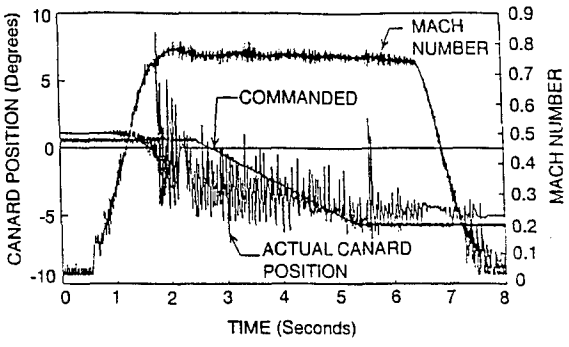

Figure 6 Mach number and canard position

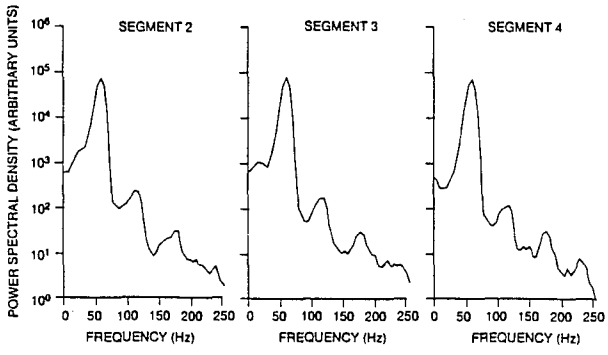

Figure 7 PSD for port canard lift

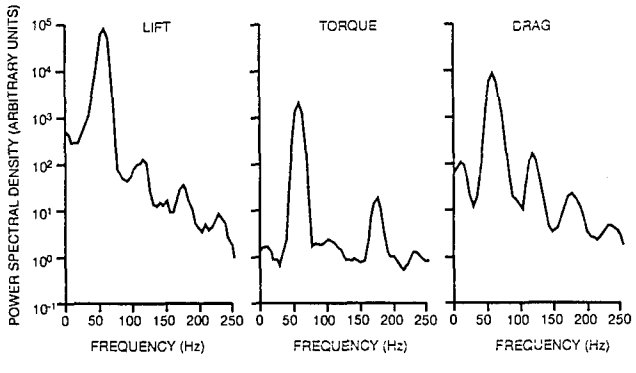

Figure 8 PSD for port canard lift, torque and drag

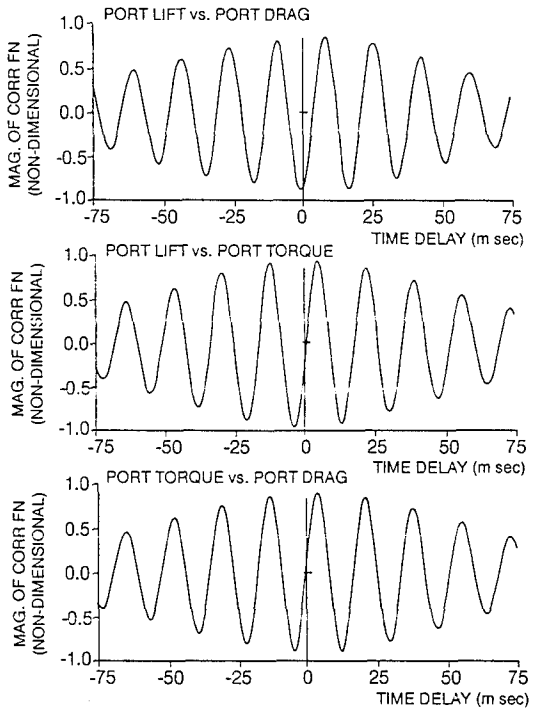

Figure 9 Cross-correlation between port canard lift, torque and drag

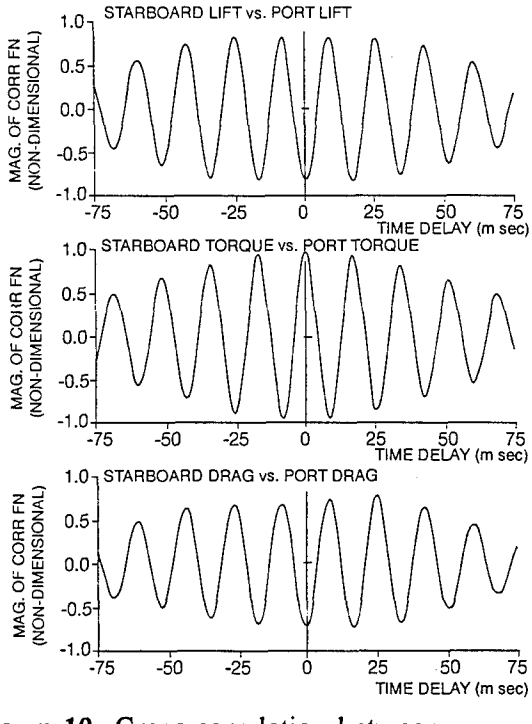

Figure 10 Cross-correlation between starboard and port canards

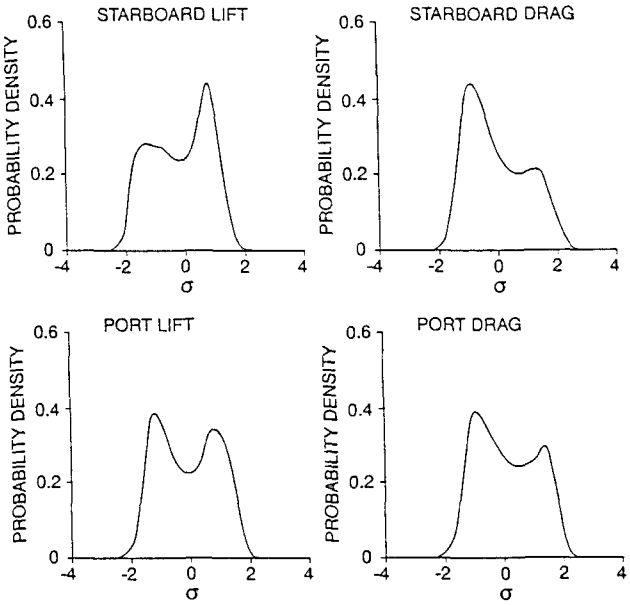

Figure 11 Probability density function for port canard lift and drag

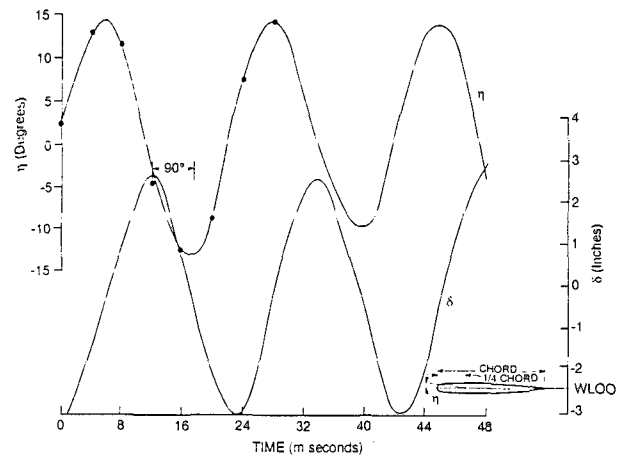

Figure 13 Canard bending and torsion deflections

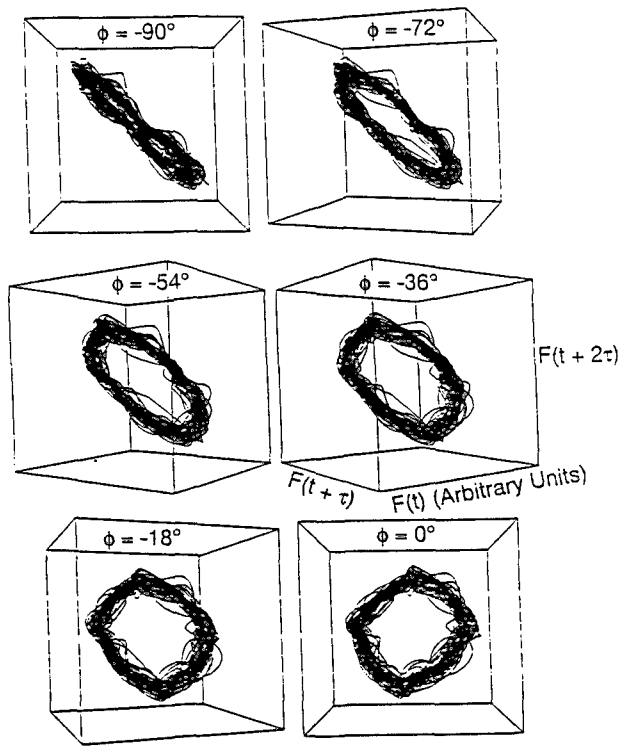

Figure 12 Phase plane plot of port canard torque

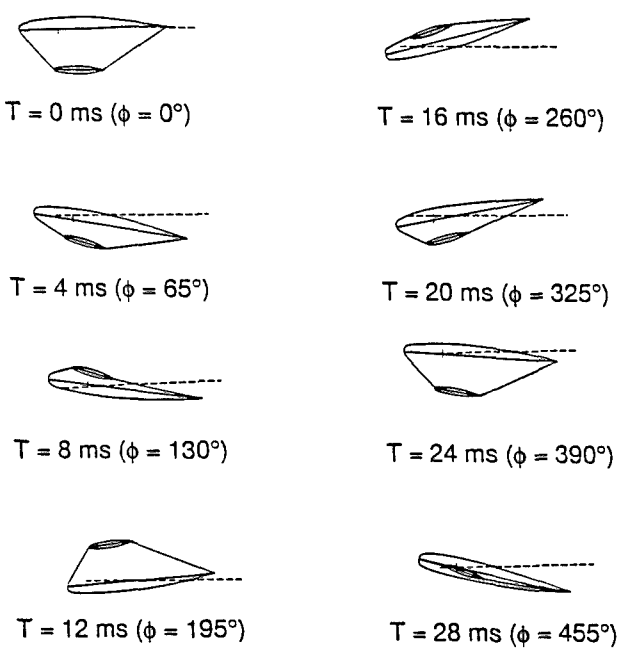

Figure 14 Canard positions at different times in an oscillation cycle

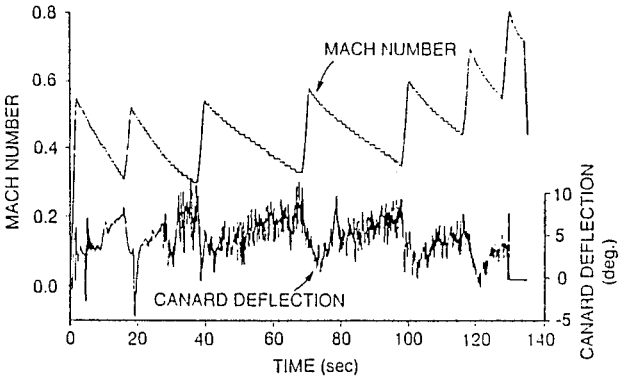

Figure 15 Flight test Mach number and canard angle

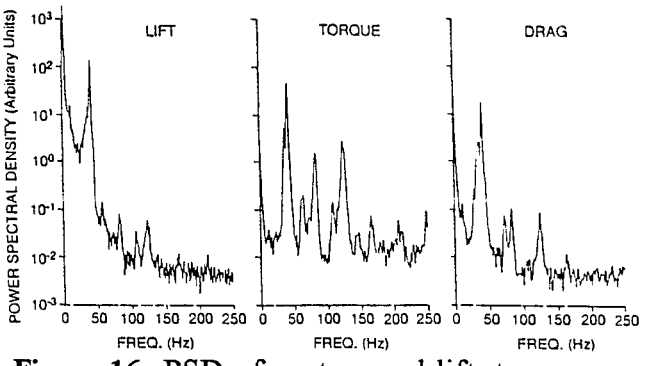

Figure 16 PSD of port canard lift, torque and drag

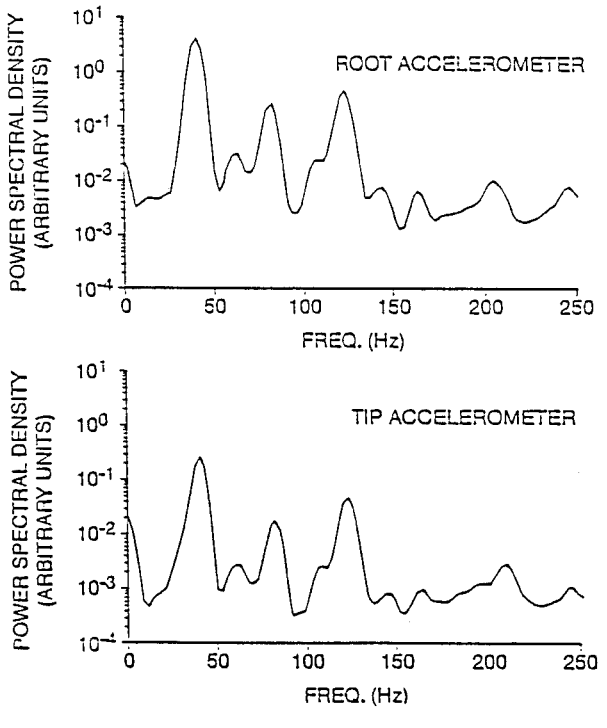

Figure 17 PSD of canard root and tip accelerometers

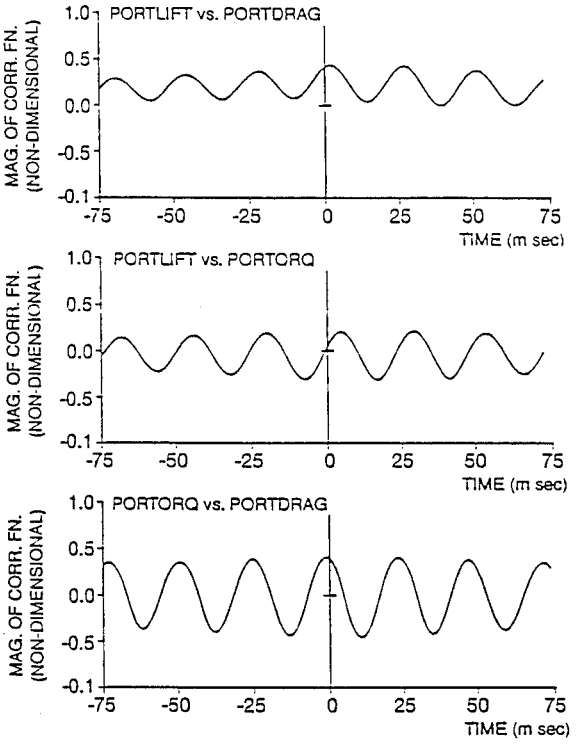

Figure 18 Cross-correlation between port canard lift, torque and drag

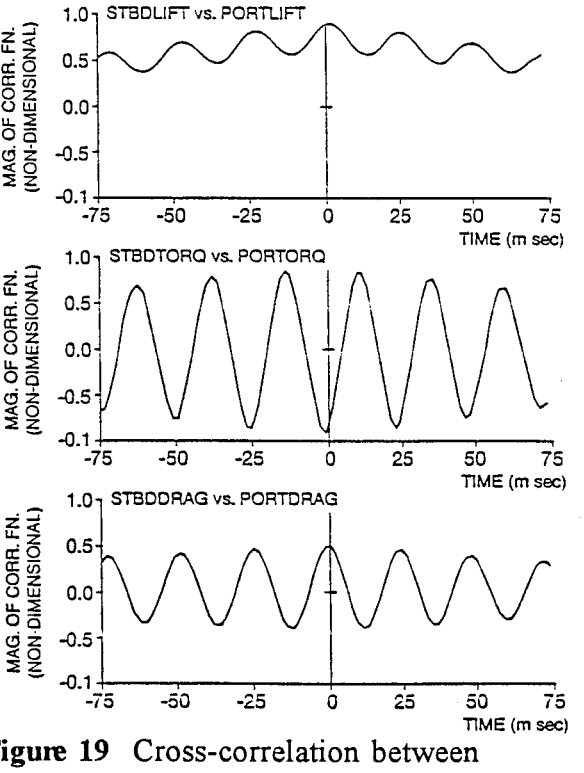

Figure 19 Cross-correlation between starboard and port lift, torque and drag

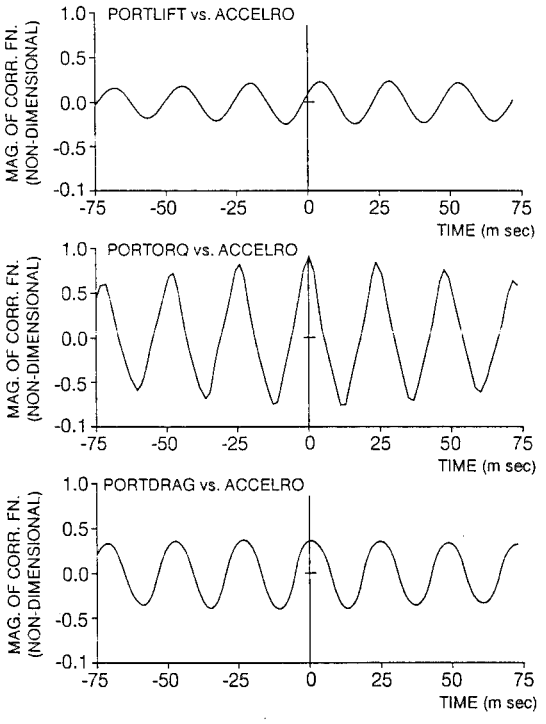

Figure 20 Cross-correlation between port canard lift, torque and drag with root accelerometer

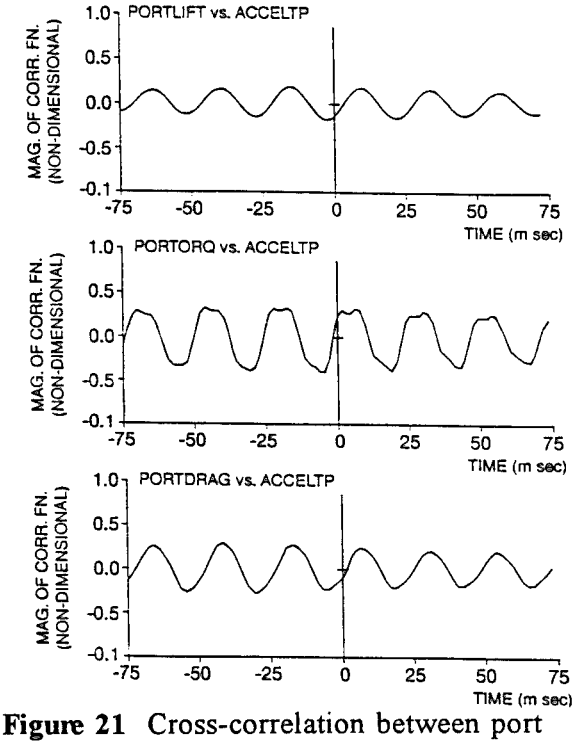

Figure 21 Cross-correlation between port canard lift, torque and drag with tip accelerometer

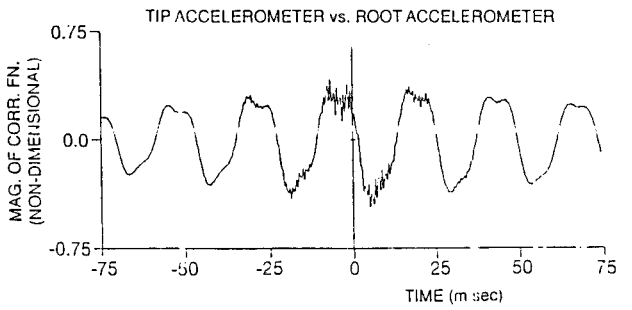

Figure 22 Cross-correlation between port canard root and tip accelerometers

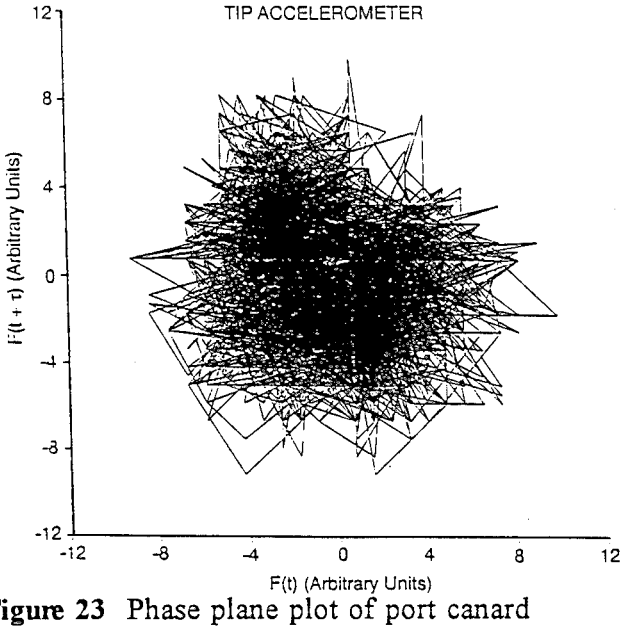

Figure 23 Phase plane plot of port canard tip acceleration

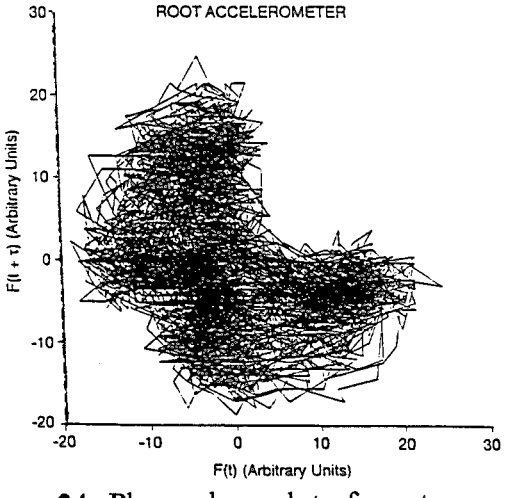

Figure 24 Phase plane plot of port canard root acceleration

Design And Testing Of An Aeroelastically Scaled Model Structure

Mark French*
Flight Dynamics Directorate
Wright Laboratory
Wright-Patterson AFB
Ohio 45433-7006, USA

F.E. Eastep**
University of Dayton
Dayton, Ohio 45405
USA

Abstract

An approach has been developed which uses optimization methods to automate wind tunnel model design. The model design process has been divided into separate stiffness design and mass design stages. Then, a sample structure was manufactured and subjected to static and modal testing using laser holographic techniques. Optical test methods are well suited to testing subscale models. A single image shows either static or dynamic out of plane deflections for the entire model. These methods reduced the time required to characterize the test specimen compared to more conventional methods and did so with improved accuracy.

Introduction

Testing aeroelastically scaled wind tunnel models is a common task in flight vehicle development programs. In some tests, the goal is simply to verify analytical methods. Then, the model must only represent the full scale vehicle in a qualitative sense. Quite often, though, the scaled model is to reproduce the response of the full scale structure[1]. This is the most general form of the aeroelastic model design problem and is the one addressed here.

Previous efforts[2,3] have been aimed at demonstrating feasibility of the basic idea and was limited to stiffness design of the model. This work has been refined and extended to include selection of tuning masses. An aeroelastically scaled model is one for which static deflection and modal behavior are related to that of a full size article by simple scaling rules[4]. The model designer must produce a structure which matches predetermined mass and stiffness properties. The problem may be treated as a parameter identification problem[5].

The design process is not complete until the resulting model has been both statically and dynamically tested to show that it reproduces the characteristics of the full scale structure. This paper discusses both the design process and the testing process.

Background

A classical form of the parameter identification problem involves determining the coefficients of a system of linear equations. The identification process is based on some system response measurement which is assumed to be a solution of the equations of the mathematical representation[6].

A body of the literature on parameter identification problems deals with model update or model improvement methods. These methods use some approximation to the desired

---

* Member AIAA

** Associate Fellow AIAA, Professor of Aerospace Engineering

Paper presented at the Structures and Materials Panel Specialists' Meeting on "Advanced Aeroservoelastic Testing and Data Analysis", held in Rotterdam, The Netherlands, from 8-10 May 1995, and published in CP-566.

system as the starting point for a procedure which uses system output to improve the accuracy of the initial model. A successful class of methods uses optimization methods to correct the mathematical representation of structures[7-10]. A concise method unifying this approach was presented by Berman and Nagy[11].

Many methods intended to isolate errors in finite element models have been proposed[12-14], all of which operate directly or indirectly on physical parameters. Wei and Janter suggest operating directly on parameters of a finite element model[15]. This basic approach has been expanded with more recent work being presented by Ewing and Venkayya[16] and Ewing and Kolonay[17]. A preliminary effort at including system identification capabilities in a general purpose finite element code is presented by Gibson[18].

The method presented here uses constrained numerical optimization methods to modify a finite element representation of the model structure so that some measure of the difference between the calculated and desired responses is minimized. By operating directly on the finite element model, orthogonality of calculated eigenvectors, symmetry of system matrices and validity of individual system matrices is assured. Also, the result of the design process is information which can be used to fabricate a model with little post-processing. The process presented here is divided into two steps. First, optimization methods are used to size the structure for stiffness only. The element sizes are then fixed and concentrated masses are added to the structure to give the desired modal response. The sizes of the masses are determined using a second optimization-based method.

Stiffness Design

The wind tunnel model designer must design a structure with a predetermined set of stiffness and mass properties. We assume for this work that the known stiffness properties come from a finite element model of the full scale structure, though perhaps one which has been tuned to agree with test results.

The stiffness design task uses an error function based on the difference between calculated and desired displacements due to a group of specified unit loads. An optimization routine to change the design so that function is minimized. When using a finite element representation of some structure, the vector of displacements due to a unit load in a single degree of freedom is just a column of the flexibility matrix. In the ideal case, the final error function value would be zero. Then, the calculated flexibility matrix of the wind tunnel model structure would match the desired one. Ideally, displacements at all grid points would be specified using unit loads applied at all grid points. However, this can result in a large and possibly overconstrained problem.

We tried several different methods for the stiffness design task. The most effective approach used an interior penalty function method as implemented in ADS[19] to minimize the objective function

$$F = \sum_{i=1}^{m} \sum_{j=1}^{n} k(\delta_{ij} - x_{ij})^2 \qquad (1)$$

where δ_{ij} is the ij term of the desired flexibility matrix and x_{ij} is the ij term of the flexibility matrix calculated for the current design. m is the number of grid points for which displacements are specified and n is the number of columns of the flexibility matrix for which displacements are specified. K is an arbitrary constant. m and n will not, in general, be identical.

We also applied constraints of the form

$$g = (\delta_{ij} - x_{ij})^2 \leq 0 \qquad (2)$$

Using the square of the displacement differences to form constraints means that the feasible region is a single point. Thus, the

optimizer is searching for a point in design space at which all constraints intersect. In general, such a point does not exist. Then, the object is to find a point in design space acceptably close to all the constraints.

Mass Design

We considered two different approaches for the mass design. Both methods assumed that the stiffness design was complete and that an acceptable level of accuracy had been obtained. The first method minimized an error function based on natural frequencies. The assumption was that tuning masses to match natural frequencies on a structure which already had nominally correct stiffness characteristics would necessarily result in correct mode shapes. While perhaps correct in a theoretical sense, this approach performed poorly in practice. We found that accurate natural frequencies could be obtained for mass selections that poorly reproduced the desired mode shapes.

The more successful of the two methods used an interior penalty function to minimize and objective function based on the difference between desired and calculated mode shapes.

$$F = \sum_{i=1}^{m} \sum_{j=1}^{n} \left[\frac{\bar{x}_{ij} - x_{ij}}{\bar{x}_{ij}} \right]^2 \qquad (3)$$

The mode shape error function was normalized in a manner similar to the frequency error function. This was to make sure the function was not biased toward areas where the displacements are large. Getting proper node line locations is critical in matching flutter behavior. The normalizing process gives equal weight to small displacements near the node lines and large displacements at antinodes.

Constraints were formed using the difference between calculated and desired natural frequencies and a total mass constraint. Frequency constraints were of the form

$$g_i = \left(\frac{f_i - \bar{f}_i}{\bar{f}_i} \right)^2 \leq 0 \qquad (4)$$

Where f_i is the calculated frequency of mode i and $\bar{f}_i$ is the desired frequency of mode i. The total mass constraint is an equality constraint of the form

$$g = \frac{m - \bar{m}}{\bar{m}} \leq 0 \qquad (5)$$

where m is the calculated total mass and the the overbar indicates the desired mass.

The total mass constraint was added to method two in order to force the design to the correct overall mass. Flutter may be considered as an energy transfer phenomenon. Kinetic energy in either the flow or the aircraft (depending of the reference frame chosen) is converted to kinetic and strain energy in the structure. Failing to properly scale the total mass of the structure would introduce unknown and potentially large differences between the kinetic energy of the model and that scaled from the full scale structure. In such a situation, it would be unreasonable to expect aeroelastic properties to scale correctly.

Model Structure

One of the goals in designing this structure was to minimize fabrication costs, so a simple all-metal structure was chosen. The structure was assumed to be made up of constant cross-section beam elements in a planar lattice. Test articles have been manufactured easily by machining the structure from a single plate of aluminum using a numerically controlled vertical end mill. Choosing this structure was not a reflection of any limitation of the method; it is valid for any structure which can be modeled using a finite element discretization.

In the stiffness design process, the heights of the elements were assigned and did not change. The widths of the elements were used as design variables. Typically, the beam heights were assigned at the maximum values that would

allow the structure to fit inside the aerodynamic envelope of the wing. This was done to keep the structure as light as possible for a given stiffness distribution. Grid point locations for the finite element representation of the wind tunnel model were fixed at the beginning of the design process and not used as design variables.

Sample Problem

A sample problem was developed to evaluate the different design methods. The wing is a clipped delta intended to simulate a common low aspect ratio fighter wing. The aerodynamic planform is presented in Figure 1. The wing is assumed to be made of aluminum with 11 spars. The finite element model of the full scale wing is presented in Figure 2.

Element sizes for the wing were determined by optimizing the structure using a minimum flutter velocity constraint using a finite element-based analysis and optimization package called ASTROS[20]. The minimum flutter speed was given as 833.3 ft/sec (10000 in/sec) at Mach .80. Heavy design variable linking was used to assign five design variables for the wing. After the design run was finished, the matched point flutter condition was determined to be Mach .75 at sea level. The calculated flutter velocity was 820.5 ft/sec and the flutter frequency was 5.81 Hz.

Modal participation factors for the full scale wing at the flutter point are given in Table 1. The modal participation coefficients are simply the complex constants by which the normal modes are multiplied to form the flutter mode. The magnitudes show that the flutter mode is composed largely of the first two normal modes. We retained the first three normal modes in all flutter calculations in case the predicted flutter mechanism changed during the design.

The model scale factors were determined without a specific wind tunnel in mind. The geometric scale factor was assigned as 1/10. The model velocity and density ratios were both assumed to be unity. Thus, we have a 1/10 scale model which will be run in a wind tunnel at Mach .75 at sea level. The scale factors are summarized in Table 2.

There is no requirement that grid point locations or element connectivities of the scaled model structure correspond to those of the full scale one. For simplicity, however, we used a subset of the grid point from the full scale structure scaled down by a factor of 10 to define the grid point for the model finite element discretization shown in Figure 3.

Selected out of plane displacements from four columns of the flexibility matrix were used for the stiffness design. The first three natural frequencies and a subset of out of plane displacements from the first three mode shapes were used for the mass design.

The first run resulted in some element sizes which were too small to be manufactured. Those element heights were reduced so that the moment of inertia in bending was unchanged and the width was not less than .050 inch. The modified design was then used as an initial design for another optimization run. This process was repeated once more so that all elements were of sizes which could be easily manufactured

Model Fabrication

After the design for the 1/10 scale model structure was completed a test specimen was manufactured. We did this to verify that assumptions made during the design process were valid. Our principal concern was excess material at the element joints. The excess material added mass at the joints which was not accounted for in the finite element model and increased the stiffness in the joint area.

Also, a slight change was made to the design to make the manufacturing process simpler. The math model was symmetric about the mid plane of the wing. This meant that there would have been steps on each side of the structure. The

actual structure was machined flat on one side and stepped on the other, making it much easier to manufacture. We assumed that resulting stiffness changes would be small. This was not borne out in testing, however, and offsets had to be included in the finite element model.

Testing Techniques

All testing was done using laser metrology. While well known, this form of testing does not seem to be widely used for validation of scaled model structures. References 21 and 22 contain excellent descriptions of the uses of holography in structural testing. Testing consisted of conventional, wet plate holography, video holography and laser vibrometry. Conventional holography was used when high resolution was desired. Figure 4 shows the layout of a typical test.

Holography can be used for mapping deformations using double exposures. The first exposure is made of the undisturbed specimen. For static testing, a load is applied and a second exposure is made and the plate developed. The interference of the two fringe patterns on the plate modifies the holographic image by superimposing fringe lines on the image. The fringe lines are lines of constant deformation. Whether the deformation is in plane or out of plane depends on the geometry of the interfering beams. We measured out of plane deformations for this work.

Just as the design process consists of stiffness design followed by the selection of tuning masses, testing is divided into static and dynamic phases.

Static testing was performed by applying either a known loading or a known displacement at selected grid points on the structure and making a double exposure hologram which showed formed fringe patterns on the image of the structure representing the deformations. Quantitative data was obtained by scanning the hologram into a PC based image processing system. Fringe lines were marked and counted automatically and the resulting data stored for plotting. A typical hologram with fringe lines is presented in Figure 5.

The imaging procedure is slightly different for modal testing. In this case, an image is captured of the structure at rest and the plate is developed. To make fringe lines, the plate is replaced in the holder and the structure excited. As with the static test, fringe lines are formed on the resulting hologram. The difference is that, since the developed plate only has the original image, the fringe lines are formed in real time and are time dependent.

Finally, the holographic method used in this effort is a slight variation of the classical holographic method. A lens was used to focus the object image on the plate. This allows reconstructing of the image with collimated white light rather than requiring a coherent beam.

In siutations where high resolution was not required, electronic test methods were employed. Some static testing was performed using Electronic Speckle Pattern Interferometry (ESPI). ESPI is similar to the photographic process except that it uses a video camera in place of a photographic slide and the fringe pattern is formed electronically. The resolution is greatly reduced, but the increased convenience often makes it attractive.

ESPI was also used for dynamic testing, particularly when only natural frequencies and node line locations were needed. A final instrument used for modal testing was a laser doppler vibrometer (LDV). The LDV illuminates the target with an unexapnded beam and compares the frequency with that of the signal reflected from the target. This Doppler shift is used to measure the instantaneous velocity of the target.

Static Test Results

We performed two sets of static tests. The first set from tests where a displacement was applied

to the various points on the structure using a probe mounted on a fine thread micrometer. Fringe lines along the spars were counted using the image processing software and the results normalized. As a result of the normalization, the stiffness can only be verified to within a constant multiplier.

The second set of static test results was obtained by applying at known load to the structure and absolute displacements measured at the various grid points on the wing. It quickly became apparent that the stiffness of the test article was significantly higher than that predicted by the finite element model. Including offsets in the finite element representation improved the agreement.

One problem with applying a known load was that the load required to generate a useful number of fringe was on the order of 0.5 grams. Applying such a small load repeatably proved to be difficult. The solution was to apply a much larger load as a tare for the first exposure and add the smaller weight for the second. In addition, the tare weight had to be immersed in a cup of glycerin to damp vibrations.

Modal Test Results

Two sets of modal tests were performed, one before the mass balancing weights were added and one after. The first three natural frequencies of the structure before mass balancing are presented in Table 3. The measured and calculated natural frequencies after the addition of the tuning masses is shown in Table 4. Agreement between experiment and analysis is good, with differences being limited to a few percent in most cases.

ESPI measurements proved to be particularly useful for modal testing. Since the fringe pattern is formed in real time, identifying the natural frequencies required little time. Once the natural frequencies were found, the image was stored digitally for comparison with calculated predictions.

Obviously, the most important measure of the quality of an aeroelastically scaled model is the degree to which it reproduces the desired aeroelastic phenomena. The full scale wing has a predicted flutter instability at 820.5 ft/sec at a Mach number of .75. The calculated flutter frequency was 5.81 Hz.

The aeroelastically scaled model has a predicted flutter speed of 759.1 ft/sec and frequency of 58.1 Hz at Mach .75. The factor of 10 difference in the flutter frequency is due to the frequency scale factor from Table 2. The predicted modal participation factors for the model are presented in Table 5. They compare well with the full scale factors from Table 1, indicating that the flutter mechanism has been well modeled.

Conclusions

Numerical and experimental results from this work indicate that a workable method of wind tunnel model design has been developed. The methods presented here are easily implemented and can result in relatively simple structures which accurately meet the mass and stiffness requirements. The example problem showed that scaled flutter velocity and frequency requirements can be satisfied and that the predicted flutter mechanism is correct as well.

The method described is applicable for any structure which can be accurately modeled using a finite element discretization. The beam lattice structure used here, is only an example.

Finally, the optical testing methods used for this work are well suited to validating the response of test structures. The ability to measure full field static and dynamic deformations with great accuracy speeds the validation process greatly. Since optical methods are well known and commercial equipment is readily available, they can be regularly incorporated into the testing process.

Acknowledgments

The authors wish to thank Mr. Gene Maddux for his invaluable assistance in the experimental work described here.

References

1. "The Graybeard Pitch" - A seminar given by Larry Felt at the Flight Dynamics Directorate, WPAFB OH, July, 1993.

2. "An Application of Structural Optimization in Wind Tunnel Model Design"; French, R.M.; AIAA 90-0956; Long Beach CA; April 1990.

3. "An Application of Compound Scaling to Aeroelastic Model Design"; French, R.M. and Kolonay, R.M.; Third Air Force/NASA Symposium on Recent Advances in Multidisciplinary Analysis and Optimization; San Francisco CA; Sept 1990.

4. Bisplinghoff, R.L., Ashley, H. and Halfman, R.L.; "Aeroelasticity"; Addison-Wesley; 1955.

5. French, R.M. and Eastep, F.E.; "Aeroelastic Model Design Using Parameter Identification"; Accepted For Publication, Journal of Aircraft.

6. Keller, C.L.; "Methods For Determining Modal Parameters and Mass, Stiffness and Damping Matrices"; AFFDL-TR-78-59; June 1978.

7. Baruch, Menahem and Bar Itzhack, Itzhack Y.; "Optimal Weighted Orthogonalization of Measured Modes"; AIAA Journal; Vol 16, No. 4, April 1978, pp 346-351.

8. Baruch, Menahem; "Optimization Procedure to Correct Stiffness and Flexibility Matrices Using Vibration Tests"; AIAA Journal, Vol 16, No 11, November 1978, pp 1208-1210.

9. Wei, Fu-Shang; "Stiffness Matrix Correction From Incomplete Modal Data"; AIAA Journal; Vol 18, No 10, October 1980, pp 1274-1275.

10. Berman, Alex; "Mass Matrix Correction Using an Incomplete Set of Measured Modes"; AIAA Journal, Vol 17, No 10, October 1979, pp 1147-1148.

11. Berman, A. and Nagy, E.J.; "Improvement of a Large Analytical Model Using Test Data"; AIAA Journal; Vol 21, No. 8, August 1983, pp 1168-1173.

12. Sidhu, J. and Ewins, D.J.; "Correlation of Finite Element and Modal Test Studies of a Practical Structure"; Proceedings, 2nd SEM International Modal Analysis Conference, Orlando, FL, pp 756-762, 1984.

13. Gysin, H.P.; "Critical Application of the Error Matrix Method for Localisation of Finite Element Modelling Inaccuracies"; Proceedings, 4th SEM International Modal Analysis Conference, Los Angeles, CA, 1986, pp1339-1343.

14. Ojalvo, I.U., Ting, T., Pilon, D. and Twomey, William; "Practical Suggestions for Modifying Math Models to Correlate With Actual Modal Test Results"; Proceedings, 7th SEM International Modal Analysis Conference, Las Vegas, NV, 1989, pp 347-354

15. Wei, Max L. and Janter, Theo; "Optimization of Mathematical Models Via Selected Physical Parameters"; Proceedings, 6th SEM International Modal Analysis Conference, Kissimee, FL, 1988, pp 73-79

16. Ewing, M.S. and Venkayya, V.B.; "Structural Identification Using Mathematical Optimization Techniques"; Proceedings, 32nd AIAA Structural Dynamics and Materials Conference; Baltimore, MD; April 1991; AIAA Paper 91-1135.

17. Ewing, M.S. and Kolonay,R.M.; "Dynamic Structural Model Modification Using Mathematical Optimization Techniques"; Proceedings, Computer Aided Optimum Design of Structures 91, Boston, MA, pp 285-295.

18. Gibson, Warren C.; "ASTROS-ID: Software For System Identification Using Mathematical Programming"; WL-TR-92-3100; September 1992.

19. "ADS - A FORTRAN Program For Automated Design Synthesis"; Vanderplaats, G.N.; NASA CR 172460; Oct 1984.

20. Johnson, E.H. and Venkayya, V.B.;" Automated Structural Optimization System (ASTROS), Volume I - Theoretical Manual"; AFWAL-TR-88-3028; December 1988.

21. Kobayashi, A.S., ed.; "Handbook on Experimental Mechanics"; Society For Experimental Mechanics, Prentice-Hall, 1987.

22. Abramson, Nils; "The Making and Evaluation of Holograms"; Academic Press, 1981.

Table 1
Modal Participation Factors for Full Scale Wing

Mode	Real	Imaginary	Magnitude	Phase (deg)
1	.9764	0.00	.9764	0.0
2	.2075	-.0494	.2132	-13.4
3	-.0173	.0309	.0354	119.2
4	.0040	.00002	.0040	.28

Table 2
Model Scale Factors

Length	1/10
Stiffness	1/10
Frequency	10
Mass	1/1000

Table 3
Natural Frequencies Before Mass Balancing

Mode	Experimental Frequency (Hz)	Predicted Frequency (Hz)	Mode Type
1	77.0	79.6	First Bending
2	227.9	226.6	Second Bending
3	262.2	261.9	First Torsion

Table 4
Natural Frequencies After Mass Balancing

Mode	Experimental Frequency (Hz)	Predicted Frequency (Hz)	Mode Shape
1	39.5	37.9	First Bending
2	127.3	118.7	Second Bending
3	164.9	150.0	First Torsion

Table 5
Modal Participation Factors For Aeroelastically Scaled Model

Mode	Real	Imaginary	Magnitude	Phase (deg)
1	.9799	0.00	.9799	0.0
2	.1907	-.0437	.1956	-12.91
3	-.0097	.0382	.0394	104.3

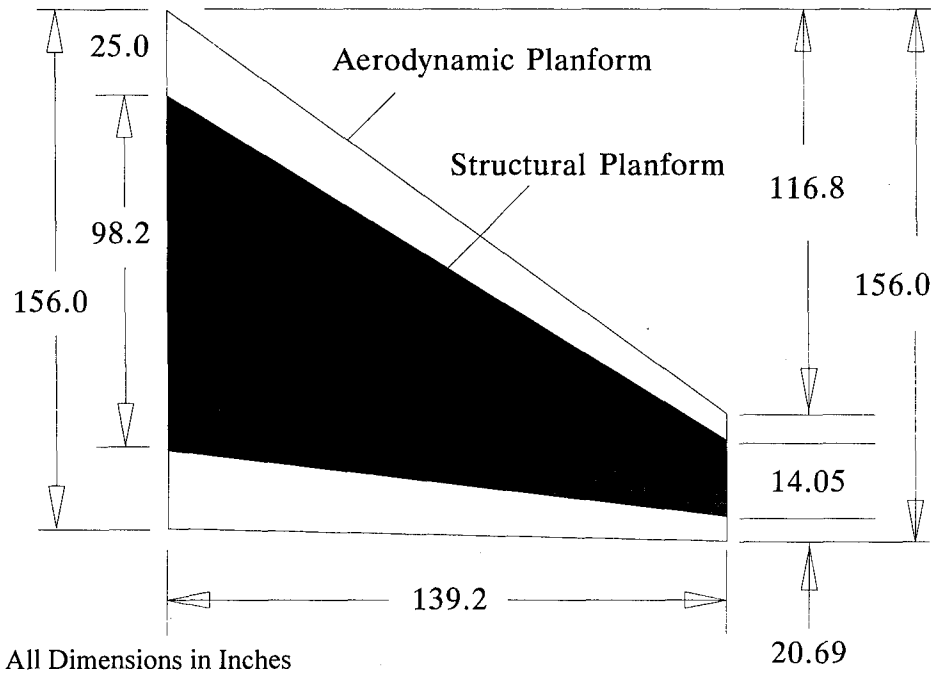

Figure 1 - Aerodynamic Planform of Full Scale Wing

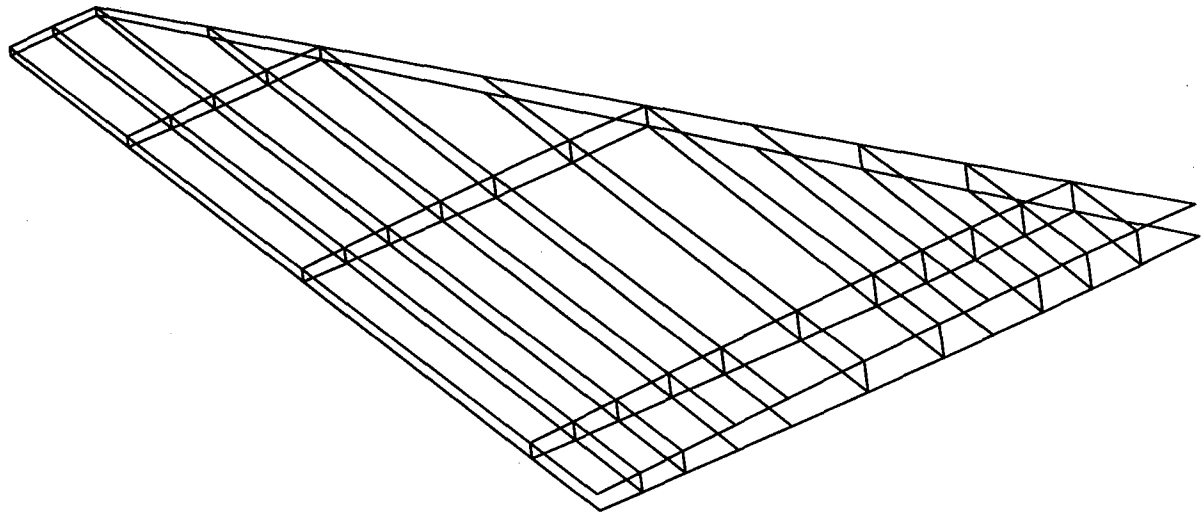

Figure 2 - Finite Element Representation of Full Scale Wing

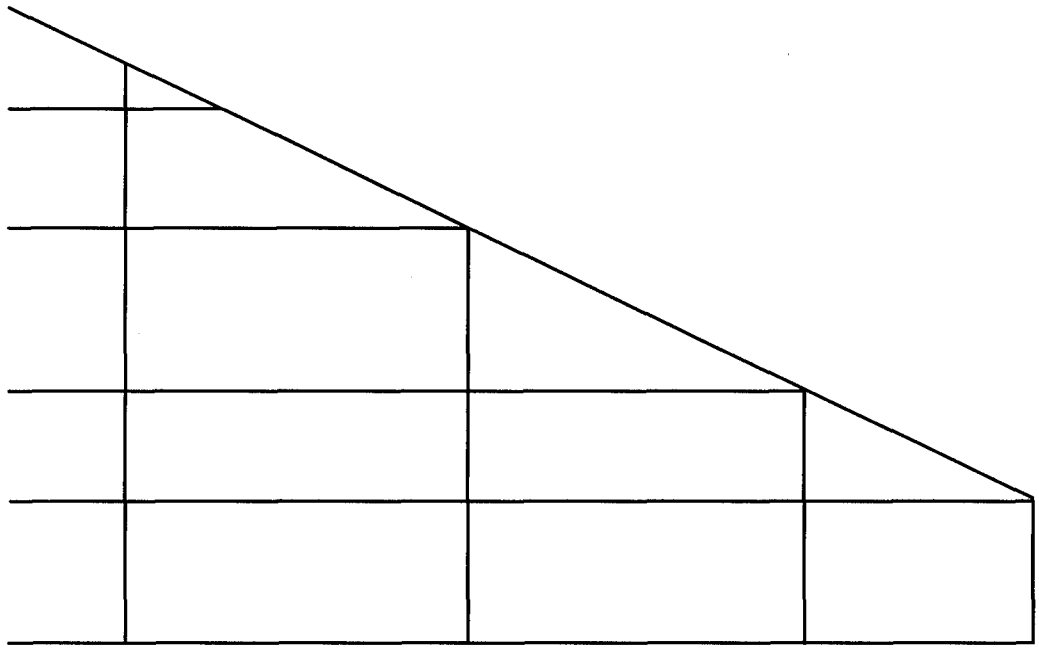

Figure 3 - Finite Element Representation of Scale Model

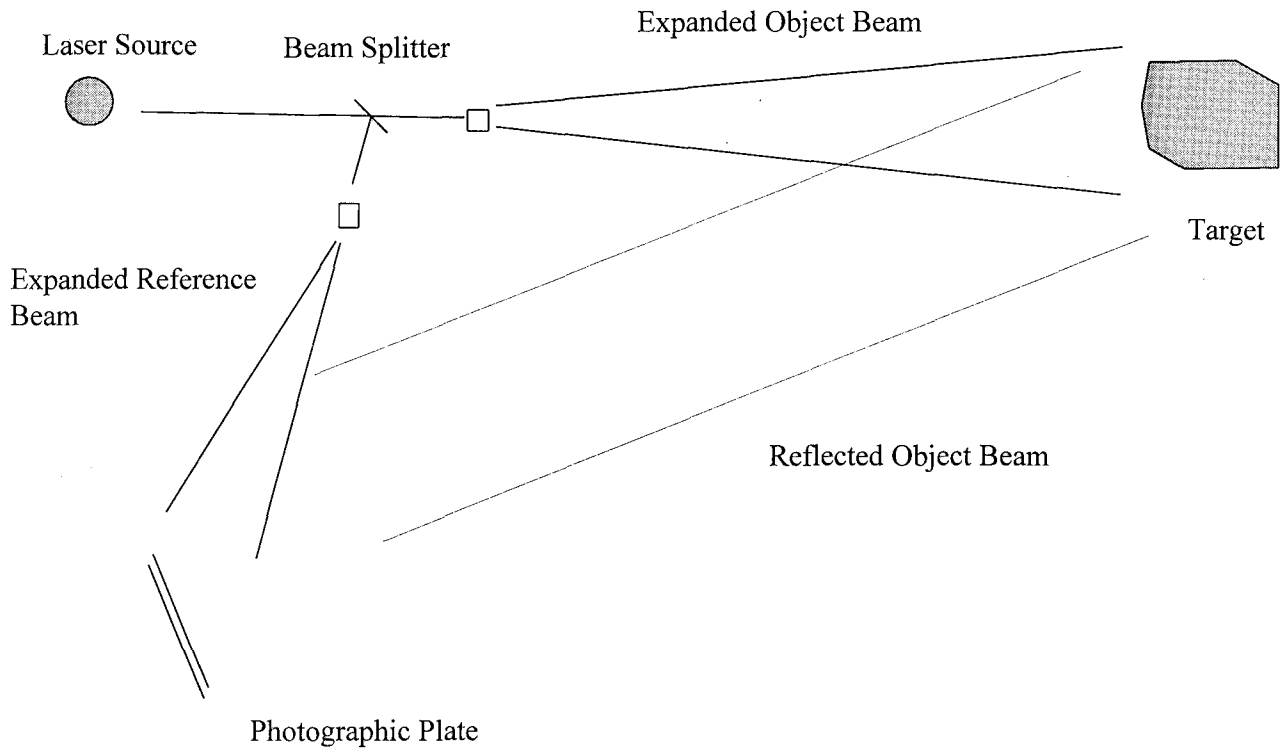

Figure 4 - Photographic Holography

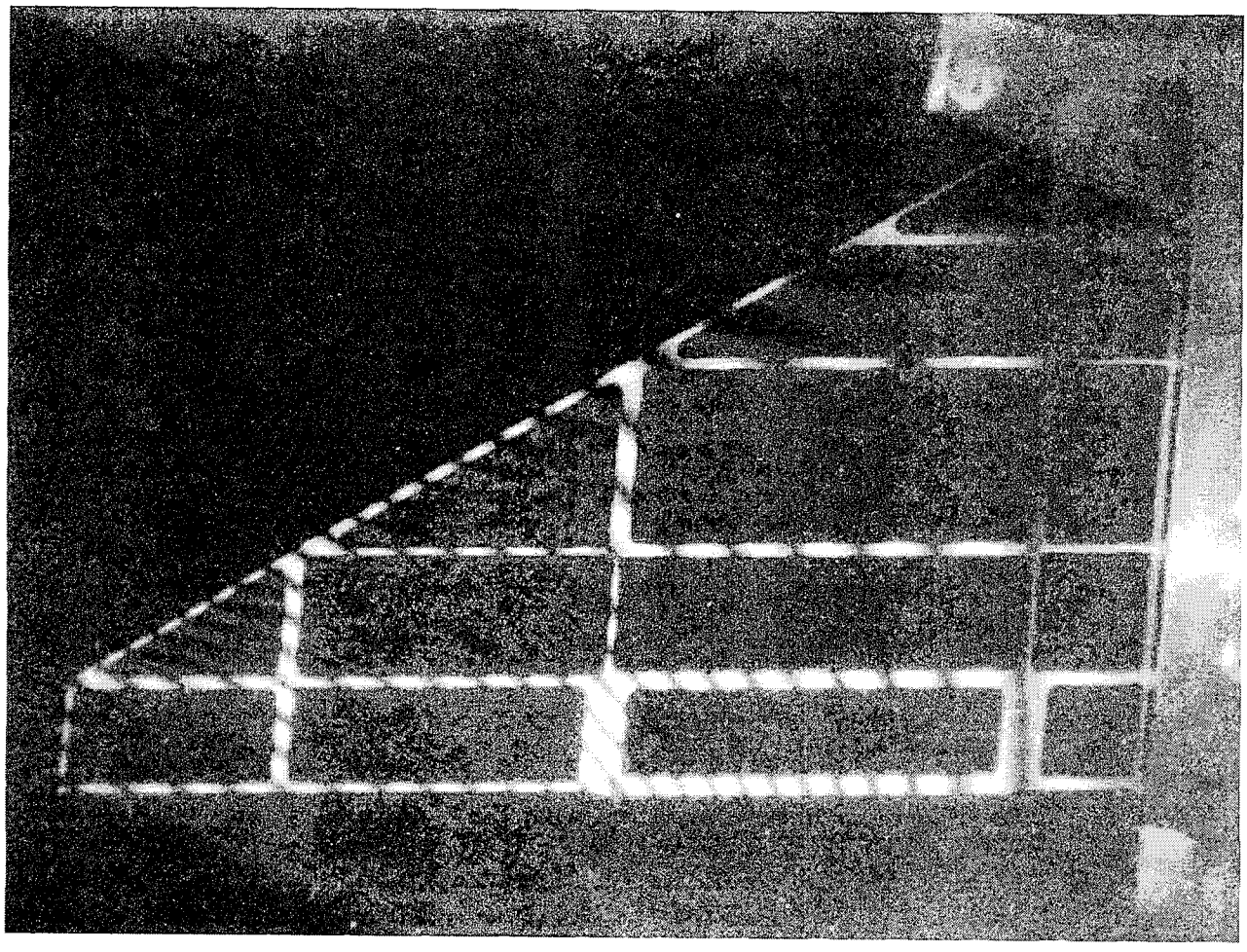

Figure 5 - Typical Double Exposure Hologram Showing Fringe Lines Due To Static Displacement.

WIND TUNNEL FLUTTER TESTING ON SHINGLES IN THE TRANSONIC AND SUPERSONIC SPEED REGIME

Albert J. Persoon
National Aerospace Laboratory, P.O. Box 90502
1059 CM, Amsterdam, The Netherlands

SUMMARY

Various types of shingles, being part of the heat protection system of re-entry vehicles, were investigated in the transonic and supersonic speed regime using NLR's High Speed (HST) and Supersonic (SST) wind tunnels. The investigations were carried out in close cooperation with Marcel Dassault Aviations (AMD) and Daimler Benz Raumfahrt Infrastruktur GmbH (DASA-RI).

A review is given of the wind tunnel experiments with emphasis on the generation and control of noise levels of the boundary layer in which the shingles were placed during the tests. The use of a spoiler or suction of the flow, both affecting the flutter characteristics of a shingle, will be discussed. The behaviour of unsteady pressures close to the shingle (upstream and downstream) is highlighted as these pressures might act as a monitoring device to define the onset of flutter or limit cycle oscillations of a panel.

1 INTRODUCTION

Since early 1990, the NLR department of unsteady aerodynamics and aeroelasticity is involved in flutter testing of prototype shingles, being part of the heat protection system of re-entry vehicles like the (proposed) European shuttle "Hermes" (Fig. 1). Flutter testing was carried out in close cooperation with Dassault Aviation (St. Cloud, France) and Daimler Benz Aerospace Raumfahrt Infrastruktur (DASA-RI, Bremen, Germany) formerly ERNO Raumfahrttechnik.
In the course of the test programme (presently MSTP) various types of shingles were investigated, namely thin aluminium pilot panels for prediction purposes and a ceramic one, manufactured by Dassault and flexible external insulation samples (FEI blankets) manufactured by DASA-RI.

The shingles of Dassault (Fig. 2a) basically consisted of thin aluminium panels of 30x30 cm^2 with a thickness of 0.7 mm to 1.3 mm, the latter being representative for the real ceramic (SI-C) shingle structure. The FEI blankets of DASA-RI (fig. 2b) were manufactured of heat resistant material covered by a coated woven top layer having dimensions of 25x25 cm^2.

Because of the vibrational characteristics of the shingles, local mass loading due to instrumentation during flutter testing was not allowed, but for monitoring purposes a miniature accelerometer or a straingage was used. During follow-up tests of FEI blankets laser equipment was applied for monitoring. The unsteady pressures upstream and downstream of a shingle were processed in more detail to evaluate a "decision criterion" for flutter onset as proposed by DASA-RI.

The main test facilities were NLR's transonic and supersonic wind tunnel (HST and SST) in which the prototype shingles were submitted to aerodynamic loads and to aeroacoustic loads, being the result of boundary layer noise. The results aimed to verify the aeroelastic (flutter) calculations of Dassault and the fatigue behaviour of FEI blankets estimated by DASA-RI.

These flutter tests are examples of aeroelastic wind tunnel testing which is rather complicated by the presence of aeroacoustic loads. They involve aspects of panel flutter and wind tunnel testing should therefore be carried out carefully.

It is the purpose of this paper to review these tests, while focusing on the realization of controlled aeroacoustic loads and appropriate measurement techniques. Further this paper deals with the preparation and execution of the flutter tests. Manipulation of boundary layer noise by suction of the flow or the use of a spoiler will be discussed as well as the use of unsteady pressures as a monitoring device for sustained oscillations of a panel. Finally, examples are presented of the flutter behaviour of an aluminium shingle (0.7 mm) and an FEI blanket.

Paper presented at the Structures and Materials Panel Specialists' Meeting on "Advanced Aeroservoelastic Testing and Data Analysis", held in Rotterdam, The Netherlands, from 8-10 May 1995, and published in CP-566.

2 SCOPE OF INVESTIGATIONS

The wind tunnel studies should reveal primarily the variation of natural frequencies and damping values of the shingles due to flow characteristics. The tests aimed to be a verification of non-linear flutter computations by Dassault (Ref. 1) as part of a study to the sensitivity of the shingles with aeroelastic coupling in the range of dynamic pressures (Q) up to 40 kPa at M=1.2 (Fig. 3). The aluminium shingles were therefore substitutes for the really to apply ceramic shingle, designed by Dassault as well.

For the FEI blankets (Fig. 4a, Ref. 2), the wind tunnel tests aimed to demonstrate the feasibility of FEI application on re-entry vehicles. Some blankets were first submitted to aging at high temperature and acoustic noise levels, resulting in a significant reduction of the mechanical properties. Such an aged blanket is assumed to be sensitive to fluctuating pressures (Fig. 4b) in a boundary layer. It had to be verified therefore that the soft woven top layer would not be damaged by a flutter type of instability up to dynamic pressures of 60 kPa at a Mach number of 2.65. The wind tunnel tests also served as a possibility to assess appropriate measurement techniques and to define a "decision criterion" for the identification of flutter onset (Ref. 3).

3 WIND TUNNEL FACILITIES

The high speed wind tunnel (HST) is a variable density closed-circuit wind tunnel with a test section of 1.6 to 1.8 x 2.6 m^2. The velocity regime ranges from M=0.2 to 1.25. The stagnation pressure can be varied between 12 and 390 kPa with a maximum dynamic pressure of around 40 kPa. The supersonic wind tunnel (SST) is of the blowdown type having a test section of 1.2 x 1.2 m^2. Compressed dried air (600m^3) of 4000 kPa (40 bar) is provided to range velocities from M=1.2 up to M=4.0. The maximum stagnation pressure is 1470 kPa; the running time varies between 12s and 40s.

4 TEST SETUP AND INSTRUMENTATION

The test setup in both wind tunnels was more or less similar. A specimen of each shingle was mounted in the floor of the test section (Fig. 5a,b). The test setup allowed to use different types of spoilers (rectangular, toothed, or "delta-wing" shaped) to increase the noise level in the boundary layer. On the contrary, the boundary layer thickness (in the HST) could be reduced by suction of the flow through pumps under the test section and a ventilated plate in front of the shingle (Fig. 5b,c). A (rectangular) spoiler caused a circulating flow above the shingle, with a maximum pressure (RMS) just behind the shingle (Fig. 5d, Ref. 5). An impression of the flow structure was obtained by pressure measurements on the floor of the test section of the HST (Ref. 6).

Close the shingle, pressure transducers were installed (Endevco 8514, 10PSI), measuring steady and unsteady pressures. They also acted as microphones to evaluate overall sound pressure levels (OASPL). Further, the aluminium shingles were provided with straingages and a small accelerometer whereas the FEI blankets only contained an accelerometer in the woven toplayer. The signals were fed into the data acquisition system "EGOIST" being similar for both wind tunnels and were real-time monitored by Fourier analysis.

5 WIND TUNNEL PREPARATIONS

Major part of the prepatory windtunnel work consisted of the accurate mounting of the various aluminium shingles in a "caisson" (tank) to avoid deformations (stresses) in the thin panel surface whereafter static loading test were carried out for straingage calibration. Next, the model was submitted to a modal survey to obtain natural frequencies and mode shapes. They appeared to agree with the modal parameters calculated by Dassault (Fig. 6).
Another point of concern in relation with aeroelastic computations dealt with the cavity effect of the caisson beneath the shingle, also discussed in reference 4. A closed cavity leads to a stiffening of the panel due to compressibility and an upwards shift of (mainly) the lowest natural frequency. Figure 7 shows some examples. Transfer functions (by a hammer test) of the 0.7 and 1.3 mm shingle are presented showing the frequency shift of the first natural frequency in case a sealing was applied around the shingle, closing the cavity.

The FEI blankets only required a verification of the "natural frequencies" of the woven top layer. No cavity effects were present as the complete blanket was glued on a stiff base plate. Mode shape measurements for a blanket had no meaning because of distinct stiffness differences in the top layer. Due to this fact a more or less local response could be expected in the boundary layer.

A modal analysis on FEI blankets would have been more useful when the base plate was able to deform in a realistic way, like the skin of a re-entry vehicle.

6 TEST PROGRAMME AND TEST PROCEDURE

The complete test programme covered a Mach number range from M=0.5 to M=1.2 (HST) and M=1.27 to M=3.12 (SST, Fig. 8). Although dynamic pressures of 40 to 50 kPa were required, the SST tests were carried out at higher dynamic pressures, from 57 to 107 kPa and two test runs at extremely high dynamic pressures of 181 and 212 kPa on request of DASA-RI to test the fatigue behaviour of the woven top layer of the FEI blanket.

The test procedure in the HST was based on entering the maximum dynamic pressure at a constant Mach number by increasing by steps the stagnation pressure (Fig. 8). Having attained a test condition where shingle responses remained stable, frequencies and damping factors were measured by a quick curve-fitter (SDOF) on power spectral densities of the panel acceleration or strain. For each new test sequence the stagnation pressure was lowered and the Mach number slowly increased.
In the supersonic speed regime (SST) the shingle response (FEI blanket) could only be monitored by the time signal of the accelerometer. Characterization of the response in terms of damping estimates was carried out by post-processing due to the short running time of the wind tunnel.

7 PRESENTATION OF RESULTS

From a large amount of data collected in the course of the various shingle tests, typical results are presented concerning the control of noise in the boundary layer (Figs. 9 to 11), the characteristics of unsteady pressures at sustained vibrations of a shingle (Figs. 12 to 14) and finally the flutter behaviour of an aluminium shingle (0.7 mm) and an FEI blanket (Figs. 15 and 16).

7.1 Control of noise in the boundary layer

Most of the shingle tests, especially the aluminium specimen, where carried out with boundary layer suction by which the boundary layer thickness was reduced in conformity with assumptions in the aeroelastic computations of Dassault. Also the effect of suction on the flutter characteristics of panels and FEI blankets was investigated. Various types of spoilers were used to generated higher noise levels to fit the ESA requirements. An example of noise levels obtained by different settings of the toothed spoiler from figure 5a is presented in figure 9. At a Mach number of about 0.8, an overall sound pressure level of about 161 dB, with reference to a pressure of 20 E-6 Pa, was reached. This level might have been even higher at a larger spoiler setting (>30 deg) but limitations were encountered in realizing the desired spectral energy distribution. As shown in figure 10, the maximum frequency level was highly dependent of the Mach number, or of the spoiler incidence introduced by a vortex shedding effect governed by some strouhal number. Increasing the free-stream Mach number yielded a linear frequency shift upwards, whereas a higher spoiler incidence led to a reduction of the frequency.
During wind tunnel testing therefore a compromise was needed in order to comply with the ESA requirements which prescribed a maximum noise level of 158 dB at about 500Hz and an overall noise level of 165 dB (Fig. 11a). Some typical results obtained in the HST (Fig. 11b,c) show pressure levels expressed in 1/1 and 1/3 octave bands (also Refs. 5,7). Although the distribution nearly fits the requirements, the overall sound pressure level was a few dB's lower, one of the limitations due to the chosen spoiler incidence.

Presently, a wind tunnel study is under progress at NLR in a continue supersonic wind tunnel (CSST) to overcome this limitation for future applications.

7.2 Unsteady pressures at shingle vibrations

As already mentioned DASA-RI proposed to evaluate a "decision criterion" for the onset of flutter by pressure monitoring in case a shingle could not be instrumented. The background lies in the assumption that a vibrating surface close to onset of flutter will influence the flow over a pressure sensor, located downstream, in such a way that the most significant frequency can be measured. Further it was discussed with DASA-RI that a difference of 10 dB (i.e. a factor of 3.2) in magnitude with the upstream pressure is the criterion by which sustained oscillations of the shingle certainly occur.
A post-analysis was therefore carried out of the pressures M1 (upstream) and M2 (downstream) at the 0.7 mm shingle test of Dassault (Fig. 12). First the time signals of both pressures are presented at a low dynamic pressure (Q=11 kPa) where no sustained oscillations were present (Fig. 12a). As can be observed, both pressure levels are nearly similar in magnitude, even with a spoiler (60 deg).
At the same Mach number but at higher dynamic pressures the shingle started to vibrate (Fig. 12b). In this case, the upstream and downstream pressures were affected by the vibrations of the shingle. Remarkable is the similarity of the shingle vibration (upper trace, Fig. 12b) and downstream pressure (lower trace) suggesting that the downstream pressure was fully dictated by the shingle oscillations (Fig. 13a).

Processing to RMS values of the first natural frequency components in the pressures (M1 and M2) indeed revealed a difference of 10 dB or more when sustained shingle vibrations occurred, which is shown in Fig. 13b. This figure shows a pressure difference of at least 10 dB at a dynamic pressure of 20 kPa, confirming the start of vibrations of the 0.7 mm shingle (as also shown in Fig. 15a). At a lower Mach number (M=1.1) no oscillations were detected and as a consequence only minor differences (< 10 dB) between the upstream and downstream pressures are present.
Thus, based on the present data, pressure monitoring seems to be an efficient means to adjust the onset of (unstable) vibrations if the panel vibrates in an overall mode.

This procedure failed however, when shingle responses were only local (FEI blanket). An example is shown in figure 14. Neither the upstream nor the downstream pressure show any response of the blanket. A reason might be the inappropriate location of pressure transducers or the very small amplitude ($5x10^{-3}$ mm) as measured during these tests.

7.3 Flutter behaviour of the shingles

The flutter behaviour of the 0.7 mm shingle where suction of the flow was applied, is presented in figure 15. The response of the shingle did not show a classical type of flutter but tended to a limit cycle oscillation. Without suction there were minor differences in frequencies and damping factors (Fig. 15a). The use of a spoiler (60 deg) which affected the boundary layer thickness, caused a stable behaviour at the same dynamic pressures. The sensitivity of a limit cycle oscillation to dynamic pressure increasing beyond 20 kPa was already predicted by Dassault (Ref. 1), and is illustrated in figure 15b.

Finally the flutter behaviour of an FEI blanket is presented in figure 16. When applying suction of the flow again minor differences in the characteristics are present (Fig. 16a). A spoiler has significant effects on the flutter behaviour resulting in much higher damping factors at lower frequencies (Fig. 16b). In the supersonic speed regime, the effects in the boundary layer on the frequencies are less. The amount of damping appeared to be high within the required Mach number range (with or without a spoiler).

8 FINAL REMARKS AND RECOMMENDATIONS

From point of view of verification of the aeroelastic and fatigue behaviour of different shingle types, the various flutter tests in HST and SST have reached this scope. Nevertheless limitations in the generated boundary layer noise are still present due to a device like a spoiler.
Appropriate measurement techniques were applied and the suggestion of DASA-RI to investigate the possibility of pressure monitoring was carried out. Pressures close to a panel, vibrating in an overall mode, can be used to define a "criterion" (10 dB) for flutter onset based on the present data.
For future applications it is recommended to use other means for noise generation in the boundary

layer to fit in with the ESA requirements. With that aim, a wind tunnel study is presently in progress at NLR. In one of the test runs an overall sound pressure level of 165 dB has already been reached (Fig. 17).

9 ACKNOWLEDGEMENT

The National Aerospace Laboratory will acknowledge the fruitful discussions and nice cooperation during wind tunnel testing with Mrs. A.L. Georges and Mr. E. Garriques of Marcel Dassault Aviation (St. Cloud, France) and with Mr. J. Bolz and Mr. N. Schummer of DASA-Raumfahrt Infrastruktur (Bremen, Germany).

10 REFERENCES

1 Georges, A.L., "Aeroelastic non-linear study for HERMES shingles", Dassault Aviation, International Conference Aeroelasticité et dynamique de structures 1993 Stasbourg.

2 Keller, K., Antonenko, J., Weber, K.H., "High-temperature insulations", ESA Bulletin 80, November 1994.

3 "Flutter test at NLR HST facility", test specifications, MBB/ ERNO, December 1991.

4 Dowell, E.H., "Panel Flutter: a review of the aeroelastic stability of plate and shells, AIAA journal, Vol. 8, March 1970.

5 Paret, A., "Essais acoustique et aeroacoustique des tuiles de la protection thermique d'Hermes; Dassault Aviation, Int. conf on acoustic and dynamic environment of space transportation systems; Jouy-en-Josas, 8-11 February 1994.

6 Persoon, A.J., Rohne, P.B., De Groot, L.F.J., "Measurement of steady and unsteady pressures in an airflow controlled by spoilers, NLR CR 92105 L, 1992.

7 Persoon, A.J., Rohne, P.B., De Groot, L.F.J., Dogger, C.S.G., "T2 flutter tests on FEI blankets in NLR's HST and SST wind tunnels, NLR CR 94054 L, 1994.

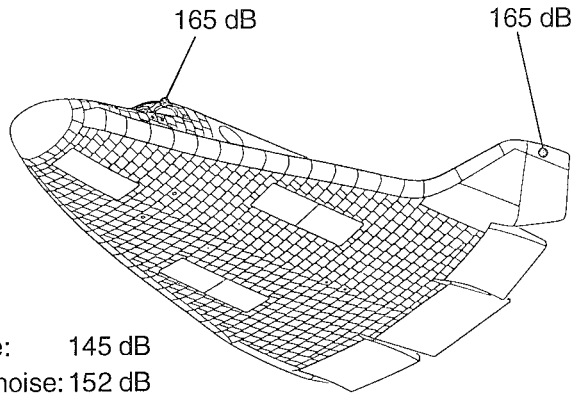

Fig. 1 Hermes thermal protection system design with (aero)acoustic noise levels (from ref. 1)

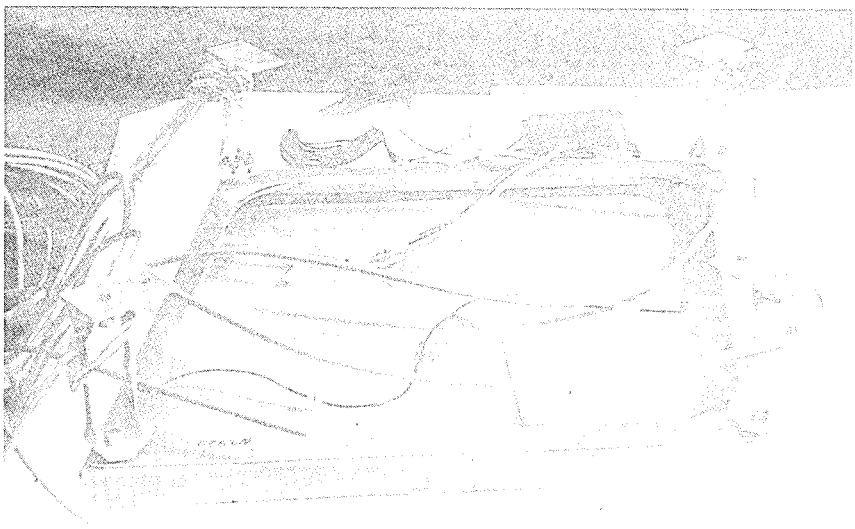

a) aluminium shingle (Dassault)

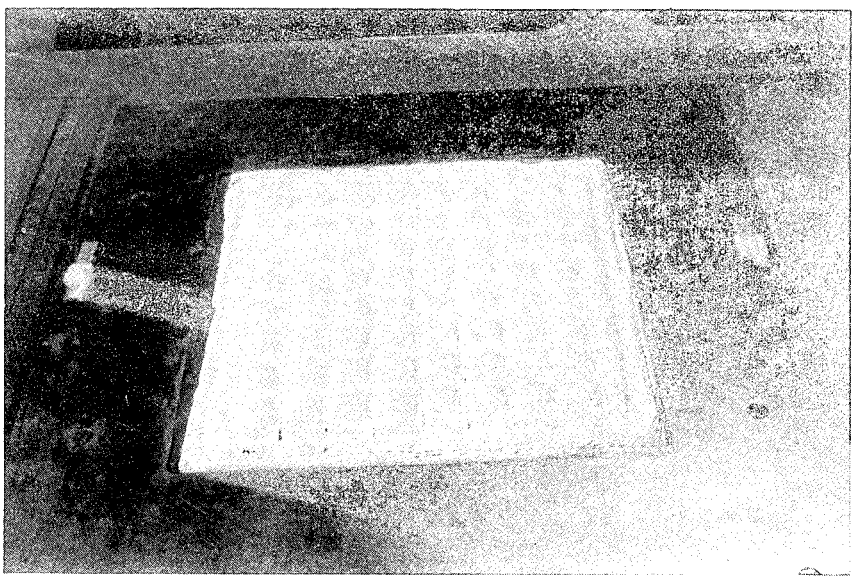

b) FEI blanket (DASA-RI)

Fig. 2 Shingles used for flutter testing

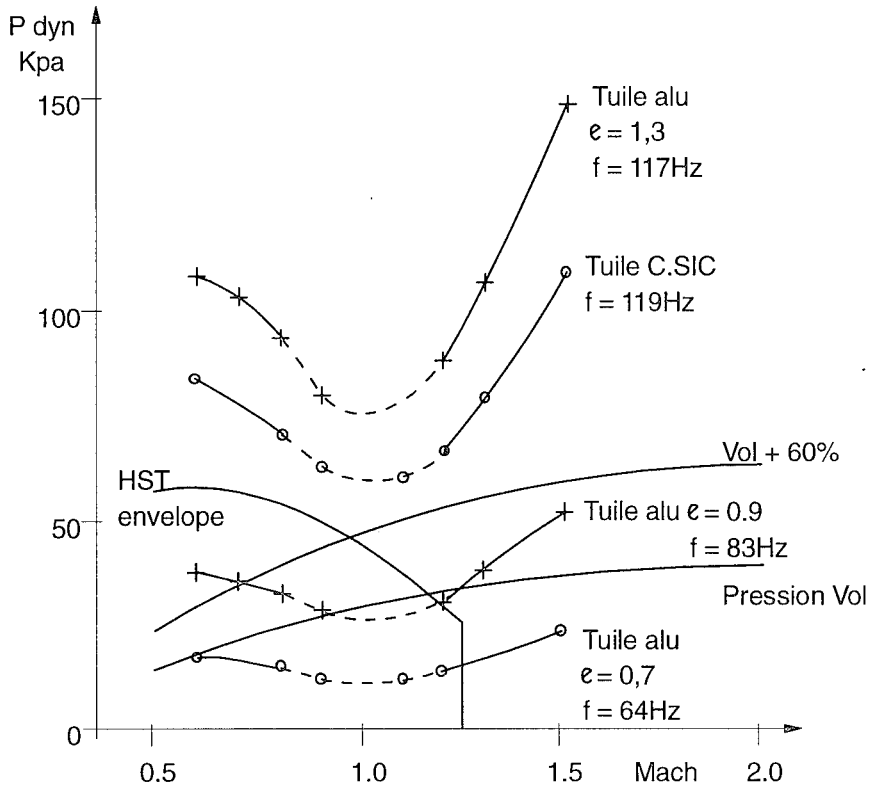

Fig. 3 Critical conditions of aeroelastic coupling for aluminium shingles predicted by Dassault (Ref. 1)

a)

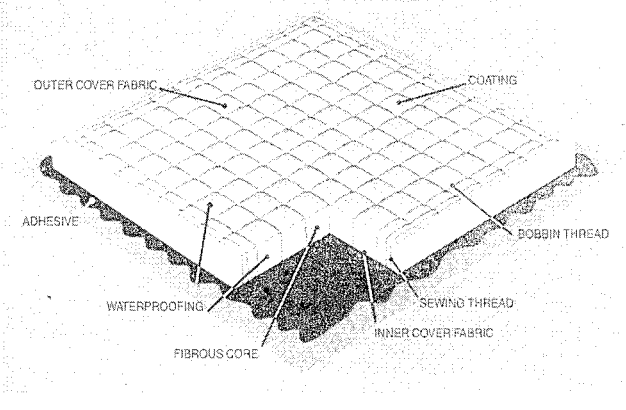

b)

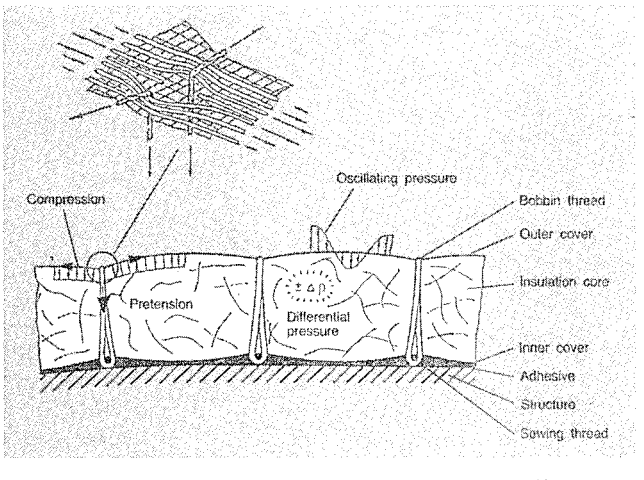

(from ref. 2)

Fig. 4 Concept of FEI blanket (a) and schematics of structural loads (b)

a)

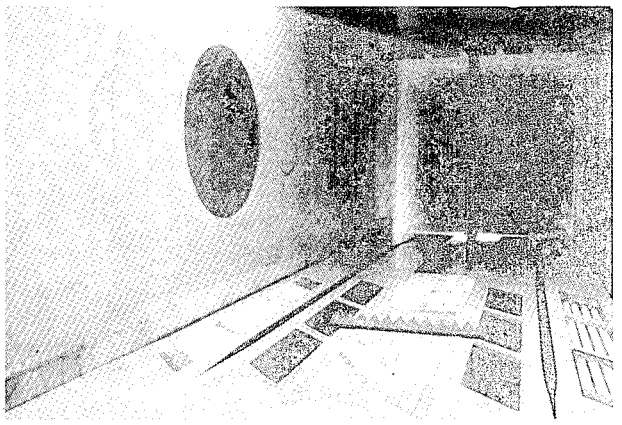

b)

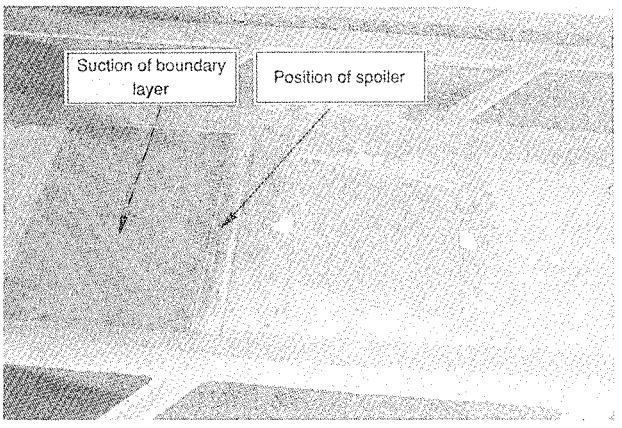

c)

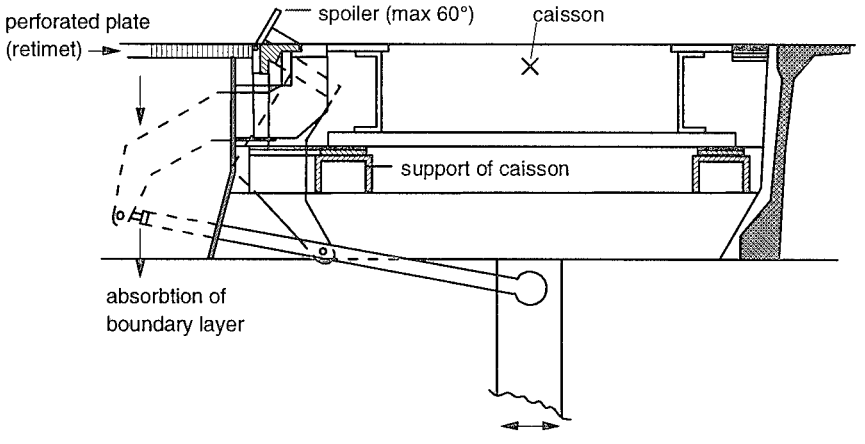

d)

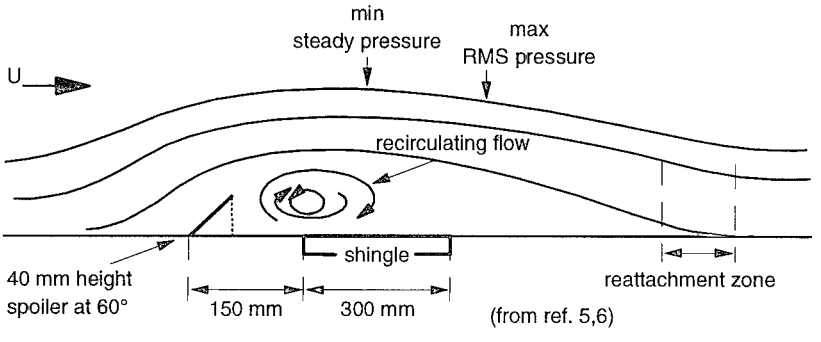

Fig. 5 Test set up of a shingle in the HST

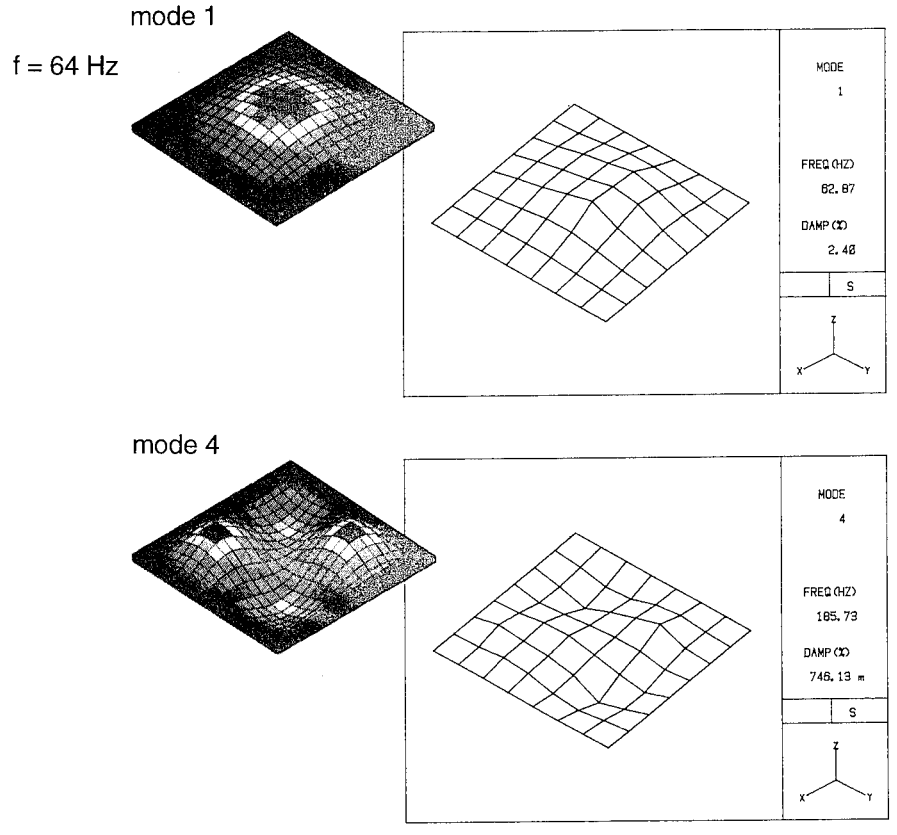

Fig. 6 Examples of mode shapes (0.7mm shingle) as computed by Dassault and measured by NLR

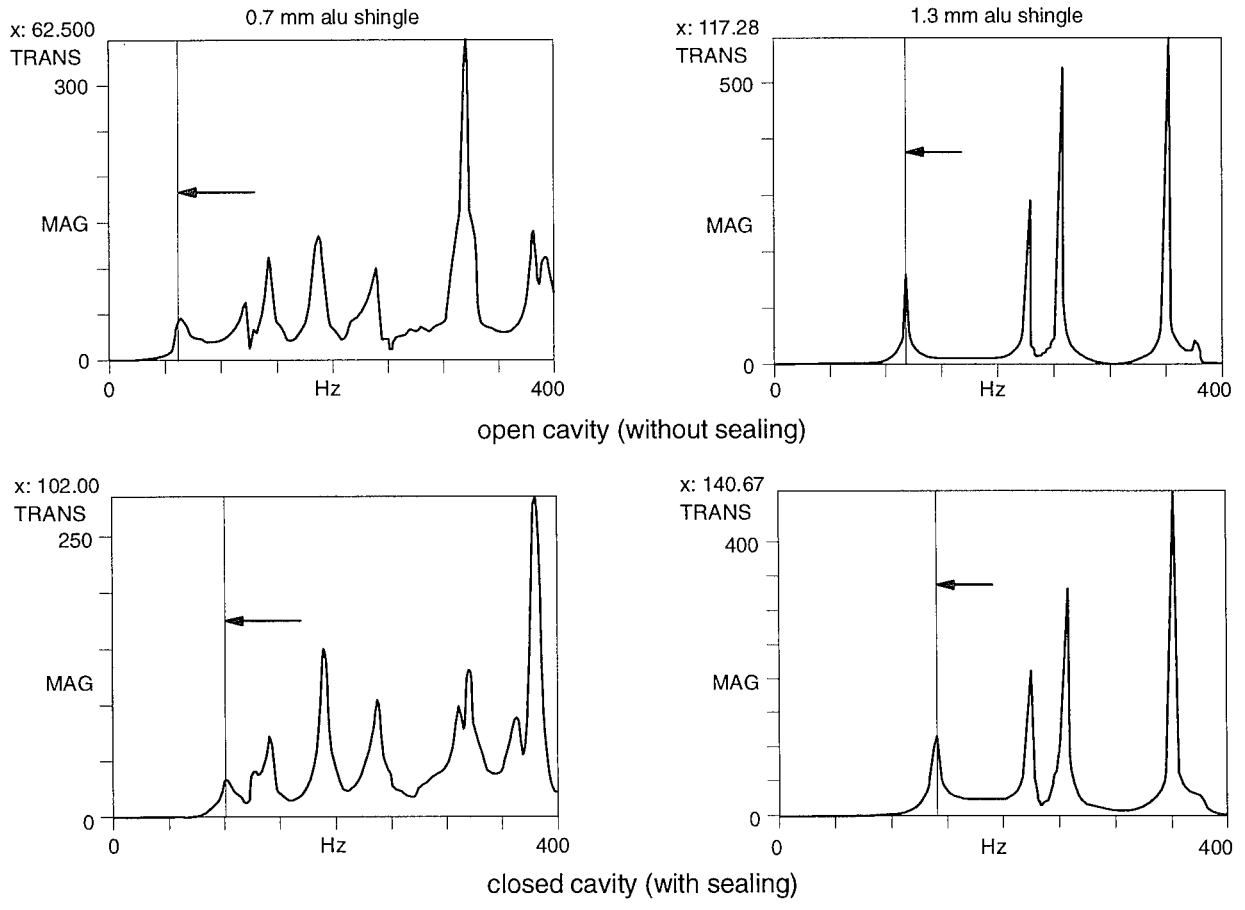

Fig. 7 Cavity effect on the lowest natural frequency for 0.7 mm and 1.3 mm shingle

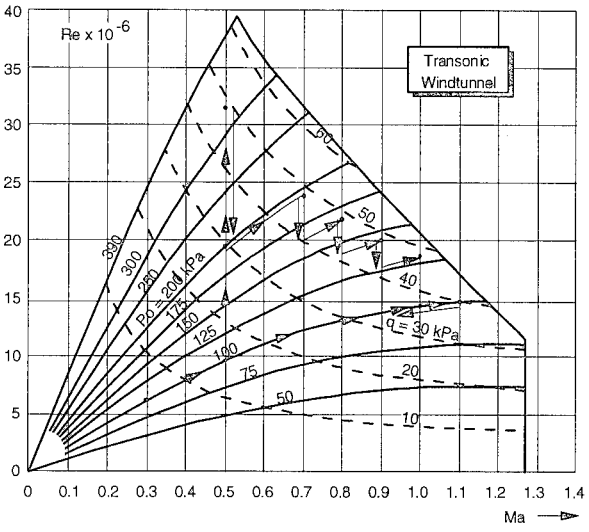

a) Transonic speed regime (alu shingles and FEI blankets)

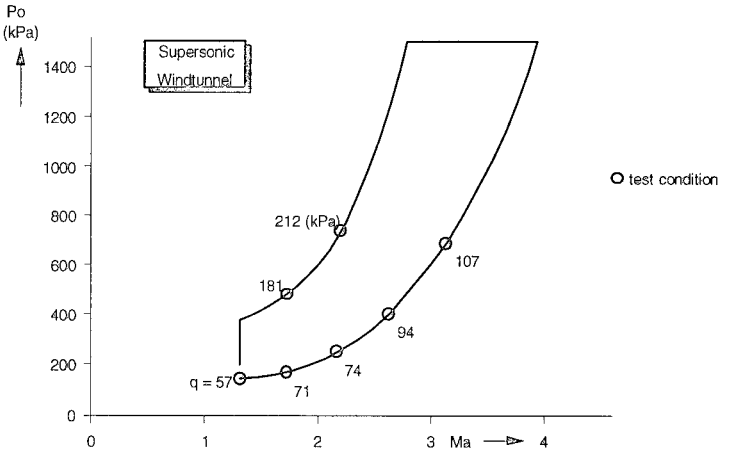

b) Supersonic speed regime (FEI blankets)

Fig. 8 Test envelope of HST and SST and example of test procedure (HST)

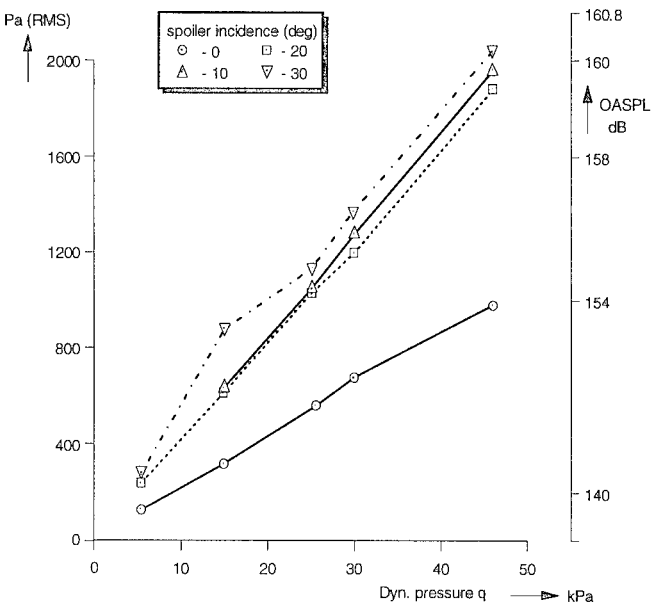

Fig. 9 Unsteady pressure (Pa) at shingle position (Ma < 0.8) at different spoiler settings (HST) and sound pressure level (OASPL)

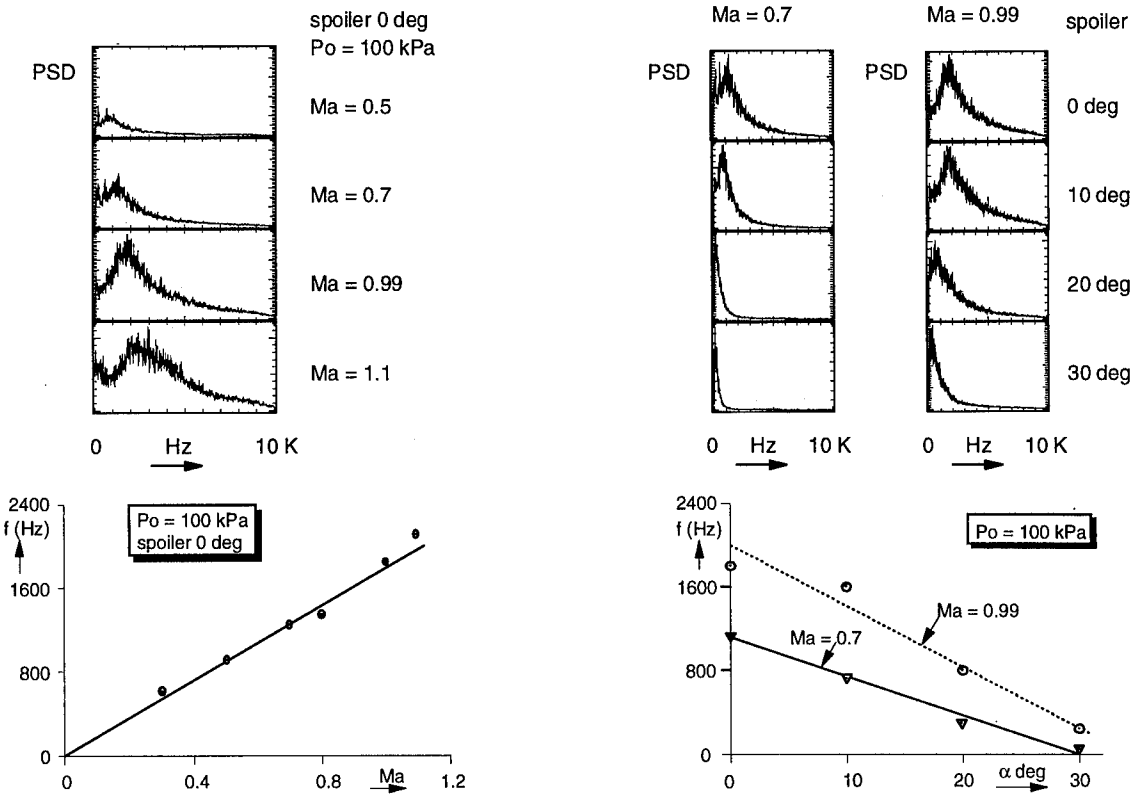

Fig. 10 Effect of mach number (left) and spoiler incidence (right) on spectral energy distribution of a pressure at the shingle position (ref. 7)

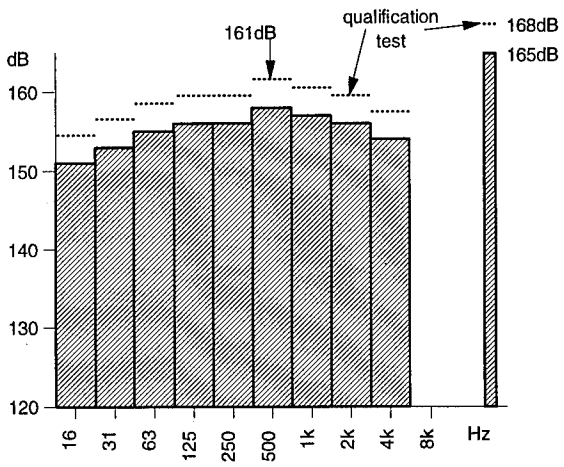

a) 1/1 octave spectrum (ESA requirement)

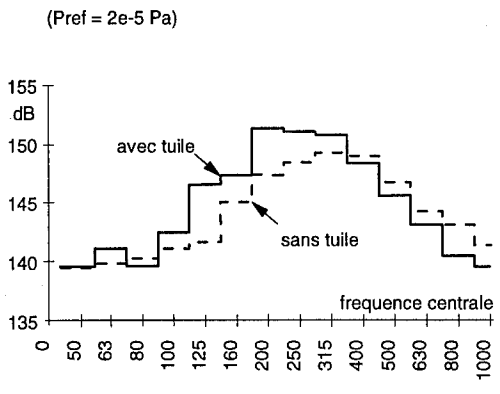

b) 1/3 octave spectrum Ma = 0.7 Q = 30kPa (from ref. 5)

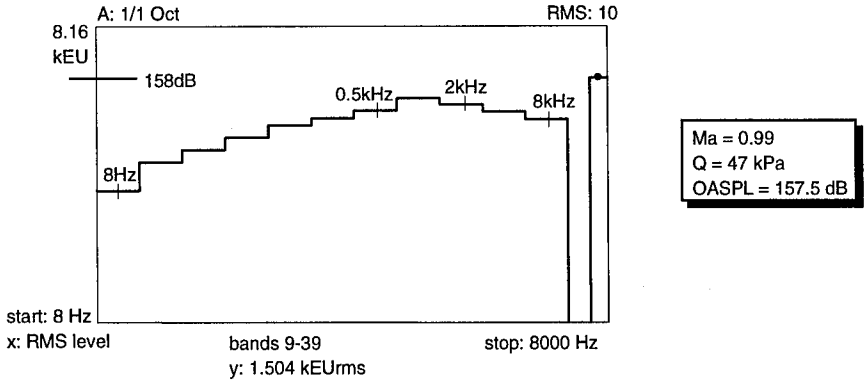

c) 1/1 octave spectrum Ma = 0.99 Q = 47 kPa (from ref. 7)

Fig. 11 Octave measurements of pressures

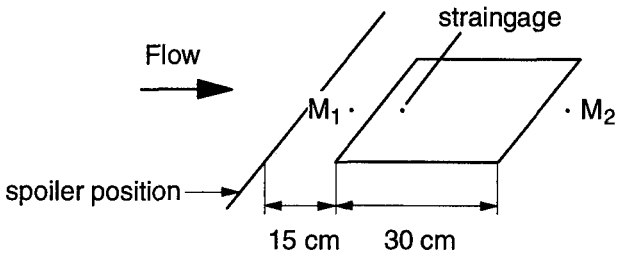

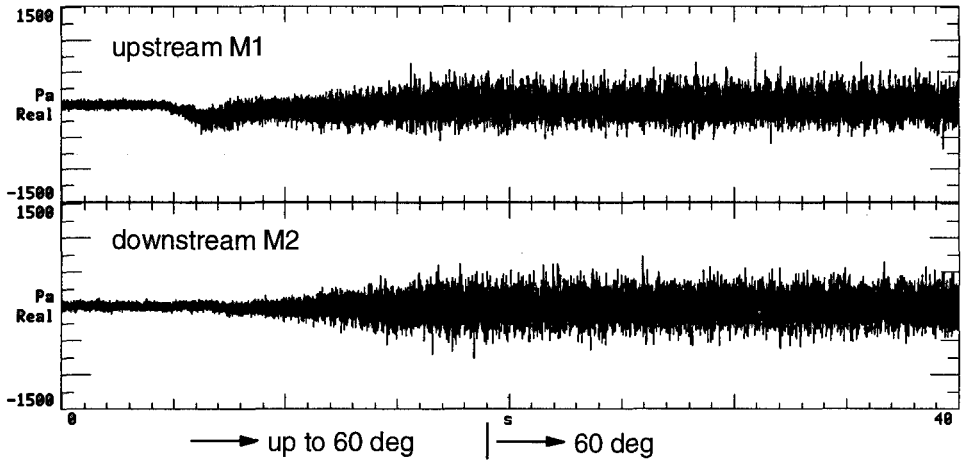

a) Effect of a spoiler (Ma = 1.2, Q = 11 kPa)

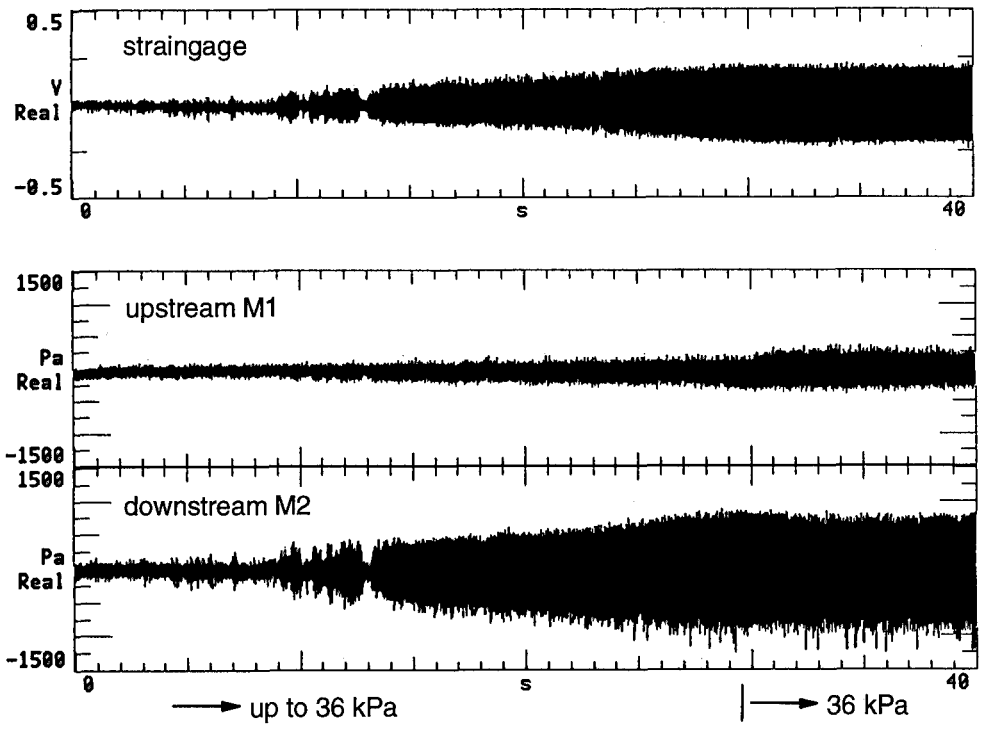

b) Effect of dynamic pressure (Ma = 1.2, Q up to 36 kPa); no spoiler

Fig. 12 Behaviour of pressures M_1 and M_2 at Ma = 1.2 (HST)

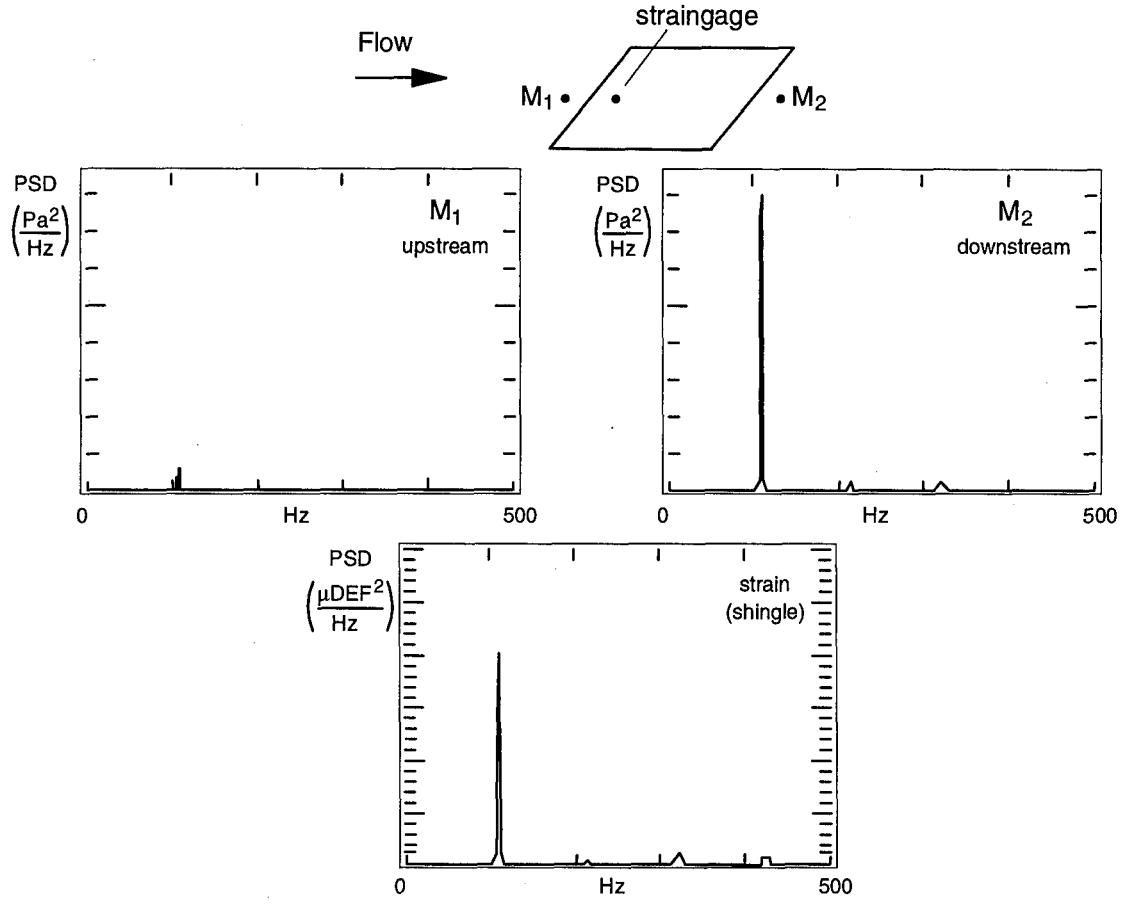

a) PSD of pressures and strain at Ma = 1.2, Q = 35.6 kPa

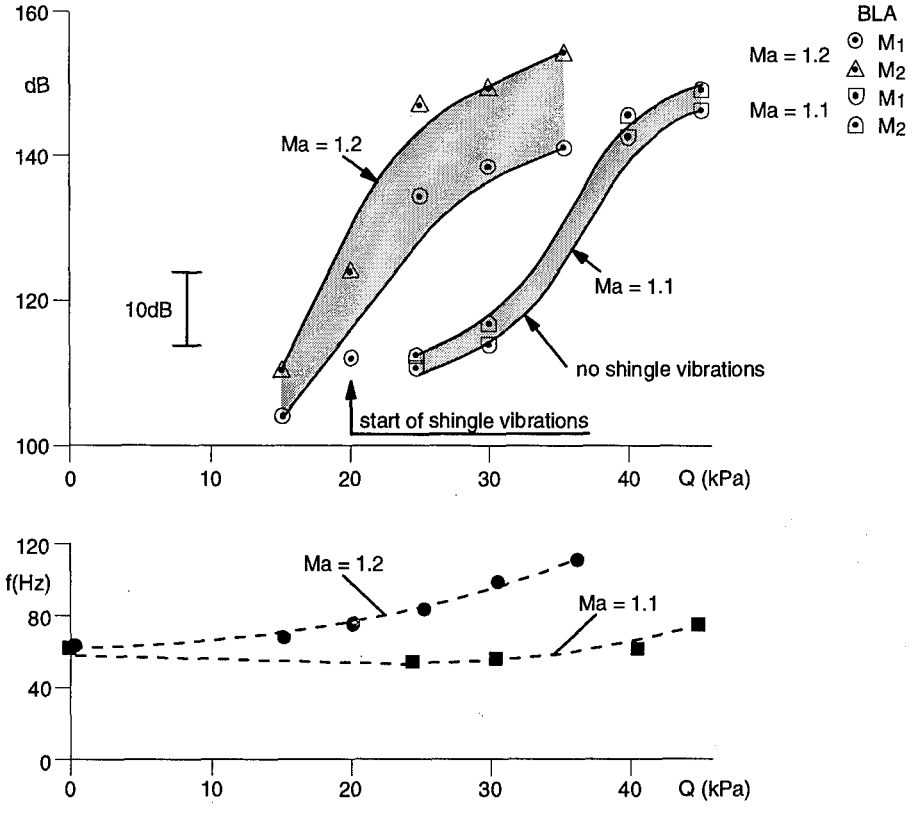

b) Pressure difference of M_1 and M_2 at the shingle first frequency

Fig. 13 Confirmation of a "decision criterion" for flutter onset by pressure monitoring as proposed by DASA-RI

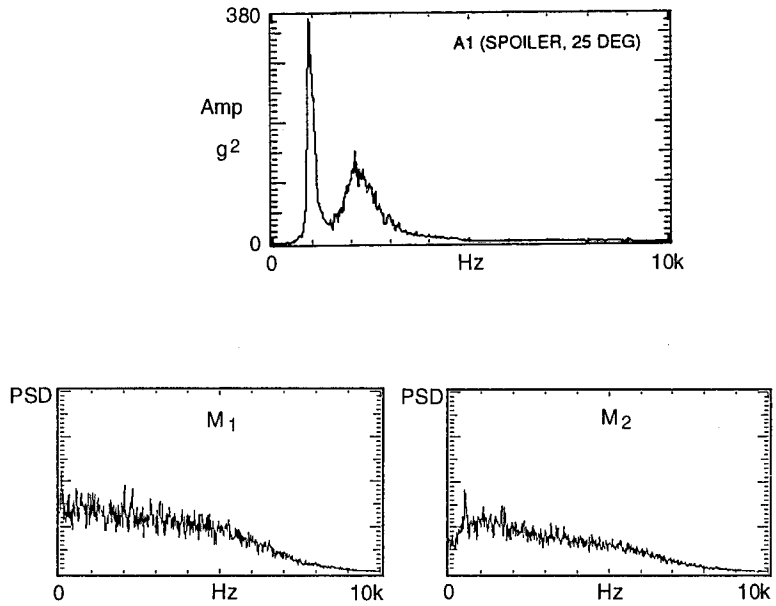

Fig. 14 Response of FEI blankets in SST (Ma = 2.18) and character of upstream and downstream pressure (M_1 and M_2)

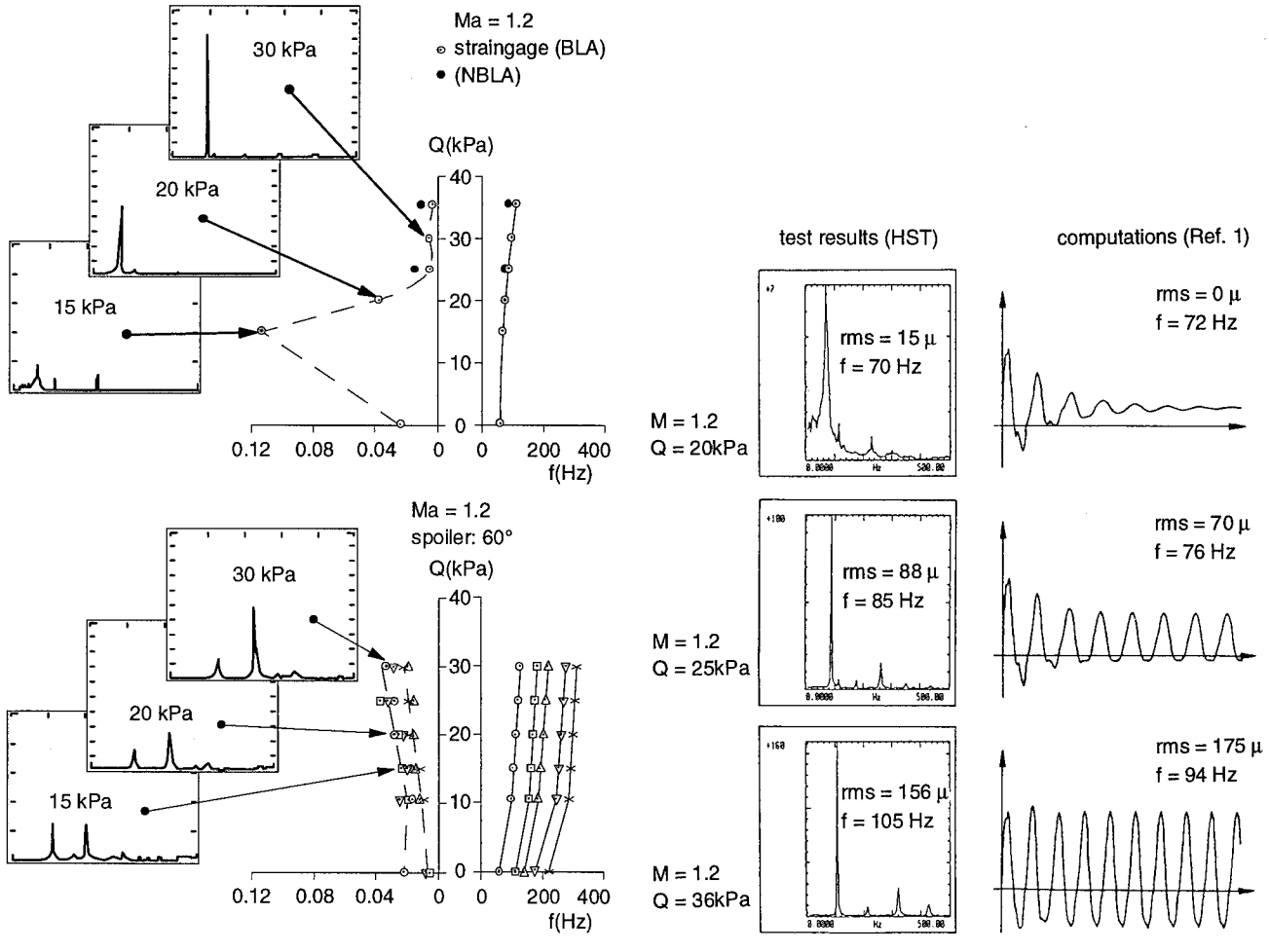

a) Flutter diagrams of 0.7 mm shingle at Ma = 1.2 without and with spoiler

b) Test results of 0.7 mm shingle and aeroelastic computations (from ref. 1) for comparison

Fig. 15 Flutter characteristics of the 0.7 mm aluminium shingle obtained by HST tests

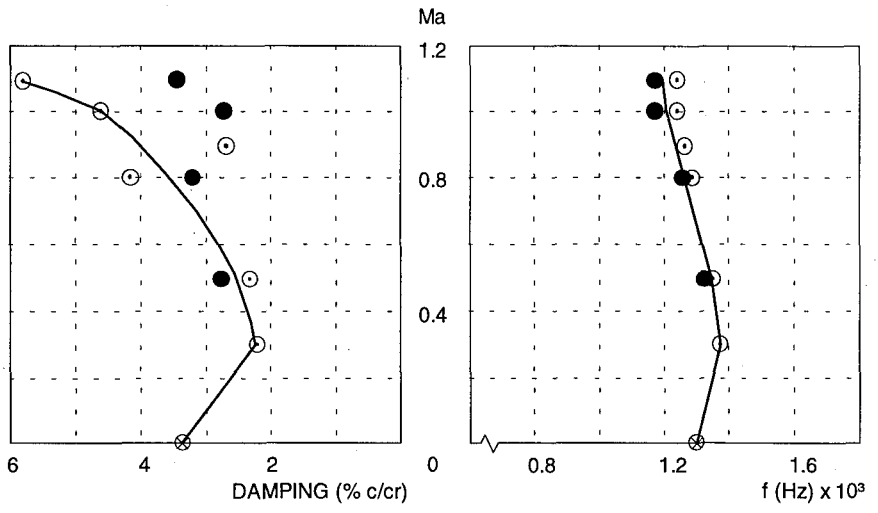

a) FEI blanket in HST at Po≈100 kPa (Boundary layer suction: ⊙ -on, ● -off)

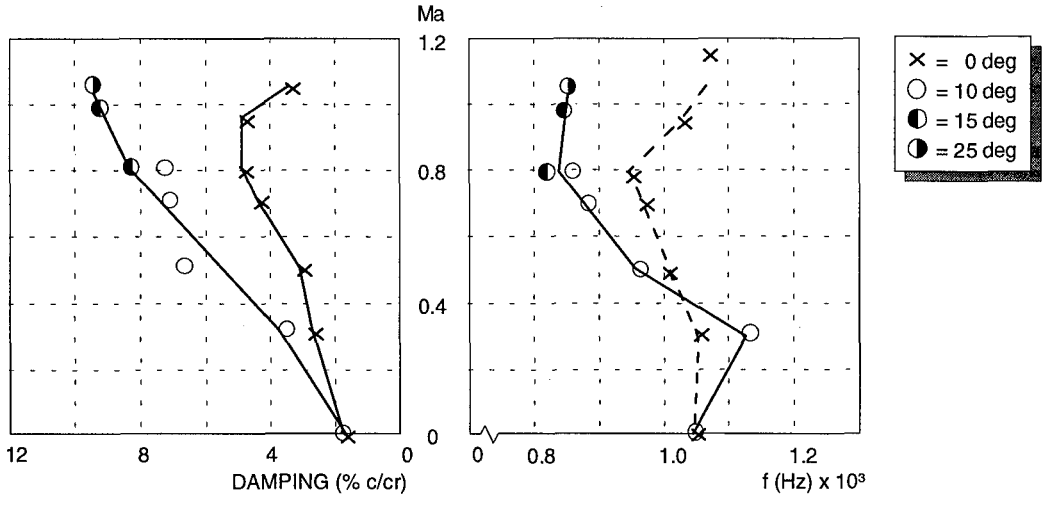

b) FEI blanket in HST at Po≈100 kPa without and with toothed spoiler

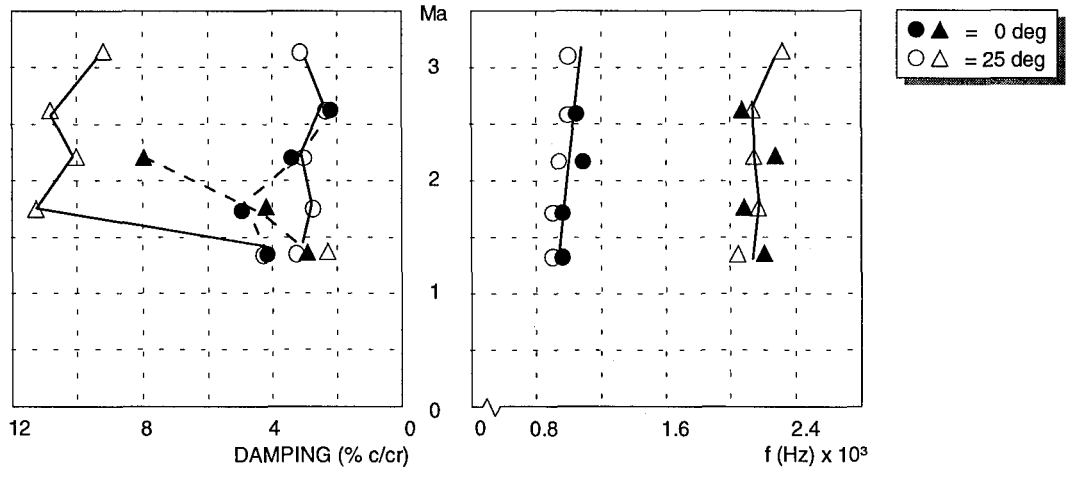

c) FEI blanket in SST without and with delta spoiler

Fig. 16 Flutter characteristics of FEI blanket obtained in HST (a,b) and SST(c) by acceleration measurements

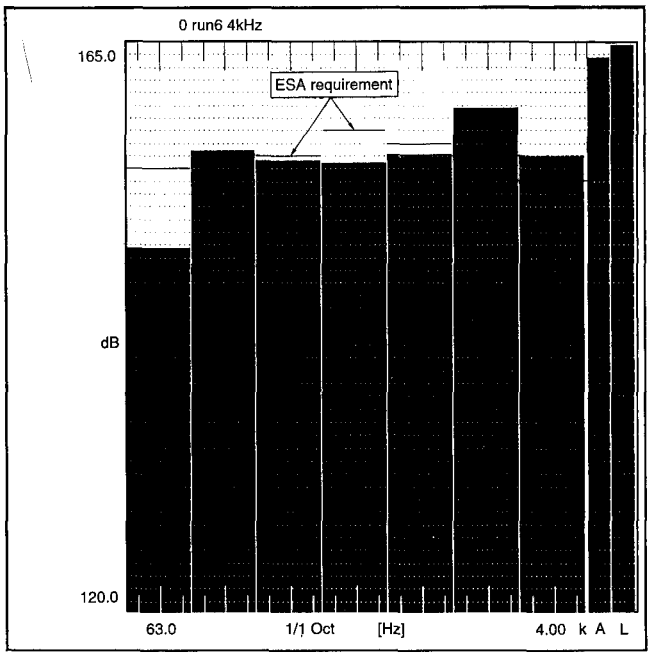

Fig. 17 Octave presentation of sound pressure levels in NLR's CSST windtunnel and comparison with ESA requirements (OASPL 165dB)

PARAMETER ESTIMATION METHODS FOR FLIGHT FLUTTER TESTING

J.E.Cooper
School of Engineering
University of Manchester
Manchester, M13 9PL, UK

1. SUMMARY

This article presents a review and assessment of the various techniques that have been used to estimate modal parameters from flight flutter test data. The relative advantages and disadvantages of the methods are examined, with particular emphasis being given to their suitability for analysing flutter test data. The problems associated with analysing non-linear and aeroservoelastic test data are highlighted. Recent advances in modal parameter identification are considered in terms of their relevance to flight flutter testing. Finally, future requirements for the analysis of flight flutter test data are discussed.

2. INTRODUCTION

Flight flutter testing is the critical part of the test programme of any prototype aircraft [1-3]. No matter how much aerodynamic and structural analysis, and wind tunnel and ground vibration testing that has been undertaken, there is always the possibility of some unpredicted aeroelastic behaviour occurring. It is a requirement to demonstrate that flutter does not occur throughout the flight envelope, and civil aircraft manufacturers typically need to demonstrate a flutter free aircraft up to a speed of 1.2 times the design dive speed. A common feature of all flutter tests is that there is pressure to complete the test as quickly as possible, however, due to the potentially catastrophic consequences of flutter, a safety first attitude to testing must be taken. Thus the ability to produce accurate frequency and damping values is crucial to the entire process, not only from the safety point of view, but also because having confidence in the estimated parameters will enable the flight envelope to be cleared more quickly.

The classical sub-critical approach to flight flutter testing is to: expand the flight envelope by performing a vibration test at constant flight conditions, curve-fit the data to estimate frequencies and dampings and, plot the frequencies and dampings against flight speed or Mach number. The damping values are then extrapolated in order to determine whether it is safe to proceed to the next test point. It is well known that the damping is the most difficult parameter to estimate accurately, as well as being the most sensitive to noise, measurement errors, etc. Unfortunately the most critical parameter in flutter testing is the damping, and therefore it is essential that damping is estimated as accurately as possible.

The curve-fitting techniques used to provide estimates of frequencies, dampings (and sometimes mode shapes) from flight flutter test data have generally been developed for modal analysis applications, such as ground vibration tests. However, there are substantial differences between the set-ups for tests performed on the ground as compared to those undertaken in the air. Substantially fewer transducers are used for flight tests and there are often significant problems involved in putting sufficient excitation energy into the airborne structure over the frequencies of interest.

A further important difference is that, in general, the amount of noise corruption in a ground test is very small and tends to consist of measurement noise. In flight flutter testing, however, there is often a considerable noise content due to turbulence, which passes through the system and therefore corrupts the measured responses in a different manner to that of measurement noise. Nevertheless, most parameter estimation techniques are formulated to minimise some error function based on noise corrupting the output data sequences. The problem of turbulence along with the difficulties in exciting the aircraft, make the task of estimating accurate modal parameters less than straightforward. It is essential to get as much energy into the structure as possible, as the resulting signal/noise ratios will be high and the task of estimating accurate modal parameters made easier.

Most parameter identification methods are used with the assumptions that the modal parameters remain constant throughout the duration of the test, and also that the structure is linear. This first assumption can be difficult to achieve where there are problems maintaining a steady flight condition, particularly towards the outer edges of the flight envelope. The linearity assumption can also be a poor approximation in flight testing, particularly where there is an active control system in operation, or if there are non-linear effects, or even when the excitation is provided via a control surface.

In the aerospace industry, the most common approach to performing a ground test is to use phase resonance methods whereby the structure is excited at a particular

Paper presented at the Structures and Materials Panel Specialists' Meeting on "Advanced Aeroservoelastic Testing and Data Analysis", held in Rotterdam, The Netherlands, from 8-10 May 1995, and published in CP-566.

resonance frequency and the amplitudes of the inputs are tuned in some manner until a normal mode is obtained. However, the shaker and control requirements of such methods has meant they have not been considered suitable for flutter testing. Their use is currently being reassessed [4]. Another development in this area is that of spatial filters [5], that are used to extract the response of individual modes through the manipulation of the responses to a number of inputs. A common application of this principle is the addition and subtraction of responses to remove symmetric or anti-symmetric modes.

So, it is usual to employ phase separation techniques for flutter testing, and this is the category of analysis methods concentrated upon in this work. The aircraft is excited over the required range of frequencies using either a random, chirp or impulsive input, and the data curve-fitted to estimate the modal parameters within that frequency range.

A number of comparisons of various parameter estimation techniques have been made over recent years on simulated and ground test data [6-12]. There is little indication as to which are the best methods on complex real structures as the truth is not known. One observation that can be made, however, is that engineers who have experience in using a particular test or analysis method will produce more accurate modal parameter estimates that those who do not. The comparative study on the Galileo Spacecraft [13] demonstrated the problems that are involved. The investigators could not even agree on the number of modes that were present, let alone what the correct values of the frequencies and dampings were. It has been suggested [9] that comparisons of various methods can be biased by the expertise of whoever is performing the test. Indeed, unbiased comparisons can sometimes be as hard to find as unbiased parameter estimates. There is a proposed round robin GARTEUR activity starting in 1995 to compare the numerous excitation techniques and analysis methods available for ground vibration testing.

There are far fewer comparisons of modal parameter estimation methods using flight flutter test data [14-18]. Reviews of the techniques used can be found in refs [19-27]. The scarcity of comparisons is partly due to the aerospace industry being extremely reluctant to publish the results of any flutter analysis that has been performed. A consequence of this unwillingness is that there is still no clear indication as to which techniques are most suitable for the analysis of flutter test data.

In this paper, parameter estimation techniques that have been used by the aerospace industry for flutter clearance will be reviewed. The relative merits and disadvantages will be discussed with particular emphasis on their suitability for analysing flight flutter test data. Some of the more recent advances in parameter estimation are considered in terms of their relevance to flutter clearance, and suggestions are made for areas where further work is required.

There has been little AGARD activity in this field since the papers by Koenig in 1983 [15,16] where different modal parameter estimation methods were compared on flutter data from a civil aircraft. It was concluded that '..the state of the art of system identification methods was insufficient for flutter testing.' This review paper, and indeed the proceedings of which it is part, will show how technology has advanced in twelve years, and will consider whether modal parameter estimation is now sufficient for flutter testing.

3. MODAL PARAMETER ESTIMATION

Parameter estimation, or system identification, methods have been developed for use in a wide variety of applications [28,29]. Essentially, a mathematical model relating inputs to outputs is taken, and data curve-fitted in order to estimate the coefficients of the assumed model. For flight flutter testing, and vibration testing in general, the input is a forcing term and acceleration generally taken as the measured output quantity.

It is assumed that controllability and observability are satisfied, ie. the modes of interest are adequately excited and that the measurement transducers are positioned correctly to capture the response. The vast majority of parameter estimation methods are intended for use on systems where linearity holds and also where the modal parameters of the system do not vary during the data acquisition period. In the modal analysis community it is considered superior to perform a 'global' curve-fit, simultaneously using data from a number (often large) of shakers and transducers (a multiple-input multiple-output (MIMO) approach). Such an approach is not recommended for flight testing, as there is a likelihood of there being a wide scatter of damping, and even frequency, estimates between individual transducers. Apart from the few studies making use of mode shape information [30,31], the methods are all intended to be used in a single-input single-output (SISO) formulation.

The following sections are by no means an exhaustive survey of modal parameter estimation methods, but review the techniques used for flutter testing in recent years and discuss their relative merits. The interested reader is directed to refs [6-9,32]. Unless otherwise stated, all of the methods are intended for use on systems that are linear and time-invariant. The methods are classified depending upon whether the curve-fit is performed using frequency domain or time domain

data, and also whether the fitted mathematical model does not allow for interaction between modes (a single degree of freedom (SDOF) model) or makes allowance for coupled modes of vibration (a multiple degree of freedom (MDOF) model.) Notice that mention will only been made regarding the accuracy of the parameter estimates, rather than the confidence with which they have been found. This topic is an area that needs to be addressed [33-37,17], particularly for the less complicated estimation methods.

4. FREQUENCY DOMAIN METHODS

The traditional approach to modal parameter estimation is to use methods based in the frequency domain. All the techniques can be related to the Kennedy and Pancu circle fitting method [38] developed in 1947. Generally, some form of the Frequency Response Function (FRF) is curve-fitted. It must be remembered that the calculation of the FRF is itself a parameter estimation procedure [39] and random noise is removed through the use of averaging. There are a wide variety of different possible approaches (eg, H_1, H_2, H_v, H^c) [40,41,2] to estimate the FRF, each based on a different assumptions regarding noise corruption. Any errors in the FRF estimation process will of course be passed onto the estimated modal parameters.

In flutter testing it can be difficult to produce smooth FRFs due to the levels of noise and also the relatively small amount of data that is obtained. Also, few averages can usually be taken, due to the difficulties of maintaining exactly the same flight condition. It has been recommended [2] that the traditional H_1 estimate is used although advanced methods such as the H^c estimate [42], which uses a third independent signal, look promising.

When using parameter estimation methods, the engineer has the choice of whether to use a simple SDOF method or the more sophisticated MDOF methods.

4.1 SDOF Frequency Domain Methods

For a MDOF system with well separated modes, the parameters of each mode on the FRF can be found by examining each circle on the Nyquist plot, or peak on the Bode plot, individually. It is usual to assume that the damping is small enough so that the damped natural frequency is the same as the natural frequency. The damping values can be found from either the half power points, or a number of points around the circle (or peak), or by curve-fitting [43].

The problems with using such methods is that the mathematical model becomes invalid if the modes becomes close (usually defined as the half-power bandwidths overlapping) and poor damping estimates will result. In the extreme case, one mode will dominate another mode to such an extent that only the parameters of the dominant mode are estimated. However, the use of such methods is still very commonplace for flight flutter testing, particularly for military aircraft, as they are easy to use, and also because the response of a mode that is close to flutter will dominate the FRF and will be estimated quite accurately. On civil aircraft, where there is a much greater likelihood of close modes due to engines, the use of such methods is not so common.

A wide variety of different approaches to filter out each of the individual modes appear in the literature [44-47,14,24]. Often a number of transformations between the time and frequency domain are required in order to isolate all of the modes. This category of methods is very popular with aircraft manufacturers and research establishments. Examples of its use can be found on the F-16 [48,49], Schweizer Sailplane [48], CF-5 Transport [50], Airbus A310 [15], F111 [51], X-31A [52], B1 [53], the F-18 and other aircraft [47,54,55].

4.2 MDOF Frequency Domain Methods

In this category, the FRF is modelled as some form of rational fraction expansion that include contributions from all of the modes. Therefore no problem arises when close modes are analysed. As well as the contribution of individual modes including complex amplitude terms, upper and lower residuals should also be included to allow for modal behaviour outside the frequency range of interest. The majority of techniques in this category [37,56-60] employ an iterative non-linear least squares curve-fit to the FRF model over the frequency range of interest. These methods require initial frequency and damping estimates for the iterative process and the convergence speed can be very sensitive to the initial estimates. The alternative approach is to produce a linearised model and to find the estimates using a direct procedure. Such methods include the Rational Fraction Polynomial method [61] and its improved implementation the Global Orthogonal Polynomial [62,63] technique. The alternative approach used in the modal analysis field of isolating each SDOF component by subtracting out the effect of the other modes on the FRF [64] appears to be seldom used for flight flutter testing.

A number of techniques developed specifically for flutter testing applications fit into this category. The method developed by Nissim and Gilyard [65] uses a model that directly estimates the physical mass, stiffness and damping matrices in a similar manner to the Direct Parameter Estimation method [66,67]. A Maximum Likelihood approach has been developed [68-69] including both input (added to the input signals - not turbulence) and measurement noise models. Theoretically such an approach should provide the best

statistical estimates of the parameters. However, there can be convergence problems when using such sophisticated methods on systems with low damping and high modal densities. An Instrumental Variables method that accounts for input noise through the structure is described in ref [70]. An alternative method [71,18] finds the spectra of an impulse taking the imperfect impulse spectrum into account as well as accounting for effects of close modes.

In the aerospace industry it is most popular to use the non-linear iterative curve-fit approach. MDOF frequency domain techniques have been used to analyse flight flutter data from the F-16 [48], Airbus [72-74] , the Mirage [75], BAe146 and BAe125 [76], Piaggio P180 [77] and YF-17 [78]. A frequency domain version of the ML technique was employed on the DLC flap system [79]. The rational fraction method was applied to data from the Boeing YC-14 [80] and Y-12 [81], as well as a frequency domain version of the instrumental variables technique [82]. Wind tunnel data from various wing models has also been used to validate some of these MDOF methods [56,83].

5. TIME DOMAIN METHODS

Time domain parameter identification became feasible with the development of the digital computer. Such methods are based upon a time series representation of the system model, which can be related to the State Space model, often used in the Control field. Although it is possible to develop methods based upon a model relating inputs and outputs, the modal analysis community has tended to use methods that curve-fit the impulse response function calculated from either: the inverse Fourier Transform of the FRF, the time response to an impulse, or generated from the response to an unknown random input. There is a bewildering number of time domain system identification methods, however, in general those used for modal analysis perform a single step least squares minimisation of a difference equation (autoregressive) model. A large number of mathematically rigorous time domain techniques exist in the Signal Processing [28,29] field however, the direct application of such methods to modal analysis or indeed flight flutter testing is fraught with difficulty due to high modal densities and low damping values. One inherent problem with the use of all time domain methods is that it is not possible to model residual effects directly, and the resulting leakage errors due to filtering modes outside the frequency range of interest can cause problems.

5.1 SDOF Time Domain Methods

Two time domain techniques exist for analysing SDOF impulse responses. The Logarithmic Decrement technique [84] uses a single exponentially damped sinusoid model. The method will give incorrect estimates if there is more than one mode in the response even if the resonances are well separated. The Moving Block method [85,86] is often employed in the helicopter industry. The Fourier Transform at the resonant frequency of successive 'blocks' of the impulse response is calculated and the resulting straight line fit leads to the damping estimate. It is possible to employ the Moving Block method on MDOF data, however, no account is taken of coupling between the modes, so errors will result as soon as the system frequencies become close.

The Log Dec method has been used to curve-fit the SDOF response from filtered FRFs in a number of approaches [24]. The technique works well if the modes are separated. The Moving Block method appears works well on simulated data [71] however, little use has been made on real flutter data.

5.2 MDOF Time Domain Methods

Curvefitting methods in this category model the impulse response as a summation of exponentially damped sinusoids. Often a least squares minimisation of a difference equation representation relating the structural response at different time instants is used. This difference equation formulation gives rise to biased estimates when the data is corrupted [87], the most common remedy being to increase the number of modes in the fitted model. Although such an approach removes most of the bias, the user then has to distinguish between the system modes and the spurious modes [88,89]. On real structures such as aircraft, this differentiation can be difficult, and a fair amount of user interpretation is required in order to get the best out of the methods.

The Polyreference technique [90] is possibly the best known in the modal analysis field, and uses a MIMO model. Its corresponding SIMO or SISO version is the Least Squares Complex Exponential algorithm [91]. The method follows a three stage procedure estimating: the coefficients of the difference equation, the frequencies and dampings, and finally the mode shapes. The final stage is most effectively undertaken in the frequency domain. The Ibrahim Time Domain (ITD) [92] technique was the method that generated the interest in time domain system identification of modal testing in the 1970s. An eigen problem is formulated from which the eigenvalues lead to the frequencies and dampings, whereas the eigenvectors give the mode shapes.

A similar approach, but based upon system realisation theory, is the Eigensystem Realisation Algorithm [93]. The main difference with the above two methods is that the Singular Value Decomposition (SVD) is a fundamental element, and theoretically all of the

spurious modes can be eliminated following inspection of the resulting singular values. However, in practice, procedures to distinguish system modes from spurious modes are still required. The Matrix Pencil method is a comparable technique developed for flutter testing [94] and other similar methods can be found in refs [95,96].

Rather than using an increased model size to reduce the bias on the estimates, an alternative approach is to formulate the problem using terms that are not affected by any noise corruption. The Instrumental Variables [28,29] technique is found in many guises ranging from simple direct methods to very complicated iterative algorithms. The Correlation Fit (CF) method [97,87] is one such approach that considers the curve fit in terms of the data correlations that are used. By using those correlations that are uncorrupted, it is possible to find unbiased estimates. As the number of correlations used is arbitrary [87], unlike the least squares based methods, a much smaller amount of model overspecification is required than the least squares based techniques. An early application of the Least Squares and Correlation Fit methods was made using Concorde data [14]. The Eigensystem Realisation Algorithm using Data Correlations (ERA/DC) [98] combines the philosophies of the ERA and CF methods resulting in a mathematically rigorous technique that takes noise corruption into account. Both ERA and ERA/DC methods have been used on stick jerk data of the BAe146-300 [99] and the ITD method has been applied to flutter data from the space shuttle [100].

An alternative approach to the above methods is to try and model the noise by including noise terms. Such approaches are very common in signal processing [28,29] however they are generally applied to systems of a low order ($\approx$ 1 or 2 modes) with very high damping ($\approx$ 50 % critical). The minimisation process then becomes non-linear and computationally intensive methods such as Maximum Likelihood and the Extended Kalman Filter [71] must be used. Gruman have devoted a lot of effort into using such techniques for flight flutter testing [17,101]. Initially a least squares method was employed [102], but this was replaced by the Maximum Likelihood / Kalman Filter type approaches on aircraft such as the F-14 and X29 [103,17,104].

An implementation of an ARMA model relating measured input to output is described in ref [105]. The technique employs a so-called 'backwards model' [106] that helps the differentiation between system and spurious modes. This approach can be used for the analysis of impulse response data as well [107].

One further approach to MDOF time domain modal parameter estimation is to directly minimise the difference between the transient data and a summation of exponentially weighted sinusoids. The resulting techniques [108,109] are iterative, require starting estimates of frequencies and dampings, and can be time consuming. The major advantage of such approaches is that spurious modes are not required to obtain unbiased estimates and the estimated frequencies and dampings are usually of a very high quality. Such methods have been used to curvefit impulse responses from control surface excitation of drones [109,110].

6. PARAMETER ESTIMATION USING RESPONSES TO TURBULENCE

The difficulties and expense of installing excitation systems for flight flutter testing have often led aircraft manufacturers to try to extract frequency and damping values using only the response to turbulence. Common instances are the testing of light aircraft, and following minor structural modifications, including different combinations of stores, where the flutter characteristics are not expected to change. There are a number of significant problems with this process. Firstly, the frequency content of the turbulence is unlikely to excite a wide range of modes, and secondly, the analysis upon which the methods stand makes the assumption the turbulence is a Gaussian white sequence, which does not occur in practice.

By far the most widely used technique to obtain a transient response from random response data is the Random Decrement method developed by Cole [111]. It is often erroneously stated that the Random Dec method provides estimates of the frequencies and dampings, it does not. The technique is used to find a scaled impulse response. Frequently, single DOF time and frequency domain methods have then been used to find the modal parameters [24,112,113]. What has not often been recognised is that the Random Dec signature can be analyzed using any of the MDOF time domain methods. Examples of this approach are where the ITD method was used to find the modal parameters from random decrement signatures on a number of aircraft [114,30].

A number of other methods exist for estimating modal parameters from the response to an unknown random input [115-117]. The autocorrelation technique has been shown to require much less data than the Random Dec technique. Other approaches include the Maximum Entropy Algorithm [118] which uses a least squares based algorithm and is often used to find the auto-spectrum, although frequencies and dampings can be calculated using the estimated auto-regressive coefficients. An approach to deal with a coloured random input is described in ref [119].

Gruman have used some of their advanced MDOF time domain algorithms to tackle the problem of obtaining modal parameters from the response to unknown random excitation [17,104].

7. FLUTTER PREDICTION

A number of techniques exist to estimate the speed at which the onset of flutter occurs. The classic flutter margin approach [120] tracks a function based upon the estimated frequency and damping values of the two modes involved (known a-priori). An extension of this method [121,122] for the trinary flutter case has been shown to be superior on data from certain aircraft. A different approach [56,65] involves taking measurements from at least two flight cases so that an estimate of the aerodynamics as well as the structural response can be made, and then the critical flutter speed is estimated. The bi-spectrum method has also been used for this application [123]. The accuracy of these methods depends on how well the parameter estimates have been found.

A further technique is to monitor the system stability. Either Jury's stability criterion [124,125], or the envelope of the impulse response [126], is estimated and the resulting function plotted against speed or Mach number and extrapolated. The advantage of this type of method is that the individual modes do not have to be estimated, however, they should be used in addition to, rather than instead of, the parameter estimation techniques described above.

8. TIME VARYING SYSTEMS

On-line, or recursive, parameter estimation methods are used to identify systems with time-varying parameters [127,128]. Such an approach is attractive to the flutter test engineer due to the difficulties sometimes experienced in maintaining a steady flight condition, or even for the tracking of frequencies and dampings over varying flight speeds or altitudes. Such techniques are formulated in the time domain. The alternative off-line approach of dividing up the time data into small segments, and assuming that the modal parameters remain constant over each segment is not considered advisable; however such an approach has been applied to space shuttle data using the Maximum Entropy algorithm [129] and also a drone aircraft [130].

A few investigations have been undertaken to track modal parameters using on-line techniques on data from the F-16, X-29A [48]. Most work in this area has been concentrated on using either Autoregressive (AR) or Autoregressive Moving Average (ARMA) models to detect on-line estimates for turbulence input [131-135]. Such techniques can also be used for a measured forcing signal and the ability to track modal parameter changes is then improved greatly as the unknown random contribution does not have to be averaged out. Recent investigations have involved the development of the Discrete Modal Filter in an on-line formulation [136,137] and an on-line estimate of the system stability using the envelope function [131]. It is somewhat surprising that little work appears to have been devoted to developing the approach of Walker et al [138-139] whose methods produce direct on-line estimates of frequency and damping rather than requiring further manipulation of the AR coefficients. One recent area of research interest applicable to time varying parameter identification is the use of Time-Frequency methods [140].

The requirement for on-line estimation techniques is likely to increase in future years, however, the difficulties that have to be overcome in order to identify accurately lightly damped, time varying systems with high modal densities from noisy data are considerable.

9. NON-LINEARITIES AND AEROSERVOELASTICITY

The presence of structural and aerodynamic non-linearities can have a major effect on flutter behaviour [141-151]. Currently, where a linear approach is usually adopted, non-linearities would often appear to be a convenient explanation for unpredicted aeroelastic behaviour . Structural phenomena of interest include friction (joints or hydraulic control actuators), backlash or free-play (control linkages), impact (physical limits of vibration) and hardening stiffness (stores attachment) whereas non-linear aerodynamic effects involve quadratic aerodynamic damping, apparent damping in the transonic region, shock and flow separation effects. Non-linearities can result in unpredicted coupling between modes due to frequency addition or subtraction effects, asymmetries in the modes affecting the flutter speed, apparent damping, chaos, non-harmonic response, limit cycles as well as flutter. Variations in frequencies and dampings are often found for the same flight case with excitation from different sources [152,49], and this can be explained by non-linearities. The non-linear aerodynamic effects are particularly difficult to predict, for instance there can be problems distinguishing between unpredicted limit cycle oscillations and classical mild flutter [150].

Aeroservoelasticity (ASE) [152-157] involves the interaction of the flexible structure, aerodynamic forces and the flight control system [153]. This interaction tends to result in non-linear behaviour which can be difficult to predict, particularly when the frequencies of the control law are close to those of the aircraft. For example, the E6 aircraft suffered a partial loss of the tail even though the linear ASE analysis did not predict a flutter problem [158]. Additional non-linearities added to those discussed above include: non-linearities in the

control laws, time delays due to signal processing, an increase of free-play and hysteresis, resolution used for the digital feedback and unsteady airloads acting on the control surfaces.

In the modal community there has been a large amount of research in recent years devoted to developing techniques for the detection, quantification and modelling of non-linearities [159,160]. The reader is referred to methods such as: the Hilbert Transform [161] and Corehence [162] used primarily to detect the presence of non-linearities, higher order FRFs[163] and Volterra Series[164] that model non-linear systems completely, restoring force surfaces[165] that are particularly useful for dealing with systems not easily modeled by polynomials (eg, backlash) and also determining what type of non-linearity is present, NARMAX models[166] that are very similar to the time domain AR and ARMA methods but with extra terms included to model the non-linearities, and higher order spectral analysis[167] which is particularly useful for the case where the input is not measured. One significant difficulty in using such methods is their sensitivity to noise.

There has been little application of such techniques to analyse non-linear flutter data, and usually a linearised approach is used. Exceptions to this rule include the use of the bi-spectrum [168] and the Hilbert transform [169,150]. The number of different flight cases that have to be considered increases quite dramatically with the use of active control technology. Also, smart structures technology is expected to play a much greater role in the future, increasing the need for accurate non-linear parameter estimation techniques.

Further work is required in this area. Indeed, it has been stated recently that ..'the inability to detect nonlinear behaviour ... is a deficiency of major significance and a grave source of concern ...' [170]. The ability to make the methods robust in the presence of noise, especially those methods used to identify some form of non-linear model, is of great importance if their use is to become standard for flutter testing.

10. FUTURE REQUIREMENTS

As well as developing improved excitation techniques in order that the quality of flutter test data may be enhanced, the following parameter estimation topics need further attention to enable the safe and efficient flight flutter testing of future aerospace vehicles:

- Estimation methods developed specifically to analyse systems with close modes corrupted by significant amounts of input noise
- Techniques for predicting error bounds on parameter estimates
- Spatial filtering techniques
- Application of phase resonance methods to flutter testing
- Non-linear estimation methods
- On-line estimation methods
- Benchmark sets of linear, non-linear and time varying flutter test data to be developed and made readily available to researchers working in these fields

Further developments in the Signal Processing and Modal Analysis fields eg, Time-Frequency Methods and Neural Networks, should be monitored to determine their suitability for flutter testing applications.

11. CONCLUSIONS

Since Koenig's work in 1983, the use of modal parameter estimation methods has increased tremendously world-wide. However, the use of the more advanced methods by the aerospace industry is still limited. It is by no means clear whether these more sophisticated techniques are superior for flutter testing, given the poor quality of the data that can occur. Non-linear parameter estimation in particular needs to be developed to a level so that aeroservoelastic systems can be identified accurately with confidence.

The state of the art of linear modal analysis is certainly more practised, and indeed better, than it was twelve years ago. However, due to the scatter of estimates still found from the analysis of flutter test data, it is still impossible to say that modal parameter estimation is now sufficient for flutter testing. It is recommended that the following exercises are undertaken:

- a survey to establish which analysis methods and excitation methods are actually used world-wide
- a round robin exercise to identify modal parameters on real flight flutter data sets involving as many different investigators and analysis techniques as possible.

12. ACKNOWLEDGMENT

The author would like to thank Mr C.W. Skingle for his encouragement to write the pilot paper version of this paper [20] presented at the AGARD SMP meeting in October 1990.

13. REFERENCES

1. Van Nunen J.W.G. & Piazzoli G., 'Aeroelastic Flight Test Techniques and Instrumentation' Agardograph 160. 1979.
2. Wright J.R.,'Flight Flutter Testing' Lecture Series on Flutter of Winged Aircraft, Von Karman Institute 1991.
3. Johnson J.,'Flutter Testing of Modern Aircraft' AIAA Student Journal Spring 1989 pp 6-11.
4. Desforges M.J., Cooper J.E. & Wright J.R.,

'Normal Mode Force Appropriation for Flight Flutter Testing' to be presented at Int Forum on Aeroelasticity & Structural Dynamics 1995.
5. Shelley S.L. & Allemang R.J., 'Calculation of Discrete Modal Filters Using the Modified Reciprocal Modal Vector Method' IMAC 10 1992 pp37-45
6. Ibrahim S.R., 'Modal Identification Techniques Assessment and Comparison' Proc IMAC 3 1985 pp 831-839.
7. Leuridan J., Brown D.L. & Allemang R.J., 'Time Domain Parameter Identification Methods for Linear Model Analysis: A Unifying Approach' J.Vib Acoustics, Stress & Reliability in Design 1985 pp 1-8.
8. Juang J-N., 'Mathematical Correlation of Modal Parameter Identification Methods via System Realisation Theory' Modal Analysis v2 n1 1987 pp 1-18.
9. Allemang R.J. & Brown D.L., 'Multiple Input Experimental Modal Analysis - A Survey' Modal Analysis v1 n2 1986.
10. Leppart E., Lee S., Chapman P. & Wada B.K., 'Comparison of Modal Test Results: Multipoint vs Single Point Random' SAE 760879 1976.
11. Andrew L.V., 'Automated Application of Ibrahim's Time Domain Method to Responses of the Space Shuttle' AIAA 81-0526 1981.
12. Cooper J.E., 'Comparison of Modal Parameter Estimation Techniques on Aircraft Structural Data' Mech Sys Sig Proc 1990 v2 n4 157-172.
13. Chen J.C., 'Evaluation of Modal Testing Methods' AIAA 94-1071 1984.
14. Wright J.R., 'Flutter Test Analysis Methods' Ph.D. Thesis University of Bristol 1975. (also BAC(CAD)GEN/b55/0322).
15. Koenig K., 'Problems of System Identification in Flight Vibration Testing' AGARD R-270. 1983.
16. Koenig K., 'Flight Vibration Test Analysis - Methods, Theory and Application ' AIAA 93-2752.2nd Flight Testing Conf 1983.
17. Perangelo H.J. & Waiseren P.R., 'Application of Advanced Parameter Identification methods for Flight Flutter Data Analysis with Comparisons to Current Techniques' AGARD CP July 1984.
18. Lee B.H.K. & Ben-Neticha Z., 'Analysis of Flight Flutter Test Data' Canadian Aeronautics and Space Journal v38 n4 1992 pp 156-163.
19. Wolfe M. & Kirkby W., 'Flight Flutter Tests' AGARD Manual of Aeroelasticity v4 ch10 1961.
20. Cooper J.E., 'Modal Parameter Identification Techniques for Flight Flutter Testing' Pilot paper presented to AGARD SMP October 1990.
21. Haidl G. & Steininger M., 'Excitation and Analysis Techniques for Flight Flutter Tests' AGARD-R-672 1978.
22. Agardograph 56, 'Several Techniques for Flight Flutter Testing' Sept 1960.
23. Koenig K.,'Flight Flutter Parameter Identification' Pilot paper presented at AGARD SMP meet April 1990.
24. NASA SP-415 'Flutter Testing Technqiues' 1975.
25. Baird E.F. & Clark W.B., 'Recent Developments in Flight Flutter Testing in the United States' AGARD Report 596 1972.
26. Natke H.G., 'Survey of European Ground and Flight Vibration Test Methods' SAE Paper 760878 1976.
27. AGARD Conf 339 Ground/Flight Testing and Correlation. 1982.
28. Soderstrom T. & Stoica P.,'System Identification' Prentice Hall 1987.
29. Ljung L.,'System Identification - Theory for the User' Prentice Hall 1987.
30. Schenk A., 'Flutter Analysis from Ambient Random Responses' Proc European Symp on Aeroelasticity & Structural Dynamics 1989 pp 245-252.
31. Schenk A., 'Die Modale Identifikation bei unbekannter Stationarer Zufallserregung' Z.Flugwiss Weltraumforsch v15 1991 pp300-130.
32. Fullekrug U., 'Survey of Parameter Estimation Methods in Experimental Modal Analysis' Proc IMAC 5 1987 pp 460-467.
33. Freudinger L. & Field R.V., 'Null Space Pole Estimation with Error Bounds' Proc IMAC 12 1994 pp 947-967.
34. Cooper J.E. Emmett P.R. & Wright J.R.,'A Statistical Confidence Factor for Modal Parameter Identification' Proc ISMA 17 1992 pp 1611-1626.
35. Longman R.W., Bergmann M. & Juang J-N., 'Variance and Bias Confidence Criteria for ERA Identified Modal Parameters' AIAA/ASS Astrodynamics Specialists Conf 1987.
36. Yao Y.X. & Pandit S.M., 'Variance Analysis of Multi-Channel Time Domain Modal Parameters' Proc IMAC 12 1994 pp200-207.
37. Copley J.C.,'Numerical Analysis of Vector Responses' RAE TR80135 1980.
38. Kennedy C. & Pancu C., 'Use of Vectors in Vibration Measurement and Analysis' J.Aero Science v14 n11 1947.
39. Cooper J.E. & Emmett P.R., 'A Non-Parametric Approach to Instrumental Variables Frequency Response Estimation' Modal Analysis v10 n2 1995 pp 84-94.
40. Rocklin G.T., Crowley J. & Vold H., 'A Comparison of H_1, H_2 and H_v Frequency Response Functions' Proc IMAC 3 1985 pp 272-278.
41. Leuridan J., Devis D., Van der Auweraer H. & Lembregts F., 'Comparison of Some Frequency Response Function Measurement Techniques' Proc IMAC 4 1986 pp 908-918.
42. Mitchell L.D., Cobb R.E., Deel J.C. & Luk

Y.W., 'An Unbiased Frequency Response Function Estimator' Modal Analysis v3 n1 1988 pp 12-19.
43. Ewins D.J.,'Modal Testing : Theory and Practice' Research Studies Press 1985.
44. Sensburg O., 'Review of Active Structural Control Systems and Flight Test Techniques for Dynamic Stability Investigations' Int Forum on Aeroelasticity & Structural Dynamics 1989 pp 1-14.
45. Houbolt J.C.,'On Identifying Frequencies and Dampings in Subcritical Flutter Testing' Flutter Testing Techniques NASA SP-415 1975.
46. Ruhlin C.L., Watson J.J., Ricketts R.H. & Doggett R.Y. 'Evaluation of Four Subcritical Response Methods for On-line Prediction of Flutter Onset in Wind Tunnel Tests' AIAA J.Aircraft v20 n10 1983 pp 835-840.
47. Bernasconi O., 'Modal Parameter Extraction from Response Power Spectral Densities' Proc 15th Int Seminar on Modal Analysis 1990 pp1147-1160.
48. Kehoe M.W., 'Aircraft Flight Flutter Testing at the NASA Ames-Dryden Flight Research Facility' 4th AIAA Flight Test Conf 1988.
49. Vernon L.,' In-Flight Investigation of a Rotating Cylinder Based Structural Excitation System for Flutter Testing' AIAA-93-1537-CP
50. Lee B.H.K., 'Determination of Subcritical Damping in CF-5 Flight Flutter Tests' J.Aircraft v22 n1 1985 pp 89-91.
51. Marshall M.A.,'Determination of In Flight Modal Characteristics of a Fighter Type Aircraft' Proc Florence IMAC 1991 pp 229-234.
52. Hodson C.H., Dobbs S.K., Brosnon M.J. & Chen J.B., 'X-31A Flight Flutter Test Excitation by Control Surfaces' AIAA-93-1538-CP.
53. Dobbs K. & Hodson C.H., 'Determination of Subcritical Frequency and Damping from B1 Flight Flutter Test Data' NASA CR-3152 1979.
54. Knauer K. & Sensburg O., 'Ground and Flight Test Techniques used for the Proof of Structural Integrity of the Tornado Combat Aircraft' AGARD Conf 339 Ground/Flight Testing and Correlation. 1982.
55. Gilyard G.B. & Edwards J.W., 'Real Time Flutter Analysis of an Active Flutter Suppression System on a Remotely Piloted Research Aircraft'. AGARD Conf 339 Ground/Flight Testing and Correlation. 1982.
56. Gaukroger D.R., Skingle C.W. & Heron K.H., 'An Application of System Identification to Flutter Testing' J.Sound & Vibration v72 1980 pp 141-150.
57. Gaukroger D.R., Skingle C.W. & Heron K.H., 'Numerical Analysis of Vector Response Loci' J.Sound and Vibration v29 n3 1973. pp 341-353.
58. Dat R., 'Determination of the Dynamic Characteristics of a Structure From an Analysis of Transfer Functions' (in French) Revue Francais de Mecanique n58-59 1976 pp 15-19.
59. Bucharles A., Cassan H. & Roubertier J., 'Advanced Parameter Identification Techniques for Near Real Time flight Flutter Test Analysis' 5th Biannual Flight Test Conf 1990 pp 118-125.
60. Wittmeyer H., 'Parameter Identification for Structures with Neighbouring Natural Frequencies Especially in the Case of Flight Resonance Tests' Z.Flugwiss. Weltraumfirsch v6 1982 pp 80-90.
61. Richardson M. & Formenti D.L., 'Parameter Estimation from Frequency Response Measurements using Rational Fraction Polynomials' Proc IMAC 1, 1982.
62. Van der Auweraer H. & Leuridan J., 'Multiple Input Orthogonal Polynomial Parameter Estimation' Mech Sys Sig Proc v1 n3 1987 pp 259-272.
63. Van der Auweraer H. & Leuridan J., 'Multiple Input Orthogonal Polynomial Parameter Estimation' Proc 11th Int Seminar on Modal Analysis 1986.
64. Goyder H., 'Structural Modelling by the Curve-Fitting of Measured Frequency Response Data' J.Sound and Vibration v68 n2 1980.
65. Nissim E. & Gilyard G.B., 'Method for Experimental Determination of Flutter Speed by Parameter Identification' AIAA 89-1324-CP 30th Structures, Structural Dynamics and Materials Conf 1989 pp 1427-1441.
66. Lembregts F., Snoeys R. & Leuridan J., 'Multiple Input Modal Analysis of Frequnecy Response Functions Based On Direct Parameter Identification' Proc 10th Int Seminar on Modal Analysis. 1985.
67. Lembregts F., Leuridan J., Zhang L. & Kanda H.,'Multiple Input Modal Analysis of Frequency Response Functions Based on Direct Parameter Identification' Proc IMAC 4 1986 pp 589-598.
68. Van der Auweraer H., Pinelon R., Leuridan J. & Schoukens J., 'Flight Flutter Data Analysis with Maximum Likelihood Estimation' IMAC 8 1990
69. Van der Auweraer H., Ishaque K. & Leuridan J., 'Signal Processing and System Identification Techniques for Flutter Test Data Analysis' Florence IMAC 1991 pp 671-681.
70. Emmett P.R., Cooper J.E. & Wright J.R., 'Improved Frequency Domain Modal Parameter Identification' to be presented at Int Forum on Aeroelasticity & Structural Dynamics 1995.
71. Lee B.H.K. & Laichi F., 'Development of Post-Flight and Real Time Flutter Analysis Methodologies' Int Forum on Aeroelasticity & Structural Dynamics 1993. pp 703-719.
72. Zimmermann H., 'Flight Vibration Testing with Tip-Vane on Airbus A310' AIAA 83-2753. 2nd Flight Testing Conf 1983.
73. Zimmermann H. & Destuynder R., 'Flight Flutter Testing with Emphasis on the Tip Vane Method' AGARD Conf 339 Ground/Flight Testing and

Correlation. 1982.
74. Lacabanne M. & Esquerre J.P., 'Correlation Between Theoretical Flutter Model and Test for Civil Aircraft' Int Forum on Aeroelasticity & Structural Dynamics 1991. pp 594-602.
75. Costard J., 'Test Techniques Adopted by Avions-Marcel Dassault-Breguet Aviation Istres' J.Aero Soc of India v39 1987 pp 61-70.
76. Woods A.G., 'The Choice of Techniques Used for Flight Flutter Clearance with Particular Reference to the BAe 146 and BAe 125' Proc 2nd int Symp on Aeroelasticity and Structural Dynamics 1985 pp 265-275.
77. Chairlone P.G. & Miranda D., 'Piaggio P180 - Aircraft Flutter Clearance Programme - Comparison Between Flight Flutter Tests and Analytical Results' Proc IMAC 6 1988 pp 679-689.
78. Winther B.A. & Cowan D.L., 'Validation of Flutter Test Analysis Method' AIAA 87-0780 1987.
79. Rohlf D. & Monnich W., 'Identification of the DLC Flap System on the Research Aircraft ATTAS' 18th Symp Soc of Flight Test Engineers 1987.
80. Imes R.S., Jennings W.P. & Olsen N.L., 'The Use of Transient Techniques in the Boeing YC-14 Flutter Clearance Programme' AIAA78-505 1978.
81. Zeng Q., Zhang L. & Zhang C., 'Signal Preprocessing and Parameter Estimation for Aircraft Flight Flutter Tests' Proc Florence IMAC 1991 pp 634-639.
82. Johnson W. & Gupta N.K., 'Instrumental Variables Algorithm for Modal Parameter Identification in Flutter Testing' AIAA.J v16 n8 1978.
83. Ghiringhelli G.L., Lanz, M. & Mantegazza P., 'A Comparison of Methods used for the Identification of Flutter From Experimental Data' J.Sound and Vibration v119 n1 1987 pp39-51.
84. Thomson W.T.,'Theory of Vibrations with Applications, Chapman and Hall 1993.
85. Bousman W.G. & Winkeler D.J., 'Application of the Moving Block Analysis' AIAA 91-0653 1981.
86. Lee B.H.K & Jones D.J., 'Comparison of Two Methods for the Reduction of Free Decaying Data in Aircraft Flutter Tests' Canadian Aerospace J v26 n4 pp 322-335.
87. Cooper J.E., 'Comparison on Some Time Domain System Identification Techniques using Approximate Data Correlations' Modal Analysis v4 1989 pp 51-57.
88. Ibrahim S.R., 'Modal Confidence Factor in Vibration Testing' J.Spacecraft & Rockets v15 1978 pp 313-316.
89. Vold H. & Crowley J., 'A Modal Confidence Factor for the Polyreference Method' Proc IMAC 3 1985 pp 305-310.
90. Deblauwe F., Brown D.L. & Allemang R.J., 'The Polyreference Time Domain Technique' Proc IMAC 5 1987 pp 832-845.
91. Brown D.L., Allemang R.J., Zimmermann R. & Mergeay M., 'Parameter Estimation Techniques for Modal Analysis' SAE790221 1979.
92. Pappa R.S. & Ibrahim S.R., 'A Parametric Study of the Ibrahim Time Domain Modal Identification Algorithm ' Shock Vib Bull v51 n3 1981 pp 43-72.
93. Juang J-N. & Pappa R.S., 'An Eigensystem Realisation Algorithm for Modal Parameter Identification and Model Reduction' J. Guidance, Dynamics & Control v8 n5 1985 pp 620-627.
94. Hui R. & Ming P.C., 'Modal Parameter Estimation for Flutter Testing using Matrix Pencil Approach' Proc IMAC 13 1995 pp1076-1080.
95. Larrimore W.E., 'Canonical Variate Analysis' American Control Conf 1983.
96. King A., Desai V. & Skelton R., 'A Generalised Approach to Q-Markov Covariance Equivalent Realisations for Discrete Systems' Automatica v24 n4 1988 pp 507-515.
97. Wright J.R., 'Flutter Test Analysis in the Time Domain Using a Recursive System Representation' J.Aircraft v11 n12 1974 pp 774-777.
98. Juang J-N., Cooper J.E. & Wright J.R., 'An Eigensystem Realisation Algorithm using Data Correlations (ERA/DC) for Modal Parameter Identification' Control -Theory and Technology v4 n1 1988 pp5-14.
99. Cooper J.E. & Wright J.R., 'Application of Time Domain Decomposition Techniques to aircraft Ground Vibration and Flutter Test Data' Proc European Symp on Aeroelasticity & Structural Dynamics 1989 pp 235-244.
100. Andrew L.V. & Park C.C., 'A Time Domain Method for Establishing Modal Parameters and Flutter Margins from Space Shuttle Data' SAE SP-596 1984.
101. Russo M.L., Richards P.T. & Perangelo H.J., 'Identification of Linear Flutter Models' 2nd Flight Testing Conf 1983. AIAA 83-2696.
102. Waiseren P.R. & Perangelo H.J., 'Real Time Flight Flutter Testing via Z Transform Technique' AIAA 72-784 1972 pp 1-15.
103. Russo M., Healy M. & Brock M., 'X-29A Flight Flutter Data Analysis by Advanced Methods' AIAA 86-9737. 3rd Flight Test Conf 1986.
104. Perangelo H.J. & Waiseren P.R., 'Flight Flutter Test Methodology at Gruman' Proc Flight Testing Technology : A State of the Art Review. 13th Annual Symp 1982 pp 91-100.
105. Batill S.M., Carey D.M. & Kehoe M.W.,'Digital Time Series Analysis for Flutter Test Data' AIAA 92-2103 1992
106. Hollkamp J.J. & Batill S.M.,'Automated Parameter Identification and Order Reduction for Discrete Time Series Models' AIAA.J v27 1991 pp 96-103.

107. Cooper J.E.,'The Use of Backwards Models for Structural Parameter Identification' Mech Sys Sig Proc v6 n3 1992 pp 217-228.
108. Smith W.R., 'Least Squares Time Domain Method for Simultaneous Identification of vibration parameters from Multiple Free Response Records' AIAA 81-0530 1981.
109. Bennett R.M. & Desmarais R.N., 'Curve Fitting of Aeroelastic Transient Response Data with Exponential Functions' NASA SP-415 1976 pp43-58.
110. Bennett R.M. & Abel I., 'Application of a Flight Test and Data Analysis Techniques to Flutter of a Drone Aircraft' Proc AIAA Dynamics Specialists Conf 1981.
111. Cole H.A., 'Detecting and Damping Measurement of Aerospace Structures by Random Decrement Signatures' NASA CR-2205 1973.
112. Schroers L.G., 'Dynamic Structural Aeroelastic Stability Testing of the XV-15 Tilt Rotor Research Aircraft' AGARD Conf 339 Ground/Flight Testing and Correlation. 1982.
113. Farrall P.A.,'Flight Flutter Test Techniques at the ARL Labs' ARL-STRUCT-TM-569 1990.
114. Ibrahim S.R., 'Application of Random Time Domain Analysis to Dynamic Flight Measurements' Shock Vib Bull v49 n2 1979 pp 165-170.
115. Coupry G., 'Random Techniques for Flutter Testing in Wind Tunnel and in Flight' Israel J. of Technology v1 1974 pp 33-39.
116. Desforges M.J., Cooper J.E. & Wright J.R., 'Spectral and Modal Parameter Estimation from Output-only Measurements' Mech Sys Sig Proc May 1995.
117. Viviers S. & McKinnel J., 'Flight Flutter Testing Without an Excitation System' Int Forum on Aeroelasticity & Structural Dynamics 1993. pp 1011-1022.
118. Ulrych T.J. & Bishop T.N.,'Maximum Entropy Spectral Analysis and Autoregressive Decomposition' Rev Geo Space Phys v31 n1 1975 pp 183-200.
119. Cooper J.E., Desforges M.J. & Wright J.R., 'Extraction of Modal Parameters From Unknown Coloured Random Input. Proc ISMA19 1994 pp 1011-1024.
120. Zimmerman N.H. & Weissenburger J.T., 'Prediction of Flutter Onset Speed Based on Flight Testing At Subcritical Speeds' J.Aircraft v1 n4 1964 pp190-202.
121. Price S.J. & Lee B.H.K., 'Development and Analysis of flight Flutter Prediction Methods' AIAA-92-2101-CP 1992
122. Price S.J. & Lee B.H.K., ' Evaluation and Extension of the Flutter Margin Methods for Flight Flutter Prediction' J.Aircraft v30 n3 1993 pp 395-402.
123. Chang J.H., Stearman R.O., Choi D. & Powers E.J., 'Identification of Aeroelastic Phenomenon Employing Bispectral Analysis Techniques' Proc IMAC 4 956 - 964 1986.
124. Matsuzaki Y. & Torii H., 'Response Characteristics of a Two-Dimensional Wing Subjected to Turbulence near the Flutter Boundary' J.Sound & Vibration v136 n2 1990 pp 187-199.
125. Matsuzaki Y. & Ando Y.,'Estimation of Flutter Boundary from Random Responses Due to Turbulence at Subcritical Speeds' J.Aircraft v19 n10 1981 pp 862-868.
126. Cooper J.E., Emmett P.R., Wright J.R. & Schofield M.J., 'Envelope Function - A Tool For Analysing Flutter Data' J.Aircraft v30 n5 1993 pp 785-790.
127. Ljung L. & Soderstrom T.,' Theory and Practice of Recursive Identification' MIT Press 1983.
128. Cooper J.E., 'Identification of Time Varying Modal Parameters' Aeronautical Journal October 1990 pp 271-278.
129. Vold H., Crowley., Geisler D. & Wolfer A., 'Maximum Entropy Frequency Response Functions' Proc IMAC 3 1985 pp 876-881.
130. Hicks J.W. & Peterson K.L., 'Real Time Flight Test Analysis and Display Techniques for the X-29A Aircraft' NASA TM 101692 1988.
131. Cooper J.E., Desforges M.J. & Wright J.R., 'The Online Envelope Function - A Guide To Aeroelastic Stability' Int Forum on Aeroelasticity & Structural Dynamics 1993. pp 981-998.
132. Walker R. & Gupta N., 'Real Time Flutter Analysis' NASA CR 170412 1984.
133. Pak C.G., Friedmann P.P. & Livne E., 'Transonic Adaptive Flutter Suppression Using Unsteady Time Domain Aerodynamics' AIAA 91-0986 1991.
134. Wendler B.H., Near Real Time Flutter Boundary Prediction From Turbulence Excited Response' AIAA 83-0814 1983.
135. Pak C.G. & Friedmann P.P., 'New Time Domain Technique for Flutter Boundary Identification' AIAA-92-2102-CP 1992.
136. Shelley S.L., Freudinger L.C. & Allemang R.J., 'Development of an Online Parameter Estimation System using the Discrete Modal Filter' IMAC 10 1992 pp 173-183.
137. Antal G., Brilhart R., Hensley D. & Freudinger L., 'Implementation of an Automated Approach for Spatial Filtering of Flight Flutter Test Data' Proc IMAC 13 1995 pp 104-111.
138. Walker R.A., Gupta N.K. & Gilyard G.H., 'Algorithms for Real Time Flutter Identification' Proc AIAA Guidance and Control Conf 1983 pp

432-437.
139. Roy R.H., Walker R.A. & Gilyard G.B., 'Real time Flutter Identification with Close Mode Resolution' AIAA 86-2019 1986
140. Newland D.E., 'An Introduction to Random Vibrations, Spectral & Wavelet Analysis' Longman 1993.
141. Fabrice P.,'Effects of Structural Non-linearities on Flutter Analysis' Int Forum on Aeroelasticity & Structural Dynamics 1993. pp 857-869.
142. Brasel O. & Eversman W., 'Application of Transient Aerodynamics to the Structural Nonlinear Flutter Problem' J.Aircraft v25 1988 pp 1060-1068.
143. Lee B.H.K. & Tron A., 'Effects of Structural Non-linearities on Flutter Characteristics of the CF-18 Aircraft' J.Aircraft v26 1989.
144. Havenstein A.J., Zara J.A., Eversman W. & Quemei I.K., 'Chaotic and Non-linear Dynamic Response of Aerosurfaces with Structural Non-linearities' AIAA 92-2547-CP 1992
145. Holden M. & Brazier R.,'Effects of Structural Non-linearities on a Tailplane Flutter Model' to be presented at Int Forum on Aeroelasticity & Structural Dynamics 1995.
146. Sensburg O. & Schoen B., 'Vibration and Flutter Investigations of Aircraft with Special Nonlinear Structural Properties' (in German) Z.Flugwiss.Weltraumforsch v2 1978 pp 395-404
147. Haidl G., 'Non-linear Effects in Aircraft Ground and Flight Vibration Tests' AGARD-R-652 1976
148. De Ferrari G., Chesta L., Sensburg O. & Lotze A., 'Effects of Non-linearities on Wing Store Flutter' AGARD Conf 339 Ground/Flight Testing and Correlation. 1982.
149. Zimmermann H., 'The Aeroelastic Challenges of the Airbus Family - Review and Prospects' Int Forum on Aeroelasticity & Structural Dynamics 1991 pp 1-11.
150. Zimmermann H., 'Aeroelastic Features of the Airbus Family' Lecture presented at the Univ of Manchester May 1994.
151. Dowell E.H.,'Nonlinear Aeroelasticity' in Flight Vehicle Materials, Structures and Dynamics - Assessment and Future Directions ASME 1993 pt2 ch4 pp 213-239.
152. Koenig K.,'On the New quality of the Flutter Problem Due to Coupling of structure and Electronic Flight Controls in Modern Large and Flexible Aircraft' Int Forum on Aeroelasticity & Structural Dynamics 1993. pp 131-150.
153. Zimmermann H.,'Aeroservoelasticity' Computer Methods in Applied Mechanics and Engineering v90 1991 pp 719-735.
154. IMechE Seminar, 'Interactions Between Aircraft Structural Dynamics and Control Systems' March 1995.
155. Knoll T.,'Aeroservoelasticity' in Flight Vehicle Materials, Structures and Dynamics - Assessment and Future Directions ASME 1993 pt2 ch3 pp 179-212
156. Kehoe M.W., 'Flutter and Aeroservoelastic Clearance of the X-29A Forwards Swept Wing Airplane' NASA TM-1000447 Sept 1989.
157. Lotze A., Sensburg O. & Kuhn M., 'Flutter Investigation of a Combat Aircraft with a Command and Stability Augmentation System' J.Aircraft v14 n4 1977 pp 368-374.
158. Borst R.G. & Strome R.W., 'E6 Flutter Investigation and Experience' AIAA-92-4601-CP.
159. Tomlinson G.R., 'Detection, Identification and Quantification of Non-linearity in Modal Analysis - A Review' Proc IMAC 4, 1986 pp 837-843.
160. Tomlinson G.R., 'Linear or Nonlinear - That is the Question' Proc ISMA19 1994 pp 11-32.
161. Tomlinson G.R, 'Developments in the Use of the Hilbert Transform for Detecting and Quantifying Nonlinearity Associated with Frequency Response Functions' Mech Syst Sig Proc v1 n2 1987 pp 151-171.
162. Rauch A.,' Corehence - A Powerful Estimator of Nonlinearity, Theory and Application' Proc IMAC 10 1992 pp 784-795.
163. Storer D. & Tomlinson G.R., 'Recent Developments in the Measurement and Interpretation of Higher Order Transfer Functions from Nonlinear Structures' Mech Sys Sig Proc v7 n2 1993 pp 173-189.
164. Schetzen M., 'The Volterra and Weiner Theories of Nonlinear Systems' John Wiley 1980.
165. Wright J.R. & Hadid M.A., 'Sensitivity of the Force State Mapping Approach to Measurement Errors' Modal Analysis v6 1991 pp 89-103.
166. Chen S. & Billings S.A., 'Representations of Nonlinear Systems : the NARMAX Model' Int J Control v49 1989 pp 1013-1032.
167. Brillinger D.R. & Rosenblatt M., 'Spectral Analysis of Times Series' J.Wiley 1967.
168. Stearman R.O., Powers E.J., Schwartz J. & Yurkovich R., 'Aeroelastic System Identification of Advanced Technology Aircraft Through Higher Order Signal Processing' Proc IMAC 10 1992.
169. Zimmermann H. & Tichy L., 'Application of the Hilbert Transform to Flight Vibration Testing' to be presented at Int Forum on Aeroelasticity & Structural Dynamics 1995.
170. Amos A.K.,'Overall Assessment of Needs and Benefits in Structural Dynamics' in Flight Vehicle Materials, Structures and Dynamics - Assessment and Future Directions ASME 1993

CF-18 Flight Flutter Test (FFT) Techniques

M.Dickinson
Department 775
Canadair Administrative Center
400 Cote Vertu Road West
Dorval Quebec H4S 1Y9
Canada

SUMMARY

The paper describes Canadair's role in the flight flutter testing of the CF-18 aircraft for the Canadian Forces. The flight test programs are flown from AETE Cold Lake Alberta, and are a partnership between Canadair and AETE. The 1992 category II 480 gallon EFT FFT program is used as a detailed example of this Canadair role. The paper emphasizes the FFT techniques currently employed, and the difficulties encountered due to non-linear modal behaviour and a transonic EFT buffet condition. The test program marked the first FFT application of AETE's LMS frequency analysis system. The paper describes the user programs developed to tailor and automate this system for CF-18 FFT use. The programs are written in the LMS UPA language and were largely developed as the FFT program progressed. The results from two separate FFT data reduction techniques (dwell-decay PSD, and FRF / MLE curvefitting) are directly compared with the pre-flight FEM predictions. The differences in the two sets of FFT results are explained by studying a simple Log-Dec analysis of a response decay.

LIST OF SYMBOLS

ADC	Analogue to Digital Converter
AETE	Aerospace Engineering Test Establishment
AIM-9	Sidewinder Air-to-Air Guided Missile
AOBSPIT	Antisymmetric Outboard Store Pitch
AW1B	Antisymmetric Wing First Bending
A_0	Initial Decay Amplitude
A_N	Decay Amplitude after N cycles
d_1	Damping of Mode 1 (1/sec)
d_2	Damping of Mode 2 (1/sec)
EAS	Equivalent Airspeed
EFT	External Fuel Tank
FECU	Flutter Exciter Control Unit
FEM	Finite Element Model
FFT	Flight Flutter Test
FM	Flutter Margin
FRF	Frequency Response Function
FTCR	Flight Test Control Room
GVT	Ground Vibration Test
HP	Hewlett Packard
LMS	Leuven Measurement Systems
MLE	Maximum Likelihood Estimator
N	Number of Cycles
PLER	Primrose Lake Evaluation Range
PSD	Power Spectral Density
q	Aerodynamic Pressure (psi)
UPA	User Programing and Acquisition
w_1	Frequency of Mode 1 (rads/sec)
w_2	Frequency of Mode 2 (rads/sec)

BACKGROUND

Canadair has been providing flutter analysis and test support to the Canadian Forces for over 25 years. In recent years, this support has involved the CE-133 (T-Bird), CF-5, and CF-18 aircraft. The flight flutter test programs are flown from AETE Cold Lake Alberta, and are a partnership between Canadair and AETE. Canadair's CF-18 FFT responsibilities are typically; (a) pre-flight flutter analysis predictions; (b) FFT plan; (c) safe flight envelope expansion; (d) post-flight data reduction; and (e) FFT report (including any flutter clearance recommendations).

FLIGHT TEST FACILITIES

AETE's CF-18 FFT facilities provide for *real-time* data monitoring and post-flight data reduction. The aircraft is excited through the primary flight control systems. The FECU is capable of generating a range of control surface (aileron, stabilator, or rudder) inputs. Up to 15 pre-programed inputs can be stored in memory. These programs specify; (a) the type of excitation (random, or sinusoidal sweep / dwell); (b) the selected control surfaces; (c) the phasing (symmetric or antisymmetric); (d) the oscillatory amplitude; (e) the DC bias; and (f) the frequency range or time duration. NB The wing / store flutter flight test programs employ aileron excitation. The airframe response to the FECU excitation is measured by 12 wing strain gauges and various fuselage / under wing store accelerometers.

The FTCR and test aircraft are in constant radio communication and data telemetry link throughout a flutter mission. The telemetry data is rebroadcast from the PLER tracking station. The data is displayed in the FTCR on various strip chart recorders and digital displays. The data is also recorded on two magnetic tapes (one on-board the test aircraft and a second in the FTCR).

The post-flight data reduction uses LMS frequency analysis software installed on a HP 9000 series 375 workstation. AETE's copy of LMS is currently at version 2.8 (ie., pre-windows). The HP / LMS system is connected to the FTCR data stream via a 40 channel DIFA Scadas ADC. Typically, 16 channels of data are acquired *real-time* using the FTCR lissajous displays inputs. NB If this *real-time* data acquisition is successful, an initial *cut* at the test point modal data can often be presented at the post-flight briefing.

FLIGHT TEST PROCEDURES

Flight flutter testing should be viewed as involving an inherent element of danger. The flight test procedures must be first and foremost concerned with flight safety. The most critical portion of the test program is the acceleration from a currently cleared EAS to the next test point. It is important

Paper presented at the Structures and Materials Panel Specialists' Meeting on "Advanced Aeroservoelastic Testing and Data Analysis", held in Rotterdam, The Netherlands, from 8-10 May 1995, and published in CP-566.

to assess the critical flutter mode damping during these EAS accelerations. This is often done with *stick-rap* inputs. The CF-18 flight flutter testing employs a *Program 15* test point build-up technique. Here, a 1 second dwell at the critical flutter frequency is placed in *Program 15* of FECU memory (as this last FECU program can be repeatedly executed by the pilot without cycling thru the other programs). The critical flutter modes can thus be readily excited during the test point accelerations. Each dwell is *CLEARED* by the lead flutter engineer in the FTCR. A qualitative check on the critical flutter mode damping can thus be obtained at 4 or 5 second intervals

The CF-18 flight flutter testing is typically performed without a pre-flight GVT. The under wing store to pylon swaybraces are manually tightened to remove all perceptible free-play. The initial flight is used to establish the flight test procedures and the low speed modal data (in lieu of a pre-flight GVT). The *straight-and-level* flight test points are then flown in order of increasing dynamic pressure (ie., EAS). The test points are typically grouped at constant Mach No's (say, .75 and .95) to allow for flutter margin extrapolations (Ref 1). A series of demonstration dives then explore the supersonic regime.

The capability of the FECU to apply a DC bias to the ailerons is of particular interest. It appears that this was originally incorporated into the FECU to accommodate free-play in the ailerons themselves. Early CF-18 flight flutter testing revealed that the outer wing panels are aerodynamically unloaded in certain flight regimes, and that this can lead to wing fold hinge free-play problems. A judicious choice of aileron bias can thus pre-load the outer wing and minimize this problem. The current flight test technique is to use positive (trailing edge down) aileron bias at low speeds, and negative (trailing edge up) bias at high speeds.

LMS UPA PROGRAMS

A suite of LMS UPA programs has been written to tailor and automate the LMS software for CF-18 FFT use. The programing is quite extensive with around 25 programs or subroutines and 20 display or plot files. The programs operate on LMS THROUGHPUT ACQUISITION time history sessions. These sessions typically contain 164 seconds of time data for 16 channels (2 aileron motion sensors, 12 wing strain gauges, and 2 store accelerometers) with a 100 Hz sample rate (ie., 16 times a 16384 channel blocksize). The suite of programs is controlled by an executive program *stack*, which can be accessed by the command *upa stack* in the Fourier Monitor. The programing currently provides the following analysis capabilities:-

1 Aileron Inputs
2 Time History Play-Back
3 Log-Dec
4 PSD
5 Automated PSD
6 FRF Generation
7 MLE FRF Curvefitter
8 Flutter Margin Prediction

Each capability is described in turn. The *Aileron Inputs* program is the key to automating the data reduction. This program searches through the aileron motion sensor time histories to find the FECU excitation inputs. The program can distinguish between symmetric and antisymmetric aileron sweeps and dwells. Figure 1 presents a typical output from the program. Each line summarizes an aileron input. These summaries give the symmetry, the type of excitation (sweep or dwell), the frequency or frequency range, the start record, the end record, and the time duration. This data is displayed to the user and stored internally as program variables.

The *Time History Play-Back* program simply allows the user to easily replay any section of a THROUGHPUT time history session. The user simply enters the blocksize and start time. The data is displayed with the Figure 2 static display format.

The *Log-Dec* program performs a logarithmic decrement analysis on selected dwell-decay time history channels. If the wing strain gauges are selected, the program analyses a left hand wing channel, the corresponding right hand wing channel, and a *symmetry* enhancement (say, LHS-RHS). The program actually performs several log-dec analyses per channel; estimating the modal frequency and damping based on 1 cycle of decay, 2 cycles, ... up to a maximum of 10 cycles. The frequency is simply estimated from the time between cycles, and the damping from:-

$$Damping\,(G) = \frac{1}{N\pi} ln\left(\frac{A_0}{A_N}\right)$$

where, (over N cycles), the amplitude decays from A_0 to A_N.

```
A-Sweep 5.0->12.0 Hz - Records:   196 to 2578  (23.82)
A-Sweep 5.0->12.0 Hz - Records:  2690 to 5074  (23.84)
A-Dwell    8.0    Hz - Records:  5420 to 5728  (3.08)
A-Dwell    8.2    Hz - Records:  6106 to 6412  (3.06)
A-Dwell    8.4    Hz - Records:  6916 to 7228  (3.12)
A-Dwell    8.6    Hz - Records:  7628 to 7936  (3.08)
A-Dwell    8.8    Hz - Records:  8344 to 8652  (3.08)
A-Dwell    9.0    Hz - Records:  9030 to 9336  (3.06)
A-Dwell    9.2    Hz - Records:  9736 to 10044 (3.08)
A-Dwell    9.4    Hz - Records: 10404 to 10708 (3.04)
```

Figure 1 *Aileron Inputs* - Typical Output Statistics

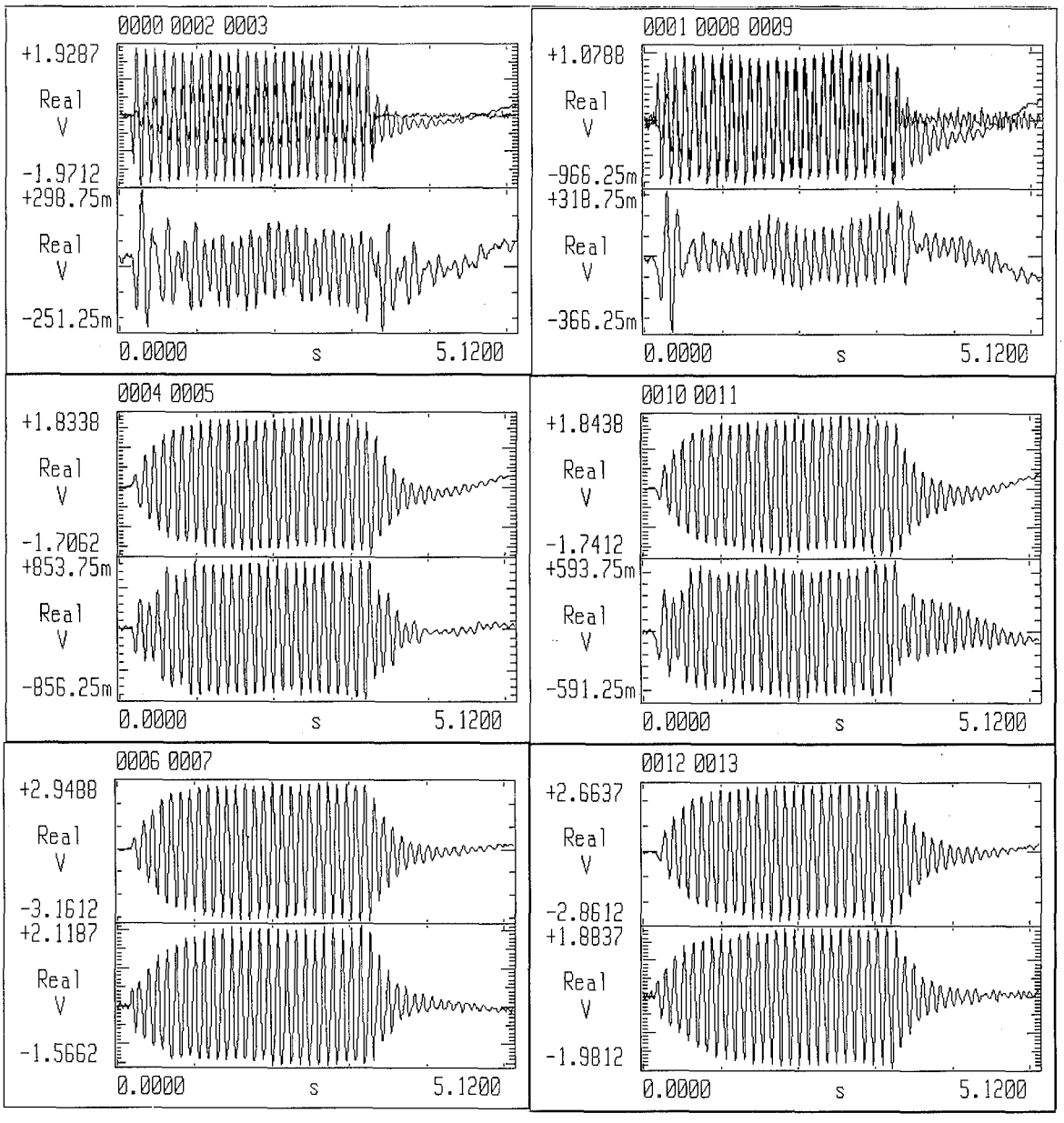

Figure 2 *Time History Play Back* - **8.4 Hz Dwell-Decay .**

Note that, parabolic interpolation of the decay cycle peaks and troughs is performed to improve the accuracy of the analysis. Clearly, this log-dec technique is mainly of use if a response channel (or a linear combination of response channels) can be found where the dwell-decay is essentially in a single mode. Indeed, Canadair has occasionally set-up modal enhancement factors based on GVT mode shape data (spatial filtering). The program summarizes the analysis results in the Figure 3 plot file format.

The *PSD* program performs a power spectral density analysis on selected dwell-decay time history channels. The program is the frequency domain counterpart of the *Log-Dec* program. Again, if the wing strain gauges are selected, the program analyses a left hand wing channel, the corresponding right hand wing channel, and a *symmetry* enhancement. Several PSD analyses are performed per channel; based on different lengths of the time decay (typically, 1.0 (0.2) 2.0 seconds). A frequency resolution of .01 Hz is obtained by using a 8192 byte analysis blocksize. The peak frequency record and two adjacent records are parabolically interpolated to give additional peak frequency accuracy. The half power point damping calculation is split into *upper* and *lower* damping estimates. The half power point frequencies are linearly interpolated between adjacent frequency records. NB Separate *upper* and *lower* damping estimates can be very useful when two closely spaced modes are present in the decay. The analysis results are summarized in the Figure 4 plot file format. The six curves are distinguished by a maximum amplitude calculation (normalized to unity).

Mid Wing Bending Strain Gauges (LHS-RHS)

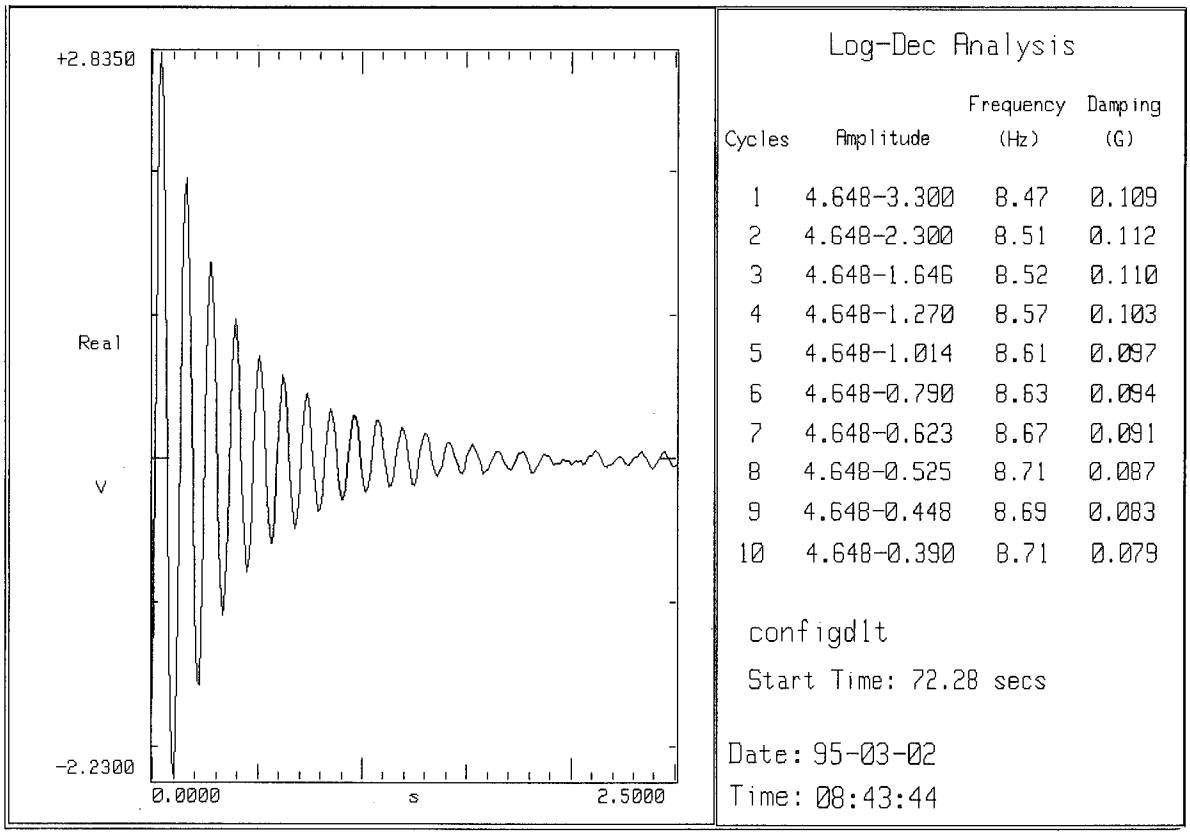

Figure 3 *Log-Dec Analysis* - **8.4 Hz Dwell-Decay**

Mid Wing Bending Strain Gauges (LHS-RHS)

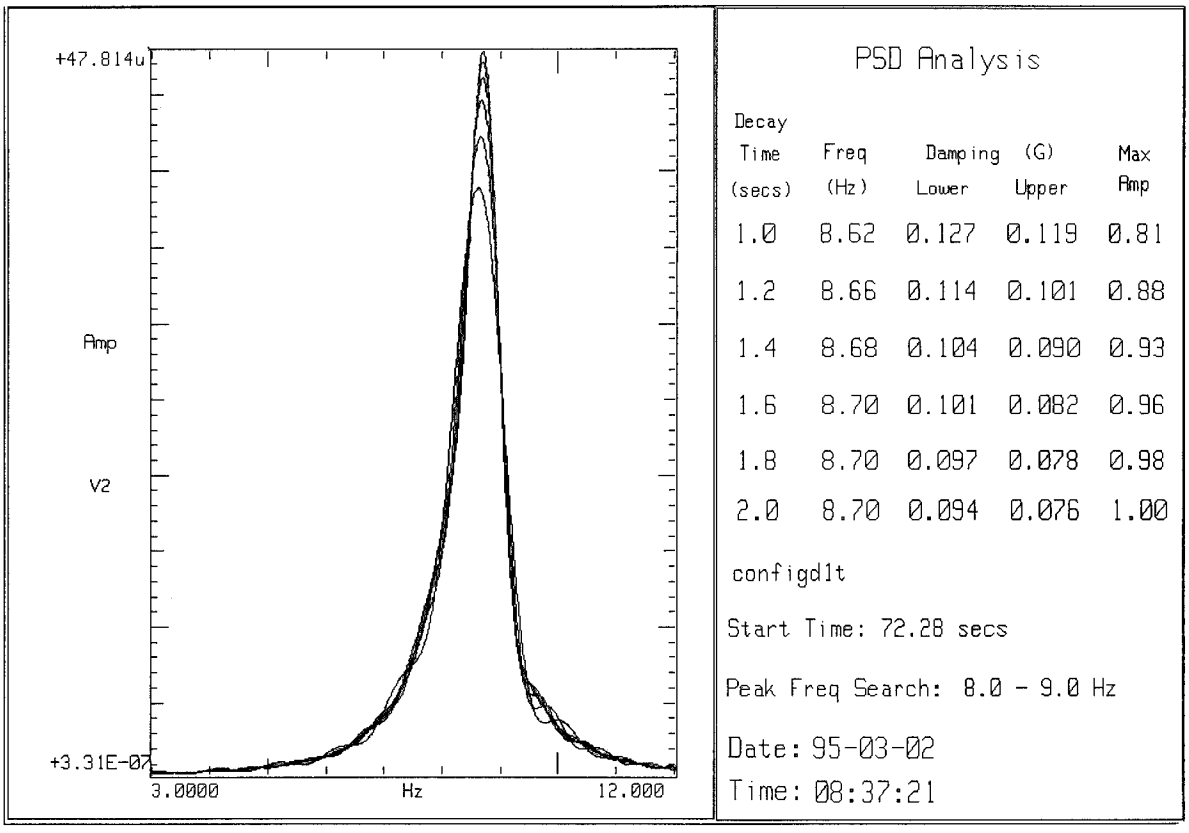

Figure 4 *PSD Analysis* - **8.4 Hz Dwell-Decay**

The *Automated PSD* program is very similar to the *PSD* program. Both programs share common analysis subroutines (eg., peak frequency and half power point damping calculation). The additional automation allows the analysis of up to six dwell decays; giving the *symmetry* enhancement of all six wing strain gauge pairs (ie., a 6 by 6 analysis matrix). The decay time and peak frequency search range can be specified by the user. The analysis results are summarized in the Figure 5 plot file format (one plot for each wing strain gauge pair).

The *FRF Generation* program calculates 14 FRF's based on the Hv estimator with Hamming windowing. The FRF's are the 14 response channels with respect to the left hand aileron motion sensor. The FRF's are calculated for aileron sinusoidal sweep excitation (typically, two 24 second back-to-back sweeps). The user specifies the analysis blocksize (say 1024), number of averages (say 9), overlap (say 50%), and start time. The resulting FRF's typically have a .1 Hz frequency resolution. NB It is important to overlap the FRF's in order to maximize the test point data.

The *MLE FRF Curvefitter* program applies a maximum likelihood estimator (Ref 2) to the FRF's. This frequency domain (single input / single output) curvefitter is applied to all 14 FRF's. The user specifies the frequency range and number of modes. Modal frequency and damping estimates are produced. The Figure 6 plot file summary can be obtained for each FRF. The curvefit is superimposed on the FRF.

The *Flutter Margin Prediction* program applies the Ref 1 flutter onset prediction equations to the sub-critical flight test modal frequency and damping trends. The method assumes a binary flutter mechanism and constant Mach flight test data. The following FM equation is obtained by applying the Routh stability criterion to the characteristic equation of the system:-

$$FM(1) = \left[\frac{w_2^2 - w_1^2}{2} + \frac{d_2^2 - d_1^2}{2}\right]^2$$

$$FM(2) = 4d_1d_2\left[\frac{w_2^2 + w_1^2}{2} + 2\left[\frac{d_2 + d_1}{2}\right]^2\right]$$

Mid Wing Bending Strain Gauges (LHS-RHS)

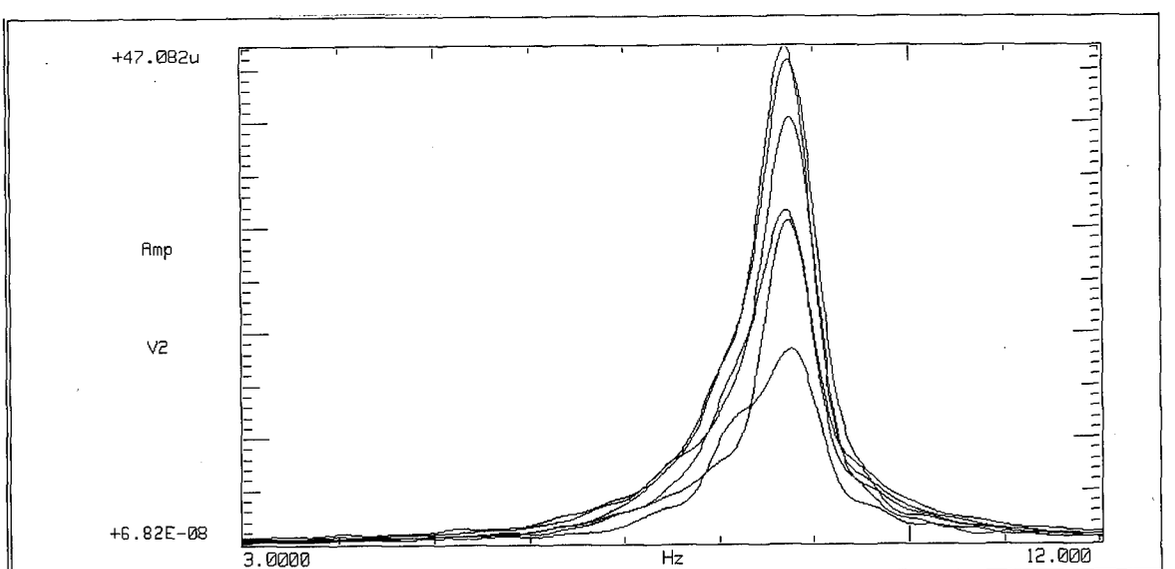

Dwell Frequency	8.0	8.2	8.4	8.6	8.8	9.0	Hz	LJ11-LM11
Decay Time	1.80	1.80	1.80	1.80	1.80	1.80	secs	3.0->12.0 Hz
Peak Frequency	8.73	8.75	8.70	8.73	8.71	8.76	Hz	configb1t
Lower Damping	0.081	0.097	0.097	0.107	0.135	0.179	G	95-02-15
Upper Damping	0.077	0.079	0.078	0.084	0.084	0.083	G	14:41:03
Max Amplitude	0.651	0.859	1.000	0.973	0.671	0.391	Norm	

Figure 5 *Automated PSD Analysis* **- 8.0 to 9.0 Hz Dwell-Decays**

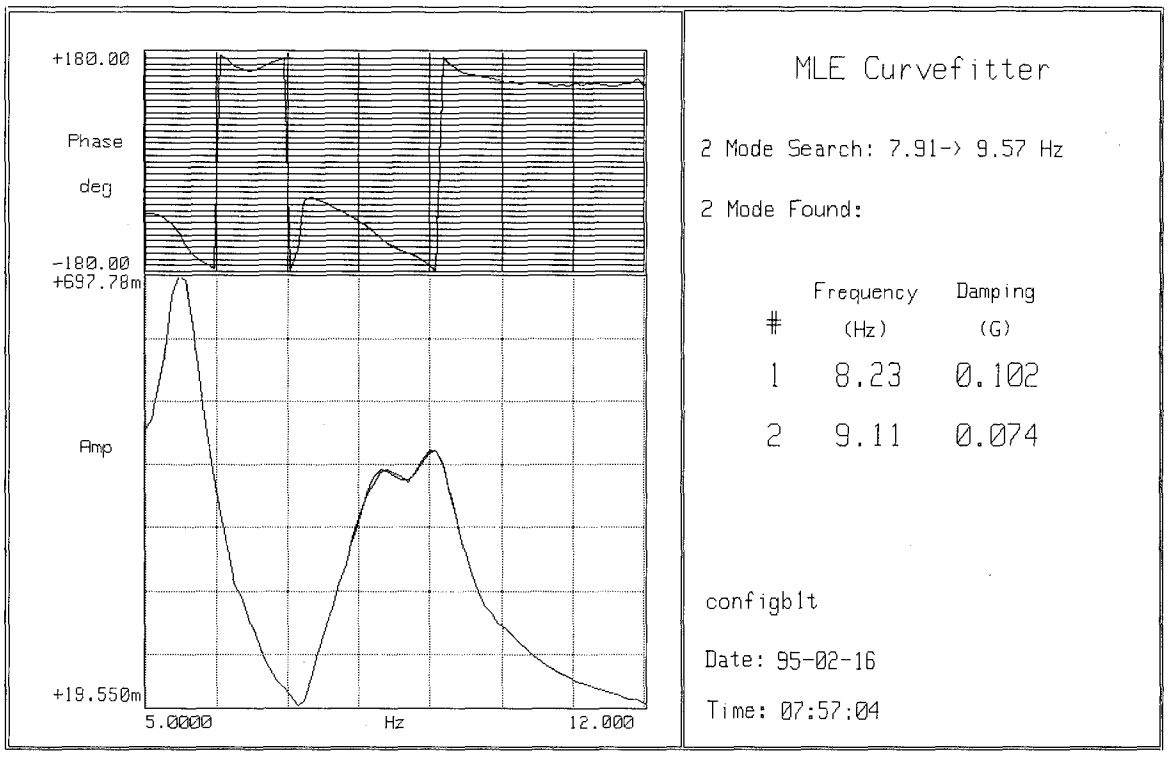

Figure 6 *MLE FRF Curvefitter*

$$FM(3) = \left[\frac{d_2 - d_1}{d_2 + d_1} \times \frac{w_2^2 - w_1^2}{2} + 2\left[\frac{d_2 + d_1}{2}\right]^2\right]^2$$

$$FM = FM(1) + FM(2) - FM(3)$$

The Ref 1 paper calls for a parabolic extrapolation of FM against q. The predicted flutter onset speed is at FM = 0. Subsequent Canadair work has shown that this method is quite sensitive to errors (or uncertainty) in the frequency data. This is particularly true when the two modes are quite close together. It is thus generally accepted that a least squares linear extrapolation of FM against EAS (or q) gives a more reliable estimate of the flutter onset speed. The LMS program currently employs a linear extrapolation against EAS. The results are presented in the Figure 7 plot file format.

CATEGORY II 480 GALLON EFT FFT DATA

The 1992 category II 480 gallon EFT FFT program assessed the flutter stability of the CF-18 aircraft with 480 gallon EFT's on the inboard wing pylons and the AIM-9 wing tip missiles off. Two outboard store loading configurations were flown (symmetric carriage of single Mk-82, and single Mk-83 bombs). Both configurations exhibit the established CF-18 8.5 Hz antisymmetric flutter mechanism; where the AW1B and AOBSPIT modes (at around 8 and 9 Hz, respectively) couple in a binary wing / store flutter mechanism. The more critical Mk-83 configuration was flight tested at three EFT fuel states (25, 50, and 100% full). The remainder of the paper describes the Mk-83 flight testing in some detail.

Ten flights were required to complete the Mk-83 testing. Thirty-six test points (ie., twelve per EFT fuel state) were flown. The aileron bias was switched from +5 to -5 degrees following test point #5 (of 12) in order to minimize the wing fold hinge free-play problems. The *safety-chase* aircraft video-taped the flight #10 test point flying. The tape confirmed that the 480 gallon EFT's exhibit a strong transonic buffet condition (EFT shock-waves, *flapping* main landing gear doors, etc). Indeed, the test aircraft lost a small fuselage access panel and experienced main landing gear door damage, as a result of the flight. It was later concluded that the fuselage damage was exacerbated by the removal of the centerline 330 gallon EFT for this flight.

Figure 8 presents the flight test modal frequency and damping trends from the Mk-83 testing with 100% full EFT's. The results from two separate data reduction techniques (dwell-decay PSD, and FRF / MLE curvefitting) are shown. The FFT data is directly compared with the pre-flight FEM predictions

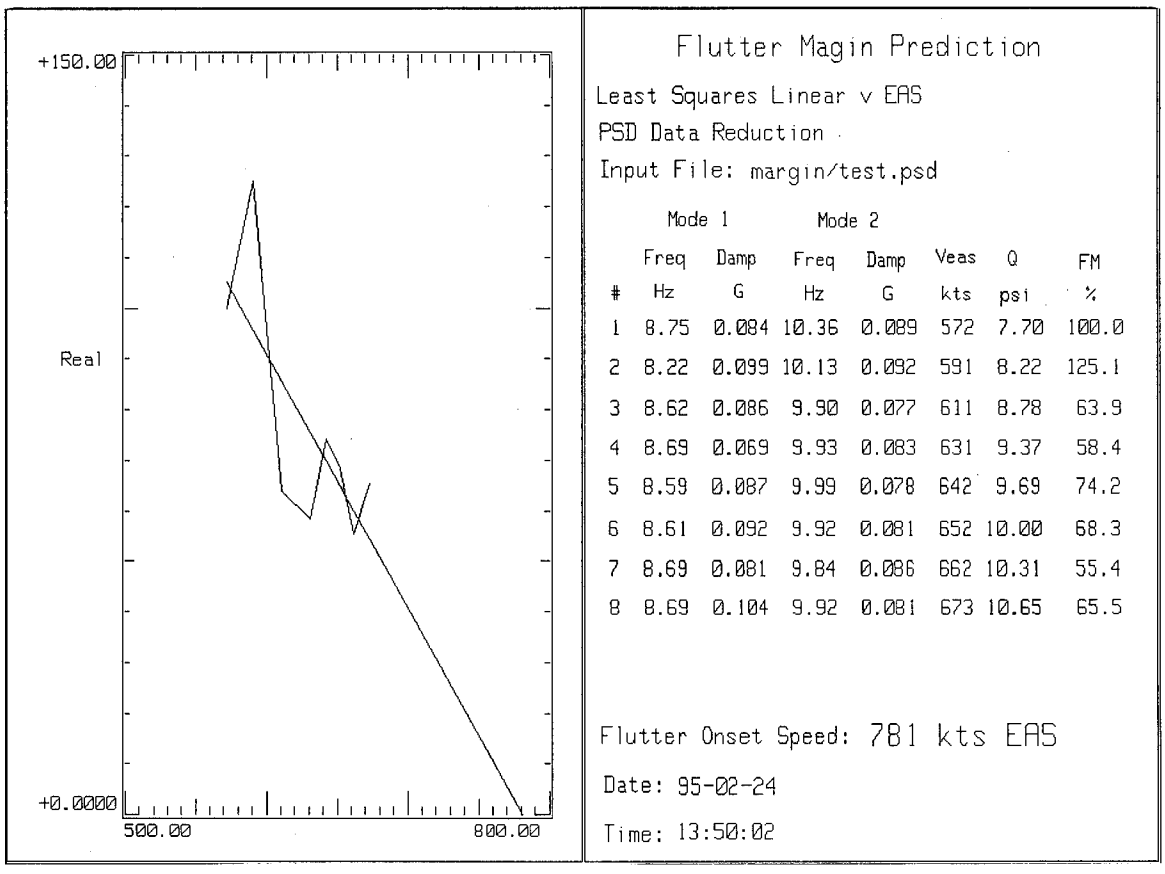

Figure 7 *Flutter Margin Prediction* - **Example Test Case**

(G=.05 structural damping). Test points 1 to 4 are at a moderate Mach number, while 5 to 12 cover a higher Mach. The modal trend plots have therefore been left unconnected between test points 4 and 5. The results from the two FFT data reduction techniques are quite different and deserve further discussion. The dwell-decay PSD analysis capability was programed early in the flight test program, and thus became the routine post-flight data reduction tool. The FRF / MLE curvefitting capability was programed later during the normal *down-time* between flights. It soon became apparent that the FRF / MLE analyses produced lower modal frequency estimates. It was thus decided to separate the two analyses, so that the flutter margin predictions would not be corrupted by these *arbitrary* frequency shifts. NB The final FFT report used the dwell-decay PSD results to set the recommended clearance envelopes.

The reason for the different modal frequency estimates became apparent fairly recently when the Log-Dec capability demonstrated the full extent of the non-linear modal behaviour. Figures 1-6 of the paper actually present test point #1 data from the Mk-83 100% full EFT testing. Figure 1 gives the test point excitation; two 5-12 Hz antisymmetric sweeps, followed by eight 3 second antisymmetric dwells (8.0 (0.2) 9.4 Hz). Figure 2 presents the 8.4 Hz dwell-decay time history data. The Log-Dec analysis of the *antisymmetric enhancement* of the left and right hand mid wing bending strain gauge channels is presented as Figure 3. The decay is essentially in a single mode (AW1B). The modal frequency and damping estimates vary (from cycle to cycle) in a fairly monotonic fashion. The initial decay frequency is quite low with high modal damping (8.47 Hz / G=.109). After 10 cycles, the average decay frequency is 8.71 Hz with G=.079 damping (ie., a modal frequency shift of 0.24 Hz and a damping reduction of G=.03). Figures 4 and 5 present the corresponding PSD analyses. Here, the modal non-linearity is not quite as evident, as all the analyses include at least 1 second of decay (ie., at least 8 cycles). Indeed, the post-flight PSD analyses were typically based on 1.5 to 2.0 seconds of decay. The PSD modal frequency estimates are thus close to the 10 cycle Log-Dec results, and can be characterized as *low amplitude* values. NB It is important not to overly truncate the decay signal as the resulting PSD modal damping estimates will be artificially high. Finally, the Figure 5 FRF / MLE analysis of the left hand mid wing torsion strain gauge response to the 2 antisymmetric sweeps gives quite low frequency and high damping estimates for both modes (AW1B and AOBSPIT). The FRF / MLE modal estimates are thus close to the 1 cycle Log-Dec results, and can be characterized as *high amplitude* values.

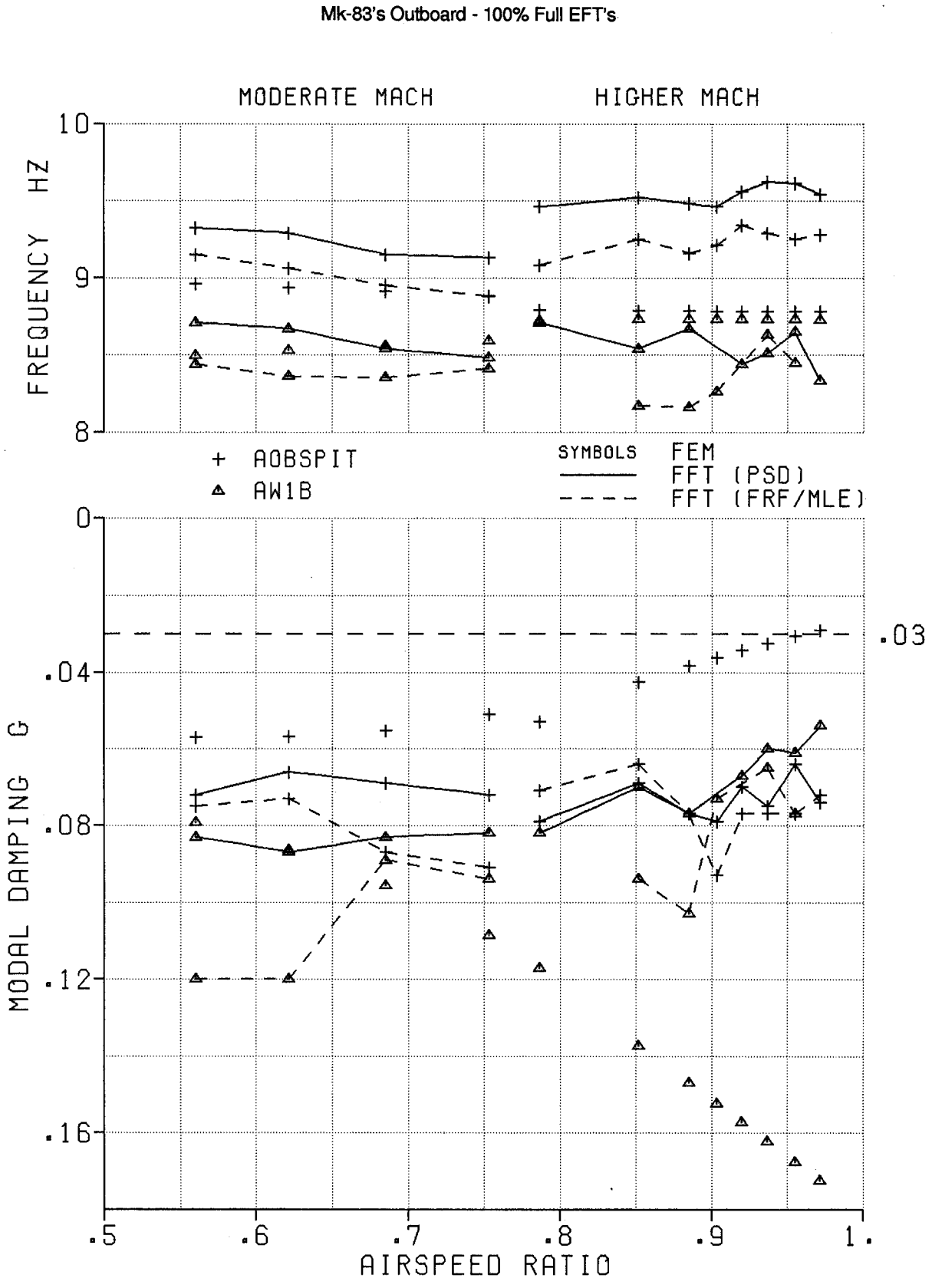

Figure 8 Category II 480 gallon EFT - Modal Trend Plots

CONCLUSIONS

The following conclusions are drawn:-

1. A suite of LMS UPA programs has been developed to tailor and automate the LMS frequency analysis system for CF-18 FFT use. The programs currently provide the following analysis capabilities; (1) aileron inputs; (2) time history play-back; (3) Log-Dec; (4) PSD; (5) automated PSD; (6) FRF generation; (7) MLE FRF curvefitter; and (8) flutter margin prediction.

2. The CF-18 FFT modal data is quite non-linear. The modal frequency and damping values vary with amplitude. For high amplitudes, the modal frequencies are *low* and the modal dampings *high*. As the amplitude decreases, the modal frequency increases and the modal damping decreases. For closely spaced flutter modes, these frequency shifts can become significant compared with the actual frequency separation of the modes. In these situations, it is extremely important to use consistent flight test data reduction techniques. This is particularly true, if the Ref 1 flutter margin equations are used to extrapolate the modal frequency and damping trends to a predicted flutter onset speed.

REFERENCES

1. Zimmerman N.H. and Weissenburger J.T. *Prediction of Flutter Onset Speed Based on Flight Testing at Subcritical Speeds* J. Aircraft Vol 1 No 4 August 1964.

2. Van der Auweraer H., Leuridan J., Pintelon R., and Schoukens J. *A Frequency Domain Maximum Likelihood Identification Scheme with application to Flight Flutter Data Analysis* LMS and Vrije Universiteit Brussel.

A MAXIMUM LIKELIHOOD PARAMETER ESTIMATION TECHNIQUE TO ANALYSE MULTIPLE INPUT/ MULTIPLE OUTPUT FLUTTER TEST DATA

H. Van der Auweraer
LMS International
Interleuvenlaan 68
3001 Leuven
BELGIUM

P. Guillaume
Vrije Universiteit Brussels
Pleinlaan 2
B-1040 Brussels
BELGIUM

INTRODUCTION

To analyse aircraft flutter characteristics, resonance frequencies and damping ratios of the appropriate flight vibration degrees of freedom must be measured at various wind-tunnel or flight test conditions within the flight envelope. Although an aircraft in principle has a large (infinite) number of degrees of freedom, there are usually only a limited number (two or three) that contribute significantly to the particular flutter mechanism and, consequently, only these modes need to be tracked as a function of the flight conditions. [1].

The actual flutter test can be performed with or without artificial excitation. In the latter case, the structural excitation from atmospheric turbulence is used to analyse the dynamic behaviour. In the former case, the structural excitation can be applied, for example, through inertial shakers, aerodynamic vanes, or with control surfaces, stick-jerks, or explosive bonkers. It is important to note that with some of these methods, the excitation (force) signal is often not available as a measured signal.

In the case of using stick jerks or bonkers, the excitation signal type is intrinsically transient. In other cases, random, sine sweeps or sine dwells may also be applied. With excitation from atmospheric turbulence, a white noise random excitation signal is assumed. An overview of a number of these techniques can be found [2,3,4].

The variety in testing and data acquisition methods also implies that the way to process and analyse data is highly dependent on the nature of these data (Fig. 1).

The present paper will further focus on the class of methods where artificial excitation is applied and the forcing signals are measurable.

In this case, both excitation and response signals can be transformed into the Fourier domain. This is generally done through the application of the Discrete Fourier transform. When sufficiently long data segments can be observed, the data can be reduced to a set of auto-, and cross-power functions by means of overlapped segment averaging. From these data, Frequency Response Functions can be estimated between the forcing excitation functions and the induced acceleration responses.

Since atmospheric turbulence is always present even when using artificial excitation, these FRF data will always be contaminated by a large amount of noise, and robust estimators for extracting the system model parameters are required.

In addition, both for safety and economical reasons, one does not always have the possibility of taking long data records. When this situation arises, the auto-, and cross-power averaging and subsequent FRF estimation cannot be performed, requiring that the parameter extraction process should start from the raw, unaveraged frequency spectra of excitation and response signals. This not only puts further demands on the robustness of the parameter extraction algorithms, but it also implies that the estimation methods must have this specific capability of starting from unprocessed frequency spectra.

MAXIMUM LIKELIHOOD ESTIMATION

It is recognised that maximum likelihood (ML) parameter identification techniques have the potential to provide a significant breakthrough in flight flutter test analysis [5]. In ref. [6], the applicability of a single input-single output (SISO) maximum likelihood estimator (MLE) in the frequency domain, which takes into account the disturbing noise on the input as well as on the output, has been demonstrated. It was shown that, compared with methods which only consider the output noise, there is a considerable gain in accuracy, especially when the measurements are very noisy. Moreover, the convergence is excellent and there is a significant reduction in the calculation time compared to the Markov estimator. In addition, the method is capable to start directly from the raw input/output spectra instead of FRFs, and it allows to generate confidence limits for the obtained modal parameters.

Thus, the two conflicting requirements of flight flutter tests, namely maximal reliability and in minimal time, are well satisfied by the proposed method. A limiting factor, however, remains the restriction to the SISO case. It is generally known that the positioning of the shaker and the response transducer plays an important role in the determination of the modal parameters of a mechanical structure. If either the excitation or the response co-ordinates happen to coincide with a node for one of the modes, then that mode will not appear as a resonance on the frequency response function (FRF). One obvious way to decrease that risk is to use

Paper presented at the Structures and Materials Panel Specialists' Meeting on "Advanced Aeroservoelastic Testing and Data Analysis", held in Rotterdam, The Netherlands, from 8-10 May 1995, and published in CP-566.

additional transducers and/or exciters. Generally, single excitation is used in flutter tests, and the transfer functions between the input and the different outputs are analysed one by one. A considerable improvement towards a consistent parameter set would already be to combine all responses in a global, SIMO (single input/multiple output) way.

However, by using multiple input excitations, the amplitude of the vibration across the structure will typically be more uniform, and thus, all parts of the structure can be excited with a smaller probability of having non-linear effects. If the input signals are uncorrelated, a SISO estimator can still be used to estimate the transfer functions among the different force and response transducers one by one. However, we will see that a multi-input, multi-output (MIMO) estimator offers supplementary advantages and is to be preferred.

In the following section, the basic formula for the MIMO estimator is summarised, a more in-depth explanation of the SISO version can be found in [6-8]. By means of simulations the superiority of the MIMO estimator over the SISO estimator is demonstrated. Finally, flight flutter data will be processed by both estimators.

THE MIMO ESTIMATION ALGORITHM

The parametric frequency domain estimator presented in this section estimates the unknown coefficients of the polynomials occurring in the transfer function matrix of the device under test (DUT).

$$H(s) = \frac{N(s)}{d(s)} \tag{1}$$

$N(s)$ is a $p \times m$ polynomial matrix with m the number of inputs and p the number of outputs of the DUT. The entries $n_{ij}(s)$ of the matrix $N(s)$ are given by

$$n_{ij}(s) = a_0^{ij} + a_1^{ij} s + \cdots + a_{\alpha_{ij}}^{ij} s^{\alpha_{ij}} \tag{2}$$

Note that all the denominators of the transfer functions in $H(s)$ are set equal to the polynomial

$$d(s) = b_0 + b_1 s + \cdots + b_\beta s^\beta \tag{3}$$

which is the least common multiple of the denominators of the entries of $H(s)$. The zeros of $d(s)$ correspond with the natural modes of the system. The indices α_{ij} $(\forall i, j)$ and β stand for the order of polynomials $n_{ij}(s)$ and $d(s)$ respectively.

The number of unknown coefficient occurring in the transfer functions is $\sum \alpha_{ij} + mp + \beta$ since one of the $\sum \alpha_{ij} + mp + \beta + 1$ coefficients in the numerators and denominator is redundant. For instance, one can set the coefficient b_0 of the denominator equal to one. The parameters to be estimated are then

$$\theta^T = \left[a_0^{11}\, a_1^{11} \cdots a_{\alpha_{11}}^{11}\, a_0^{12} \cdots a_0^{21} \cdots a_{\alpha_{pm}}^{pm}\, b_1\, b_2 \cdots b_\beta \right] \tag{4}$$

The perturbations induced by the measurement and the process noise are represented by the following frequency domain error-in-variables (EV model)

$$\begin{cases} x_M(k) = x(k) + v(k) \\ y_M(k) = H(k)x(k) + w(k) \end{cases} \tag{5}$$

where $x(k)$ and $x_M(k)$ are $m \times 1$ vectors respectively the exact and the measured Fourier coefficients of the inputs, $y_M(k)$ represents a $p \times 1$ vector with the measured Fourier coefficients of the outputs as entries, and the vectors $v(k)$ and $w(k)$ stand for noise on the input and output coefficients respectively. All these quantities are evaluated at the frequencies f_k $(k = 1, 2, \cdots, F)$.

Assuming that the noise on the real and imaginary part of the spectra of the input and output signals are independent, zero mean, Gaussian random variables, it can be proven that the Maximum Likelihood (ML) estimate $\hat{\theta}_{ML}$ of the modal parameters is found by minimising the cost function

$$(K) = \frac{1}{2} \sum_{K=1}^{F} e_M^H(k) C_e^{-1}(k) e_M(k) \tag{6}$$

where $(\cdot)^H$ represents the complex conjugate transpose operator and,

$$e_M(K) = N(k)x_M(k) - d(k)y_M(k) \tag{7}$$

The matrix $C_e^{-1}(k)$ in equation (6) is found by inverting the following Hermitian matrix

$$C_e(k) = N(k)C_x(k)N^H(k) + |d(k)|^2 C_y(k) \tag{8}$$

where $C_x(k)$ and $C_y(k)$ represent the covariance matrices of the perturbation noise of the inputs and the outputs respectively at the frequency f_k [9]. These can be determined from a priori measurements [7,11].

A critical step in the estimation process is the selection of he order of the numerator and denominator polynomials. This can be done from a visual inspection of the FRFs, or through the application of more advanced analysis tools such as multi-frequency singular value decomposition [14]. Using the property that the expected value of the cost function, when no model errors occur, equals [13].

$$Ek = pF - \frac{n}{2} \tag{9}$$

with n the number of unknown parameters, the validity of the suggested model can be tested and order modifications can be done if necessary.

Notice that the cost function is a strong non-linear function of the unknown parameters. Solving the equations requires an efficient and accurate iterative procedure. It has been observed that the Gauss-Newton method can be useful to determine the minimum of the cost function. The least squares (LS) solution $\hat{\theta}_{LS}$ [12], obtained by setting $C_e(k)(\forall(k))$ equal to the identity matrix in equation (6), can be used as a start value for the iterative Gauss-Newton process.

COMPARISON OF THE SISO AND MIMO MLE BY MEANS OF SIMULATIONS

The estimates of the MIMO method described in the previous section will now be compared with these of the SISO algorithm for the estimation of linear systems (ELiS) [6-8]. Thereto, synthetic data for a DUT with one input and three outputs is generated. The exact parameters of DUT are given in Table 1.

Table 1 Exact modal parameters

Numerator of transfer functions	Zero		Natural frequency (Hz)	Damping ratio (%)
	Re	Im		
1	-0.8	±250.0	39.78893949	0.32999836
2	-1.2	±180.5	28.72810208	0.66480525
3	-0.5	±150.0	23.87337409	0.33333148
Denominator of transfer functions	**Pole**		**Natural frequency (Hz)**	**Damping ratio (%)**
	Re	Im		
1, 2 and 3	-1.5	±180.0	28.64888446	0.83330440
	-1.0	±300.0	47.74674817	0.33333148

The exact FRFs are shown in Fig. 2. Note, in the second transfer function, the presence of a pole and a zero which are very close to each other. As the input signal we use a multi-sine formed by summing sine waves with equal amplitudes and with frequencies uniformly distributed in the range of interest. To simulate the measurement inaccuracies, zero mean coloured Gaussian noise is added to the exact Fourier coefficients of the input signal and the three output signals. The FRFs derived from these noise signals, with a mean signal-to-noise ratio per spectral line of 17 dB, are shown in Fig. 3. Note that, due to the addition of noise, the first pole and the zero of the second transfer function are no longer apparent in the plot.

For the SISO and MIMO estimations, 25 spectral lines, uniformly distributed between 15 and 60 Hz of the noisy input and output signals are selected.

The model orders for the SISO estimations are given in Table 2.

Note that due to a pole-zero cancellation, the model order of the transfer function had to be reduced in order to obtain good estimates [6]. The results of the SISO estimator, averaged over 100 experiments, are shown in Table 3. The standard deviations are given in parentheses.

The results of the MIMO estimator are summarised in Table 4. Polynomials of order two were used for the numerator of all the transfer functions $(\alpha_{11} = \alpha_{21} = \alpha_{31} = 2)$ and the order of the polynomial $d(s)$ was set equal to four $(\beta = 4)$.

Notice that the MIMO estimator is able to find good estimates of the closely positioned pole and is zero in the second transfer function where the SISO estimator failed. The good results of the MIMO estimator have to be attributed to the fact that all the measurements of one experiment are processed together, and to the addition of links among some of the parameters (e.g. equal denominators). The introduction of links among the coefficient of the different transfer functions not only reduces the number of parameters to be estimated, its main purpose is to relate the information present in the input-output data as closely as possible to each other. Without these links, the MIMO estimator loses a lot of its power.

The simulation results given in this section clearly illustrate the role of the links. By stating that the denominator of all transfer functions are equal to $d(s)$, it is even possible to estimate accurately the zero of the second transfer function. We found -1.27628 ± j180.552 which is close to the exact value -1.2 ± j180.5. Indeed, the input-output data of the three transfer functions are used together to estimate the coefficients of $d(s)$. From the first and the third FRF of Fig. 3 it is clear that there is a pole around 28.7 Hz. So, the MIMO estimator knows that the second subsystem must also have a zero in the immediate vicinity of that pole to obtain a flat course of its FRF plot in that region. The SISO estimator, on the other hand, processes the input and the output Fourier coefficients of the different transfer functions one by one. So, the data of the other transfer functions do not contribute to the improvement of the accuracy of the estimated transfer function parameters.

Table 2 SISO model orders

Transfer function	Order numerator	Order denominator
1	2	4
2	0	2
3	2	4

In Tables 3 and 4, the standard deviation of the SISO and MIMO estimates are given between parentheses. It is noticeable that the standard deviation of the SISO estimates are on average 25% larger than for the MIMO case. Thus the SISO estimator is no longer efficient when used to estimate the MIMO system. Notice, however, that the estimates of the denominator, obtained with the SISO estimator, can be averaged over the different transfer functions to obtain better estimates.

Table 3 Results of the SISO estimator

Numerator of transfer functions	Zero		Natural frequency (Hz)	Damping ratio (%)
	Re	Im		
1	-0.792 (0.048)	± 249.919 (0.047)	39.7761 (0.0074)	0.317 (0.019)
3	-0.468 (0.040)	± 149.972 (0.039)	23.87337409	0.312 (0.026)

Denominator of transfer functions	Pole		Natural Frequency (Hz)	Damping ratio (%)
	Re	Im		
1	-1.525 (0.045)	± 180.016 (0.044)	28.6515 (0.0070)	0.847 (0.024)
	-1.006 (0.064)	± 299.968 (0.059)	47.7416 (0.0093)	0.335 (0.021)
2	-1.040 (0.056)	± 299.970 (0.054)	47.7419 (0.0086)	0.347 (0.018)
3	-1.534 (0.039)	± 180.013 (0.039)	28.6511 (0.0061)	0.852 (0.022)
	-0.978 (0.060)	± 300.025 (0.057)	47.7507 (0.0090)	0.326 (0.020)

Table 4 Results of the MIMO estimator

Numerator of transfer functions	Zero		Natural frequency (Hz)	Damping ratio (%)
	Re	Im		
1	-0.819 (0.032)	± 249.943 (0.032)	39.7799 (0.0050)	0.328 (0.013)
2	-1.276 (0.040)	± 180.552 (0.041)	28.7364 (0.0065)	0.707 (0.022)
3	-0.443 (0.030)	± 149.946 (0.031)	23.8648 (0.0050)	0.296 (0.020)

Denominator of transfer functions	Pole		Natural Frequency (Hz)	Damping ratio (%)
	Re	Im		
1, 2 and 3	-1.537 (0.036)	± 180.012 (0.036)	28.6509 (0.0057)	0.854 (0.020)
	-1.007 (0.048)	± 299.983 (0.047)	47.7440 (0.0074)	0.336 (0.016)

The standard deviation will not however decrease with the square root of the number of samples as is the case for stochastic independent variables. To be more specific, consider the following example. Take for instance two stochastic variables u_1 and u_2 with standard deviation σ. When the two variables are uncorrelated the standard deviation of the sample mean $\overline{u}$ equals $\frac{\sigma}{\sqrt{2}}$ but when correlations exist, the standard deviation of $\overline{u}$ is given by

$$std\,\overline{u} = \sqrt{\frac{\sigma^2 + \mathrm{cov}(u_1, u_2)}{2}} \qquad (10)$$

Thus, if the positive correlation exists, the standard deviation will decrease less or possibly not at all if the variables are totally correlated $\left[\mathrm{cov}(u_1, u_2) = \sigma^2\right]$.

Due to the fact that the same input signal is used to excite the three subsystems, positive correlations are introduced among the different SISO estimates. Even when averaged, the standard deviation of the SISO estimates will not become smaller than the MIMO ones.

COMPARISON OF THE NATURAL FREQUENCIES AND DAMPING RATIOS WITH THE SISO AND THE MIMO ESTIMATOR WHEN APPLIED TO REAL MEASUREMENTS

In this section flutter data is processed by the two estimators and the results are compared. The data was obtained by shaking a wing of an aeroplane and recording the applied force and the response signals at several points. A burst sine excitation was applied. The signals are given in Fig. 4. The Fourier coefficients are determined with a DFT algorithm

(see Fig. 5). Only the 36 most significant spectral lines, which all lie between 7.8 and 8.8 Hz, are used for the estimations.

Via an a priori noise analysis, it is found that the power spectra of the input and output noise are approximately flat [8,10].

A transfer function matrix model, with numerators and denominators of second order, is used to estimate the DUT. All the denominators are assumed to be equal during the MIMO estimation. Table 5 summarises the results of the estimated poles. The standard deviations are given in parentheses.

Notice that the standard deviation of the SISO estimates are approximately 50% larger than the MIMO standard deviations. Notice also that, due to the smaller ratio of the number of unknown parameters to the number of processed input-output data, the MIMO estimator is more likely to have reached its asymptotic behaviour than the SISO estimator. Thus, the bias on the MIMO estimates is suspected to be less important than the SISO ones.

Table 5 Flutter data results

SISO estimator applied to input 1 and output 1	
Re (Pole)	-1.013 (0.078)
Im (Pole)	50.679 (0.070)
f_0	8.067 (0.011)
ω_0	50.689 (0.071)
ζ	0.0200 (0.0015)
MIMO estimator applied to all the measurements	
Re (Pole)	-1.015 (0.051)
Im (Pole)	50.991 (0.046)
f_0	8.1171 (0.0074)
ω_0	51.001 (0.046)
ζ	0.0199 (0.0010)

CONCLUSIONS

In this paper, the formulation of the Maximum Likelihood SISO (Single Input / Single Output) estimator, (ELiS) is generalised for MIMO (Multiple Input / Multiple Output) systems. The behaviour of the two ML estimators is compared when applied to real and synthetic data. The following conclusions can be drawn:

When a mechanical structure is excited at different places or/and the response is monitored at several points, the MIMO estimator can extract more information out of the measurements than the SISO estimator. The gain obtained by using the MIMO estimator is essentially due to the assumption of global parameters in the transfer function matrix. The result is independent of the estimation method used. Usually it is assumed that the transfer functions of the transfer function matrix equation (1) all have common poles. The more links the better the interaction among the measurements. In one of the test cases, it was therefore possible to estimate a pole-zero pair which was completely hidden by the noise thanks to the information present in the input-output measurements related to the other transfer functions.

Due to the relatively large amount of data processed by the MIMO estimator, the asymptotic properties of the ML estimators are reached sooner. When the input signals are correlated, the SISO estimator cannot be used without introducing supplementary errors.

REFERENCES

[1] C.W. Skingle, 1981, "Practical Applications of System Identification in Flutter Testing", DGLR Bericht 82-01, Proc. Int. Symposium on Aeroelasticity, Nurnberg (FRG), Oct. 5-7, 1981, pp. 121-129.

[2] H. Zimmerman, R. Destuynder, 1982, "Flight Flutter Testing with Emphasis on the Tip Vane Method", AGARD Conf. 339 on Ground Flight Testing & Correlation, 1982.

[3] K. Koenig, 1990, "Flight Flutter Parameter Identification", presented at the AGARD meeting, Spring, 1990.

[4] H. Van der Auweraer, K. Ishaque, J. Leuridan, 1990, "Signal Processing and System Identification Techniques for Flutter Test Data Analysis, Proc. 15-th Int. Seminar on Modal Analysis, K.U. Leuven, Mech. Eng. Dept., Leuven (B), Sept. 17-21, 1990, pp. 517-538.

[5] G.L. Ghiringhelli, M. Lanz and P. Mantegazza, 1987, "A Comparison of Methods used for the Identification of Flutter from Experimental Data", Journal of Sound and Vibration 119, 39-51, 1987.

[6] R. Pintelon, J. Schoukens and P. Guillaume, 1989, "Parametric Frequency Domain Modelling in Modal Analysis", Mechancial Systems and Signal Processing 3, 398-403, 1989.

[7] J. Schoukens, R. Pintelon and J. Renneboog, 1988, "A ML Estimator for Linear and Non-Linear Systems - A Practical Application of Estimation Techniques in Measurement Problems", IEEE Transactions on Instrumentation and Measurement, IM37;10-17, 1988.

[8] R. Pintelon, 1988, "Analysis and Application of A Maximum Likelihood Estimator for Linear Systems", PhD Dissertation, Vrije Universiteit Brussels, 1988.

[9] J. Schoukens and J. Renneboog, 1985, "Study of the Noise Influence on the Fourier Coefficients after a Discrete Fourier Transform", IEEE Transactions on Instrumentation and Measurement, IM35, 278-286, 1985.

[10] J. Schoukens, 1985, "Parameterestimatie in Lineaire en Niet-Lineaire Systemen met Behulp van Digitale Tijdsdomein Metingen"; PhD Dissertation, Vrije Universiteit Brussels, 1985.

[11] J. Schoukens, R. Pintelon, E. Van Der Ouderaa and J. Renneboog, 1988, "Survey of Excitation Signals for FFT Based Signal Analysers", Proc. of the 13th Seminar of Modal Analysis, September 19-23, Leuven (B), 1988.

[12] E.C. Levi, 1959, "Complex Curve Fitting", IRE Transactions on Automatic Control, 37-43, 1959.

[13] J. Schoukens and R. Pintelon, 1988,"On the Limits of Order Estimation", Proc. of the 8th Symposium on Identification and System Parameter Estimation, August 27-31, 1988, Beijing, pp. 1026-1031.

[14] D. Otte, 1994, "Development and Evaluation of Singular Value Analysis Methodologies for Studying Multivariate Noise and Vibration Problems", PhD Dissertation, Katholieke Universiteit Leuven, 1994.

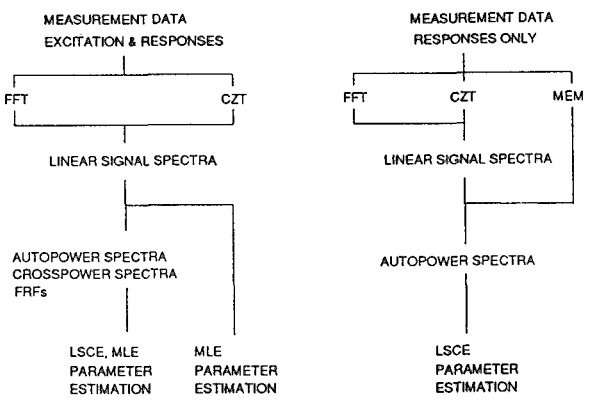

Figure 1 Flutter data analysis approaches

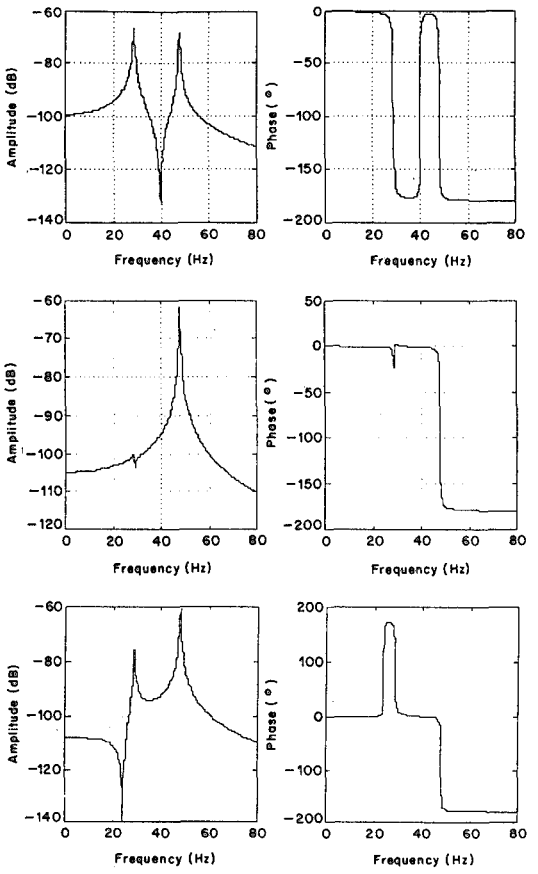

Figure 2 Simulations- Exact FRFs

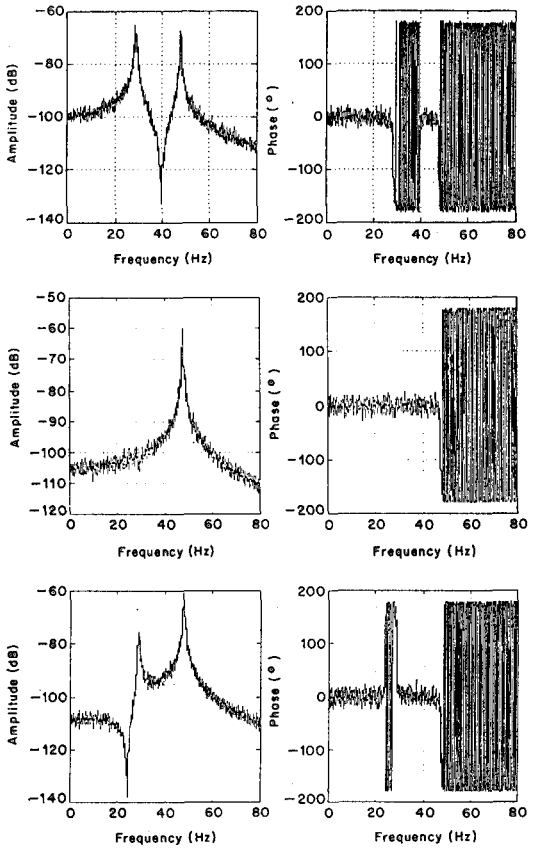

Figure 3 Simulations - Perturbed FRFs

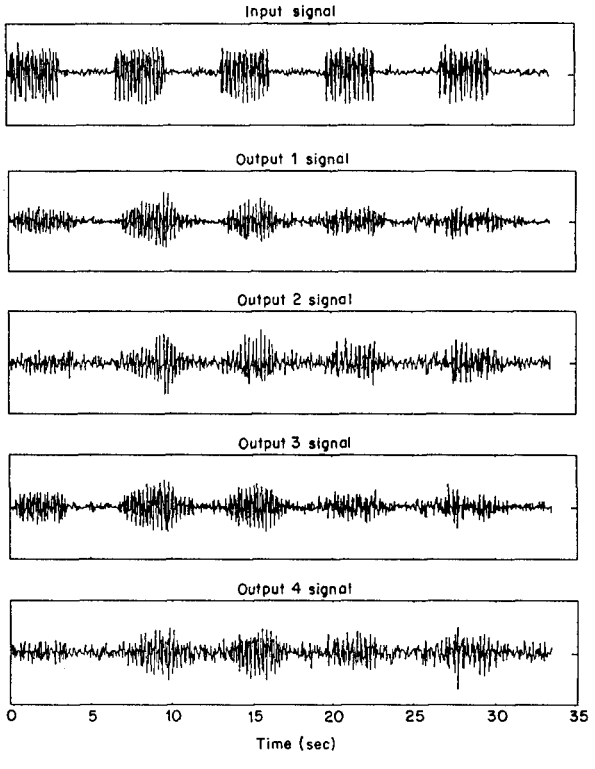

Figure 4 Flutter data - Time histories

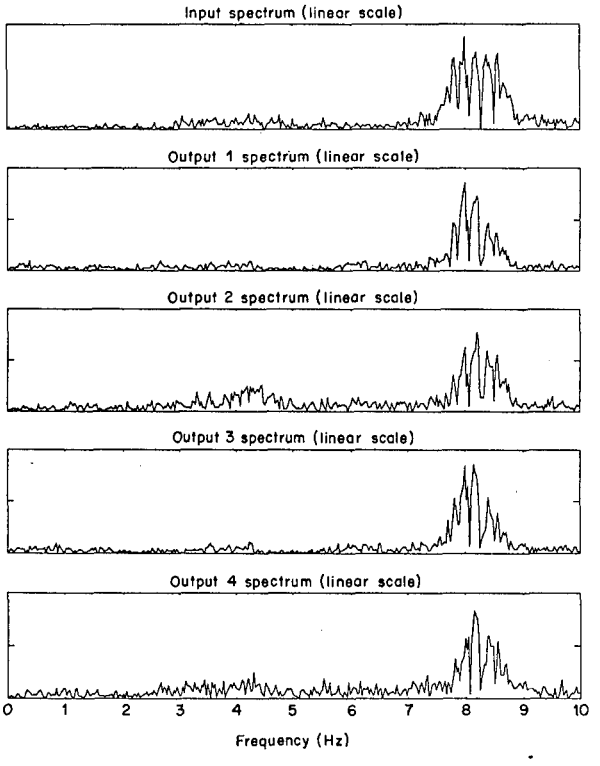

Figure 5 Flutter data - Spectra

ADVANCES IN THE ANALYSIS OF FLIGHT FLUTTER TEST DATA

J.E. Cooper, M.J. Desforges, P.R. Emmett & J.R. Wright

School of Engineering
University of Manchester
Manchester M13 9PL, UK.

1.SUMMARY

A number of methods developed with the aim of improving the analysis and interpretation of flight flutter test data are described. The approaches are divided into improved curvefitting techniques and methods for enabling increased confidence in the flutter clearance procedure. Real and simulated flight flutter data are used to illustrate the various approaches.

2.INTRODUCTION

Flight flutter testing [1,2] is a critical stage in the development of any prototype aircraft. The requirement is for a flight envelope to be cleared safely and with confidence; however, the flutter clearance needs to be completed in as few flights as possible. The data analyzed in flight flutter tests is often corrupted significantly with the effects of turbulence and also tends to suffer from inadequate excitation of the aircraft, a limited number of transducers and problems with maintaining a steady flight condition at the extremes of the flight envelope. It is therefore critical that high quality system identification methods are employed to produce accurate frequency, damping and, possibly, mode shape estimates. Damping is the most critical parameter for flight testing; however, it is the most difficult parameter to identify accurately, especially where modes are very close in frequency. Hence, the analysis of flight flutter test data is seldom straightforward.

The usual approach to flight flutter testing is to test at a particular point in the flight envelope and to extrapolate frequency and damping trends in order to establish whether it is safe to proceed to the next test point. Traditionally this process has been performed manually, depending greatly upon the test engineer's experience and interpretation of the results.

This paper is divided into two sections. The first section deals with advanced system identification methods employed for the analysis of flight flutter data. One method, the Eigensystem Realisation Algorithm using Data Correlations (ERA/DC) [3,4], is based in the time domain whereas the other, the Instrumental Variables Output Error Method (IV/OEM) [5], performs a curve-fit in the frequency domain. An approach is also described that produces confidence bounds on the frequency and damping estimates that are obtained [6].

The second section of this work describes a number of methods that are intended to improve the confidence in the overall flight flutter testing process. The 'envelope function' is a tool for assessing the overall stability of the aircraft without explicitly performing any curve-fitting [7]. An approach for automating the tracking of modes making use of the Modal Assurance Criterion [8], and an approach utilising a force appropriation method [9] to enable modes with very close natural frequencies to be excited individually, are also described.

It is intended that these developments can be used to improve the confidence in flight flutter testing procedures, thereby not only making the process safer, but also enabling the test schedule to be carried out more efficiently.

3. CURVE FITTING

Due to the difficulties associated with obtaining good flight flutter test data, it is imperative that robust parameter identification methods, able to deal with noisy data from systems with high modal densities, are used. In this section, two curve-fitting techniques are described that meet these criteria, together with a method for obtaining statistical error bounds on the parameter estimates.

3.1 Eigensystem Realization Algorithm using Data Correlations (ERA/DC)

3.1.1 Introduction

The ERA/DC method [3] is a time domain system identification technique that can be used to estimate the parameters of a state space model from decay response time data. These parameters can then be used to estimate the natural frequencies, damping ratios and mode shapes. The technique can produce accurate modal parameter estimates for systems with very close natural frequencies, and is a global identification method in that multiple responses from a number of separate input cases can be analyzed simultaneously to

Paper presented at the Structures and Materials Panel Specialists' Meeting on "Advanced Aeroservoelastic Testing and Data Analysis", held in Rotterdam, The Netherlands, from 8-10 May 1995, and published in CP-566.

provide a single set of damping and frequency estimates. The method has been compared with a number of different system identification approaches and performed very well in terms of accuracy and computational requirements.

For flight flutter testing, the decay response used can be one of the following:

1. Inverse Fourier Transform of the Frequency Response Function (FRF),
2. response to an impulse such as a stick jerk or pyrotechnic device, or
3. decaying response function generated from the response to an unmeasured random input using, for example, the Autocorrelation or Random Dec methods.

Unlike the original Eigensystem Realisation Algorithm (ERA) approach, where the fundamental component of the method is a least squares minimisation of a difference equation response model, the ERA/DC method permits the user to perform the curve-fit using response data correlations. Those correlations considered most likely to cause bias errors can be eliminated from the curve-fitting process. Compared to the ERA approach, it has been found that the ERA/DC method enables accurate estimates to be found for modes close in frequency using smaller model orders, as well as requiring smaller matrices to be manipulated, thereby reducing the required computational time.

A key element in the ERA/DC method, that differs from other popular time domain system identification methods such as Polyreference, is the use of the Singular Value Decomposition (SVD) in order to produce a 'minimum order realisation' which, theoretically, enables all of the spurious modes to be eliminated during the estimation process rather than attempting to eliminate them once the modal parameters have been found. In practice, it is not feasible to discard all of the spurious modes; however, a large proportion of them can be rejected through the use of the SVD.

3.1.2 Mathematical Model

The ERA/DC method models the response of an m mode system to an impulse for (ni) input and (no) measurement stations at time instant (k+1) as

$$Y_{k+1} = CA^{k}B \tag{1}$$

where Y is an (no*ni) block data matrix, A is the (2m*2m) system matrix, and C and B are the (no*m) output and (m*ni) input state space matrices respectively. The technique finds a realisation (i.e. estimate) for matrices A,B and C.

Define the block Hankel matrix H_k as

$$H_k = \begin{bmatrix} Y_{k+1} & Y_{k+2} & . & . & Y_{k+\eta+1} \\ Y_{k+2} & Y_{k+3} & . & . & Y_{k+\eta+2} \\ . & . & . & . & . \\ . & . & . & . & . \\ Y_{k+\zeta+1} & Y_{k+\zeta+2} & . & . & Y_{k+\eta+\zeta+1} \end{bmatrix} \tag{2}$$

where ζ and η determine the number of data points involved. Then the correlation matrix R_k can be defined as

$$R_k = H_k H_o^T \tag{3}$$

and block correlation Hankel matrix U_q constructed such that

$$U_q = \begin{bmatrix} R_q & R_{q+r} & . & . & R_{q+\beta r} \\ R_{q+r} & R_{q+2r} & . & . & R_{q+(\beta+1)r} \\ . & . & . & . & . \\ . & . & . & . & . \\ R_{q+\alpha r} & R_{q+(\alpha+1)r} & . & . & R_{k+(\alpha+\beta)r} \end{bmatrix} \tag{4}$$

where α and β determine the size of the matrix. Parameter q is set so that the low lag value correlations that rise to biased estimates can be omitted from the fit. The r parameter enables the U_q matrix to be set up without any overlap between the R_k blocks.

The SVD of matrix U_q is found in the form

$$U_q = P D Q^T \tag{5}$$

where the matrix D of singular values has been truncated to only contain those singular values that are non-zero (i.e. significant); thus zero, and in practice

very small, singular values are ignored. The P and Q matrices of singular vectors have dimensions consistent to those of the D matrix. The realization can be shown to give the following expression for the system matrix

$$A = D^{-1/2} P^T U_{q+1} Q D^{-1/2}$$

and the eigenvalues of this matrix lead to the system frequencies and dampings.

3.1.3 Application to Flight Flutter Test Data

Over a number of years the ERA/DC technique has been applied successfully to the analysis of flutter test data of both commercial and military aircraft [4], using both stick jerk data and also impulse response functions generated from FRFs between measured input and output time signals.

As an example, consider the stick jerk response and corresponding Spectrum Amplitude of flight flutter test data from a four-engined commercial aircraft, shown in Figures 1 and 2. Figure 3 shows the resulting stabilisation diagram from the analysis for differing amounts of truncation in the number of singular values used in the analysis; the stabilisation diagram shows how estimates from different model orders converge in frequency and damping. It can be noted how little overspecification of the mathematical model is required before stabilised results are achieved. Finally, Figure 4 shows the estimated damping trends for a number of flight speeds indicating that the aircraft remains stable and that results are consistent between flight points.

3.2 Instrumental Variables Output Error Method (IV/OEM)

3.2.1 Introduction

An ideal modal parameter estimator for use in flight flutter testing would possess a number of qualities. The method should be fast in application, make efficient statistical use of data, and provide the test engineers with a reliable assessment of the accuracy with which each modal parameter has been identified. The Instrumental Variables Output Error Method (IV/OEM) approach, used in conjunction with the confidencing techniques described below, performs well in terms of these criteria when compared to methods in current use. The method is formulated in the frequency domain. A full description and assessment of the approach is presented in [5].

3.2.2 Theory

The response $Y(\omega)$ of a transducer to a measured input signal $U(\omega)$ in the frequency domain may be approximated by the following relation

$$Y(\omega) = \frac{p_o + p_1 i\omega \ldots + p_{np}(i\omega)^{np}}{1 + q_1 i\omega \ldots + q_{nq}(i\omega)^{nq}} U(\omega) + N(\omega) \quad (6)$$

where p and q are coefficients of the numerator and denominator polynomials, np and nq define the polynomial orders and the term $N(\omega)$ represents the total influence of errors due to measurement noise and the response to unmeasured aerodynamic excitation. By multiplying through by the denominator polynomial, the set of such equations obtained for each frequency of interest may be written,

$$b = [\Delta]x + \nu \quad (7)$$

where $b_k \triangleq Y(\omega_k)$ is the kth element of b, and the parameter vector $x \triangleq (q_1, q_2, \ldots, q_{nq}, p_0, q_1, \ldots, p_{np})^T$. The kth row of $[\Delta]$, which will be denoted δ_k, is defined by

$$\delta_k \triangleq \left(-i\omega_k Y, -(\omega_k)^2 Y, \ldots, -(i\omega_k)^{nq} Y, \; U, i\omega_k U, \ldots, (i\omega_k)^{np} U \right) \quad (8)$$

The method of linear least squares, commonly applied to solve for the unknown polynomial coefficients x in (7), may be shown to produce parameter estimates which do not approach the true values, even with an infinite amount of data; the estimates are then said to be biased. In order to overcome this problem, a method of solution known as instrumental variables may be employed; the solution of equation (7) now becomes,

$$\hat{x}_{iv} = \left([Z]^T [\Xi][\Delta] \right)^{-1} \left([Z]^T [\Xi] \right) b \quad (9)$$

where an instruments matrix [Z] and filter, or weighting, matrix $[\Xi]$ are chosen so that,

$$E\left([Z]^T \nu \right) = 0$$

and $$\text{Rank}\left(E\left([Z]^T [\Xi][\Delta] \right) \right) = n$$

where n is (nq+np+1), ie, the number of parameters in x. It may be shown that x_{iv} is unbiased. In addition, it may be shown that in order for the method to make optimum use of the data (i.e. be efficient), the weighting matrix $[\Xi]$ should be diagonal, with elements,

$\chi_{ii} = (E(|\nu(\omega_i^2)|))^{-1}$ for some frequency ω_i, where E represents mathematical expectation. If, in addition, [Z] obeys the relation $[Z] = E([\Delta])$, the method will be optimally efficient among all unbiased estimators. The question remains how to construct matrices $[\Xi]$ and

[Z], in a manner suitable for use in flight flutter testing.

It is possible to employ standard spectral analysis methods to obtain optimal χ_{ii}, but such an approach brings attendant problems. In order to circumvent these, the IV/OEM method employs a matrix whose diagonal elements are of the form

$$\chi_{ii} = |Q(\omega)|^2 \qquad (10)$$

where $Q(\omega)$ is the polynomial denominator in equation (6).

All parameters associated with this matrix are contained in the transfer function, and so there is no additional labour involved in its construction. Little statistical efficiency is lost when this simplification is applied to the analysis of flight flutter test data; the benefits are considerable. It may be shown that this approach is still unbiased, and is in fact optimal if the noise $N(\omega)$ is white; however, whilst measurement noise may be nearly white, the response to turbulence will not be.

A good set of parameter estimates may be obtained using an iterative process in which the instruments matrix [Z] is updated based on predictions of the response using the current model. On data from the flight flutter test of a twin-propeller light passenger aircraft, exhibiting noise to signal ratios of approximately 30%, it was found that 30-40 iterations were sufficient to ensure good efficiency.

Modal parameters may be obtained from the polynomial coefficients by a number of means. Experience has shown that the best of these is the companion matrix approach. In this method, the roots of the denominator polynomial are found as the eigenvalues, λ_j, of the companion matrix,

$$[\Omega] = \begin{bmatrix} \frac{-q_{nq-1}}{q_{nq}} & \frac{-q_{nq-2}}{q_{nq}} & \cdots & \frac{-q_1}{q_{nq}} & \frac{-q_0}{q_{nq}} \\ 1 & 0 & \cdots & 0 & 0 \\ 0 & 1 & \cdots & 0 & 0 \\ \vdots & \vdots & \cdots & \vdots & \vdots \\ 0 & 0 & \cdots & 1 & 0 \end{bmatrix} \qquad (11)$$

The natural frequencies ω_r and dampings ζ_r of the modes contained in the transfer function are obtainable from the following relationships,

$$\omega_r = |\lambda_{2r}| \; ; \; \zeta_r = \Re(\lambda_{2r})/\omega_r \quad r=1,2 \ldots \qquad (12)$$

where it has been assumed that the roots λ_j are ordered in complex conjugate pairs. Similar assignments may be made for real roots (non-oscillatory modes). The associated (complex) modal amplitudes are found via polynomial division.

3.2.3 Evaluation using Simulated Data

A mathematical model of a four-engined commercial aircraft was used to test the method. The response of the model to a linear chirp was simulated 300 times, each time including randomly generated total noise contributions of atmospheric turbulence and transducer noise set at 14% of signal levels. The FRF exhibiting the dominant modes in the region of interest is shown in Figure 5. Modal parameters for the 4-7 Hz range were estimated using the IV/OEM approach and the standard Least Squares method. There are four modes in the region, and two out-of-range modes with strong residual effects; in practice, these model orders are often not known a-priori, and so the estimators were applied using various numbers of modes in the fit.

The mean prediction error is defined as $\sum_{k=1}^{N} (Y_T(\omega_k) - \hat{Y}(\omega_k))^2/N$, where $\hat{Y}$ denotes the predicted output based on the estimated modal parameters and Y_T is the response to the deliberate excitation only. The mean prediction error for the two estimators, averaged over the 300 simulated responses, is presented in Figure 6. It is clear that the IV/OEM results are considerably more accurate than those for the standard Least Squares, for the same model order; a zero prediction error corresponds to correct parameter estimates.

3.3 Errors and Confidence Intervals

3.3.1 Introduction

As well as estimating the modal parameters, it is also of interest to calculate the confidence intervals, thereby enabling the flutter test engineer to decide how much reliance can be put on a particular damping value. It is possible to arrive at estimates of the statistical errors on the modal parameters by a variety of methods. An approach which is simple to compute, and has been found useful in practice, is to assume that the estimated parameter, $\hat{x}$, is reasonably close to the true vector, x_T. The method is outlined here for the case of natural frequencies and dampings, but is easily expanded to account for modal amplitudes.

3.3.2 Mathematical Background

We seek the first order term in the Taylor series relating the estimated modal parameters to the noise ν in (7). This term is simply the product of those first order terms arising from the operations, (9), the eigenvalue solution of [Ω], and (12). The term arising from (10) is simply given by

$$[T] = ([Z]^T[\Xi][\Delta])^{-1}[Z]^T[\Xi].$$

Since the matrix of eigenvectors, [L], of [Ω] is available, the first order terms in the Taylor series are given by

$$\frac{\partial \lambda_j}{\partial [\Omega]_{uv}} = [L]^{-1}_{jv}[L]_{uj} \qquad (13)$$

The matrix of such terms is denoted [S]. The first order Taylor terms associated with (12) are easily found by differentiation, and the matrix of such terms is denoted [R]. Hence, if the deviation from x_T is small, the variance matrix associated with the estimated modal parameters is given by

$$[V] = RST\Psi T^T S^H R^H$$

where $[\Psi] = E(\nu\nu^T)$. T is known, and R and S are obtained using estimated parameter values, since x_T is not known in advance. [Ψ] may be estimated using standard times series methods. For some purposes, for example selection of model order, the assumption that $N(\omega)$ is white is found to give perfectly acceptable results.

If the number of data points is very large, then the estimates will be Normally distributed about their true values, with variance matrix equal to [V]. Standard statistical methods may therefore be used to obtain any confidence interval desired for any given parameter. In practice, data capture times are limited and the distribution is not Normal. In such circumstances, a different approach may be taken which accounts for the fact that the precise distribution is not known.

The above approach may be applied to obtain error bounds on modal parameters arising from estimation of rational polynomial coefficients obtained using any estimator, as long as the errors on the coefficients are calculable.

3.3 Application to Simulated Flight Test Data

The above approach was applied to the estimation of two modes in the system shown in Figure 5. Results are shown in Tables 1 and 2 for 20% and 40% noise. The actual and estimated standard deviations (σ and σ_e - obtained from 200 realisations) respectively for the natural frequencies (ω) and bandwidths ($2\zeta\omega$) are compared. The difference between these two values (Δ) expressed as a percentage indicates that the method shown is promising. Application to data from the flight flutter test of a twin propeller commercial aircraft supports this finding.

4. CLEARANCE

The ability to estimate frequencies and dampings accurately is only part of the testing process. The addition of other techniques to the conventional flight flutter testing methodology that can be used to: obtain good quality data, to detect whether there has been a significant change in stability without performing a curve-fit, and also to improve the mode tracking procedures will be of immense value. In this section, a number of approaches is discussed that are intended to improve the confidence with which flight flutter testing can be carried out.

4.1 The Envelope Method - A Tool for Detecting the Onset of Flutter

Whilst much effort has been expended towards development of more sophisticated analysis methods, it is often difficult to identify modal parameters accurately (especially when modes are close in frequency and data noisy). Therefore damping against speed trends are not always very illuminating. Sometimes the analyst has to revert to visual inspection and comparison of time histories (especially responses to stick jerk and pyrotechnic devices) to see if the overall stability is changing between two flight conditions.

The envelope method [6] associates an overall stability parameter with a particular decaying response without attempting to extract modal parameters. The approach is seen as an aid to flutter clearance, not a substitute for traditional methods.

The idea is to obtain the envelope for a particular decay using the Hilbert Transform (HT). If y(t) is the measured decay then the HT is given by,

$$y_H(t) = \frac{1}{\pi}\int_{-\infty}^{+\infty} \frac{y(\tau)}{t-\tau} d\tau \qquad (14)$$

and the signal $y_H(t)$ is essentially the same as y(t) with all frequency components shifted in phase by 90°. It may then be shown that the envelope function $y_E(t)$ is given by

$$y_E(t) = [y(t)^2 + y_H(t)^2]^{1/2} \quad (17)$$

An envelope function for a system with a single mode is shown in Figure 7.

It would be possible to overlay the envelopes from different speeds in order to check for changes in stability, but the presence of multiple modes makes interpretation of the envelopes difficult. Instead, any reduction in the overall stability of the aircraft modes is likely to lead to a reduction in the rate of decay of the envelope; a measure of this effect can be obtained via the shape factor

$$S = 1/\bar{t} \quad (18)$$

where

$$\bar{t} = \frac{\int_0^{t_{max}} y_E(t)tdt}{\int_0^{t_{max}} y_E(t)dt} \quad (19)$$

is the time centroid of the area under the envelope between 0 and t_{max} as shown in Figure 8. Note that $\bar{t}$ could be estimated directly from the sampled time values of y(t) without needing to obtain the envelope function. For a single mode of natural frequency ω_n and damping ratio ζ, it can be shown that S is the decay rate ($\zeta\omega_n$) if $t_{max} = \infty$. For finite t_{max}, then S tends to $2/t_{max}$ when damping is zero so the shape factor will clearly not cross zero at flutter; instead, it will simply drop in value and reach a threshold. When more modes are present, this threshold will differ and will not be known but a significant reduction in S provides a warning of a reduction in stability.

Using simulated impulse response data for a two mode flutter system with dampings plotted in Figure 9 , the variation in shape function in Figure 10 shows the onset of flutter without any curvefitting having been performed.

The method has also been applied to simulated data obtained from the theoretical aeroelastic model of a four-engined commercial aircraft, having an artificially low flutter speed of around 390 knots (flutter frequency 4 Hz). A typical noisy displacement impulse response and envelope are shown in Figure 11 and the wing tip shape parameter is shown in Figure 12 for noise-free and noise-corrupted data; the reduction in stability with speed is apparent. Because the flutter occurred at a low frequency then displacement rather than acceleration data were used in order to enhance the critical behaviour. The method has been applied to real data but not yet where flutter is encountered.

The best choice of t_{max} and any preprocessing (e.g. exponential weighting to deal with noise) need further consideration but the method shows some promise.

4.2 Mode Tracking using the Modal Assurance Criterion

The tracking of the modes of an aircraft through changing flight conditions can prove difficult; this is particularly the case if the modal density is high, as is often the case with aircraft, or if the modes cross in frequency. A method of comparing the modes at consecutive flight test conditions using mode shape information and the Modal Assurance Criterion (MAC), is presented to help alleviate some of the problems of mode tracking.

Natural frequencies and damping ratios can be estimated from multiple response flight test data at a single flight condition using any of a wide range of time or frequency domain identification techniques. Mode shape vectors can also be estimated by an extension of the curve-fitting approach used. Note that the modes are complex due to the aerodynamic coupling present.

The moment (or weighted correlation) between two mode shape vectors relating to modes q and r, estimated at flight conditions c and d respectively, is given by

$$mom(q,r) = \phi(c,q)W\phi^H(d,r) \quad (19)$$

where ϕ is an (no) row vector of mode shape terms, and no is the number of response transducers used. W is a weighting matrix allowing the relative confidence in each response measurement to be included. The Modal Assurance Criterion (MAC) between the two modes is calculated from

$$MAC(q,r) = \frac{|mom(q,r)|^2}{mom(q,q)\ mom(r,r)} \quad (20)$$

A value of MAC(q,r) equal to one implies that the shapes of the two modes compared are identical. A value of zero indicates two orthogonal mode shapes.

Under the assumptions that the aircraft mode shapes are distinct - implying that sufficient response positions are

used to define distinct modes - and that the mode shapes vary only slightly between the changes in flight conditions used during flutter testing, the value of the MAC alone can be used to 'pair-off' the modes estimated at consecutive sets of flight conditions. Displaying the MAC values between all possible pairs of modes as a greyscale grid, where black indicates a MAC value of one and white indicates zero, allows the degree of similarity between any pair of modes to be clearly visualised for the purpose of mode tracking.

Table 3 shows the natural frequencies of six modes of the four-engined commercial aircraft model used earlier, relating to airspeeds of 130 and 150 m/s. Figure 13 shows the comparison of the estimated mode shapes derived from 17 responses using the MAC approach. Despite the closeness of modes 3 and 4 in frequency, the modes are clearly distinguishable by their mode shapes. Figure 13 also shows that modes 1 and 2 cross in frequency, an effect which would complicate a mode tracking procedure based on natural frequencies alone. Furthermore, the coupling of modes 1 and 3 - the flutter modes - is indicated by the higher MAC values between these modes.

Figure 14 shows the MAC values derived between the four modes estimated from real flight test data at constant Mach number and increasing airspeed using six response transducers. The clear pairing of the modes between consecutive flight conditions demonstrates the robustness of the MAC approach in mode tracking with flutter test data over realistic changes in flight condition.

The MAC approach [8] is capable of tracking modes up to the flutter condition on the basis of mode shapes alone. However, as the flutter condition approaches, the coupling of the two flutter modes increases and high MAC values occur between the two less distinct mode shapes at consecutive flight conditions. Also, the change in modeshapes between flight conditions is significantly greater near to the flutter condition. The combination of these effects at conditions close to flutter could lead to a failure of the mode-tracking, if based on the MAC value alone. In reality, the small changes in flight condition considered at the extremes of the flight envelope would tend to prevent the MAC approach from breaking down; also, a suitable choice of weighting matrix could place particular emphasis upon transducer locations where mode shapes were different. Additional consideration of modal frequency and damping estimates would reinforce the mode-tracking procedure.

4.3 Use of Force Appropriation in Flutter Testing

4.3.1 Introduction

During flight flutter testing, it is essential that the damping ratios of all significant modes be estimated as accurately as possible. The aeroelastic behaviour of aircraft often leads to a high modal-density which makes system identification difficult, particularly in cases when modes are badly excited or response data are corrupted. In traditional modal testing, such as aircraft Ground Vibration Tests, normal mode force appropriation is used to alleviate the problems of high modal density and poor excitation.

4.3.2 Force Appropriation

Force appropriation is a method of exciting a single normal mode of a structure, by applying forces in a certain pattern at the particular natural frequency. The natural frequency and the ideal pattern of excitation for a given mode are estimated by a procedure such as the Multivariate Mode Indicator Function (MMIF) [10]. Once a suitable pattern of forces has been obtained, an estimate of the modal damping can be made by exciting the mode at a set of frequencies around resonance.

A normal mode is defined as one for which all the responses to excitation at the natural frequency are in quadrature with the excitation signal. Thus, if we assume a purely real input $F(\omega)$ at the natural frequency, the response of a normal mode $Y(\omega)$ will be purely imaginary. A normal mode can thus be identified by minimising the magnitude of the real part of the response with respect to the magnitude of the total response. After some simplification, the minimisation of the ratio $\lambda = \|Y_R\|^2 / \|Y_R + iY_I\|$ results in the eigenvalue problem,

$$[H_I^T H_I]\, F = [H_R^T H_R + H_I^T H_I]\, F\, \lambda \qquad (21)$$

where H_R and H_I are the real and imaginary parts of the FRF matrix $H(\omega)$. The frequencies at which eigenvalues reach a minimum value are sought. A plot of the solutions for the eigenvalues (λ) against frequency (ω) will thus drop to zero at the natural frequencies of the system. The corresponding eigenvectors at these frequencies give the force patterns which can be used to best excite the normal modes.

The Modal Purity Indicator (MPI) is a method of evaluating numerically the degree to which a normal mode is appropriated. The MPI is found by summing the responses over all measurement points, thus

$$MPI = 1 - \frac{\sum_{k=1}^{nt} \Re[Y(k)]\,|Y(k)|}{\sum_{k=1}^{nt} |Y(k)|^2} \qquad (22)$$

An MPI value of 1 indicates a perfectly appropriated normal mode such that all points on the modeshape will be in quadrature.

4.3.3 Extension to Flutter Testing

The theory introduced above applies to the aircraft on the ground at zero speed. In flight, the aerodynamic effects cause the net damping and stiffness matrices to be non-symmetric. It is still possible to excite the aircraft at a single frequency with a particular force pattern with quadrature phase. However, this condition will occur at frequencies of the undamped aircraft but with aerodynamic stiffness effects included. The corresponding modes will not be classical 'normal' modes, but will be essentially the modes of interest at that flight condition. Thus, force appropriation may be applied as a means of enhancing the response of a particular mode [9].

In such an application, it is no longer practical to excite the aircraft at several frequencies around resonance. Instead, damping may be estimated by exciting at resonance (i.e. resonance dwell) and then allowing the response to decay. This decay will tend to include some contribution from other modes due to damping coupling effects.

4.3.4 Application to Simulated Aircraft Data

A model of the four-engined commercial aircraft was used to demonstrate the application of force appropriation to flutter testing. The optimal positions at which it would be realistically possible to excite the aircraft were found to be the nose, wing-tip and tailplane. The MMIF was estimated between using these three excitation positions and 17 response positions around the aircraft and is shown in Figure 15. The frequencies were found to a high accuracy from the minima of the eigenvalue plots. Reapplication of the estimated force vectors allowed the modal damping to be estimated from a single mode decay, and the MPI to be calculated. The results of the theoretical force appropriation procedure are shown in Table 4. The frequencies of the first six modes were all estimated well and the application of the force vectors allowed the modes to be appropriated and the modal damping estimated with a high level of accuracy.

A flight test was simulated using sweep excitation at the nose and wing-tip only. The MMIF was estimated from excitation response measurements corrupted by white noise and is shown on Figure 16. The frequencies were estimated to the resolution of the FRFs obtained (0.01 Hz), and the force vectors reapplied for estimation of the modal damping. All results are given in Table 4. It was not possible to appropriate mode 3, a predominantly tailplane mode, due to the lack of a tailplane exciter and its proximity in frequency to mode 4. The remaining five modes were estimated with reasonable accuracy.

The application of force appropriation to flight flutter testing is theoretically possible, and would improve the accuracy with which modes could be estimated. However, in order to appropriate all of the aircraft modes, this technique requires the simultaneous application of excitation at several positions, which is not currently common practice. Such a process would tend to be slow, and would probably only be used in practice for particularly difficult and important modes. It is worth pointing out that classical modal testing leans heavily upon the use of multiple exciter methods because of the close mode problem. It may be argued that flutter testing is considerably more difficult than modal testing and has a severe penalty for error; perhaps flutter testing should follow suit.

An extension of the approach is to perform the force appropriation process upon data obtained separately from several excitation positions (often available), determine the proportion of each excitation required in order to enhance a particular mode and then to linearly combine the FRFs rather than excite the actual aircraft. This approach is analogous to modal filtering.

5. CONCLUSIONS

A number of methods for curve-fitting and clearance have been described that can be used to improve the confidence with which flight flutter testing can be carried out.

6. ACKNOWLEDGEMENTS

The authors are grateful for the financial support of British Aerospace (Commercial Aircraft Division), EPSRC, and British Aerospace (Military Aircraft Division).

7. REFERENCES

1. Wright J.R., 'Flight Flutter Testing' VKI Lecture Series 1992-01 ISSN0377-8312
2. Cooper J.E,' Parameter Estimation Techniques for Flight Flutter Testing' AGARD SMP Paper 10. 1995.
3. Juang J-N, Cooper J.E. & Wright J.R., 'An Eigensystem Realization Algorithm using Data

Correlations (ERA/DC) for Modal Parameter Identification' Control - Theory and Advanced Technology v4 n1 pp 5-14 1988.
4. Cooper J.E. & Wright J.R.,' Application of Time Domain Decomposition Techniques to Aircraft Ground and Flutter Test Data' Proc European Forum on Aeroelasticity and Structural Dynamics pp 235 - 243 1989.
5. Emmett P.R., Cooper J.E. & Wright J.R., 'Improved Frequency Domain Modal Parameter Identification' Int Forum on Aeroelasticity & Structural Dynamics, June 1995.
6. Cooper J.E., Emmett P.R. & Wright J.R., 'A Statistical Confidence Factor for Modal Parameter Identification' 17th Int Seminar on Modal Analysis 1992 pp 1611 - 1626.
7. Cooper J.E., Emmett P.E., Wright J.R. & Schofield M.J., 'Envelope Function - A Tool for Analysing Flutter Data' AIAA J of Aircraft v30 n5 1993 pp 785 - 790.
8. Desforges M.J., Cooper J.E. & Wright J.R., 'Mode Tracking during Flutter Testing using the Modal Assurance Criterion' Trans I.Mech.E - Aerospace Sciences 1995.
9. Desforges M.J., Cooper J.E. & Wright J.R. 'Force Appropriation for Flight Flutter Testing' Int Forum on Aeroelasticity & Structural Dynamics, June 1995.
10. Williams R., Crowley J. & Vold H.,'The Multivariable Mode Indicator Function in Modal Analysis' IMAC 4, 1986 pp 66-70.

Mode	Parameter	σ	σ_e	Δ %	σ/parameter(%)
1	ω	1.54E-02	1.63E-02	+6	3E-01
1	$2\zeta\omega$	2.94E-02	3.04E-02	+3	6E-00
2	ω	1.06E-03	1.06E-02	+0	2E-02
2	$2\zeta\omega$	1.93E-03	2.04E-03	+5	2E-00

Table 1. EPT Estimates. 20% Noise.

Mode	Parameter	σ	σ_e	Δ %	σ/parameter(%)
1	ω	8.65E-02	7.70E-02	-10	2E-00
1	$2\zeta\omega$	1.10E-01	1.04E-01	-5	2E+01
2	ω	2.48E-03	1.88E-03	-20	4E-02
2	$2\zeta\omega$	4.50E-03	4.14E-03	-8	4E-00

Table 2. EPT Estimates. 40% Noise.

Mode	Frequency (Hz)	
	130 m/s	150 m/s
1	3.2524	3.3652
2	3.2919	3.2841
3	3.6348	3.6101
4	3.6530	3.6467
5	4.5078	4.4969
6	4.8446	4.8334

Table 3. First Six Natural Frequencies of Aircraft Model

Mode	Theoretical Appropriation			Simulated Flight Test		
	ω (Hz)	ζ (%)	MPI	ω (Hz)	ζ (%)	MPI
1	3.116	4.275	0.8610	3.106	3.603	0.8076
2	3.297	1.069	0.9758	3.301	1.245	0.9226
3	3.634	2.407	0.8887			
4	3.658	0.629	0.9727	3.662	0.638	0.9019
5	4.515	1.662	0.8917	4.512	1.729	0.8957
6	4.845	2.861	0.8434	4.834	2.128	.07807

Table 4. Appropriated Modes From Aircraft Model.

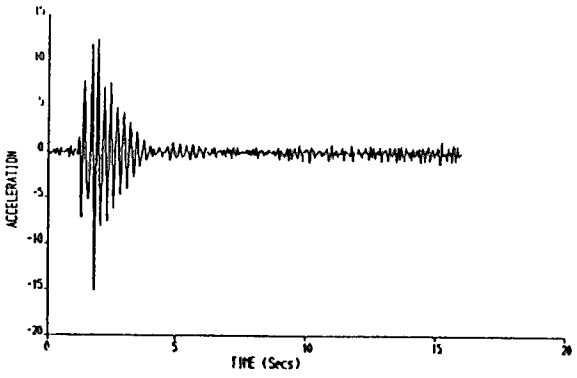

Fig 1. Response to Stick Jerk.

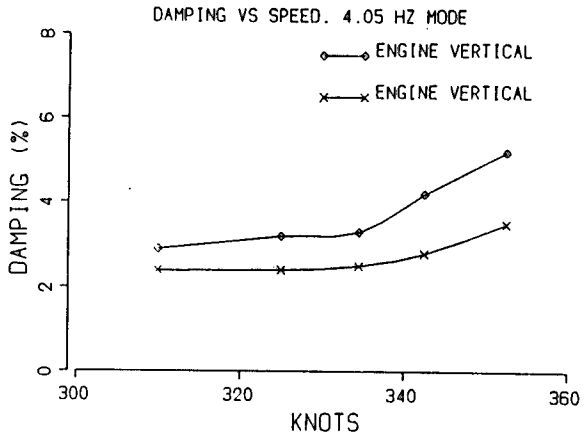

Fig 4. Typical Damping Trends.

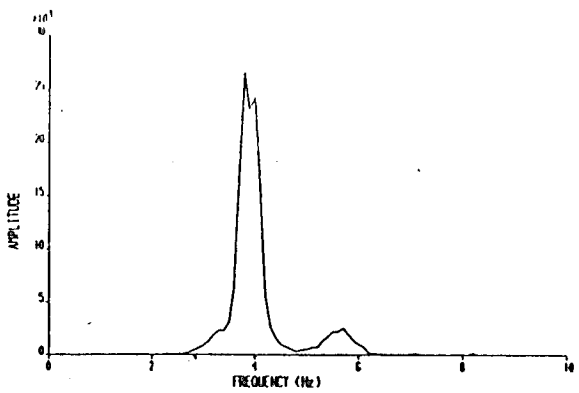

Fig 2. Spectra of Decay Response.

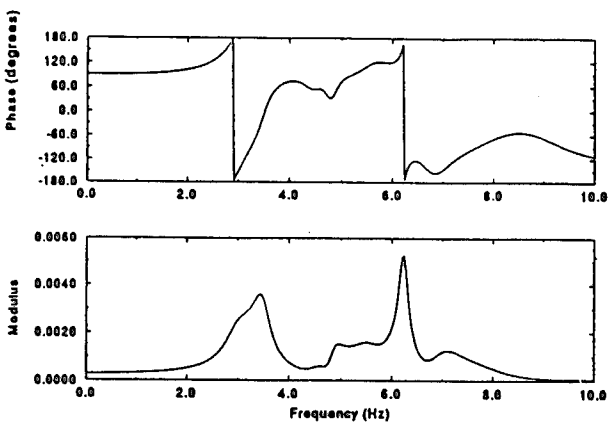

Fig 5. FRF of Aircraft Model.

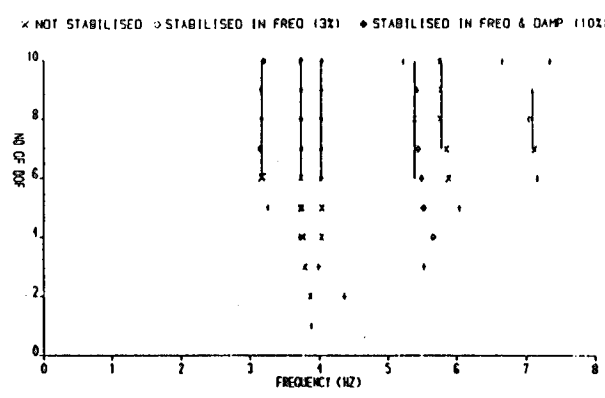

Fig 3. Stability Plot.

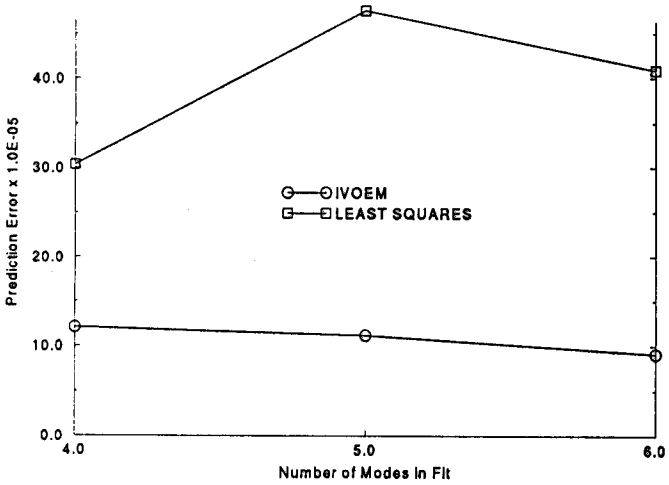

Fig 6. Mean Prediction Errors.

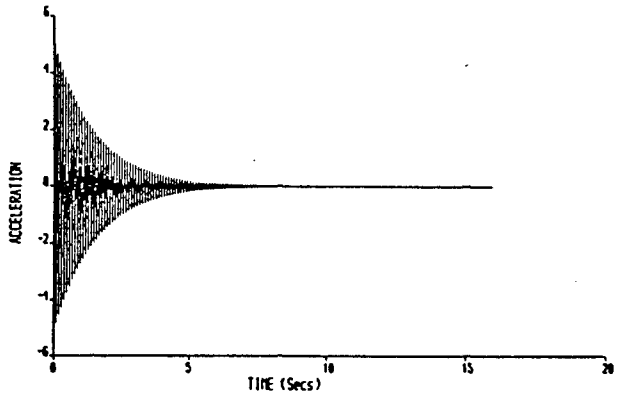

Fig 7. Impulse Response. Single Mode.

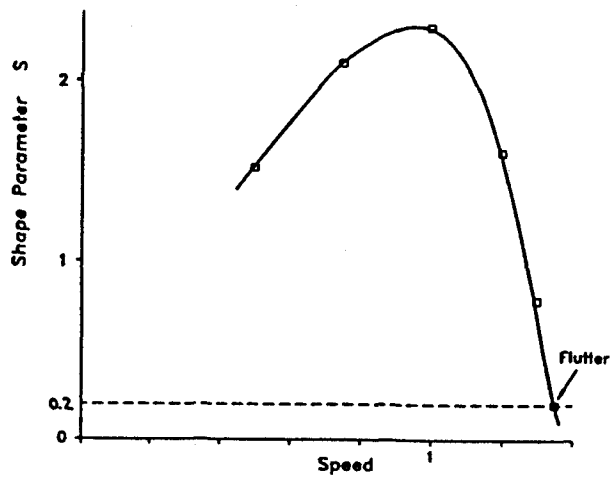

Fig 10. Shape Functions of Two Mode System.

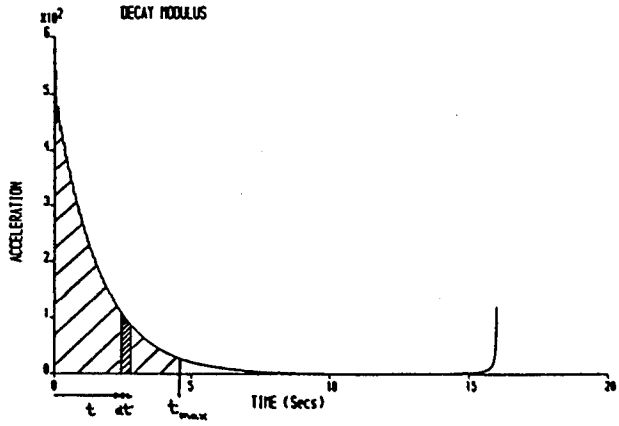

Fig 8. Shape Function Definition.

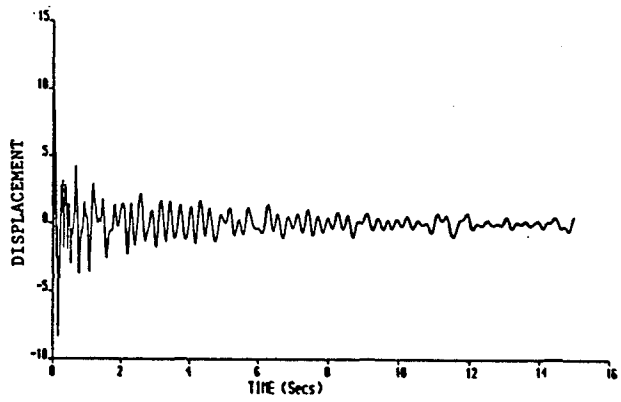

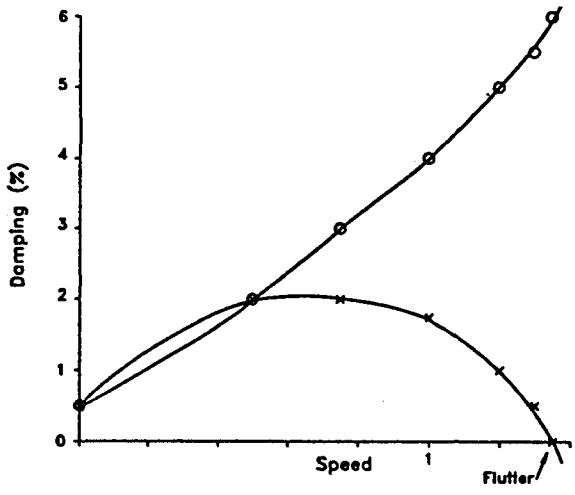

Fig 9. Dampings of Two Mode Flutter System.

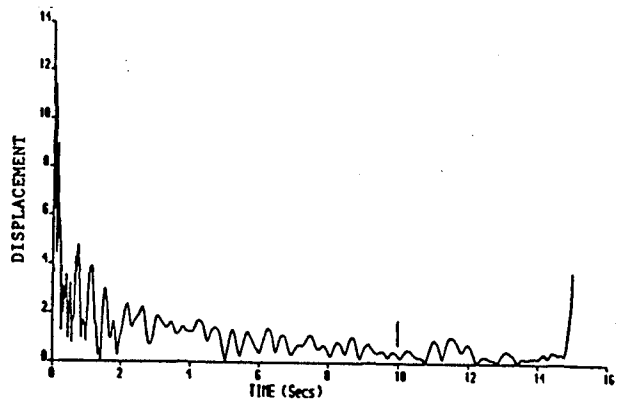

Fig 11. Typical Impulse Response & Envelope.

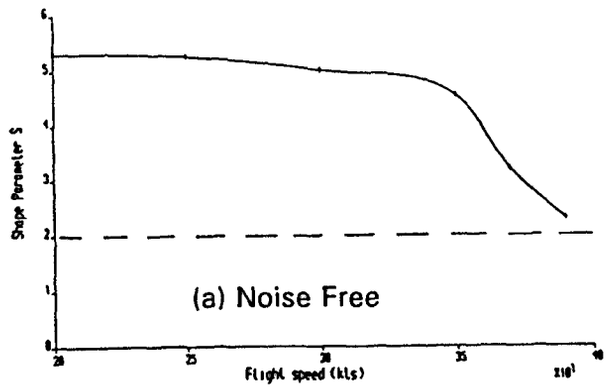

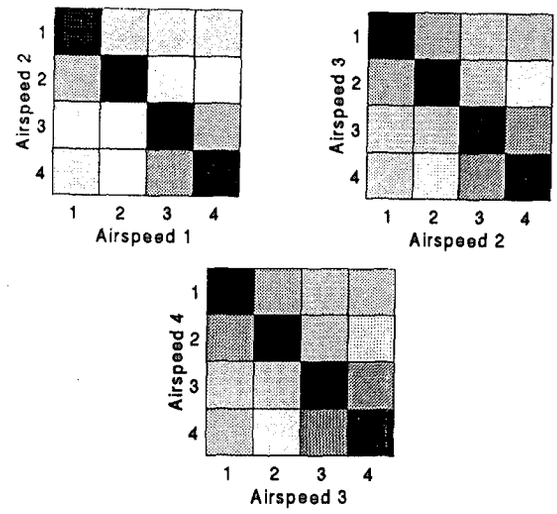

Fig 14. MAC Values. Real Flutter Test Data.

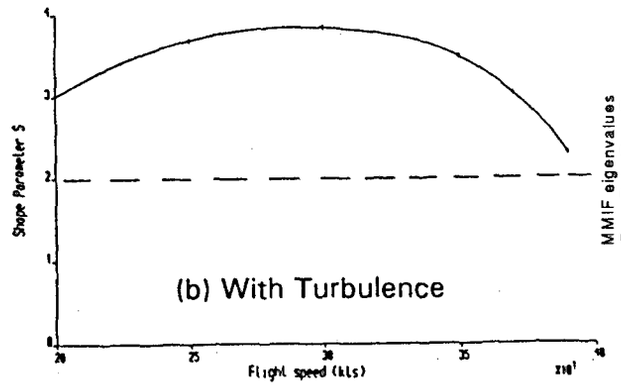

Fig 12. Wing Tip Shape Parameter.

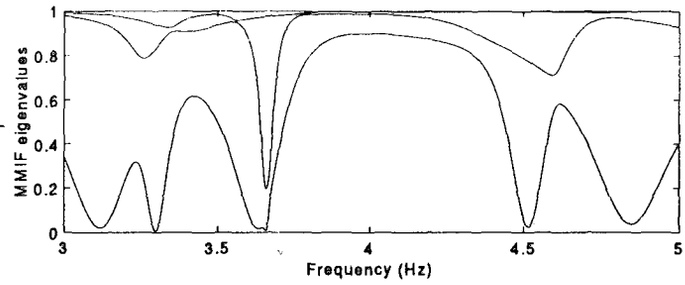

Fig 15. Aircraft Model MMIF. No Noise.

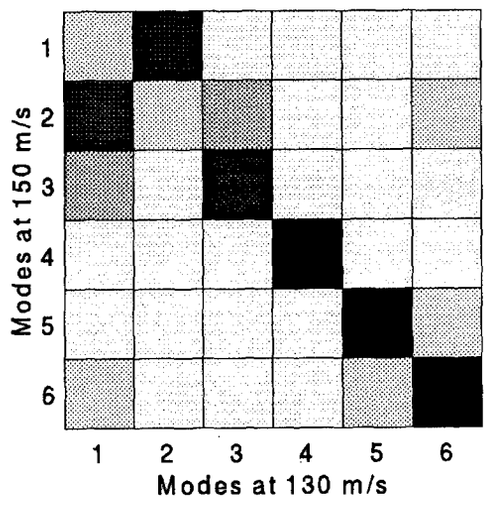

Fig 13. Mode Shape Comparison. Simulated Data.

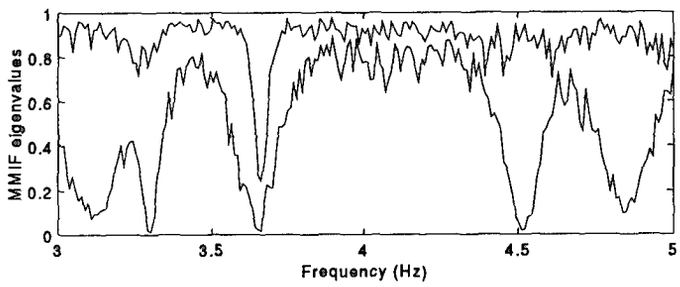

Fig 16. MMIF. Simulated Flight Test.

A QUARTER CENTURY OF NASA WIND-TUNNEL AND FLIGHT EXPERIMENTS INVOLVING AEROSERVOELASTICITY

Thomas E. Noll and Boyd Perry III
NASA Langley Research Center
Mail Stop 340
Hampton, Virginia, 23681-0001
United States

and

Michael W. Kehoe
NASA Dryden Flight Research Center

1. SUMMARY

Over the past quarter century, the NASA Langley Research Center (LaRC) and the NASA Dryden Flight Research Center (DFRC) have played major roles in the development, demonstration, and validation of aeroservoelastic modeling, analysis, design, and testing methods. Many of their contributions resulted from their participation in wind-tunnel and flight-test programs aimed at demonstrating advanced active control concepts that interact with and/or exploit the aeroelastic characteristics of flexible structures. Other contributions are a result of their interest in identifying and solving adverse aeroservoelastic interactions that allow unique flight-test demonstrations or flight envelope clearance programs to be successfully completed. This paper provides an overview of some of the more interesting aeroservoelastic investigations conducted in the Transonic Dynamics Tunnel (TDT) at LaRC and in flight at DFRC. Four wind-tunnel and four flight-test projects are reviewed in this paper. These test projects were selected because of their contributions to the state-of-the-art in active controls technology (ACT) or because of the knowledge gained in further understanding the complex mechanisms that cause adverse aeroservoelastic interactions.

2. INTRODUCTION

Aeroservoelasticity (ASE) is a multidisciplinary technology that deals with the interactions of an aircraft's flight control systems (FCS), its flexible structure, and the steady/unsteady aerodynamic forces resulting from its rigid-body and flexible motions. The disciplinary interactions commonly associated with ASE are summarized in the diagram shown in Figure 1 (Ref. 1). These interactions can be either adverse, ranging from being mild (an annoyance) to serious (affecting flight safety), or beneficial, resulting in improvements in aircraft performance and/or reductions in aircraft weight. The factors that determine the difference between adverse and beneficial are the ability of the FCS designer to take properly into account many complex modeling issues and the designer's ingenuity in exploiting ACT.

Historically, the recognition of ASE as a serious design issue evolved as a result of advancements within independent technical disciplines, all aimed at improving the performance of flight vehicles. For example in the technical disciplines of structures and materials, structural efficiency and weight minimization resulted in very flexible structures which satisfied aeroelastic and strength requirements. In the technical discipline of flight controls, the use of ACT to improve stability, maneuverability, ride comfort, etc., resulted in higher frequency actuator bandwidths. There were also advancements in fly-by-wire and digital FCS technologies that further increased the performance and capability of ACT. As a result of these advancements, the previously separated natural frequencies of the aircraft structure (originally high frequencies) and those of the FCS (originally low frequencies) began to approach and then overlap each other. Through the interaction of the third technical discipline, unsteady aerodynamic forces, the now overlapping modal frequencies had the potential to, and at times did, couple to produce large magnitude adverse aeroservoelastic responses and instabilities.

Figure 2 attempts to illustrate some of the complex relationships that exist in ASE. At the top of the figure is ACT, below which are listed five of the many possible types of active control systems (ACS). The dots suggest other types of ACS not listed here. The broad shaded double-headed arrow near the top of the figure represents the continuum of aircraft natural modes and suggests that at one end of the continuum rigid-body modes play a more important role in the ACS design and, at the other, elastic modes are more important. Below each control system are listed a potential problem and the major benefit associated with that particular control system. Adverse ASE interactions is the common potential problem for all ACS.

There have been many documented cases of adverse ASE interactions encountered during flight; Reference 2 describes a few cases that occurred in the 1960s and 70s. The impetus that spurred significant interest in the adverse-side of ASE interactions came during the United States Air Force (USAF) Lightweight Fighter (LWF) Program. The USAF contracted General Dynamics and the Northrop Corporation to design and build two prototype LWF aircraft, the YF-16 and the YF-17, for a fly-off competition. The YF-16 (Ref. 3) was the first of the two prototypes to be flight-tested. Although detailed ASE analyses were performed prior to first flight, at what was thought at the time to be the most critical flight conditions, the YF-16 encountered two unexpected ASE instabilities in flight at conditions not analyzed. Post-flight analyses for these conditions accurately predicted the instabilities. With the YF-16 experience in

Paper presented at the Structures and Materials Panel Specialists' Meeting on "Advanced Aeroservoelastic Testing and Data Analysis", held in Rotterdam, The Netherlands, from 8-10 May 1995, and published in CP-566.

hand, ASE analyses on the YF-17 prototype were successful in predicting ASE adverse interactions (Ref. 4) prior to first flight and in defining modifications to the vehicle to avoid the instabilities. This side of ASE was perceived by the aircraft designers as problems that needed to be identified and corrected; the other side offers opportunities to improve aircraft performance.

By the 1960s, researchers began to investigate the feasibility of using ASE interactions in some positive fashion for increasing the capabilities of military aircraft. Since then many researchers, too numerous to mention, have investigated and demonstrated the usefulness of ACT for favorably modifying the aeroelastic response characteristics of flight vehicles. As a result, ASE has entered the limelight as a viable tool for answering some very difficult design questions and has the potential for obtaining further structural weight reductions, optimizing maneuvering performance, and satisfying the multimission requirements being imposed on future military and commercial aircraft designs.

ASE today is becoming even more multidisciplinary, expanding beyond its original technical disciplines of controls, structures, and aerodynamics into the disciplines of structural fatigue, thermodynamics, and propulsion. New issues to resolve and/or opportunities to exploit include: control laws designed to suppress flutter, alleviate loads, improve ride quality, or provide other benefits that, at the same time, affect fatigue life; high surface temperatures during flight at hypersonic speeds that result in changes in material properties and thus vehicle stiffness and flutter; and ACT concepts that use thrust vectoring as the closed-loop force producer. Another technical discipline ripe for inclusion in ASE is smart materials. The unique feature of smart materials is that under certain stimuli (voltage, temperature, etc.) the structural properties of these materials can be altered. If these properties are properly tailored, the resulting internal structural interactions can be very beneficial for reducing vibrations or alleviating undesirable aeroelastic responses.

Over the past quarter century, NASA LaRC and NASA DFRC have played major roles in developing ACT through their participation in many wind-tunnel and flight-test programs. These programs were conducted for the purposes of: (1) establishing concept feasibility; (2) demonstrating proof of concept; and (3) providing data for validating new modeling, analysis, and design methods. This paper provides an overview of some of the more interesting ASE investigations conducted in the TDT at LaRC and in flight at DFRC. Four wind-tunnel and four flight-test projects are reviewed in this paper. These projects were selected because of their contributions to the state-of-the-art in ACT or because of the knowledge gained in further understanding the complex mechanisms that cause adverse ASE interactions.

For the wind-tunnel test projects, the ACS investigated could all be placed in the modal frequency band near the middle and right side of Figure 2, implying that the deliberate beneficial interaction of the elastic modes of the wind-tunnel model and its ACS was an important aspect of the test. An "ASE success" for such tests would be a strong indication that the appropriate "primary benefit" would be possible in a flight vehicle. Although during the wind-tunnel tests unexpected "adverse ASE interactions" were sometimes experienced, and usually eliminated, these occurrences will not be discussed herein.

With one exception, the flight-test projects discussed in this paper had significantly different emphases than the wind-tunnel test projects. Three of the flight projects involved systems designed to improve the flight control and maneuvering capabilities of the aircraft. Since these control systems were designed to interact with the rigid body modes of the aircraft, they generally fall in the modal frequency band that begins to far left side of Figure 2 and extends toward the middle. An "ASE success" for such flight-tests would be the elimination of the adverse ASE interaction so that the flight-test could resume. Although each flight project was successful in its primary purpose, those details are beyond the scope of this paper and may be found in the appropriate references.

For each program discussed herein, the objectives of the effort, the testing techniques, the test results, any significant findings, and the lessons learned with respect to ASE testing are presented.

3. DESCRIPTION OF TEST FACILITIES

3.1 NASA LaRC's Transonic Dynamics Tunnel

The TDT (Ref. 5) is a "National Facility" dedicated almost exclusively to identifying, understanding, and solving aeroelastic problems. A photograph of the TDT is shown in Figure 3. The TDT is a closed-circuit, continuous-flow wind tunnel capable of testing at stagnation pressures from near zero to atmospheric and over a Mach number range from zero to 1.2. The test section of the TDT is 16 feet square with cropped corners. Varying the pressure in the tunnel simulates variations in flight altitude. One feature of the TDT which is particularly useful for aeroelastic testing is a group of four bypass valves connecting the test section area to the opposite leg of the wind-tunnel circuit downstream of the drive fan motor. In the event of a model instability, such as flutter, these quick-actuating valves are opened, causing a rapid reduction in the test section Mach number and dynamic pressure. Other features that make the TDT uniquely suited for aeroelastic and ACT testing include: high visibility of the model from the control room; a highly sophisticated computer-controlled data acquisition system; oscillating vanes upstream of the test section that can be used to generate sinusoidal gusts; a variety of model mounting and suspension systems ranging from cantilever sidewall mounts for component models to a two-cable suspension system for full-span "free-flying" models; safety screens that protect the tunnel fan blades from debris in case of a model failure; state-of-the-art instrumentation and test equipment; and a full-time staff of experienced aeroelastic research engineers and technicians.

Tests can be performed using air as the test medium, however, the most distinguishing feature of the tunnel is the use of a heavy gas, presently R-12 refrigerant, as the primary test medium. R-12 is four times as dense as air and has a speed of sound half that of air. These properties of R-12 have beneficial effects on the design, fabrication, and testing of aeroelastically scaled wind-tunnel models. Other advantages of using R-12 are a nearly three-fold

increase in Reynolds number and lower tunnel drive horsepower.

3.2 NASA DFRC's Flutter Test Laboratory

DFRC traces its origin to the early post World War II period and the first attempts to fly faster than the speed of sound. Since that time, DFRC has served as a focal point for flight-test activities associated with all aspects of aeronautical research and development (Ref. 6).
Within DFRC is the Western Aeronautical Test Range (WATR) which consists of a highly automated complex of computer-controlled tracking, telemetry, and communications systems and control room complexes that are capable of supporting any type of mission.
Each control room provides the research engineer with fast and complete access to communications data, tracking data, telemetry data, timing data, and video data. This provides real-time analysis of test results to assure flight safety and that data is of sufficient quantity and quality to meet research objectives.

The need frequently arises to monitor the aeroelastic and ASE characteristics of new or modified aircraft and control systems designs to ensure that no undesirable resonant modes or instabilities exist within the intended flight envelopes. The WATR's Spectral Analysis Facility (SAF) is intended to assist the engineers in analysis tasks associated with these investigations. The SAF provides a combination of hardware and software designed to minimize the amount of flight-test time needed to safely test an aircraft throughout a specified flight envelope. Normally, the aircraft's modal characteristics are monitored by exciting the structure and measuring the response of the structure. These responses are received in real time on the ground, decommutated, and displayed on strip charts and spectrum analyzers. Monitors also provide graphics, numeric, discrete, and flight mode annunciator displays. The telemetered data are also processed by parameter identification algorithms to estimate the vehicle's aeroelastic and ASE stability.

4. WIND-TUNNEL TEST ACTIVITIES

In the past 25 years there have been about a dozen active controls demonstrations in the TDT, too many, unfortunately, to describe in the limited space of this document. This section of the paper contains a selection, spanning the entire 25 years, of four of the more noteworthy of these demonstrations. A common thread among these four projects is that each has had a significant impact on the state-of-the-art of ACT. Recall from earlier comments, this section emphasizes the performance gains that can be realized through beneficial ASE interactions and deliberately omits any discussion regarding adverse ASE interactions.

4.1 B-52 CCV Full-Span Model Program

The success of ACT flight investigations in the 1960s to reduce the dynamic response of the XB-70 (Ref. 7) and the B-52E (Ref. 8) aircraft due to gusts opened the gateway to a multitude of ACT studies and applications that continue to this day. In conjunction with the B-52E flight investigation, a 1/30th scale, full-span, free-flying B-52 aeroelastic wind-tunnel model was constructed and tested in the TDT. The model was dynamically scaled (stiffness and mass distribution) to match the first nine symmetric elastic vibration modes of the flight vehicle (frequency range from 0 to 25 Hz). The model was equipped with active ailerons and elevators and demonstrated in the wind tunnel what had already been demonstrated in flight: the ability of active controls to alleviate structural dynamic response caused by turbulence.

In the early 1970s, the U.S. Air Force Flight Dynamics Laboratory (AFFDL) initiated a research program with the Boeing Company to further develop and demonstrate ACT. This program was named the Controlled Configured Vehicles (CCV) Program (Ref. 9). For this program the B-52E vehicle reported on in Reference 8 was modified to serve as the testbed to evaluate several advanced control concepts through analyses and flight-testing. One such concept was active flutter suppression (AFS), attractive because of its promise of requiring smaller structural weight penalties to meet flutter margin requirements.

In parallel with the CCV flight-test program, an investigation sponsored by AFFDL with Boeing and in cooperation with NASA LaRC was initiated to: 1) develop active control concept evaluation techniques through wind-tunnel testing; 2) demonstrate that aircraft ACS can be simulated with wind-tunnel models; 3) obtain experimental data for validating analysis results and methods; and 4) obtain data for correlation with the B-52E flight-test results. The impetus behind this investigation was the availability of the previously tested 1/30th-scale B-52 aeroelastic wind-tunnel model. This program was the B-52 CCV wind-tunnel test program (Ref. 10), and the remainder of this subsection of the paper addresses this program.

The B-52 wind-tunnel model was modified to dynamically match equivalent changes made to the full-scale aircraft. In addition, to properly represent the AFS and the vertical ride control (VRC) systems being evaluated in flight, the wind-tunnel model was further modified to include new outboard ailerons, flap segments, and horizontal canards. These control surfaces were driven by an electromechanical system consisting of d.c. torque motors mounted within the fuselage and crank-pushrod linkages and shafting from the motors to the control surfaces. Figure 4 shows the B-52 wind-tunnel model installed in the TDT on the two-cable mount system.

The AFS system consisted of two independent feedback loops: an aileron loop and a flaperon loop. Since both systems were designed to separately provide a 30 percent increase in flutter speed, they were considered redundant systems. With the exception of scaling differences, the AFS systems on the wind-tunnel model and on the B-52E aircraft were very similar over the frequency range of interest.

The wind-tunnel test data, scaled up to corresponding flight-test conditions, are compared with flight-test results in Figure 5. Concentrating first on the wind-tunnel results only (open symbols), it can be seen that the AFS-on tests were performed to conditions only slightly above the open-loop flutter point of 253 m/s. However, at the highest velocity for AFS-on, the damping in the flutter mode showed a large improvement compared to that for AFS-off and also showed the potential for a significant increase in flutter speed. Comparing, now, the AFS-on

wind-tunnel results (open square symbols) with the AFS-on CCV flight-test results (closed square symbols, taken from Reference 11) the damping trends are seen to agree quite well. These comparisons provided further encouragement that dynamically scaled wind-tunnel models may be useful testbeds for investigating potential AFS systems on full-scale flight vehicles.

The VRC system on the full-scale aircraft was designed to reduce, by at least 30 percent, the gust-induced vertical acceleration at the pilot's station. This system used vertical acceleration, sensed at the pilot's station, and the horizontal canards. The VRC system on the wind-tunnel model was a scaled-down version of the actual flight system. Test results indicated that the VRC system reduced the magnitude of the 6th and 8th mode peaks on the model by about 60 percent and 75 percent respectively, and on the airplane by about 56 percent and 73 percent respectively.

The most significant finding that resulted from the B-52 CCV full-span model program was the knowledge that dynamically scaled, actively controlled wind-tunnel models were extremely useful in studying and developing advanced active control concepts. From that time forward, wind-tunnel models were destined to play the following important roles in the development of active-control concepts: increase the confidence level in these concepts by providing data to verify analytical models and methods; and eliminate the risks and lower the costs associated with flight-testing these concepts.

4.2 YF-17 Semispan Model Program

During the early 1970s McDonnell-Douglas Corporation, under AFFDL sponsorship, performed analytical studies (Ref. 12) to define the feasibility of applying AFS concepts to flutter problems associated with military aircraft. The elimination of flutter placards associated with the carriage of wing-mounted external stores on fighter-attack aircraft was identified as the most promising application of AFS because of the significant payoffs in aircraft performance. As a direct result of these studies, AFFDL in cooperation with NASA LaRC, began an aggressive series of wind-tunnel test investigations, spanning about 10 years, to develop and demonstrate wing/store AFS.

The Northrop Corporation was contracted by AFFDL for the first wind-tunnel demonstration of wing/store AFS.
The objective of this program was to perform several series of tests to evaluate a multitude of control concepts based on different design philosophies. These concepts began with simple nonadaptive analog controllers and evolved into digital adaptive controllers. For this program, a 30-percent-scale, semispan, aeroelastic model of the YF-17 aircraft was designed for testing in the LaRC TDT.
The wind-tunnel model consisted of a wing, a fuselage, and a horizontal tail. The model was very unique in that it was side-wall mounted using cables and a set of bars and linkages that simulated rigid-body pitch and plunge degrees-of-freedom. The horizontal tail, attached to an electric motor located within the fuselage, was used for trimming the model at various tunnel conditions. The wing had leading- and trailing-edge control surfaces powered by electro-hydraulic actuators. Three different external store configurations having widely different flutter characteristics (flutter frequency, modal coupling, and flutter-mode violence) were also available.

The first series of wind-tunnel tests was conducted in three entries: June, August, and December of 1977. For these tests, a different AFS control law, each employing a single control surface, was developed for each external store configuration. These wind-tunnel tests were quite successful, particularly for AFS systems that used the leading-edge surface. For the configuration with the most violent flutter characteristics, the model was tested 18 percent above the unaugmented flutter dynamic pressure without incurring an instability. Based on damping trends at this condition, the model was projected to be stable up to about 29 percent in dynamic pressure above the unaugmented flutter condition (Ref. 13). This program demonstrated that active suppression of wing/store flutter was a feasible and practical application for ACT.
The program also demonstrated for the first time that leading-edge surfaces acting alone are viable AFS surfaces.

For the second series of tests, conducted during October 1979, the use of multiple loops with multiple control surfaces acting simultaneously was investigated. For this series of tests only the wing/store configuration with the most violent flutter mode was available as a testbed.
To reduce the risk of losing the model during flutter or other unexpected ASE instabilities, the store was modified to include an internal electro-mechanical system that served as a flutter stopper. This system would passively suppress flutter by moving an internal mass very rapidly, thereby changing the wing/store structural frequencies in such a manner as to decouple the critical elastic modes.
Whenever an instability was encountered the system could be triggered either automatically or manually.

Research organizations from three European countries were invited to participate in the second series of tests through the auspices of USAF data exchange agreements or information exchange programs. These organizations included British Aerospace and the Royal Aeronautical Establishment from the United Kingdom, the Office National d'Etudes et de Recherches Aerospatiales from France, and Messerschmitt-Bolkow-Blohm GmbH from West Germany. Control laws from each of the organizations varied greatly in their design philosophy, and in the number of sensors and control surfaces used.
All control laws were highly successful in suppressing flutter (Ref. 14). One control law was tested to a dynamic pressure 70 percent above the passive flutter condition. Post-test evaluation of damping trends indicated that this control law could have stabilized the model up to about 131 percent above the passive condition.

Some "firsts" demonstrated in this portion of the program included the ability to switch from one control law to another above the unaugmented flutter condition and the ability to switch from a control law that used a trailing-edge control surface to one that used a leading-edge control surface above the unaugmented flutter condition.
The ability to switch control laws above flutter without experiencing any noteworthy transient motions on the model laid the groundwork for adaptive control. In addition to the test demonstrations, advancements in test procedures and measurement techniques were also accomplished. Procedures to calculate model open-loop characteristics

from measured closed-loop transfer functions were demonstrated at conditions below and above flutter. Also, techniques developed and used to extract system gain and phase margins from Nyquist plots provided a measure of model stability and were useful in identifying ways to improve the control law performance.

The next step in the logical progression of AFS was to transition from analog nonadaptive systems to digital adaptive controllers. The demonstration of an AFS digital adaptive controller was accomplished in two phases. During the first phase, several of the analog control laws tested previously were digitized and implemented on a digital controller. These control laws were then retested during November 1981. The performance of the digital control laws and the improvement in flutter speed demonstrated was comparable to the metrics obtained during the analog control test demonstrations. Although sampling time was identified as a critical parameter, the control laws performed adequately down to a sampling rate of 100 samples per second (Figure 6), which was typical of sampling rates for aircraft digital FCS under development in the late 1970s.

During the second phase of these tests, a relatively simple adaptive controller was developed and tested during April 1982 (Ref. 15). The first level of adaptation consisted of discriminating between possible flutter modes (based on a priori knowledge) and selecting the appropriate control law; the second level consisted of adapting the control law to changes in flight condition. In addition, the ability of the controller to adapt rapidly following a store release was demonstrated. For this unique demonstration, a wing-tip mounted store was abruptly released transforming the model from a stable condition to a violent flutter condition. The adaptive controller recognized the unstable behavior, implemented a new control law, and stabilized the model in a small fraction of a second.

4.3 F-16 Full-Span Model Program

To assist in identifying a large number of critical wing/store flutter modes for the F-16, a 1/4-scale, full-span, free-flying flutter model was designed and fabricated by General Dynamics for testing in the TDT. This model was tested successfully many times in the 1970s and 80s to support the USAF F-16 flutter clearance program.

General Dynamics took advantage of the existing 1/4-scale flutter model, by then a mature and reliable testbed, to investigate the potential of applying AFS to the F-16. A new set of wings, equipped with accelerometers positioned at key locations and flaperon surfaces powered by hydraulic actuators, was fabricated. In addition, ballast in the fuselage was replaced with a hydraulic pump to power the wing servoactuators. For the next 8 years the F-16 model (Figure 7) with the new wings became a testbed for evaluating AFS systems that ranged from analog to complex digital adaptive concepts. This program, the F-16 full-span model program, was carried-out by a team of researchers from General Dynamics, the U.S. Air Force Wright Aeronautical Laboratories (AFWAL), and NASA LaRC and involved three wind-tunnel test entries in the TDT.

The objective of the first test conducted in February 1979 was to demonstrate the ability of flaperons for suppressing antisymmetric flutter (Ref. 16). Other research issues included: the effects of asymmetry between left and right wing sensor signals and actuators; the simultaneous implementation of symmetric and antisymmetric control laws; switching of control laws above open-loop flutter; and determining if open-loop frequency response functions (FRF) could be measured accurately enough to provide useful information. Important accomplishments from the first test included: successful modifications to control laws (gain/phase changes and sensor changes) during testing to maximize AFS effectiveness; successful switching of control laws above the unaugmented flutter condition without experiencing any threatening transient motions; and testing closed loop to a dynamic pressure 100 percent above the unaugmented flutter dynamic pressure (with flaperon displacements never exceeding 0.6 degrees).

The second test was accomplished in October 1981 (Ref. 17). The objectives of this test were to: determine the accuracy of measured FRF and define approaches for improving the accuracy; investigate the feasibility of suppressing flutter with a single flaperon while simulating a failure in the other; and demonstrate the ability of flaperons for suppressing symmetric flutter. The accuracy of the measured FRF was determined by actually varying gain and phase angles and measuring the gain and phase margins up to an unstable condition. Both the direct (actual measurement of open-loop data) and the indirect methods (extraction of open-loop data from closed-loop responses) of obtaining FRF were found to provide reasonable measures of model stability. The AFS was found to perform satisfactorily with one flaperon locked out; however, the gain margin was reduced by a factor of one-half. Finally, AFS systems employing flaperons performed equally well for both symmetric and antisymmetric flutter modes.

With successful conventional AFS wind-tunnel test demonstrations on the F-16 wind-tunnel model and successful adaptive AFS test demonstrations on the YF-17 model in hand, the AFWAL, General Dynamics, and NASA LaRC team became directly involved in developing and demonstrating a totally digital adaptive (no prior knowledge of the aircraft configuration) system. The objectives of this investigation included: demonstrating digital adaptive flutter suppression for three different external store configurations, each having widely different flutter-mode characteristics; demonstrating a 30-percent improvement in flutter speed with the AFS operating for each store configuration; and demonstrating the suppression of flutter following the separation of a store from the wing. These tests were accomplished during December 1986, and the results are summarized in Reference 18. These tests demonstrated, for the first time, the feasibility of using a digital adaptive AFS system having no prior knowledge of the wing/store configuration. For one test run, the adaptive controller updated the control law over 2500 times without losing control of the flutter mode. The controller also performed satisfactorily during simulated single actuator failures and with rapidly changing test conditions. In addition, the system performed very well in adapting and stabilizing the model following the release of a wing-tip missile that

immediately resulted in a post-flutter condition. In this unstable condition, the system was able to identify the unstable plant, design a nominal control law, and suppress flutter in less than a second.

Besides successfully demonstrating adaptive control of wing/store flutter, some of the more significant accomplishments of the program included: the use of control laws developed by the adaptive controller as a backup analog safety system; the launching of missiles from a free-flying model at conditions below and above the unaugmented flutter boundary; and the use of advanced computer architecture employing multiple processors and multitasking to permit high speed asynchronous parallel processing.

4.4 Active Flexible Wing Full-Span Model Program

In the early 1980s Rockwell International Corporation developed a concept it named the Active Flexible Wing (AFW) Concept (Ref. 19), and in 1985, in cooperation with AFWAL and NASA LaRC, Rockwell undertook a research program to demonstrate this concept. The AFW concept exploits, rather than avoids, wing flexibility by employing active leading- and trailing-edge control surfaces, up to and beyond control-surface reversal. A high-performance aircraft designed using the AFW concept achieves its high roll rates using wing control surfaces only, thereby eliminating the need for a "rolling tail" and, consequently, eliminating the additional structural weight associated with a rolling tail. In an AFW design an active roll control (ARC) system is required to efficiently manage the rolling of the vehicle. An ARC system monitors flight conditions and, based on those conditions, chooses the most effective control surfaces to roll the vehicle and also chooses the proper sign for control-surface deflections (one sign if below reversal, the opposite if above). In an AFW design further weight savings can also be achieved by the additional use of active controls. Taken alone or in combination, flutter suppression, gust load alleviation, and maneuver load control all have the potential for further reductions in vehicle weight. By taking full advantage of ACT and the AFW concept, Rockwell predicted that, compared to conventionally designed high-performance vehicles, weight savings of at least 15 percent of take-off gross weight could be achieved for an advanced fighter configuration.

An AFW Program grew out of the AFW Concept. The testbed for the AFW Program was a full-span, aeroelastically scaled, wind-tunnel model (Figure 8) of an advanced fighter configuration. The model, referred to as the AFW wind-tunnel model, was designed and built by Rockwell for testing in the LaRC TDT. The model was sting-mounted utilizing an internal ballbearing arrangement, allowing the model freedom to roll about the sting. A roll degree-of-freedom brake was employed for those cases when a fixed-in-roll condition was required. The model had two leading-edge and two trailing-edge control surfaces on each wing panel driven by rotary-vane, electro-hydraulic actuators powered by an onboard hydraulic system. A variety of sensors were available including accelerometers, strain gages, rotary variable differential transducers, and a roll rate gyro.

The model was tested on four different occasions (1986, '87, '89, and '91). The first two tests involved Rockwell, the Air Force, and NASA and focused on demonstrating the AFW Concept. The results from these tests are reported in References 19. The second two tests involved only Rockwell and NASA and focused on the demonstration of aeroelastic control (consistent with the AFW concept) through the application of digital ACT. For these tests the model was fitted with wing-tip ballast stores to lower the model flutter speed into the operational capabilities of the TDT. Active control concepts considered during these tests included AFS and rolling maneuver load alleviation (RMLA). These ACS were designed to be compatible with each other such that they could be tested simultaneously, even at conditions above the passive flutter speed of the wind-tunnel model.

The design goal of AFS control laws was to penetrate the passive flutter boundary and proceed to the tunnel operating limit. For the wind-tunnel model in the fixed-in-roll configuration symmetric and antisymmetric flutter boundaries had to be penetrated to demonstrate anything more than a trivial increase in flutter dynamic pressure. Maximum test dynamic pressures (26 percent above the antisymmetric flutter condition and 17 percent above the symmetric flutter condition) were limited by high dynamic response of the wing surfaces, however, analysis of the experimental measurements indicated that the control law was still stabilizing both flutter modes at these maximum conditions.

An important goal of the AFW Program was the demonstration of multiple-input, multiple-output, multiple-function control law testing. This goal was accomplished through the simultaneous operation of AFS and RMLA control laws. The design goal of RMLA control laws was to reduce or control wing loads during rolling maneuvers of 90 degrees. Important design considerations were to maintain stability, acceptable control-surface deflections and rates, and constant roll performance. These control laws were implemented with the wind-tunnel model in the free-to-roll configuration, for which only one flutter boundary (symmetric) was within the tunnel operating envelope. For these demonstrations, aggressive roll maneuvers were performed and wing loads were controlled at conditions 17 percent in dynamic pressure above the open-loop flutter condition. The results of these tests are summarized in Reference 20.

5. FLIGHT-TEST ACTIVITIES

Out of the many ACT related flight-test programs conducted at DFRC during the last 25 years, four have been selected for discussion in this section. These four programs span the entire range of ACT applications. The first program involves an active control system that was intentionally designed to interact with the flexible modes of the vehicle; the emphasis in this discussion is on the performance of the AFS rather than the adverse interactions of the system with other rigid body or elastic modes of the vehicle. For the other three programs, the systems were designed to interact only with the rigid body modes of the vehicle; the emphasis in this discussion is on the adverse ASE interactions encountered in flight and the modifications performed to the FCS to allow testing to continue and objectives of the test to be met.

5.1 DAST Drone Program

In the early 1970s NASA embarked on an ambitious high-risk flight-test program (Ref. 21) whose primary objectives were to validate analysis and synthesis methods for the active control of aeroelastic response and analysis techniques for aerodynamic loads prediction. This program was called DAST - Drones for Aerodynamic and Structural Testing. It was conceived and implemented at LaRC with flight-tests conducted at DFRC. The flight-test vehicle was an unmanned Firebee II target drone whose standard wing had been replaced with an aeroelastic research wing (ARW). The flight-tests associated with the DAST Program were referred to, at the time, as "a wind tunnel in the sky" because these tests retained some of the best features of wind-tunnel and piloted-flight-testing while removing some of the limitations of each. The DAST flight-tests: achieved realistic combinations of Mach number and dynamic pressure; achieved more realistic Reynolds numbers; included realistic inertial effects; removed the restriction of small model size; eliminated any questions concerning tunnel interference effects with walls and model mountings; and eliminated the risks to the test pilot associated with flutter testing.

The DAST flight-tests were conducted after an air launch from a B-52 and were concluded via a parachute recovery system and helicopter mid-air retrieval. Because of limitations on the fuel capacity of the Firebee II test vehicle, these means of launch and recovery allowed the maximum amount of flight-test time (typically 15-30 minutes) per flight. During a flight the test vehicle was controlled by a test pilot located in a ground cockpit.

The ARW-1 wing was designed to have both symmetric and antisymmetric classical bending-torsion flutter modes within the flight envelope. It had a supercritical airfoil, an aspect ratio of 6.8, and a cruise Mach number of 0.98. The primary objective of the ARW-1 flight-tests was to verify transonic flutter prediction techniques and to validate predicted AFS system performance (Ref. 21) Figure 9 is a planview of the ARW-1 flight-test vehicle showing the major features of the vehicle. The AFS system consisted of analog compensation, feedback signals from both wing and fuselage accelerometers, summing and differencing networks to obtain both the symmetric and antisymmetric components of the wing accelerations, and trailing-edge control surfaces driven by hydraulically powered rotary-vane actuators. For safety purposes, an ejectable ballast was installed on the trailing edge of each wing tip to serve as a flutter-stopper safety device.

Six flight-tests were originally envisioned, but only three were conducted. The flight-tests were to have been performed at three different altitudes (10, 15, and 25 thousand feet), with a progression in risk from approaching the open-loop flutter boundary, to slightly penetrating (with AFS engaged) the flutter boundary, to deeply penetrating (20 percent in Mach number beyond) the boundary. As described in Reference 22, during the second flight, at an altitude of 25,000 feet, the vehicle was flown, with AFS off, to Mach 0.91. At this altitude both symmetric and antisymmetric flutter were predicted to occur at Mach 0.92.

Between the second and third flights of the test vehicle the control laws of the AFS system were updated and reinstalled on the vehicle. Inadvertently and unknowingly to the entire test team, during this update a very serious error occurred: an erroneous factor of one-half was inserted into the control law, effectively halving the gain in both symmetries of the AFS system, and thereby lowering the closed-loop flutter Mach number at all altitudes. During the third flight the vehicle was to be flown at an altitude of 15,000 feet and tested with the AFS system on. Based on experimental data from the first two flight-tests, the open-loop flutter Mach number at this altitude was estimated to be between 0.76 and 0.77. Based on analysis, and using the nominal values of AFS gain, the closed-loop flutter Mach number at this altitude was predicted to be above 1.0, considerably higher than the highest Mach number to be tested. As the vehicle was accelerating from Mach 0.8 to its next test point at Mach 0.825, it encountered destructive symmetric closed-loop flutter, resulting in the separation of the right wing from the vehicle and the complete destruction of the vehicle after ground impact. An extensive post-test analysis and investigation determined that the inadvertent factor of one-half in the AFS control law was the primary cause of the flutter incident (Ref. 22).

As stated earlier, from its inception the DAST Program was recognized as an ambitious flight-test program with a high degree of risk accepted as part of the program. In spite of the fate of the ARW-1 test vehicle, valuable data was acquired and valuable lessons were learned from the DAST Program. The last flight was video taped from a chase plane and NASA has in its archives the only known video tape of in-flight, destructive, bending-torsion flutter with the wing separating from the vehicle. A flight-test technique and a "wind tunnel in the sky" flight-test facility were successfully developed and demonstrated.
Lessons learned the hard way from the DAST experience are the critical importance of end-to-end checks, which would have revealed the erroneous factor of one-half prior to the ill-fated flight and the critical importance of accurate on-line predictions of damping in the flutter mode, which would have alerted flight-test engineers of the impending danger.

5.2 X-29A Program

The X-29A aircraft is a single-seat fighter-type vehicle with thin, supercritical airfoil, forward swept wings. The wings are covered with aeroelastically tailored, graphite-epoxy, composite skins for controlling the divergence of the forward swept wing. For improved maneuverability, the aircraft was designed to be 35-percent statically unstable in the longitudinal axis. The aircraft is controlled using active, all-movable canards, strake flaps, and flaperons commanded by a triplex redundant, high-gain, digital, fly-by-wire control system. During the flight-testing of the X-29A aircraft during the 1980s, several unexpected ASE interactions were observed as described in the next few paragraphs.

Buffet-Induced Structural/FCS Interaction:
While conducting flight-tests to investigate the flying characteristics of the X-29A at high angles-of-attack, unexpected ASE interactions were encountered.
During envelope expansion up through 45 degrees angle-

of-attack, an ASE interaction occurred between the buffeting on the aircraft, the structural mode response, and the FCS in the lateral-directional axis (Ref. 23). Power spectral density (PSD) plots of the rudder trailing-edge accelerometer signal, the roll and yaw rate outputs, and the rudder and flaperon control surface positions indicated the presence of three structural modes: an antisymmetric wing bending mode at 11 Hz, a fuselage lateral bending mode at 13 Hz, and a vertical fin bending mode at 16 Hz. The PSD plot of the roll rate gyro showed considerable energy in the frequency range from 11 to 16 Hz, while the yaw rate signal over the same frequency band was approximately three orders of magnitude less. This difference was partially attributed to a structural notch filter at 11.2 Hz in the yaw rate path. The PSD plots of the rudder and flaperon control surface positions also showed considerable response over the 11 to 16 Hz frequency band. This ASE interaction contributed to the control surface actuator commands being miscompared in the hydraulic logic of the flaperon actuator. This miscomparison resulted in a reconfiguration of the flaperon actuator settings during the flight. Although this interaction did not produce an instability, increased flight-test time was required to repeat maneuvers already accomplished with the earlier flaperon setting. This occurrence was one of the catalysts for implementing a notch filter into the roll rate gyro path of the FCS. The lesson was that subsystems of an airplane can be adversely affected by ASE. Although this flight incident did not result in significant changes in the way ASE testing is performed, it did add another data point to our knowledge base dealing with the complex mechanisms associated with ASE.

Canard/FCS Interaction: After completing the envelope expansion tests without experiencing further ASE interactions, several changes in the FCS were made to improve the airplane handling qualities. On subsequent flight-tests a higher-than-expected response at 13.5 Hz was observed on the canards (Ref. 24). This response was also observed in the time history signals of the canard position feedback, the canard command, the flaperon command, and the strake command. Other longitudinal feedback paths, such as pitch rate and normal acceleration, and the lateral-directional axis did not contain any unusually high response at 13.5 Hz. It was determined from analytical and test data that the lowest canard mode (canard pitch) was at 26.5 Hz, and that this mode was aliased to the lower frequency of 13.5 Hz by the FCS. The A/D converter sampling rate was 40 samples/second and, therefore, provided a Nyquist frequency of 20 Hz. The FCS was somewhat prone to aliasing because the 32 Hz antialiasing filter break frequency used in the off-the-self flight computer hardware was not modified for the X-29A airplane.

It was also determined that amplitude of the forced response at 13.5 Hz was a function of the amount of wear on the canard aerodynamic seals fitted between the canard root and the fuselage. The canard responses for ships 1 and 2 are shown in Figure 10 for Mach numbers of 0.40, 0.60, and 0.80 at 15,000 feet. The data for ship 1 is with worn seals (174 hours) while the data for ship 2 is with new seals (2 hours). Each airplane had identical control laws in the FCS. It is thought that as the canard seals for ship 1 wore, less force was exerted between the canards and the fuselage which consequently allowed the structural response of the canards to become larger. This increase in structural response amplitude was sensed by the canard linear variable displacement transducer, aliased to a frequency of 13.5 Hz, and then amplified in the FCS. The overall effect was to have more power at a frequency of 13.5 Hz in both the canard position feedback path and the canard command path. For ship 2, the tightness of the new seals was found to add damping to the canard structure thereby reducing the response of canard pitch mode.

The canard structural response was also found to be affected by the canard aerodynamic loading. Flight test results showed that structural response was largest when the normalized canard lift coefficient was nearly zero and decreased as the normalized canard lift coefficient was increased. This data suggested that ASE testing should be accomplished at an angle-of-attack for which the surface of concern is at or near zero lift.

Based on these X-29A experiences, the lesson learned is to recognize how essential it is to consider all changes to aircraft subsystems, however insignificant. These changes may directly or indirectly impact the structural dynamic characteristics of the vehicle and have a significant effect on ASE interactions. Also, the correct placement of the FCS antialiasing filter break frequencies is important. Incorrect placement can cause aliasing of structural response signals that result in unwanted forced excitations of the aircraft structure.

5.3 AFTI/F-16 Program

The F-16 aircraft was a testbed for the Advanced Fighter Technology Integration Program (AFTI) (Ref. 25). The modifications made to the airplane provided improved weapon system effectiveness and survivability in air-to-air and air-to-surface combat situations. There were eight pilot-selectable digital flight control modes and one analog back-up mode. Structural modifications included the addition of canards under the engine inlet duct and the addition of a dorsal structure on the upper fuselage.

One pilot-coupled ASE instability was encountered during the flight-test program. The resultant unstable oscillation was limited in amplitude and involved the antisymmetric missile pitch mode (5.8 Hz) coupling with the lateral-directional axis of the FCS. This oscillation was induced by a roll command from the pilot and was sustained when the pilot applied more than 0.7 pounds of lateral stick force. When the pilot reduced the lateral stick force, the oscillation dissipated. The oscillation occurred at altitudes of 10,000 to 30,000 feet and between Mach numbers of 0.78 and 0.90. Efforts to excite the oscillation at 45,000 feet were unsuccessful. A time history of the oscillation at Mach 0.85 at an altitude of 20,000 feet is shown in Figure 11. Note that when the lateral stick force was less than 0.7 pounds, the oscillations on the flaperons decreased. The oscillation was a result of a high-gain, but low-authority, roll-command channel in the lateral-directional axis that bypassed the roll-notch filter designed to filter out the 5.8 Hz antisymmetric missile pitch mode. This loop was activated with lateral stick forces equal to or greater than 0.7 pounds.

This program illustrated the need to thoroughly model the FCS architecture in the ASE analysis. The analysis in this case had not modeled stick inputs, resulting in the loop not being accurately represented, which, in turn, resulted in inaccurate analytical predictions of closed-loop stability. In addition, this program illustrated that ASE instabilities can occur in any portion of the flight envelope and not only at the high speed, high dynamic pressure extremes.

5.4 F-18 HARV Program

An F/A-18 aircraft was modified at DFRC to perform flight research at high angles-of-attack using thrust vectoring. Control law concepts for agility and performance enhancement were also incorporated to provide data for correlation with computational fluid dynamics solutions. This vehicle is referred to as the High Angle of Attack Research Vehicle (HARV). Modifications included the addition of vanes in each engine exhaust for thrust vectoring and a research FCS containing high angle-of-attack control laws (Ref. 26).

During the aircraft ground tests, considerable freeplay in the turning vane assembly mechanism in the engine was identified. The freeplay was a concern, and frequency response and fatigue analyses were performed to determine the effect of the vibration levels on the aft fuselage structure. Analysis results indicated that the fatigue life of the structure was adequate for the number of flight hours required to complete the flight research program. The aircraft was initially flown with the standard F-18 FCS. For these tests, the thrust vectoring turning vanes were positioned at the edge of the engine exhaust plume. In this position, the vanes were found to have considerable movement due to the freeplay since they were not aerodynamically loaded. However, no unusual problems were encountered due to vane movement.

After these initial flight-tests, a set of research flight control laws that used aircraft normal acceleration in the feedback loop and the thrust vectoring turning vanes were implemented. During subsequent flight-tests, the pilot reported feeling a high frequency vibration each time the research FCS was engaged. He also reported that the vibrations dissipated when he maneuvered the aircraft. Figure 12 shows the time history signals of a vane strain gage and the airplane normal accelerometer. The oscillation is shown to begin as the research FCS was engaged. At approximately 8 seconds, the pilot commanded a pitch maneuver which deflected the vanes into the exhaust plume. The oscillation dissipated while the vanes were immersed in the plume. When the vanes were retracted to the edge of the exhaust plume, the oscillation began again.

The power spectrum of the airplane normal accelerometer signal indicated high response at two frequencies, 18.5 Hz and 21.5 Hz. The 21.5 Hz mode was the turning vane rotation mode. The sampling rate in the FCS was 40 samples/second which yields a Nyquist frequency of 20 Hz. Antialiasing filters were placed in the FCS, however, not all of the response of the 21.5 Hz mode was filtered out and some of the signal was sensed by the airplane normal accelerometer which was then digitized to a frequency of 18.5 Hz. The turning vanes were then commanded to oscillate at a frequency of 18.5 Hz. The ASE problem was resolved by installing a notch filter at these two frequencies. Subsequent flight-testing revealed that the oscillation was eliminated.

6. THE NEXT QUARTER CENTURY

As the next quarter century begins, there are several ongoing or planned NASA wind-tunnel and flight-test projects that have the potential for making significant contributions of their own to the state-of-the-art of ACT.

Several wind-tunnel test projects are now underway to develop and demonstrate new avenues for exploiting ASE interactions. One project is investigating the use of piezoelectric actuators embedded in the structure to suppress undesirable subcritical aeroelastic response and to prevent flutter. With the advent of neural network technology and its promising role of providing significant advances in future ACT concepts, these tests will include neural-network-based AFS concepts. Neural networks can provide the adaptation required to change control laws to not only changes in flight condition but, more importantly, for reconfiguring the FCS following a failure of an actuator or a feedback sensor. Other wind-tunnel test projects are underway to investigate the feasibility of using spoilers for flutter suppression and for using aerodynamic and/or smart materials to alleviate the structural response associated with buffeting tails.

In the area of flight-testing, a full-scale flight investigation utilizing a high performance fighter is required to demonstrate the benefits of AFW technology. Successful completion of a flight-test program is required to mature the basic technology and provide aircraft designers with the confidence to use the technology on future air vehicles. A program, using an F-18 airplane at DFRC, is presently being proposed and advocated by the USAF Wright Laboratory. Flight testing is expected to begin in 1999.

7. REFERENCES

1) Newsom, J., "An Overview of the NASA/LaRC Aeroservoelasticity Branch," Proceedings of the Aeroservoelastic Specialists Meeting, AFWAL-TR-84-3105, Vol. 1 and 2., October 1984.

2) Felt, L., Huttsell, L., Noll, T., and Cooley, D., "Close Encounters of the Aeroservoelastic Kind," 19th AIAA/ASME/ASCE/AHS Structures, Structural Dynamics, and Materials Conference, May 1978.

3) Peloubet, R. P., "YF-16 Active Control System/Structural Dynamics Interaction Instability," 16th AIAA/ASME/ASCE/AHS Structures, Structural Dynamics, and Materials Conference, May 1975.

4) Arthurs, T. D. and Gallagher, J. T., "Interaction Between Control Augmentation System and Airframe Dynamics on the YF-17," 16th AIAA/ASME/ASCE/AHS Structures, Structural Dynamics, and Materials Conference, May 1975.

5) "The Langley Transonic Dynamics Tunnel," LWP-799, September 1969.

6) Moore, A. L., "The Role of a Real-Time Flight Support Facility in Flight Research Programs," NASA TM 86805, January 1986.

7) Wykes, J. and Kordes, E., "Analytical Design and Flight Test of a Modal Suppression System on the XB-70 Aircraft," AGARD CP-46, 1970.

8) Burris, P. M. and Bender, M. A., "Development of Active Flutter Suppression Wind-Tunnel Testing Technology," AFFDL-TR-74-126, January 1975.

9) "B-52 CCV Program Summary," AFFDL-TR-74-92, Vol. 1, 1974.

10) Sevart, F., "Development of Active Flutter Suppression Wind-Tunnel Testing Technology," AFFDL-TR-74-126, January 1975.

11) Roger, K., Hodges, G., and Felt, L., "Active Flutter Suppression—A Flight Test Demonstration," 15th AIAA/ASME/ASCE/AHS Structures, Structural Dynamics, and Materials Conference, April 1974.

12) Triplett, W., Kappus, H., and Landy, R., "Active Flutter Suppression Systems for Military Aircraft—A Feasibility Study," AFFDL-TR-72-116, February 1973.

13) Hwang, C., Winther, B., Noll, T., and Farmer, M., "Demonstration of Aircraft Wing/Store Flutter Suppression Systems," AGARD Report No. 668, April 1978.

14) Hwang, C., Johnson, E., Mills, G., Noll, T., and Farmer, M., "Wind-Tunnel Test of a Fighter Aircraft Wing/Store Flutter Suppression System, An International Effort," AGARD Report No. 689, April 1980.

15) Johnson, E., Hwang, C., Joshi, D., Harvey, C., Huttsell, L., and Farmer, M., "Adaptive Flutter Suppression—Analysis and Test," AGARD Report No. 703, September 1982.

16) Peloubet, R. and Bolding, R., "Summary of Active Flutter Suppression Research at General Dynamics Fort Worth Division," AFWAL-TR-83-3082, April 1983.

17) Peloubet, R. and Haller, R., "Wind-Tunnel Demonstration of an Active Flutter Suppression Using F-16 Model with Stores," AFWAL-TR-83-3046, April 1983.

18) Peloubet, R., Bolding, R., and Penning, K., "Adaptive Flutter Suppression Wind-Tunnel Test Demonstration," AFWAL-TR-87-3053, October 1987.

19) Miller, G. D., "Active Flexible Wing (AFW) Technology," AFWAL-TR-87-3096, 1987.

20) "Special Section: Active Flexible Wing," AIAA Journal of Aircraft, Vol. 32, No. 1, pp. 9-76 and pp. 205-207, January-February 1995.

21) Murrow, H. N. and Eckstrom, C. V., "Drones for Aerodynamic and Structural Testing (DAST) - A Status Report," AIAA Journal of Aircraft, Vol. 16, No. 8, pp. 521-526, August 1979.

22) Edwards, J. W., "Flight Test Results of an Active Flutter Suppression System," AIAA Journal of Aircraft, Vol. 20, No. 3, pp. 267-526, March 1983.

23) Voracek, D. F. and Clarke, R., "Buffet Induced Structural/Flight Control System Interaction of the X-29A Aircraft," NASA TM 101735, April 1991.

24) Kehoe, M. W., Laurie, E. J., and Bjarke, L. J., "An In-Flight Interaction of the X-29A Canard and Flight Control System," NASA TM 101718, April 1990.

25) Bennett, W. S. and Ramage, J. K., "AFTI/F-16 Automated Maneuvering Attack System Configuration Development And Integration," National Aerospace Electronics Conference, May 1986.

26) Regenie, V., Gatlin, D., Kempel, R., and Matheny, N., "The F-18 High Alpha Research Vehicle, A High-Angle-of-Attack Testbed Aircraft," NASA TM 104253, September 1992.

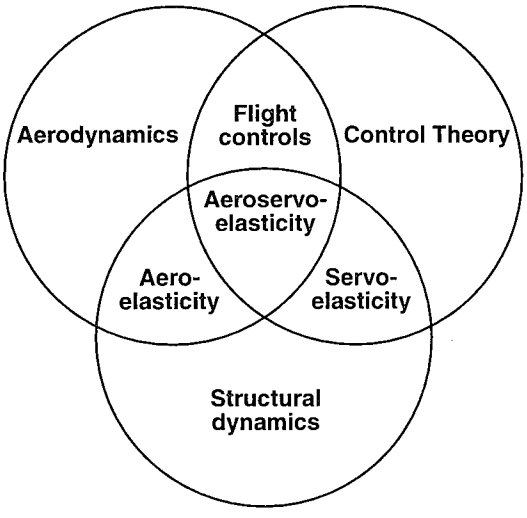

Figure 1. Aeroservoelasticity interaction triangle.

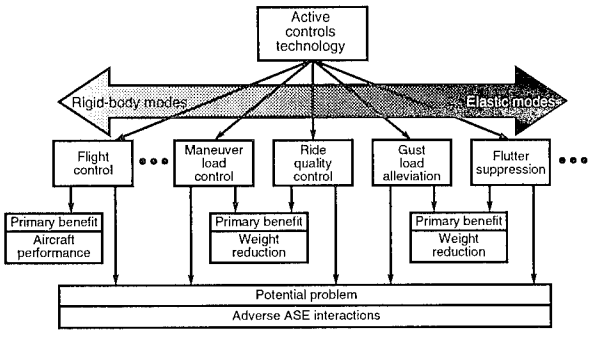

Figure 2. Active controls technology.

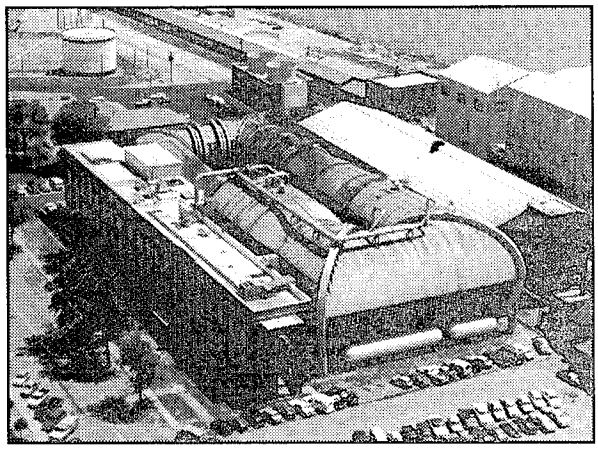

Figure 3. Photograph of the Transonic Dynamics Tunnel.

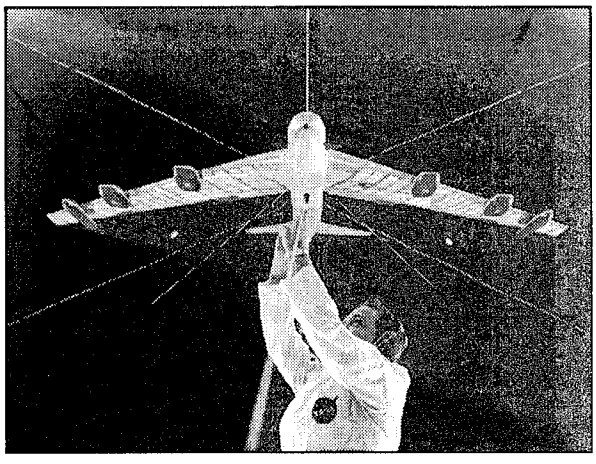

Figure 4. B-52 full-span model mounted in the Transonic Dynamics Tunnel.

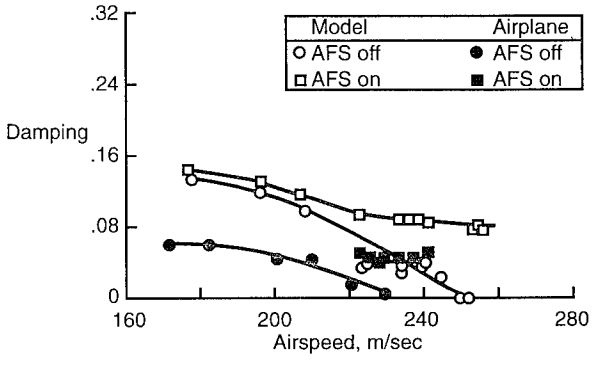

Figure 5. Comparison of B-52 wind-tunnel and flight test results, AFS system off and on.

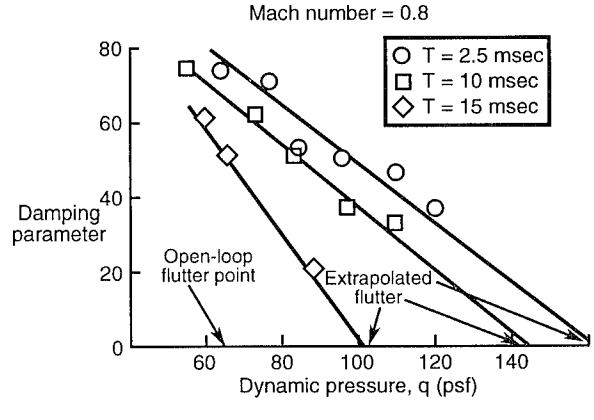

Figure 6. Effects of sampling time on digital control law performance.

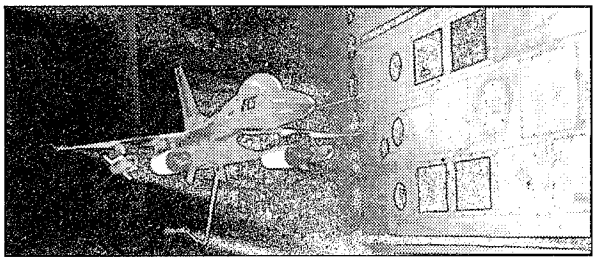

Figure 7. F-16 full-span model mounted in the Transonic Dynamics Tunnel.

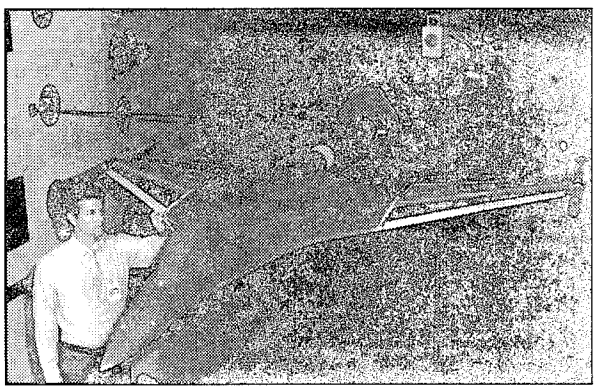

Figure 8. AFW full-span model mounted in the Transonic Dynamics Tunnel.

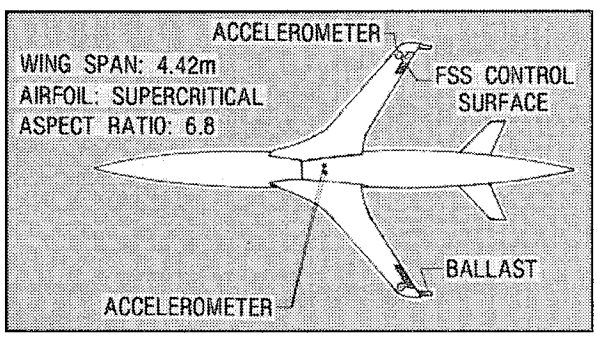

Figure 9. Planview of the DAST flight test vehicle.

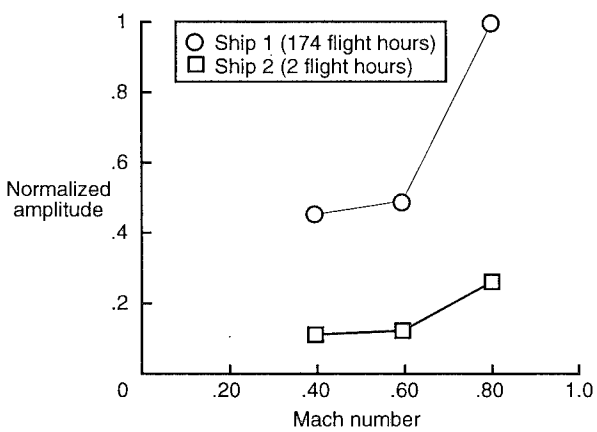

Figure 10. Effects of X-29A canard aerodynamic seal wear on structural response.

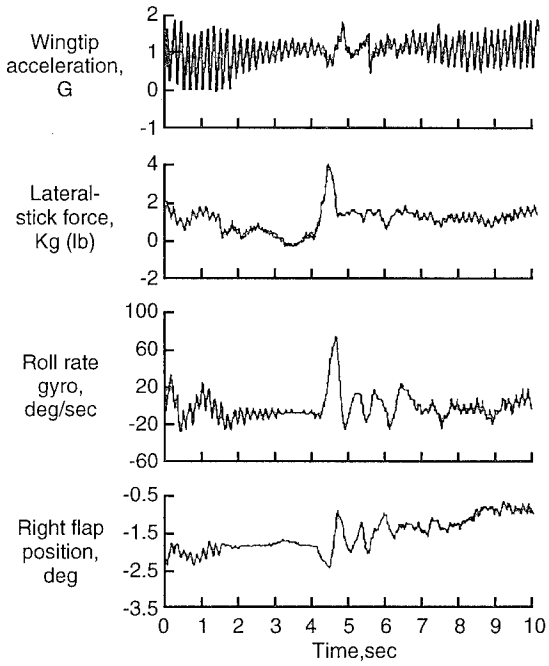

Figure 11. Effects of stick force on the AFTI/F-16 antisymmetric missle pitch mode.

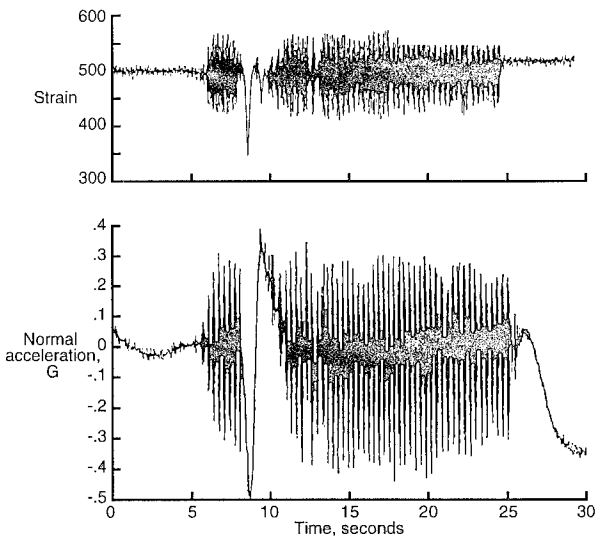

Figure 12. F-18 HARV thrust vectoring vane strain and normal acceleration.

SYSTEM OF AEROSERVOELASTIC EXPERIMENTAL AND NUMERICAL INVESTIGATIONS FOR AIRCRAFT DESIGN AND CERTIFICATION

M.Ch. Zitchenkov
V.I. Dovbishchuk
V.N. Popovsky
Central Aero-Hydrodynamic Institute (TsAGI)
Zhukovsky, 140160
Moscow Region, Russia

SUMMARY

Solving practical problems of modern aeroservoelasticity (ASE) presumes accomplishing reasonable synthesis and reliable analysis of nonlinear analogue-digital multi-dimensional electromechanical objects characteristics in frequency and time domains. The paper describes shortly the system of experimental and analytical research and certification used in Russia aircraft industry to ensure aircraft safety from vibrations of various types due to interaction between airframe and flight control system as well as active control of aeroelastic dynamic deformations. The system provides qualitative determination and analysis of ASE characteristics for all aircraft development stages. Some real results obtained in ASE research programs on wide body civil and aerospace aircraft are presented as an illustration.

1. INTRODUCTION

The experience of flying technique design and production shows that ASE is an important general aeroelasticity problem considered together with flutter, control reversal, divergence, buffeting, etc. All phenomena connected with influence of automatic flight control system (FCS) on aircraft structure aeroelastic behavior for different operating regimes compose ASE subject of interest. The significant amount of different publications and reports at the international conferences was devoted to this problem and, in particular, in recent years. Some foreign publications are given as examples below in the reference.

As flexible aircraft/FCS interaction is a complex problem including aeroelasticity and flight control dynamics, expert cooperation and adequate understanding of theoretical/technical aspects in both scientific subjects is required for successful solution of ASE problems as far as a specific aircraft is concerned. Thanks to a great amount of practical activities in this field in TsAGI, Flight Test Institute, design bureaus and other organizations of Russia since the 50th (starting point of applying hydraulic actuators in aircraft) up till now, ASE has been formed and developed as aircraft applied scientific direction. A team of experts in ASE was brought up developing theoretical models, software, hardware and methodology of solving ASE problems for different types of flying technique. Some results of such research are presented in references [1÷9].

The following ASE study directions should be noted:

- ensuring flexible structure/FCS aeroelastic stability;
- estimation of FCS influence on aircraft loading and aircraft structure flutter;
- synthesis and development of special active control subsystems (ACS) for load alleviation, flutter characteristic improvements, and vibration level decrease.

The flexible structure/FCS aeroelastic stability ensuring was historically the first significant problem requiring practical solution. Active control application for improvement of aircraft technical and strength characteristics has lately become quite urgent.

2. AEROELASTIC INTERACTION SCHEME

Flight and investigation experience shows that at the unfavorable combination of aerodynamic, elastic, inertia structural characteristics and dynamic control system parameters (Fig. 1) in the multi-connection closed-loop "flexible aircraft - FCS" self-oscillations occur that may result in control malfunction and dangerous stresses generating in the structural elements. As a rule oscillation forms at ASE instability differ greatly from the forms of common airframe flutter. In some cases the instability in the loop "flexible structure - FCS" can take place due to inertia-kinematics connections in the ground regimes where airspeed is equal to zero. The general scheme of aeroelastic interaction of the structure with control system can be presented in the following way. Kinematics parameters of elastic structural oscillations are responded by FCS sensors and transformed by the flight computer (digital or analogue) in accordance with the given control algorithms and then transferred to the input of actuators deflecting control surfaces which in turn affect the structure both aerodynamically and by inertia (Fig. 2). The structure is also affected by different commands from the pilot and external disturbances due to air gusts. In general practice two types of problems are to be solved, i.e. defining stability degree of closed system and its response to the external disturbance.

Mathematical model describing the dynamics of modern aircraft having multi-function FCS in the frequency range of elastic oscillations is rather complicated. For example, wide body passenger aircraft structure with engines on the under-wing pylons can have about 20 closely spaced symmetrical and antisymmetrical elastic modes (Fig. 3) in the transmissibility range of control system. When the ASE parameters of modern highly maneuverable aircraft are

Paper presented at the Structures and Materials Panel Specialists' Meeting on "Advanced Aeroservoelastic Testing and Data Analysis", held in Rotterdam, The Netherlands, from 8-10 May 1995, and published in CP-566.

investigated it is necessary in some cases to consider the problem of aeroelastic interaction at large disturbances (maneuver, gust), so the united model of aircraft trajectory movement and its elastic vibrations is required.

The distant analogue-digital system of automatic control realizes the control algorithms and parameters depending on flight conditions. It is significantly non-linear in the common case and uses different sensors and control surfaces. Non-linear control relationships valuable for aeroelastic interaction analysis are often caused by the parameters of actuators and servoactuators like the dead zone, deflection rate limitation, loading effect (hinge moment). Including the digital computer into the control contour also causes the specific properties in the oscillatory processes that are defined by discrete control signals by time and level. The effect of transposition of higher harmonics into the low-frequency domain (in the case of relatively low sample frequency) enables the interaction of elastic modes with dispersed frequencies and their great influence on the dynamics of aircraft trajectory movement.

Considering the difficulty of the problem a complex of experimental and analytical investigations is developed and operated for its practical solution. These studies are performed during the whole period of aircraft development and include the analysis, physical simulation and full-scale tests.

3. SYSTEM OF COMPLEX INVESTIGATIONS

Many years of activities in ensuring the required ASE parameters for many airplanes of various types and applications resulted in the modern system for investigations and certification including the following sections.

CERTIFICATION REQUIREMENTS, RECOMMENDATIONS AND DATA BASES.

The requirements to aeroelastic stability including the structure/FCS interaction are formulated in the section C - "Strength" of Aviation regulations (AR-25.629) [10]. As a rule certification materials are prepared and analyzed together with design bureaus, thereafter the TsAGI Department of aeroelasticity prepares the specific conclusion. Aviation regulations (AR-25.302) also prescribe to consider the effect of control systems on the strength parameters.

The recommendations contain the proposals dealing with the methods and the volume of investigations that are to be performed at various stages of aircraft development. In particular, at the technical proposal stage it is recommended to evaluate the validity of using special active load alleviation systems; at the conceptual design stage the analytical and/or model studies in wind tunnel are to be carried out to select the control structure and parameters, efficiency and stability evaluation; during the detailed design the margins of aeroelastic stability are specified together with dynamically scaled model tests (in the presence of active control system) and bench tests of FCS elements; then the experimental aircraft with FCS is tested on the ground and sometimes (see below in section 4) in a specific flight; and finally, frequency characteristics of FCS of the first production aircraft are defined.

Experts have various data containing all kinds of results in ASE that help to outline investigation program at the early stage of development and to define reasonably the study volume considering structural and control peculiarities of every specific aircraft.

ANALYTICAL METHODS AND SOFTWARE.

Theoretical model of flexible aircraft/FCS movement includes the definition of aerodynamic forces affecting vibrating deformed surface, elastic-mass structural scheme, mathematical models of actuators and analogue-digital control elements. The problems are solved of stability boundary definition, response to the external disturbance, optimal synthesis of active control systems, identification of structure and control parameters. The developed software enables to effectively solve the problems of aeroelastic interaction using test results in the frequency and time domains by means of various general-purpose computer complexes including personal computers.

PHYSICAL SIMULATION.

The problem of simulating ASE phenomena on physical models in wind tunnels can be separated in three parts: generating a dynamically similar model of flexible aircraft structure, control system simulation, and flight conditions simulation, including gust effect. Widely used flutter models are utilized, assembled by miniature electrohydraulic fast actuators and control linkage, providing the deflection of the required control surfaces (ailerons, spoilers, elevators, rudders, etc.). Control linkage is manufactured so that it could not influence the rigidity of structural elements. The sensors of accelerations, angular speed, bending and torsion moments are mounted on the model. To realize the models of active control system (ACS) and control law algorithms a mobile analogue-digital computer laboratory is used also equipped with measuring and test result processing system. Atmospheric turbulence effect is simulated by means of profiles controlled by hydraulic actuator and mounted at the entrance of wind tunnel test chamber.

GROUND AND FULL-SCALE AIRCRAFT/FCS TESTS.

The methods are used enabling to get frequency parameters of non-linear analogue-digital FCS channels and elements during the ground tests of full-scale aircraft or at the control bench in the frequency range of elastic structural oscillations. To determine these parameters special facilities are used simulating FCS sensors oscillations and measuring laboratories with data acquisition and processing system.

FLIGHT TESTS.

During the flight tests the following problems can be solved:

- determination of structural frequency characteristics by the signals of FCS sensors at the forced oscillations of control surfaces;
- confirmation of aeroelastic stability margins;
- efficiency evaluation of active control systems for loads and elastic oscillation damping.

During these activities recommendations are given and necessary changes are introduced. Investigations and

analysis resulted in generating the whole analytical-experimental model of ASE. It should be noted that though analytical methods and tools are highly developed, the direct experiment is still very valuable for receiving final certification papers.

4. FREQUENCY RESPONSE METHOD AND ASE REQUIREMENTS

The experience in design of aviation technique had shown the frequency response functions (FRF) analysis to be the most reasonable and suitable method for structure/FCS aeroelastic stability investigations. The aircraft FRF connect amplitude and phase of the structure frequency response (displacement, angle velocity, acceleration) in FCS sensors locations with harmonical deflections of control surfaces. On the other hand FCS frequency response functions are defined as relationships between amplitude and phase of control surface oscillations and harmonical deflections of FCS sensors. For solving the flexible aircraft/ FCS stability problem FRF must be determined in the whole frequency range where ASE interaction can take place.

One of the frequency response method advantages, that is important for practical applications, is the possibility of independent determination of structural FRF $S_{ik}(j\omega)$ and those of the FCS - $L_{ki}(j\omega)$, where i is a serial number of sensor and k is a serial number of control surface. Some part of arrays $S_{ik}(j\omega)$ and $L_{ki}(j\omega)$, for example, may be determined by calculations, another part - by bench tests or in the wind tunnels and the third part - by ground tests of full scale aircraft. Then all FRF may be used together to determine these functions of open-loop contour $W_o^c(j\omega) = S_{ik}(j\omega)L_{ki}(j\omega)$ (where c is the contour number) and to analyze general multi-loop ASE stability and active control efficiency.

The special certification standards which act in Russia for providing aircraft structure/FCS aeroelastic stability are formulated in Aviation regulations (AR-25.629 [10]). The basic principle is the absence of aeroelastic instability (continuous oscillations) for all possible aircraft configurations and flight regimes and the presence of essential stability margins. To ensure aircraft safety and stability from the ASE point of view the open-loop FRF should meet the following requirements (Fig. 4): within the phase range from -60° to $+60^\circ$ amplitude of response should not exceed 0.5 (here the (+1,0) point is considered as critical). If it is found out by numerical analysis or in ground tests that open-loop FRF is situated in the right semi-plane and, simultaneously, the amplitude of response exceeds 0.3 (the 2nd zone in Fig. 4), the stability margins should be confirmed by flight test results.

The criterion to define a control law of active damping system (ADS) used for load alleviation and aeroelastic stability characteristics improving, may be formulated in the frequency domain as for the above stability requirements. For the effective operation of ADS (in accordance with Nyquist criterion) it is necessary to provide maximum phase stability margin ($K_{ph} = 180^\circ$) in active control loop at the frequency of the vibration mode ω_d to be damped. Choice of active control loop gain is governed by the system functions and stability requirements.

5. WIDE BODY CIVIL AIRCRAFT ASE INVESTIGATIONS

The ASE experimental and numerical investigations for IL-96-300 were conducted beginning from technical proposal stage aiming active reduction of loads in root and middle parts of the wing and also meeting the requirements to aeroelastic stability margins. Special small aileron end sections having the ability of symmetrical and antysymmetrical deflections as well as the elevator were provided for active control.

During the first stage of dynamically scaled model (length scale 1/10) tests in the subsonic wind tunnel, the possible ADS algorithms and parameters were chosen with preliminary efficiency/stability estimations.

Multi-loop digital nonlinear ADS that is now installed on full-scale aircraft for actual operation was simulated during the second stage of these tests (after aircraft and control system detailed design). Fig. 5 illustrates ADS model efficiency in decreasing wing root bending moments under random turbulence disturbances, the influence of control surfaces (ailerons) rate limit on ADS efficiency and the satisfaction of ASE stability requirements.

The open-loop FRF of one aircraft/FCS configuration is shown in Fig. 6 for the case of operating conventional autopilot and rigid body stability improving system. The aircraft structure FRF in this case was calculated for the maximum flight speed (V_D), and control system frequency response was obtained experimentally in ground full-scale tests. For providing aeroelastic stability special additional filters in FCS sensors channels were introduced. The aircraft structure calculated FRF were confirmed by flight test results. The total open-loop FRF considered as an example meets to ASE stability certification requirements.

6. AEROSPACE AIRCRAFT DYNAMICALLY STABILITY

The significant amount of analytical/experimental investigations was performed in cooperation of several organizations and numerous specialists to provide sufficient ASE stability characteristics for Russian aerospace aircraft (ASA). The scheme of ASA preflight investigation and certification procedure is shown in Fig. 7. The relatively high gains in multi-regime remote digital FCS channels and four heavy unbalanced elevons (and rudder) were the main reasons of ASE stability problem for ASA being complicated and urgent in the ground and flight regimes.

The detailed ground structure/FCS vibration tests of full-scale ASA were carried out (simultaneously with modal vibration tests) with the following objectives:

- confirmation of the correspondence between experimental FCS control channel dynamic characteristics and technical requirements;

- determination of structure FRF using oscillations of control surfaces and application of concentrated external exciting forces, that is necessary for additional verification of ASA mathematical model and possible correction of control laws;
- determination of ASA structure/FCS dynamic stability boundaries by analysis of open-loop experimental FRF without consideration of aerodynamic forces;
- direct proof of sufficient dynamic stability margins of ASA structure/FCS closed-loop system by means of external excitation.

During two stages of tests ASA was installed on special low frequency air support system and on landing gear. Block-diagram of the experiment is illustrated by Fig. 8. The results shown as an example in Fig. 9 illustrate the existence of amplitude margin $K_{mod} > 2$ in the roll channel for one flight regime (yaw channel is closed) in the frequency range containing five vibration modes. The decay of oscillations in the closed system with nominal gains after switching off the external excitation as well as the absence of decay at the two-time increase of the gain in the roll angular velocity channel is shown in Fig. 10.

During the ground test stage the data were received necessary for the correction of mathematical dynamic structure model and control law parameters. The discovered differences between experimental and analytical FRF of the structure and control system were caused by the strong cross-interaction between FCS channels and structure asymmetry, differences in individual dynamic characteristics of actuators with elevons and nonlinear properties of landing gear.

After stability margins were specified by using numerical and experimental characteristics and some necessary corrections were made, ASA "Buran" was certified according to ASE and other problems and a successful orbited flight with fully automatic landing was, as well known, carried out.

7. CONCLUSIONS

The paper contains short description (review) of methodology and procedures for applied investigations in ASE, carried out starting from the stage of aircraft outlook determination till its series production and certification. The utilized system approach to the problem considered gives the enough degree of reliability in ensuring aircraft safety in spite of various types of dynamic instability, connected with aeroelastic interaction between structure and control system. Analytical and experimental results enable effective following aircraft design, up to date formulating recommendations, in-time introduction of necessary changes of structure and control system, as well as wide application in solving the neighboring problems in the field of strength and flight dynamics. Study methods and certification requirements are continuously improved and modified with aircraft becoming more complex and acquiring new functional possibilities. The agreement of requirements and methods for producing certification documents, aeroservoelasticity problems at transonic speeds, active control concept developments seem to be advanced directions for investigations and cooperation among experts from various countries and organizations today and in the future.

REFERENCES

1. A.F.Minaev. Theory of Oscillations in Uncommon Systems and its Application to Control Systems.- Trudy TsAGI, issue 2200, 1983.
2. F.Z.Ishmuratov, A.F.Minaev, V.N.Popovsky. Method of Frequency Response Characteristics Calculations for Flexible Aircraft in Longitudinal Maneuver. -Trudy TsAGI, issue 2226, 1984.
3. V.I.Dovbishchuk, M.Ch.Zitchenkov. Experimental Investigations of Active Damping System for Heavy Aircraft Dynamically Scaled Model in Wind Tunnel.- Papers of the 6th Symposium in Elastic Vibrations of Structure with Liquid. SibNIA, Novosibirsk, 1990.
4. S.F.Alferov, V.I.Dovbishchuk, L.S. Kooksa, V.N.Popovsky. Aeroelastic Stability of Modern Civil Aircraft with Automatic Control.-Proceedings of International Conference "Aircraft Flight Safety", held in TsAGI. Zhukovsky, Russia, 1993.
5. B.I.Smirnov. Development of Optimal Active Flutter Suppression System for Flexible Aircraft. - Trudy TsAGI, issue 1966, 1977.
6. M.Ch.Zitchenkov, V.I.Dovbishchuk. Determination of Structure and Modern Control System Dynamic Characteristics for Aircraft Aeroservoelastic Certification. - A Collection of Reports of Russian-Chinese Aircraft Strength Conference. Peking, 1994.
7. K.S.Kolesnikov, V.N.Sukhov. Flexible Aircraft as an Object for Automatic Control.- Moscow, Mashinostroenie, 1974.
8. O.A.Kuznetsov, V.V. Politov. Determination of Loads Acting on Flexible Aircraft with Automatic Control System During Flight in Atmosphere Turbulence. - Trudy TsAGI, issue 2135, Moscow, 1974.
9. S.M.Belotserkovsky, Yu.A. Kochetkov, A.A. Krasovsky, V.V. Novitsky. Introduction in Aeroautoelasticity. - Moscow, Nauka, 1980.
10. Aviation regulations. Part 25. Airworthiness Standards: Transport Category Airplanes. Russia, 1994.
11. H.Zimmermann, S.Vogel, D.Schierenbeck. Aeroelastic Investigations as Applied to Airbus Airplanes. ICAS-92-5.5.1.
12. T.Noll, E.Austin, S.Donley, G.Graham, T.Harris, I.Kaynes, B.Lee, J.Sparrow. Impact of Active Controls Technology on Structural Integrity. - Technical Papers of AIAA/ASME/ASCE/AHS/ASC 32nd Structures, Structural Dynamics, and Materials Conference. Part.3. Baltimore, USA, 1991.
13. K.Seyffarth, M.Lacabanne, H.K.Koenig, H.Cassan. Comform in Turbulence (CIT) for a Large Civil Transport Aircraft.- A Collection of Papers of "International Forum on Aeroelasticity and Structural Dynamics". - Strasbourg, France, 1993.
14. J.Abel, J.R.Newsom. Langley Research Center Contributions in Advancing Active Control Technology. - NASA CP 2172, 1981.
15. W.Grice. An Airline View of Experience With the L 1011 TRISTAR 500 System. - Convention Proceedings. The Royal Aeronautical Society, 1987.

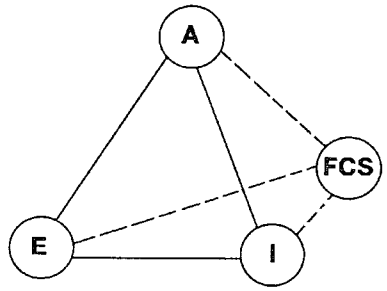

A aerodynamic
E elastic
I inertia
FCS forces from control

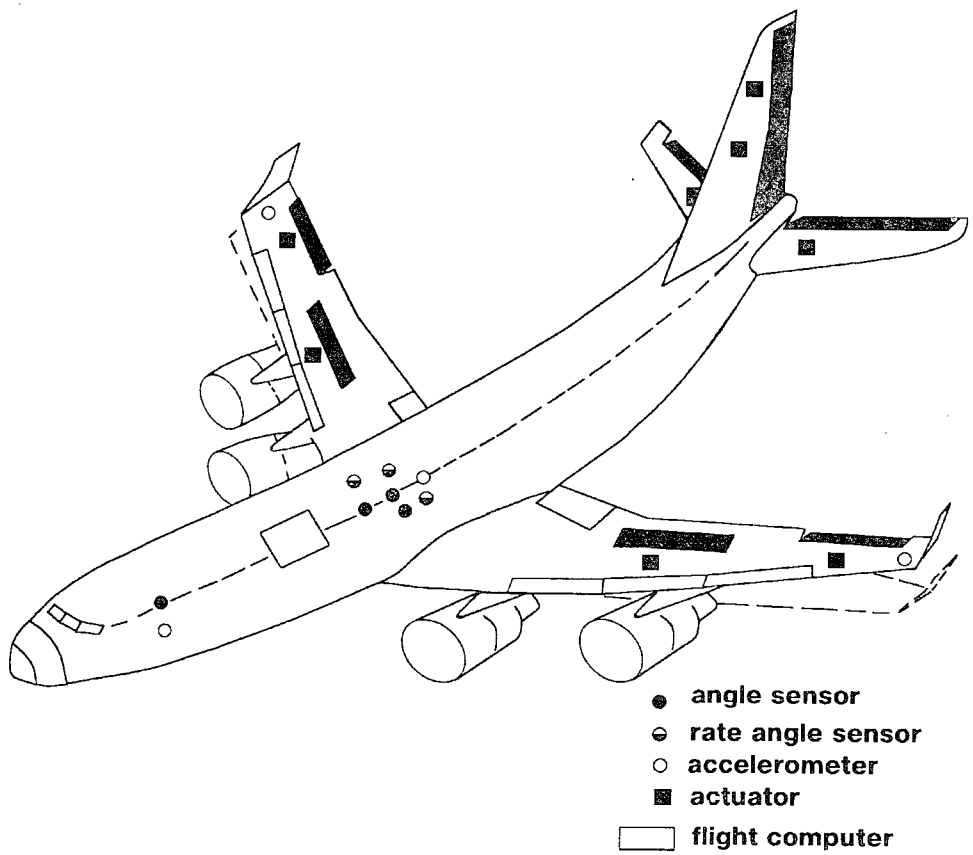

Fig. 1 ASE problem

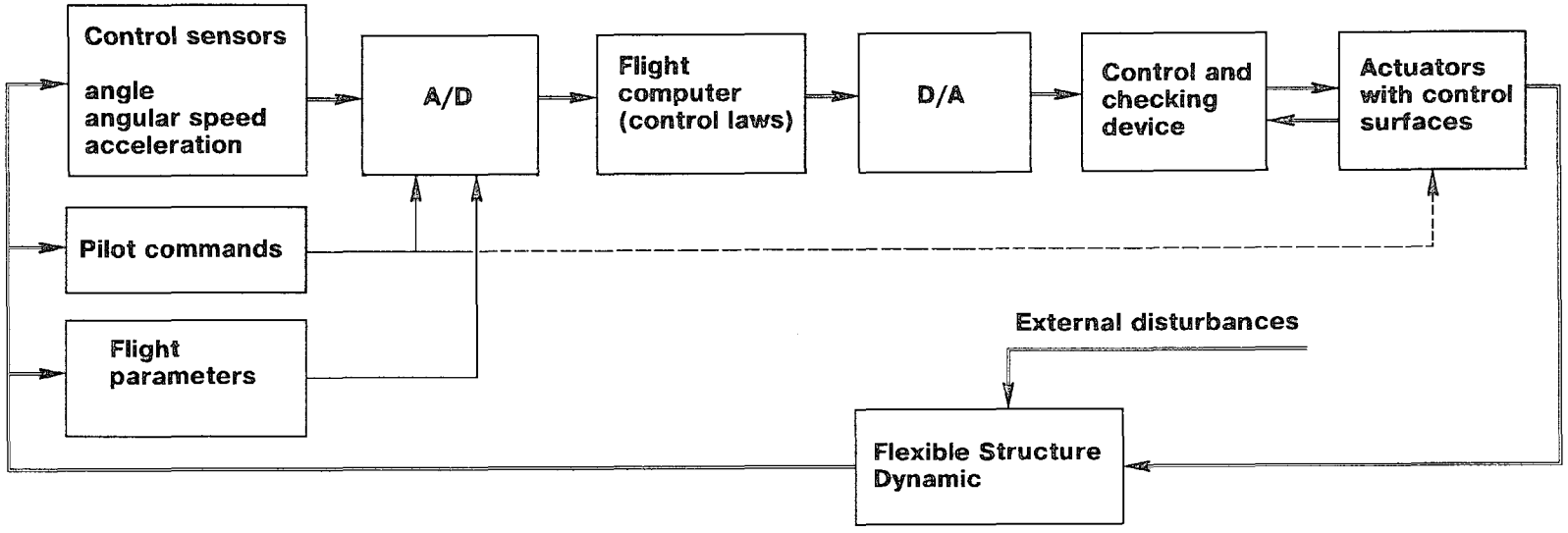

Fig. 2 Scheme of aeroelastic interaction

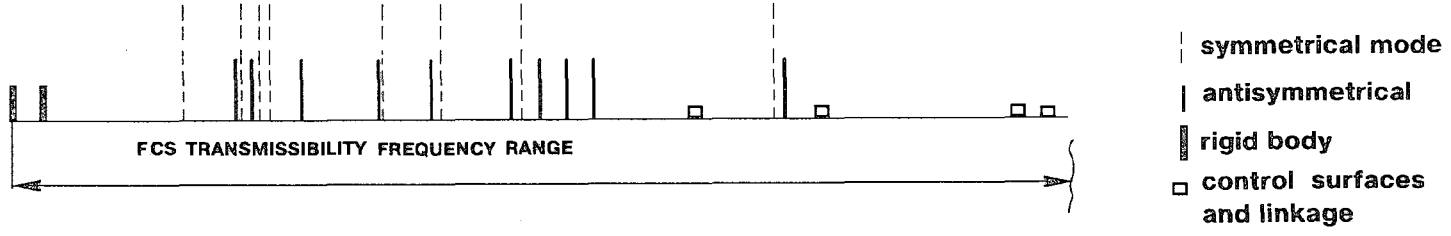

Fig. 3 Natural frequencies of wide body civil aircraft

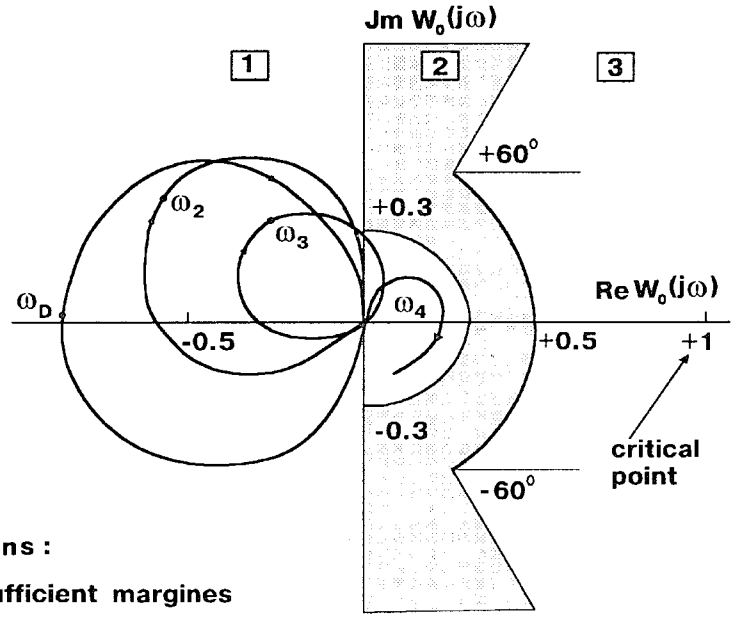

Domains :

1 sufficient margines

2 special flight test are required

3 margines are absent

Fig. 4 ASE stability requirements.

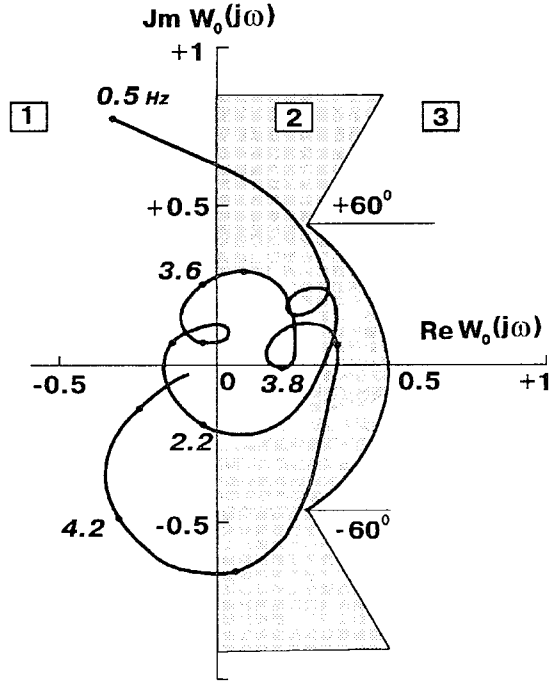

Fig. 6 Wide body civil aircraft, open-loop FRF.

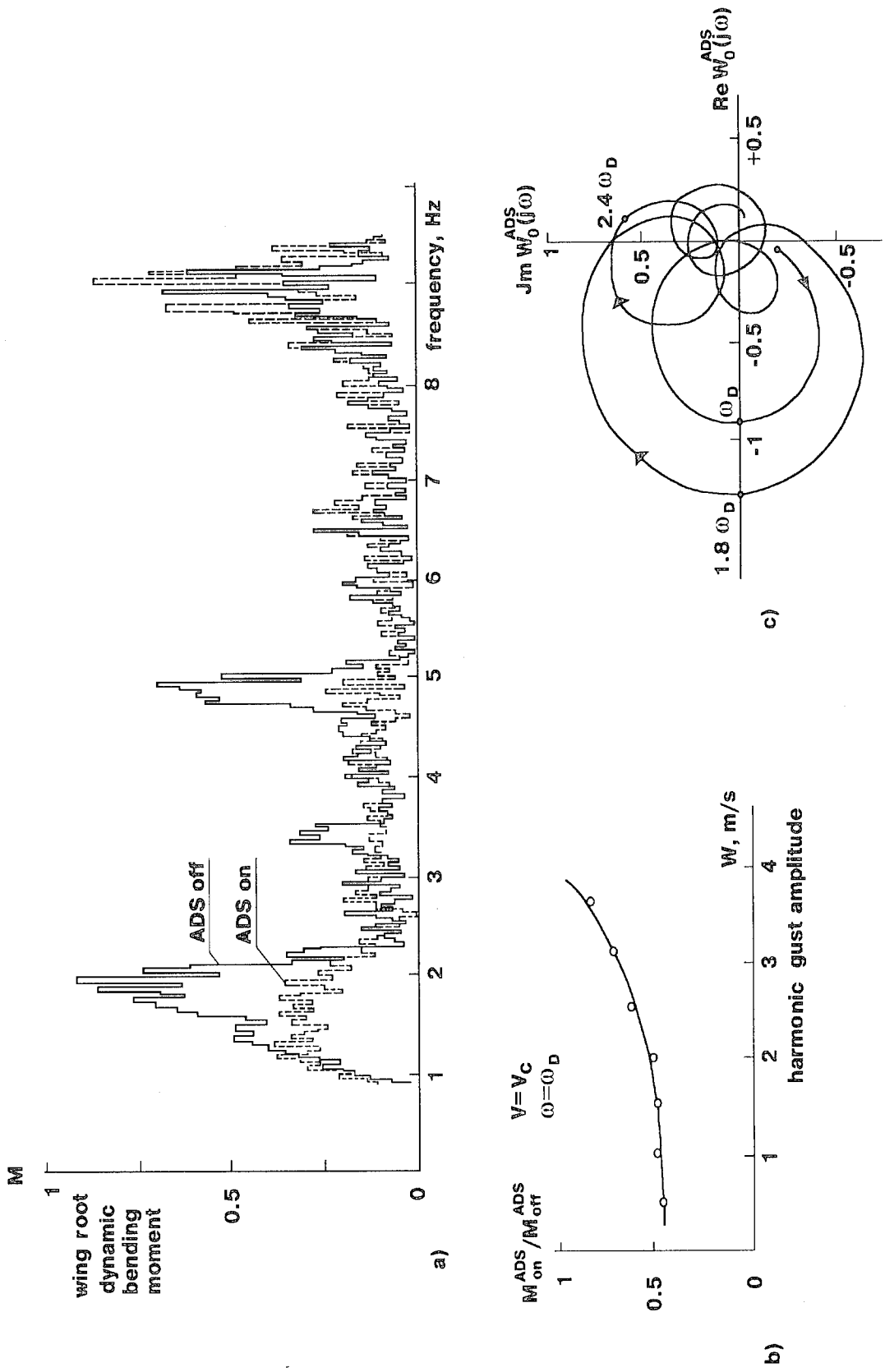

Fig. 5 ADS model efficiency (a), influence of ailerons rate limit (b), satisfaction of stability requirements (c).

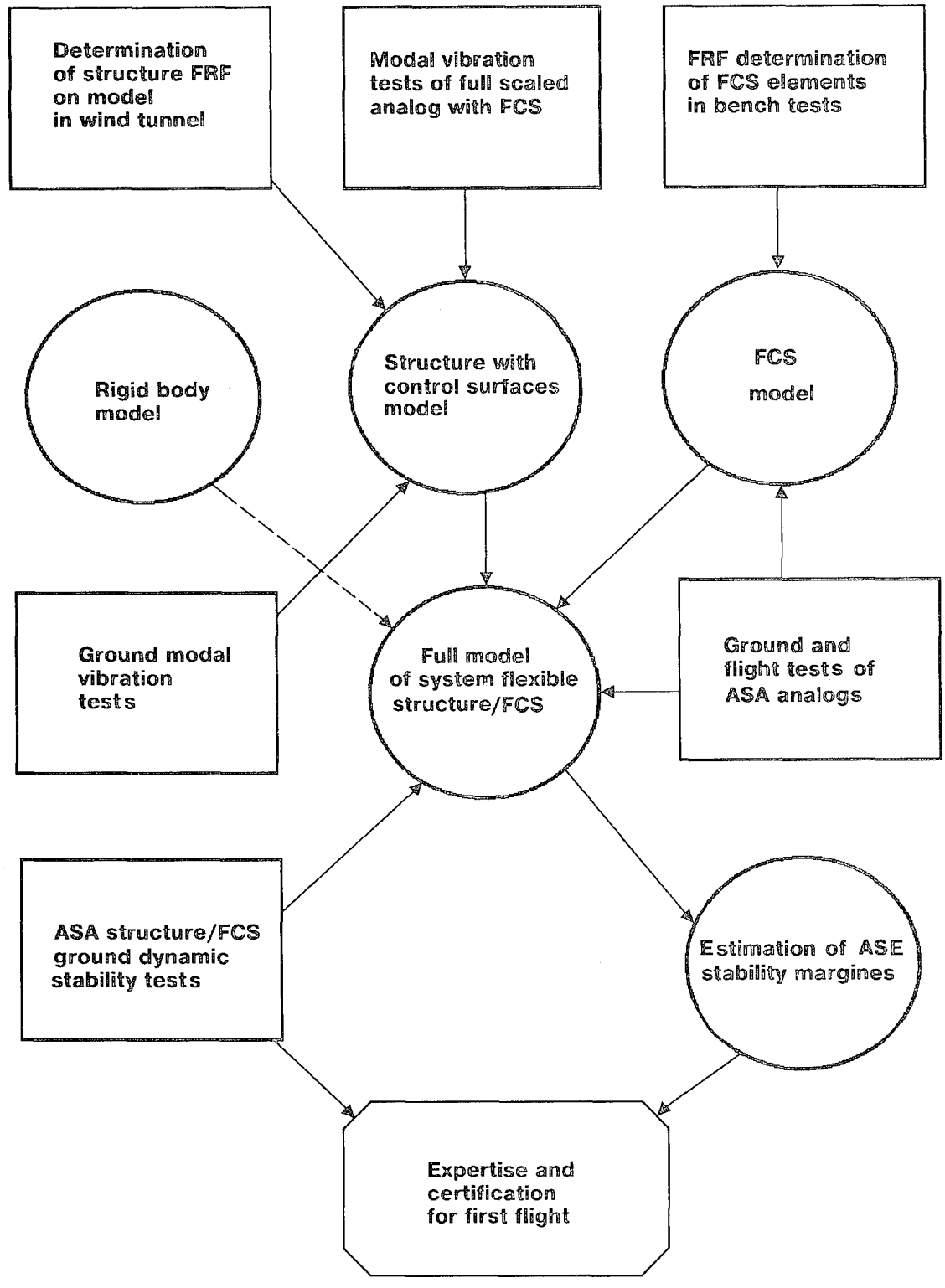

Fig. 7 Procedure of ASA preflight ASE investigations.

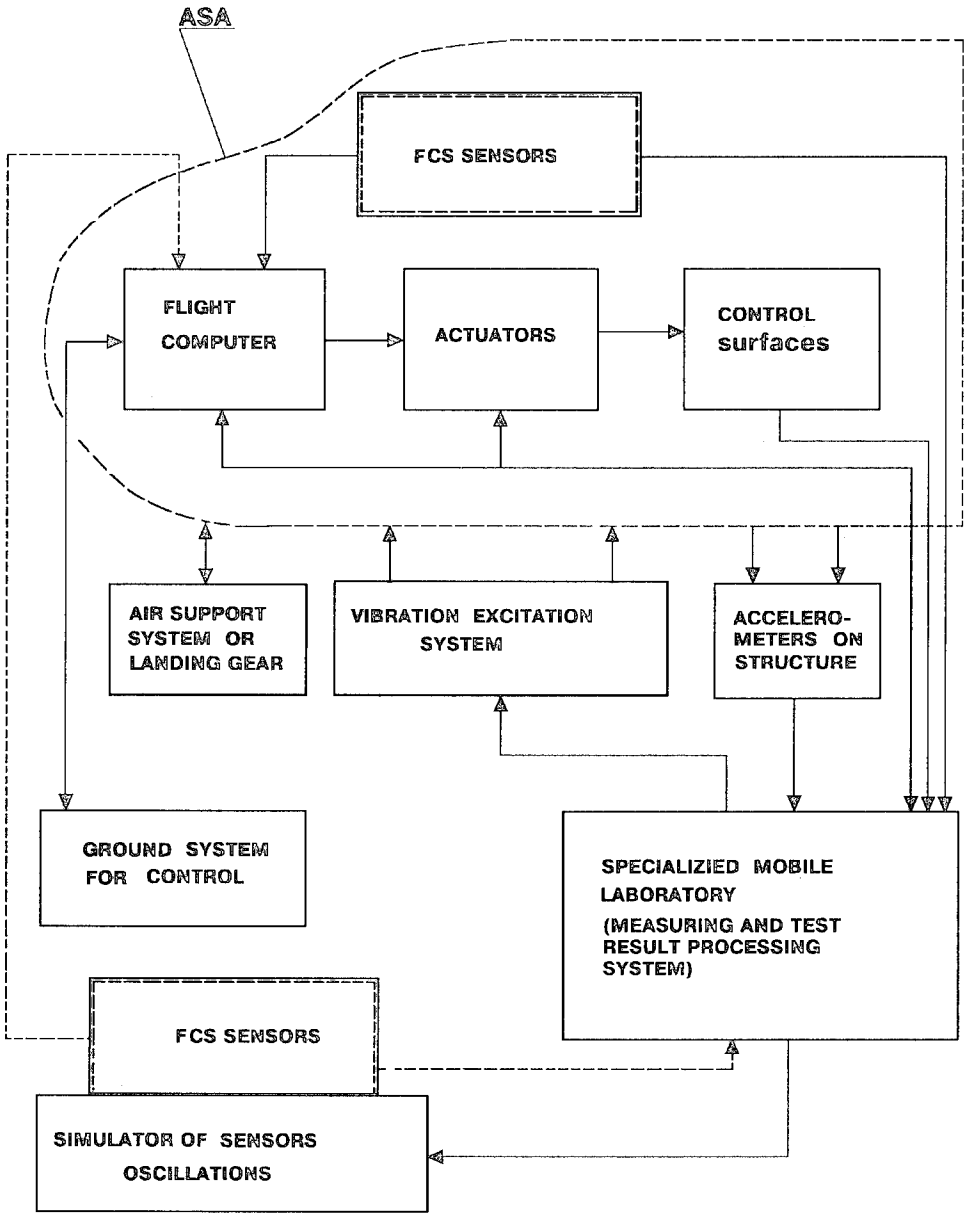

Fig. 8 Scheme of ASA structure/FCS ground vibration tests.

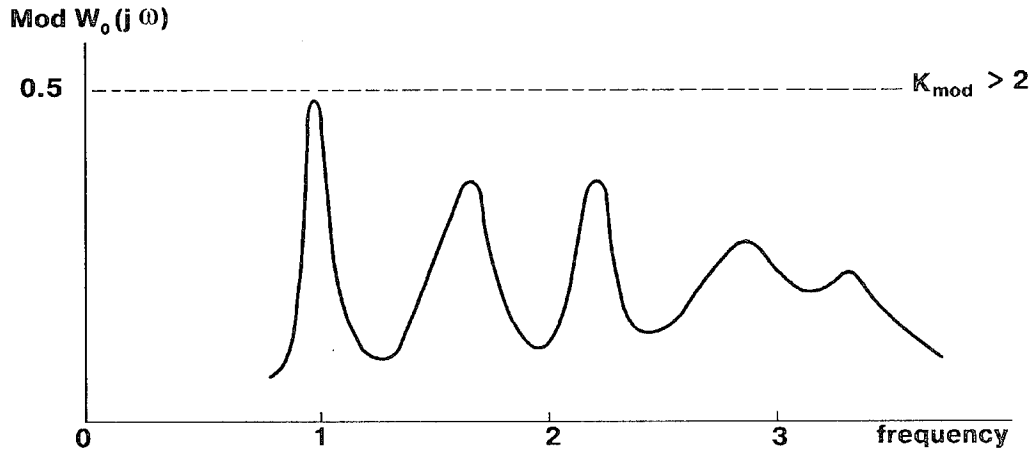

Fig. 9 ASA, roll channel, open-loop amplitude FRF.

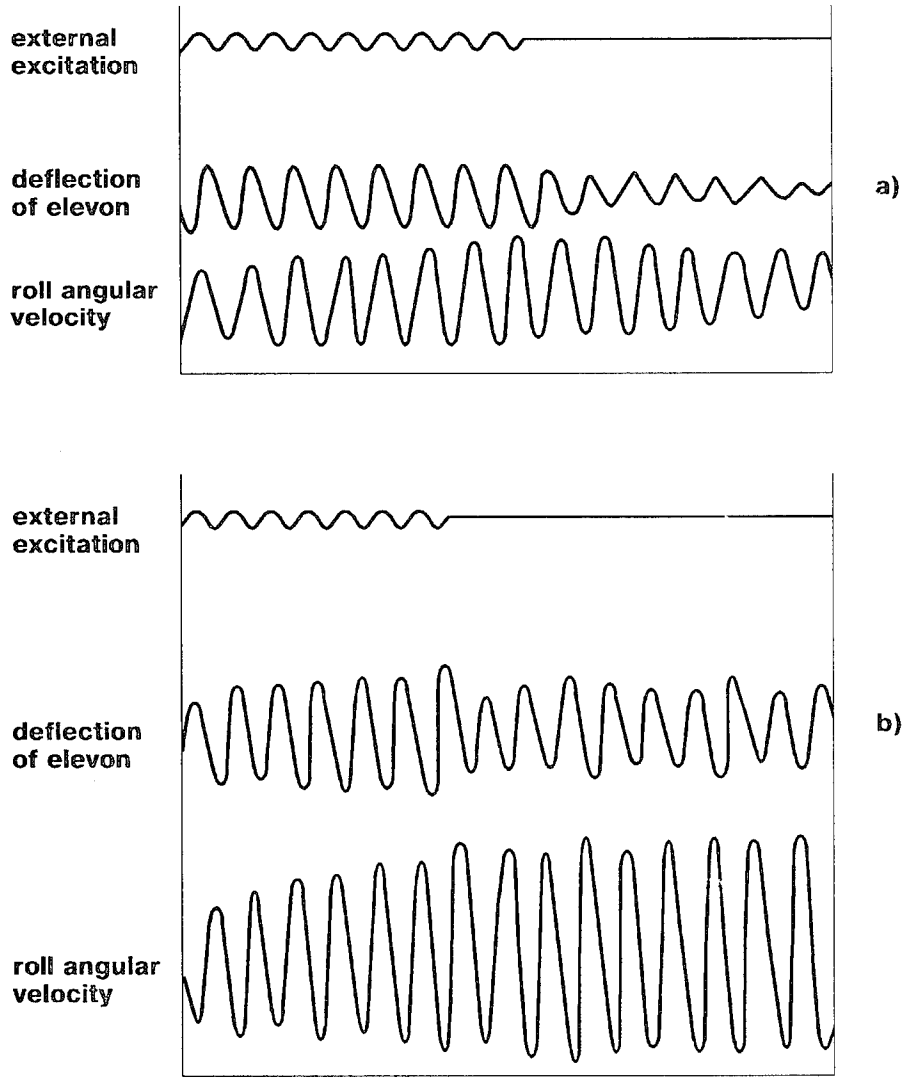

Fig. 10 ASA, closed system: a) nominal gains in FCS,
b) two-time increase of the gain in the roll angular velocity channel.

Essais en vol de flottement sur avions de transport civil munis de commandes de vol électriques

M. Lacabanne
AEROSPATIALE
A/BTE/EG/ST/D - M0132/2
316, route de Bayonne
31060 Toulouse Cedex 03
France

RÉSUMÉ

Le développement sur avions civils de commandes de vols électriques a eu pour conséquence de faire évoluer la stratégie d'ouverture du domaine de vol pendant les essais en vol de flottement, mais a également posé de nouveaux problèmes relatifs à la stabilité aéroélastique de l'avion asservi par les lois de pilotage ou par des lois agissant sur la dynamique de la structure.

Cette présentation a pour but de montrer l'intérêt de l'utilisation des commandes de vol électriques (CDVE) pendant les essais en vol de flottement et d'illustrer à partir d'exemples la stratégie d'essais de vibrations en vol sur avions à CDVE.

Quelques réflexions sur la stratégie d'ouverture du domaine de vol d'avions subsoniques futurs de très grande capacité sont faites.

1. INTRODUCTION

Les essais en vol de flottement sont une étape essentielle dans le processus de certification des avions civils. Les règlements JAR/FAR 25 qui s'appliquent aux avions de type Airbus précisent que ces essais doivent être conduits jusqu'à V_{DF}/M_{DF} lorsque M_D est supérieur ou égal à 0.8, ce qui est le cas pour tous les avions de transport civils actuels de capacité supérieure à 100 places.

Le constructeur doit donc définir une stratégie d'ouverture du domaine de vol garantissant la sécurité des équipages d'essais dans tout le domaine. Cette stratégie doit tenir compte des problèmes classiques de flottement mais aussi des problèmes de stabilité aéroservoélastique.

Pour les avions de type Airbus, cette stratégie a évolué en raison de l'introduction des CDVE. Les changements de stratégie sont apparus à partir de l'A320, se sont poursuivis sur les A340/A330 et A321 et ont essentiellement porté sur les points suivants :

- Il est devenu naturel de solliciter l'avion par les gouvernes en injectant des ordres calibrés sur les servocommandes dans la gamme des fréquences des modes structuraux à analyser. Cette possibilité d'excitation calibrée de la structure par les gouvernes est complémentaire des moyens d'excitation traditionnels et est facile à mettre en oeuvre.
- La vérification d'absence d'instabilité aéroservoélastique par couplage entre aérodynamique, structure et lois de commande de vol est devenue la règle. De nouveaux essais, complémentaires des essais classiques de flottement, ont donc été inclus dans les programmes d'essais en vol d'ouverture du domaine.
- Les lois de pilotage sont conçues de façon à minimiser l'interaction avec les modes de structure, donc à éviter les instabilités aéroservoélastiques.Mais, dans certains cas, les ordres élaborés par les lois de commande de vol modifient la dynamique des modes de structure pour assurer, par exemple, des fonctions telles que l'atténuation des charges de rafale ou l'amélioration du confort des passagers en turbulence.
  L'exemple du CIT (Comfort In Turbulence) sur A330 illustrera la stratégie d'essais dans le cas de lois agissant sur la dynamique de la structure.

Malgré toute l'expérience acquise dans la conduite des essais de flottement des avions Airbus et, depuis 1987, sur les avions à commandes de vol électriques, de nouvelles questions se poseront pour les avions subsoniques futurs de très grande capacité. A la fin de cette présentation, nous essaierons de mettre en évidence les difficultés propres à l'ouverture du domaine de vol de ces avions et nous nous interrogerons sur la stratégie à adopter pour les essais de flottement.

2. MOYENS D'EXCITATION EN VOL

Les vols de flottement ont pour objectif de déterminer les fréquences et amortissements des modes structuraux en différents points du domaine de vol. La progression dans le domaine de vol peut être conduite à Mach constant en augmentant pas à pas la vitesse.

La meilleure méthode pour obtenir les fréquences et amortissements consiste à exciter la structure, à calculer les fonctions de transfert entre les réponses et l'entrée excitatrice enfin, à faire une analyse modale des fonctions de transfert.

Dans ce processus, l'excitation de la structure est essentielle. La comparaison des différents moyens d'excitation en vol a fait l'objet de nombreux articles (1), (2) et je ne reviendrai pas dans cet exposé sur la revue comparée des méthodes d'excitation en vol. J'expliquerai, par contre, l'évolution dans le choix des moyens d'excitation en relation avec l'introduction des CDVE.

Paper presented at the Structures and Materials Panel Specialists' Meeting on "Advanced Aeroservoelastic Testing and Data Analysis", held in Rotterdam, The Netherlands, from 8-10 May 1995, and published in CP-566.

2.1 Excitation en vol sur avion "conventionnel"

Sur les avions dits "conventionnels", pour lesquels il y a transmission mécanique des ordres de pilotage vers les gouvernes, les aéroélasticiens ont essentiellement eu recours à des excitations appliquées par le pilote sur les organes de pilotage, à des excitations par impulseurs et à des excitations calibrées par des surfaces auxiliaires conçues spécialement pour les essais de flottement.

Parmi tous ces moyens, l'excitation par des surfaces auxiliaires telles que les palettes d'extrémité de surfaces portantes est, pour un avion nouveau, la plus satisfaisante. En effet, ce moyen d'essai utilisé pour l'excitation d'une voilure par exemple, modifie peu les caractéristiques dynamiques de la structure ; il permet une excitation calibrée dont le niveau de forces est réglable et mesurable ; il permet de développer une force d'excitation de niveau à peu près indépendant de la fréquence d'excitation sur une grande plage de fréquences.

2.2 Excitation en vol sur avion à CDVE

Sur ce type d'avion, les moyens d'excitation des avions "conventionnels" peuvent être utilisés, mais aussi, l'excitation par ordres calibrés sur les servocommandes. Cette évolution est liée à la définition des commandes de vol. En effet, bien que l'excitation calibrée de la structure soit possible sur avion conventionnel en injectant un ordre au travers du servomoteur, lui même actionnant la timonerie mécanique puis la servocommande, cette technique n'est généralement pas retenue par l'aéroélasticien à cause de la limitation en bande passante de l'ensemble servomoteur-timonerie mécanique-servocommande. La fonction de transfert entre la position de la gouverne de profondeur et l'ordre injecté sur le servomoteur (figure 1) illustre sur un Airbus A300 cette limitation.

Par contre, sur avion à CDVE pour lequel les ordres peuvent être transmis directement aux servocommandes, les bandes passantes sont plus élevées et permettent d'envisager l'excitation de la structure par ordres calibrés sur les servocommandes. La figure 2 montre les fonctions de transfert des servocommandes d'aileron et de profondeur sur A320 et met en évidence une bande passante suffisante pour l'excitation des modes structuraux jusqu'à environ 10 Hz. L'attaque directe de la servocommande a de plus l'avantage de réduire l'influence des non linéarités (jeux, hystérésis) apportées par la timonerie mécanique.

Les signaux d'excitation utilisés le plus souvent sont les balayages sinusoïdaux à fréquence variable et les impulsions. La figure 3 montre l'évolution en fonction de la vitesse des accélérations obtenues en extrémité d'empennage et de gouverne de profondeur pour une impulsion symétrique sur les gouvernes de profondeur de l'A320.

Les figures 4a et 4b montrent, sur l'Airbus A321, les réponses temporelles obtenues par balayage symétrique sur les ailerons, et sur la profondeur entre 2 et 8 Hz. Ces exemples montrent que l'excitation par les gouvernes sur avion à CDVE donne des niveaux de réponse très satisfaisants, tout à fait adaptés pour extraire les paramètres modaux par analyse modale.

3. ANALYSE MODALE

Les essais en vol de flottement des Airbus ont lieu sur le site d'essais en vol de Toulouse. Depuis l'A320, ces vols sont suivis et analysés en télémesure. La description des méthodes d'analyse des essais en vol de flottement par suivi télémesure sur Airbus a fait l'objet de présentations (3), (4). Nous rappelons que l'identification des fonctions de transfert et l'analyse modale sont effectuées en temps réel. La validation de l'analyse modale et la synthèse modale sont faites par les spécialistes en temps différé en attribuant un critère de qualité à l'analyse.

La figure 5a montre les résultats de l'identification des fonctions de transfert sur les capteurs de voilure, moteur et fuselage avant en vertical pour l'excitation par les ailerons en symétrique sur l'A321.

La figure 5b montre ces résultats pour l'excitation par la profondeur.

Le tableau 1 donne les résultats de l'analyse modale sur les capteurs ci-dessus pour les deux types d'excitation. Le critère de qualité de l'identification est donné avec la signification suivante :

- ** bon
- * acceptable
- \- moyen (amortissement non retenu)

Certains "modes" ne sont pas retenus à cause d'une mauvaise identification. Ils n'apparaissent pas dans le tableau.

Excitation	Mode	1	2	3	4	Capteur
Aileron	f (Hz) A (%) CQ		3.42 8.4 -	4.09 3.6 *		Voilure
Profondeur	f (Hz) A (%) CQ			4.15 4.3 *		Voilure
Aileron	f (Hz) A (%) CQ	3.13 4.3 **		4.11 3.8 **	4.89 4.4 -	Moteur en Z
Profondeur	f (Hz) A (%) CQ			4.12 4. **	4.93 4.1 **	Moteur en Z
Aileron	f (Hz) A (%) CQ	3.16 3.7 *		4.11 3.9 **	4.92 3.5 **	Fuselage avant
Profondeur	f (Hz) A (%) CQ			4.12 4.5 *	4.91 4.1 *	Fuselage avant

Synthèse modale sur 3 capteurs	f (Hz) A (%)	3.14 4.1	3.42	4.11 4.0	4.91 3.8

Tableau 1 : Analyse modale sur A321 avec excitation par les gouvernes.

Ces résultats montrent la complémentarité des excitations permettant d'identifier 4 modes entre 2 et 8 Hz avec seulement 3 capteurs pour 5 modes présents dans le modèle aéroélastique. La synthèse de l'analyse modale donne 4 modes :
f = 3.14 Hz amorti à 4.1 %, f = 3.42 Hz
f = 4.11 Hz amorti à 4 %, f = 4.91 Hz amorti à 3.8 %

La synthèse de l'analyse modale avec excitation aileron sur 22 capteurs donne 5 modes :

Synthèse modale sur 22 capteurs Excitation aileron	f (Hz) A (%)	3.14 4.4	3.43 8.6	4.10 3.7	4.91 3.7	7.44

On retrouve donc par analyse modale sur l'ensemble des capteurs, les 5 modes du modèle aéroélastique. Le mode à 7. 44 Hz est difficile à identifier car c'est le mode de coplanaire voilure.

L'intérêt de l'excitation en vol par les CDVE ayant été montré, nous allons traiter les problèmes spécifiques à l'ouverture du domaine de vol sur ce type d'avion.

4. STRATÉGIE D'OUVERTURE DU DOMAINE DE VOL SUR AVION À CDVE.

Les avions à CDVE sont asservis par des lois intégrées dans les calculateurs de vol et qui assurent un grand nombre de fonctions. Nous distinguerons, pour simplifier, les fonctions de pilotage et celles conçues pour agir sur la dynamique des modes de structure.

La stratégie d'essais en vol aéroservoélastiques est différente selon les fonctions intégrées dans les CDVE et les caractéristiques géométriques, inertielles et de rigidité de l'avion. Ces différences seront expliquées dans les exemples décrits ci-dessous.

4.1 Essais sur avions avec couplage CDVE - structure faible.

Dans le cas où les CDVE intègrent des fonctions de pilotage sur des avions pour lesquels les modes de la mécanique du vol et les modes de la structure détectés par les capteurs utilisés pour les retours des lois CDVE n'ont pas des fréquences très proches, le couplage entre lois CDVE et structure peut être minimisé par filtrage passe bande des modes structuraux sans dégradation des caractéristiques de pilotage. Un écart supérieur à 2 Hz permet de réduire simplement le couplage par filtrage.

Les solutions de filtrage sont étudiées et validées sur le modèle aéroservoélastique rebouclé par les lois CDVE.

Il faut ensuite vérifier par essais en vol que la stabilité aéroélastique n'est pas remise en cause par le bouclage des lois CDVE.

La procédure d'essais est la suivante :
- la première phase consiste à étudier le comportement aéroélastique en lois directes, c'est à dire le comportement en flottement de l'avion "conventionnel".

- la deuxième phase consiste à étudier l'influence des lois CDVE sur la stabilité aéroélastique. Dans la mesure où l'interaction CDVE-Structure est faible, une simple vérification en vol de la stabilité est faite pour l'avion rebouclé par les CDVE à plusieurs points du domaine de vol. Ces vérifications sont faites à grandes mais aussi à basses vitesses en raison de la variation des gains de retour en fonction de la vitesse.

La figure 6 compare sur l'A321 les fonctions de transfert obtenues par excitation de la gouverne de profondeur en lois directes et en lois normales rebouclées en croisière. Ces résultats confirment que les solutions de filtrage passe-bas des modes de structure sont satisfaisantes et garantissent la stabilité de l'avion rebouclé par les CDVE. On peut néanmoins noter une petite influence de la loi de pilotage longitudinal sur le mode de flexion du fuselage à 4.1 Hz.

4.2 Essais sur avions avec lois agissant sur la dynamique structurale.
Pour illustrer les essais en vol d'aéroservoélasticité dans le cas de lois conçues pour agir sur la dynamique des modes de structure, nous prenons l'exemple du C.I.T. (Comfort In Turbulence) sur A340.

Le C.I.T. a pour objectif de réduire les réponses le long du fuselage en turbulence (ref. 5). Dans le cas longitudinal, la loi C.I.T. élabore un ordre sur la profondeur à partir de l'accélération verticale mesurée au fuselage avant (figure 7). La conception de ce type de lois est faite à partir du modèle aéroservoélastique constitué du modèle aéroélastique de l'avion et du modèle de servocommandes.

Une première validation du modèle de servocommandes est faite à partir de mesures de réponses en fréquences au sol. Le comportement aéroélastique de l'avion est identifié en vol en mesurant, dans le cas de sollicitations sur les gouvernes utilisées pour la commande, les réponses dynamiques de l'avion sur les capteurs de retour des lois. On peut également vérifier que les ordres numériques élaborés par la loi et injectés sur les servocommandes sont conformes aux spécifications.

Dans le cas du C.I.T. longitudinal, qui est une commande mono-entrée mono-sortie, l'excitation sur la servocommande de profondeur entre 2 et 4 Hz donne en boucle ouverte les réponses de la figure 8 sur la position de la gouverne, l'ordre C.I.T. et l'accéléromètre de retour au fuselage avant. Au point de vol et pour le cas de chargement considérés, les fonctions de transfert en boucle ouverte essentielles pour la validation du modèle aéroservoélastique sont calculées en temps réel.

La figure 9 montre sous forme de Nyquist le transfert aéroélastique accélération fuselage/ordre générateur et le transfert ordre loi/ordre générateur. Pour une loi mono-entrée mono-sortie, on peut donc juger en temps réel des marges de stabilité de la loi. On peut donc, si le réglage de la loi paraît satisfaisant, effectuer, au cours du même vol, des essais en boucle fermée. Sur l'exemple ci-dessus, les essais en boucle fermée ont été faits dans le même vol et on a pu comparer, sur excitation de palette d'extrémité de voilure, les fonctions de transfert boucle ouverte et boucle fermée pour 2 valeurs de gain différentes (figure 10).

Il est important de noter que l'adéquation de la loi aux objectifs visés et la rapidité de sa mise au point dépend de la qualité du modèle aéroélastique utilisé pour la conception. Pour juger de la qualité de ce modèle, la figure 11 compare les Nyquist ordre loi/ordre générateur pour quatre cas de masse donnant des réponses dynamiques caractérisées par des glissements de fréquences et des amplitudes différentes. Cette comparaison prouve la qualité du modèle aéroservoélastique dans la gamme des fréquences utiles pour le contrôle.

Il est donc indispensable, pour valider des lois de commande actives sur la structure, de mesurer en vol, aussi bien à basses qu'à grandes vitesses, les réponses dynamiques des capteurs de retour sur des sollicitations par les gouvernes utilisées pour la commande. Il faut ensuite comparer les fonctions de transfert mesurées sur l'avion à celles données par le modèle aéroélastique pour plusieurs points de vol et plusieurs cas de masse. Le réglage final ne pourra être obtenu qu'après validation du modèle aéroélastique avion et des modèles servocommandes. Le réglage final de lois actives doit être effectué en temps différé, en particulier dans le cas multi-entrées multi-sorties.

Dans le cas du C.I.T., les ajustements de la loi ont été minimes après essais en vol. En effet, le C.I.T. étant mono-entrée mono-sortie, la définition et la validation des lois est plus simple que dans les cas multi-entrées multi-sorties ; de plus, la qualité du modèle aéroélastique n'a pas conduit à modifier significativement les lois définies avant vol.

Dans la procédure d'essais de lois actives, on peut également étudier le comportement de l'avion dans le cas de modifications programmées de gain et de phase créant une instabilité dynamique. Ce type d'essais a montré qu'une oscillation à cycle limite, dont l'amplitude correspond à la limitation de l'ordre C.I.T., apparait et ne met pas en cause la sécurité (figure 12).

En résumé, la validation et la mise au point de lois actives sur la structure nécessite d'exciter la structure par les gouvernes, de mesurer la réponse dynamique sur les capteurs de retour, de comparer les fonctions de transfert mesurées à celles du modèle aéroélastique, de modifier les lois si nécessaire pour atteindre les objectifs de stabilité et performances visés et de procéder à la validation finale par essais en vol et à l'aide du modèle aéroélastique.

5. Essais aéroservoélastiques sur avions subsoniques futurs de très grand capacité.

Ces avions auront des caractéristiques géométriques et inertielles telles que les fréquences des modes structuraux se rapprocheront des modes de la mécanique du vol. Les avions de très grande capacité (600 places et au delà) équipés de CDVE présenteront très certainement des couplages CDVE-structure forts. Les lois CDVE auront donc un effet sur les modes structuraux et il devra être étudié sur le plan théorique mais aussi pendant les essais en vol. Il devrait être plus difficile que sur les avions actuels de réduire ces couplages.

Afin de distinguer les problèmes de flottement classiques des problèmes d'aéroservoélasticité, les essais en vol seraient menés en deux phases :

- la première phase permettra d'analyser les phénomènes aéroélastiques à grandes vitesses et, en particulier le flottement de l'avion dit "conventionnel" en lois directes, dans l'hypothèse où la stabilité de l'avion serait satisfaisante pour voler dans cette configuration. Cette phase est identique à celle du § 4.1. Les fonctions de transfert seront mesurées à l'aide d'excitations par les gouvernes à grandes, mais aussi à basses vitesses afin de préparer la phase d'essais aéroservoélastiques ;
- la deuxième phase sera celle des essais d'aéroservoélasticité avec engagement des lois CDVE. Elle aura lieu après analyse, à l'aide des modèles aéroservoélastiques et de mécanique du vol du comportement de l'avion avec CDVE vis à vis des objectifs de stabilité, performances et robustesse fixés.

Contrairement au cas d'avions à couplage CDVE-structure faible, une simple vérification de la stabilité aéroélastique de l'avion couplé par les CDVE ne sera pas suffisante. Les critères de performances et de robustesse des lois CDVE devront être analysés vis à vis du pilotage et du comportement de la structure. Cette phase sera similaire à celle décrite au § 4.2, mais les difficultés de validation des lois seront augmentées à cause de la proximité des modes structuraux et des modes de la mécanique du vol et, à cause d'une architecture de lois multi-entrées multi-sorties.

6. CONCLUSION

Le concept de commandes de vol électriques a fait évoluer, sur avions civils, les essais d'ouverture du domaine de vol, dits de flottement, en rajoutant des essais dits d'aéroservoélasticité.

L'expérience acquise sur les avions à CDVE depuis l'A320 doit permettre de définir une stratégie d'essais aéroélastiques adaptée aux avions de transport subsoniques de très grande capacité.

Une grande part de ces essais sera bien sûr consacrée aux essais de flottement pour étudier la stabilité aéroélastique de l'avion en lois directes. Les excitations calibrées par les gouvernes devront être utilisées en complément des moyens d'excitation traditionnels.

Il faudra aussi, à cause d'un risque de couplage CDVE-structure vraisemblablement plus difficile à résoudre que sur avions actuels, spécifier des essais d'aéroservoélasticité dans le but d'analyser le comportement de l'avion avec CDVE vis à vis des objectifs de stabilité, performances et robustesse.

Il faudra donc faire preuve d'imagination afin d'aboutir à la définition optimale de lois CDVE sans trop augmenter le nombre d'essais, tout en garantissant la sécurité.

7. RÉFÉRENCES

1. H. Zimmermann, R. Destuynder
   "Flight flutter testing with emphasis on the tip vane method".
   AGARD-CP339, October 1982.

2. R. B. Ramsay
   "In flight structural mode excitation system for flutter testing".
   AGARD-CP-519, May 1992.

3. A. Bucharles, G. Lignon, H. Cassan
   "Flutter test analysis by telemetry system".
   AGARD, 73rd Symposium FMP, October 1988.

4. A. Bucharles, H. Cassan, J. Roubertier
   "Advanced parameter identification techniques for near real time flight flutter test analysis".
   AIAA/SFTE/DGLR/SETP, Fifth biannual flight test conference, Ontario May 1990.

5. K. Seyffarth, M. Lacabanne, K. König, H. Cassan
   "Comfort in Turbulence for a large civil transport aircraft".
   International forum on aeroelasticity and structural dynamics, May 1993.

6. B. D. Caldwell
   "The FCS structural coupling problem and its solution".
   AGARD-CP-560, May 1994.

7. H. Hönlinger, H. Zimmermann, O. Sensburg, J. Becker
   "Structural aspects of active control technology".
   AGARD-CP-560, May 1994.

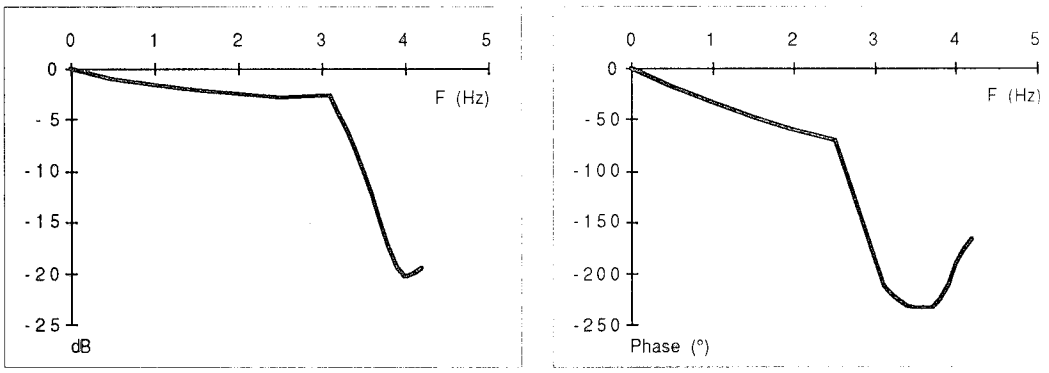

Figure 1: Réponse en fréquences position profondeur/ordre servomoteur PA sur A300-600

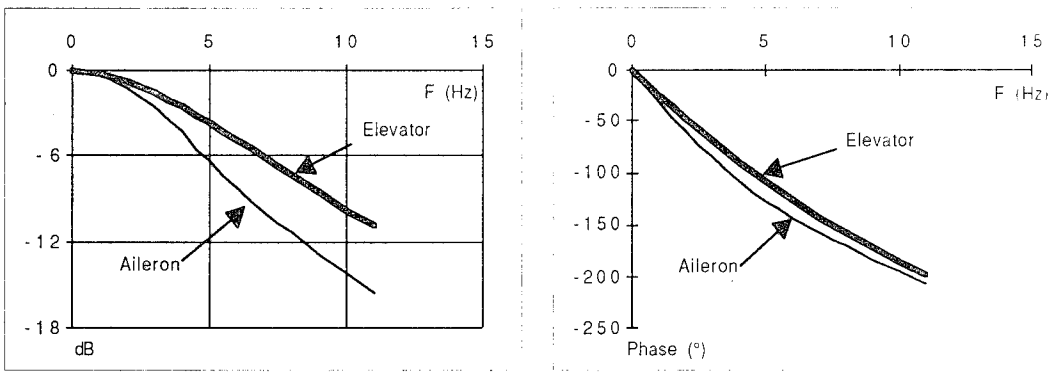

Figure 2: Réponses en fréquences des servocommandes de profondeur et d'aileron A321

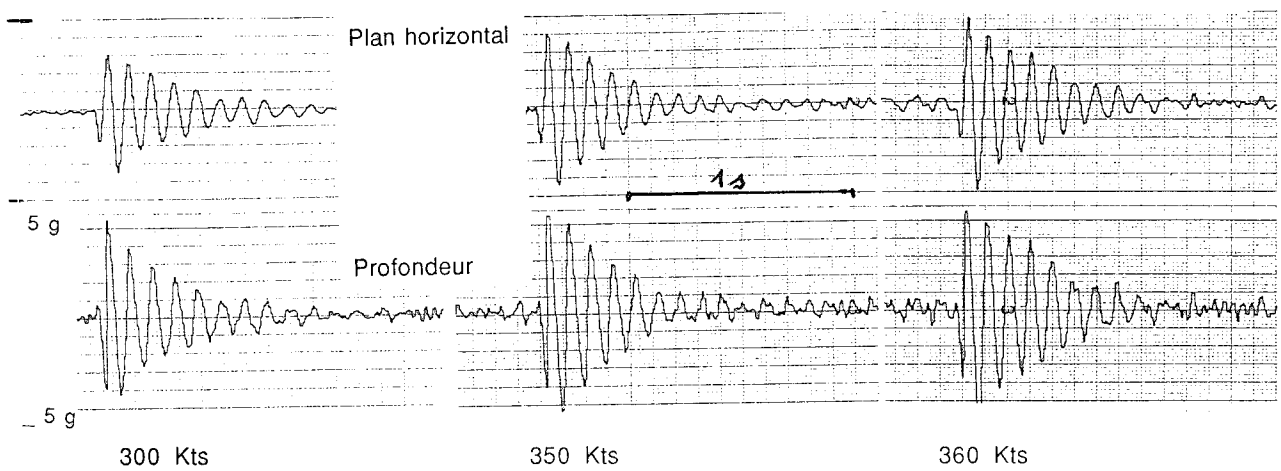

Figure 3: Réponses du plan horizontal A321 sur une impulsion profondeur

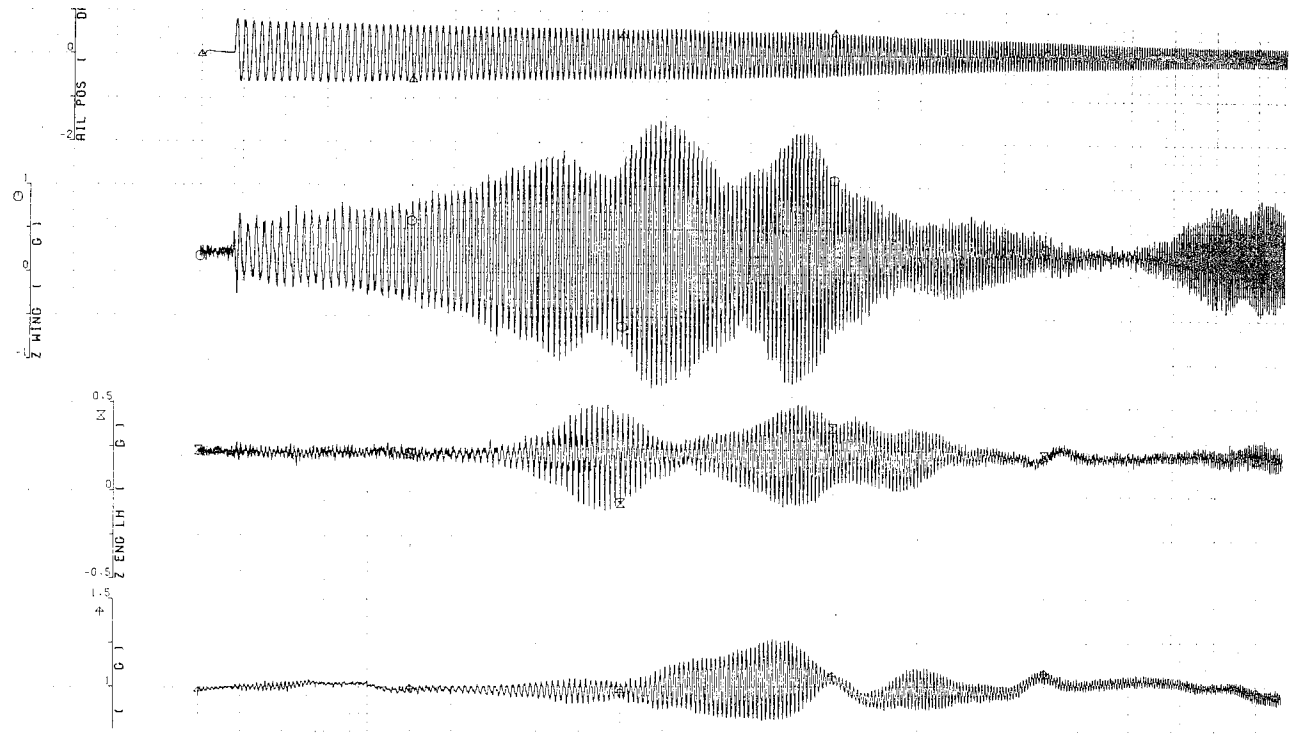

Figure 4a: A321-Accélérations voilure,moteur,fuselage sur excitation ailerons en symétrique

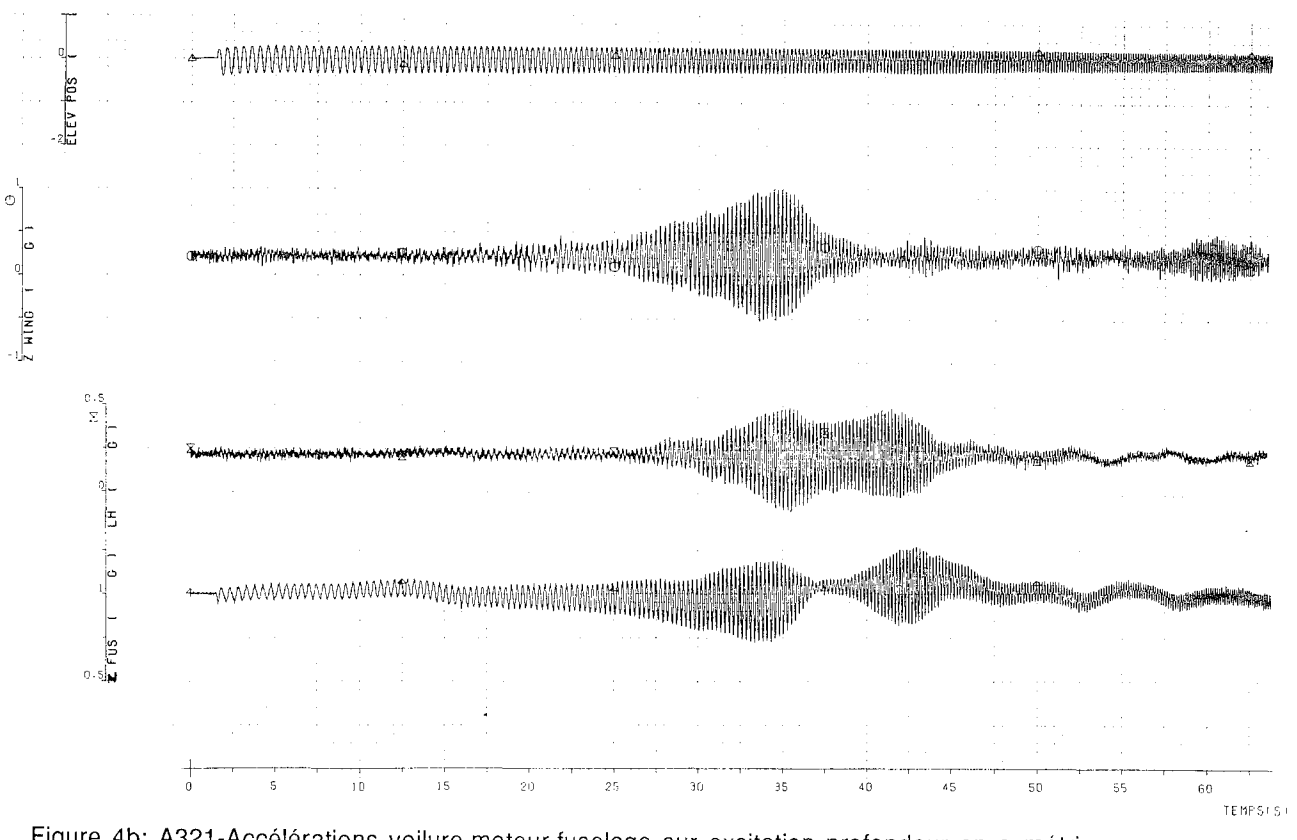

Figure 4b: A321-Accélérations voilure,moteur,fuselage sur excitation profondeur en symétrique

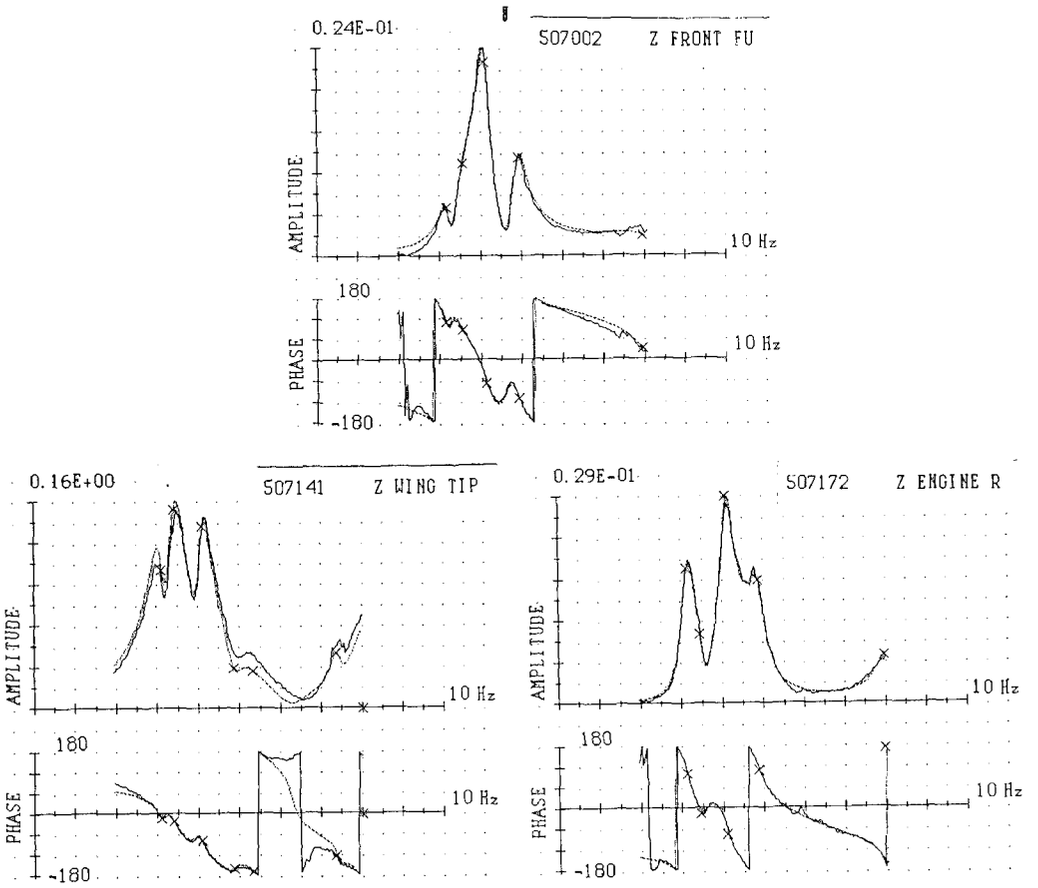

Figure 5a: A321-Identification des fonctions de transfert sur excitation ailerons en symétrique

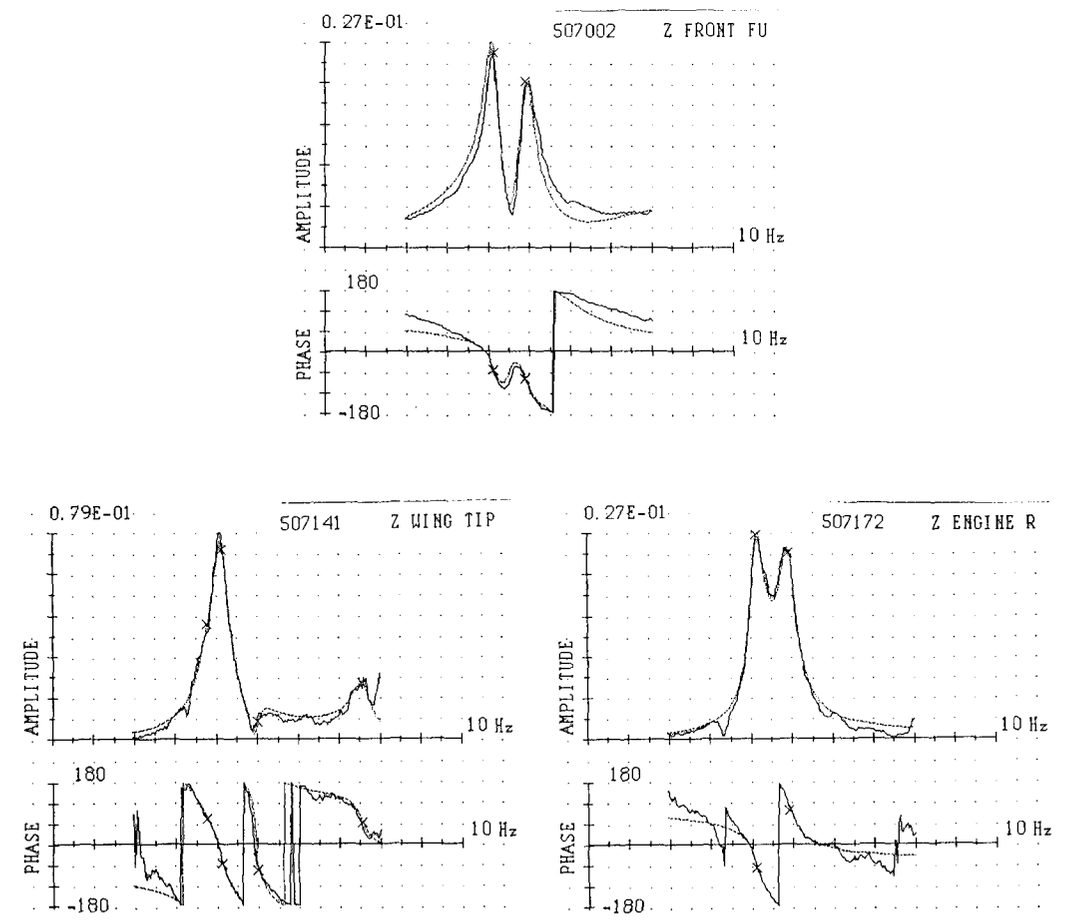

Figure 5b: A321-Identification des fonctions de transfert sur excitation profondeur en symétrique

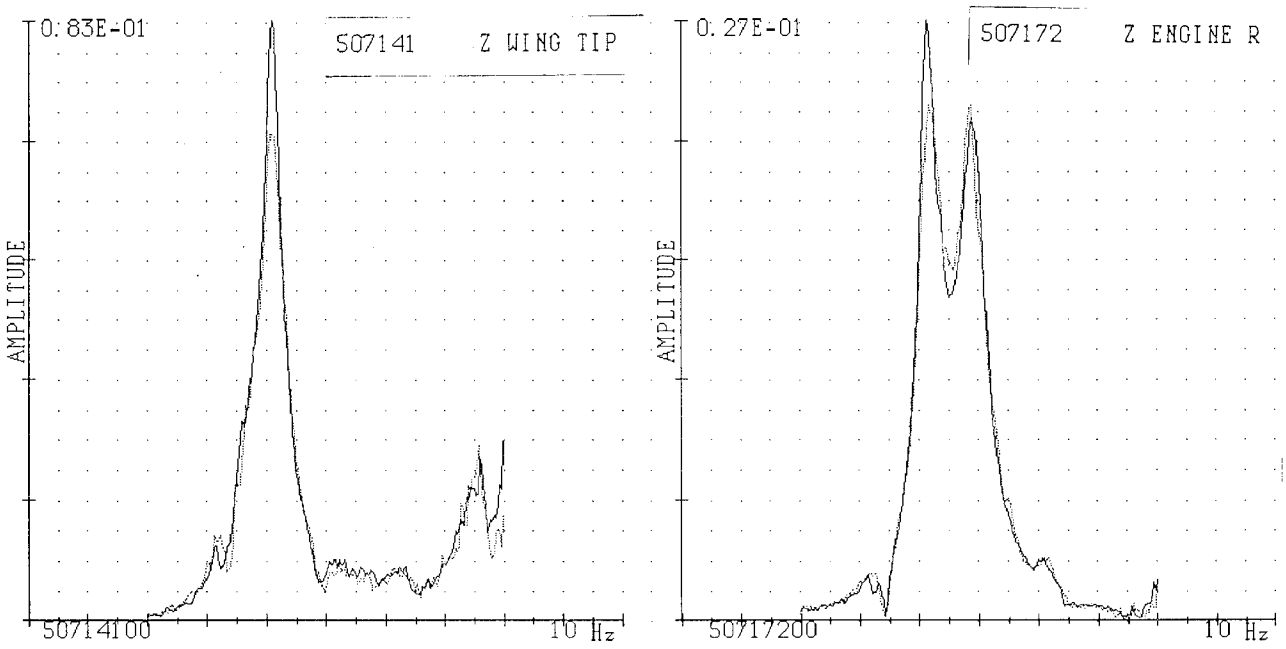

Figure 6: A321-Fonctions de transfert en lois directes et lois normales en symétrique

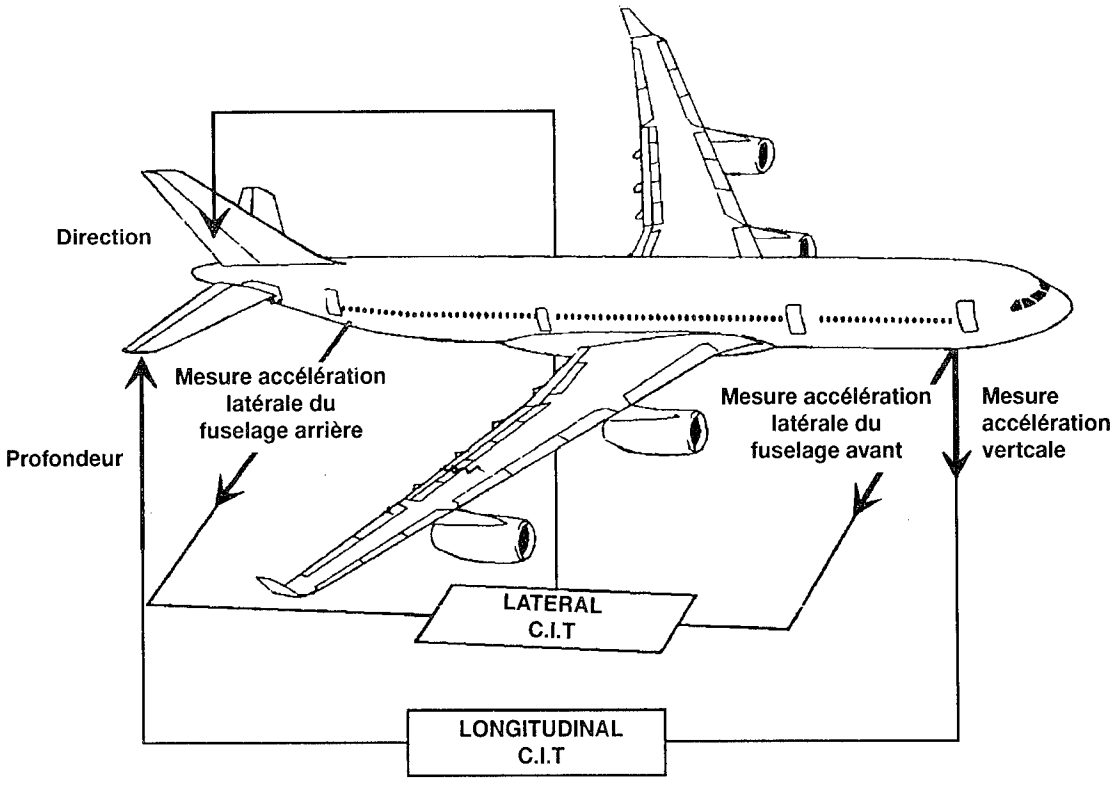

Figure 7: Principe du CIT (COMFORT IN TURBULENCE) sur A340

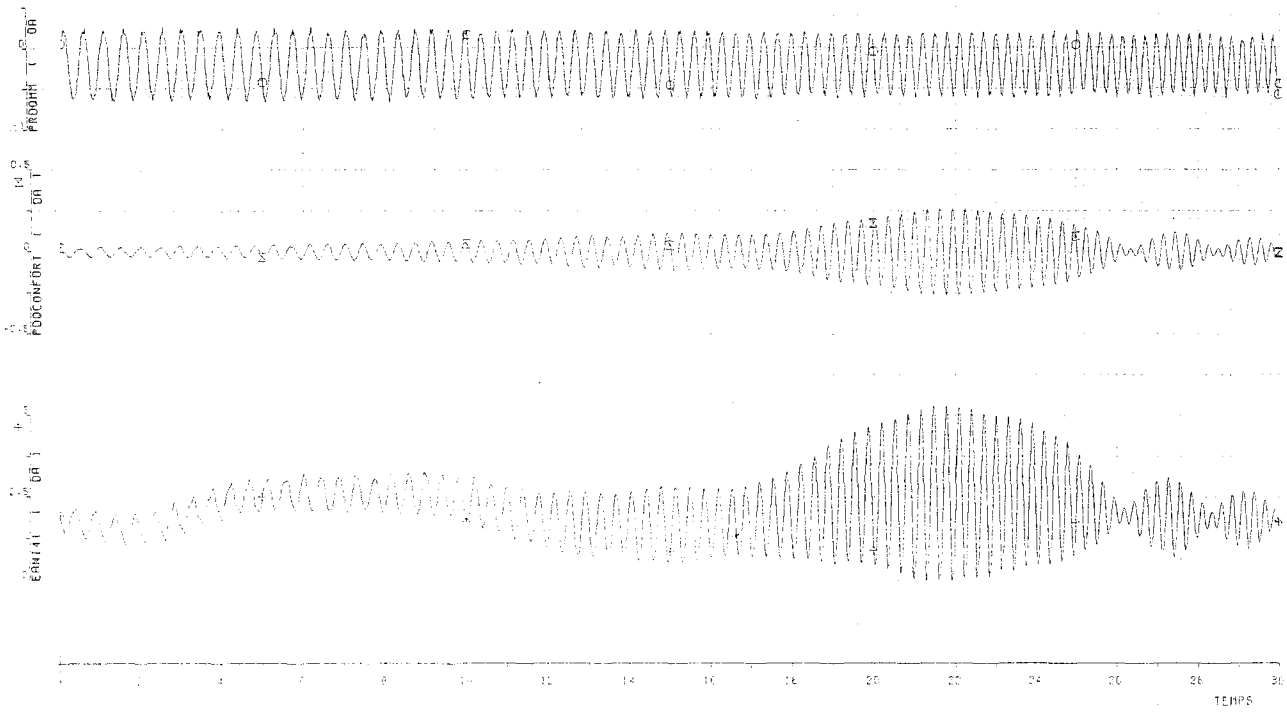

Figure 8: Réponse temporelle du CIT en boucle ouverte entre 2 et 4 Hz

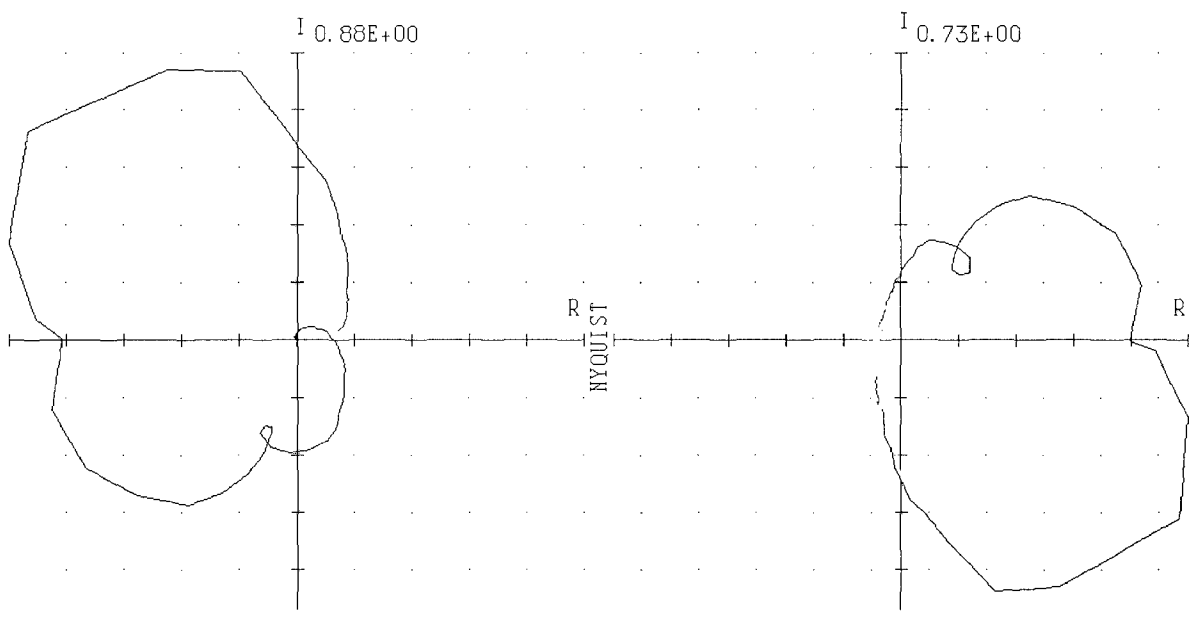

Ordre loi / Ordre générateur

Accélération fuselage / Ordre générateur

Figure 9: Nyquist du CIT longitudinal en boucle ouverte entre 1 et 4 Hz

Transfert fuselage avant

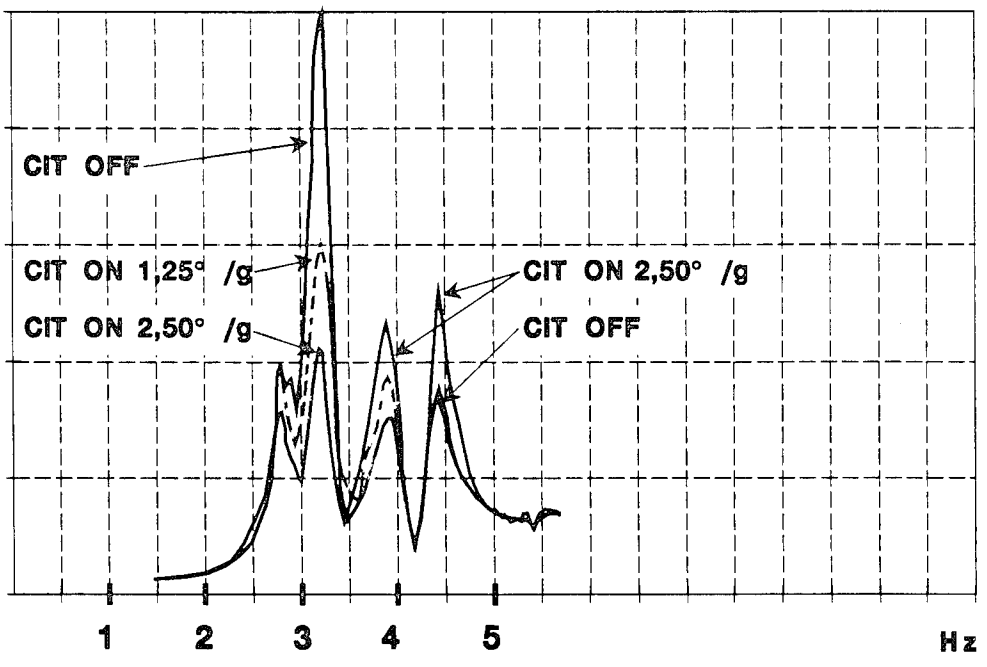

Transfert fuselage arrière

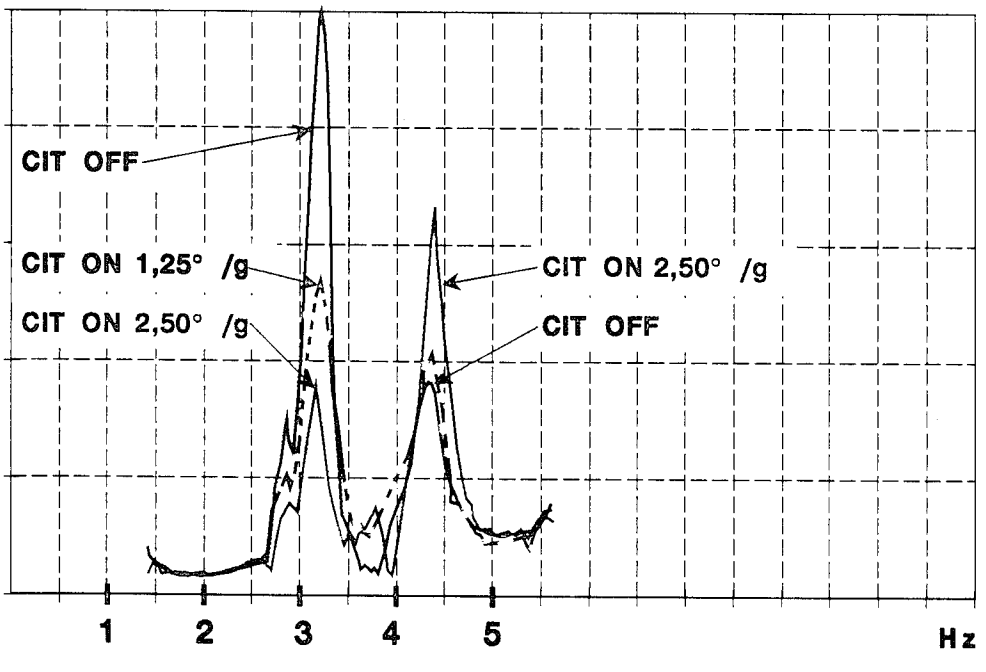

Figure 10: Comparaison des transferts CIT,fuselage/effort palette,en boucle ouverte et fermee

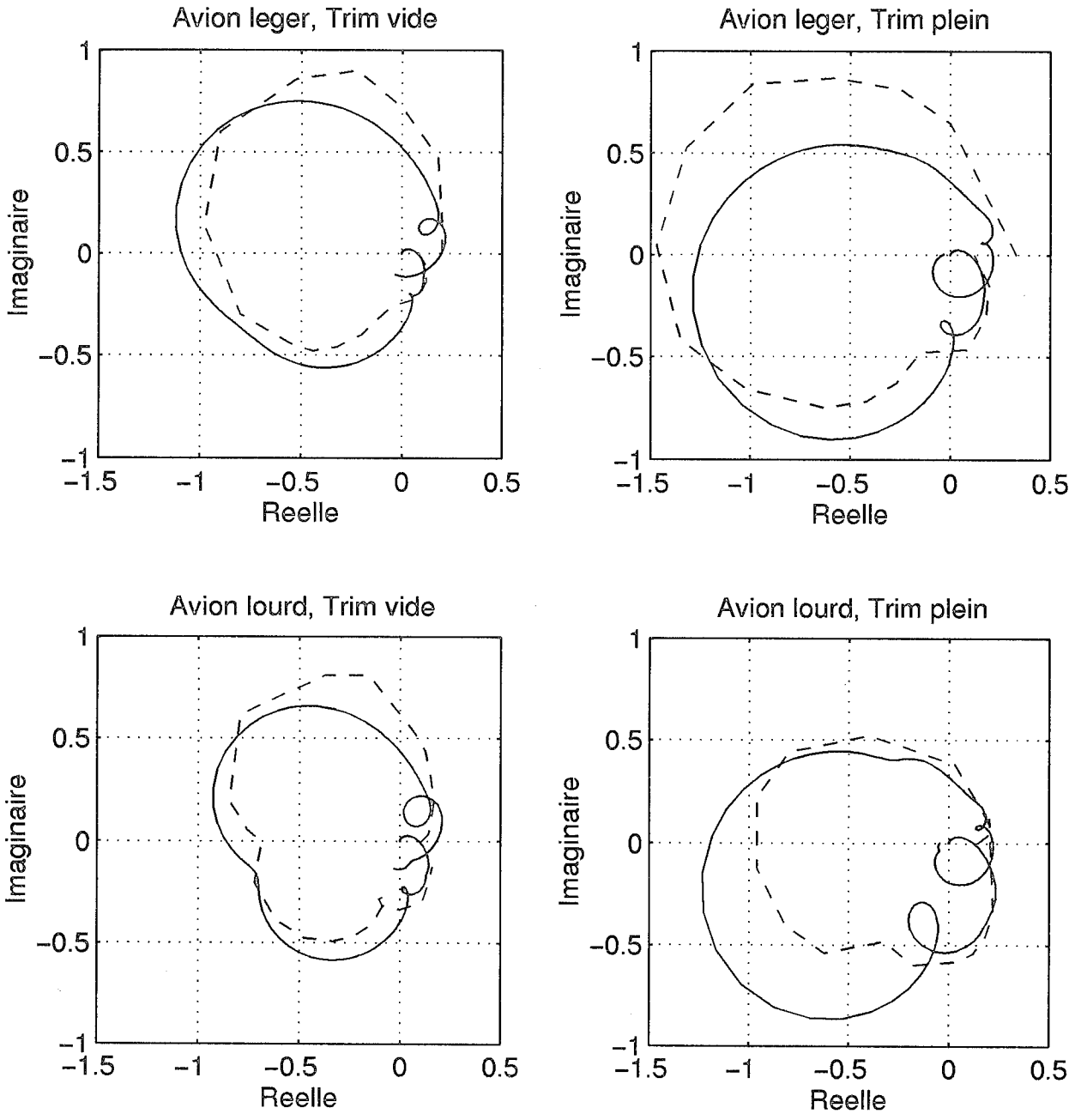

Figure 11: Comparaison essai vol/modèle aéroélastique sur 4 cas de chargement

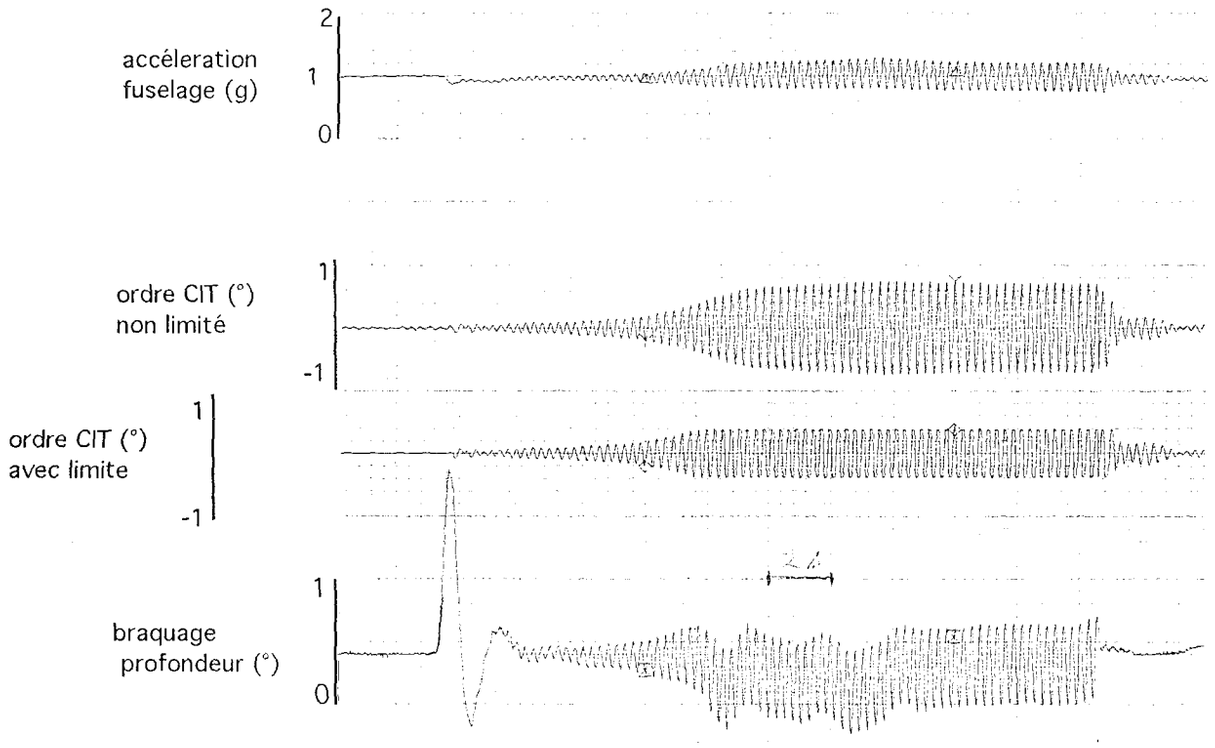

Figure 12:Cycle limite avec modifications du CIT

Pretension and Reality of Flutter-Relevant Tests

Klaus Koenig
Deutsche Aerospace Airbus GmbH
Hünefeldstraße 1-5
28183 Bremen
GERMANY

SUMMARY

The paper gives a short review of all flutter–relevant tests of an a/c and discusses differences between the wanted and the reached reliability of the measured data.
This includes weight measurements, stiffness tests, actuator impedance tests, tests of the electronic flight control systems (EFCS), ground vibration tests (GVT), flight vibration tests (FVT), in–flight measurements of unsteady airloads and safety tests for active control systems.
The conclusions are that most of the tests need some improvements, some tests should be better exploited and at least one test – the in–flight measurement of unsteady airloads – should become standard practice to close a gap in the logic of flutter certification.

1. INTRODUCTION

The proof of the freedom from flutter for an aircraft (a/c) type is eventually based on computations. This is possible due to the "assumed" reliability of the computation and caused by the huge number of cases to be demonstrated.

Of course the reliability of the computation must be substantiated by hardware checks allowing to confirm or to correct the mathematical model used for the computations.
Due to the contribution of different elements to the physics of flutter, logic requires to check the individual elements and their interaction for a complete and reliable substantiation. If only component tests were performed, one could not conclude that the coupling is correctly modeled and if only coupling tests were performed, one could not conclude that different failures of the elements don't compensate each other in just the tested configuration but become critical in another one.
Fig. 1–1 shows the different elements of the computation and all the relevant tests. This is a large number of tests but with one or two exceptions they are usually executed. The classical flight vibration test is only the final and crucial test. So, if one wants to discuss advanced aeroelastic testing, if seems reasonable to have a look at all the tests mentioned. They all are flutter–relevant and contribute to the reliability of aeroelastic demonstrations.

2. REVIEW OF FLUTTER–RELEVANT TESTS

In the following, a short review of the different tests is given to reveal differences between pretension and reality of aeroelastic testing.
For each test the following questions are of interest and will be discussed in more or less detail.

- ❑ Are all the necessary data measured?
- ❑ Is the accuracy of the measurement sufficient?
- ❑ What is the difference between measured and predicted data?

2.1 Measurement of Masses

These are the first tests. Each individual part, instrument, assembly and the finished a/c are weighed.
The accuracy of the measured data is out of question. But weighing confirms just the masses. The moments of inertia are only measured for some individual units such as the control surfaces but not for the complete a/c.
That is the first deficit to be mentioned.
Compared with the predictions, an accuracy of about the following is reached:

- *less than 1% (down to 0.2%) for the total a/c weight*
- *less than 1% of the mean aerodynamic chord for the centre of gravity position of the complete a/c*
- *about 5% for the moments of inertia of control surfaces*

That should be a rather reliable basis for flutter computations if the available mass distribution were consequently used.
About 100000 local masses and also about 100000 individual grid points in the finite element (FE) model of a larger a/c are available. But a reasonable allocation of all the masses to all the grid points and a subsequent reduction of the degrees of freedom is often substituted by a separated mass condensation and a separated stiffness condensation down to about 1000 points where masses and stiffnesses are brought together. This may be a waste of available information and may reduce the accuracy of the computation. So it may be another difference between pretension and reality.

2.2 Stiffness of the Structure

Contrary to the masses, often no separately measured stiffnesses are used for the substantiation of the final flutter calculations.
There may be several reasons for this but in the opinion of the author it is an unacceptable deficit since :

- The logic of flutter–relevant tests requires also the measurement of the stiffness.
- Static strength tests are done anyway so that the hardware costs for the test specimens, the instrumentation and the test execution are already paid.
- The local stiffness is as important as the mass distribution.
- Stiffness tests can be performed at separated parts (such as pylons, horizontal tails etc.) so that the corrections of the theoretical data most often necessary can be much more precisely localized than with test results from the GVT.
- Local stiffnesses of special importance e.g. attachment points of actuators may be better taken from measurements than from crude FE models.
- If intelligently arranged, stiffness test results should be available earlier than GVT test results.

Paper presented at the Structures and Materials Panel Specialists' Meeting on "Advanced Aeroservoelastic Testing and Data Analysis", held in Rotterdam, The Netherlands, from 8-10 May 1995, and published in CP-566.

- Non–linear stiffnesses, frictions or other non–linear behaviour may be recognized much more simply and precisely.

So it may be worth considering some improvements especially if one realizes that corrections of the FE model stiffness by up to

40% for engine pylon sideward
20% for wing fore & aft
10% for wing vertical and fuselage sideward

are not unrealistic.

2.3 Actuators of Control Surfaces

The mathematical description of actuators deals primarily with three variables: the (nowadays often electrical) command signal u, the actuator deflection z_A and the actuator load p_A.

A simple equation could read

$$z_A = H_{zA,u} \cdot u + H_{zA,pA} \cdot p_A$$

were H.. are transfer (frequency response) functions. This equation already implies that signal and load influences are separable which is, of course, already a linear approximation.

But actuators are highly non–linear mainly (due to the throttle equation $p \sim \dot{x}^2$) and show a large scatter range.

The influencing parameters are:

- temperature
- supply and return pressure
- servo control law (gain)
- activated mode
- amount of mass to be moved
- constant load in working point
- static position in working point
- amplitude and frequency of command signal
- amplitude and frequency of externally exciting loads
- backlash, wear and/or ageing
- failure conditions as
  - *supply pressure decrease*
  - *leakage*
  - *wrong activation status*
  - *desynchronisation of multiple actuators*
  - *mechanical blocking or fractures*

Fig. 2.3–1 gives an example of the influence of some of these parameters. The envelope of all these curves and more must be covered in the demonstration of freedom from flutter. This means that not only one but several tests are necessary to measure the actuator characteristics.

In addition, it must be mentioned that the importance of reliable actuator data has increased in the last years with the introduction of the "fly by wire" and active control technology as can be imagined.

2.4 Transfer Functions of EFCS

The electronic flight control system (EFCS) comprises a larger number of control laws.

Accelerations, velocities and deflections together with other signals are measured, combined in the EFCS computer and finally given to the actuators of the control surfaces. The control laws define the modifications of the measured signals between the connection points "pickup" and "actuator". The total number of flutter–relevant connections may be in the order of 15 connecting pick–ups of n_z, n_y, ϕ, Θ, α, p, q, r with aileron, elevator and rudder actuators.

The total number of different control laws to be distinguished for flutter analyses may be in the order of 20 (normal, flare, direct, autopilot, load alleviation, comfort law all depending on velocity, Ma–number, altitude, payload, fuel, pilot command and other conditions as failures). This may sum up to about 300 different transfer functions between pick–ups and actuators to be covered. Fig. 2.4–1 shows an example of a normal pitch law.

All of the laws are well defined by the theoretical control laws. Nevertheless, their realization should be checked by tests for several reasons:

- *the general safety, to eliminate simple errors*
- *to compare the measured non–linear test results with the linearized approximations used in the flutter calculation*
- *to measure the time delay caused by signal processing in the EFCS and its computers.*

With respect to the last reason, it must be mentioned that data transfer, computation time and other delays may sum up to about 150 or 300 ms in normal or failure case as was explained in ref. 1. These delays cause phase shifts which are additional to the well defined control laws. The amount of the additional phase shift may reach complete sign changes and –what is the most important– they may have a scatter of the same order in failure cases. This is of fundamental importance for the flutter calculations especially if active control laws intend to interfere with the modal damping. So the measurement of control law transfer functions is a must.

Usually the measurement is performed in the iron bird anyway for the safety of the control laws themselves but the results must also be checked by the flutter specialists what may be a new requirement for them. Therefore there is not much experience available but it seems that the predicted data are confirmed by the test results.

2.5 The Classical GVT

The classical GVT is the GVT without EFCS feed back. In this test for the first time the complete a/c is tested and reveals the result of stiffness and weight coupling. Measurements are to be made of: frequency, generalized mass, mode shape and modal damping of all modes up to about 50 Hz. The reliability should be sufficient at least up to the control surface torsion modes which may play an important roll in the flutter mechanism and which reach perhaps 20 to 25 Hz in a larger a/c.

For the execution of the test the a/c must be suspended in a weak suspension for a sufficient separation of rigid body and structure frequencies. This can not always be realized but can be compensated if the suspension is included in the eigenfrequency calculation so that no deficit should result.

For the mode shape measurement, the a/c is equipped with accelerometers. Their number must be large enough to allow comparison with heave, pitch and roll movement of all the individual aerodynamic panels used in the theoretical flutter calculation. So for a larger a/c about 700 pick–ups are used. This is in the same order as the number of panels and means that pitch and roll angles of each panel must be interpolated from the heave values of the neighboured panel – which should be just sufficient but

gives no redundancy in case of pick–up failures. For more details of the GVT execution, reference should be made to the literature like for example ref. 2 . But at least one further question should be mentioned. It concerns the excitation. Usually it is the intention to measure the real modes of the conservative system, that means those modes of the a/c structure which would occur without damping. This is realized by a mode excitation with up to 6 or even more harmonically driven shakers acting at the same time in phase at different locations on the a/c structure to compensate the energy dissipation and the complex movement with different phases at different locations.
Whether the "true" real mode shape is really measured by this forced vibration is at least dependent on the carefulness of the test team. So it should be allowed to ask whether modern test and computation facilities don't suggest to aim at the complex modes in GVT. Perhaps only an aged tradition has to be overcome.
The accuracy of the test results of a GVT reachs only 20% for the generalized masses and the modal dampings but should be very good for most of the frequencies.
Unfortunately for some important modes such as the control surface rotation modes there are sometimes some larger non–linear influences causing a frequency scatter of about 20% for different vibration amplitudes.
If the measured frequencies are compared with the computed ones larger differences are found and massive stiffness corrections become necessary. After these corrections an average difference of about ±5% may remain – which is not an excellent result.
The necessary corrections are large as already mentioned in chapter 2.2 and their introduction on the basis of the GVT test results is a blind one since one can no longer distinguish between the influence of the mass and the influence of the stiffness or other reasons.
In general, most often the mode shapes themselves are not sufficiently exploited for the correction of the FE model though theoretical methods are available. As a consequence, there is also no value of the deviation of the measured mode shapes from the predicted ones available.
The most common application of the measured mode shapes is just their direct introduction into flutter calculations to allow a comparison of such flutter results with pure theoretical ones.

2.6 Actuators in the GVT

The non–linear actuators are special elements so they need special attention.
There are different possibilities of dealing with the actuators in the classical GVT. First, one can substitute each actuator by a piece of steel during the basic tests to avoid the influence of the non–linearities. The stiffness of the substitute can be fitted to the equivalent stiffness of the actuator. Later the actuators can be installed and especially the control surface modes can be excited once more to see the differences.
This more expensive method reveals the influence of the local connection stiffnesses in the basic test and should show the influence of the actuator characteristics in the additional tests. So this method is recommended in critical cases.
On the other hand, it is cheaper to perform the tests with installed and activated actuators from the beginning. This should work if the actuators mainly behave as springs (as for smaller amplitudes due to the overlaps of the control valves) or if complex modes are acceptable already in the GVT. Up to now for larger flexible civil a/c the second method together with the excitation of real modes worked without major problems.
For mechanically controlled actuators, the influence of the elastic deformations on the control signal positioning elements must be checked. It could cause problems if, for example, fuselage bending would result in an actuator activation due to control cable movement.

2.7 Measurement of Damping in GVT

Nowadays the measurement of the structural damping in the GVT is more important than in the past due to the contribution of the damping to the magnitude and phase of the active control feed back. Fig. 2.7–1 shows the unwanted signal content of the classical rigid body control signals Nz, Ny, P, Q, R at higher frequencies due to structural vibration. The magnitude of each peak is inversely proportional to the square root of its modal damping and the structural damping may contribute to a larger extent to the amount of the total damping.
Unfortunately, the scatter of the measurement of modal dampings in GVT reaches about ±20% (s. ref. 2) depending on the modes. That is not very good but what is even worse is that the amount of damping depends strongly on the load distribution and this means that the modal dampings of an airborne a/c in flight shape may differ considerably from the values measured at the a/c while standing on the ground.
The necessary consequence is that the structural damping during GVT must be measured for different loading conditions to get a feeling of their influence but, additionally, one must try to measure also at the flying aircraft during FVT – which is not usual, and at least difficult.

2.8 The Extended GVT

For a/c with fly by wire technique the classical GVT must be extended the check the coupling of structure and flight control already on ground and before first flight. This is the first time the coupling can be checked and it is the last chance to find a coupling which is too strong or other failures without possible catastrophic consequences.
The absence of airloads is of course a deficit for these tests but nevertheless their significance for the safety and reliability of all the further work and tests cannot be rated highly enough.
This coupling test should include frequency sweep excitations by electrical signals in the EFCS and by loads on the control surfaces with open and closed EFCS.
The efficiency of the inertia loads excited by the electrical signals is large enough to give reasonable response values so that a good comparison with the theoretically predicted transfer functions can be performed (s. for example Fig 2.8–1).
Such tests are simply to be performed but they are new and therefore there is still some resistance against them which must be overcome.

2.9 Unsteady Airload Measurement

Tests to measure the unsteady airloads in flight on the real a/c are unusual. But a rational analysis of the necessary steps to demonstrate the freedom from flutter of a newly developed a/c type reveals that such a test is a necessary link in the logical chain of duties as already shown in Fig. 1–1.

Unsteady airloads are sometimes measured on a/c models in wind tunnels. But the deficits of such test results are well known.

Therefore usually these loads are only computed and later on corrected on the basis of measured frequencies and damping values from the flight vibration test.

If one proceeds in such a way it is once again neither proved that the correction is applied in the right place nor that, in case no correction seems to be necessary, two failures don't compensate each other. This fact is not only of theoretical importance. The author remembers a case where the mass of bonkers installed in the tail plane of an a/c to excite it during FVT, hid the deficits of local unsteady airloads. All the FVTs were finished without problems, no tendency of flutter was found. But then another a/c of the same newly developed type but without flight test equipment installed showed real flutter to the surprise of the crew expecting no evil. One may imagine the resulting danger, the problems for a/c certification and the amount of work, time and money to find the true reason of this flutter case. The repair later on was simple: about 8 kg of mass placed in the right location.

Typical cases of necessary corrections of unsteady airloads computed, for example, by the doublet lattice method are known from the measured hinge moments of control surfaces. Though there are examples of good agreement of predictions and test results, sometimes correction factors of 0.5 are necessary to meet the measured hinge moments on the control surfaces of larger civil a/c in the transonic region.

Such large corrections indicate the amount of uncertainty and they are really a strong reason to perform unsteady pressure measurements.

Further the correction of the hinge moment alone is not sufficient. As one can see from Fig. 2.9–1 taken from ref. 3. The airloads arise not only on the control surface itself but in its whole neighbouring area.

Fig. 2.9–2 shows for another theoretical example the influence of these neighboured loads on flutter results if the corrections are only applied directly on the control surface.

The modal damping of a fuselage mode modified by an active control system can be influenced even if the loads on the active elevator itself are set to zero as indicated by the modal damping of the elevator rotation mode. A rather unrealistic result.

Finally, it should be mentioned that for transonic wings such measurements are more important since precise shock positions or local disturbances of the airflow are more difficult to predict.

2.10 The Classical Flight Vibration Test

The FVT is the highlight of the flutter analysis, its crucial test. For large modern a/c, the FVT is becoming more and more extensive, dangerous and more difficult to analyse but requires more precise test results.

The FVT has different purposes:

- *to confirm that the aircraft really is free from flutter*
- *to measure the amount of damping – the final criterion of safety*
- *to prove that the mathematical model used predicted what was later measured so that this model may be used also for predictions in other cases not tested.*

Therefore, the FVT first of all needs some excitation of vibrations with larger amplitudes to show that these amplitudes really decrease without further excitation.

The tests should cover the whole envelope of flight conditions and a/c configurations which are required for justification and/or which are possible. Furthermore, in the tests all modal data, such as frequency, damping and mode shape of all relevant modes should be measured at least up to the control surface torsion modes like in the GVT.

That is the pretension. But practice is much more modest.

2.10.1 The Scope of the Classical FVT

In principle, critical failure cases are excluded from the tests even if their justification is required since they are possible with a probability of being in failure state of more than 10^{-9}.

In addition, the total number of combined flight conditions and a/c configurations is too large to test all of them. A representative and conservative selection is necessary. This should include minimum and maximum payload, and fuel cases as well as other important conditions. At least the configuration which is known from calculation as the most critical one should be tested.

The flight envelope – velocity and Mach number – must be completely covered up to V_D/M_D at least for one mass configuration. Fig. 2.10.1–1 gives an example of test points. Other configurations are most often only checked at V_{MO}/M_{MO} and V_D/M_{MO} if possible in stationary flight. Unsteady flight conditions are of course flown but most often without special measurement or excitation of vibrations.

2.10.2 The Excitation of Vibrations

An effective excitation is especially important for the success of a FVT since the quality of excitation is fundamental for the quality of the test results. Different methods have been used. A survey is given in Table 2.10.2–1. Typical hardware is shown in Fig 2.10.2–1,–2,–3.

Modern a/c use mainly the control surfaces or externally installed devices as tip vanes (Fig. 2.10–1) or rotating cylinders (Fig. 2.10–3). A detailed comparison of wing mounted tip vane and control surface excitation as used on a large civil a/c is given in Table 2.10.2–2.

This table shows that both methods have their advantages and disadvantages. But if the actuator transfer functions allow to excite with a sufficiently high frequency the control surfaces are recommended.

In Fig. 2.10.2–4 one can see of course that both methods excite the different modes at different locations with different intensity but there is no fundamental difference. All

the tests were performed within one flight and at the same velocity and Mach number. (By chance the bandwith of the tip vane excitation was not quite identical with the bandwith of the control surface excitation).
Fig. 2.10.2–5 shows the results of the modal analysis of these tests. All modal data could not always be analyzed from the control surface excitation but no principal difference is visible which could be allocated to the excitation method.
The maximum excitation frequency applied in these tests was 16 Hz for both the exciters (not shown). But the quality of test results reduces with increasing frequency at least if sweeps with constant sweep velocity [octaves/sec] are used. Harmonic excitations may be more effective but they are also more expensive. So the accuracy of the FVT and its analysis reduces with increasing frequency under normal circumstances.
From the principles of the flutter mechanism it is known that control surface torsion modes may play a role which is not negligible. But the above–mentioned upper excitation frequency of 16 Hz does not reach these torsion frequencies which are at about 20 to 25 Hz for larger a/c. This shows one of the largest and most dangerous gaps between pretension and reality in FVT.

2.10.3 Pick–Ups in FVT

An opposite situation is often found for the pick–ups. Most often more accelerometers are installed (s. Fig. 2.10.3–1) than could or should be used for the test analysis. This is due to the difficulties of a subsequent installation in case of problems during the test phase and by the necessity of redundant pick–ups to avoid expensive test doubling in case of pick–up failure.
Up to now, not much profit can be gained from this situation because the inclusion of pick–ups which are not well excited into the modal analysis does not increase the reliability of the analysis result. On the contrary, additional mathematical computation effort is needed to eliminate the measurement deficits of these pick–ups.

2.10.4 Modal Analysis of Test Results

Several theories and softwares are available for the modal analysis of FVTs and there have been some improvements in the last years but the reliability of the test results is still not sufficient. Fig. 2.10.2–5 gave an example of scatter. One can read about 0.1÷5% for the frequencies and 7÷60% for the dampings. These data resulted from "multi output" analyses of a test in 1993. About 10 years ago a more detailed study of the author (s. ref. 4) resulted in a scatter of about 2% for frequencies and 35% for damping values. So the progress was obviously not too large. The comparison of different analyses results of one single test as given in ref. 4 but now extended to 16 different analyses is shown in Tab. 2.10.4–1 as a reminder. This example was a rather simple one. Conditions where clusters of nearly equal eigenfrequencies are to be analyzed are more difficult. This may occur, for example, at a/c with four equal engines on four equal pylons and the situation may be even worse if, in addition, the a/c is slightly asymmetric so that a symmetric excitation excites both the "symmetric" and the "antisymmetric" modes. That would double once more the number of modes within the cluster. The analysis may be rather cumbersome since the additional unintentionally excited modes are not well excited. They show a poor noise–to–signal ratio but nevertheless disturb the response (example s. Fig. 2.10.4–1).The resulting reliability of the analyzed frequency and damping values may be rather poor.
The modal deformation as the third modal data is becoming more and more important nowadays and is included in the LMS analysis method – offered on the market. Experience with the reliability of the measured modal deformations is not available. The only fact that is known is that their accuracy is even worse in comparison with the accuracy of frequency and damping.
So one can conclude that FVT results are not the best ones with the consequence that firstly there is no really reliable proof of the accuracy of the theoretical flutter model and secondly that there is still a larger danger for the prediction of the flutter boundary during the FVT.
Some further improvement is obviously necessary. The question is only how to get it. In the opinion of the author there are at least two things which could be done. First each analysis could be performed by basically different methods, for example the one in time, the other in frequency domain. This would allow immediately to judge the individual reliability of the test results. Since the principle failures introduced by the different analysis methods are different a good agreement of the results should indicate a larger reliability.
Secondly, available knowledge of the a/c under investigation could be better exploited i.e. coupled with the pure mathematical analysis method. Systematic information given as a priori knowledge to the analysis program should help to improve the test results. In other words the evaluation of the results performed after the analysis by the test engineer should at least partially be transferred to the computer. If, for example, one knows that there are n modes within the tested frequency range the program should know this also and should at least try to find them.
Another question concerns the so–called lag states of the airloads and the actuator modes. If they exist and if they contribute to the test result they should be visible in the analysis result or at least their existence should be taken into account by the analysis method.
Finally and as already mentioned in chapter 2.7 the ana–lysis should distinguish between the structural and aerodynamic portions of the modal damping.
This perhaps could be done by measurements at high and low flight velocities and by extrapolation to the zero velocity – again requiring an increasing amount of flight, test and analysis expense.

2.11 The Extended FVT

For modern a/c using EFCS, the FVT must be extended by a large amount.
The EFCS signals given to the control surfaces always contain information of the structural vibration since this information is included in some measured input signals.
Even low pass filtering can not avoid this totally. So the closed loop feed back may cause a flutter instability due to coupling of structure and EFCS and the danger of cou-

pling increases especially for large and flexible a/c with closer rigid body and structural eigenfrequencies.
To check this, additional tests and measurements on top of the classical FVT are necessary.
The additional tests are:

- tests with and without EFCS to check the influence of EFCS
- checks of the large number of different control laws or law conditions, which may even change during or after the FVT phase due to law development.
- checks of flight conditions at lower speed and/or with deflected flaps where the control law gain –that means the electronical coupling– is larger than at higher speeds.

The additional measurements are:

- the main EFCS signals (at least the final commands) which are, in principle, digital while classical acceleration signals were analog (besides, it may be difficult to build transfer functions between digital and analog data)
- the open loop Nyquist diagrams (most often measured in closed loop from control surface actuator input to law command output) for evaluation of robustness margins.
- the in–flight signal transfer function of the actuators as a last check under real flight conditions
- the modal deformation at the position of feed back pick ups since this defines the strength of the coupling between EFCS and structure (and that means the third modal data, the residuum can no longer be neglected in the modal analysis and is of fundamental importance)

Fig. 2.10.2–4 and 2.10.2–5 included three different laws the "direct" law (D) with nearly no feed back, the normal EFCS law (N) and the autopilot law (A). As one can see in this case there is not much influence; only one of the antisymmetric modes gets a reduction of damping due to EFCS and autopilot. Fig. 2.11–1 shows another example from an other a/c with a larger influence. The intention of these laws was to modify only the rigid body behaviour of the a/c. But in these a/c there were additional ride comfort laws (C laws) which were intended to increase the modal damping of some of the fuselage modes. These laws coupled strongly as one can see in Fig. 2.11–2 where transfer functions from input signals of a control surface actuator to accelerometers in the fuselage with C law open and closed are shown.
As a further example of the actuator scatter, in–flight measurements of the transfer function $H_{zA,u}$ (from signal input to actuator deflection) are compared with rig test results (s. Fig. 2.11–3). The differences are remarkable and indicate the amount of accuracy of computations of the EFCS feed back influence.

2.12 Safety Tests for Active Control

As already mentioned it was not usual to test critical failure cases in FVT. But with the introduction of active control laws as the C law described above, it should be discussed whether it is necessary to do some tests of the safety equipment which must be installed if critical failures of the active control law can not be excluded with a probability of being in failure state of less than 10^{-9}.
Fig. 2.12–1 shows an example. The C law was intentionally modified by an increase of gain and phase so that it should lead to a flutter instability as in failure case. As one part of the safety device the C law signal is limited so that no really critical vibration can occur and the C law can be switched off.
During the test at a constant altitude the a/c speed was carefully increased up to a level where flutter was expected. But first it did not occur.
The pilot tried to excite it by stick jerks, failed two times, but initiated an explosive vibration with the third and largest jerk. After a certain amount of elevator signal amplitude was reached, its limitation became active and the vibration remained constant up to the final switch off of the device.
So the safety could be proved and the related maximal amount of disturbance could be measured.
Such tests should increase the confidence in the a/c and it may be appropriate to check a case which is not completely improbable with test pilots on board instead of with paying passengers.

3. CONCLUSION

The reality of flutter–relevant tests does not fit completely to its pretension. Most of the tests could win by some possible improvements. For the GVT, the question of complex mode measurement should be discussed again. For the FVT the reliability of modal data analysis needs continuous updating and for fly by wire a/c the new EFCS tests need special attention. Furthermore, the exploitation of static stiffness tests is strongly recommended. But measurements of unsteady airloads on the flying a/c and especially on its control surfaces should be a must.

REFERENCES

1. Koenig, K.
"On the New Quality of the Flutter Problem due to Coupling of Structure and Electronic Flight Control in Modern Large and Flexible Aircraft"
Forum International Aeroelasticite et Dynamique de Structures 1993, Strasbourg p131–150

2. Niedbal, N.
"Survey of the State of the Art in Modern Ground Vibration Testing" DGLR–Bericht 82–01, 1982

3. Roos, S. and Zwaan, R.J.
"Calculation of Instationary Pressure Distributions and Generalized Aerodynamic Forces with the Doublet–Lattice–Method" NLR–TR–72037U

4. Koenig, K.
"Problems of System Identification in Flight Vibration Testing" AGARD–R–720 (1983)

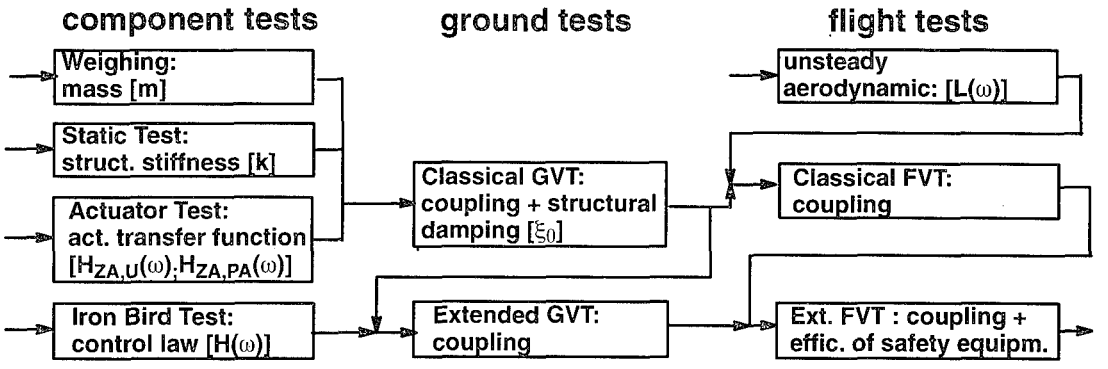

FIG. 1–1 LOGIC OF MODEL VALIDATION
by individual checks of contributing components and of coupling mechanisms

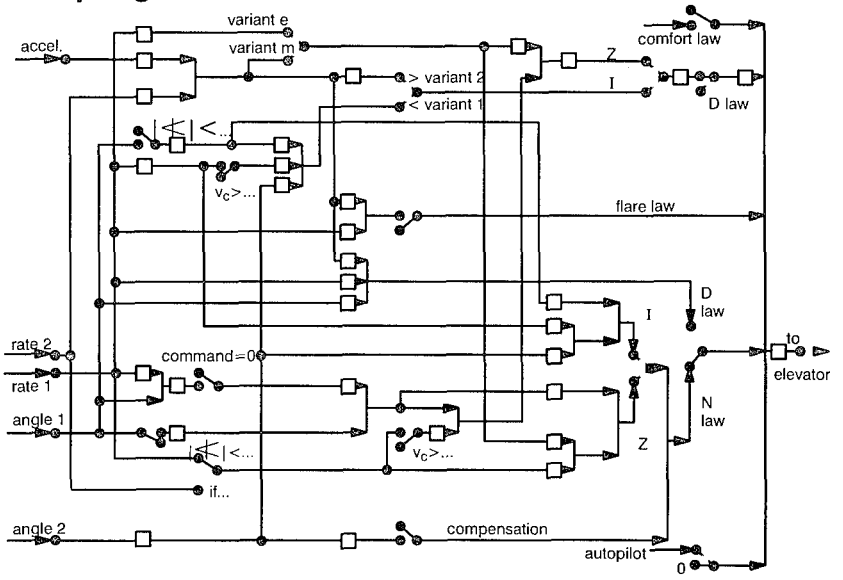

FIG. 2.4–1 VARIABLE SIGNAL FLOW IN AN EFCS PITCH LAW
(switches as for normal flight with large velocity)

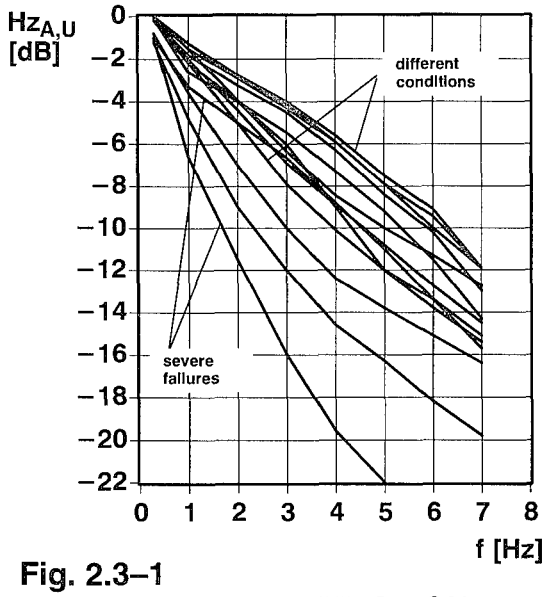

Fig. 2.3–1
PARAMETER INFLUENCE ON TRANFER FUNCTION
(rudder with 3 active actuators)

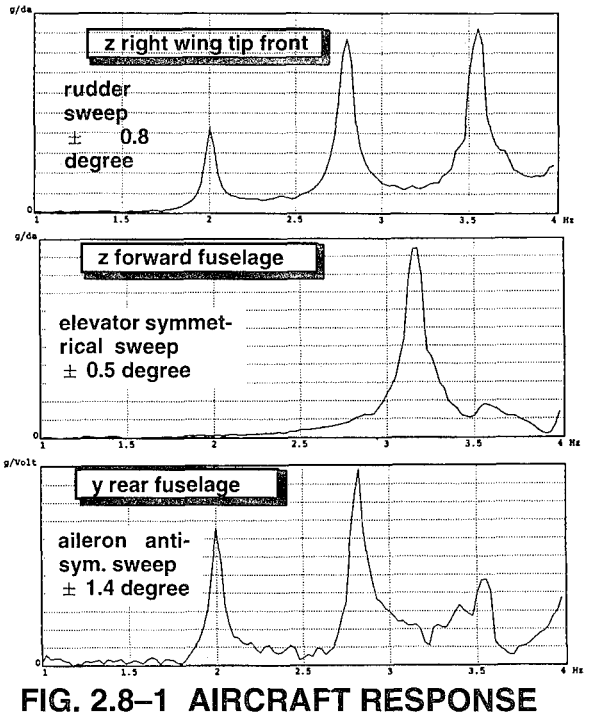

FIG. 2.8–1 AIRCRAFT RESPONSE TO SIGNAL EXCITATION

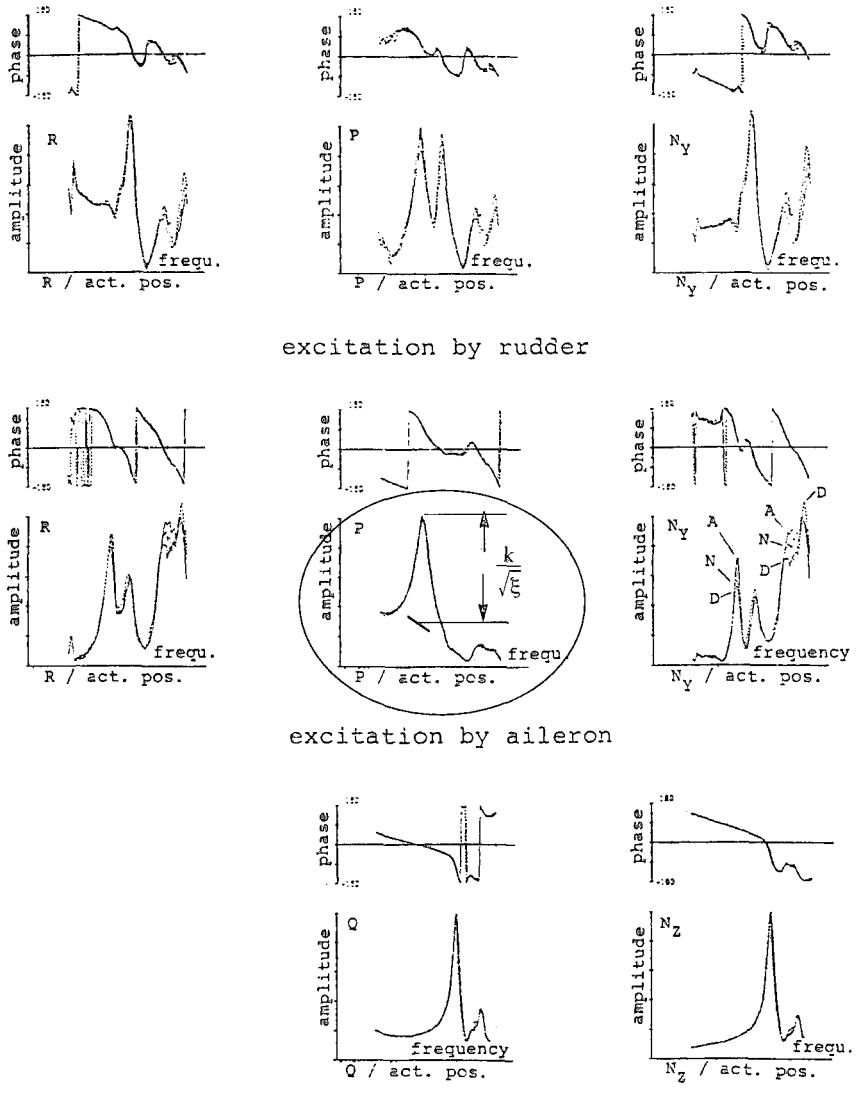

FIG. 2.7–1 TRANSFER FUNCTIONS FROM CONTROL SURFACE DEFLECTIONS TO PICK UP SIGNALS OF EFCS (measured with different control laws D,N,A activ)

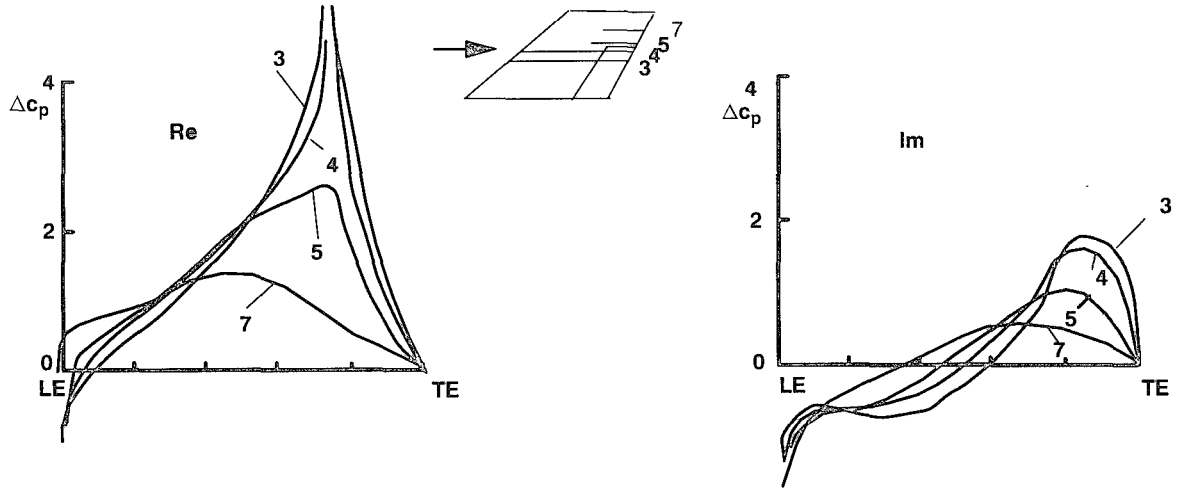

FIG. 2.9–1 INSTATIONARY PRESSURE DISTRIBUTIONS ON A WING WITH OSCILLATING CONTROL SURFACE

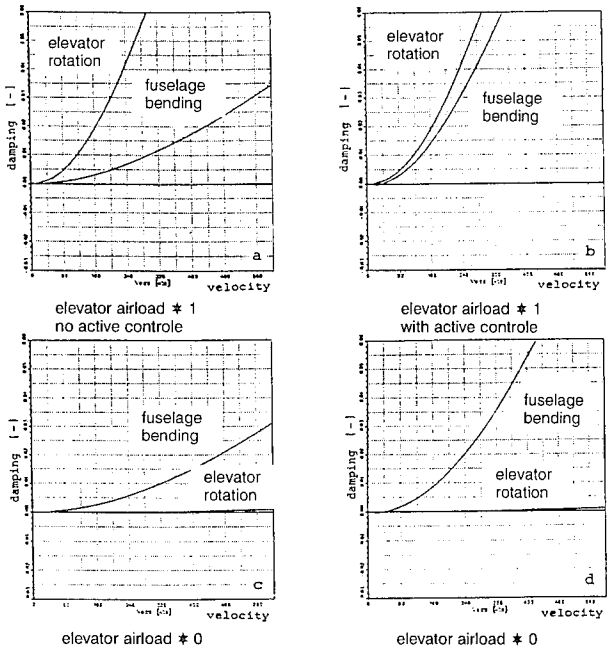

FIG. 2.9–2 INFLUENCE OF AIRLOAD CORRECTIONS

	Tip Vane	Control Surfaces
additional costs	– large	+ small
actuator transfer function	+ constant in gain and phase	– gain reduction and phase shift with frequency
disturbances caused by backlash	+ small	– larger
changes due to installation or use	– additional masses	– aerodynamic loads of steady state flow
sample rate	+ high	– smaller; limited by sample rate of control
interference of excitation and control	+ no	– possible due to non–linear effects
useful for establishing of open loop Nyquist diagrams	– not applicable	+ mandatory
flexibility of use during one flight	+ flexible	– fixed to predefined program for safety reasons
excitation measurement	+ close to response (load by strain gauge)	– remote from response (signal)
No. of excited modes	+ sometimes larger with one measurement	– sometimes smaller even with 2 measurements (e.g. aileron + rudder)
signal–to–noise ratio	+ independent	– influenced at resonances of control law feed back

Table 2.10.2–2
DETAILED COMPARISON OF TIP VANE AND CONTROL SURFACES

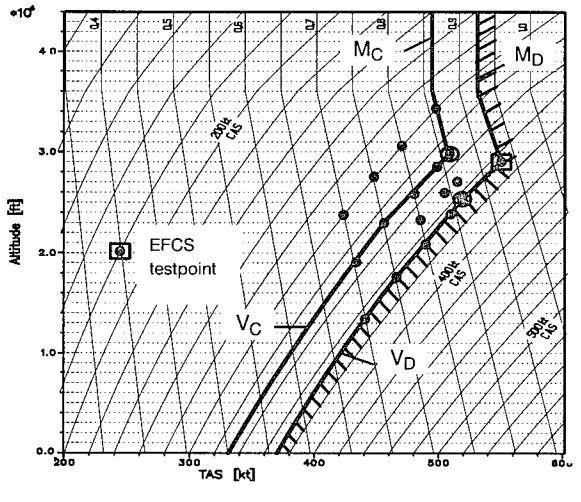

FIG. 2.10.1–1
FVT – CONDITIONS WITHIN FLIGHT ENVELOPE

typ:	natural turbulence	control surface movement		bonkers	inertia loads	aerodynamic loads from added devices	
additonal device to be installed:	no	no		rocket	mass + motor	movable vane + motor (+ hydr.pipe)	rotating cylinder+ motor
additional mass:	0	0		moderate	heavy	moderate	moderate
typical energy supply:	turbulence +a/c velocity	hydraulical		gunpowder	electrohydraulic	hydraulic or electric	electric
typical excitation mode:	random	pulse (stick jerk)	sweep of electr. signal	pulse	harmonic	sweep	sweep
excitation measurable?	no	yes	yes	difficult	yes	yes	yes
main disadvantages:	•dependent on weather •small amplitudes •restricted analysis	•restricted excitation •poor analysis	•gain reduction and phase shift with increasing frequency	•restricted No. of tests within one flight •response sensitive to burning time •poor analysis	•too large, too heavy •location in fuselage	•costs	•costs •no variable amplitude within flight
main advantages:	•no costs	•no costs	•cheep •mandatory for fly by wire a/c	•most locations •excitation level independent on flight velocity	•excitation level in dependent on flight velocity	•effective •good analysis	•good analysis

TAB. 2.10.2–1 SURVEY OF DIFFERENT EXCITATION DEVICES

FIG. 2.10.2–1 AIRCRAFT WITH TIP VANES

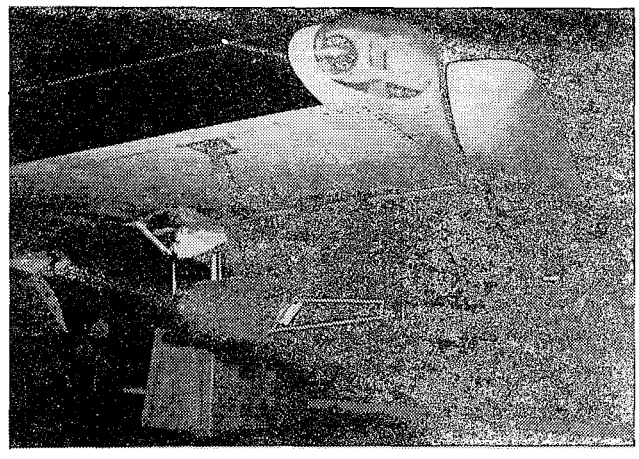

FIG. 2.10.2–2 COLIBRI EXCITER INSTALLED ON A WING

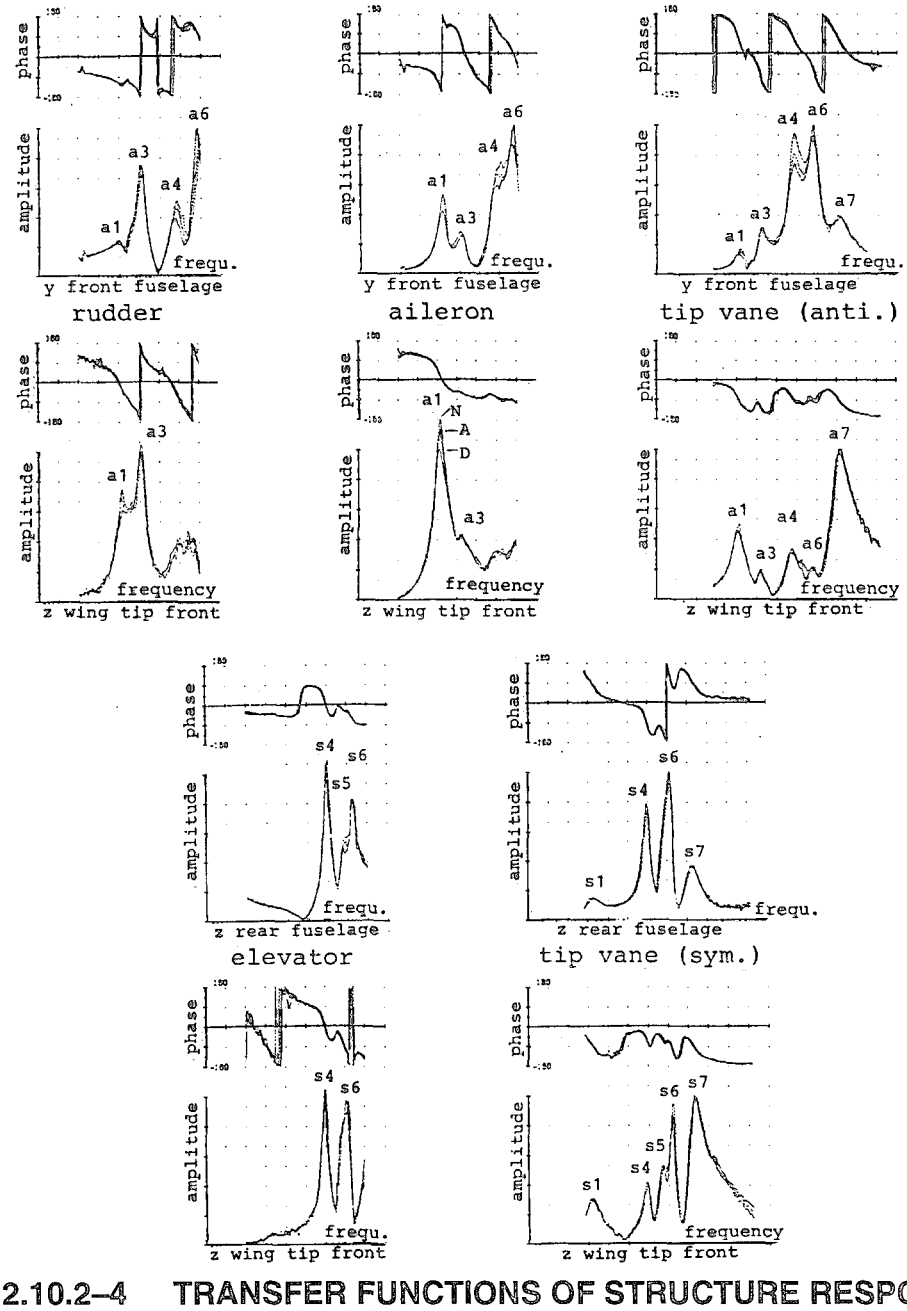

FIG. 2.10.2–4 TRANSFER FUNCTIONS OF STRUCTURE RESPONSE DUE TO DIFFERENT TYPES OF EXCITATION (measured with different control laws D,N,A active)

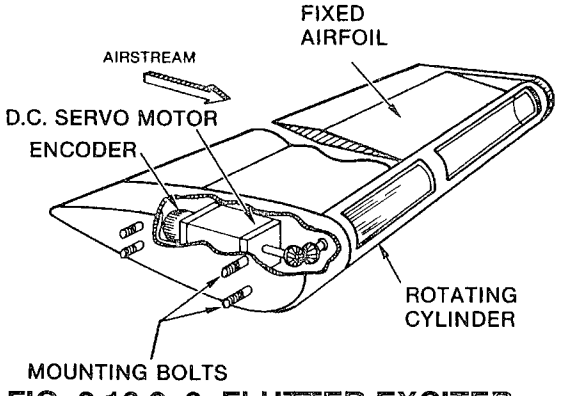

FIG. 2.10.2–3 FLUTTER EXCITER

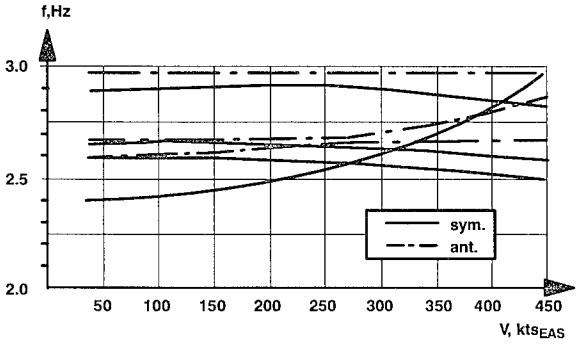

FIG. 2.10.4–1
EXAMPLE OF FREQUENCY CLUSTER
(mainly vertical and lateral engine modes of a 4 engine a/c)

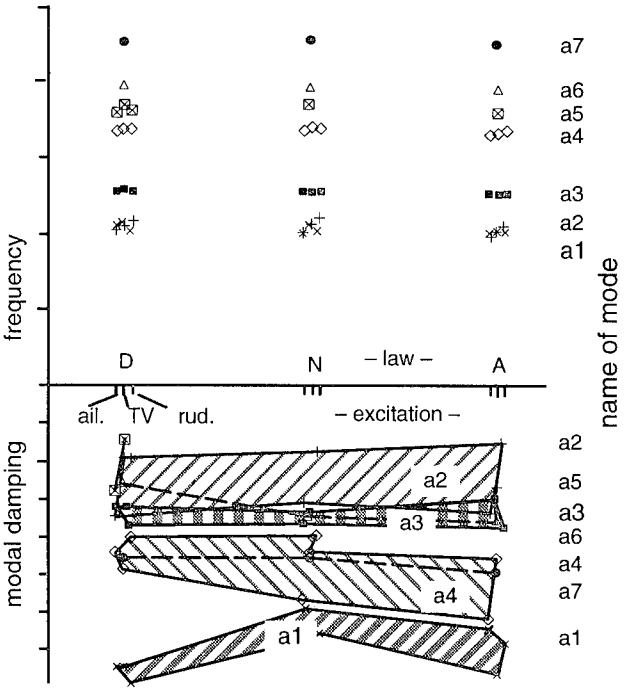

Fig. 2.10.2–5
RESULTS OF MODAL ANALYSIS FROM FIG. 2.10.2–4
(influence of different laws D,N,A and excitations ail. TV, rud.)

method	No of analysed output signals	mode						remarks
		1.WZ	EY	EZ	1.FZ	2.FZ	2.WZ	
		frequency [Hz] / damping [% of critical]						
1	1	1.75 / 6.2	2.08 / 7.2	–	3.89 / 2.9	4.24 / 1.2	5.01 / 4.6	HP single mode analysis
2	1	1.88 / 5.8	1.95 / 10.8	–	3.98 / 4.2	4.22 / 2.6	5.00 / 4.4	Gan Rad
3	1	1.79 / 7.3	2.04 / 5.0	–	3.94 / 4.9	4.24 / 1.9	5.03 / 4.5	Nicolet
4	1	1.84 / 11.2	1.97 / 4.3	–	3.99 / 3.9	4.23 / 2.5	5.01 / 4.3	
5	1	1.84 / 10.7	1.93 / 4.5	–	3.87 / 4.3	4.24 / 1.6	5.00 / 3.8	
6	2	1.84 / 8.9	1.96 / 6.8	–	3.95 / 2.9	4.29 / 2.6	5.01 / 4.8	one transferfunction as No.1
7	1	1.75 / 10	1.99 / 5	–	–	–	5.07 / 5	
8	1	1.82 / 7.0	1.98 / 7.7	–	3.95 / 4.7	4.20 / 2.7	5.04 / 4.2	author, transff.of No.1
8.1	1	1.84 / 8.3	1.97 / 7.4	–	3.98 / 6.4	4.21 / 3.5	5.05 / 4.4	auth. other transff.
9	1	1.82 / 10.3	1.92 / 7.5	–	3.98 / 5.0	4.29 / 3.0	5.02 / 5.o	
10	>2	– –	– –	–	3.97 / 4.5	4.25 / 2.7	5.01 / 4.7	
11.1	1	1.87 / 7.2	2.03 / 7.8	–	4.01 / 3.0	4.25 / 2.0	5.02 / 4.3	LMS; MLE
11.2	1	1.81 / 6.2	2.03 / 6.3	–	3.95 / 4.2	4.24 / 2.5	5.02 / 4.5	LMS; LSCE
11.3	8	1.90 / 9.1	2.00 / 6.1	3.12/3.4	3.95 / 4.5	4.25 / 2.8	5.01 / 5.0	LMS; LSCE
11.4	1	1.81 / 9.2	1.99 / 6.3	–	4.02 / 3.3	4.27 / 2.2	5.03 / 4.4	LMS; OPOL
12	5	2.01 / 16.7	1.82 / 2.9	–	3.98 / 4.9	4.28 / 2.7	5.06 / 4.6	
$\bar{x}$ mean		1.84 / 8.9	1.98 / 6.4		3.96 / 4.2	4.25 / 2.4	5.02 / 4.5	
δx stan.dev.		.06 / 2.7	0.06 / 1.8		0.04 / 0.9	0.03 / 0.6	0.02 / 0.3	
δx [% of $\bar{x}$]		3.3 / 30	3.0 / 29		1.0 / 22	0.6 / 23	0.4 / 7	
max scatter −/+ [% of $\bar{x}$]		−4.9/9.2/−35/88	−8.1/5.1/−55/69		−2.3/1.5/−31/52	−1.2/0.9/−50/46	−0.4/1.0/−16/11	

TABL: 2.10.4–1 COMPARISON OF DIFFERENT ANALYSES OF ONE SINGLE FVT

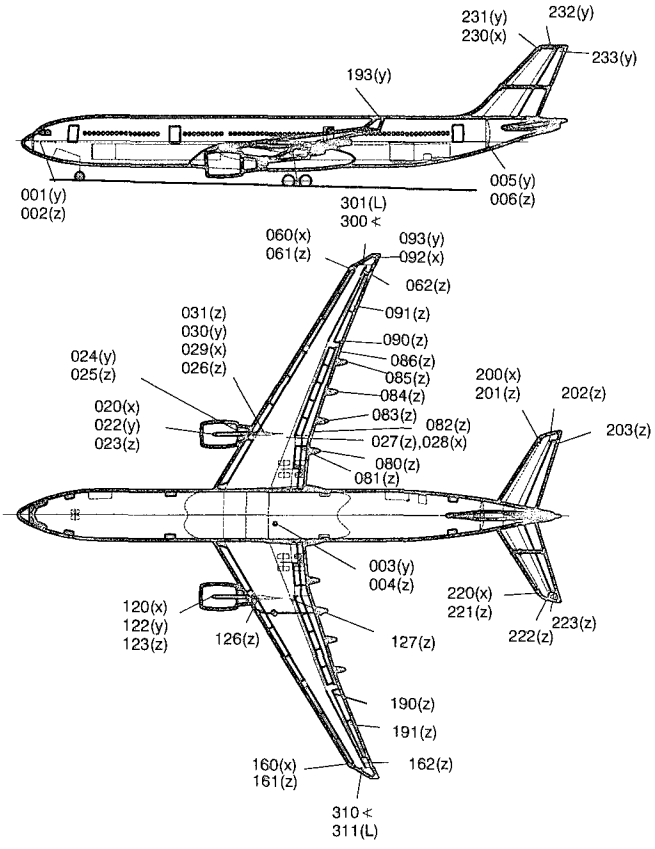

FIG. 2.10.3–1 PICK–UPS FOR FVT

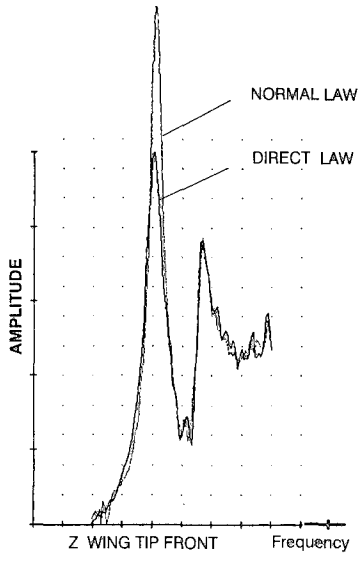

Fig. 2.11–1
INFLUENCE OF CONTROL LAW
(antisym. excitation by aileron)

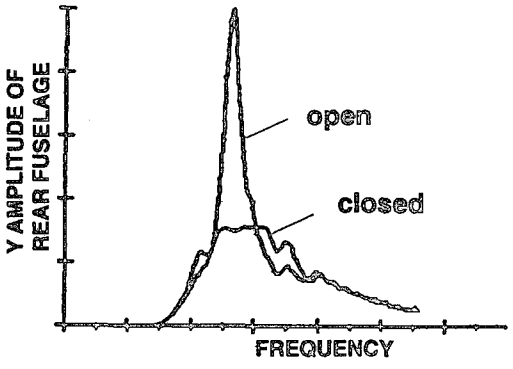

FIG. 2.11–2 INFLUENCE OF C LAW

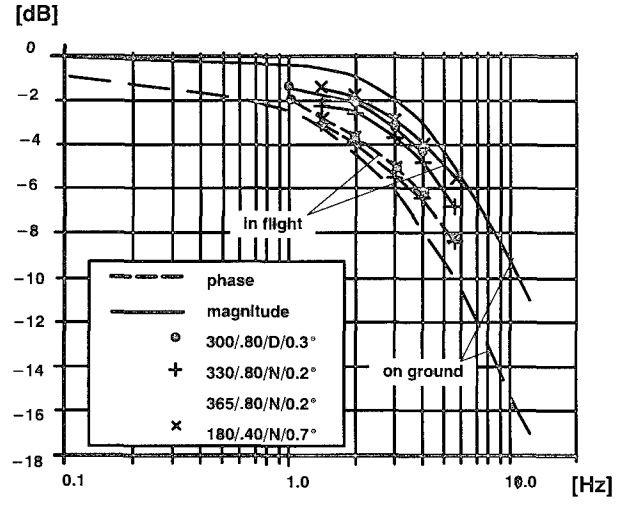

FIG. 2.11–3
$H_{ZA,U}$ TRANSFER FUNCTION OF
ELEVATOR ON GROUND AND IN FLIGHT

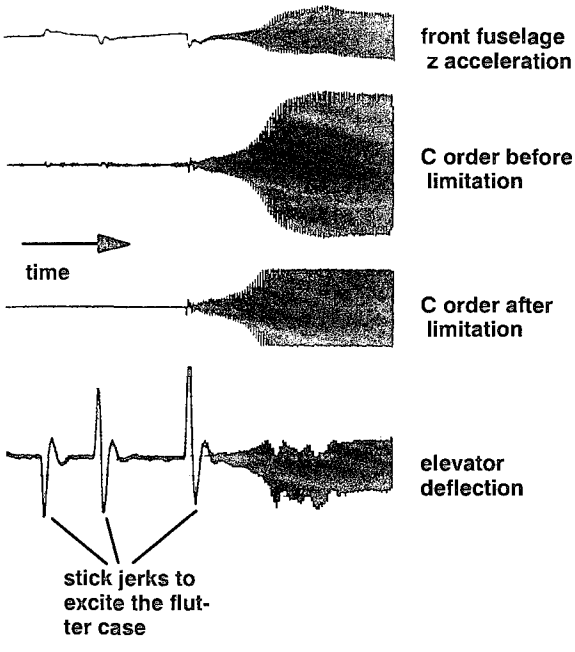

Fig. 2.12–1 SAFETY TEST OF C LAW

FLIGHT FLUTTER TESTING OF COMBAT AIRCRAFT

R.B. Ramsay

British Aerospace Defence Ltd (Military Aircraft Division)

Warton Aerodrome, Preston

Lancashire, England PR4 1AX

UNITED KINGDOM

SUMMARY

A computer system for analysis and display of flutter parameters during flight flutter testing of an unstable digitally controlled fly-by-wire combat aircraft is presented.

The system is being developed by BAe in conjunction with Parsytec GmbH, a computer company specialising in parallel processing hardware and software and applied to the Eurofighter 2000 (EF2000). The benefits will increase aircraft safety by identifying critical parameters involved in the flutter mechanisms during flight flutter testing, by increasing the visibility of data to the test engineer.

The Parsytec system, which is part of the Flight Test ground station, is fully integrated with the telemetry facility and is capable of analysing, confidencing and displaying test data for comparison with prediction in near-real time. This facility, which includes parallel processing transputers combined with high performance digital signal processing devices, will enable the engineer to assess analysed data quickly and efficiently in order to decide whether or not the aircraft can safely progress the envelope expansion.

In addition, an aircraft excitation system is being developed which will permit predefined waveforms, generated within the Flight Control Computers (FCC) to be summed into the Flight Control System (FCS) actuation loops under cockpit control.

The overall clearance philosophy for identifying critical flutter parameters through calculations, ground testing and flight testing is also presented.

1. BACKGROUND

During the initial stages of flight flutter testing a new type of aircraft, the flight envelope is opened progressively in terms of Mach number and airspeed. The rate of expansion is determined by the need to establish that the aircraft is safe and free from potential interactions between aerodynamic forces and structural servoelastic characteristics.

Such interactions, from any initial disturbance caused by a gust or turbulence, could result in vibration and coupling of structural modes resulting in the destruction of the airframe.

To avoid encountering this phenomenon, known as flutter, flight tests are performed to establish the aircraft frequency and damping characteristics. A number of accelerometers are positioned on the airframe and their response to specific excitation monitored in-flight and analysed to assess the stability and give a basis for clearance to a higher airspeed or Mach number test point.

Previous in-flight flutter analysis has been restricted to performing analysis on two accelerometers, from a possible twenty transmitted, to determine frequency and damping, using a Hewlett-Packard 5451C Fourier analysis system. Results were hand plotted to identify airspeed and Mach number trends to compare with prediction.

The analysis is supported by analogue pen playouts of the twenty accelerometers to visually check structural responses resulting from known excitation inputs. Full analysis of all parameters was carried out post-flight.

As a result of these restrictions, flight envelope expansion was slow to progress due to the limited number of test points achieved per flight, because it became necessary to analyse the recorded data prior to issuing a clearance for an increase in airspeed or Mach number.

The introduction of a parallel processing capability into the analysis facility enables twenty accelerometers to be analysed simultaneously instead of sequentially, as previously. The use of parallel processing will therefore result in an increased efficiency in flight clearance and reduce the costs of flutter clearance by reducing the number of flights, time scales and manpower requirements.

Included in the specification for the parallel processor was the requirement to reduce the time taken for the analysis of twenty accelerometers by 80-90%.

The timescale for implimenting and commissioning of the computer system was based on the EF2000 flutter test programme.

Paper presented at the Structures and Materials Panel Specialists' Meeting on "Advanced Aeroservoelastic Testing and Data Analysis", held in Rotterdam, The Netherlands, from 8-10 May 1995, and published in CP-566.

This paper describes the computer system which is capable of analysing, confidencing and displaying telemetered flutter test data in near-real time.

The overall clearance philosophy for identifying critical flutter parameters through calculations, ground testing and flight testing is also presented.

In conjunction with the flutter ground station an aircraft excitation system is being developed which will permit predefined waveforms generated within the FCC's to be summed into the FCS actuation loops under cockpit control. This development work is presented in Reference 1.

2. CLEARANCE PHILOSOPHY

For flutter it is necessary to provide evidence of qualification or verification of fitness of purpose to ensure safe flight, adequacy for the flight testing task and verification against the specification.

In general, qualification is to demonstrate that the aircraft shall be free from flutter or aeroservoelastic instabilities at all speeds up to 1.15 (airspeed limit) for all flight conditions.

Flutter qualification is achieved by :-

- Theoretical calculations, including the characteristics of the FCS supported by
- Ground tests: static stiffness, actuator impedance, ground vibration and structural coupling testing.
- Wind Tunnel tests : Flexible and rigid model testing.
- Flight Flutter tests.

Figure 1 shows schematically the flutter qualification route to flight clearance. Calculations are performed using component finite element models which are assembled into a total aircraft model with inputs from ground testing.

Sensitivity studies are performed on components and total aircraft to identify the critical parameters involved in the flutter mechanisms, including the effects of the FCS. Results from aircraft ground resonance testing (GRT) are used to update the model and flight clearances issued, subject to flight flutter testing.

The flight flutter test requirements are integrated into the overall envelope expansion programme and testing performed to identify the critical flutter parameters. Flight testing and analysis is performed in near-real time on the flutter designated development aircraft and a formal flight clearance issued following completion of the envelope expansion flying.

Formal clearance will apply to all other aircraft with the same design build standard and configuration. Additional key configurations will then be flight tested to an agreed test schedule.

3. FLIGHT TEST GROUND STATION

3.1 Flutter Ground Station

A computer system is being developed by BAe Aerodynamics in conjunction with Parsytec GmbH, a computer company specialising in parallel processing hardware and software, to analyse, confidence and display telemetered flight flutter data for comparison with predictions in near-real time. A post-flight facility is available for analysis and display of data.

The system enables the engineer to access analysed flutter data following continuous and impulsive excitation within seconds of completion of a test point in order to decide whether or not the aircraft can safely progress to the next test point.

In order to demonstrate the system, results from flight flutter testing of the Experimental Aircraft Program (EAP) have been used. The EAP was used to develop a flutter excitation system suitable for use on EF2000. The results are from impulsive and frequency sweep excitation, covering subsonic and supersonic flight conditions.

The results in the form of plots of frequency and damping against airspeed have been compared directly with predictions matched to GRT results.

3.2 System Structure Overview

Figure 2 shows the general layout of the Flight Test ground station designed primarily for EF2000 flight testing

Telemetered PCM data is received, calibrated and elaborated by the ADYIN front end computer. The data is then passed to the APTEC input/output computer which acts as a databus for peripheral display and analysis devices.

The flutter station is hosted by a MicroVax 3500 which provides a user interface for control of the Parsytec transputer system. The front end processor of the transputer system is located within a Sun-server linked directly to the APTEC. The processor accesses data for analysis by the transputer system either from the real-time PCM data stream, or from a disc file on the MicroVax 3500 (post-flight analysis mode).

3.3 System Components

Figure 3 shows schematically the flutter ground station system and the interface with Flight Test. The Parsytec system comprises of a transputer system, supporting three monitors, and controlled by a MicroVax 3500.

3.3.1 MicroVax 3500

The MicroVax 3500 runs the VMS operating system and supports a menu driven workstation. The MicroVax provides the user with an interface for control of the

transputer system. Via the MicroVax, the user inputs flight instrumentation details, analysis display order, test point conditions, excitation type, analysis parameters, filters and data storage file names. The start of data acquisition is also controlled through the MicroVax.

3.3.2 Transputer System

The transputer system comprises one BBK-V2 VMEbus T800 board for data input located in the Sun-server, one DBT-8 T800 piggy-back board for data buffering, one TPM-SIG T800 ZORAN DSP (digital signal processing) board for data analysis and three GDS-2 T800 G300 boards for graphics output, each with a piggy back board for mouse control.

The network of the transputers, except the front end board, which is located in the Sun-server, are housed in a dedicated expansion cabinet.

Three 19 inch EIZO Flexscan colour monitors are used for display of analysed data.

Figure 4 shows the transputers arranged in a pipeline configuration with overall control of the system maintained by a program running on the MicroVax. Individual control of the graphical processors is via a mouse pointing device and a "pop-up" menu system.

3.4 Software

The user has access to all stored data on the system. The data is filed under analysed data, flight data, prediction data and VAX set-up data (Figure 5). In addition, there is separate controlled access to the source code of the Parsytec system.

Entry into the system is controlled by a menu driven "command file" program which gives the user a series of options, which control access to executable code (e.g. flutter analysis) and provides other "utility" functions (e.g. tape transfer). Inputs to this menu system are by keyboard input as either numerical selections from a list or character string to select other options. The three main options are flutter analysis, data conversion and analysed data review.

3.4.1 Flight Flutter Analysis

Each transputer, and the MicroVax, run a separate software component of the system responsible for a separate function. The software components are :

1. MicroVax user interface.
2. Front end data receiver.
3. Data buffer.
4. Data analysis.
5. Analysis display.
6. Auto data monitor.
7. Trend display.

The code is written in a mixture of C and Occam for the transputers and exclusively in C for the VAX.

3.4.1.1 MicroVax User Interface

The code running on the MicroVax has two functions :-

1. Booting of the transputer system.
2. User control of the transputer system.

The control of the system is via a menu driven user interface. This enables the user to easily set up the system by input of textual and numerical information. Runs are started from the menu system, at the time the relevant set-up information is forwarded to the transputer system.

3.4.1.2 Front End

The function of the front end module is to accept, reformat and precondition the raw data from the APTEC system and to pass it on to the buffer processor. For testing and post-flight analysis the front end can be run in a mode where it reads data from the VAX disk instead of the APTEC system.

The front end converts the data from the APTEC system (or VAX disk) to 32-bit floating point format and then the data is checked for "drop out", "dc-offset" and "dead channels". Each block of data has a header block associated with it and the results of the data checks are stored in this header for forwarding to the analysis screen where warning messages are displayed.

3.4.1.3 Data Buffering Module

The function of the module is to buffer the data stream from the front end system and feed the data into the analysis module. There are three components in the module which run in parallel with each other : the input process, the buffer manager and the output process.

The input process maintains a separate buffer for each channel. It informs the buffer manager when data has been received for a channel. The buffer manager keeps track of the data in each channel data buffer. The output process sends blocks of data for each channel in turn to the analysis module (cycling through each channel, up to a maximum of 20, sampling at 512 samples/second).

3.4.1.4 Analysis Module

The main analysis of the flight data is performed by this module. The analysis module can accept and analyse up to twenty channels of digital time history data for random, continuous and impulsive excitation methods. For continuous excitation one of the channels contains the excitation signal, with the remaining 19 channels containing the responses. For impulsive and random excitation the channels contain just the response signals.

For random excitation (e.g. atmospheric turbulence) the autocorrelation technique is used. This technique assumes that the random forcing applied to the structure has a flat power spectrum over the frequency range of interest. Thus, an approximate transfer function and power spectral density (PSD) is obtained for each channel by correlation of the response data only.

For continuous excitation, transfer functions for each channel are calculated using a block-overlap technique: the data are segmented into overlapping blocks and the average frequency response is calculated from the Fourier Transforms of these blocks. The response is cross-correlated with the excitation frequency to generate the PSD and the coherence is then calculated. For impulsive excitation the PSD is calculated, but with no need to use block-overlapping or cross-correlation.

From the PSD the dominant modes of oscillation for each channel are extracted using the following technique. The mode with the largest power is extracted, re-scaled and re-phased with respect to the original complex frequency domain transform and subtracted in the frequency domain. This process is repeated until no more significant modes exist (based on the PSD), up to a maximum of four modes. The damping of the modes is then calculated by fitting a line to the logarithm of the time progression of the mode.

After the modes have been extracted, the confidencing level for each mode is calculated (see section 3.6), and the frequency, damping and confidencing values are passed to the analysis screen for display.

3.4.1.5 Analysis Screen

The analysis screen has a layout as shown in Figure 6. It displays data for four channels at a time showing the impulse response, PSD, Argand plot and the frequencies and logarithmic damping of the four extracted modes. Numeric values for the frequency, damping and confidencing are written to the screen for each mode.

Continuous display of selected air data (e.g. altitude, Mach number, airspeed) are available in order to check the test point conditions against that scheduled.

The display is menu controlled with a menu bar being displayed at the top of the screen. Scrolling backward and forward through the 20 channels is performed using the mouse. Using the mouse on the extracted modes on the screen causes the screen to "zoom in" and display the data for that mode.

The user has the capability to change the confidencing level of a particular data point in the "zoomed" screen and, when the data are deemed acceptable it can be passed to the auto data monitor.

3.4.1.6 Auto Data Monitor

The monitor is used for displaying the results of the analysis along with the results from previous test points and theoretical data. The monitor display comprises four graphs showing frequency and damping against airspeed for two ranges of confidence level (Figure 7). When new data is acquired the traces on the plots are extended to include the new data. Colour coding of the symbols and lines plotted on each trace will take place to separate modes and show "warning levels".

The monitor runs grouping and warning algorithms. When new data points are calculated it is necessary to assign them to an existing mode (from previous test points). The grouping algorithm does this by comparison of frequency values with previous data to determine whether the new data can be grouped with an existing mode. Once the data has been assigned to modes the warning algorithm examines damping values and gradients and frequency separation to determine what colour code warning is displayed.

The operator has the capability to display different confidence levels and save displayed data in a plot file for all confidence levels. Access to predicted data for display is also available.

3.4.1.7 Trend Display

The trend screen monitors the analysed data independently of the main analysis chain. It has essentially the same functionality as the auto data monitor (Figure 7). However, it can display theoretical and acquired data for different surfaces to those being analysed in the main data acquisition, giving the operator the opportunity to review critical surface or other test cases. It also gives the capability to look at Mach number and altitude trends and compare data from different excitation cases.

3.4.1.8 Data Conversion

This section of the system gives the user access to programmes which convert previously stored digital flight data (from the HP9000) into a format which can be read by the transputer. Note that the digital data could have been created by analogue data being converted to this form. This would enable analysis of data from non-digital sources, e.g. Panavia Tornado flight flutter test data.

Multiple test points can be processed at the same time and the options are selected from a menu system. The user can store data on a TK70 tape in a backup format. Use is made of the Flight Test programmes and a C programme which interfaces with the transputer system.

3.4.1.9 Analysed Data

This section of the system gives the user access to data previously analysed using the flight flutter analysis programme. Options to browse a specific test point (i.e. frequencies, dampings and confidences for each channel), edit a file, print a file and save a number of files onto the TK70 tape drive are controlled via a menu system. The browse facility uses a simple C programme and the other functions are controlled by a "command file".

As further post-flight facilities become available they will be added in under this menu item.

3.5 Main Vax Menus

The Vax main menu is shown in Figure 8. Each test case needs a specific set up which defines all textual and numeric parameters required for analysis, display and storage of the data. This set up file has a unique identifier which is used to call up all the relevant information for the test "user program", prior to "initialise the transputer system" and "start acquisition".

3.5.1 Test Definition Files

This is the primary menu which identifies other menu files for input to the Parsytec system for analysis, display and storage. Each test definition file represents a flight test point and is identified with a file name (e.g. E2451216: E=EAP, 245=flight number, 12.16=schedule item). A typical test definition file is shown in Figure 9.

The primary menu identifies the flight test instrumentation (FTI) group, FTI analysis group, excitation type (impulsive or continuous) and plot file directory names.

3.5.2 Instrumentation Files

In order to perform the flutter analysis the aircraft flight test instrumentation used to measure input excitation and output structural response signals is required to be input via the Parsytec menus.

The FTI channels in the order transmitted or recorded on the aircraft are input in the form of an identifier number, calibration, measurement units and description. This information is stored under an aircraft and FTI group number identifier (e.g. EAP3).

In addition to the FTI group, the order in which the channels are analysed and displayed have to be identified. The analysis group is identified as a group letter and therefore the complete FTI input file can be described (e.g. EAP3A).

It is recommended that the FTI channel analysis order is arranged to display the expected maximum structural responses for the particular surface being excited. For near-real time analysis a limited number of analysis channels should be displayed, sufficient to identify the modes involved in the flutter mechanism. This will enable the engineer to quickly assess the analysis data for the important accelerometers.

3.5.3 Analysed Data Files

Following analysis of the flight data, frequency and damping versus airspeed (Mach number and altitude are also available) plots are displayed for the test point analysed together with previously stored data. The current data being displayed can be stored on a plot file which is identified by the type of excitation and surface being excited e.g. symmetric wing impulsive excitation (EAPPHASE1.SYMWG.IMP).

3.5.4 Prediction Data Files

Prediction data can be stored on the VAX and accessed and plotted using the options available on the auto data monitor and trends screen. It is recommended that flutter critical surface modes involved in the flutter mechanism only are plotted for clarity when comparison is made with measured data.

Prediction data is stored for a particular Mach number and called up independent on the current test point Mach number.

3. 6 Confidence Algorithm

An algorithm has been developed to assess analysis output data and assign a confidence level (0 to 5) to each response accelerometer. In any trial the weighting functions in the algorithm can be changed to reflect the quality of data being analysed due to different excitation inputs and covering a wide airspeed and Mach number range.

Algorithm changes are based on the expected quality of data from predictions due to the position and type of instrumentation, effect of airspeed and Mach number and, in particular, transonic effects. Results using this algorithm have been compared to previously analysed data which uses the same method for extraction of the modes from the power spectral density and engineering experience in deciding confidence levels.

The algorithm confidence values are made up from a number of factors for continuous and impulsive excitation :

Continuous Excitation.

Confidence:-

$$((1.9 \times C_A) + (1.2 \times C_{SEP}) + (1.9 \times C_{LD})) \times C_{COH} \times C_M$$

Impulsive Excitation:-

$$((1.9 \times C_A) + (1.2 \times C_{SEP}) + (1.9 \times C_{LD})) \times C_M$$

3.6.1 Modal Amplitude Factor (C_A)

The extracted modes are confidenced, based on the maximum absolute value in the mode compared with the maximum absolute value in the original signal.

3.6.2 Frequency Separation Factor (C_{SEP})

The confidence factor is based on three frequency checks, these are :

1. The frequency of the peaks above a specified amplitude in the PSD are identified.

2. The frequency separation, in terms of frequency resolution, of all extracted peaks is calculated.

3. The minimum frequency separation for each identified peak with respect to all other peaks is determined.

3.6.3 Logarithmic Decrement Line Fit (C_{LD})

The confidence factor is based on how well a straight line fits the peaks of the logarithmic decrement of the extracted mode (i.e. the error of the least squares polynomial fit).

3.6.4 Coherence Factor (C_{COH})

The coherence at the modal peak is used to calculate the coherence factor (0 to 1) for continuous excitation only.

3.6.5 Signal Magnification Factor (C_M)

The factor is based on the ratio of the maximum absolute value in the original signal compared to the full scale deflection for that channel. This ensures that channels with a small response are given a lower confidence than channels with larger response.

The decision to manually over-ride the calculated confidence values can be made via a menu on the analysis screen.

4. FLUTTER EXCITATION SYSTEM

The problem of developing and qualifying a suitable excitation system to measure the frequency and damping of modes of vibration during flight flutter testing on flying surfaces with small thickness/chord ratios was part of the development of the EAP in support of the EF2000 programme, Figure 10.

The excitation system developed on EAP (Ref.1) is the basis of the EF2000 system which has been extended to include all primary control surfaces with input functions suitable for assessing flutter, structural coupling, air data calibration and inter-manoeuvre stability assessment for a number of aircraft configurations.

Figure 11 summarises the excitation types available. The bias function operates for a fixed period of time and when complete the aircraft control surfaces will be offset at the commanded position. The general time functions (3-2-1-1, doublet, impulse, frequency sweep) operate for a predefined time, directing the selected function to the injection points selected through the test specification. The test specification identifies the injection points and the test data (amplitude and frequency break points).

Figure 12 summarises the available functions and injection points. For flutter excitation single impulses and frequency sweeps are available for individual surfaces, symmetric and differential pairs and full flaps. Combination of controls are available for impulses and double frequency sweeps.

The excitation system structure is shown in Figure 13. The injection point is within that part of the forward path of the outer actuation loop that is computed at 320 HZ. The figure also indicates the command control surface selection and safety protection functions that control the interaction of the excitation system with the primary actuator functions.

5. FLUTTER EXCITATION SIMULATION

In order to optimise the amplitude profile of the frequency sweeps to be used for flight flutter testing an aircraft response model formed from a structural model and actuator forcing function is used to assess the aircraft structural response at various flight conditions.

The forcing functions represents the actuator inputs into the structure and use of the actuator stiffness and a displacement function which represents the ram output demand of the actuator. The actuator output demands are determined from rig and aircraft ground testing by injecting into the FCS known input demands.

5.1 Aircraft Predicted Responses

Figure 14 shows a typical wing response at two accelerometer positions due to symmetric outboard trailing edge flap excitation. The accelerometer positions represent a wing tip pod rear position in the vertical sense and an outboard underwing missile nose in the lateral sense. The wing bending and torsion mode responses increase with airspeed for the same forcing input, due to the effect of the aerodynamics. The tip missile yaw mode is easily identified due to symmetric excitation.

6. FLIGHT TEST INSTRUMENTATION

The instrumentation used to record structural vibration in the range of interest are piezo-electric accelerometer transducers with a power unit amplifier. The instrumentation requirements are defined by Aerodynamics and they include the positioning of the accelerometers and the expected response range. Aircraft installation drawings have to be approved by the originator to avoid local structural responses and non-linearities.

Figure 10 shows the typical positioning of the instrumentation on the aircraft to measure structural responses in the fundamental modes for the wing, foreplane and fin. In addition to accelerometer responses the FCS primary actuator input demands are recorded in order to perform transfer function analysis.

6.1 Instrumentation Positioning

Modal predictions based on the configuration to be tested are the basis for deciding the instrumentation positioning to record the structural response. In particular, the mode shape and position of the nodal line of the modes involved in the flutter mechanism are used to define the position of the instrumentation.

In addition the structural response of a mode together with its frequency due to a known input demand (impulse or actuator sweep) will define the instrumentation calibration and recording range.

7. FLUTTER TEST ANALYSIS

7.1 Flight Trials Data

The flight test data used here were measured during dedicated flight flutter testing and the flying concerned with the development of the in-flight structural mode excitation system on EAP. Frequency and damping trends with airspeed are presented for impulsive and continuous frequency sweep excitation inputs to the wing and foreplane.

Impulsive and continuous transfer function analysis have been performed on the data to extract frequency and damping for the modes involved in the flutter mechanisms.

7.1.1 Wing Impulsive Excitation

Figures 15,16 show the symmetric wing frequency and damping trends versus airspeed for M=0.9 and 1.2 due to impulsive excitation.

The frequency trends for the bending and torsion modes show good agreement with prediction. The torsion mode frequency (WT1) at M=1.2 identifies both port and starboard wings. During the aircraft ground resonance testing individual port and starboard wing torsion frequencies were measured.

The damping trends for the bending mode show good agreement with prediction. The torsion mode damping shows quite separate port and starboard wing trends, particularly at M=1.2. Within the separate component damping there is minimum scatter even at high airspeed. Any scatter shown is the result of the analysis of a number of accelerometer responses which respond differently, depending on the mode being excited and the position on the wing.

7.1.2 Foreplane Continuous Excitation

Figures 17,18 show the symmetric foreplane frequency and damping trends versus airspeed at M=0.9 and 1.2 due to continuous frequency sweep excitation of 2-25 Hz and 25-80 Hz.

The frequency trends for the bending and torsion modes show good agreement with predictions.

The damping trends, in general, for both bending and torsion modes show good agreement with prediction. At M=0.9 and 1.2 individual port and starboard foreplane torsion mode damping has been identified. This is probably due to the different amounts of backlash in the system between port and starboard foreplanes. This effect is quite significant at M=1.2.

8. ANALYSIS METHOD DEVELOPMENT

At present the flutter identification method used was developed by Potter (Ref.2). With this method estimates of frequency and damping, in particular damping, become steadily worse on mechanisms with progressively closer modes.

In order to compliment the existing method, two advanced system identification techniques are being developed in conjunction with the Victoria University of Manchester (VUM), for incorporating into the existing flutter suite.

8.1 Time Domain Methods

Two time domain methods are being considered, these are the Eigensystem Realisation Algorithm (ERA) and the Eigensystem Realisation Algorithm using Data Correlations (ERA/DC).

8.1.1 ERA Method

The method was developed by Juang and Pappa at NASA Langley in the mid 1980's. The technique is based in the time domain and uses decay responses, which may be generated either: by applying an impulse to the structure, by inverse Fourier transforming the frequency response function, or generating the decay response from the response to an unknown random input using methods such as random decrement.

The fundamental element of the algorithm is the Least Squares technique applied to a difference equation model and therefore over-specification of the mathematical model is required to eliminate any statistical error due to noise. The ERA technique incorporates the Singular Value Decomposition (SVD) in its formulation and therefore produces a so called Minimum Order Realisation. Therefore, most of the theoretical computational modes resulting from the over specified solution can be eliminated during the calculation.

8.1.2 ERA/DC Method

The method was developed by Juang, Cooper and Wright in 1987. The method follows a similar formulation to the standard ERA approach except that the analysis is performed on correlations of the impulse response rather than the impulse response data itself. Effectively, the Least Squares element in the ERA is replaced with another technique, the Correlation Fit method, that reduces the statistical error problem.

As well as producing a Minimum Order Realisation, the technique has the advantage in that the amount of model order over-specification that is required is reduced greatly.

8.2 Frequency Domain Methods

Two frequency domain methods are being considered, developed by British Aerospace Civil Aircraft Division, and referred to as the Plot and Prediction Analysis (PAPA) and the Instrumental Variables (IV/OEM).

8.2.1 PAPA Method

The PAPA or Transfer Function Analysis (TFA) in its implementation, is an estimator of a class known as the "Output Error Methods". It works on the principle that the

turbulence and transducer noise components are not correlated with the input signal. A transfer function is fitted to the data in such a way that it fits the data as closely as possible.

If the noise is white, then this approach is almost statistically efficient. In practice, turbulence noise has been filtered through the aircraft structure, and so is non-white. The fact that the noise is not white means that PAPA is not optimal, but in practice the loss of efficiency is not very great, partly because noise is never ideal anyway.

Because the transfer function is a non-linear function of the modal frequencies and dampings, PAPA must solve the least squares problem iteratively. Hence the algorithm which estimates the modal parameters has some undesirable properties. Principal among these are a requirement for starting estimates for the modal frequencies and dampings, and the fact that the algorithm is not guaranteed to converge within a reasonable time.

8.2.2 IV/OEM Method

The Instrumental Variables approach attempts to perform exactly the same operation as PAPA, and is called the Instrumental Variables/Output Error Method algorithm. The IV/OEM approach attempts to overcome the problems associated with an iterative solution to the least squares minimisation. It does this by linearising the problem, and using a compensating procedure (Instrumental Variables) to overcome the undesirable statistical effects of the linearisation. Because the heart of the approach is linear, start-up estimates are not required, and convergence is guaranteed.

In comparisons on flutter test data the IV/OEM approach was found to be on average 15-30 times faster than the PAPA method.

9. ACKNOWLEDGEMENTS

This work has been carried out with the support of the Procurement Executive, Ministry of Defence and Parsytec UK Ltd.
The author would like to thank his colleagues, in particular, Mr Tom Kelly for his help in preparing this paper.

10. REFERENCES

1. R.B.Ramsay

In-Flight Structural Mode Excitation System for Flutter Testing, Flight Mechanics Panel Symposium, Crete, 11-14th May 1992.

AGARD CP-519.

2. D.K.Potter

The Interpretation of Complex Signals from Mechanical Systems. Institute of Mechanical Engineers, London, 24th February 1976.

11. FIGURES

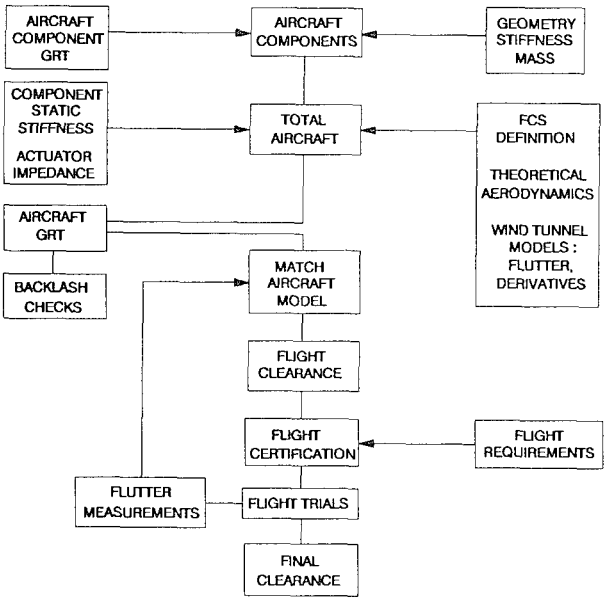

Figure 1: Flight Certification Route

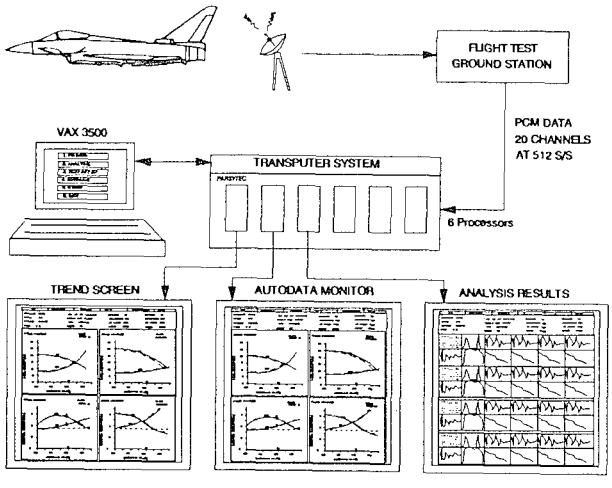

Figure 3: Flight Flutter Ground Station

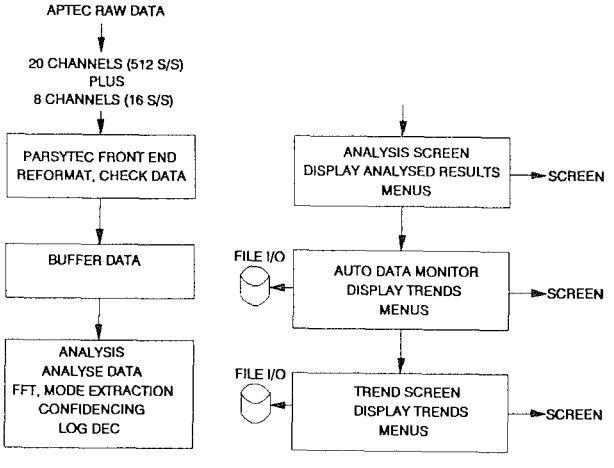

Figure 4: Transputer System Structure

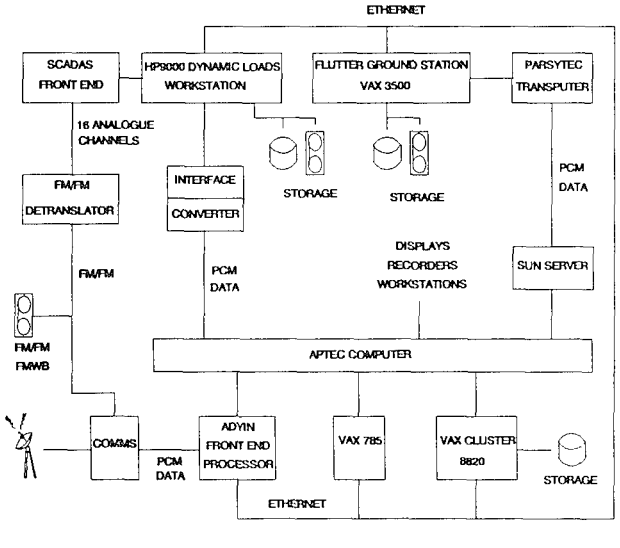

Figure 2: Flight Test Layout

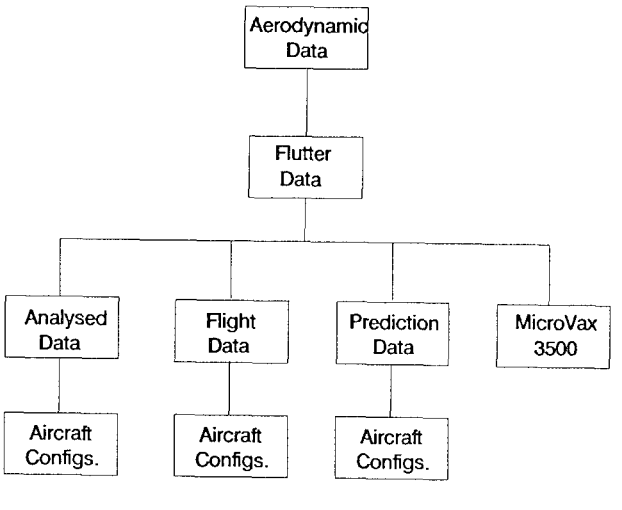

Figure 5: Parsytec Software Layout

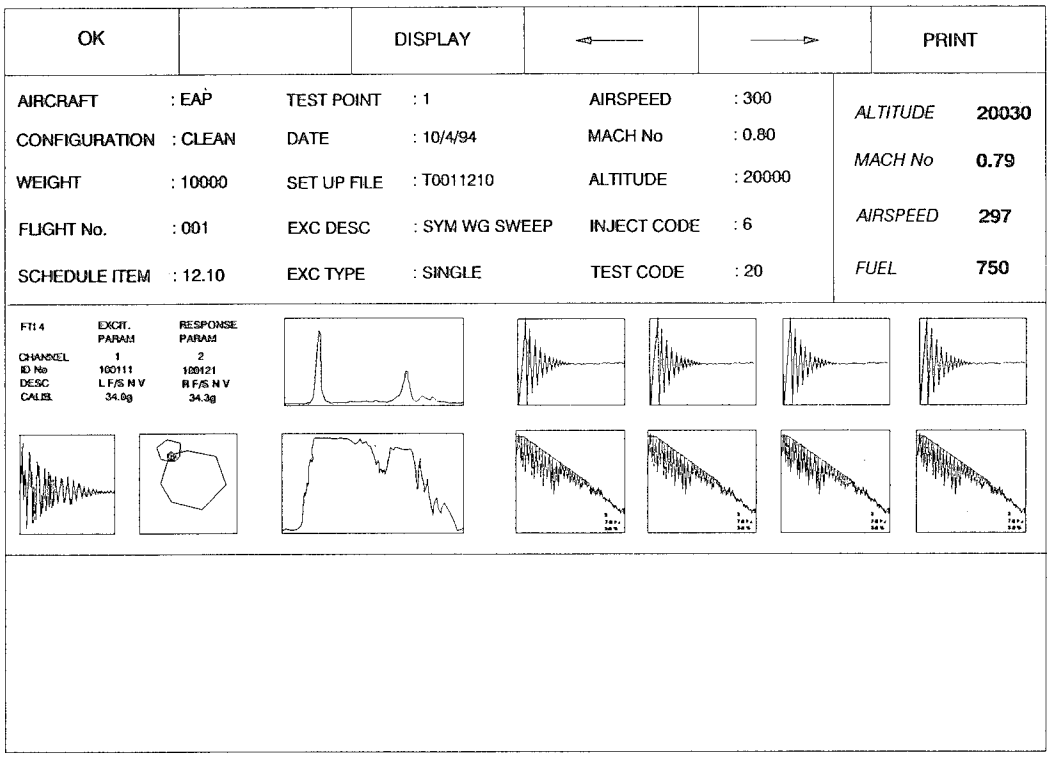

Figure 6: Analysis Screen Layout

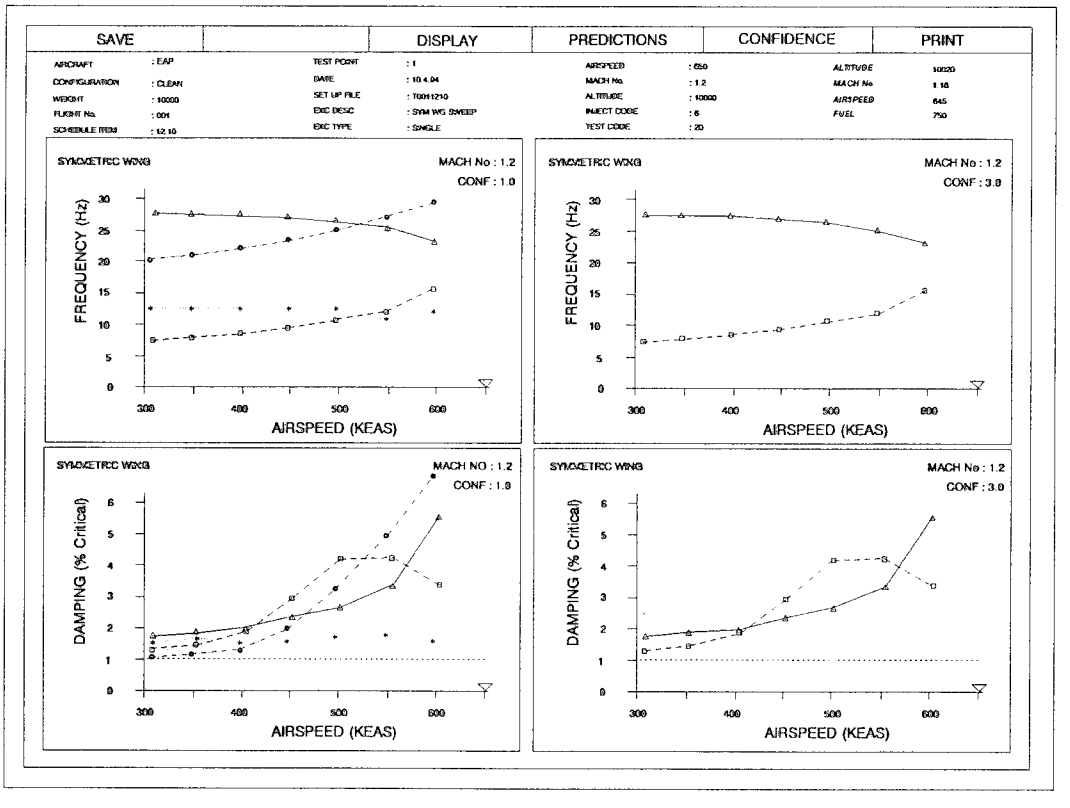

Figure 7: Autodata Monitor and Trends Screen Layout

FLIGHT FLUTTER ANALYSIS MAIN MENU

1. FTI GROUP PARAMETER DEFINITION
2. ANALYSIS GROUP DEFINITION
3. TEST ROUTINE DEFINITION
4. USER PROGRAM
5. INITIALISE TRANSPUTER SYSTEM
6. START ACQUISITION
7. HELP
8. EXIT SYSTEM

Figure 8: Main Menu Layout

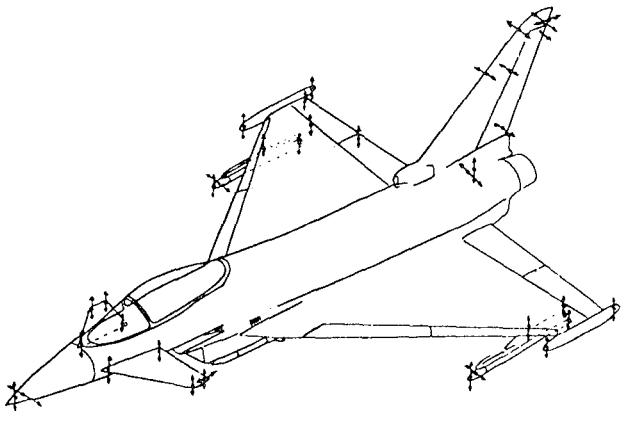

Figure 10: EF2000 Flutter Instrumentation

Test Set-Up Edit Definition

File Name : E1171401 OPEN CONTINUE QUIT

Test ID No.	: 1	Weight (kg)	: 15000	FTI Group No.	: 3
Aircraft	: EAP	Schedule Item	: 14.1	Ex. File Name	: EAPEXCIT
Flight No.	: 117	Mach No.	: 1.20	Ex. Test No.	: 1
Config.	: CLEAN	Airspeed (KIAS)	: 500	Plot File Dir.	: EAPPHASE1
Date	: 7.12.87	Altitude (ft)	: 20000	AirD File Name	: EAP
Crit. Damp	: 1.0	Trend Scr File	: EAP	Sampling Freq.	: 512
DC Offset	: 0.10	Dead Chan Lim	: 0.0001	Drop out Limit	: 0.10

Figure 9a: Aircraft Test Set-up Definition

Continue

Single Impulsive Excitation

SAVE QUIT

Block Period (secs)	:	2
Exc. Duration (ms)	:	50
Analysis Group Letter	:	A
High Pass Filter (Hz)	:	2.0
Low Pass Filter (Hz)	:	25.0
Plot File Name	:	SYMWG

Figure 9b: Aircraft Test Set-up Definition

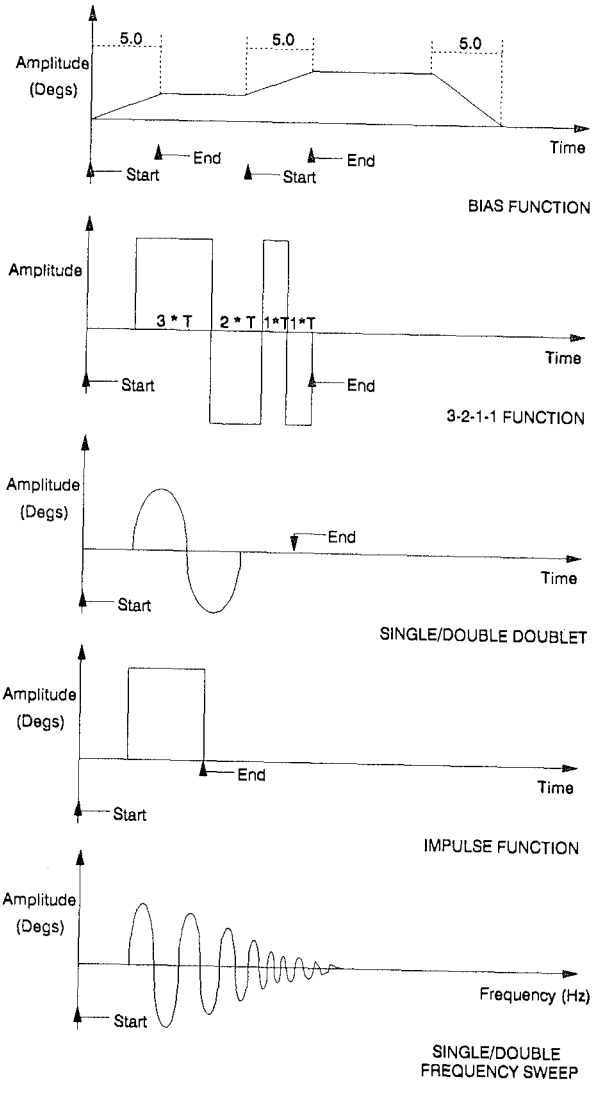

Figure 11: Excitation System Functions

INJECTION POINT	BIAS	DOUBLET SINGLE	DOUBLET DOUBLE	3-2-1-1	IMPULSE	FREQ SWEEP SINGLE	FREQ SWEEP DOUBLE
L.E. DROOP	*						
PITCH STICK		*		*			
ROLL STICK		*		*			
RUDDER PEDALS		*		*			
LEFT O/B FLAP		*			*	*	
LEFT I/B FLAP		*			*	*	
RIGHT I/B FLAP		*			*	*	
RIGHT O/B FLAP		*			*	*	
LEFT FOREPLANE					*	*	
RIGHT FOREPLANE					*	*	
RUDDER		*			*	*	
SYMMETRIC I/B FLAPS		*			*	*	
SYMMETRIC O/B FLAPS		*			*	*	
SYMMETRIC FULL FLAPS	*	*			*	*	
SYMMETRIC FOREPLANES	*	*			*	*	
DIFFERENTIAL I/B FLAPS		*			*	*	
DIFFERENTIAL O/B FLAPS		*			*	*	
DIFFERENTIAL FULL FLAP		*			*	*	
DIFFERENTIAL FOREPLANE					*	*	
SPLIT FLAPS (SYMM)	*						
SYM F/P + O/B FLAPS			*		*		*
SYM F/P + I/B FLAPS			*		*		*
SYM F/P + FULL FLAPS			*		*		*
DIFF O/B FLAPS + RUDDER			*		*		
DIFF I/B FLAPS + RUDDER			*		*		
DIFF FULL FLAP + RUDDER			*		*		

Figure 12: Excitation System Control Inputs

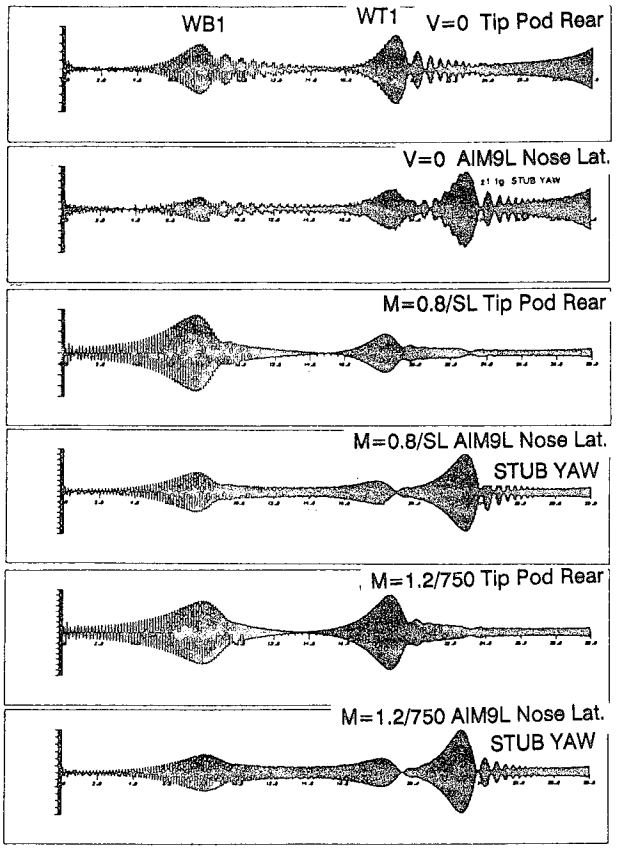

Figure 14: Simulated Wing Responses

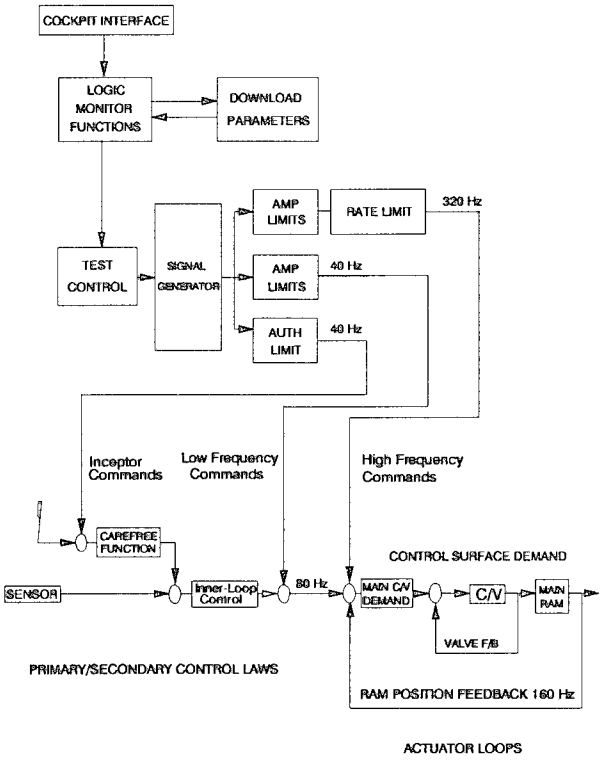

Figure 13: Excitation System Structure

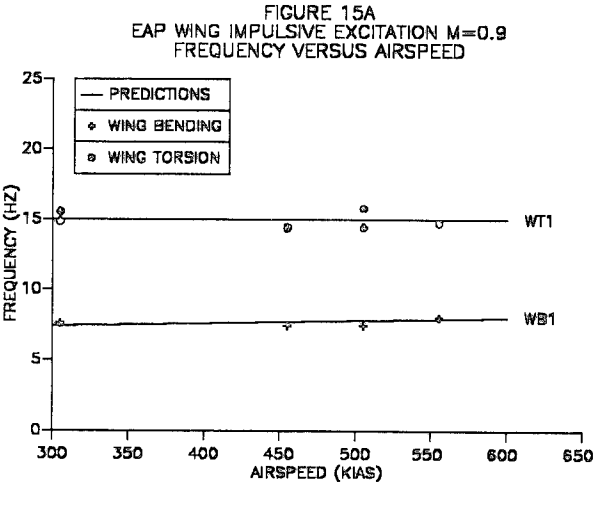

FIGURE 15B
EAP WING IMPULSIVE EXCITATION M=0.9
WING BENDING DAMPING VERSUS AIRSPEED

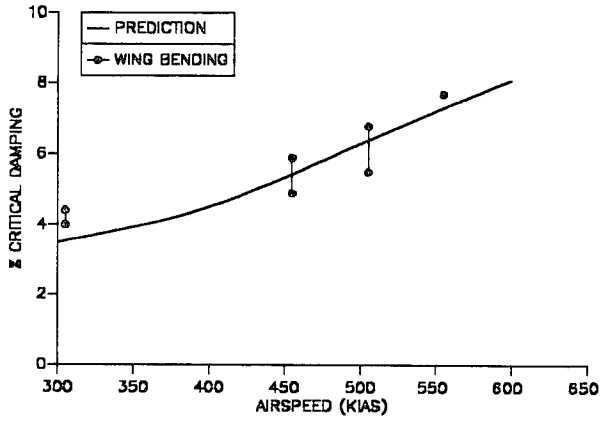

FIGURE 16B
EAP WING IMPULSIVE EXCITATION M=1.2
BENDING MODE DAMPING VERSUS AIRSPEED

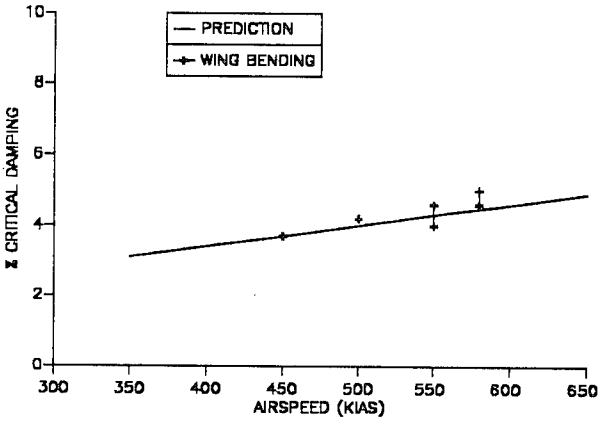

FIGURE 15C
EAP WING IMPULSIVE EXCITATION M=0.9
WING TORSION DAMPING VERSUS AIRSPEED

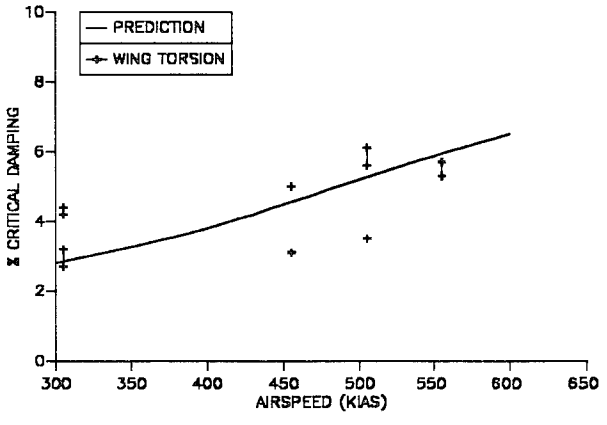

FIGURE 16C
EAP WING IMPULSIVE EXCITATION M=1.2
TORSION MODE DAMPING VERSUS AIRSPEED

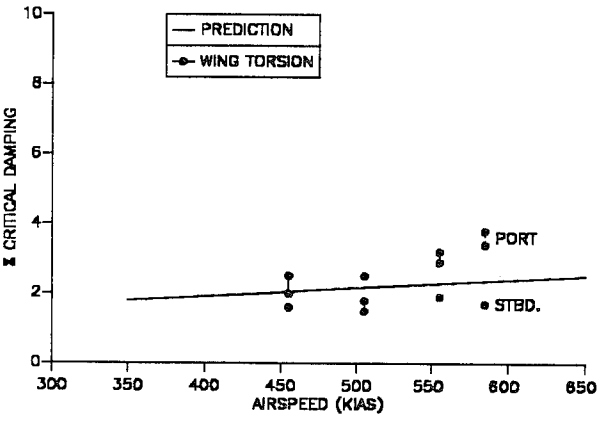

FIGURE 16A
EAP WING IMPULSIVE EXCITATION M=1.2
FREQUENCY VERSUS AIRSPEED

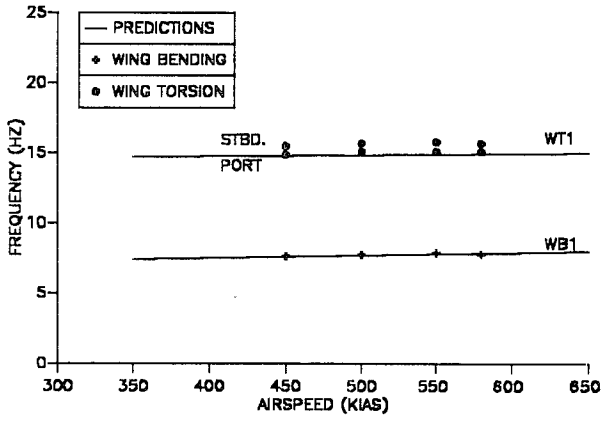

FIGURE 17A
EAP FOREPLANE SWEEP EXCITATION M=0.9
FREQUENCY VERSUS AIRSPEED

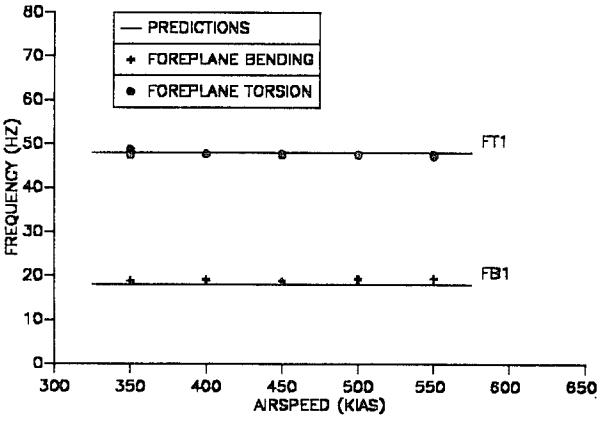

FIGURE 17B
EAP FOREPLANE SWEEP EXCITATION M=0.9
BENDING MODE DAMPING VERSUS AIRSPEED

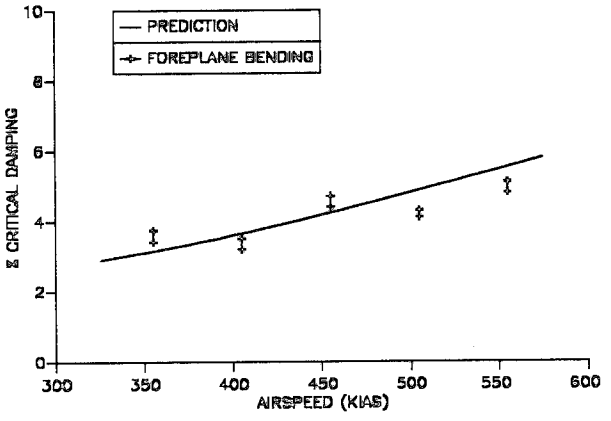

FIGURE 18B
EAP FOREPLANE SWEEP EXCITATION M=1.2
BENDING MODE DAMPING VERSUS AIRSPEED

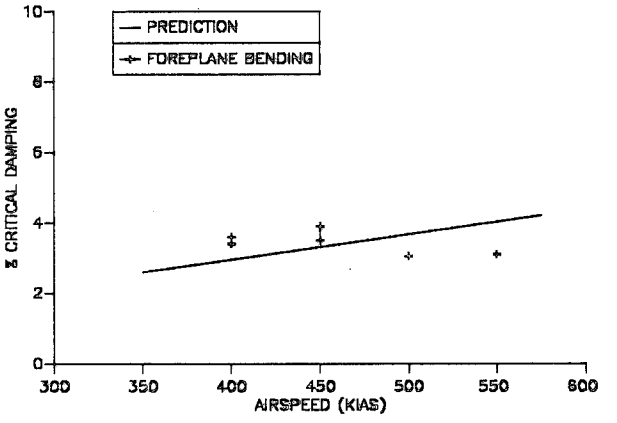

FIGURE 17C
EAP FOREPLANE SWEEP EXCITATION M=0.9
TORSION MODE DAMPING VERSUS AIRSPEED

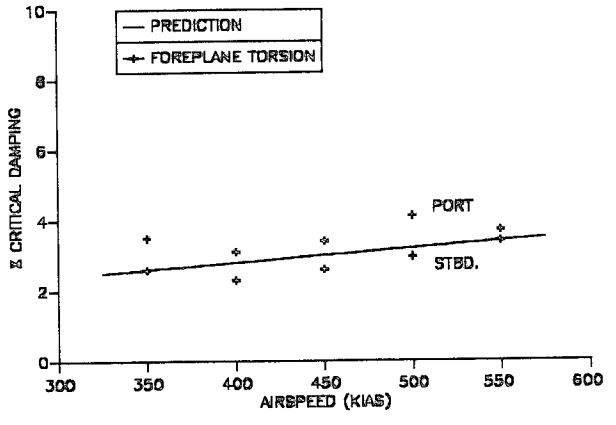

FIGURE 18C
EAP FOREPLANE SWEEP EXCITATION M=1.2
TORSION MODE DAMPING VERSUS AIRSPEED

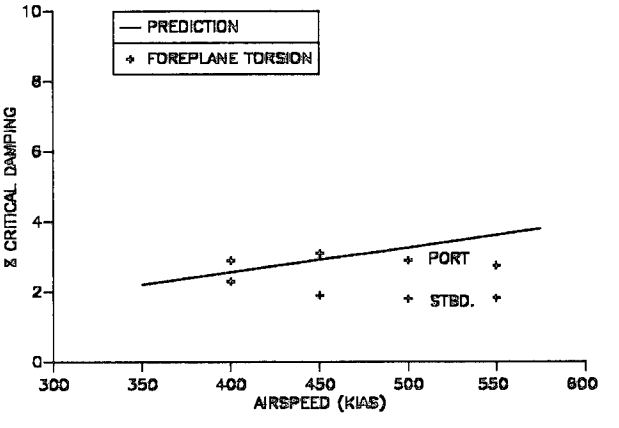

FIGURE 18A
EAP FOREPLANE SWEEP EXCITATION M=1.2
FREQUENCY VERSUS AIRSPEED

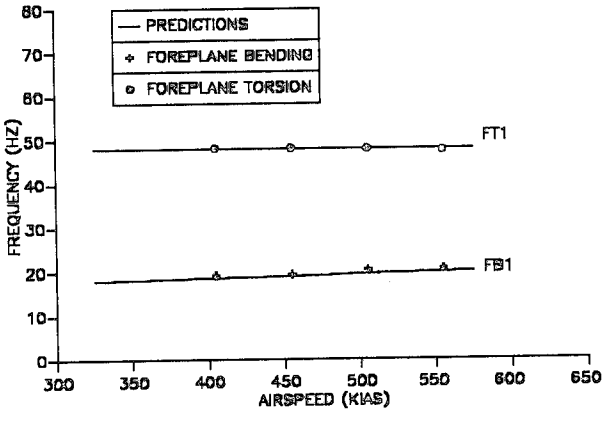

The Evolution of Flight Vehicle System Identification†

Peter G. Hamel and Ravindra V. Jategaonkar
Institut für Flugmechanik
Deutsche Forschungsanstalt für Luft- und Raumfahrt e.V., (DLR)
Lilienthalplatz 7, 38108 Braunschweig, Germany

1. SUMMARY

Aircraft parameter estimation is probably the most outstanding and illustrated example of the system identification methodology, which provides answers to the age-old inverse problem of model determination and validation given a set of observations. After providing a brief account of historical background, the paper traces chronologically the evolution of flight vehicle system identification starting from determination of aircraft frequency and damping ratio from flight data in the early twenties to the present day advanced applications such as estimation of high fidelity aerodynamic data bases for flight simulators or evaluation of highly augmented unstable flight vehicles of unconventional configurations. Through selected examples, it is demonstrated that the system identification methods have reached a maturity level that makes them a powerful and useful tool to support not only research but also industry activity in model validation, handling qualities evaluation, control law design, and flight vehicle design, and thus contribute significantly to risk and cost reduction in the optimal deployment of the existing aircraft and in the development of new generation aircraft. Although the paper focuses mainly on the applications in the area of flight mechanics, some aspects of interdisciplinary flight vehicle modeling, for applications such as aeroservoelasticity or high bandwidth rotorcraft modeling, are addressed as well.

2. HISTORICAL BACKGROUND

System identification, as it is termed today, is a scientific discipline which provides answers to the age-old inverse-problem of obtaining a description in some suitable form for a system given its behaviour as a set of observations. The inverse-problem and, hence, system identification has been fundamental to the evolution of human being, who is characterized by his inquisitive nature not only to know more about the principle underlying (i.e. model formulation of) the process he is observing but also in adequate details (i.e. analysis and parameter estimation).

In a very broad sense, several of the physical laws are outcome of system identification methodology. For example, the inference of the acceleration due to gravity by Newton was an outcome of his exploring an answer to the observation he had made, namely that of a free-falling apple. Although this example may appear less justifying, the roots of the modern system identification can definitely be traced back to the 18th century. In the year 1795, Gauss invented the Least Squares method to compute the orbit of a planet from astronomical observations [1]. Gauss applied Bayes rule and the method of maximum likelihood, as it is called today, to derive the least squares principle.

Although Gauss used the maximum likelihood principle, the earliest reference to it is found in a paper *"The most probable choice between several discrepant observations and the formation therefrom of the most likely induction"* by Bernoulli in the year 1777 [2]. The terms 'likelihood function' and 'maximum likelihood' were not explicitly introduced; also no rigorous proof, a hallmark of today's approach, was provided, but clearly these concepts together with the solution obtained by differentiating the likelihood function were introduced thus providing the foundation for the evolution of the system identification methodology.

Even though the ideas of likelihood function were introduced by Bernoulli and Gauss during the 18th century, the method of maximum likelihood was first introduced as a general statistical parameter estimation method by Fisher in the year 1912 [3]. Until the early forties, much of the work on parameter estimation was deterministic in nature. With the work of Wiener in 1942 and that of Kolmogorov in 1941, however, the focus essentially changed from deterministic to stochastic estimation [4,5]. Following the pioneering work of Wiener, it was in the year 1960 that Kalman provided a recursive solution to filtering problem [6]. The recursive solution being directly amenable to digital computations, the Kalman filter quickly became popular and is today the most widely used approach to stochastic estimation.

It was in the year 1965 that Åström and Bohlin first implemented the maximum likelihood method on a digital computer and applied the same to estimate parameters of an industrial plant based on the difference equation representation [7]. This marked the beginning of the modern era of system identification methodology for which Zadeh had already provided a classical definition in 1962 [8]:

> *"Identification is the determination, on the basis of input and output, of a system within a specified class of systems, to which the system under test is equivalent".*

Today, the fascinating field of system identification covers applications in the areas of biology, chemical processes, economics, geology, materials, mechanical systems, flight vehicles et cetera. A cursory glance at the published literature makes it evident that the aircraft parameter estimation is the most outstanding and illustrated example of system identification methodology.

The highly successful application of system identification to flight vehicle is possible partly due to the advances in measurement techniques and data processing capabilities provided by the digital computers, partly due to the ingenuity of the engineers in advantageously using the devel-

† Interpanel AGARD-FVP contribution

Paper presented at the Structures and Materials Panel Specialists' Meeting on "Advanced Aeroservoelastic Testing and Data Analysis", held in Rotterdam, The Netherlands, from 8-10 May 1995, and published in CP-566.

opments in the other fields like estimation and control theory, and partly due to the fairly well-understood basic physical principles underlying the flight vehicles enabling adequate modeling and possibility of carrying out proper flight tests [9-11]. Today, these tools have reached such a level of maturity that they are an integral part of any aircraft development and assessment program, Fig. 1.

3. PARAMETER ESTIMATION IN FLIGHT MECHANICS

Flight mechanics is that branch of engineering which deals with motion of a flight vehicle. The central issue in flight mechanics is to predict and evaluate the performance and dynamical characteristics of a flight vehicle, be it a conventional transport aircraft, highly augmented unstable aircraft flying at high angles of attack, rotorcraft or missile. Representation of motion of a flight vehicle, which is in general free to move in any direction, involves coupled equations of motion. The basic equations of motion are derived from the Newtonian mechanics, usually considering flight vehicle as a rigid body. These equations, defining the characteristic motion, involve the fundamental assumption that the forces and moments acting on the flight vehicle can be synthesized. Validity and utility of the mathematical models depend to a large degree on the adequacy and accuracy with which these external forces and moments acting on the flight vehicle can be modeled.

Various forces and moments acting on a flight vehicle can be broadly classified into: i) aerodynamic, ii) inertial, iii) gravitational, and iv) propulsive forces. Determination of the aerodynamic forces, the problem recognized in the early 20th century, constitutes the most difficult problem in flight mechanics even today in spite of the significant advances made in the field of modeling. The present challenge to flight vehicle system identification is the determination of an aerodynamic model of high performance, highly augmented vehicle from rapid, large amplitude maneuvers. Such a model is, in general, of unknown structure, highly nonlinear and affected by elastic modes, unsteady aerodynamics and erroneous air data measurements.

The aerodynamic modeling, which provides a means to obtain relationships between the three forces X, Y, Z along the three cartesian coordinates and the three moments L, M, N about these axes as functions of linear translational motion variables u, v, w and rotational rates p, q, r was introduced by Bryan in the early 20th century [12]. This marks the beginning of evolution of flight vehicle system identification. The developments over the last nine decades have led to three different but complementary techniques of determining aerodynamic coefficients, namely i) analytical methods, ii) wind-tunnel methods, and iii) flight test methods.

The first two techniques are employed to generate basic information about the flight mechanical parameters. The analytical estimations, however, have doubtful validity and also have disadvantage of being based on inadequate theory. Nevertheless, computational fluid dynamics have in recent years positively influenced the analytical scenario by providing numerical solutions of total configuration via sophisticated and advanced Euler and Navier-

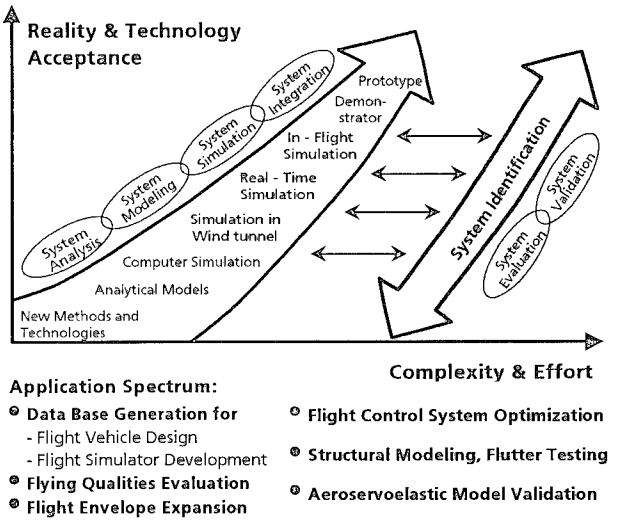

Fig. 1: The key role of system identification

Stokes flow solvers [13,14]. Experimental methods are essential to corroborate the analytical predictions. Wind-tunnel techniques, which are relatively inexpensive, have provided in the past a huge amount of data on innumerable flight vehicle configurations and are, as a rule, a basis for any new design. These techniques are, however, often associated with certain limitations of validity arising out of, for example, model scaling, Reynold's number, dynamic derivatives, cross coupling and aeroservoelasticity effects. Moreover, these measurements could also be affected by tunnel unsteadiness or model support vibrations and interferences. Determination of aerodynamic derivatives from flight test measurements is, therefore, important and necessary to reduce limitations and uncertainties of the aforementioned two methods [15]. It is for this reason that this paper focuses on aircraft parameter estimation from flight data, although the other two techniques have contributed in ample measure to the objective of flight vehicle modeling.

4. ESTIMATION TECHNIQUES OF THE PAST

The importance of obtaining flight derived aircraft parameters was recognized early. A couple of years after introduction of the classical stability approach by Bryan, Glauert's work in 1919 on the analysis of phugoid motion and that of Norton et al during 1919-1923 on estimating a number of derivatives such as (L_p, Y_v, L_v, N_v, M_w) marks the beginning of experimental investigation of dynamic stability in actual flight [16-18]. The interest in dynamic behaviour of aircraft grew steadily over the period. During the late forties and early fifties several techniques were introduced, such as steady-state oscillatory excitations by Milliken [19,20], pulse-input methods incorporating Fourier analysis by Seamans et al [21], and weighted least-squares [22]. Although Shinbrot had introduced during this time the response curve fitting method [23], which is equivalent to the today's output error method, it was then found to be impracticable due to the lack of adequate (digital) computational means. The time-vector method which also became popular during this period of time [24-28], was first applied to analyze the aircraft dynamic stability problem by Doetsch through his familiarity with electrical engineering [27]. The analog matching techniques were also applied

towards the end of this era [29,30]. An excellent account of dynamic stability and control research during this early period is found in Ref. 20 and a survey of methods for determining stability and control derivatives from dynamic flight measurements in Ref. 31. The techniques of the forties to early sixties were frequency response methods, and either limited to estimation of incomplete sets of coefficients, to simple motions, or restricted due to other reasons [32].

The aforementioned sketch of the historical background is, by no means, exhaustive. Nevertheless, in view of the authors, they represent the important milestones in the history of aircraft parameter estimation prior to the advent of digital computers. Nostalgically, a brief account of some of these early methods, which have practically become techniques of the past, is provided here. A brief discussion of these techniques in comparison with the modern methods of system identification may also be found in Refs. 33-34.

4.1 First Dynamic Flight Test

During the investigation of dynamic stability in flight, which had started during 1919-1923 [17,18], flight tests were carried out applying specific control inputs, either generated by the pilot or by some additional device mounted on the aircraft. For example, Norton used a 'step function' generated by dropping sand boxes from the wing tips. In other application, applied known moments were generated by parachutes at the wing tips. It is interesting to point out that the ideas behind applying specific inputs to excite the characteristic aircraft motion for parameter estimation were well appreciated even in those early days. As will be discussed later, the aspect of optimal control inputs is one of four important aspects for successful application of modern system identification techniques (see section 5). The test aircraft JN4 (Fig. 2) on which this pioneering work on dynamic flight testing was carried out at N.A.C.A. is of equal historical importance as the estimates of the damping-in-roll obtained from flight data shown in Fig. 3.

4.2 Longitudinal Oscillation Method

This test technique was first used during the late forties to determine the full-scale aerodynamic stability and control data from flight tests [19,20]. The test procedure consisted of stabilizing the aircraft at a given flight condition and establishing steady-state pitching oscillations of small amplitude at a chosen frequency by applying continuous sinusoidal input to the elevator. Several oscillation cycles, typically five or more, were recorded with the help of a strip-chart recorder or an oscillograph. At the same flight condition, the procedure was repeated typically 25 times for several frequencies up to about 8 rad/s. This sequence was then carried out at different flight conditions.

The recorded data enabled to check between the measured response and the conventional theory in terms of frequency response characteristics. Further analysis or fairing of the experimental response data with the so-called "Circle Diagram" led to determination of the effective damping and spring constants. However, more significantly, the analysis method also provided a means to directly obtain the aerodynamic derivatives, which could then be inserted into the classical equations.

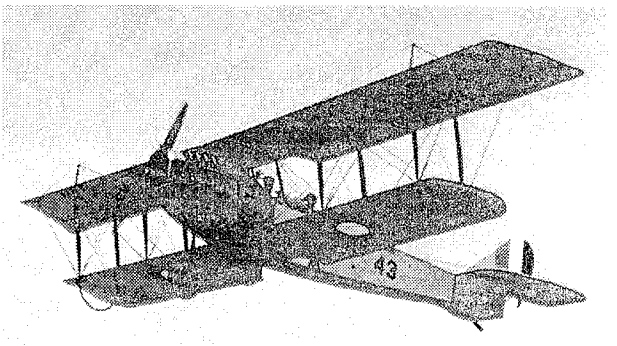

Fig. 2: Test aircraft JN4
(Photo: Courtesy NASA Ames Research Center)

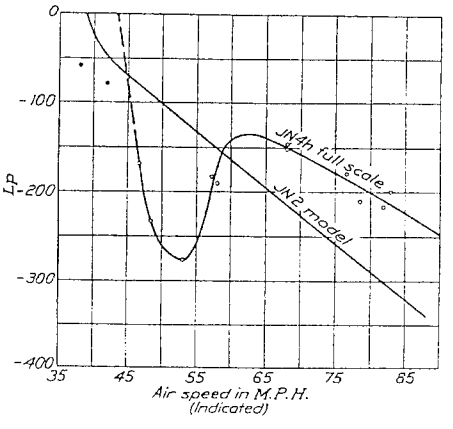

Fig. 3: Damping-in-roll from JN4h flight test
(Reproduced from Ref. 17)

4.3 Pulse Method of Dynamic Response Testing

As an alternative to the time consuming and in some cases undesirable sinusoidal response testing, the transient response method was introduced during the early fifties [21]. The technique was based on the evaluation of performance function, which is the ratio of the Fourier Transform of the aircraft response to that of the input. Approximation of a continuous function by a series of delayed triangular functions provided a convenient means to obtain the necessary information from the oscillograph records. Although an electro-mechanical Fourier Synthesizer was developed at M.I.T., the method was well suited for paper and pencil computation.

4.4 Time-Vector Method

During the fifties and sixties, the Time-Vector method was one of the commonly applied graphical procedures of determining aerodynamic derivatives [25-28]. The test procedure consisted of stabilizing the aircraft at a given flight condition and initiating a free oscillation by an abrupt pulse. With the controls held fixed, the resulting free-oscillation was allowed to damp out. The time-vector decomposition, carried out separately for each moment or force equation, required substituting the amplitude and phase relationships, which were obtained from the locations of the peaks of the oscillatory motion.

To illustrate the method, consider the yawing moment equation:

$$I_Z \dot{r} - I_{XZ} \dot{p} = \bar{q} S b \left(C_{n\beta} \beta + C_{np} pb/2V + C_{nr} rb/2V + C_{n\dot{\beta}} \dot{\beta} b/2V + C_{n\delta r} \delta_r \right) \quad (1)$$

For the free-oscillation portion of the recorded flight data, neglecting the contribution due to the control input, Eq. (1) can be reformulated in terms of the amplitude ratios and phase relations as:

$$\frac{I_Z}{\bar{q}Sb}\frac{|\dot{r}|}{|r|}e^{i\phi_{\dot{r}r}} - \frac{I_{XZ}}{\bar{q}Sb}\frac{|\dot{p}|}{|r|}e^{i\phi_{\dot{p}r}} - C_{np}\frac{b}{2V}\frac{|p|}{|r|}e^{i\phi_{pr}} - C_{n\beta}\frac{|\beta|}{|r|}e^{i\phi_{\beta r}} - (C_{nr} - C_{n\dot{\beta}})\frac{b}{2V}\frac{|r|}{|r|}e^{i\phi_{rr}} = 0 \quad (2)$$

where, for example, $|p|/|r|$ is the amplitude ratio and ϕ_{pr} is the phase angle between the variables p and r. The first two terms on the left hand side of Eq. (2) do not involve any unknown derivative, and assuming that the derivative C_{np} is known, the third term can be computed. Starting from yaw rate, r, the contributions due to these three terms are plotted as shown by solid lines in Fig. 4. The vector polygon satisfying Eq. (2) is now completed based on the other two phase angles. The lengths of these two vectors shown by dotted lines yield the contributions of the last two terms. From the known amplitude ratios $|r|/|r|$ and $|\beta|/|r|$ the unknown parameters $C_{n\beta}$ and $C_{nr} - C_{n\dot{\beta}}$ can now be obtained by simple arithmetic.

The method provided an insight into the comparative contributions of the various terms to the particular mode. It was also amenable in the absence of sideslip angle measurement. It was, however, associated with certain disadvantages: i) as discussed in the above illustration, the method allowed estimation of only two of the three derivatives in the lateral moment equation, ii) as is the case with any graphical procedure, the method was time consuming in generating consistent set of results, and iii) it was difficult to apply it to a heavily damped aircraft.

4.5 Analog Matching

Prior to the advent of digital computers, in the early sixties analog matching was a popular technique of updating and validating wind-tunnel predictions of stability derivatives based on flight tests [29,30]. It provided a means of determining stability derivatives that was simple and straightforward, providing the operator an insight into vehicle response characteristics.

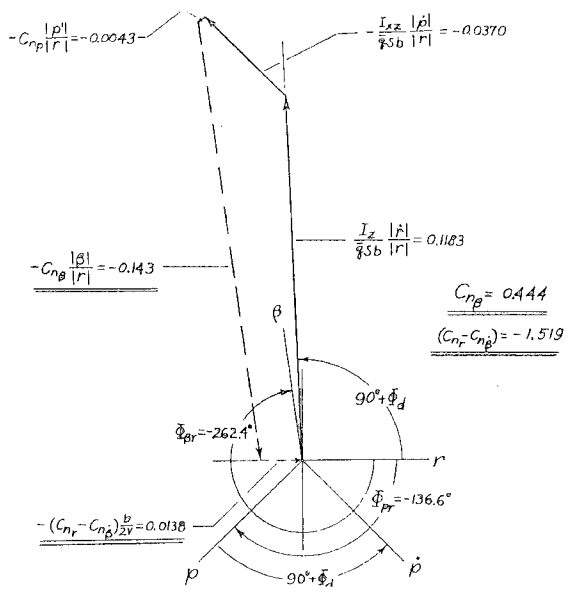

Fig. 4: Time vector diagram for yawing moment (Reproduced from Ref. 28)

To briefly state, mathematical model, in several instances the decoupled equations of aircraft motion, was programmed on an analog computer, incorporating theoretical or wind-tunnel predictions of the stability derivatives as first approximations. The flight recorded control inputs, duplicated through function generators incorporating diodes, amplifiers etc., were fed to the simulation. Comparing qualitatively the simulated response with the actual aircraft response, the stability parameters were manually tuned to reduce the differences.

The analog matching technique, although appealing, had several shortcomings, namely i) the success or failure depended on the ingenuity of the operator in adjusting the proper parameter, ii) time consuming, iii) restricted by the quality of the flight data, iv) involved qualitative judgement of the operator, and v) limited to a few number of primary derivatives.

5. MODERN METHODS OF AIRCRAFT PARAMETER ESTIMATION

The automatic data processing capability provided by the digital computers dramatically changed the focus of the flight data analysis from frequency domain methods to time domain methods. It became possible to obtain significantly more number of stability and control derivatives from a single flight test. A coordinated approach based on the flight test techniques, flight test instrumentation and methods of data analysis gradually evolved for flight vehicle system identification. Research activities at several organizations, like NASA Dryden and Langley RC, US Army Aeroflightdynamics Directorate at NASA Ames RC, USA; Institute of Flight Mechanics, DLR, Germany; NLR and TU-Delft, The Netherlands; DRA, England; NRC, Canada; et cetera, have culminated into the present state of maturity. During this evolution, AGARD played a significant role through dissemination of information, see Appendix 1. Many individuals contributed to the progress, and although it may be unjust to mention a few names, in view of the authors, Fig. 5 provides a retrospective of important contributions during the last three decades.

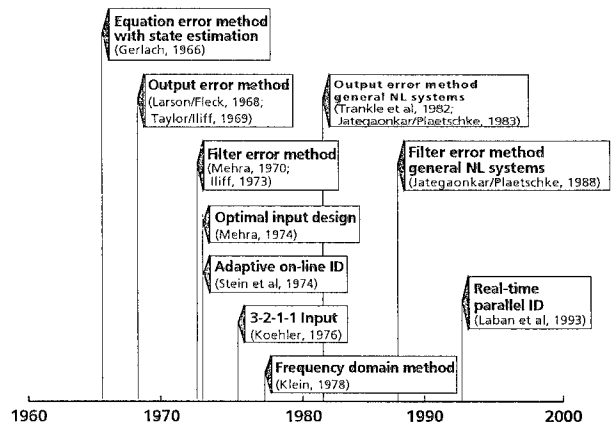

Fig. 5: Retrospective of important first contributions to the advancements of flight vehicle parameter estimation methods

The coordinated approach to flight vehicle system identification can be divided into three major parts [35]:

- **Instrumentation and Filters** which cover the entire flight data acquisition process including adequate instrumentation and airborne or ground-based digital recording equipment. Effects of all kinds of data quality have to be accounted for.

- **Flight Test Techniques** which are related to the selected flight vehicle maneuvering procedures. The input signals have to be optimized in their spectral composition in order to excite all response modes from which parameters are to be estimated.

- **Analysis of Flight Data** which includes the mathematical model of the flight vehicle and an estimation criterion which devises some suitable computational algorithm to adjust some kind of starting values or a priori estimates of the unknown parameters until a set of best parameter estimates is obtained which minimizes the response error.

Corresponding to these strongly interdependent topics, four important aspects of the art and science of system identification have to be carefully treated, Fig. 6.

- Design of the control input shape in order to excite all modes of the vehicle dynamic **motion**.

- Selection of instrumentation and filters for high accuracy **measurements**.

- Type of flight vehicle under investigation in order to define the structure of a possible mathematical **model**.

- Quality of data analysis by selecting the most suitable time or frequency domain identification **method.**

These **"Quad-M"** requirements must be carefully investigated for each flight vehicle from a physical standpoint, and is the key to the successful flight vehicle system identification. These requirements fall within the framework of the contemporarily and widely accepted definition provided by Zadeh [8]. A systematic treatment of these key-issues has been provided by Maine and Iliff [10], Klein [11], Hamel [9], and Mulder et al [36]. A survey of contributions to flight vehicle system identification up to 1980 has been provided by Iliff [33].

6. OPTIMAL INPUT DESIGN

The accuracy and reliability of parameter estimates, obtained applying either the recent modern methods like maximum likelihood or the methods of the past such as forcing function, depend heavily on the amount of information available in the vehicle response. This fact was recognized early during the evolution stages as evident from the Milliken's statement in 1951 [20]:

> *"It would appear that the optimum input in a given case is that which best excites the frequency range of interest, and hence the harmonic content of the input should be examined before the test to ensure that it is suitable".*

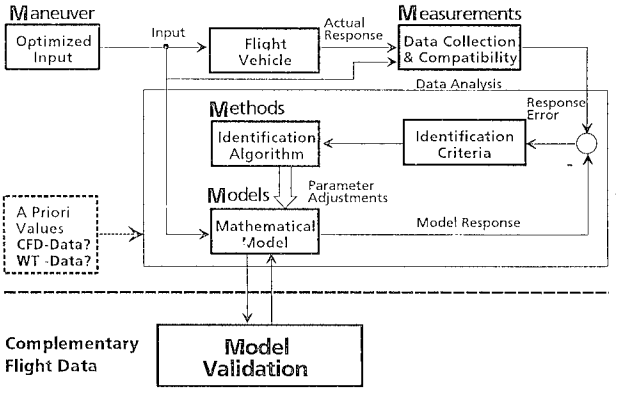

Fig. 6: The Quad-M basics of flight vehicle system identification

Throughout the history of flight vehicle system identification this has been, in essence, the guiding principle in designing a proper flight test maneuver for extracting aerodynamic parameters.

The early developments in the mid-forties and early fifties led to design of input signals such as continuous sinusoidal input, step input, or pulse input. These designs were mainly governed by the method of analysis applied to extract stability and control derivatives from flight data. In the general field of system identification, the theoretical developments on input design were started during the sixties by Levin [37], Litmann and Huggins [38], and Levadi [39]. Around the same time, optimal input design for flight vehicle system identification started with the work of Gerlach [40,41]. In the seventies, Mehra, Gupta, Koehler, et al have significantly contributed to the optimal input design [42-46]. Considering the aircraft as a linear multi-variable system, the inputs were optimized with respect to the information or covariance of the parameters, the design carried out either in time or frequency domain. The work on optimal input signals for aircraft parameter estimation continued in the following decade as well [47-50].

References 48 and 49 provide a thorough comparison of five input signals, namely i) Doublet, ii) Multi-step 3211, iii) Mehra, iv) Schulz, and v) DUT signal. With regard to the accuracy of parameter estimates, it was conclusively established that the 3211, Mehra and DUT signals have the same efficiency. The more recent Langley-input design also compares favourably with these inputs [50]. Fig. 7 shows the 3211 input and its spectrum in comparison to the other two commonly applied input signals. The multi-step input signal developed by Koehler at DLR is, however, easily realizable and relatively easy to fly manually by pilots, see Fig. 8 [9]. In addition, the frequency contents could be readily adapted to match the changing flight conditions.

Although sporadic developments on optimal input design have been reported since then, for example as recently as in 1992 [51], as evident from Table 1, the 3211 signal remains todate as the one most accepted worldwide and utilized by the international flight test community, mainly because of its two aforementioned advantages. An overview on optimal input and maneuver design is also provided by Mulder et al [52].

The frequency sweep test techniques, although rarely used for fixed-wing aircraft, has found renaissance in the field of rotorcraft system identification during the recent past through the work of Tischler and few others [53]. These techniques are useful and necessary not only for the next generation specification requirements [54], but are also an integral part of the interdisciplinary modeling aspects discussed later in this paper (see section 14). Critical flight incidences have, however, occurred while sweep testing due to, for example, exceeding the aeroservoelastic range or the flight permissible maximum loads [55]. Proper coordination is, hence, necessary through careful preparation, buildup, real-time monitoring and analysis to prevent possible structural damage and to avoid any increase in the risk factor.

7. FLIGHT TEST INSTRUMENTATION

The accuracy of the parameter estimates is directly dependent on the quality of the flight measured data, and hence high accuracy measurements of the control inputs and of the motion variables is a pre-requisite for successful application of the modern methods of flight vehicle system identification. Classical information on flight test instrumentation for parameter identification is provided by Wolowicz [30] and also found in, for example, Ref. 56. Furthermore, the V/STOL flight test instrumentation requirements have been described by Hill et al [57]. During the seventies the various aspects of flight test instrumentation have been investigated in detail [58]. The pioneering work carried out at NLR and DUT, The Netherlands, has resulted into a sophisticated level of flight instrumentation. The measurements are further refined through a data pre-processing, generating at the same time any unmeasured flow variables. Based on the high quality data, the subsequent aerodynamic modeling carried out in those institutions is mostly based on the regression analysis, which is the simplest of various parameter estimation methods discussed next. Although, more recently flight instrumentation systems based on commercially available sensors and standard signal processors have been developed, the flight instrumentation is a laborious and time consuming job. In addition, particularly when the full-fledged data gathering for the purpose of high-fidelity flight simulators is desired, more often than not, flight certification of the installed hardware through proper authorities is necessary.

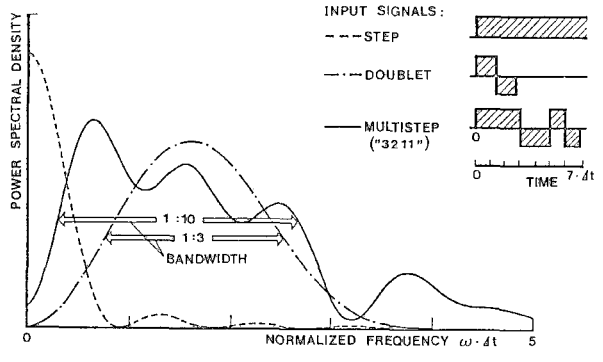

Fig. 7: Frequency domain comparison of input signals

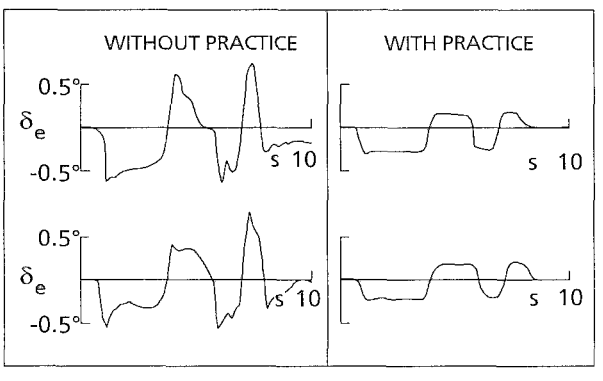

Fig 8: Pilot flown 3211 input signal (CASA C-212)

Period	Flight Vehicle	Organization
Fixed Wing		
1974 - '83	HFB 320 FLISI	DFVLR
1974 - '76	CASA C-212	INTA
1976 - '82	DHC-2 Beaver	DUT / NLR
1978 - '80	Tornado P11	E-61
1980 - '81	Alpha Jet TST	E-61
1980 - '81	CCV F104 G	MBB
1981 - '83	DO-28 TNT	Dornier
1983 - '84	Alpha Jet DSFC	E-61
1984	F-8 DFBW	NASA
1984	A 300-600	AI
1984 - '86	Do-28	TU, BS
1985 - '90	VFW 614 ATTAS	DLR
1987	A 310-300	AI
1987	Cessna Citation 500	NLR
1990	Dash 8 Series 100	NRC
1991	Dash 8 Series 300	NRC
1992 - '93	C160 'Transall'	DLR
1993	Convair VV580	NRC
1990 - '95	X-31A	RI/DASA
1994	Challenger CL601/3	NRC
1994	Gulfstream G IV	NRC
1994	A 300/600 "Beluga"	SATIC
1994 - '95	EF 2000	WTD-61
WT Models		
1980 - '82	Do-28 TNT, OLGA	DFVLR
1980 - '82	DO-28 TNT	IMFL
Rotorcraft		
1977	BO 105 S3	MBB
1978 - '87	BO 105 S123	DFVLR
1980 - '87	BO 105 ATTHeS	DFVLR
1982	UH 60A	US-Army
1983	CH-53 A	US-Army
1983	RSRA	NASA
1985	Bell 206A	NRC
1986	Bell205A-1	NRC
1986	PUMA	RAE
1986 - '87	XV-15	US-Army
1992	Bell 412HP	NRC

Table 1: Application statistics of 3211 input signal

8. METHODS OF DATA ANALYSIS

The various parameter estimation methods can be broadly classified into three categories: i) equation error methods, ii) output error methods, and iii) filter error methods. Choice of a particular method is generally dictated by the model formulation and assumptions made regarding the measurement and process noise, both of which are unavoidable in practical cases. The above three methods belong to a class called "direct approach". The other approach to aircraft parameter estimation is called the "indirect approach" in which a nonlinear filter provides estimates of the unknown parameters which are artificially defined as additional state variables. The equation error methods represent a linear estimation problem whereas the remaining methods belong to a class of nonlinear estimation problems. The equation error and the output error methods are deterministic methods whereas the other two are statistical. More recently the neural network approach to aircraft parameter estimation has also been investigated.

8.1 Equation Error Method

Synthesis of aerodynamic forces and moments acting on a flight vehicle through Taylor series expansion invariably leads to a model that is linear in parameters. To this class of problems, the classical regression techniques can be conveniently applied [11,36,59]. Application of the regression technique requires measurements of the dependent variables, for flight vehicle they are the aerodynamic forces and moments. Though these variables are not directly measurable, they can be computed with relative ease from the measurements of the linear and angular accelerations.

At any instant of the time t_k, the dependent variables, in this case the aerodynamic forces and moments, $y(t)$ can be expressed in terms of the independent variables, $x(t)$, for example the angular rates, flow variables etc., as:

$$y_i(k) = \theta_{i1}\, x_1(k) + \ldots \quad . + \theta_{ir}\, x_r(k) + e_i(k) \tag{3}$$

where e_i denotes the stochastic equation-error, and hence the synonymously used name "equation error method" From N discrete measurements of the dependent and independent variables, for $N>r$ the unknown parameters can be estimated applying the Least-Squares method.

$$\hat{\theta} = \left(X^T X\right)^{-1} X^T Y \tag{4}$$

where θ is the rx1 vector of parameters, Y is the Nx1 vector of measured values of y_i, and X is the Nxr matrix of independent variables. Considering one dependent variable at a time, the parameters of the three aerodynamic forces and three aerodynamic moments acting on the aircraft are estimated separately.

Alternatively, concatenation of the three forces and three moments, which anyway dependent upon the same set of independent variables, namely the aircraft motion variables, Eq. (3) can be extended to the following form:

$$y(k) = \Theta\, x(k) + e(k) \tag{5}$$

Eq. (5) is exactly in the form of an observation equation characterizing a dynamic system in state-space. In this case the parameters for the six dependent variables can as well be estimated simultaneously applying the output error method described in the next subsection.

The main advantage of the regression technique is its simplicity. For a given model structure, the least-squares estimates are obtained with minimal computation in one shot. One of the regression techniques is the stepwise regression. This method, including statistical evaluation of the residuals, is particularly helpful in efficiently arriving at unknown aerodynamic model structure through successive augmentation of the postulated model [60]. Several aspects of model structure determination have been discussed by Hall, Gupta and Tyler [61] and by Klein, Batterson and Murphy [60,62]. Furthermore, since the method does not rely on the temporal relation between the data points, several separate maneuvers can easily be concatenated to estimate a single set of derivatives common to all the time segments [63]. Based on this property, the 'Data Partitioning' approach can be applied to analyze large amplitude maneuver by dividing the maneuver into several smaller portions to which a simplified model can be fitted [11,64,65].

The main disadvantage of the regression method, however, is that in the presence of measurement errors in the independent variables, the least-squares estimates are asymptotically biased, inconsistent and inefficient [59]. Nevertheless this method has found several applications to aircraft parameter estimation, providing acceptable results compared to the more complex methods introduced later in this paper. It is mainly because of two reasons. First, the high quality sensors and instrumentation system minimize these errors. Secondly, prior to applying the regression method, more reliable signals can be generated through a data pre-processing step. The well defined kinematic equations of aircraft motion provide a sound basis for this step, which is often called as flight-path-reconstruction or aircraft state estimation [66-68]. The separation of the state estimation and aerodynamic modeling is called in the literature as Two-Step method [52] or Estimation Before Modeling, EBM [69,70] .

8.2 Output Error Method

The output error method is a nonlinear optimization method which has been most widely used for aircraft parameter estimation ever since its introduction around the seventies. The modified Newton-Raphson method introduced by Taylor and Iliff in 1969 [71] is equivalent to the quasilinearization method applied by Larson and Fleck in the year 1968 [72]. A schematic of the output error method which accounts for measurement noise only is provided in Fig. 9.

The equations of aircraft motion are formulated in state space as:

$$\dot{x}(t) = A(\beta)\, x(t) + B(\beta)\, u(t) + b_x \tag{6a}$$

$$y(t) = C(\beta)\, x(t) + D(\beta)\, u(t) + b_y \tag{6b}$$

$$z(k) = y(k) + v(k) \tag{6c}$$

where x is the state vector, y the observation vector, and u the control input vector. The matrices A, B, C, and D contain the unknown parameters β, which represent the stability and control parameters, and b_x and b_y are the bias terms accounting for the nonzero initial conditions and possible systematic errors in the measurements of output and control variables [73-75].

The estimates of parameter vector $\Theta^T=[\beta^T, b_x^T, b_y^T]$ are obtained by minimizing the cost function [73]:

$$J = \frac{1}{2}\sum_{k=1}^{N}[z(k)-y(k)]^T R^{-1}[z(k)-y(k)] + \frac{N}{2}\ln|R| \qquad (7)$$

where R is the measurement noise covariance matrix. Eq. (7) is the negative logarithm of the likelihood function (probability density of the measurement vector) which, for a given R, reduces to the output error cost function. Starting from suitably specified initial values, the new updated estimates of Θ are obtained applying the Gauss-Newton method [73].

$$\Theta_{i+1} = \Theta_i + \Delta\Theta \qquad (8a)$$

$$\Delta\Theta = \left\{\sum_k \left[\frac{\partial y}{\partial\Theta}(k)\right]^T R^{-1} \frac{\partial y}{\partial\Theta}(k)\right\}^{-1} \left\{\sum_k \left[\frac{\partial y}{\partial\Theta}(k)\right]^T R^{-1}[z(k)-y(k)]\right\} \qquad (8b)$$

where the subscript i indicates the i-th iteration. The first term in braces on the right-hand side of Eq. (8b) is an approximation of the second gradient $\partial^2 J/\partial\Theta^2$ suggested by Balakrishnan [76]. This approximation helps to reduce the computational costs without significantly affecting the convergence [77].

Implementation of the output error method requires computation of the state variables, x, of the response variables, y, and of the response gradients $\partial y/\partial\Theta$ based on the postulated model of Eq. (6). The computational aspects of the maximum likelihood function and of the sensitivities are discussed by Gupta and Mehra [78] and by Maine and Iliff [73]. The state space approach and the matrix representation readily enable computation the of states using the state transition matrix. Computation of the response variables is then a simple matter of plugging the right quantities in Eq. (6b). Computation of the response gradient is little more complex requiring the sensitivity equations $\partial x/\partial\Theta$ and $\partial y/\partial\Theta$ obtained by partial differentiation of the system equations with respect to the unknown parameters. Linear representation facilitates solution of $\partial x/\partial\Theta$ using the same state transition matrix already computed for state variable computations.

8.2.1 Extension of output error method to general nonlinear systems

During the seventies the output error method developed for linear systems became much popular due to its simplicity. A number of estimation software packages were developed the world over [74,75,77,79-82] and applied to a multitude of cases, for bibliography see Ref. 83. During this period the need for estimation of nonlinear aerodynamics was also developing. Logically, it was attempted to extend the then well established output error method for linear systems to nonlinear system as well. The two most commonly adapted approaches were: i) to consider the nonlinear terms in aerodynamic coefficients such as w^2, α^2, ... $\alpha\delta_e$ as pseudo control inputs, computing these prior to estimation and thereby retaining basically the linear system representation [84-87] and ii) augmentation of the state vector with nonlinear terms α^2, $\alpha\delta_e$ using the computed variables, which principally retains the nonlinear equations of motion [88]. The second approach, although more justified, was limited in the scope of application since it often involved modifications in the estimation program for different nonlinear terms considered. In the presence of measurement errors, the first approach of pseudo-control inputs yielded biased estimates. Thus a more complete approach to aircraft parameter estimation based on the use of nonlinear equations of motion and/or aerodynamic model postulates with nonlinear terms was still necessary.

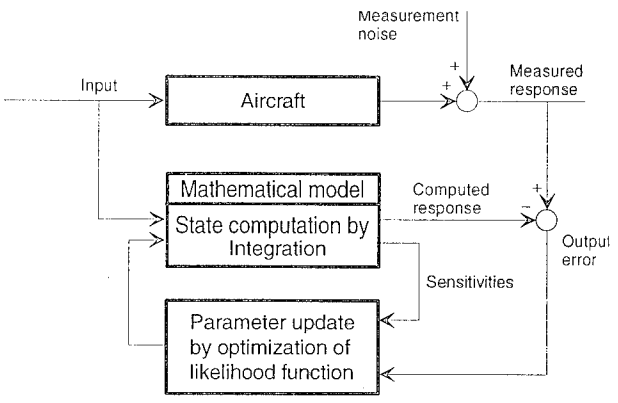

Fig. 9: Schematic of output error method

The difficulty of applying the output error method to nonlinear systems was one of practice. Any time the structure of the postulated nonlinear model was changed, it entailed tedious and laborious algebraic derivation and software implementation of the sensitivity equations. The sensitivity coefficients are essential in the optimization of the cost function. A numerical approach investigated for Levenberg-Marquardt method by Trankle et al [89] and for Modified Newton-Raphson method by Jategaonkar and Plaetschke [90] provided the much needed solution to this general problem during the early eighties.

In a general case, the dynamic system is represented as:

$$\dot{x}(t) = f[x(t), u(t), \Theta] \qquad x(t_0) = x_0 \qquad (9a)$$

$$y(t) = g[x(t), u(t), \Theta] \qquad (9b)$$

where f and g are general nonlinear real valued vector functions. Numerical integration methods, for example a fourth order Runge-Kutta, are now required to compute the state variables. The response gradients are approximated by finite-differences. The procedure is fairly straightforward. Perturbing one parameter at a time, and each time solving the perturbed state equations by numerical integration, the perturbed response variables $y_{pi}(\theta_j)$ are computed. The response gradient for this parameter can be approximated as [90]:

$$\left[\frac{\partial y}{\partial\Theta}(k)\right]_{ij} \approx \frac{y_{pi}(k) - y_i(k)}{\delta\Theta_j} \qquad (10)$$

Concatenation of these response gradients yields the sensitivity matrix. Several estimation packages catering to general nonlinear systems have been since then developed based on the aforesaid approach of numerical-approximation of the sensitivities [91-93]. An alternative approach based on surface fitting is also possible to approximate the sensitivities [94,95]. The Modified New-

ton-Raphson method with numerical approximation of the sensitivities is found to be far more efficient than the derivative free direct search methods [96,97].

8.3 Filter Error Method

Filter error method is the most general stochastic approach to aircraft parameter estimation, which accounts for both process and measurement noise, and was proposed by Balakrishnan [98]. With the pioneering work of Mehra [99-101] and of Iliff [102] during the early seventies, these techniques provided capabilities to estimate aircraft parameters from flight data in turbulent atmosphere, Fig. 10. Several applications have been since then reported [103-106].

The dynamic system is assumed to be described by the following stochastic equations:

$$\dot{x}(t) = A(\beta)\,x(t) + B(\beta)\,u(t) + F\,w(t) + b_x \tag{11a}$$

$$y(t) = C(\beta)\,x(t) + D(\beta)\,u(t) + b_y \tag{11b}$$

$$z(k) = y(k) + G\,v(k) \tag{11c}$$

where w and v represent the process and measurement noise respectively and F and G represent the noise distribution matrices.

In this case, the cost function, Eq. (7), gets modified to:

$$J = \frac{1}{2}\sum_{k=1}^{N}[z(k)-\tilde{y}(k)]^T\,\tilde{R}^{-1}\,[z(k)-\tilde{y}(k)] + \frac{N}{2}\ln|\tilde{R}| \tag{12}$$

where $\tilde{y}$ is the filter predicted observation vector and $\tilde{R}$ is the covariance matrix of the innovations. Computation of $\tilde{y}$ requires the predicted state vector $\tilde{x}$. The Kalman filter, which is an optimal state estimator for linear systems, provides predicted state variables:

$$\tilde{x}(k+1) = \Phi\,\hat{x}(k) + \Psi\,B\,u(k) + \Psi\,b_x \tag{13a}$$

$$\tilde{y}(k) = C\,\tilde{x}(k) + D\,u(k) + b_y \tag{13b}$$

$$\hat{x}(k) = \tilde{x}(k) + K\,[z(k) - \tilde{y}(k)] \tag{13c}$$

where $\tilde{x}$ and $\hat{x}$ denote the predicted and corrected state vectors respectively, K denotes the Kalman filter gain matrix, $[z(k)\text{-}y(k)]$ is the residual (innovation), and Φ and Ψ are the state transition matrix and its integral respectively. In many applications, particularly for time-invariant systems, it is often adequate to use a steady-state filter for state estimation [73]. This simplification results in significant reduction of computational burden. Even under this assumption, computation of the gain matrix K is the complex part of the filter error method.

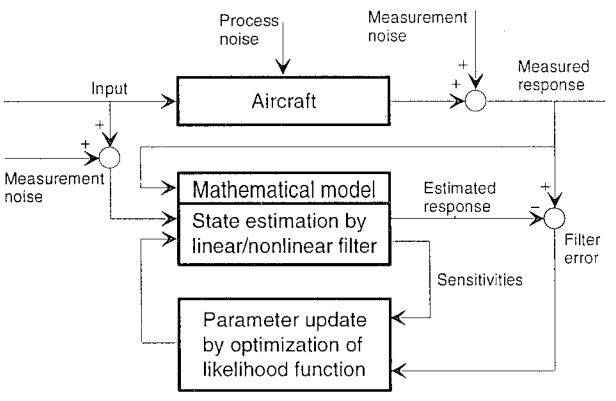

Fig. 10: Schematic of filter error method

Partial differentiation of Eq. (11) yields the sensitivity equations in this case, which can be solved using the same state transition matrix Φ and its integral Ψ. This computation requires computation of the gradient of covariance matrix, which requires solving Lyapunov equations. It would suffice here to mention that in the case of linear systems the Riccati equation and Lyapunov equations can be solved efficiently, although with some computational complexity. The algorithmic details are found in Ref. 105.

8.3.1 Extension of filter error methods to general nonlinear systems

Difficulties of extending the aforesaid filter error method to nonlinear systems are twofold: i) efficiently implementing the computations which provide flexibility to handle conveniently different model structures without software modifications and ii) to derive a suitable filter for nonlinear state estimation. The numerical approach of finite-difference approximation, which was already found to be working efficiently in the case of output error method, can be extended to the filter error method to compute the response gradients. Since optimal filters for nonlinear systems are practically unrealizable, an Extended Kalman Filter based on a first-order approximation of the state and measurement equations can be used for nonlinear filtering; flexibility for different nonlinear model postulates without requiring software programming changes being implicit in the implementation.

Without going into any further detail, it can be stated that the algorithmic development is on the similar lines as that of linear systems. It turns out that the algorithm in this case requires numerical integration of perturbed state equations and additionally the computation of the perturbed gain matrices for each unknown parameter. These extensions proposed and validated by Jategaonkar and Plaetschke are found to work well for practical purposes of estimating stability and control derivatives from flight data in the presence of process and measurement noise [107,108].

8.4 Estimation in Frequency Domain

Although since last three decades the time domain methods have dominated the field of aircraft parameter estimation, there are a few cases, for example rotorcraft identification, in which frequency domain approach demonstrated by Klein may be preferable [109].

Applying the Fourier transformation, the system equations get transformed into:

$$j\omega\,x(\omega) = A(\beta)\,x(\omega) + B(\beta)\,u(\omega) \tag{14a}$$

$$y(\omega) = C(\beta)\,x(\omega) + D(\beta)\,u(\omega) \tag{14b}$$

$$z(\omega_l) = y(\omega_l) + v(\omega_l) \tag{14c}$$

The cost function to be minimized is then given by:

$$J_{FR}=\sum_{l=1}^{M}[z(\omega_l)-y(\omega_l)]^{*}S_{vv}^{-1}[z(\omega_l)-y(\omega_l)]+\log|S_{vv}| \quad (15)$$

where $\omega_l=2\pi l/T$ is the l-th discrete frequency, M is the number of frequencies to be evaluated, and S_{vv} is the spectral density matrix of the measurement noise. Minimization of Eq. (15) by the Gauss-Newton method yields the maximum likelihood estimates of the system parameters. The scope of the frequency domain method has been extended to include non-periodic signals and to enable multi-run evaluation [110,111].

The transformation of system equations into frequency domain leads to a set of algebraic equations, i.e. no integration is involved in frequency-domain. This makes the method suitable for unstable systems for which numerical integration in time-domain leads to numerical divergence problems. Furthermore, without affecting the estimation results the 'zero-frequency' can be neglected in the evaluation, which can be advantageous not only in eliminating the need to account for a large number of bias parameters and thereby drastically reducing the total number of parameters to be estimated but also to overcome the problems of correlation between the bias parameters and the aerodynamic bias terms. For multi-run evaluation, bias parameters often far exceed the number of aerodynamic derivatives. The aforementioned advantages of the frequency-domain method are, however, associated with a substantial disadvantage of the method being applicable to only linear systems.

8.5 Parameter Estimation by Filtering Approach

In this indirect approach the parameter estimation problem is transformed into a state estimation problem by artificially defining the unknown parameters as additional state variables. Considering the constant system parameters Θ as output of an auxiliary dynamic system:

$$\dot{\Theta}=0 \quad (16)$$

and by defining an augmented state vector $x_a^T=[x^T, \Theta^T]$, the extended system can be represented as:

$$\dot{x}_a(t)=\begin{bmatrix} f[x_a(t),u(t)] \\ \hline 0 \end{bmatrix}+\left[\begin{array}{c|c} F & 0 \\ \hline 0 & 0 \end{array}\right]\begin{bmatrix} w(t) \\ \hline 0 \end{bmatrix} \quad (17a)$$

$$y(t)=g[x_a(t),u(t)] \quad (17b)$$

$$z(k)=y(k)+v(k) \quad (17c)$$

The Extended Kalman Filter yields the solution to this combined state and parameter estimation problem [112]. As in the case of filter error methods for nonlinear systems, a numerical approach to compute the first order system matrices leads to a flexible software which can be easily applied to general nonlinear systems [108].

The filtering approach to identification of aerodynamic derivatives was introduced at Calspan [84,113], but is only seldom used, mainly because the performance strongly depends upon the statistics of the measurement and process noise, i.e. on the covariance matrices, which are in general unknown. The approach is, however, well suited for on-line application [114] and applicable to unstable systems as well. It has found some application with renewed interest in the very recent [115,116].

Recognizing early the need for adequate analytical tools for analysis of flight data from flight vehicles of increasing complexity, as a long term perspective the research and development work on aircraft parameter estimation was initiated at the DLR Institute of Flight Mechanics in the early seventies. In the eighties this developmental work was pursued jointly with the special research project SFB-212 of the Technical University, Braunschweig. This collaborative effort has resulted in several extensively tested and validated estimation algorithms, see Table 2, providing a sound foundation for advanced applications of aerodynamic modeling.

Methods	Time domain						Frequency domain	
	ML Output error (*)		ML Filter error			State augmentation	Output error	Filter error
DLR Software code	LINHP7	NLHP1L	KALML7	NLKAL (†)	MLEKF	XAEKF	PIFREQ	PIFRFF
Linear systems	☺	☺	☺	☺	☺	☺	☺	☺
Nonlinear systems		☺		☺	☺	☺		
Measurement noise	☺	☺	☺	☺	☺	P	☺	☺
Process noise			☺	☺	P	P		☺
Multi-run evaluation	☺	☺	☺				☺	
Time delays		☺		☺			☺	☺
Unstable systems	☺	☺	☺	☺	☺	☺	☺	☺

☺ : Features available; P : Pre-definition of covariances required.
* : Optionally enables least-squares estimation.
† : Optionally enables output-error and least squares estimation.

Table 2: Summary of aircraft parameter estimation programs

8.6 Neural Network Based Methods

Artificial neural network (ANN), sometimes called as perceptron, is an information processing system which can be made to learn through examples, and can be adopted thereafter for other purposes such as prediction. Through a flexible set of basic functions, also called hidden units, nodes or neurons, having certain properties the ANNs provide a means of nonlinear-mapping the given input-output subspace, and thus provide an overall characterization of a system. There are two types of networks which have found some application in aircraft identification. They are: i) Feed Forward Neural Network and ii) Recurrent Neural Network [117-119].

The feed forward neural network is, as implied by the name, characterized by the unidirectional flow of the signals. Typically, it contains a number of hidden layers between the input and output layers. The input and output layers define the given data subspace which is to be modeled, Fig. 11. In the context of estimation of aerodynamic coefficients, the input variables are typically the variables pertaining to the aircraft motion such as angle of attack, angle of sideslip, or angular rates, and the control inputs exciting the aircraft motion. The output variables are the aerodynamic force and moment coefficients. The size of the neural network is determined by the number of hidden layers and by the number of nodes in each layer, the nodes in the input and output layers being fixed through the data subspace being modeled. The weights or parameters of the network, defining the forward and cross connectivities, are estimated by back propagation method [120,121]. In contrast to the conventional approach of aircraft parameter estimation based on the well understood basic principles underlying the aircraft dynamics and aerodynamic forces and moments, the neural network approach leads to a black-box model to which no physical significance can be attributed, either to the structure or to the weights [121-124].

In contrast to the feed forward neural network in which the nodes represent some neural variables, in the recurrent neural network the outputs of the nodes represent the unknown parameters of the dynamic system. The outputs of the nodes are some nonlinear function of the internal states of the network, which are evolved in time through differential equation describing dynamics of the network. The recurrent neural network has a fixed number of mutually connected nodes equal to the number of

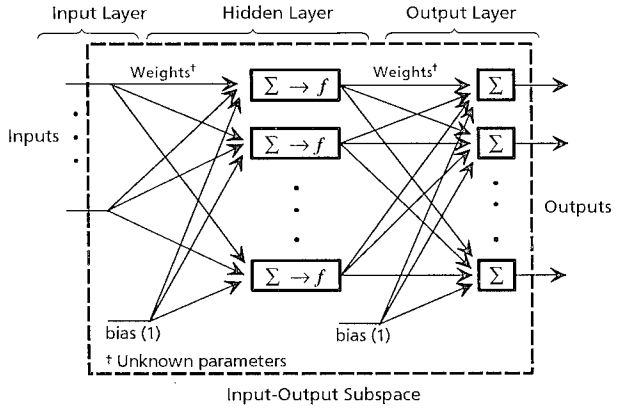

Fig. 11: Feed forward neural network with one hidden layer

unknown parameters of the postulated state space model [119]. Conceptually, the recurrent neural network can be compared with the Extended Kalman Filter in which the unknown system parameters are propagated in time by defining them as additional states, see section 8.5.

Although the recurrent neural network is amenable to state space models, its performance is found to critically depend upon tuning of the sigmoid nonlinearity which can, at best, be carried out on heuristic basis. It is partly due to this reason and partly due to the fixed structure of the network that the applicability of the recurrent neural network to practical cases of aircraft identification is very limited in scope [119]. From this viewpoint, the feed forward neural networks, although leading to a black-box model structure without physical interpretation of the estimated weights, may prove to be more flexible and may have somewhat wider application than the recurrent neural networks.

9. MODEL VALIDATION

As depicted in Fig. 6 the parameter estimation and the model validation are an integral part of system identification. The parameter estimation methods provide an answer to the question:

"Given the system responses, what is the model?"

whereas model validation tries provide an answer to the related question:

"How do you know that you got the right answer?".

Several criteria, to be used in conjunction with each other, help to validate the model: i) standard deviations of the estimates (i.e. estimation uncertainties in terms of Cramer-Rao bounds), ii) goodness of fit (i.e. value of the cost function being minimized, for example, the determinant of the covariance matrix of the residuals), iii) correlation coefficients among the estimates, iv) plausibility of the estimates from physical understanding of the system under investigation or by comparison with other predictions such as wind-tunnel or analytical methods, and v) model predictive capability.

The predictive capability of the identified model is determined by comparing the flight measured responses with those predicted by the model for the same control inputs. In this proof-of-match process, the aerodynamic model is kept fixed. The initial conditions have to be suitably adjusted to match the flight conditions being tested. The flight maneuvers used for model validation are, as a general rule, not used in estimating the aerodynamic model. The complementary flight data, often called as validation test data, for which the model predictive capability has to be demonstrated is an important part of the flight simulator certification and acceptance.

To eliminate the subjective evaluation, the FAA (Federal Aviation Administration) has specified guidelines in terms of the tolerance values for each variable depending upon the nature of the validation test [125]. For example, in the case of short period dynamics, the tolerances are $\pm 2°/s$ for the pitch rate, $\pm 1.5°$ for the pitch attitude, and $\pm 0.1\ g$ for the vertical acceleration. For the roll response

the tolerances are ±2°/s for roll rate and ±2° for bank angle. The flight measurements with these tolerances define a band within which the model predicted response must lie to meet the specified accuracy requirement. Although majority of the validation tests are verified in time domain either through time histories or in terms of period and damping ratios of the oscillatory modes such as phugoid or dutch roll, it is also possible to extend the verification to frequency domain, which may bring out more clearly the range of applicability of the identified model. This is particularly important for high authority flight control systems or in cases where aeroservoelastic effects may be dominant.

10. PRACTICAL UTILITY OF FILTER ERROR METHODS

For flight data gathered in turbulence the filter error methods are inevitable, since the output error method is known to yield biased estimates in the presence of atmospheric turbulence [11,73]. Even in the case of flight maneuvers in smooth air, the filter error method could lead to better estimation results, since some of the unavoidable modeling errors are then treated as process noise characterized by low frequency contents rather than as measurement noise [105]. Moreover, although it is generally argued that the flight tests for aircraft parameter estimation could be carried out in calm air, in any practical exercise one has no control over the prevailing atmospheric conditions or due to very tight time schedules and due to cost factors involved in a time-bound project very little choice of waiting for steady atmospheric conditions.

As a typical example, the estimates of the weathercock stability, derivative C_{n_β}, obtained by applying the output error and the filter error method to the same set of flight data are provided in Fig. 12 [126]. The C-160 data analyzed here was gathered from eight flights carried out during a span of less than two weeks, the seven of them being in seemingly steady atmosphere whereas one encountered moderate amount of turbulence. It is clearly visible that the estimates provided by the output error method, particularly those for flight 223 during which moderate turbulence was encountered, differ much from those for other flights at same nominal flight conditions. Moreover, a fair amount of scatter is observed in the estimates from other flights in seemingly steady atmosphere making the final conclusion regarding the nature of the nonlinearity or fairing of data difficult. On the other hand, the filter error method yields clearly grouped estimates with much less scatter and the estimates from flight 223 match well with the other estimates. The nonlinear dependency of the weathercock stability on the angle of attack is now to be observed much better.

Another example for which the estimation methods accounting for process noise are essential pertains to X-31A identification. At high angles of attack, the forebody vortices, which are shed stochastically from the aircraft nose, act as process noise exciting randomly the lateral-directional motion. The results presented later in this paper demonstrate that the filter error method was well suited for this application, whereas the output error method provided estimation results which could not be completely resolved.

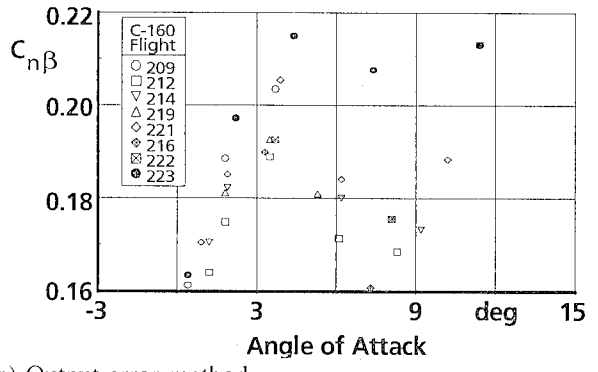

a) Output error method

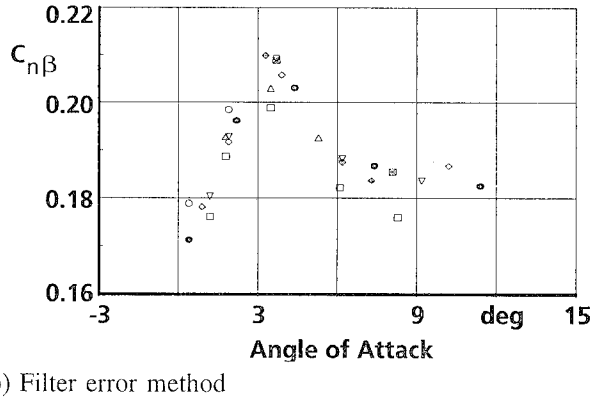

b) Filter error method

Fig. 12: Flight estimates of weathercock stability

The filter error method, due to its formulation, contains a feedback proportional to the fit error. This feedback stabilizes numerically the filter error algorithm and also helps to improve the convergence properties. The stabilizing property of the filter error algorithm, as will be discussed in this paper subsequently, makes it suitable for open-loop identification of unstable aircraft.

These few selected typical examples provide an answer to the question often raised regarding the practical utility of the filter error method. It can be pragmatically concluded that these method can yield better estimates, are no more limited to linear systems, and are indispensable for many future applications such as high angle of attack identification or to unstable aircraft. These advantages outweigh the disadvantage of higher computational overheads. Even in such a case it needs to be reminded that in any exercise on parameter estimation the actual cpu-time is only a minor part of the total time, the major part being consumed by mundane tasks such as checking of flight data, collecting and analyzing the results, and generating plots et cetera.

11. UNSTABLE AIRCRAFT IDENTIFICATION

The demands of high performance characteristics have led to aerodynamically unstable aircraft configurations. Although unstable aircraft can be flown only with the aid of a flight controller, i.e., in closed loop, the determination of aerodynamic characteristics of the basic unstable aircraft, i.e., of the open-loop plant, is of primary interest in several instances.

The simplest approach to identification of unstable aircraft is to use linear regression in the time domain or as

already mentioned, the maximum-likelihood method in the frequency domain. Application of the other time-domain methods to such cases, however, needs some consideration. The most widely used output error method in this case encounters numerical difficulties of diverging solution. Some special techniques and modifications are, hence, necessary to prevent the growth of errors introduced by poor initial values, round-off or discretization and propagated by inherent instabilities of the system equations. Several solution such as: i) S-plane transformation [127], ii) output error method with artificial stabilization [128,129], iii) equation decoupling [130], and iv) a relatively new approach called multiple-shooting based on efficient techniques for the solution of two-point boundary value problems are possible [131]. These approaches, although provided solutions in particular cases, were either found to involve engineering judgement, or require considerable effort or the results could not be completely resolved [131]. On the other hand, the filter error method having the stabilizing property due to its formulation and the regression method appear to be more readily applicable to unstable aircraft. The filter error method may have some advantages, particularly in the presence of considerable measurement noise in which case the regression analysis yields biased estimates. In any case, a method which accounts for process noise is preferable, since the controller feeds back the measured variables containing measurement noise, and thereby introduces a component of stochastic input.

Apart from the choice of a suitable method, yet another serious difficulty encountered in the unstable aircraft identification is that of parameter identifiability. The controller tends to suppress the oscillatory and transient motion. This is what the controller is anyway designed for. It is, however, detrimental to the identifiability and accuracy of the parameter-estimates, since the information contend in the data is drastically reduced. Furthermore, the feedback results in correlated inputs and also correlated motion variables. The combined solution to both these problems is to introduce controlled inputs directly deflecting the control surfaces. This is often called in the literature as Separate Surface Excitation.

As a typical example, Fig 13 shows the estimates of the canard control effectiveness obtained from the X-31A flight test data for two cases, namely the pilot input maneuvers and the separate surface excitation [65]. As evident from Fig. 13a, the pilot input maneuvers yield estimates with a large standard deviations and moreover the scatter is also large. This is definitely attributed to the aforementioned difficulties of insufficient information content and of correlated variables. On the other hand, the separate surface excitation maneuvers yield well identifiable estimates, Fig. 13b.

As demonstrated, the separate surface excitation eliminates the problems due to the correlated inputs and correlated motion variables. The separate surface excitation is, however, a complex procedure requiring hardware modifications and often flight certification. The alternative approach would be to attempt parameter-estimation based on data-collinearity and biased estimation [11,132].

Although the aspects of parameter identifiability and data-collinearity have been discussed in the context of

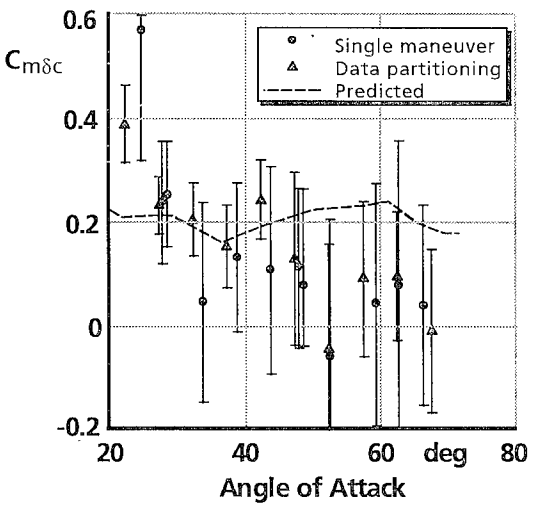

a) Pilot input maneuvers

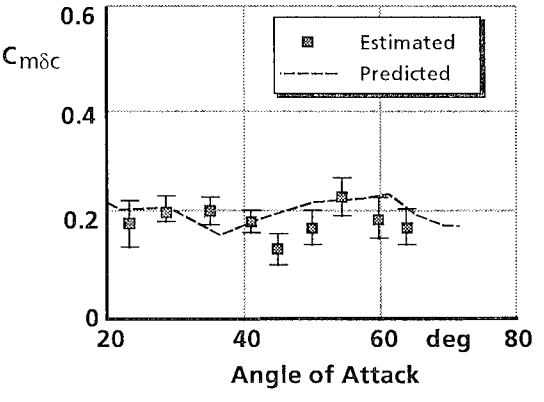

b) Separate surface excitation maneuvers

Fig. 13: Estimates of canard control effectiveness from X-31A flight data

unstable aircraft, these issues are equally applicable to stable aircraft as well.

Identification of open-loop unstable aircraft via closed-loop identification, although feasible, is rather impractical. From such an attempt, to obtain the open-loop parameters of the basic aircraft, it would require incorporating the models for the controller and actuator dynamics in the estimation procedure. The overall system being stable, any standard parameter estimation method can be applied without encountering any serious difficulty. With the current state of the art, even the increased model size should not be a serious problem. The primary difficulty is to obtain the exact models for the complex control laws containing discrete nonlinearities, and that the actuator performance and controller gains may be flight dependent. Moreover, this approach may result in open-loop parameter estimates with low accuracy.

12. ON-LINE AIRCRAFT IDENTIFICATION

The primary motivation for on-line identification is adaptive control, although other minor benefits can also be derived from the immediate knowledge of the aircraft model. The adaptive control investigations in flight on the X-15 aircraft dates back to 1971 [133], which were

based on the concepts of analogue computation. The modern methods of parameter estimation were investigated by Stein et al and others during the year 1977 for adaptive control of F-8 DFBW aircraft [134]. The scope of identification was then restricted mainly to a sub set of aircraft parameters from decoupled and simplified equations of aircraft motion. Recently, based on parallel processing Laban and Mulder have successfully extended the on-line identification capabilities to a complete set of aerodynamic derivatives during the flight [34,135]. In other investigations the near real time approach has been adopted to check the simulation accuracy and for flight test planning purposes [136,137].

13. SELECTED EXAMPLES OF FLIGHT VEHICLE SYSTEM IDENTIFICATION

Few selected applications presented in this paper pertain to determination of aerodynamic data bases for high-fidelity simulators, verification of stability and control characteristics of a commercial transport aircraft, identification of highly augmented unstable flight vehicle, and high bandwidth rotorcraft modeling.

13.1 Aerodynamic Data Bases for High-Fidelity Flight Simulators

Prior to the advent of digital computers, the accuracy of aircraft simulation was marginal due to the inherent limitations of analog computers. The development of digital computers opened up new horizons not only in the field of aircraft parameter estimation but also in the field of flight simulators [138]. With the evolution of high performance modern aircraft and with the spiralling developmental and experimental costs, the importance of ground-based flight simulators and that of in-flight simulators has increased significantly in the recent past. Simulators are increasingly used not only for pilot training but also for other applications such as flight planning, envelope expansion, design and analysis of control laws, handling qualities investigations, and pilot-in-the-loop studies. Many of these applications demand a high-fidelity flight simulator. It is generally known that the fidelity of a simulation depends to a large extent on the accuracy of the mathematical model and of the aerodynamic data base representing the flight vehicle.

Although validation and update of aerodynamic data bases derived from analytical predictions and wind-tunnel measurements through flight test is a viable approach [139], such updates are possible only through repetitive procedure involving considerable engineering judgements. Moreover, incremental modifications of aerodynamic predictions may not lead to a homogeneous data base. On the other hand, system-identification methodology provides an alternative and efficient approach to derive flight validated data base covering the entire operational flight envelope [140-143].

Estimation of a comprehensive aerodynamic model suitable for a flight simulator is an iterative process, which starts with point-identification at all the points flight tested. Point-identification results in a model related to specific trim conditions. Based on this bulk of the estimation results, the aerodynamic model postulates can be extended to include angle of attack or Mach number dependencies, coupling derivatives, and nonlinearities. Through multi-point-identification several flight conditions can be analyzed simultaneously to arrive at comprehensive model. This general approach is followed in both the examples presented below.

13.1.1 Aerodynamic data base for ATTAS In-flight simulator

The research aircraft ATTAS, Fig. 14, is an in-flight simulator of the DLR. A comprehensive flight test program covering the fly-by-wire operational envelope was carried out to enable identification of both the aerodynamics and the actuation systems.

As a typical example of aerodynamic model identification, the flight estimates of the lift due to the Direct-Lift-Control (DLC) flaps are shown in Fig. 15. It is found that they are somewhat less effective than designed for, the difference being pronounced for larger positive, i.e. the downward, deflections. Even for relatively smaller deflections of 10-15°, the influence of flow separation is evident, particularly for the landing flap of 14°. Moreover, apart from the static characteristics shown in Fig. 15, the transient effects of the downwash generated by the DLC-flaps due to the dynamic motion has a considerable influence on the aircraft pitching motion (not shown here), both for small and large deflections [144].

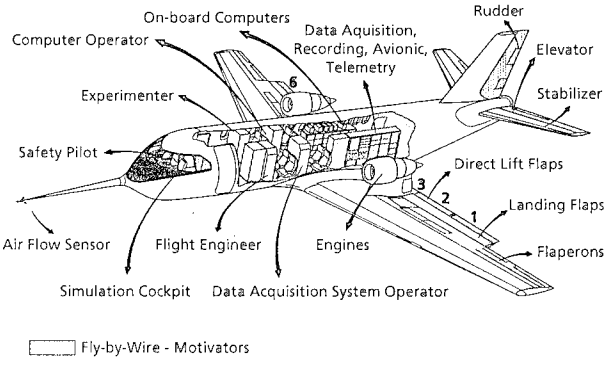

Fig. 14: ATTAS In-flight simulator

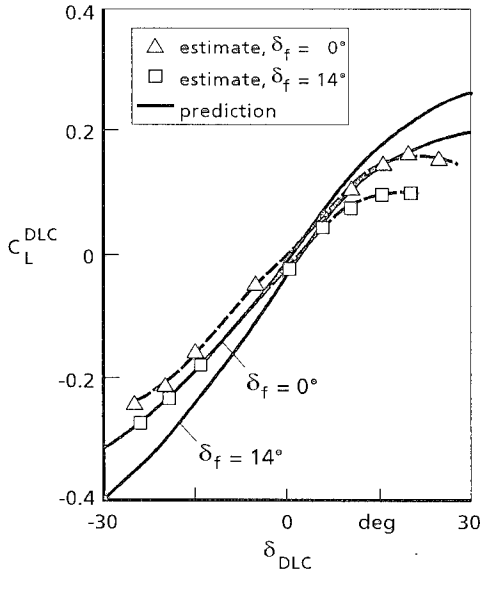

Fig. 15: Estimates of DLC-flap effectiveness

It was also found that the wind-tunnel predictions of the pitch damping and roll damping derivatives are comparable to the flight estimates. On the other hand, the identification results from flight data analysis indicate that the sidewash effect (derivative C_{n_β}), the effect which was not accounted for in the wind-tunnel predictions, contributes significantly to the dutch roll damping [145].

The identification results indicate that the DLC flap actuation system can be adequately modeled by a second order system with rate and displacement limitation, see Fig. 16. The possible maximum deflection is limited and depends upon the landing flap position and aerodynamic loads acting on the aircraft, see Fig. 17.

13.1.2 Aerodynamic data base for C-160 flight simulator

The C-160 "Transall" is a military transport aircraft capable of carrying troops, casualties, freight, supplies, and vehicles, and serves the needs of the German as well as French Air Force. To meet the current demands of improved pilot training at reduced cost and increased safety, as well as of optimal deployment of existing fleet of aircraft, a modern high performance flight simulator was required by the German Air Force. Although the wind-tunnel measurements of the "Transall", made in the sixties, are still available, this wind-tunnel generated data base was found to be unsuitable for a flight simulator which has to meet the Level D quality standards specified by the FAA.

The complete Data Gathering program, carried out with the instrumented aircraft, Fig. 18, consisted of flight tests for: i) Calibration of air data system, ii) Estimation of aerodynamic data base, iii) Ground tests (taxiing, ground acceleration/deceleration, stopping distances), iv) Validation tests for simulator certification and approval according to FAA guidelines, v) Sound data, vi) C-160 specific operational characteristics (load drop, landing and takeoff on unprepared terrain and short field, single engine flights), and vii) stall dynamics. Altogether 28 flights were carried out, totalling to a flight test time of 79 hours. A total of 350 trim conditions and 964 system-identification maneuvers including 22 stall maneuvers were investigated covering altitudes upto 26000 *ft* and Mach numbers upto 0.52. Test points were judiciously chosen to span the entire operational envelope and possible configurations: i) Clean configuration (η_K = 0°, nominal CG of 28% MAC), ii) Landing flaps (η_K = 20°, 30°, 40°, 60°), iii) CG locations (forward 23%, nominal 28%, and aft 33% MAC), iv) Landing gear, v) Ramp door, and vi) Single engine.

A detailed description of aerodynamic modeling and of all other pertaining issues is found in Refs. [142,146-149]. For illustration purposes, the estimates of the dihedral effect, derivative C_{l_β}, obtained by point-identification are shown for four landing flap positions in Fig. 19. The estimates are clearly a function of angle of attack and also of landing flap. The multi-point identification results are also shown in the same figure [142].

From the quasi-steady and dynamic stall maneuvers an unsteady aerodynamic model for high-lift including flow separation and stall was identified. Based on the Kirchhoff's

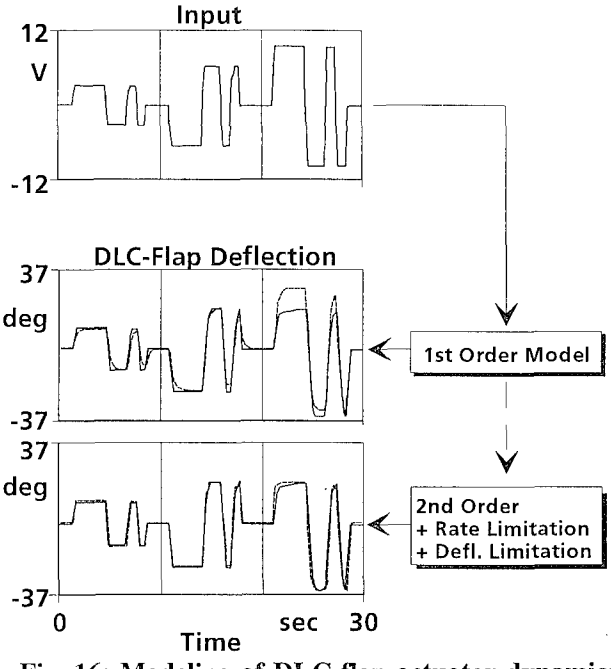

Fig. 16: Modeling of DLC-flap actuator dynamics
(——— measured, ------- estimated)

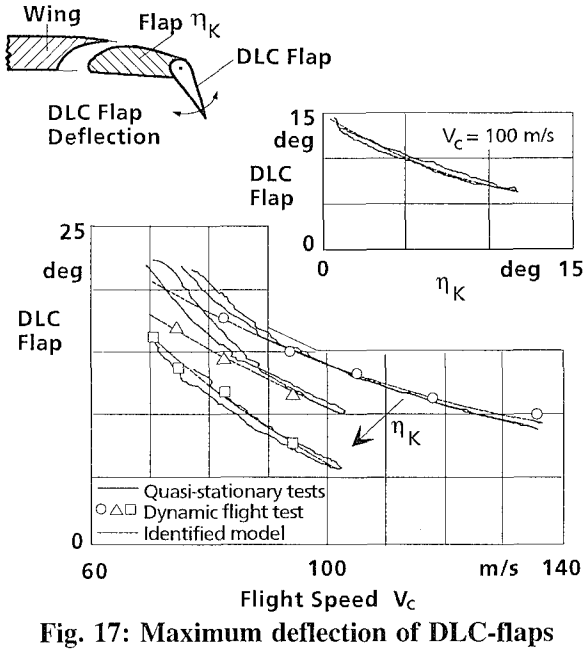

Fig. 17: Maximum deflection of DLC-flaps

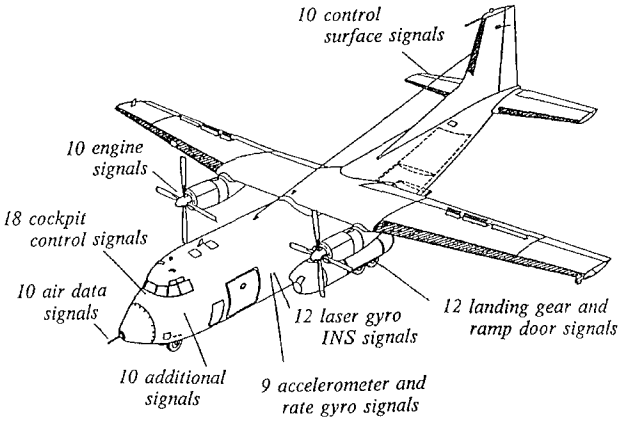

Fig. 18: Instrumented C-160 "Transall"

theory of flow separation, the wing lift can be modeled as a function of angle of attack and flow separation point X [150,151].

$$C_L(\alpha, X) = C_{L\alpha} \left\{\left(1+\sqrt{x}\right)/2\right\}^2 \alpha \qquad (18)$$

Based on an approximation of the Wagner or Theodorson function [152,153], the time-dependent flow separation point can be expressed as:

$$\tau_1 \frac{dX}{dt} + X = X_0(\alpha - \tau_2 \dot{\alpha}) \qquad (19)$$

The steady flow separation point, X_0, may be determined from static wind-tunnel tests or can also be identified from the flight tests from the approximation:

$$X_0 = 1/2 \left\{1 - \tanh[a_1(\alpha - \alpha*)]\right\} \qquad (20)$$

The model in terms of the two parameters (a_1, α^*) appearing in Eq. (20) and two time constants appearing in Eq. (19) yields the identified lift coefficient and the separation point shown in Fig. 20 [151].

Simulation of aircraft takeoff and landing is yet another complex modeling aspect which requires combining of aerodynamic model, ground effects, and ground handling model. In addition, at low altitudes the aircraft performance is severely affected by the wind. In such cases it is essential not only to account for the constant wind but also for the wind profile [149].

The parameter estimation techniques were also applied to identify the ground effects, which have a dominant influence on the landing and takeoff performance. In general, it is known that three main effects of the ground effect are: a reduced downwash angle at the tail, an increase in the wing-body lift curve slope, and an increase in the tail lift curve slope. Fig. 21 shows the identified ground-effect parameters as a function of ratio of aircraft altitude to wing span (h/b) and landing flap deflection η_K. A linear model was found adequate to model the flight performance, since the altitudes for which the ground effect changes nonlinearly, ($h<\bar{c}$), are not reached for the top-wing configuration [149].

The accuracy of the flight derived aerodynamic data base is verified through predictive capability of the identified model. Typical results are presented in Fig. 22 for the short period dynamics. The model predicted responses shown by solid lines are well within the specified band obtained from the flight measurement plus/minus the tolerances defined by the FAA. For the same maneuver, the validation in frequency domain is shown in Fig. 23. Matching of the long period phugoid dynamics, which has to complete three full cycles of oscillation is one of a more difficult task [154]. Even this objective was achieved within the margins specified for frequency and damping terms. As evident from Fig. 24 pertaining to the validation test for stall maneuver, the identified model yields acceptable match. For the same maneuver, neglecting the unsteady aerodynamic effects leads to discernible deviations in the response match, see Fig. 24a. The model predictive capability in terms of plots such as Fig. 22 is often referred to in the flight simulator context as the proof-of-match data. It demonstrates the suitability of the identified data base for a flight simulator which has to meet the standards specified by the regulatory authorities, in the present case Level D.

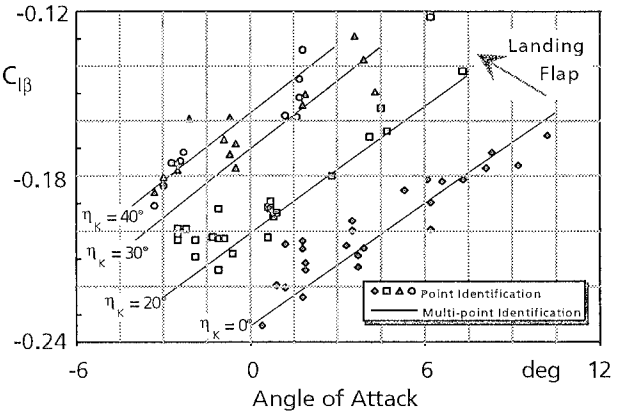

Fig. 19: Flight estimates of dihedral effect

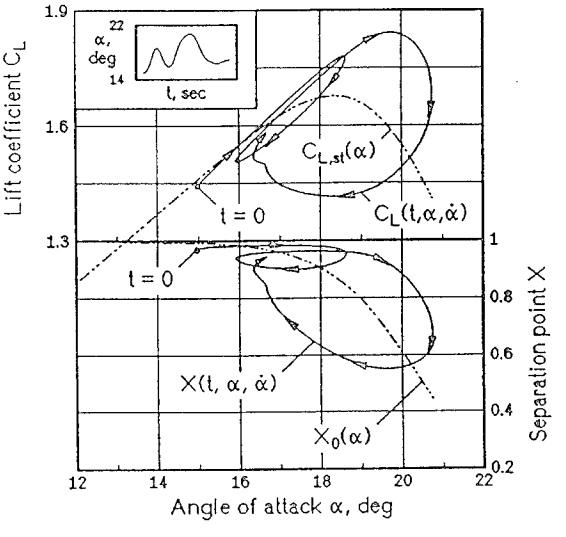

Fig. 20: Estimated lift coefficient and flow separation point

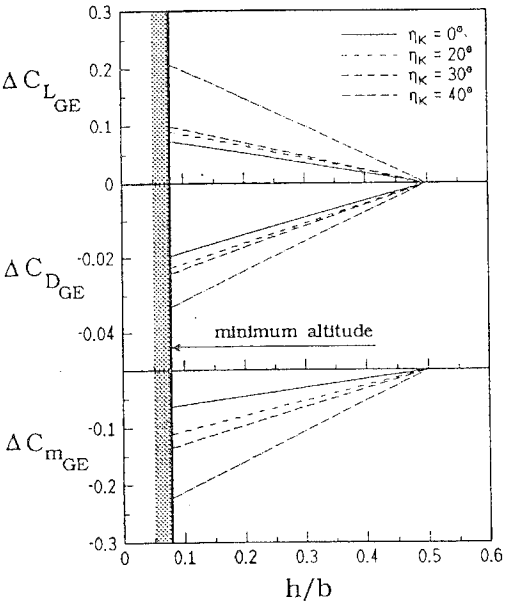

Fig. 21: Estimated ground effect (GE)

Starting from specification of a flight instrumentation system, calibration and certification of the installed hardware, proposing and carrying out the flight test program, analysing the huge amount of flight data, generating the aerodynamic characteristics valid over the entire operational envelope, and providing the simulator manufacturer with appropriate documentation, the complete Data Gathering project was carried out successfully within a short period of about 13 months. The broad spectrum of C-160 system identification results demonstrate in ample measure that the system identification methods have reached a maturity level, which enables to generate homogeneous data bases suitable for high quality flight simulators. Such applications, under the severe constraints of time put by the industry, however, demand dedicated efforts from a group of engineers and are possible only through a team work.

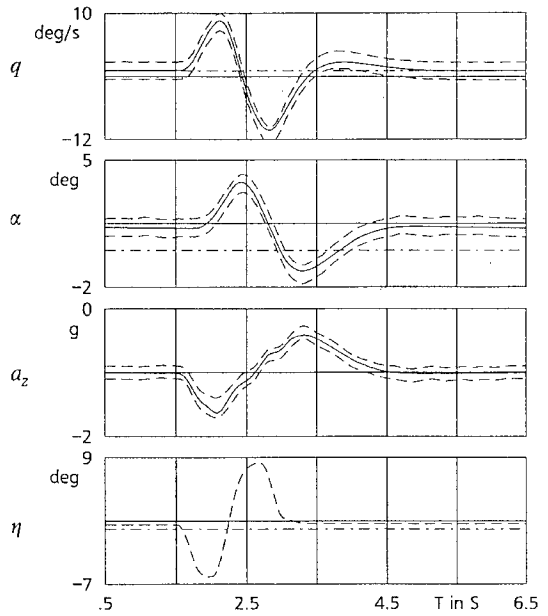

Fig. 22: Proof-of-Match for short period dynamics
(- - - - - measured ± tolerance; ———— estimated)

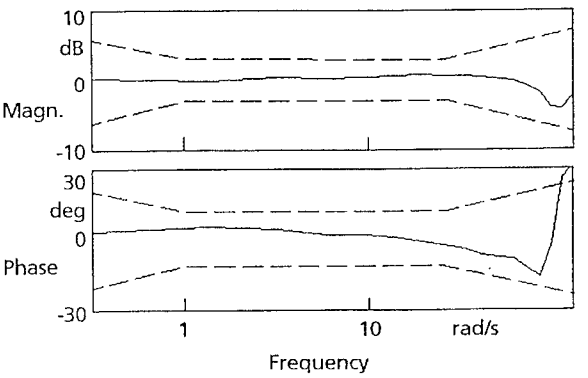

Fig. 23: Proof-of-Match in frequency domain for pitch rate (short period dynamics)
(- - - - tolerance band of unnoticeable dynamic effects; ———— $q_{estimated}$ / $q_{measured}$)

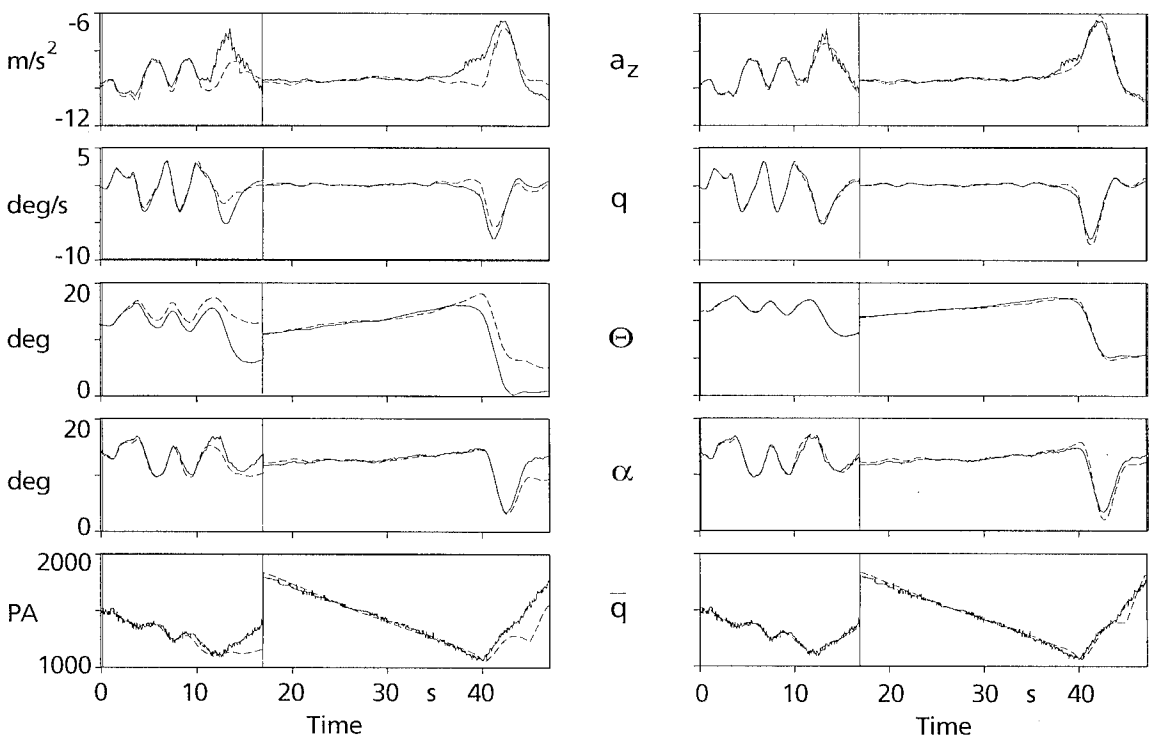

a) Neglecting unsteady effects

b) Accounting for unsteady effects

Fig. 24: Validation of C-160 "Transall" stall dynamics (———— flight measured; - - - - - estimated)

13.2 X-31A System Identification

The U.S./German experimental aircraft X-31A (Fig. 25) is a highly control augmented fighter with enhanced maneuverability. Post-stall maneuvering is enabled by applying advanced technologies like high angle-of-attack aerodynamics and flight control system integrated thrust vectoring [155,156]. System identification methods were employed: i) to predict aerodynamic behaviour at new flight conditions and ii) to validate and update the predicted aerodynamic data base [157]. The X-31A posed several challenges in aircraft system identification mainly because the uncontrolled basic airframe is aerodynamically unstable, because the integrated flight control laws lead to correlated deflections of the control surfaces and of the thrust vector vanes, and because the flight tests were not optimized for system identification purposes.

The thrust vector (TV) system consists of three vanes which can be moved into the aircraft's jet engine exhaust thus deflecting the thrust vector and thereby providing additional control in pitch and yaw. Two pitch doublet maneuvers flown with TV-engaged are analyzed. To this data with TV-engaged, applying the aerodynamic model obtained at the same flight condition without engaging TV yields the response match shown in Fig. 26a (TE: Trailing edge deflection; CAN: Canard deflection; σ: thrust deflection angle in pitch). A discernible mismatch is visible in pitch acceleration, $\dot{q}$, pitch rate, q, and pitch attitude, θ, which is attributed to the thrust deflection in pitch. On the other hand, modeling of the thrust vector influence on pitching motion yields the response match shown in Fig. 26b. From the two figures, the effect of thrust-vector modeling on the system-identification quality is apparent [158].

The thrust vector control effectiveness in pitch and in yaw were identified from flight data. It was found that

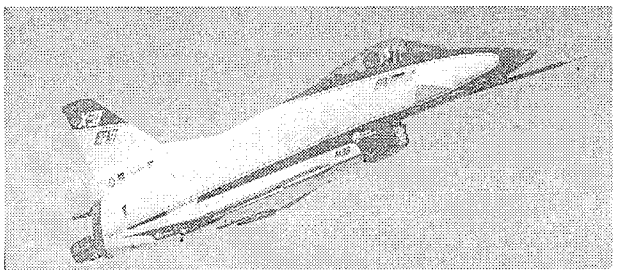

Fig. 25: X-31A aircraft
(Photo: Courtesy NASA Dryden)

the TV-effectiveness in pitch, $C_{m\sigma}$, in general follows the prediction. On the other hand, the TV-effectiveness in yaw, $C_{n\kappa}$, is somewhat lower than predicted, see Fig. 27. Once again, as in the case of Fig. 13, the pilot input maneuvers yield estimates which are scattered having large uncertainty levels due to the problems of correlation and insufficient excitation, whereas the separate surface excitation maneuvers provide more accurate results.

Although the output error method with artificial stabilization was successfully applied to the TV-modeling and to the longitudinal case, the approach was tedious due to the iterations required to eliminate diligently the effect of stabilization on the estimates. Application of this method to the lateral-directional mode was, however, feasible only on a part of bank-to-bank maneuver. Moreover the estimation results could not be completely resolved. A necessity for application of other methods was indicated. The filter error method and regression analysis were applied. It is interesting to note that the simpler approach of regression and the more complex filter error method yield approximately the same results, except that the

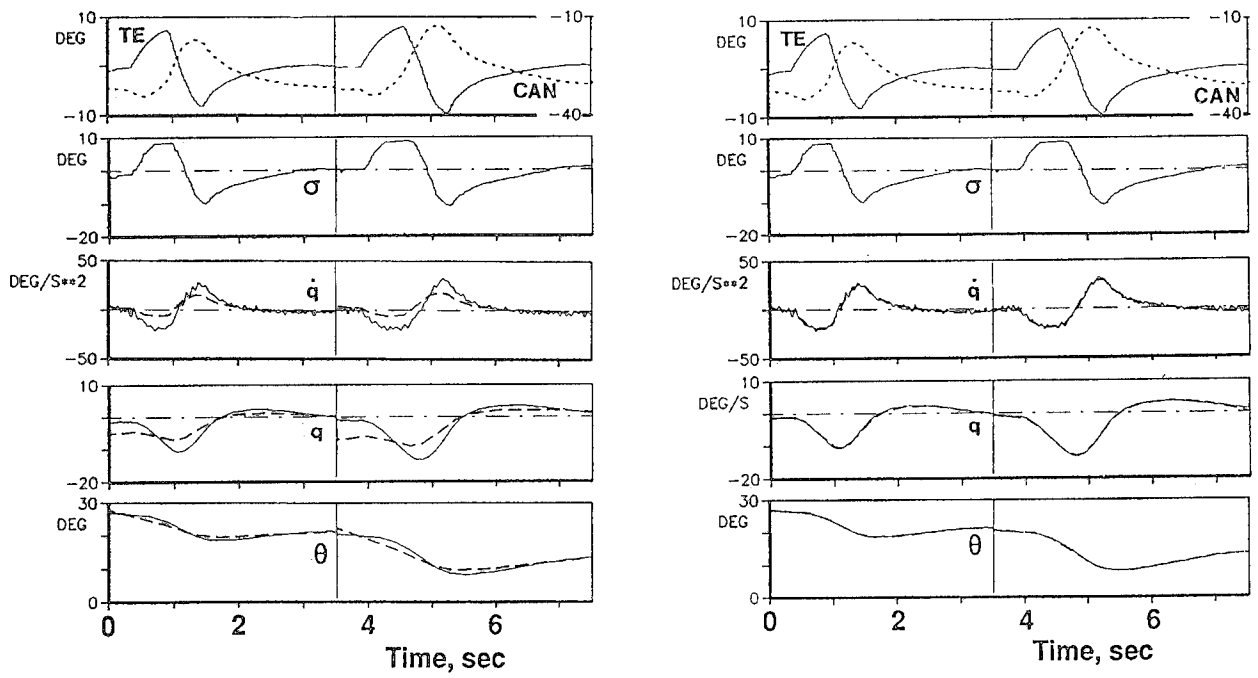

a) Neglecting TV-effects

b) Accounting for TV-effects

Fig. 26: Identification of thrust vector effects (———— measured; - - - - - - estimated)

uncertainty levels are somewhat larger for regression [159]. The frequency domain method also provided viable approach to unstable aircraft identification [160].

The results of X-31A system identification have been by and large used to validate and in several cases update the wind-tunnel predicted data base. Two typical examples have been provided in Fig. 28 [65]. As evident from Fig. 28a, the flight estimates did not confirm the wind-tunnel predicted large value of the dihedral effect between 30° and 45° of angle of attack (SSE: Separate Surface Excitation). Similarly, considerable discrepancies were also observed in the estimates of the directional stability, Fig. 28b (QT: Quasi Tailless configuration).

In conclusion, diligent modeling and a wide variety of estimation techniques provided flight validated aerodynamic characteristics, including post-stall regime and thrust vector control. Furthermore, the crux of the problem pertaining to highly augmented aircraft was the data correlation and insufficient excitation, and an efficient solution to this problem was provided by separate surface excitation.

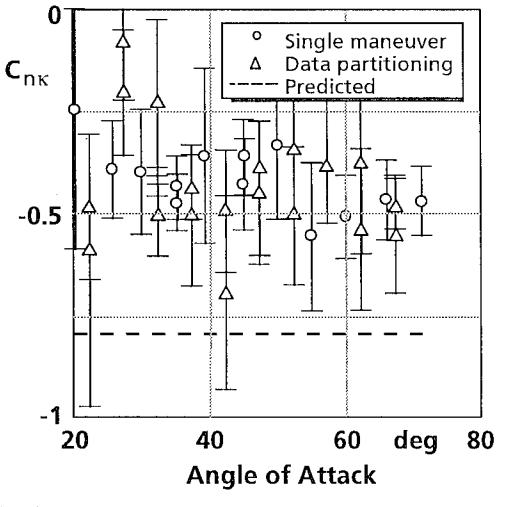

a) Pilot input maneuvers

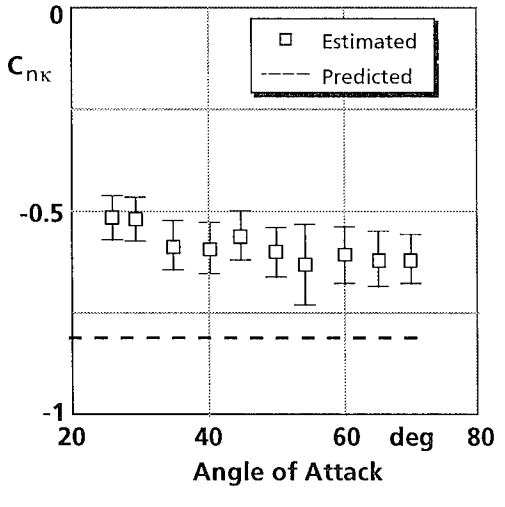

b) Separate surface excitation

Fig. 27: Thrust vector effectiveness in yaw

System identification provided improved results for flight test planning, expansion of flight envelope, and data base for simulation and control law modifications and validation, and thus catered to actual needs of the aircraft industry.

14. SYSTEM IDENTIFICATION APPLIED TO RELATED TOPICS

As set out at the beginning of the paper, having briefly traced the evolution of flight vehicle system identification and also having provided some typical examples in the area of flight mechanics, it is now attempted to illustrate some applications in the related areas. This attempt neither traces the history in these areas nor is it claimed to be exhaustive in nature. These examples serve the sole purpose of indicating some possibilities of applying system identification methods, and hoping that these methods would also become in these and other related fields as popular, as successful, and as indispensable as they have become in flight mechanics.

14.1 Aircraft Accident Analysis via Wind Estimation

The well defined kinematic equations of aircraft motion can be effectively used not only for the classical purpose of estimating unmeasured or poorly measured variables like angle of attack and for checking instrument accuracies, but also for more difficult applications such as estimating winds along a flight trajectory.

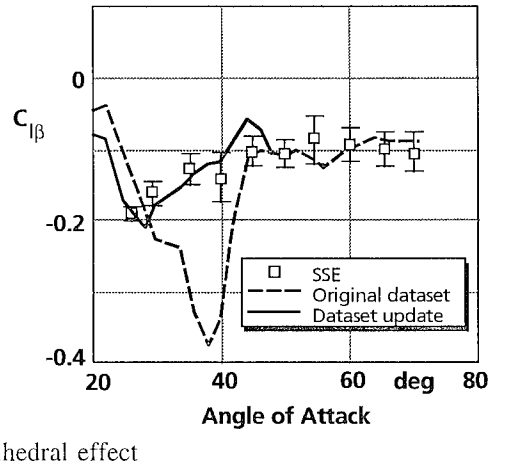

a) Dihedral effect

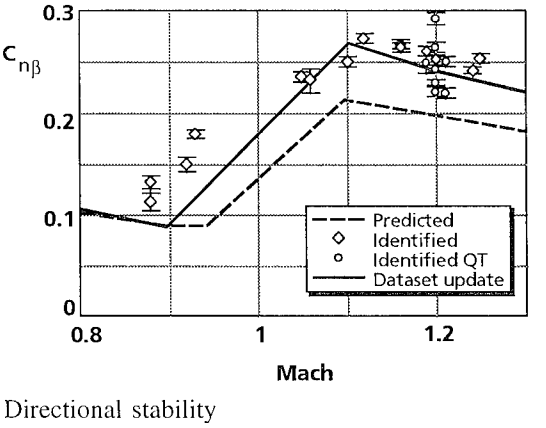

b) Directional stability

Fig. 28: Some examples of X-31A data base updates

Fig. 29 shows the concept of wind estimation as a difference between the aircraft velocities with respect to Earth and air mass in the Earth frame. Although dedicated flight test instrumentation, a basis for many investigations on estimation of stability and control derivatives, is often not available with the commercial aircraft, a combination of digital flight data recorder (DFDR) and air-traffic control (ATC) data provides sufficient amount of information. These advanced applications of the state estimation methodology, reported by Bach and Wingrove [162,163], have proved to be useful in assisting the analysis of aircraft accident.

14.2 In-Flight Estimation of Airload Parameters

Determination of airload parameters from flight tests of a prototype aircraft is required not only for flight certification of that particular aircraft by the regulatory bodies but also for prediction of loadings on a new airplane of similar design. The system identification methods have been employed in the past to obtain airload parameters in conjunction with identification of aerodynamic parameters from the same set of flight test data. This combined approach leads to significant reduction in total flight test time required for certification. A typical example of estimating the aerodynamic parameters pertaining to the lateral-directional motion and the airload parameters is found in Ref. 164. For such applications, however, in addition to the rigid-body motion variables the measurements of horizontal tail rolling moment, the vertical tail sideforce, and pilot rudder pedal force are necessary.

14.3 Flutter Testing

The main aim of flutter testing is to identify the frequency and damping of the structural modes either from flight test on a prototype or from wind tunnel tests on a scaled model. In several instances the wind tunnel flutter model testing has become an integral part of the aircraft development [165,166]. In the early days, classical methods of analysis like power spectral density, peak-hold spectrum method, or randomdec method were applied to measure the frequency and damping from model response assuming that the response can be approximated by that of a single-degree-of-freedom system. During the last decade or two, however, the advanced system identification methods have also been applied to flutter test data analysis. For example, Perangelo and Waisanen apply the maximum-likelihood method to the randomly excited fin response of F-14A aircraft, identifying a 13th order model to characterize the power spectral density up to about 70 Hz [165].

Compared to the least-squares flutter analysis, the maximum likelihood method yields more accurate estimates and moreover can be successfully applied to flutter test data in the presence of atmospheric turbulence. The more accurate estimates of the modal characteristics enable better extrapolation of flutter margins.

14.4 Aeroservoelastic Modeling

In contrast to the purely flight mechanical models characterized adequately by low-order dynamics or purely structural models by higher-order dynamics, the aeroservoelastic (ASE) models cover both the low frequency as well as high frequency range. An interdisciplinary flight vehicle modeling approach shown in Fig. 30 is, hence, necessary to arrive at appropriate models for the

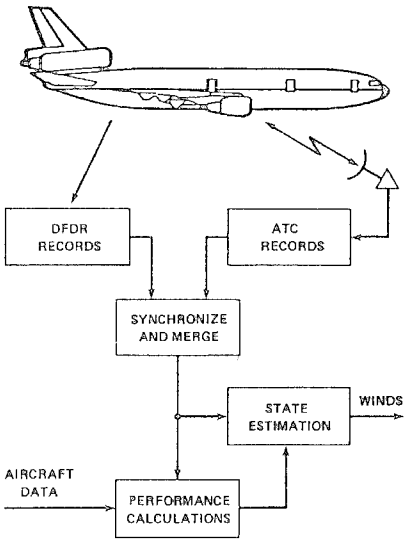

Fig. 29: Wind estimation from airline flight records
(Reproduced from Ref. 159)

aeroservoelastic applications. The ASE dynamics include coupling due to structural, control, sensor, aero, and actuator dynamics. Since accurate models can be obtained for structural dynamics through ground vibration tests, for the control dynamics through the design knowledge, and for the sensor dynamics through airdata calibration, the ASE-modeling uncertainties are predominantly dictated by the actuator and aerodynamic models [167].

The aerodynamic models must include both the rigid body modes as well as the unsteady effects. The typical examples presented in this paper clearly demonstrate that the modern methods of system identification provide adequate tools to obtain high-fidelity flight-mechanics models. Hence, it would be desirable to include such flight derived models in terms of aerodynamic derivatives instead of those based on the generalized aerodynamic forces.

Determination of actuator models from flight data is mostly restricted to equivalent models. Such flight derived models are usually low-order models, typically second to fourth order, and are obtained either in frequency domain by fitting a transfer function to measured

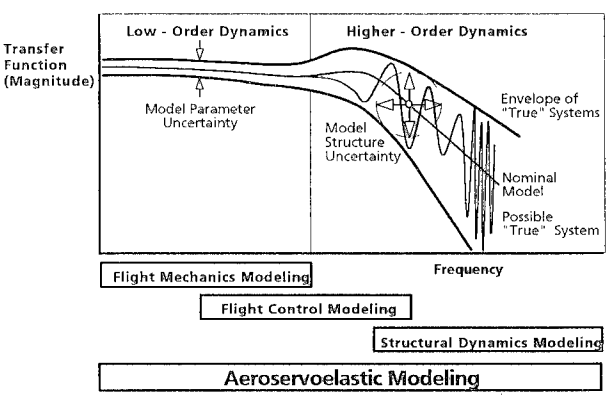

Fig. 30: Interdisciplinary flight vehicle modeling

data or in time-domain through state space representation as shown in Figs. 16 and 17. However, for some applications it may be necessary to incorporate higher order actuator models based on the physical properties of the system (main ram, servovalve, ram feedback etc.) and its compliance with the structure [167].

The structural modes, particularly in the case of an aeroelastic airplane, can influence the accuracy of the flight mechanics models, i.e. of the stability and control derivatives. Rynaski et al report such investigations during the late seventies [168], and also others more recently [169,170]. Techniques based on removal of structural effects through filtering of data, pseudostatic structural modeling and dynamic structural modeling have been discussed by Iliff [171]. Acree and Tischler report successful identification of several structural modes from frequency sweep flight data of an XV-15 Tilt-Rotor aircraft [172].

14.5 Rotorcraft System Identification

Another application which demands extended mathematical models pertains to helicopter in-flight simulator incorporating modern concepts of active control technology. The philosophy of model following control based on feed forward regulation provides safer and more accurate mode control; the performance, however, depends strongly on the validated mathematical model of the host flight vehicle. The high bandwidth requirements of the rotorcraft flight control system demand augmentation of rigid-body model through higher-order rotor dynamics [173-175]. The flight test and system identification results of Figs. 31 and 32 obtained with the BO-105

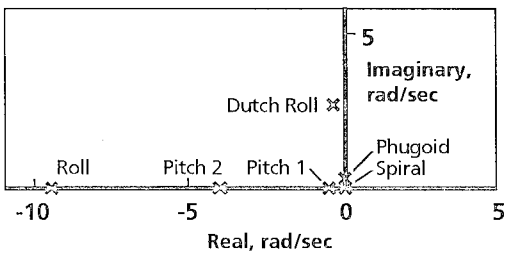

a) Rigid-body dynamics

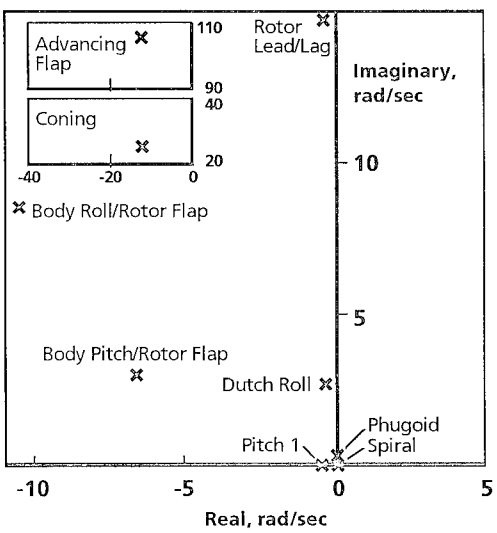

b) Rigid-body and rotor dynamics

Fig. 31: Eigenvalues of different model structures (BO-105 data)

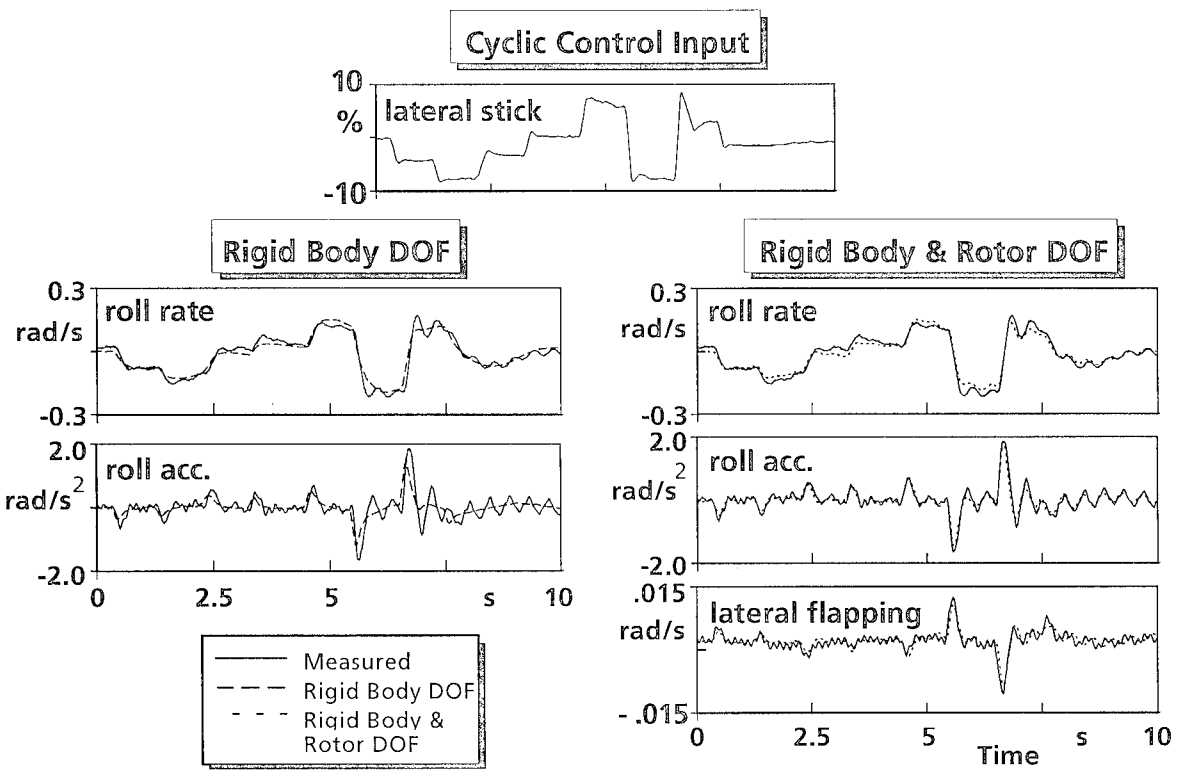

Fig. 32: Comparison of BO-105 helicopter flight test data with 6 DOF rigid-body and 9 DOF extended model responses

ATTHeS in-flight simulator clearly indicate the effect of unmodelled rotor modes on the identification quality [176-177].

Fig. 31 illustrates that the low frequency rotorcraft eigenvalues (phugoid, spiral, dutch roll, and pitch) are the same for both the models, whereas the higher frequency behavior is characterized by the more refined description of the 9 DOF model. Fig. 32 compares the roll axis time history responses for both the models to the measured data. It can be observed that only the 9 DOF model can match the amplitude peaks and the high frequency lead-lag rotor dynamics of the roll acceleration data. The model differences become even more obvious, when the results (not shown here) are compared in frequency domain [177].

An excellent repertoire of various aspects of rotorcraft identification is provided by the Working Group 18 of the FVP panel of the AGARD [176,177]. By ingeniously extending the system identification methods to this complex problem this group has significantly enlarged the application domain of these methods.

In all of the examples presented in this paper, and for that matter in any exercise on flight vehicle system identification, it is obvious that the inverse principle is applied to arrive at the model description. To this inverse-principle the following remarks by the renowned NASA expert Iliff are most appropriate [178]:

"Given the answer, what are the questions?"

which in his words is nothing but:

"We look at the results and try to figure out what situation caused those results".

Compared to the classical definition based on the technical aspects by Zadeh [8] (see section 2), the aforesaid remarks provide the philosophical definition to system identification.

15. CONCLUDING REMARKS

From the nostalgic remembrance of the first dynamic flight test the paper traces several milestones in the history of flight vehicle system identification. A brief overview is provided of the Quad-M key-issues and of the various modern methods of parameter estimation. The paper demonstrates successful application of the system identification methodology to a broad spectrum of flight vehicle modeling problems. The selected examples focus on: i) development and update of data bases from flight test data including nonlinear and unsteady aerodynamics for high-fidelity flight or in-flight simulators, for flight control law optimization, or for other applications, ii) identification of a highly augmented unstable aircraft incorporating modern concepts of thrust vectoring and high angle of attack aerodynamics, and iii) interdisciplinary modeling aspects of rigid-body and rotor dynamics for high bandwidth requirements. From the high quality of the results presented in this paper, and that of the several other applications reported during the recent past, it can be concluded that many of the application areas which were considered as emerging areas a decade ago have now been, more or less, well established; and that the system identification methods have reached a high level of maturity, making it a sophisticated and powerful tool not only for the research purposes but also to support the needs of the aircraft industry. Since the quest for better understanding of aerodynamic phenomena will continue in the future, it can be said that today the scope of the flight vehicle modeling will mainly be limited by the imagination and innovative approach of the analyst and little by the methods of parameter estimation.

16. ACKNOWLEDGEMENT

The authors would like express their appreciation to V. Klein of the George Washington University, JIAFS, NASA Langley RC, Hampton, Va, USA for his valuable comments on the manuscript of this paper

17. REFERENCES

[1] Gauss, K. F., "Theoria Motus", 1809; Also: "Theory of the Motion of the Heavenly Bodies Moving About the Sun in Conic Section", Dover, NY, 1963.

[2] Bernoulli, D., "The Most Probable Choice Between Several Discrepant Observations and the Formation Therefrom of the Most Likely Induction", Acta. Acad. Petrop., 1777, pp. 3-33. English Translation: M. G. Kendall, 'Daniel Bernoulli on Maximum Likelihood' in Biometrika, Vol. 48, No.1, 1961, pp. 1-18.

[3] Fisher, R. A., "On an Absolute Criterion for Fitting Frequency Curves", Messenger Math., Vol. 41, 1912, pp. 155-160.

[4] Wiener, N., "The Extrapolation, Interpolation and Smoothing of Stationary Time Series", OSRD 370, Report to the Services, Research Project DIC-6037, MIT, Feb. 1942.

[5] Kolmogorov, A. N., "Interpolation und Extrapolation von stationären zufälligen Folgen", Bull. Acad. Sci. USSR, Ser. Math. 5, 1941, pp. 3-14.

[6] Kalman, R. E., "A New Approach to Linear Filtering and Prediction Problems", Transactions ASME, Series D, Journal of Basic Engineering, Vol. 82, March 1960, pp. 35-45.

[7] Åström, K. J. and Bohlin, T., "Numerical Identification of Linear Dynamic Systems from Normal Operating Records", Proceedings of the 2nd IFAC Symposium on Theory of Self-Adaptive Control Systems, England, 1965, Editor: P. H. Hammond, Plenum Press, NY, 1966, pp. 96-111.

[8] Zadeh, L. A., "From Circuit Theory to System Theory", Proceedings, IRE, Vol. 50, 1962, pp. 856-865.

[9] Hamel, P. G., "Aircraft Parameter Identification Methods and Their Applications - Survey and Future Aspects", AGARD LS-104, Nov. 1979, Paper 1.

[10] Maine, R. E. and Iliff, K. W., "Identification of Dynamic Systems - Applications to Aircraft. Part 1: The Output Error Approach", AGARD AG-300-Vol. 3, Part 1, Dec. 1986.

[11] Klein, V., "Estimation of Aircraft Aerodynamic Parameters from Flight Data", Progress in Aerospace Sciences, Pergamon Press, Oxford, Vol. 26, 1989, pp. 1-77.

[12] Bryan, G. H., "Stability in Aviation", McMillan, London, 1911.

[13] Kroll, N., Radespiel, R., and Rossow, C.-C., "Accurate and Efficient Flow Solvers for 3D Applications on Structured Meshes", VKI Lecture Series 1994-05, Brüssel, Belgium, March 1994.

[14] Slooff, J. W. and Schmidt, W. (Editors), "Computational Aerodynamics Based on the Euler Equations", AGARD AG-325, Sept. 1994.

[15] Hamel, P. G., "Determination of Aircraft Dynamic Stability and Control Parameters from Flight Testing", AGARD LS-114, May 1981, Paper 10.

[16] Glauert, H., "Analysis of Phugoids Obtained by a Recording Airspeed Indicator", A.R.C. R&M No. 576, Jan. 1919.

[17] Norton, F. H., "The Measurement of the Damping in Roll on a JN4h in Flight", NACA Report 167, 1923.

[18] Norton, F. H., "A Study of Longitudinal Dynamic Stability in Flight", NACA Report 170, 1923.

[19] Milliken, W. F. Jr., "Progress in Dynamic Stability and Control Research", Journal of the Aeronautical Sciences, Vol. 14, No. 9, Sept. 1947, pp. 493-519.

[20] Milliken, W. F. Jr., "Dynamic Stability and Control Research", Proceedings of the 3rd Anglo-American Aeronautical Conference, Brighton, UK, 1951, pp. 447-524.

[21] Seamans, R. C. Jr., Blasingame, B. P., and Clementson, G. C., "The Pulse Method for the Determination of Aircraft Dynamic Performance", Journal of the Aeronautical Sciences, Vol. 17, No. 1, January 1950, pp. 22-38.

[22] Shinbrot, M., "On the Analysis of Linear and Nonlinear Dynamical Systems from Transient Response Data", NACA TN-3288, Dec. 1954.

[23] Shinbrot, M., "A Least-Squares Curve Fitting Method with Applications to the Calculation of Stability Coefficients from Transient Response Data", NACA TN 2341, April 1951.

[24] Mueller, R. K., "The Graphical Solution of Stability Problems", Journal of the Aeronautical Sciences, Vol. 4, No. 8, Aug. 1937, pp. 324-331.

[25] Breuhaus, W. O., "Resume of the Time-Vector Method as a Means for Analyzing Aircraft Stability Problems", WADC TR-52-299, Wright Air Development Center, US Air Force, Nov. 1952.

[26] Doetsch, K. H., "The Time Vector Method for Stability Investigations", RAE Report, Aero 2495, Aug. 1953.

[27] Sternfield, L., "A Vector Method Approach to the Dynamic Lateral Stability of Aircraft", Journal of the Aeronautical sciences, Vol. 21, No. 4, April 1954, pp. 251-256.

[28] Wolowicz, C. H. and Holleman, E. C., "Stability Derivative Determination from Flight Data", AGARD Report 224, Oct. 1958.

[29] Rampy, J. M. and Berry, D. T., "Determination of Stability Derivatives from Flight Test Data by Means of High Speed Repetitive Operation Analog Matching", FTC-TDR-64-8, Edwards, CA, USA, May 1964.

[30] Wolowicz, C. H., "Considerations in the Determination of Stability and Control Derivatives and Dynamic Characteristics from Flight Data", AGARD AR-549, Part 1, 1966

[31] Greenberg, H., "A Survey of Methods for Determining Stability Parameters of an Airplane from Dynamic Flight Measurements", NACA TN-2340, April 1951.

[32] Rynaski, E. G., "Application of Advanced Identification Techniques to Nonlinear Equations of Motion", Proceedings of the Stall/Post-Stall/Spin Symposium, Wright-Patterson AFB, OH, Dec. 1971. pp. 0.1 - 0.18.

[33] Iliff, K. W., "Parameter Estimation for Flight Vehicles", Journal of Guidance, Control, and Dynamics, Vol. 12, No. 5, Sept.-Oct. 1989, pp. 609-622.

[34] Laban, M., "On-Line Aircraft Aerodynamic Model Identification", Ph. D. Thesis, Delft University of Technology, Delft, The Netherlands, May 1994.

[35] Hamel, P. G., "Flight Vehicle System Identification - Status and Prospects", In: DFVLR-Mitt. 87-22, Nov. 1987, pp. 51-90.

[36] Mulder, J. A., Jonkers, H. L., Horsten, J. J., Breeman, J. H., and Simon, J. L., "Analysis of Aircraft Performance, Stability and Control Measurements", AGARD LS-104, Nov. 1979, Paper 5.

[37] Levin, M. J., "Optimal Estimation of Impulse Response in the Presence of Noise", IRE Transaction on Circuit Theory, Vol. CT-7, No. 1, March 1960, pp. 50-56.

[38] Litmann, S. and Huggins, W. H., "Growing Exponentials as a Probing Signal for System Identification", Proceedings, IEEE, Vol. 51, June 1963, pp. 917-923.

[39] Levadi, V. S., "Design of Input Signals for Parameter Estimation", IEEE Transactions on Automatic Control, Vol. AC-11, No. 2, April 1966, pp. 205-211.

[40] Gerlach, O. H., "Analysis of a Possible Method for the Measurement of Performance and Stability and Control Characteristics of an Aircraft in Non-Steady Symmetric Flights", In Dutch with Summary in English, Report VTH-117, Dept. of Aerospace Engineering, Delft University of Technology, Delft, The Netherlands, Nov. 1964.

[41] Gerlach, O. H., "Determination of Performance, Stability and Control Characteristics from Measurements in Non-Steady Manoeuvres", AGARD CP-17, Sept. 1966, pp. 499-523.

[42] Mehra, R. K. "Optimal Inputs for Linear System Identification", Preprints, JACC, Stanford, California, 1972.

[43] Stepner, D. E. and Mehra, R. K., "Maximum Likelihood Identification and Optimal Input Design for Identifying Aircraft Stability and Control Derivatives", NASA CR-2200, March 1973.

[44] Gupta, N. K and Hall, W. E. Jr., "Input Design for Identification of Aircraft Stability and Control Derivatives", NASA CR-2493, Feb. 1975.

[45] Koehler, R. and Wilhelm, K., "Auslegung von Eingangssignalen für die Kennwertermittlung", DFVLR-IB 154-77/40, Dec. 1977.

[46] Plaetschke, E. and Schulz, G., "Practical Input Signal Design," AGARD LS-104, Nov. 1979, Paper 3.

[47] Proskawetz, K. O., "Optimierung stufenförmiger Eingangssignale im Frequenzbereich für die Parameteridentifizierung", ZFW, Vol. 9, No. 6, Nov.-Dec. 1985, pp. 362-370.

[48] Plaetschke, E., Mulder, J. A., and Breeman, J. H., "Results of Beaver Aircraft Parameter Estimation", DFVLR-FB 83-10, Feb. 1983.

[49] Mulder, J. A., "Design and Evaluation of Dynamic Flight Test Manoeuvres", Ph. D. Thesis, Delft University of Technology, Delft, The Netherlands, Oct. 1986.

[50] Morelli, E. A., "Practical Input Optimization for Aircraft Parameter Estimation Experiments", Ph. D. Thesis, The George Washington University, Washington, DC, 1990.

[51] Young, P. and Patton, R. J., "Frequency Domain Identification of Remotely-Piloted Helicopter Dynamics Using Frequency-Sweep and Schroeder-Phased Test Signals", AIAA 88-4349, 1988.

[52] Mulder, J. A., Sridhar, J. K., and Breeman, J. H., "Identification of Dynamic Systems: Applications to Aircraft. Part 2: Nonlinear Analysis and Manoeuvre Design", AGARD AG-300, Vol. 3, Part 2, May 1994.

[53] Tischler, M. B., Fletcher, J. W., Diekmann, V. L., Williams, R., A., and Cason, R. W., "Demonstration of Frequency-Sweep Testing Techniques Using a Bell 214-ST Helicopter", NASA TM-89422, April 1987.

[54] Kolwey, H.,
Tech Memo for the AHS T&E Committee, March 1994.

[55] Ham, J. A., "Frequency Domain Flight Testing and Analysis of an OH-58D Helicopter", Journal of the AHS, Vol. 37, No. 4, Oct. 1992, pp. 16-24.

[56] Borek, R. W. and Pool, A. (Editors), "Basic Principles of Flight Test Instrumentation Engineering", AGARD AG-160, Vol. 1 (Issue 2), March 1994.

[57] Hill, R. W., Clinkenbeard, I. L., and Bolling, N. F., "V/STOL Flight Test Instrumentation Requirements for Extraction of Aerodynamic Coefficients", AFFDL-TR-68-154, Dec. 1968.

[58] Breeman, J. H., Woerkom, van, K., Jonkers, H. L., and Mulder, J. A., "Aspects of Flight Test Instrumentation", AGARD LS-104, Nov. 1979, Paper 4.

[59] Klein, V., "Identification Evaluation Methods", AGARD LS-104, Nov. 1979, Paper 2.

[60] Klein, V., Batterson, J. G., and Murphy, P. C., "Determination of Airplane Model Structure from Flight Data by Using Modified Stepwise Regression", NASA TP-1916, Oct. 1981.

[61] Hall, W. E. Jr., Gupta, N. K., and Tyler, J. S., "Model Structure Determination and Parameter Identification for Nonlinear Aerodynamic Flight Regime", AGARD CP-172, May 1975, Paper 21.

[62] Klein, V. and Batterson, J. G., "Determination of Airplane Model Structure from Flight Data Using Spline and Stepwise Regression", NASA TP-2126, 1983.

[63] Breeman, J. H., Erkelens, L. J. J., and Nieuwpoort, A.M.H., "Determination of Performance and Stability Characteristics from Dynamic Manoeuvres with a Transport Aircraft Using Parameter Identification Techniques", AGARD CP-373, July 1984, Paper 4.

[64] Batterson, J. G. and Klein, V., "Partitioning of Flight Data for Aerodynamic Modeling of Aircraft at High Angles of Attack", Journal of Aircraft, Vol. 26, No. 4, April 1989, pp. 334-339.

[65] Weiss, S., Friehmelt, H., Plaetschke, E., and Rohlf, D., "X-31A System Identification Using Single Surface Excitation at High Angles of Attack", AIAA 95-3436, 1995.

[66] Klein, V. and Schiess, J. R., "Compatibility Check of Measured Aircraft Responses Using Kinematic Equations and Extended Kalman Filter", NASA TN D-8514, Aug. 1977.

[67] Keskar, D. A. and Klein, V., "Determination of Instrumentation Errors from Measured Data Using Maximum Likelihood Method", AIAA 80-1602, 1980.

[68] Evans, R. J., Goodwin, G. C., Feik, R. A., Martin, C., and Lozano-Leal, R., "Aircraft Flight Data Compatibility Checking Using Maximum Likelihood and Extended Kalman Filter Estimation", Proceedings of the 7th IFAC/IFORS Symposium on Identification and System Parameter Estimation, York, UK, July 3-7, 1985, pp. 487-492.

[69] Stalford, H. L., "High-Alpha Aerodynamic Model Identification of T-2C Aircraft Using the EBM Method", Journal of Aircraft, Vol. 18, No. 10, Oct. 1981, pp. 801- 809.

[70] Sri-Jayantha, M. and Stengel, R. F., "Determination of Nonlinear Aerodynamic Coefficients Using the Estimation-Before-Modeling Method", Journal of Aircraft, Vol. 25, No. 9, Sept. 1988, pp. 796-804.

[71] Taylor, L. W. Jr. and Iliff, K. W., "A modified Newton-Raphson Method for Determining Stability Derivatives from Flight Data", In: Computing Methods in Optimization Problems, Editor: Zadeh, L. A., Neudstadt, L. W. and Balakrishnan, A. V., Academic Press, NY, 1969, pp. 353-364.

[72] Larson, D. B. and Fleck, J. T., "Identification of Parameters by the Method of Quasilinearisation", Cal. Report 164, Cornell Aeronautical Lab., Buffalo, NY, 1968.

[73] Maine, R. E. and Iliff, K. W., "Identification of Dynamic Systems", AGARD AG-300, Vol. 2, Jan. 1985.

[74] Taylor L. W. Jr. and Iliff, K. W., "System Identification Using a Modified Newton-Raphson Method - A FORTRAN Program", NASA TN D-6734, May 1972.

[75] Plaetschke, E., "Kennwertermittlung mit Maximum-Likelihood-Verfahren", DFVLR-IB 154-74/20, Dec. 1974.

[76] Balakrishnan, A. V., "Communication Theory", McGraw Hill, NY, 1968.

[77] Maine, R. E. and Iliff, K. W., "A FORTRAN Program for Determining Aircraft Stability and Control Derivatives from Flight Data", NASA TN D-7831, April 1975.

[78] Gupta, N. K. and Mehra, R. K., "Computational Aspects of Maximum Likelihood Estimation and Reduction in Sensitivity Function", IEEE Transaction on Automatic Control, Vol. AC-19, No. 6, Dec. 1974, pp. 774-783.

[79] Maine, R. E. and Iliff, K. W., "User's Manual for MMLE3, a General FORTRAN Program for Maximum Likelihood Parameter Estimation", NASA TP 1563, Nov. 1980.

[80] Groves, R. D., Bowles, R. L., and Mayhew, S. C., "A Procedure for Estimating Stability and Control Parameters from Flight Test Data by Using Maximum Likelihood Method Employing Real-Time Digital System", NASA TN D-6735, May 1972.

[81] Ross, A. J. and Foster G. W., "FORTRAN Program for the Determination of Aerodynamic Deri-

vatives from Transient Longitudinal or Lateral Responses of Aircraft", RAE TR 75090, Sept. 1975.

[82] Bentley, D. B., "FORTRAN Program RE90: A Program for the Identification of Longitudinal Stability Derivatives from Flight Data", Hawker Siddeley Aviation, MAE-R-CHP-00002, 1976.

[83] Iliff, K. W. and Maine, R. E., "A Bibliography for Aircraft Parameter Estimation", NASA TM 86804, Oct. 1986.

[84] Eulrich, B. J. and Rynaski, E. G., "Identification of Nonlinear Aerodynamic Stability and Control Parameters at High Angles of Attack", AGARD CP-172, May 1975, Paper 2.

[85] McBrinn, D. E. and Brassell, B. B., "Aerodynamic Parameter Identification for the A-7 Airplane at High Angles of Attack", Proceedings of the 3rd AIAA Atmospheric Flight Mechanics Conference, Arlington, Tex., Aug. 1976, pp. 108-117.

[86] Galbraith, I. J. and Petersen, T. J., "Nonlinear Parameter Identification and Its Application to Transport Aircraft", AGARD CP-235, Nov. 1978, Paper 18.

[87] Ross, A. J., "Identification Experience in Extreme Flight Regimes", AGARD LS-104, Nov. 1979, Paper 8.

[88] Iliff, K. W., "Maximum Likelihood Estimation of Lift and Drag from Dynamic Aircraft Maneuvers", Journal of Aircraft, Vol. 14, No. 12, Dec. 1977, pp. 1175-1181.

[89] Trankle, T. L., Vincent, J. H., and Franklin, S. N., "System Identification of Nonlinear Aerodynamic Models", AGARD AG-256, March 1982, Paper 7.

[90] Jategaonkar, R. V. and Plaetschke, E., "Maximum Likelihood Parameter Estimation from Flight Test Data for General Nonlinear Systems", DFVLR-FB 83-14, March 1983.

[91] Weiss, S., "Ein Program zur Maximum-Likelihood Parameterschätzung für nichtlineare Systeme", DFVLR-IB 111-87/29, July 1987.

[92] Murray, J. E. and Maine, R. E., "pEst Version 2.1 User's Manual", NASA TM 88280, Sept. 1987

[93] Blackwell, J., "A Maximum Likelihood Parameter Estimation Program for General Non-Linear Systems", ARL-AERO-TM-392, Jan. 1988.

[94] Murphy, P. C., "An Algorithm for Maximum Likelihood Estimation Using an Efficient Method for Approximating Sensitivities", NASA TP 2311, June 1984.

[95] Cui, P.-Y., "A New Algorithm of Approximating Sensitivities for Maximum Likelihood Estimation", Proceedings of the 10th IFAC Symposium on System Identification, Copenhagen, Denmark, July 4-6, 1994, pp. 2.601-2.604.

[96] Jategaonkar, R. V. and Plaetschke, E., "Non-Linear Parameter Estimation from Flight Data Using Minimum Search Methods", DFVLR-FB 83-15, March 1983.

[97] Murphy, P. C., "A Methodology for Airplane Parameter Estimation and Confidence Interval Determination of Nonlinear Estimation Problems", NASA CP 1153, April 1986.

[98] Balakrishnan, A. V., "Stochastic System Identification Techniques", Stochastic Optimization and Control, H. F. Karreman (Ed.), Wiley, London, 1968.

[99] Mehra, R. K., "Maximum Likelihood Identification of Aircraft Parameters", Proceedings of the 11th Joint Automatic Control Conference, Atlanta, GA, June 1970, pp. 442-444.

[100] Mehra, R. K., "Identification of Stochastic Linear Dynamic Systems Using Kalman Filter Representation", AIAA Journal, Vol. 9, Jan. 1971, pp. 28-31.

[101] Tyler, J. S., Powell, J. D., and Mehra, R. K., "The Use of Smoothing and Other Advanced Techniques for VTOL Aircraft Parameter Identification", Final report, Naval Air Systems Command Contract N00019-69-C-0534, Systems Control, Inc., Palo Alto, CA, June 1970.

[102] Iliff, K. W., "Identification and Stochastic Control with Applications to Flight Control in Turbulence", Ph. D. Dissertation, Univ. of California, Los Angeles, CA, May 1973.

[103] Schulz, G., "Maximum-Likelihood-Identifizierung mittels Kalman-Filterung: Kleinste-Quadrate Schätzung. Ein Vergleich bei der Bestimmung von Stabilitätsderivativa unter Berücksichtigung von Böenstörungen", DLR-FB 75-74, Aug. 1975,

[104] Yazawa, K., "Identification of Aircraft Stability and Control derivatives in the Presence of Turbulence", AIAA 77-1134, 1977.

[105] Maine, R. E. and Iliff, K. W., "Formulation and Implementation of a Practical Algorithm for Parameter Estimation with Process and Measurement Noise", SIAM Journal of Applied Mathematics, Vol. 41, Dec. 1981, pp. 558-579.

[106] Foster, G. W., "The Identification of Aircraft Stability and Control Parameters in Turbulence", RAE TR-83025, March 1983.

[107] Jategaonkar R. V. and Plaetschke, E., "Identification of Moderately Nonlinear Flight Mechanics systems with Additive Process and Measurement Noise", AIAA 88-4347, 1988.

[108] Jategaonkar, R. V. and Plaetschke, E., "Algorithms for Aircraft Parameter Estimation Accounting for Process and Measurement Noise", Journal of Aircraft, Vol. 26, No. 4, April 1989, pp. 360-372.

[109] Klein, V., "Aircraft Parameter Estimation in the Frequency Domain", AIAA 78-1344, 1978.

[110] Fu, K.-H. and Marchand, M., "Helicopter System Identification in the Frequency Domain", 9th European Rotorcraft Forum, Sept. 13-15, 1983, Stresa, Italy, Paper 96.

[111] Marchand, M. and Fu, K.-H., "Frequency Domain Parameter Estimation of Aeronautical Systems without and with Time Delay", Proceedings of the 7th IFAC Symposium on Identification and System Parameter Estimation, York, UK, July 3-7, 1985, pp. 669-674.

[112] Kashyap, R. L., "A New Method of Recursive Estimation in Discrete Linear Systems", IEEE Transactions on Automatic Control, Vol., AC-15, No. 1, Feb. 1970, pp. 18-24.

[113] Chen, R. T. N., Eulrich, B. J., and Lebacqz, J. V., "Development of Advanced Techniques for the Identification of V/STOL Aircraft Stability and Control Parameters", Cornell Aeronautical Lab., Inc., Report No. BM-2820-F-1, 1971.

[114] Speyer, J. L. and Crues, E. Z., "On-Line Aircraft State and Stability Derivative Estimation Using the Modified-Gain Extended Kalman Filter", Journal of Guidance and Control, Vol. 10, No. 3, May-June 1987, pp. 262-268.

[115] Plaetschke, E., Jategaonkar, R. V., Rohlf, D., and Weiss, S.,"Methoden zur Schätzung der Parameter eines Flugzeugs im Post-Stall-Bereich", Proceedings of the Symposium on 'Sicherheit im Luftverkehr', Technical Univ. of Braunschweig, Germany, Sept. 13-15, 1994, pp. 297-306.

[116] Kokolios, A., "X-31A Lateral Aerodynamic Characteristics Determined from Flight Data by Two Estimation Techniques", M. S. Thesis, The George Washington Univ. Washington, DC, July 1993.

[117] Sjöberg, J., Hjalmarsson, H., and Ljung, L., "Neural Networks in System Identification," Proceedings, 10th IFAC Symposium on System Identification, July 4-6, 1994, Copenhagen, pp. 2.49-2.72.

[118] Hopfield, J. J., "Neural Networks and Physical Systems with Emergent Collective Computational Abilities", Proc. National Academy of Science, Vol. 79, 1982, pp. 2554-2558.

[119] Raol, J. R. and Jategaonkar, R. V. " Aircraft Parameter Estimation Using Recurrent Neural Networks - A Critical Appraisal", AIAA 95-3504, 1995.

[120] Dreyfus, S. E., "Artificial Neural Networks, Back Propagation, and the Kelly-Bryson Gradient Procedure", Journal of Guidance, Control, and Dynamics, Vol. 13, No. 5, Sept.-Oct. 1990, pp. 926-928.

[121] Hess R. A., "On the use of Back Propagation with Feed-Forward Neural Networks for the Aerodynamic Estimation Problem", AIAA 93-3638, 1993.

[122] Linse, D. J. and Stengel R. F., "Identification of Aerodynamic Coefficients Using Computational Neural Networks", Journal of Guidance, Control, and Dynamics, Vol. 16, No. 6, Nov.-Dec. 1993, pp. 1018-1025.

[123] Rokhsaz, K. and Steck, J. E., "Use of Neural Networks in Control of High-Alpha Maneuvers", Journal of Guidance, Control, and Dynamics, Vol. 16, No. 5, Sept.-Oct., 1993, pp. 934-939.

[124] Youssef, H. M. and Juang, J.-C., "Estimation of Aerodynamic Coefficients Using Neural Networks", AIAA 93-3639, 1993.

[125] Anon., "Airplane Simulator Qualification", FAA Advisory Circular, AC 120-40B, Feb. 1991.

[126] Jategaonkar, R. V., "A Comparison of Output Error and Filter Error Methods from Aircraft Parameter Estimation Results", In: DLR-Mitt. 93-14, Dec. 1993, pp. 63-87.

[127] Lebacqz, J. V. and Govindaraj, K. S., "Implicit Model Following and Parameter Identification of Unstable Aircraft", Journal of Guidance and Control, Vol. 3, No. 2, March-April 1980, pp. 119-123.

[128] Maine, R. E. and Murray, J. E., "Application of Parameter Estimation to Highly Unstable Aircraft", Journal of Guidance, Control, and Dynamics, Vol. 11, No. 3, May-June 1988, pp. 213-219.

[129] Plaetschke, E., "Identifizierung instabiler flugmechanischer Systeme mit einem Ausgangsfehlerverfahren", ZFW, Vol. 16, No. 4, July-Aug. 1988, pp. 233-240.

[130] Preissler, H. and Schäufele, H., "Equation Decoupling - A New Approach to the Aerodynamic Identification of Unstable Aircraft", Journal of Aircraft, Vol. 28, No. 2, Feb. 1991, pp. 146-150.

[131] Jategaonkar, R. V. and Thielecke, F., "Parameter Estimation Methods for Unstable Aircraft", Journal of Aircraft, Vol. 31, No. 3, May-June 1994, pp. 510-519.

[132] Klein V. and Morelli, E. A., "Parameter Estimation of a Highly Augmented Aircraft from Flight Data", Proceedings of the 9th IFAC Symposium on Identification and System Parameter estimation, Budapest, Hungary, July 8-12, 1991, pp. 538-543.

[133] Anon, "Experience with the X-15 Adaptive Flight Control System", NASA TN D-6208, March 1971.

[134] Stein, G., Hartmann, G. L., and Hendrick, R. C., "Adaptive Control Laws for F-8 Flight Test", IEEE Transaction on Automatic Control, Vol. AC-22, No. 5, Oct. 1977, pp. 758-767.

[135] Laban, M. and Mulder, J. A., "On-Line Identification of Aircraft Aerodynamic Model Parameters", Proceedings of the 9th IFAC Symposium on Identification and System Parameter estimation, Budapest, Hungary, July 8-12, 1991, pp. 556-561.

[136] Quanwei, J. and Qiongkang, C., "Dynamic Model for Real-Time Estimation of Aerodynamic Characteristics", Journal of Aircraft, Vol. 26, No. 4, April 1989, pp. 315-321.

[137] Bauer, J. E., Crawford, D. B., Gera, J., and Andrisani II, D., "Real-Time Comparison of X-29A Flight Data and Simulation Data", Journal of Aircraft, Vol. 26, Feb. 1989, pp. 117-123.

[138] Allen, L. D., "Evolution of Flight Simulators", AIAA 93-3545, 1993.

[139] Neville, K. W. and Stephens A. T., "Flight Update of Aerodynamic Math Model", AIAA 93-3596, 1993.

[140] Baillie, S. W., Hui, K., and DeLeeuw, J., "The Flight Test and Data Analysis Program for the Development of a Boeing/deHavilland Dash 8 Simulator Model", AGARD CP-519, Oct. 1992, Paper 30.

[141] Mulder, J. A., Baarspul, M., Breeman, J. H., Nieuwpoort, A. M. H., Verbraak. J. P. T., and Steeman, P. S. J. M., "Determination of the Mathematical Model for the New Dutch Government Civil Aviation Flying School Flight Simulator", Proceedings of the 18th Annual Symposium of the Society of Flight Test Engineers, Amsterdam, The Netherlands, Sept. 28 - Oct. 2, 1987, Paper 15.

[142] Jategaonkar, R. V., Mönnich, W., Fischenberg, D., and Krag, B., "Identification of C-160 Simulator Data Base from Flight Data", Proceedings of the 10th IFAC Symposium on System Identification, Copenhagen, Denmark, July 1994, pp. 3.67-3.74.

[143] Trankle, T. L. and Bachner, S. D., "Identification of a Full Subsonic Envelope Nonlinear Aerodynamic Model of the F-14 Aircraft", AIAA 93-3634, 1993.

[144] Jategaonkar, R. V., "Identification of Actuation System and Aerodynamic Effects of Direct-Lift-Control Flaps", Journal of Aircraft, Vol. 30, No. 5, Sept.-Oct. 1993, pp. 636-643.

[145] Jategaonkar, R. V., "Determination of Aerodynamic Characteristics from ATTAS Flight Data Gathering for Ground-Based Simulator", DLR-FB 91-15, May 1991.

[146] Krag, B., Jategaonkar, R. V., Mönnich, W., and Fischenberg, D., "Estimation of an Aerodynamic

Data Base for a New C-160 'Transall' Flight Simulator from Flight Data", Proceedings of the RAeS Symposium on 'Data Issues for Flight Simulators - An On-Going Problem?", Nov. 10-11, 1993, London, pp. 7.1-7.12.

[147] Jategaonkar, R. V., Mönnich, W., Fischenberg, D., and Krag, B., "Data Gathering for C-160 "Transall" Flight Simulator. Part 1: Math Model and Aerodynamic Data Base", DLR IB 111-93/37, May 1993.

[148] Jategaonkar, R. V., Mönnich, W., Fischenberg, D., and Krag, B., "Identification of Speed Brake, Ramp Door, Air-Drop and Landing Gear Effects from 'Transall' Flight Data", AIAA 94-3473, 1994.

[149] Fischenberg, D., Mönnich, W., Krag, B., and Jategaonkar, R. V., "Aspects of C-160 Simulator Model Determination and Validation On and Close to the Ground", AIAA 94-3404, 1994.

[150] Leishman, J. G. and Nguyen, K. Q., "State-Space Representation of Unsteady Airfoil Behavior", AIAA Journal, Vol. 28, No. 5, May1990, pp. 836-844.

[151] Fischenberg, D., "Identification of an Unsteady Aerodynamic Stall Model from Flight Test Data", AIAA 95-3438, 1995.

[152] Wagner, H., Über die Entstehung des dynamischen Auftriebs von Tragflügeln", Zeitschrift für die angewandte Mathematik und Mechanik, Vol. 5, No. 1, Feb. 1925, pp. 17-35.

[153] Goman, M. and Khrabrov, A., "State-Space Representation of Aerodynamic Characteristics of an Aircraft at High Angles of Attack", Journal of Aircraft, Vol. 31, No. 5, Sept.-Oct. 1994, pp. 1109-1115.

[154] Neville, K. W., "Simulator-To-Flight Validation - Methods, Problems and Dilemmas", Proceedings of the RAeS Symposium on 'Data Issues for Flight Simulators - An On-Going Problem?', Nov. 10-11, 1993, London, pp. 14.1-14.7.

[155] Anon, "Experimentalflugzeug Rockwell/MBB X-31A in Erprobung", Luft und Raumfahrt, Vol. 11, No. 4, 1990, pp. 8-14.

[156] Ross, H., "X-31 Enhancement of Aerodynamics for Maneuvering beyond Stall", AGARD CP-497, Nov. 1991, Paper 2.

[157] Rohlf, D., Plaetschke, E., and Weiss, S., "X-31A Model Evaluation and Validation via System Identification", AIAA 91-2875, 1991.

[158] Plaetschke, E. and Weiss, S., "Identification of Thrust Vector Effectiveness from X-31A Flight Test Data", ZFW, Vol. 17, No. 4, Aug. 1993, pp. 235-238.

[159] Plaetschke, E., Weiss, S., and Rohlf, D., "Identification at High Angles of Attack Applied to X-31A Flight Test Data", In: DLR-Mitt. 93-14, Dec. 1993, pp. 181-198.

[160] Kaletka, J. and Fu, K.-H., "Frequency Domain Identification of Unstable Systems Using X-31A Aircraft Flight Test Data", AIAA 93-3635, 1993.

[161] Rohlf, D., Plaetschke, E., and Weiss, S., "X-31A System Identification Applied to Post Stall Flight - Aerodynamics & Thrust Vectoring", AGARD CP-548, March 1994, Paper 14.

[162] Bach, R. E. Jr. and Wingrove R. L., "Analysis of Windshear from Airline Flight Data", Journal of Aircraft, Vol. 26, No. 2, Feb. 1989, pp. 103-109.

[163] Wingrove R. L. and Bach, R. E. Jr.,"Analysis of Severe Atmospheric Disturbances from Airline Flight Records", AGARD CP-470, Sept. 1989, Paper 3.

[164] Park, G. D., "Parameter Identification Technology Used in Determining In-Flight Airload Parameters", Journal of Aircraft, Vol. 14, No. 3, March 1977, pp. 251-256.

[165] Perangelo, H. J. and Waisanen, P. R., "Application of Advanced Parameters Identification Methods for Flight Flutter Data Analysis with Comparison to Current Techniques", AGARD CP-373, July 1984, Paper 5.

[166] Bucharles, A. and Roubertier, H. C.-J., "Advanced Parameter Identification Techniques for Near Real Time Flight Flutter Test Analysis", AIAA 90-1275, 1990.

[167] Brenner, M. J., "Actuator and Aerodynamic Modeling for High-Angle-of-Attack Aeroservoelasticity", NASA TM-4493, June 1993.

[168] Rynaski, E. G., Andrisani II, D., and Weingarten, N. C., "Identification of the Stability Parameters of an Aeroelastic Airplane", AIAA 78-1328, 1978.

[169] Zerweckh, S. H. and Flotow, A. H. von, "Flight Testing a Highly Flexible Aircraft - Case Study on the MIT Light Eagle", AIAA 88-4375, 1988.

[170] Ghosh, A. K. and Raisinghani, S. C., "Parameter Estimates of an Aeroelastic Aircraft as Affected by Model Simplifications", Journal of Aircraft, Vol. 31, No. 2, March-April 1994, pp. 452-454.

[171] Iliff, K.W., "Aircraft Identification Experience", AGARD LS-104, Nov. 1979, Paper 6.

[172] Acree, C. W., Jr. and Tischler, M. B., "Identification of XV-15 Aeroelastic Modes Using Frequency Sweeps", Journal of Aircraft, Vol. 26, No. 7, July 1989, pp. 667-674.

[173] Hamel, P. G., "Aerospace Vehicle Modelling Requirements for High Bandwidth Flight Control", In: Aerospace Vehicle Dynamics and Control, (Ed.) M. V. Cook and M. J. Rycroft, Clarendon Press, Oxford, 1994, pp. 1-31.

[174] Kaletka, J. and von Grünhagen, W., "System Identification of Mathematical Models for the Design of a Model Following Control System", Vertica, Pergamon Press, Oxford, Vol. 13, No. 2, 1989, pp. 213-228.

[175] Tischler, M. B., "Identification Requirements for High-Bandwidth Rotorcraft Flight Control System Design", Journal of Guidance, Control, and Dynamics, Vol. 13, Sept.-Oct. 1990, pp. 835-841.

[176] Hamel, P. G. (Editor), "Rotorcraft System Identification", AGARD AR-280, Sept. 1991.

[177] Hamel, P. G. and Kaletka, J., "Rotorcraft System Identification - An Overview of AGARD FVP Working Group 18", AGARD CP-552, 1995, Paper 18.

[178] Anon, "He has a Question for any Answer", (An interview with Kenneth Iliff by Staff Writer M. McCall), Antelope Valley Press (Newspaper), CA, USA, Nov. 1, 1994.

Appendix 1: Review of AGARD publications during the last two decades in field of aircraft parameter estimation

Year	Title	Reference
1975	Methods for Aircraft State and Parameter Identification	CP-172; (1 to 29)
1976	Flight / Ground Testing Facilities Correlation	CP-187; (6,8,13)
1977	Flight Test Techniques	CP-223; (5,11,12,13)
1978	Rotorcraft Design	CP-233; 20
1978	Dynamic Stability Parameters	CP-235; (14,15,17,18)
1978	Excitation and Analysis Technique for Flight Flutter Tests	RP-672
1979	Aeroelastic Flight Test Techniques and Instrumentation	AG-160; 9
1979	High Angle of Attack Aerodynamics	CP-247; 1,14
1979	Stability and Control	CP-260; 16
1979	Aerodynamic Characteristics of Controls	CP-262; (2,3,16)
1979	Parameter Identification	LS-104; (1 to 10)
1981	Dynamic Stability Parameters	LS-114; 10
1982	Advances in the Techniques and Technology of the Application of Nonlinear Filters and Kalman Filters	AG-256; 7
1984	Flight Test Techniques	CP-373; 5
1985	Identification of Dynamic Systems	AG-300-Vol. 2
1985	Unsteady Aerodynamics - Fundamentals and Applications to Aircraft Dynamics	CP-386; (24, S2)
1986	Identification of Dynamic Systems - Applications to Aircraft, Part 1: The Output Error Approach	AG-300-Vol. 3, Part 1
1991	Rotorcraft System Identification	AR-280
1991	Rotorcraft System Identification	LS-178
1991	Manoeuvring Aerodynamics	CP-497; 14
1992	Flight Testing	CP-519; (14,29,30)
1994	Technologies for Highly Manoeuvrable Aircraft	CP-548; 18
1994	Identification of Dynamic Systems - Applications to Aircraft, Part 2: Nonlinear Model Analysis and Manoeuvre Design	AG-300-Vol. 3, Part 2

ELEMENTS OF THE B-2 FLIGHT FLUTTER TEST PROGRAM

By
R. T. Britt, et al
Northrop Grumman B-2 Division

Presented at the
AGARD Structures and Materials Panel
Specialists' Meeting
ADVANCED AEROSERVOELASTIC TESTING
AND DATA ANALYSIS
Rotterdam, The Netherlands
(8-10 May 1995)

FLIGHT FLUTTER TEST SYSTEM

- Introduction
- Flight Test Approach
- Description of Flutter Data Analysis System
- Typical Results
- Acknowledgements

Paper presented at the Structures and Materials Panel Specialists' Meeting on "Advanced Aeroservoelastic Testing and Data Analysis", held in Rotterdam, The Netherlands, from 8-10 May 1995, and published in CP-566.

FLIGHT FLUTTER TEST SYSTEM

Introduction

- Approach Dictated by Flight Test Requirements
  - Integrated Test Blocks
  - Real Time Point to Point Clearance
  - Minimum Test Modifications to Air Vehicle
- Composed of Elements Utilized in YF-17 and F-20 Flight Flutter Test Programs
- System used in Flutter Clearance of B-2 Aircraft

FLIGHT FLUTTER TEST SYSTEM

Flight Test Approach

- Vehicle Excited Via Control Surface Inputs
  - All Surfaces
  - Pre-Programmed Excitations
  - Sinusoidal Sweeps and Random
    - » Frequency To 16 Hz.
    - » Deflections To 2 Deg.

- Measurands
  - Accels, Strain Gages, Control Surface Displacement
  - Locations Chosen From Analysis & GVT Considerations

FLIGHT FLUTTER TEST SYSTEM

Flight Test Approach(Continued)

- Flutter Data Acquisition
  - Data Telemetered From Measurands on Vehicle
  - Converted to Engineering Units
  - Buffered Into Selected Data Blocks

- Flutter Data Processing and Analysis
  - Generate Frequency Response Function (FRF)
  - Apply Parameter Estimation Techniques
  - Interactive Curve-Fit of FRF's
  - Compute And Store Estimated Frequencies and Dampings

- Point to Point Clearance (Near Real Time)

FLIGHT FLUTTER TEST SYSTEM

Description of Flutter Data Analysis System

- Composed of 3 Modules

  - USER Program: Interface Between Host Computer and Other Program Functions
  - ACQUISITION Program: Acquires And Real-Time Transforms Data Into FRF Format
  - ANALYSIS Program: Three Techniques Available For Fitting Data/Estimating Frequency And Damping

- System Installed At Edwards Air Force Base(Real-Time Application) and At B-2 Division For Post Flight Analysis

FLIGHT FLUTTER TEST SYSTEM

Acquisition Program

- Acquires and Real-Time Transforms Data
- Sets Acquisition Parameters
  - Reference Input
  - Sampling Rate of 100 SPS
  - Set Block Size (Maximum 2048 Samples/Block)
  - Noise Reduction Features
    - » Number of Averages
    - » Overlapping Blocks
- Compute Fourier Transform and Power Spectra

FLIGHT FLUTTER TEST SYSTEM

Acquisition Program(Continued)

- Store Acquired Data in Data Files
  - Auto Spectra, FRF, Coherence Function
  - Time History Data
- Data May Be Reprocessed Post Flight(Time History File)
  - Change Block-Size, Noise Reduction Parameters, Filtering

FLIGHT FLUTTER TEST SYSTEM

Data Analysis Program

- Extracts Frequencies and Dampings via Three Methods
  - Sanathanan Parameter Estimation Technique(SPET)
  - Least Squares Complex Exponential Curve Fit(LSCEXP)
  - Modal Parameter Estimation Technique(MPET)

- SPET The Primary Analysis Tool
  - Demonstrated Several Advantages Over Other Methods
    - » Fit Multiple Modes Over Wide Frequency Range
    - » Simultaneously Fit Closely Spaced Modes
  - Important Under Time Constraints of In-flight Extraction
  - Consistent Results

FLIGHT FLUTTER TEST SYSTEM

Sanathanan Parameter Estimation Technique

- Fits Polynomial Coefficients of FRF $G(j\omega)$

$$FRF = G(j\omega) = \frac{P(j\omega)}{Q(j\omega)}$$

- Computes Coefficients Then Determines Roots of $G(j\omega)$ For Frequencies and Dampings

- Reference: Sanathanan, C.K., and Koerner, J., "Transfer Function Synthesis as a Ratio of Two Complex Polynomials", IEEE Transactions on Automatic Control, pp. 56-58, January 1963

FLIGHT FLUTTER TEST SYSTEM

Typical Results/Applications

- Surface Deflection Auto Spectrum
- Frequency Response and Coherence Functions
- Fitted FRF
- Frequency and Damping Extraction Summary

FLIGHT FLUTTER TEST SYSTEM

Surface Deflection Auto Spectrum

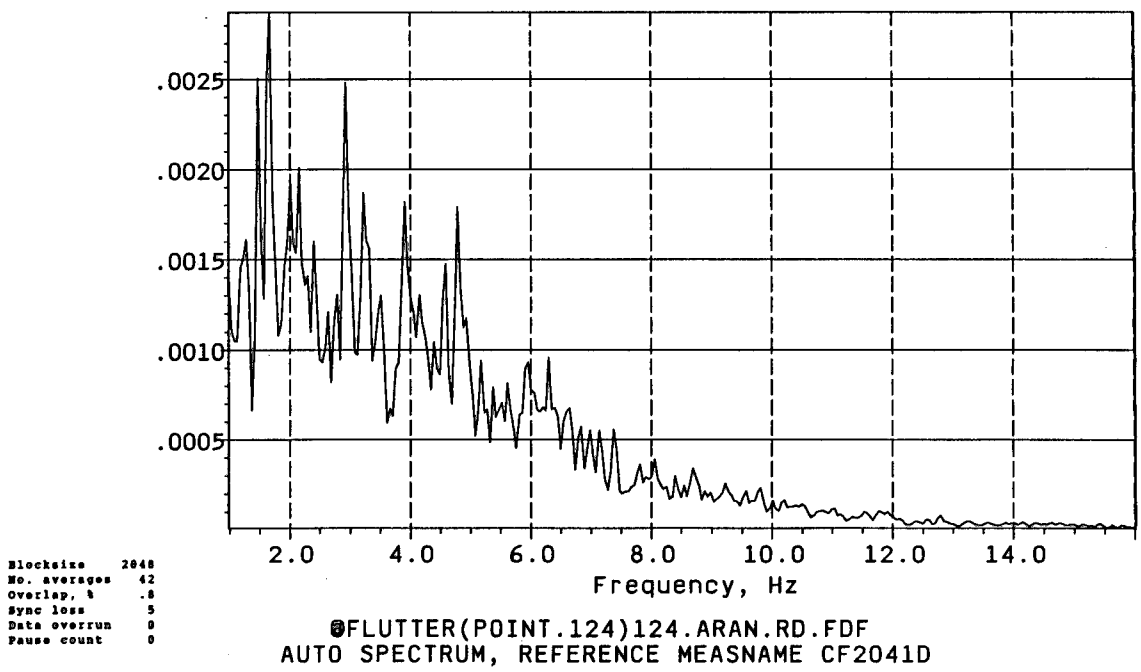

FLIGHT FLUTTER TEST SYSTEM

Frequency Response and Coherence Functions

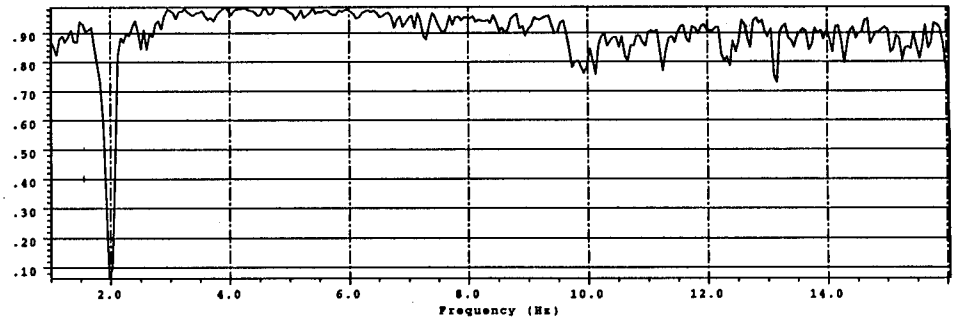

Magnitude

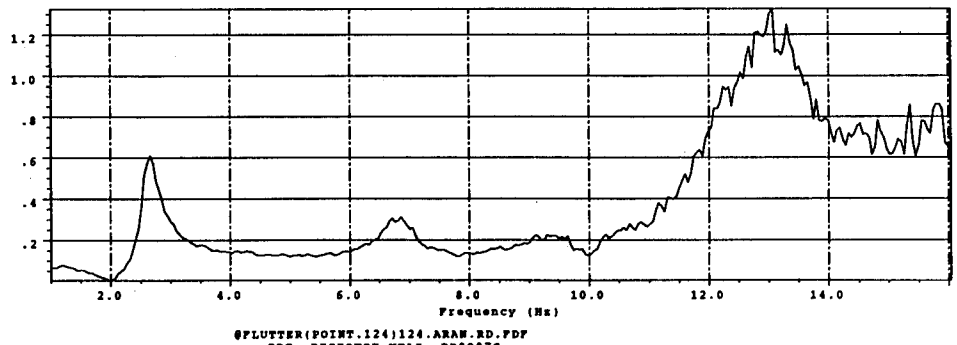

FLIGHT FLUTTER TEST SYSTEM

Fitted FRF

Magnitude

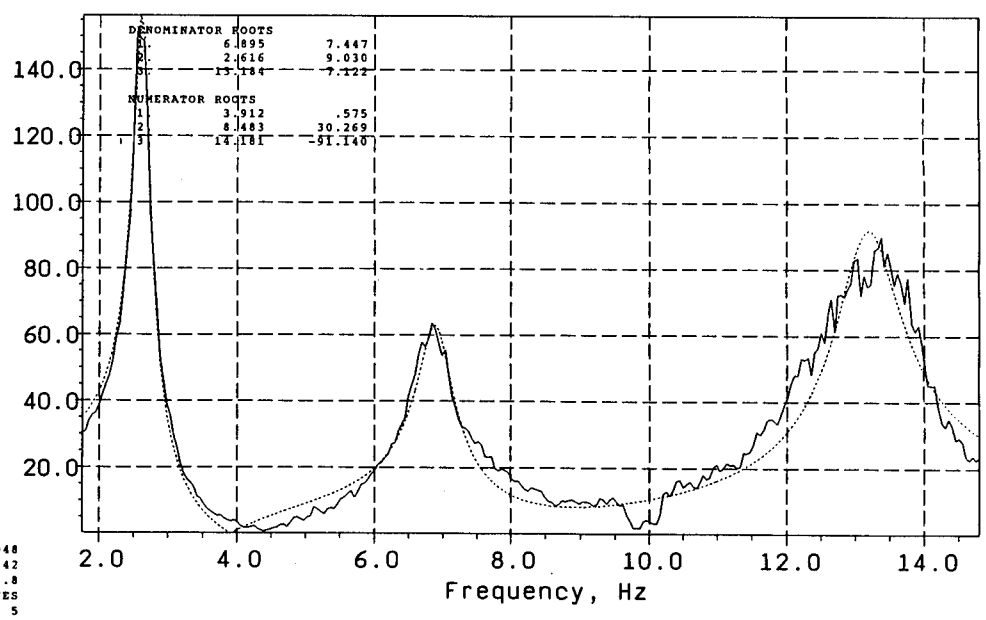

Blocksize 2048
No. averages 42
Overlap, % .8
Hanning window YES
Sync loss 5
Data overrun 0
Pause count 0
Error action: continue

@FLUTTER(POINT.124)124.ARAN.RD.FDF
FRF, RESPONSE MEASNAME BD0016S

FLIGHT FLUTTER TEST SYSTEM

Frequency/Damping Extraction Summary

MEAS. NAME	MODE 1		MODE 2		MODE 3		MODE 4		EXCITATION		ANAL METH
	f	g	f	g	f	g	f	g	TYPE	SURF	
BC0001G	2.81	16.4					13.1	7.60	RAN	RD	SPET
BC0002G	2.82	16.2							RAN	RD	SPET
BC0009G					9.53	14.3	13.7	8.07	RAN	RD	SPET
BC0010G	2.79	16.0	7.71	8.92					RAN	RD	SPET
BC0017S	2.81	16.6					13.1	8.10	RAN	RD	SPET
BC0018S	2.80	15.8					13.3	7.93	RAN	RD	SPET
BD0001G	2.82	15.9					13.1	8.27	RAN	RD	SPET
BD0009G	2.81	16.3	7.73	6.98	9.50	11.2	13.7	7.73	RAN	RD	SPET
BD0010G	2.79	16.3	7.71	9.04					RAN	RD	SPET
BD0017S	2.81	16.0					13.1	7.99	RAN	RD	SPET
BD0018S	2.81	16.0					13.6	8.63	RAN	RD	SPET
BC0004G	2.82	16.2					13.4	12.8	RAN	RD	SPET
BC0005G	2.82	16.2					13.2	9.43	RAN	RD	SPET
BC0015S	2.81	15.7	7.60	9.84			13.4	8.54	RAN	RD	SPET
BC0016S	2.81	16.2	7.72	9.09			13.6	8.62	RAN	RD	SPET
BC0020S	2.81	16.1	7.57	7.68					RAN	RD	SPET
BC0014G	2.80	16.1	7.48	9.45	10.3	16.8	13.4	7.32	RAN	RD	SPET
BD0004G	2.82	16.0							RAN	RD	SPET
BD0005G	2.82	15.8					13.2	9.13	RAN	RD	SPET
BD0006G	2.83	15.9	7.69	6.86	10.4	7.14			RAN	RD	SPET
BD0007G	2.84	15.5	7.74	7.95			13.3	9.59	RAN	RD	SPET
BD0011G	2.81	16.1	7.67	9.62	9.89	8.48	13.1	11.6	RAN	RD	SPET
BD0014G	2.81	16.0	7.55	6.55	10.4	8.65	13.2	9.33	RAN	RD	SPET
BD0016S	2.81	16.0	7.72	8.79			13.4	8.27	RAN	RD	SPET
BH0002G	2.80	16.5	7.62	8.02					RAN	RD	SPET
BH0012G	2.80	17.1			10.8	11.6	13.0	16.3	RAN	RD	SPET
BI0105S	2.81	15.6	7.68	7.06					RAN	RD	SPET
BI0106S	2.82	15.5	7.71	7.58					RAN	RD	SPET

AVERAGE	2.81	16.1	7.7	8.2	10.1	11.9	13.3	9.3
SIGMA	0.01	0.3	0.1	1.1	0.4	3.6	0.2	2.2
N	33	33	21	21	9	9	23	23

Aeroservoelastic Design, Test Verification and Clearance of an Advanced Flight Control System

J. Becker
Daimler Benz Aerospace AG
Military Aircraft Devision
Postfach 80 11 60
81663 München, Germany

V. Vaccaro
Alenia
Defense Aircraft Engineering
Corso Marche 41, Turin, Italy

SUMMARY

The design of notch filters is based upon a model of the aircraft describing the coupled flight dynamic, flight control dynamics and structural dynamic behaviour and on ground and in flight structural coupling tests. The paper outlines design procedures, design and clearance requirements, correlation between model predictions and structural coupling tests and model update for on ground and in flight.

1. INTRODUCTION

The development of advanced digital flight control systems for a modern military aircraft as shown in Fig. 1 is strongely influenced by aeroservoelastic effects. The flexible aircraft behaviour especially for artificial unstable aircraft con-figurations with outer wing missiles, tip pods and heavy under wing stores and tanks has significant effects on the flight control system (FCS). The signals of the inertia measuring unit (AMSU) - the gyro platform - contain besides the necessary information of rigid aircraft rates and accelerations also flexible aircraft rates and accelerations in the frequencies of the aircraft elastic modes. The 'flexible' aircraft rates and accelerations measured by the inertia measuring unit are passed through the flight control system control paths, they are multiplied by the FCS gains and FCS filters and inserted in the control surface actuator input which then drives the controls in the frequencies of the elastic modes of the aircraft. The flexible aircraft is excited by the high frequency control deflections and might also experience aeroservoelastic instabilities i.e. flutter can occur or limit cycle oscillations may occur, and dynamic load and fatique load problems can arise. The FCS design therefore has to minimize all structural coupling effects through the available means like optiminium sensor positioning, notch filtering and additional active control. This paper describes the major aspects, problem areas to be considered in the FCS design with respect to aeroservoelastic effects, it outlines notch filter optimisation technique and mentiones possible flight verification procedures. Many of the design and clearance aspects described here have been adressed in previous publications, see Ref.s 1 to 5.

2. AEOROSERVOELASTIC DESIGN FOR ADVANCED FLIGHT CONTROL SYSTEMS

2.1 Design philosophy

The FCS shall be designed to cover the full rigid, flexible aircraft frequency range with respect to aircraft rigid mode and structural mode coupling stability requiremtents for each control system individual loop for on ground and in flight. The structural coupling influences shall be minimised by FCS notch filters.The FCS shall be designed to be as robust as possible with respect to all possible aircraft configurations and configuration changes, (missiles on, off, tanks on and off etc) .That includes that all structural coupling changes with configuration should be covered by a constant set of notch filters to avoid system complexity due to configuration switches for different sets of notch filters. In addition any scheduling of notch filters with flight conditions should be avoided in a wide range of the flight envelope but not excluded for critical structural coupling areas. In order to avoid problems in the notch filter design due to nonlinear unsteady elastic mode and control surface aerodynamics and nonlinear actuator dynamics the elastic mode stability requirements should mainly be based on gain stabilisation of the flexible modes. Phase stabilisation shall only be applied to low frequency elastic modes in order not to create too complex design and clearance procedures. Phase stabilisation of low frequency elastic modes might not be avoided, it is used as tool to meet handling requirements.

The notch filter design can be based upon an analytical model of the aircraft structure including a linear FCS model. The analytical model must however be verified through ground test results both from ground resonance and structural coupling testing and from in flight flutter and structural coupling testing. The model should be updated by the test results for different configurations. Due to restrictions in the accuracy of the analytical model predictions on ground and in flight mainly at high frequency elastic modes where the prediction becomes more and more unrealistic the analytical model data with respect to inertia shall be replaced by on ground measured data. In order to cover all possible sets of aircraft store configurations a selection of critical configuration has to be established by analytical model investigation in advance.

The critical selected configurations have to be introduced into the design of the structural filters.

The notch filter design shall cover the full range of stores and fuel states for the absolute worst case of FCS gain for trimmed aicraft conditions and shall also take into account worst gain situations in out of trim conditions.

2.2 Design Requirements

2.2.1 Stability Requirements

The design requirements are primarily stability requirements for all flight control rigid/flexible aircraft modes. The stability are achieved by the introduction of notch filters.. The open frequency response requirements are demonstrated in Fig. 2 for the cases A and B.

case A describes in a Nichols diagram the gain and phase margin requirement for early prototype

Paper presented at the Structures and Materials Panel Specialists' Meeting on "Advanced Aeroservoelastic Testing and Data Analysis", held in Rotterdam, The Netherlands, from 8-10 May 1995, and published in CP-566.

flying and indicate that all elastic modes shall be gain stabilised.

case B describes gain and phase margins for production aircraft for configurations which are flight tested on prototypes including structural coupling flight tests. The first frequency low flexible modes are phase stabilised and higher frequency flexible modes are gain stabilised.

e MIL Spec. MIL-F-9490 D FCS requirements shall be met.

2.2.2 Vibration Requirements/Dynamic Load Requirements

In addition to the stability requirements for the structural coupling unacceptable vibration levels must be avoided including noise levels. The vibration levels induced by structural coupling might create high fatique loads to actuators and to aircraft structure. The notch filters together with noise filters have to be designed to meet the specific vibration requirements.

2.2.3 Flutter Requirements

The FCS design for elastic mode coupling reduction with notch filters has to fulfill the flutter requirements of the aircraft without FCS. The aircraft with FCS shall meet the 15 % flutter speed margin as well as the minimum elastic mode damping requirements as described in MIL SPEC MIL-A-0087A.

2.3 Design Tools

The FCS design for the flexible aircraft is possible with the assumption that the aircraft characteristics are predictable to the necessary accuracy to optimize notch filters which meet the requirements. The characteristics of the controlled flexible aircraft shall be described in the form of open loop frequency transfer functions of the FCS control path feedback loops to a sufficient high frequency, see blockdiagram in Fig. 3. In detail for the longitudinal control system the pitch rate, the normal acceleration and the flow sensor α open loop signal at the control opening point has to be known. For the lateral control the roll rate -, yaw rate-. lateral acceleration - and flow sensor signal β - open loop signal has to be described. The open loop signal consists of the transfer function of the aircraft due to control surface input sensed at the inertia measuring unit (rates and accelerations) and sensed at the flow sensors and the transferfunction of the FCS from the sensor to the opening point and from the opening point to the actuators.

The individual transferfunction can be derived from two different methods the first using the analytical dynamic model calculation, the second using on ground measured sensor to actuator input transfer functions from the structural coupling test superimposed with calculated magnitudes of unsteady aerodynamic transfer functions. The applicability of the analytical dynamic model calculation pends on the accuracy of the modelling and its verification. Both methods depend on the accuracy of the unsteady aerodynamic transfer functions which are in both methods derived from theoretical predictions of unsteady aerodynamics for elastic modes and control surface deflection.

2.3.1 Analytical Model of the Flexible Aircraft with Flight Control System

The analytical model of the flexible aircraft with FCS consists of the linear dynamic description of the flight mechanic equations of motion, the description of the flexible aircraft through modal description using generalized coordinates, generalised masses, stiffness and model structural damping and generalised aerodynamic forces of the flexible modes and generalised control surface inertia and unsteady aerodynamic terms, the FCS is described through linear differential equations. In addition hardware and software, i.e. all sensors, actuators computer characteristics are described by differential equations. The flexible aircraft with control FCS can be demonstrated in a matrix form, see below

The equations of motion for the forced dynamic response of an aeroelastic system can be written in matrix differential equation form:

$$m_r b_r^2 \begin{bmatrix} M_{qq} & M_{q\delta} \\ M_{\delta q} & M_{\delta\delta} \end{bmatrix} \begin{Bmatrix} \ddot{q} \\ \ddot{\delta} \end{Bmatrix} + \frac{s_R}{kV} \left\{ \omega_r^2 m_r b_r^2 \begin{vmatrix} gK_{qq} & 0 \\ 0 & K''_{\delta\delta} \end{vmatrix} + \right.$$

$$+ \frac{\rho}{2} V^2 F s_R \frac{b_r}{s_R} \begin{vmatrix} c''_{qq} & c''_{q\delta} \\ c''_{\delta q} & c''_{\delta\delta} \end{vmatrix} \begin{Bmatrix} \dot{q} \\ \dot{\delta} \end{Bmatrix} + \left\{ \omega_r^2 m_r b_r^2 \begin{vmatrix} K_{qq} & 0 \\ 0 & K'_{\delta\delta} \end{vmatrix} + \right.$$

$$+ \frac{\rho}{2} V^2 F s_R \frac{b_r}{s_R} \begin{vmatrix} c'_{qq} & c'_{q\delta} \\ c'_{\delta q} & c'_{\delta\delta} \end{vmatrix} \begin{Bmatrix} q \\ \delta \end{Bmatrix} = \begin{Bmatrix} Q(t) \end{Bmatrix},$$

where m_r, b_r and ω_r are the reference mass, length and frequency and M, K and C are referred to as the generalized mass, stiffness and aerodynamic matrices which are nondimensional. The generalized mass and stiffness matrices are calculated using a finite element mode (FEM) of the total aircraft, see Fig. 4. For dynamic response calculation the FEM is reduced, see Fig. 5. The true airspeed V and semispan s_n of the reference plane are used to form the reduced frequency $k = (\omega s_R)/_V$. F is the area of reference plane and g is the structural damping of the elastic modes. The generalized forces Q are equal to zero for the conventional flutter problem. The generalized coordinate q describes the amplitude of the elastic airplane modes including elastic control surface modes for a system with actuators whereas δ_0 denotes the rotation of the rigid control surface according to the complex actuator stiffness represented by the impedance function of equation (2).

$$K_{\delta 0 \delta 0} = K'_{\delta 0 \delta 0} + iK''_{\delta 0 \delta 0}.$$

For the controlled aircraft the servo-induced control deflection $\Delta\delta$ has to be introduced as an additional degree of freedom for each control surface. The generalized forces generated by the servoinduced con-trol deflections $\Delta\delta$ can be described as the right-hand term of equation (1) by

$$\left\{Q(t)\right\} = -m_r b_r^2 \begin{Bmatrix} Mq_{\Delta\delta} \\ M_{\dot\delta_o \Delta\delta} \end{Bmatrix} \Delta\ddot\delta$$

$$- \frac{\rho}{2} V^2 F s_R \frac{b_r^2}{s_R^2} \frac{s_R}{k \cdot V} \begin{Bmatrix} c''q_{\Delta\delta} \\ c''_{\dot\delta_o \Delta\delta} \end{Bmatrix} \cdot \Delta\dot\delta$$

$$- \frac{\rho}{2} V^2 F s_R \frac{b_r^2}{s_R^2} \begin{Bmatrix} c'q_{\Delta\delta} \\ c'_{\dot\delta_o \Delta\delta} \end{Bmatrix} \Delta\delta.$$

Assuming normalized rigid control surface modes δ_o and $\Delta\delta$, the rotation of each control surface can be superimposed by

$$\delta = \delta_o + \Delta\delta$$

δ is used here as abbreviaion of foreplane and inboard and outboard flap or for rudder and differential inboard and outboard flap

The state-space-description of (1) is as follows:

$$\{x\} = [A]\{x\} + \{B\}x_i$$

The matrix in equation (1) describing the flexible aircraft with FCS is enlarged by linearized rigid flight mechanic equations. For example the state vector for longitudinal control includes then rigid aircraft state variables

$$X = {}_L\Delta v/v,\ \Delta\alpha,\ \Delta\omega y,\ \Delta 0,\ q,\ \delta_o,\ \Delta\delta,\ q,\ \delta_o,\ \Delta\delta$$

The flight mechanic equations may in a first approximation contain elastified aerodynamic derivatives as function of incidence, Mach number and they are for low frequency assumed to be decoupled from the flexible aircraft equations. In another approximation the flight mechanic equations are fully rigid and theoretical inertia and unsteady aerodynamic coefficients are introduced.

The flight mechanic equations for longitudinal control are described below:

Rigid aircraft equations with flexible compling terms
Normal Force equations

$$\Sigma Z = -\varrho/2\, V^2 F \left[c'_{z\alpha}(\omega)\cdot\alpha + c''_{z\alpha}(\omega)/\omega\cdot\dot\alpha\right]$$

$$- mV\cos\alpha\omega_y - \varrho/2\, V^2 F\bar c\left[c'_{zq}(\omega)\omega_y + c''_{zq}(\omega)\dot\omega_y\right]$$

$$- mg\sin\alpha\,\Theta$$

$$- \varrho/2\, V^2 F\left[c'_{z\dot\delta}(\omega)\,\delta + c''_{z\dot\delta}(\omega)/\omega\cdot\dot\delta\right] - Z_{m\dot\delta}\ddot\delta$$

$$- \varrho/2\, V^2 F\left[\Sigma_j c'_{zqj}(\omega)\,q_j + \Sigma_j c''_{zqj}(\omega)\,q_j\right] = 0;$$

Elastified 'rigid' aircraft equations

$$\Sigma Z = -\varrho/2\, V^2 F\, c_{zq}(\alpha)\alpha - mV\cos\alpha\omega_y - \varrho/2\, V^2 F\bar c\, c_{zq}\,\omega_y$$

$$- mg\sin\alpha\,\Theta$$

$$- \varrho/2\, V^2 F\cdot c_{z\dot\delta}(\alpha)\,\delta = 0;$$

Pitch Moment equation witch flexible compling terms

$$\Sigma M = -\varrho/2\, V^2 F\bar c\left[c'_{m\alpha}(\omega)\,\alpha + c''_{m\alpha}(\omega)\cdot\dot\alpha\right]$$

$$- I_y\dot\omega_y$$

$$- \varrho/2\, VF\bar c^2\left[c'_{mq}(\omega)\,\omega_y + c''_{m}(\omega)\,\dot\omega_y\right]$$

$$- \varrho/2\, V^2 F\bar c\left[c'_{m\dot\delta}(\omega)\,\delta + c''_{m\dot\delta}(\omega)/\omega\,\dot\delta\right] - M_{m\dot\delta}\ddot\delta$$

$$- qFs\left[\Sigma_j c'_{mqj}(\omega)\,q_j + c''_{mqj}(\omega)/\omega\,\dot q_j\right] = 0$$

Elastified Pitch Moment 'rigid' aircraft

$$\Sigma M = -\varrho/2\, V^2 F\bar c\, c_{m\alpha}\cdot\alpha + I_y\dot\omega_y - \varrho/2\, V^2 F\bar c\, c_{m\dot\delta}(\alpha)\,\delta$$

$$- \varrho/2\, V^2 F\bar c^2\, c_{mq}\,\omega_y$$

$$- \varrho/2\, V^2 F\bar c^2\, c_{m\dot\alpha}\cdot\dot\alpha = 0;$$

c'	Real part of calculated aerodyn. coefficient
c''	Imag. part of calculated aerodyn. coefficient
$\varrho/2\, V^2$	dynamic pressure
F	reference area
$\bar c, s$	reference length
q_j	generalized coordinate

Conservative Assumptions

The assumptions to be made for dynamic modelling including hardware have to be conservative in order to cover any system failure.

Actuator Characteristics:

The transfer function of the actuators shall meet the upper gain boundary. The actuator phase characteristic shall include both extremes for minimum and worst phase boundaries. Nonlinear actuator characteristics with amplitude reduce structural coupling.

The actuator phase characteristic is important for the phase stabilisation concept. An example of actuator transfer function is shown in Fig. 8.

Inertia Measuring Unit:

The transfer function of the sensor platform has to describe the upper gain boundary and the minimum and maximum phase boundary. Only the upper linear boundary is necessary to be represented.

Flow Sensors:

Approximated measured flow sensor transfer functions shall be used.

Structural Modelling:

Consideration of the full travel of the flexible mode frequencies with flight condition, fuel contents and actuator failure cases is necessary. The minimum experienced structural damping shall be applied. In order to be accurate, the analytical model has to updated from ground resonance test results mainly with respect to mode frequencies.

In addition the aircraft identification test results from structural coupling test shall be adopted. Flexible mode frequency shifts with actuator demand amplitude shall be adopted to the modelling to represent minimum and maximum possible mode frequency.

Unsteady Aerodynamic Modelling:

The unsteady forces used in the dynamic model calculation shall be represented in a conservative manner.
The magnitude of the unsteady aerodynamic forces:
The magnitude (modulus) of the unsteady forces of the flexible modes and of the control surface defection shall be predicted to represent a realistic high value for all Mach numbers and incidences. Since flow separation at higher incidences is leading to alleviation in the motion induced pressure distributions of the flexible modes and of the control surface deflections the introduction of unsteady aerodynamic forces from pure linear theory is regarded to be conservative. Special attention has to be put to transonic effects on the unsteady aerodynamic forces. Since however the structural coupling critical conditions which are related to the worst gain condition of the FCS are high incidence conditions, because the FCS gains result from low control surface efficiencies at high incidence, the assumption of linear unsteady subsonic and supersonic aerodynamics derived by linear theory or numerical Euler code calculations in the linear range is believed to be conservative throughout the full flight envelope.

The magnitude for the unsteady aerodynamic forces is sufficient for the design of high frequency elastic mode notch filters, because only a gain margin requirement is requested.
It shall be stated that the unsteady forces must be calculated for a number of reduced frequencies to cover the full frequency range.

The Phase of the Unsteady Aerodynamic forces:

For the phase stabilisation of low frequency flexible modes like the first wing/fin bending the unsteady aerodynamic phase shall be represented in a conservative manner. A reasonable approach for the phase of the first elastic mode is again the application of linear theory. The argumentation is that at high incidence and combined high FCS gains the aerodynamic damping is increased compared to low incidence from experience found for different wing configurations. In terms of phase stability margin Ref. 3. explains the difference in a Nichols diagram, where linear theory shows the more critical condition..

FCS Modelling:

In order to design in a robust manner the calculation of open loop transfer functions shall consider the worst FCS gain conditions. The worst trimmed end to end gain conditions have to be included into the model calculations. Special consideration shall be also put to the maximum out of trim gain conditions with respect to structural coupling criticality.

2.3.2 Ground Test Result

Ground vibration test results and structural coupling tests are needed to verify or update the calculated results from dynamic model predictions. In general the total aircraft structural dynamic model consisting of subcomponents can be updated by updating the subcomponent stiffness and damping using the results from component ground resonance tests and aircraft ground resonance and structural coupling tests. The update of the analytical model is described separately in the ALENIA paper, see Ref. 6.
A typical result of the comparison of ground test to prediction is shown in Fig. 9

2.3.3 Flight Test Results

Flight test results from structural coupling/flutter tests are needed to verify or update the predicted results of open loop frequency response functions by the update of unsteady aerodynamic forces used in the dynamic model. This can be achieved through the comparison of predicted and flight test measured closed loop converted into open loop frequency transfer functions.

The comparison there is not only restricted to loop signals, also predicted accelerations at significant aircraft locations are compared, i.e. outer wing, front, rear

fuselage upper fin.

The flight test results are derived through frequency sweep excitation of the control surfaces which should be possible through a special software in the FCC's.

2.5 FCS Design with Optimisation of Structural Decoupling

Different means are available to minimize structural coupling effects in the Flight Control System. The practical usable tools are to minimize structural coupling are:

- optimum sensor location
  The AMSU shall be put to the antinode of the first fuselage bonding mode, the elastic pitch-yaw angle/pitch-yaw rate is there minimum. Optimum sensor location is meaningless for first wing bending mode coupling since, the fuselage counteracts with a linear pitch, see Fig. 6, 7.

- Stiffening of the AMSU platform:
  A very high stiffness of the sensor platform is favourable, since local medium to high frequency elastic rates will not occur. A frequencies optimum shall be as high as possible

- Actuator transfer function:
  A strong decay in the actuator transfer function at medium to high frequencies would minimize coupling effects. Actuator frequencies at medium frequencies (10 - 30 Hz) shall be well damped, see Fig. 8. Actuator phase shifts at low elastic mode frequencies shall be known for the absolute minimum and maximum value

- Minimum weight/inertial of control surfaces,
  High frequency 20 - 80 Hz structural coupling effects are small using light weight controls.

- FCS Optimisation:
  Fig.'s 3 demonstrate schematically the feed-back paths for the longitudinal and laterial stabilisation. After the measurement of the vertical, laterial accelerations, the pitch rate, the roll rate and yaw rate, the flow sensor signals α and β, these signals are filtered first in the AMSU by notch filters which minimize the signals at high frequencies, then the signals are filtered by the flight control computer notch - and phase advance filters. After multiplication with the FCC gains the signals are passed to the different control surface actuators. In front of the actuator input the signals are filtered by flap, canard and rudder notch filters. A certain optimisation is achieved by putting a number of notch filters in the feedback paths and to use also in the paths to the control additional filters. With this concept a better minimization of phase shifts at low frequency, which is necessary to meet the handling criteria, is possible.

- Optimisation of phase advance filters:
  Phase advance filters used in the FCS shall be configured that low frequency phase shifts due to notch filtering and other delays are put to zero at low frequency. In addition to minimize elastic mode coupling the well known dB increase of advance filters at higher frequencies shall be minimized. The optimisation of phase advance filter should be combined with the notch filter optimisation. This might be performed in a iterative manner or in a combined optimisation with the frequency response functions including rigid aircraft response.

- Optimisation of notch filters:
  The notch filter optimisation is the major tool for decoupling the aircraft control from aero-servoelastic influences. Since the coupling is of severe impact on the FCS on delta wing unstable aircraft a mathematical filter optimisation had to be developed in order to achieve flight dynamic requirements. The optimsation is described here.

In order to optimize the filters it is necessary to establish the open loop frequency response functions at the opened summation points of the longitudinal and lateral control S_{L1}, S_{L2} and S_{A1}, S_{A2}, see Fig.

For example the open loop frequency response function at the longitudinal open loop point S_{L1} can be formulated using the seperate transfer functions of the loop response without notch filters due to flap and canard excitation (S_{L1} closed) and by putting for each separate flap or canard excitation the gains of the loops in a sequence to zero

a) $G_{nz} = 0,\ G_\alpha = 0,\ G_q \neq 0$

a1) flap excitation only to generate F_F^q at S_{L1}

a2) canard excitation only to generate F_c^q at S_{L1}

b) $G_{nz} = 0,\ G_\alpha \neq 0,\ G_q = 0$

b1) flap excitation only to generate F_F^α at S_{L1}

b2) canard excitation only to generate F_c^α at S_{L1}

c) $G_{nz} \neq 0,\ G_\alpha = 0,\ G_q = 0$

c1) flap excitation only to generate F_F^{nz} at S_{L1}

c2) canard excitation only to generate F_c^{nz} at S_{L1}

The total open loop transfer function F at S_{L1} can be formu-lated

$$F(f) = [F_F^q\ F_{NF} + F_C^q\ F_{NC}] * F_A^q$$
$$+ [F_F^\alpha\ F_{NF} + F_C^\alpha\ F_{NC}] * F_{AD}^\alpha$$
$$+ [F_F^{nz}\ F_{NF} + F_C^{nz}\ F_{NC}] * F_A^{nz}$$

where

F_{NF} = Flap notch filters transfer function

F_{NC} = canard notch filters transfer function

F_A^q AMSU notch filters transfer function

$F_A^{n_z}$ AMSU notch filters transfer function

F_{AD}^{α} Flow sensor signal notch filter transfer function

A similar formulation can be derived for all other summation points S_{L2}, S_{A1} and S_{A2}.

The open loop frequency response functions F_F and F_C can be calculated at arbitrary frequency steps using the dynamic model response programme or the dynamic model response programme for the aerodynamic open loop response functions calculation only which are then superimposed to the relevant frequency response functions measured during structural coupling tests on ground factorised by the FCS path gains and filter transfer function.

Digital effects in the design.
The notch filter transfer functions are designed and specified as second order numerator and denominator functions in the continuous Laplace domain but take into account frequency warning effects.

$$\acute{\omega}_z = \frac{2}{T} \tan \frac{\acute{\omega}_L T}{2}$$

$\acute{\omega}_L$ is the Laplace domain frequency

$\acute{\omega}_z$ is the digital domain frequency

T is the sample period

$$F = \frac{1 + As + Bs^2}{1 + Cs + Ds^2}$$

The notch filter transfer function in its analog form is

$$F = \frac{1 + as + bs^2}{1 + cs + ds^2}$$

$$A = a \frac{\omega_n T}{2 \tan\left(\frac{\omega_n T}{2}\right)}; \qquad B = b \left(\frac{\omega_n T}{2 \tan\left(\frac{\omega_n T}{2}\right)} \right)^2$$

$$C = c \frac{\omega_n T}{2 \tan\left(\frac{\omega_n T}{2}\right)}; \qquad D = d \left(\frac{\omega_n T}{2 \tan\left(\frac{\omega_n T}{2}\right)} \right)^2$$

The notch filter transfer function in its prewarped specification is

The frequency in the continuous domain corresponds to a downward frequency warping in the digital domain.

The digital effects caused by AMSU sensor signal processing transmission delay and sampling of the AMSU output by the FCC's is represented in the dynamic model by AMSU hardware assumptions using a defined transfer function.

The aliasing is included in the analysis by a folding back procedure.

The notch filter coefficients are optimized using a notch filter optimisation programme. The computer programme is based on the Schittkowski FORTRAN subroutine solving constrained nonlinear programming problems, see Ref. 7 A finite difference gradient approach is applied.

From the total open loop frequency response function the phase shift at low frequency due to notch filters can be derived which shall be minimized.

min Phase (F(f ≈ 1Hz))

The total open loop frequency response function including optimized notch filters shall meet the stability requirements, -9 dB for gain stabilisation or the gain/phase requirements described in 2.2.

With these requirements the constraints of the optimisation can be formulated. The total number of constraints is defined by the number of frequencies at which the requir-ement has to be fulfilled.

The number of variables is known from the number of notch filters. Initial guess of the solution is prescribed in the input and used after initial optimisation runs. Lower and upper bounds of the variables are prescribed.

Notch filter numerator, denominator frequencies are selected using the frequencies response peak characteristic for the selection of numerator frequencies, the asymtotic behaviour of the notch filters at high frequencies for the denominator frequency and the denominator critical damping for each notch filter. The notch filter critical damping for AMSU filters is prescribed to be > 0.25 for FCC the minimum value is prescribed to be > 0.1A scaling matrix is used for the variables.

Examples of optimisation:
The result of a optimisation of notch filters is demonstrated in Fig. 10. The Bode- and Nichols diagram show the open loop frequency response with and without notch filters for special configurations and flight conditions.

The figure also includes variation in parameters for which the notch filters are applied but not optimized. This situation due to the following circumstances may happen

- the structural coupling test on ground shows different frequencies of the elastic modes than assumed in the design (for instance a special configuration was not included in the design etc.)
- the in flight structural coupling test shows different db's and different phase of the low frequency elastic modes than assumed during design, see for example Fig. 11
- the on aircraft actuator characteristics are different from design assumptions
- Redesign of structural parts local weight changes,

change of pylon stiffnesses etc. during development phase

It is the task of the structural coupling/notch filter design and clearance procedure to treat this situation.

4. DESIGN AND CLEARANCE PROCEDURE

Fig. 12 shall explains the design and clearance procedure which is based upon a series of on aircraft tests and on rig tests for identification and clearance and consequently a series of dynamic model updates from testing and from updated FCS definitions. Reiteration of the full process of ground tests, prediction model updates and notch filter optimisation is necessary for new configuration etc.

5. CONCLUSIONS

The structural coupling/notch filter design and clearance procedure as described has demonstrated the complexity in the dynamic modelling resulting from the finite element modelling technique and its update resulting from aircraft component tests, aircraft ground vibration tests and on ground structural coupling tests and also from updates of actuator impedance and frequency response functions from rig and on aircraft tests as well as unsteady aerodynamic modelling of elastic modes and of control surface rotations at all flight conditions and its validation by structural coupling flight tests.

It was demonstrated that a robust FCS notch filter design has to be adopted which includes the description of all worst case assumptions for the structure, the FCS gains and FCS minimum and maximum phase at low elastic mode frequencies, and worst case assumption for actuator and sensor hardware. Digital effects have to be fully included.

In order to achieve a realistic clearance procedure the notch filters coefficients shall not be dependent on flight condition and aircraft configuration.

To design a common notch filter set for configurations and flight conditions the design concept of phase stabilisation of low frequency flexible aircraft modes has to be applied in order to meet the requirements for aircraft handling. In addition if this concept is not fully sufficient notch filter scheduling with flight condition for extreme flight condition shall be considered.

6. REFERENCES

1. A. Lotze, O. Sensburg, M. Kühn
   Flutter investigations on a combat aircraft with a command and stability augmentation system
   AIAA Paper No. 75-1025, AIAA 1975 Aircraft Systems and Technology Meeting

2. O. Sensburg, J. Becker, H. Hönlinger
   Active Control of Flutter and Virbrations of an aircraft
   Proceedings of the International IUTAM, Symposium on Structural Control, University of Waterloo, Ontario, Canada, 4th - 7th June 1979

3. J. Becker
   Aeroservoelastic Stability of aircraft at high Incidence
   68th AGARD Fluid Dynamics Panel Specialist Meeting, May 1991

4. B.D. Caldwell
   The FCS-Structural Coupling problem and its solution, AGARD Conference Proceedings on Active Control Technology,
   FMP Symposium held at Turin, May 1994

5. H. Hönlinger, H. Zimmermann, O. Sensburg, J. Becker
   Structural Aspects of Active Control Technology
   AGARD Conference Proceedings on Active Control Technology, FMP Symposium held at Turin, May 1994

6. V. Vaccaro, J. Becker
   Ground structural coupling testing and model updating in the aeroservoelastic qualification of a combat aircraft AGARD 80th SMP Meeting on Advanced aero-servoelastic testing and data analysis, Rotterdam 7th 12th May 1995.

7. Schittkowski, K., NLPQL: AFORTRAN
   Subroutine solving constraint nonlinear programming problems, Annuals of Operations, 5, 485-100 (edited by Clyde L. Mouna)

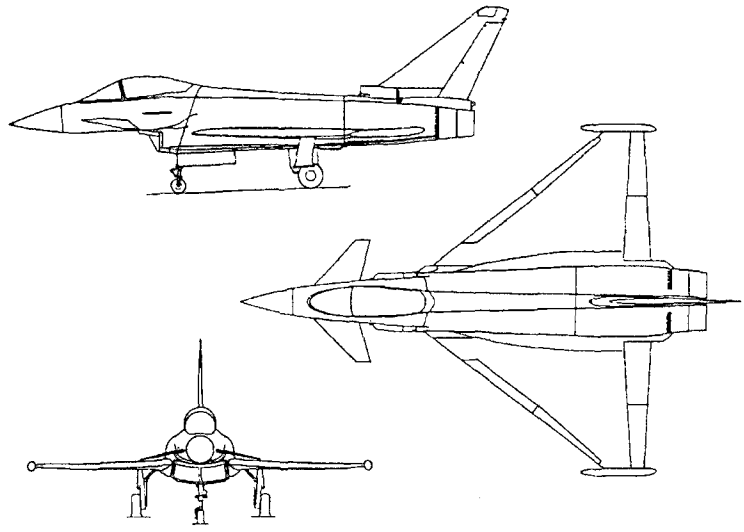

FIG. 1 MODERN MILITARY AIRCRAFT

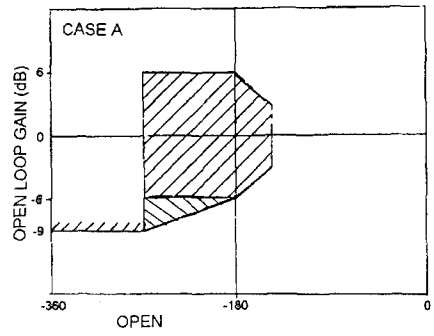

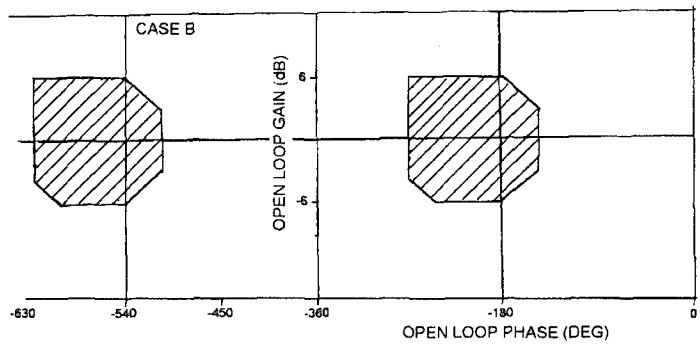

FIG. 2 STABILITY REQUIREMENTS FOR OPEN LOOP (NICHOLS DIAGRAM FREQUENCY RESPONSE FUNCTIONS CASE A EARLY PROTOTYPE FLYING CASE B PRODUCTION AIRCRAFT

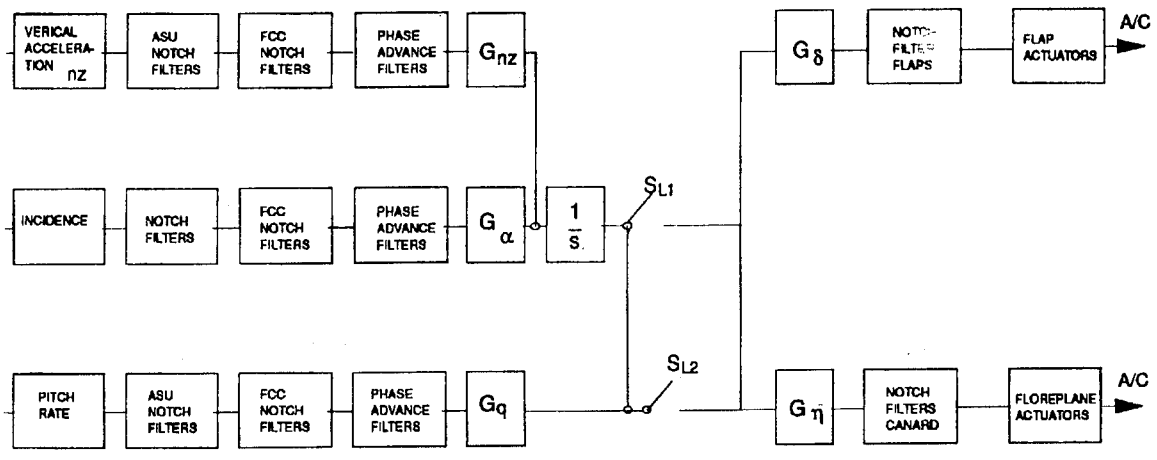

G_{n2}, G_2, G_q, G_δ, G_η CONTROL FEEDBACK GAINS

AMSU Aircraft Motion Sensor Unit

FCC Flight Control Computer

BLOCKDIAGRAM OF LONGITUDINAL CONTROL
STABILISATION PATHS (SCHEMATIC)

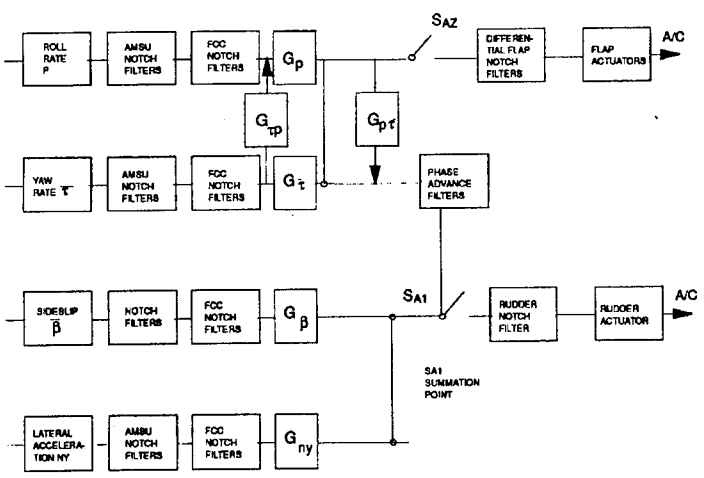

BLOCKDIAGRAM OF LATERAL CONTROL
STABILISATION PATHS (SCHEMATIC)

FIG. 3

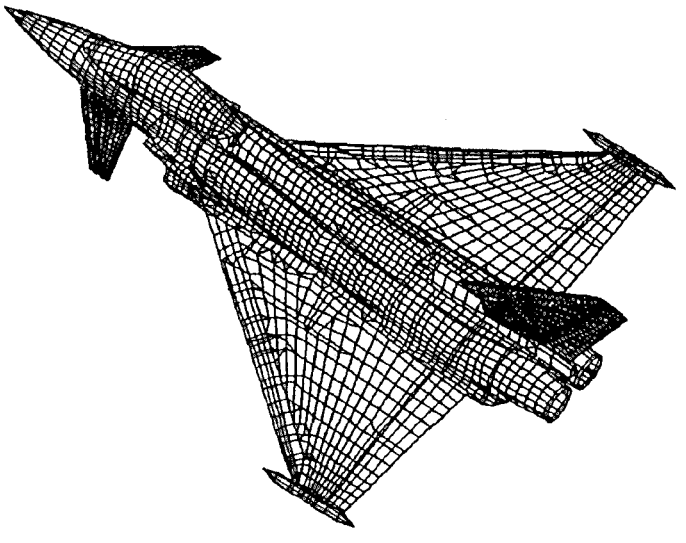

FIG. 4 FINITE ELEMENT MODEL OF THE AIRCRAFT
(STATIC ASSEMBLY)

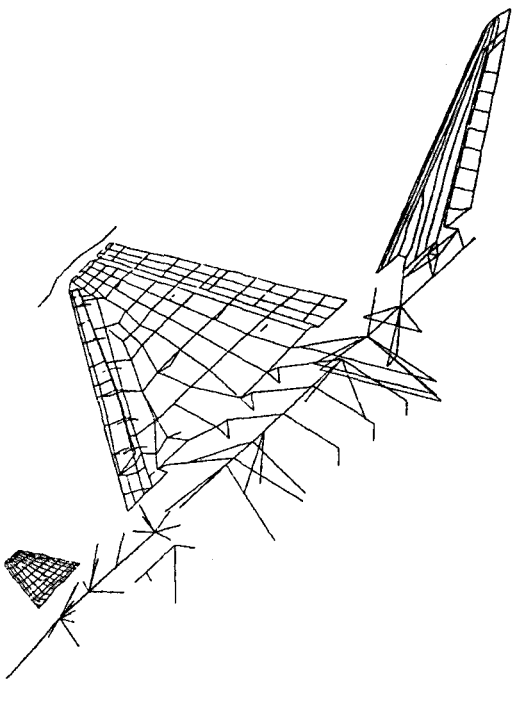

FIG. 5 STRUCTURAL GRID FOR DYNAMIC CALCULATIONS
(DYNAMIC ASSEMBLY)

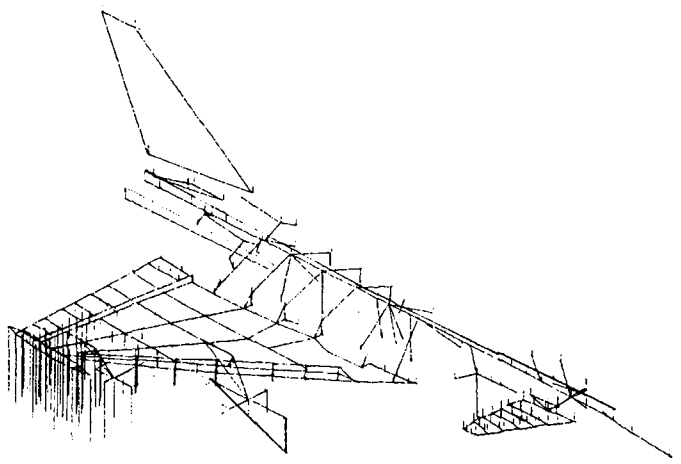

FIG. 6 TYPICAL SYMMETRIC FIRST WING BENDING MODE FOR AIRCRAFT WITH UNDERWING TANK

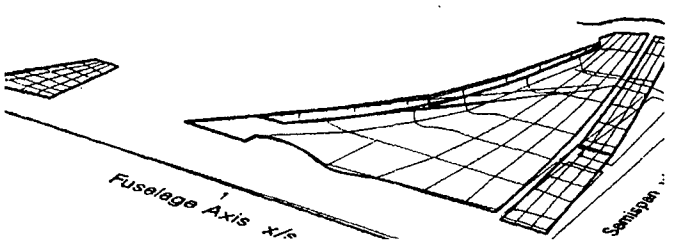

FIG. 7 APPROXIMATION OF FLEXIBLE MODE UNSTEADY AERODYNAMIC CALCULATIONS

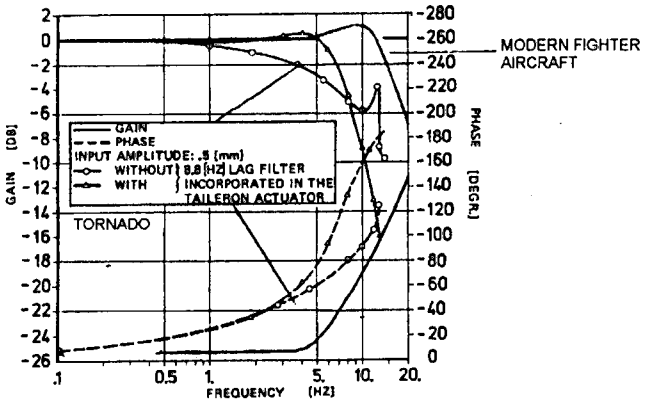

FIG. ACTUATOR TRANSFER FUNCTION COMPARISON OF TORNADO TO MODERN FIGHTER

FIG. 8 ACTUATOR TRANSFER FUNCTION COMPARISON OF TORNADO TO MODERN FIGHTER

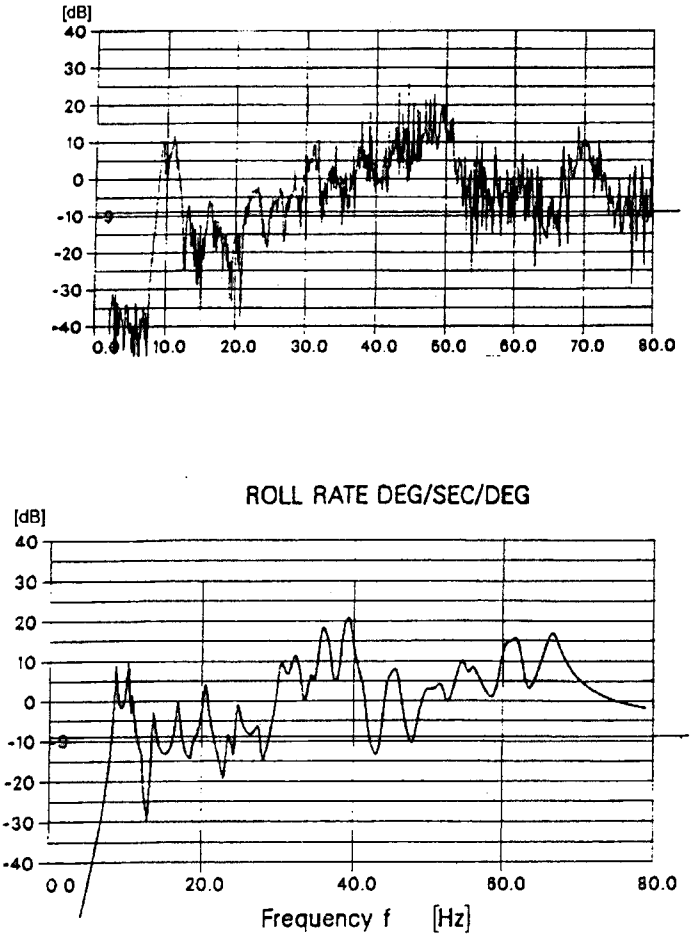

FIG. 9 COMPARISON OF AMSU ROLL RATE DUE TO RUDDER FREQUENCY RESPONSE FUNCTION PREDICTION VERSUS TEST RESULT ON GROUND

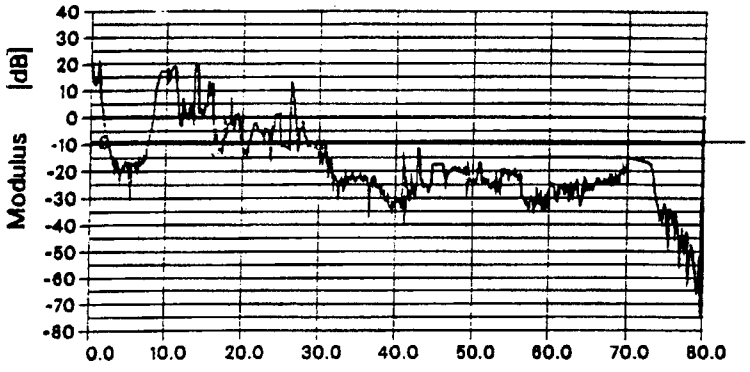

FIG. 10A OPEN LOOP FREQUENCY RESPONSE WITHOUT FCC NOTCH FILTERS BUT WITH AMSU NOTCH FILTERS

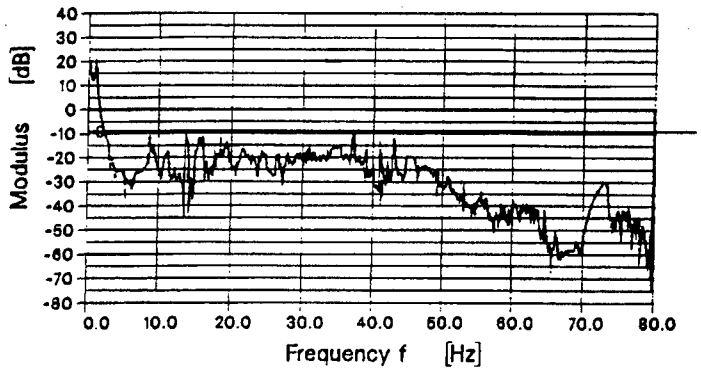

FIG. 10B OPEN LOOP FREQUENCY RESPONSE WITH NOTCH FILTER (AMSU and FCC)

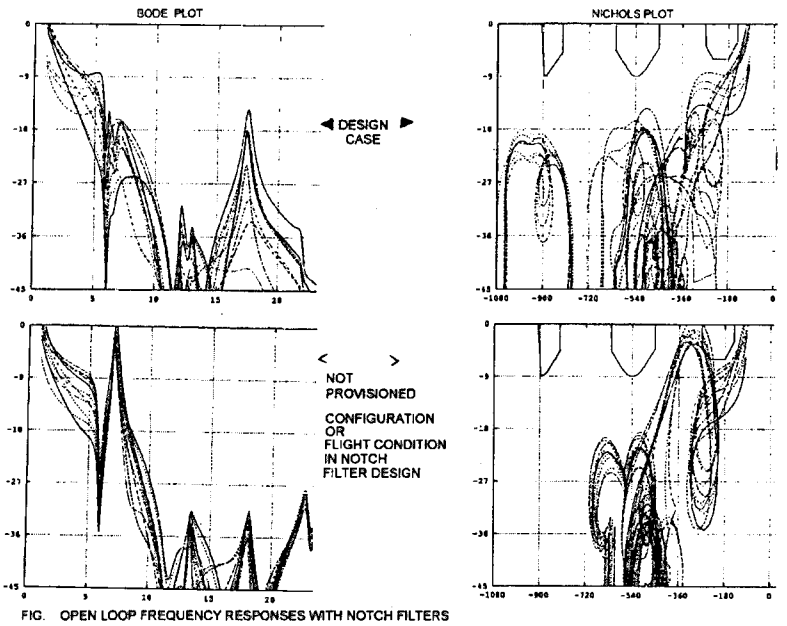

FIG. OPEN LOOP FREQUENCY RESPONSES WITH NOTCH FILTERS

FIG. 11 OPEN LOOP FREQUENCY RESPONSES WITH NOTCH FILTERS

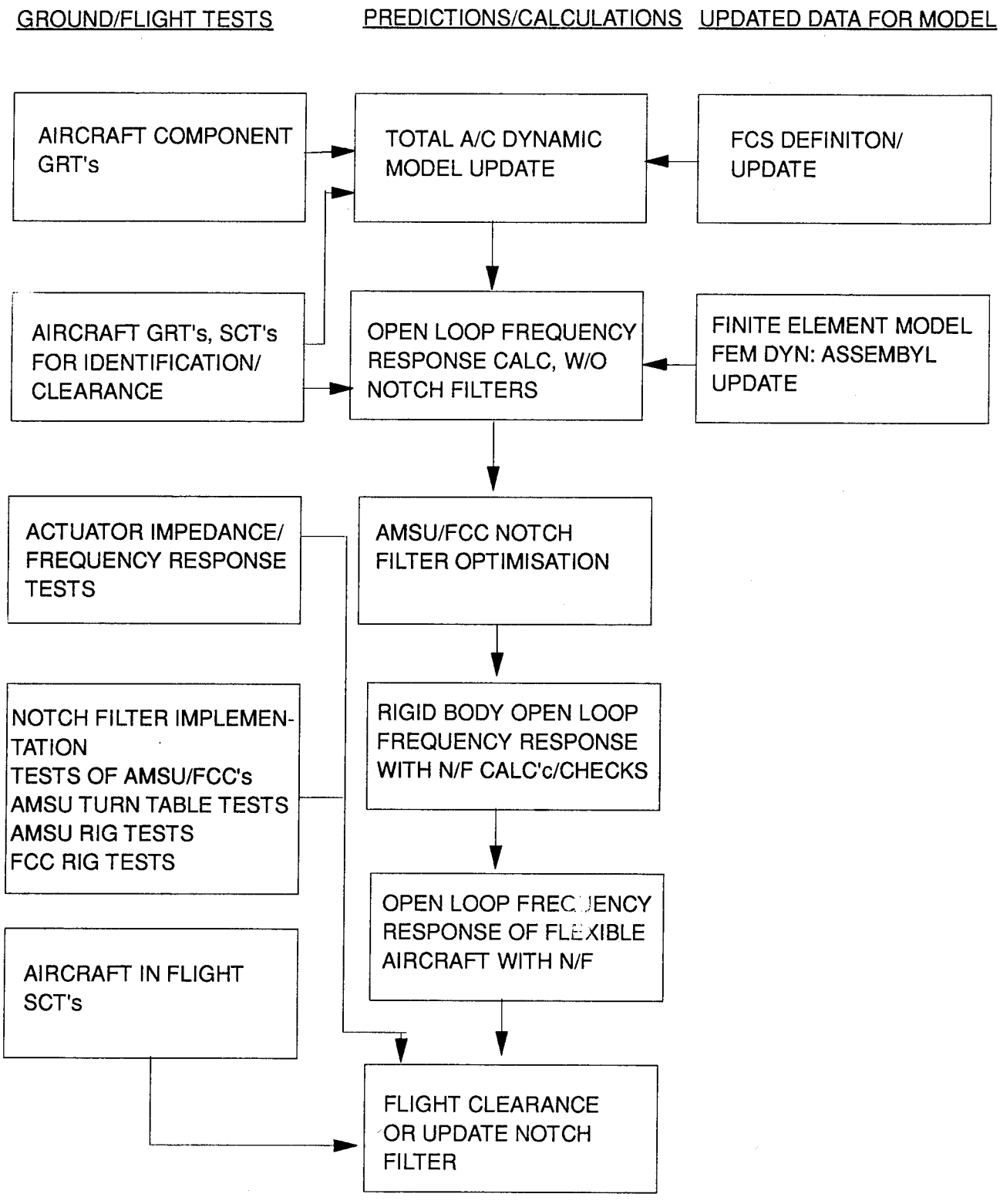

FIG. 12 DESIGN AND CLEARANCE PROCEDURE

GROUND STRUCTURAL COUPLING TESTING AND MODEL UPDATING IN THE AEROSERVOELASTIC QUALIFICATION OF A COMBAT AIRCRAFT

V. Vaccaro
Defence Aircraft Engineering
Alenia Aeronautica
Corso Marche 41, Turin, Italy

J. Becker
Military Aircraft Division
Daimler-Benz Aerospace
Hugo Junkers Strasse, Ottobrunn, Germany

1. SUMMARY

This paper is concerned with the role played by the ground Structural Coupling Test (SCT) and the update of the aeroservoelastic model in the qualification process of a modern combat aircraft.

Most of modern combat aircraft are equipped with fly-by-wire and electronic flight control systems (FCS). The problem of interaction between the dynamic response of the airframe and the FCS is usually solved through an appropriate set of notch filters, designed to attenuate the level of structure vibrations picked up by the FCS sensors. Fundamental part of the qualification of the notch filter set is the ground testing activity, generally known as ground Structural Coupling Test.

The main subject of this paper is the description of the test procedure followed for a delta-canard fly-by-wire aircraft. The peculiar aspect of this test was the identification of the coupling characteristics of the aircraft in the configuration with external stores. The final part of the paper deals with the utilisation of the test results in the updating of the aeroservoelastic model. Emphasis is placed upon the necessity of an adequate model, in order to reduce the test activity to a limited set of external store configurations.

2. NOTATION

AMSU	Aircraft Motion Sensor Unit
ATE	Automatic Test Equipment
C.G.	Centre of Gravity
DOF	Degree of Freedom
FCC	Flight Control Computer
FCS	Flight Control System
FEM	Finite Element Model
GRT	Ground Resonance Test
LMS	Loads Monitoring System
NF	Notch Filter
OLFRF	Open Loop Frequency Response Function
PC	Personal Computer
SC	Structural Coupling
SCT	Structural Coupling Test
TBD	To Be Defined
TFA	Transfer Function Analyser
U/W	Under Wing

3. INTRODUCTION

The new generation of high performance fighter aircraft rely upon digital controls, which improve their handling and manoeuvre capabilities, and allow unstable aeroplanes to fly. To achieve these performances the aircraft FCS is designed to generate a feedback based on the analysis of signals coming from AMSU sensors. Since the AMSU is fitted to the elastic airframe, its sensors, besides the aircraft rigid body motion parameters, pick up also the structure vibrations. The concept of system stability must be therefore extended to the full system, including the aerodynamic and mass characteristics of the aircraft, the FCS and the structural dynamics of the airframe.

Among the forces that cause the airframe dynamic response, the aerodynamic and inertial forces induced by oscillating control surfaces play a fundamental role. They in fact give rise to a very dangerous loop when exciting the structure near a resonance. This can occur when signals from AMSU are not appropriately filtered of the structure vibration contents, inducing, through the feedback to control surface actuators, those oscillations that must be avoided.

SC is the discipline developed to study the coupling between the dynamic response of the airframe and the FCS, and plays a very important role in the qualification of aircraft with digital controls. The usual solution to SC problems is to implement a set of NF in the FCC and AMSU control laws, in order to attenuate to a safe level the airframe vibration contents in the signals running in the FCS. Reference 1 illustrates the procedure developed and applied to design and qualify the NF. A fundamental step of this procedure is the ground SCT stage, the aim of which is to identify the SC characteristics of the aircraft. Data from SCT are required for the updating of the aeroservoelastic model to be used for the NF upgrade.

4. GROUND STRUCTURAL COUPLING TEST

The amount of analysis to be carried out using the aeroservoelastic model is really huge. Calculations are in fact required for NF design and optimisation, and subsequently for flight clearance purposes. Considering the wide possibility of combinations of external stores for a modern aircraft, which strongly influence the dynamic response characteristics of the airframe, it is evident that only a limited set of external store

Paper presented at the Structures and Materials Panel Specialists' Meeting on "Advanced Aeroservoelastic Testing and Data Analysis", held in Rotterdam, The Netherlands, from 8-10 May 1995, and published in CP-566.

configurations can be tested on ground, the rest being studied only through calculations. The consequence is the need of an adequate mathematical model for SC analysis.

The main objective of the ground SCT is therefore to get all information needed to evaluate how the model simulates the SC characteristics of the aircraft in absence of aerodynamics, and then to update the model and the preliminary NF, if necessary. Additionally, the test is very important to assess the influence on the aircraft response of structure non-linearity, hydraulic failures, control surface trim position, actuator hinge backlash, undercarriage support, etc., not implemented in the linear model.

Essentially the test consists in measuring the AMSU signals in response to the excitation of the aircraft obtained by means of sinusoidal rotation of control surfaces about their hinge axes. This gives rise to inertial forces due to the surface C.G. offset with respect to the hinge axis, as shown in the sketch of figure 1, and makes the structure respond at the same frequency of the surface oscillation. The relevant vibration levels are picked up by the AMSU sensors, measured and then used to calculate the transfer functions corresponding to those already employed for the preliminary NF design. This kind of test is carried out in open loop, avoiding that AMSU signals are sent to the FCC and therefore to the control surface actuators. This stage of testing is defined *Identification Test*, because it serves to identify the SC aircraft characteristics and it must be carried out quite early with respect to the flight date, depending on the time required for the updating of notch filters. Another SCT stage is usually foreseen in the route to clearance just before the first flight, called *confirmatory test*, the aim of which is to verify that the updated NF satisfy the requirement for the aircraft in the pre-flight standard. This test is necessary when significant changes are detected, above all in the mass distribution, between pre-flight and identification test aircraft standard.

The following paragraphs will be devoted to describe more in detail all the aspects which are typical of ground SCT.

4.1. Aircraft Build Standard

The aircraft to be tested must be representative of the flight standard with regard to the mass distribution and the airframe stiffness. Since the identification test is usually carried out several months prior to the first flight, it might be that some equipment are missing or not available at that time. If this is the case ballast are to be fitted to substitute the missing items which with their weight can influence the aircraft response. One of this is, for instance, the pilot with his flight equipment.

Concerning with the stiffness, it is essential that all panels and doors carrying loads must be closed and fixed. Since during the test it is required the access to some equipment for cable connection (FCC, AMSU), power supply and inspection, it might be necessary to build spare structural panels with stiffened holes, in order to maintain the stiffness characteristics and fulfil the access requirements.

The peculiarity of the SCT is the excitation, that is obtained by means of the oscillation of the control surfaces. For this reason it is necessary to have the hydraulic and electrical plant perfectly functioning and the flight actuators installed. The power supply to these systems is obtained by means of external devices that will be connected to the aircraft.

Other essential components needed for the test are the FCC and the AMSU, each one with the appropriate hardware and software standard. The FCC at this stage is only needed to manage the excitation signal generated from the test equipment, driving it to the actuators. Since the control laws are not involved in the test procedure a preliminary FCC software version can be accepted.

4.2. Aircraft Suspension

The aircraft must be tested in free-free condition, and this can be accomplished using an elastic suspension or pneumatic supports. The suspension must be designed with a response frequency quite below the lowest modal frequency of the aircraft, in order to avoid any interference with the airframe response.

Some test runs might also be repeated on undercarriage, to evaluate the influence of this system on the aircraft response. This approach can result to be very helpful for the confirmatory test phase, when very few runs are required and therefore the test could be carried out, in order to save time, using the undercarriage support. The aircraft response in free-free condition can then be derived from the differences between free-free and on-undercarriage responses measured during the identification test.

4.3. Special Requirements

During SCT some parameters must be kept under control, in order to avoid damage to the aircraft. For instance, control surface actuators operate at frequencies that are higher than those required during the flight for the aircraft control, and some actions are to be undertaken to avoid an excessive drying of actuator ram seals. The risk is in fact that these parts are not lubricated as required, because of the short run of the ram at high frequency. The solution to the problem is to interrupt the test after that the actuator rams have performed a certain number of cycles, defined by the relevant specification, and lubricate the sealing carrying out a run characterised by few cycles at wide amplitude and very low frequency. Considering that the number of cycles allowed between the lubricating cycles is reached quite rapidly, above all at high frequency, the lubricating cycles are expected to be carried out rather frequently during the SCT. This of course slows down the test and compels to split it into several runs.

Engines are other items that need attention during the test, in order to distribute effects of vibration wear on bearings and rotating parts, that during the test are obviously at rest. This is usually accomplished by rotating periodically the shafts of the engine during the test, using crank systems or any other device that allows the rotation of the engine shafts.

During SCT high vibration levels might be reached in some parts of the airframe and maintained for several cycles. For this reason it is necessary to monitor these levels by means of a set of accelerometers and strain gauges, located at aircraft structure critical points. These sensors send the signals to a device, which automatically cuts out the excitation when it realises a dangerous situation for the aircraft. In particular, each channel is set to the level of acceleration or stress, that must not be exceeded at the relevant airframe point and a continuos comparison is performed between these thresholds and the signals coming from the sensors. Whenever a threshold is exceeded, the device generates a signal which causes the cut-out of the excitation. Usually the thresholds correspond to the *fatigue negligible limits* of the elements of the structural component: if they are not exceeded during the test no fatigue damage is caused to the structure. If the excitation is not high enough to obtain an adequate response of the structure it is necessary to increase the excitation level beyond these limits: in this case the signals coming from the sensors must be recorded for subsequent evaluations on the fatigue damage caused to the structure. The thresholds in this case are increased up to a certain percentage of the negligible limits, never exceeding the *maximum limits*, provided together with the negligible limits. The set of accelerometers, strain gauges and the logic device constitute the Loads Monitoring System (LMS), the scheme of which is illustrated in figure 2. The ATE is the device which manages the generation and the interruption of the excitation signal and will be described in the next paragraphs.

4.4. Excitation Procedures

SCT is peculiar for the way adopted to shake the airframe in order to get the dynamic response. The inertial forces which excite the aircraft are generated making the control surfaces oscillate about their hinge axis. To do this a sinusoidal signal is generated by the test equipment and then sent to the control surface actuators through an appropriate setting of FCC. The control surfaces are not moved all at the same time, but they operate in couple or alone, depending whether they are symmetrically located on both sides of the aeroplane or not (rudder). Two different types of excitation can be considered: symmetric, sending the same signal to the two surfaces of the couple; anti-symmetric, sending signals with same amplitude but shifted in phase of 180 degree. With this approach it is possible to excite separately the symmetric and anti-symmetric modes of the airframe. Figures 3 and 4 show the different combinations of control surfaces and the relevant AMSU signals measured to calculate the OLFRFs.

Since the aim of the test is to identify how the principal modes of the aircraft respond to this kind of excitation, it is necessary to excite the aircraft in the relevant frequency range. To fulfil this task a sine step sweep procedure has been adopted, changing the frequency of the signal with discrete steps and maintaining the same signal for a certain number of cycles, during which signals from AMSU are measured. The Sine Step method has shown to be more appropriate than a sine continuous sweep with logarithmic frequency variation, because it allows to gather data for more cycles at each frequency and consequently a better average of the aircraft response.

The amplitude of the oscillation must be chosen wide enough to obtain the level of forces needed for a proper response of the aircraft. It must change with frequency: it is wide at low frequency, and it diminishes as frequency increases, in order to respect the LMS constraints. The approach normally followed to obtain the best response of the structure is to maintain the level of the excitation amplitude as high as allowed by the LMS constraints. Some preliminary runs are dedicated to optimise the amplitude of the sine sweep: starting from a TBD value at low frequency, the run is repeated increasing every time the level of amplitude, until the LMS cuts off the input signal. On the basis of this level an appropriate amplitude profile versus frequency can be defined, following two opposite necessities: to keep the amplitude as high as possible and to avoid a continuos interruption of the test by the LMS. Figure 5 shows an example of how the amplitude profile, of the signal sent to the control surface actuators, can change with frequency . It can be seen that, due to LMS constraints it might be necessary to reduce the amplitude also at some resonance.

4.5. Preliminary Checks

Many checks must be carried out prior to start with the SCT, in order to verify that all test equipment and instrumentation items are working in accordance to the SCT specifications.

An assessment of the mass characteristics of the aircraft is required in order to update the representation of mass in the mathematical model. At least the total weight and the C.G position of the aircraft should be measured.

Control surface actuator hinge backlash tests are required prior and after the test, to verify that the surface oscillations have not caused any damage to the hinges.

It must be verified that the FCC feedback loops are opened, and this can be done by simply *hand rocking* the aircraft in pitch, yaw and roll. From the analysis of FCC signals that indicate the position of control surfaces it can be deduced whether they are moving or not: of course, since no external signal is sent to the actuators, a movement of the surfaces would mean that a feedback signal is sent by the FCC to them, and that therefore the loop is closed. Since the test must be carried out in open loop, the FCC setting has to be reviewed and the check repeated if the open loop condition is not verified.

Another important check regards the by-pass of the AMSU NFs . Preliminary NFs are in fact implemented in the FCC and AMSU control laws and all facilities provided for their by-pass must be activated. To verify the effectiveness of the by-pass procedure, some runs must be repeated in the frequency range where AMSU NFs are active, with the by-pass on/off: if the NFs are correctly by-passed the appropriate attenuation has to be found when comparing the OLFRF measured with the by-pass active with respect to the one without by-pass.

The last stage before starting the SCT consists in measuring the transfer function of each actuator, to verify that the relevant performances are in accordance with previous rig tests.

4.6. Aircraft Identification Test

The OLFRFs to be measured are defined by the procedure for the NF design , and can be deduced from the sketches reported in figure 3 and 4. They must be measured in a frequency range extended up to the sampling rate which characterises FCC digital signals. This is necessary to take into account the folding-back effect of the high frequency range due to digitalisation.

To carry out the SCT it is necessary to exchange data with the FCC and this function is carried out by the ATE, a device designed for pre-flight FCC checks and able to perform the following operations during SCT:

- set up and read/write FCC parameters
- injection of the excitation signal in the FCC
- reading of AMSU sensor signals from FCC facilities
- real time presentation of FCC signals

The excitation signal is generated by a TFA, incorporated in the ATE and interfaced with an external PC. The same TFA performs the calculation of the OLFRFs and sends the relevant data to the PC for storing and subsequent analysis. Figure 6 illustrates the layout of the test, showing the links among the test items and the exchanged data. During the test measured OLFRFs are compared with theoretical predictions, in order to check whether unexpected or unwanted effects are influencing the test.

It is very important to verify the degree of non linearity of the aircraft response during the test, looking at the shape of AMSU and LMS sensor time histories traced in real time by a brush recorder. More detailed information are obtained repeating some runs, usually for the most important normal modes, at different amplitude levels. The lesson learnt from the SCT is that the highest amplitude levels compatible with LMS constraints should be used, to keep non linearity effects to a minimum level. Figure 7 shows the same OLFRF measured at different amplitude levels in the first wing bending frequency range, highlighting that the main effect of non linearity is on the amplitude of the peak, with small influence on the frequency.

Besides the influence of amplitude other test runs are to be carried out, in order to investigate the influence of failures of one or two of the four redundant hydraulic systems and FCCs. These checks are needed as in this case the actuator performances can present significant changes, influencing the OLFRFs and thus the NF design.

4.7. Confirmatory Test

The *identification test* covers all the aspects necessary to identify the SC characteristics of the aircraft required for the NF design. It is very detailed and carried out for different aircraft configurations, regarding both external stores and internal fuel. This is done to verify the theoretical predictions relevant to the influence of mass characteristics on the aircraft response.

On the contrary, the *confirmatory test* is intended to be a very short test, with the aim of verifying that the aircraft in the ready-to-fly standard does not present significant changes in the response with respect to the *identification test*. The test is therefore to be carried out when the aircraft is in the flight configuration. The verification is normally limited to the modes that are very sensible to mass distribution changes and that play a leading role in the NF design. It consists in a short *identification test*, limited to few modes, selected as most critical from the NF design point of view.

The confirmatory test is the last step in the NF qualification route before flying the configuration under assessment. It is needed to issue the SC flight clearance: from the analysis of the test results it will come out whether the NFs, based on data from the *identification test*, can be confirmed for flight or not, and a reassessment for flight conditions can be necessary. In the worst case flight limitations might result for some regions of the flight envelope.

5. UPDATING OF THE AEROSERVOELASTIC MODEL

To accomplish the NF design procedure the OLFRFs relevant to external store configurations are required. Considering the number of configurations and the possible sub-configurations deriving from store release, it is essential the development of a reliable aeroservoelastic model to carry out the amount of calculations required for the NF design.

Among the components of the aeroservoelastic model there is the aircraft structural dynamic model, the updating of which is discussed in this paper. The basis of this model is the Nastran Superelement Technique, which allows to design simpler models and then to assemble the final model with a linking procedure. In the case of the canard-delta the airframe has been divided in the following superelements:

- wing including flaperons and slats
- fuselage
- foreplane
- fin and rudder

Each superelement consists in a mass and stiffness matrix, calculated using the relevant FEM and applying a reduction to a set of DOFs. The dynamic reduction of the model is a very important stage, as it allows to reduce drastically the number of DOFs, leading to a much *lighter* model. The DOFs selection must be performed following the guideline that the reduced model has to simulate adequately the structural dynamic characteristics of the component in a certain frequency range. Some trials might be required before a satisfactory result can be achieved.

The GRT results represent the basis for the updating of the dynamic model. All the remarks that follow about the model updating, are based on the activity performed after the GRT

and SCT campaign, mainly devoted to study the U/W subsonic tank configuration.

Considering that component GRT for wing, fin, foreplane and pylons, had already been carried out and the relevant superelements updated, the GRT on the assembled aircraft was required to gather data for the update mainly of the fuselage superelement and of all the elastic elements used to simulate, in the assembled model, the links among the superelements. Figure 8 is a sketch of the superelement model updating activity performed before the GRT on the aircraft. At this stage a preliminary updated model was available and it was used to predict the response of the aircraft during GRT and SCT. It was also employed to carry out all calculations required for the preliminary NF design. Figure 9 illustrates the next step, carried out after the GRT and concluded with the delivery of the final updated model, including all the effects not covered during previous superelement GRTs.

From a first rough look to the aircraft GRT results it came out that the model had the general trend to predict lower modal frequencies with respect to test results. The differences between test results and predictions indicated that a model update was necessary. The consequent correction consisted in a correction of the superelement stiffness matrices and in the update of the mass distribution of the model, the latter based on the assessment of the aircraft mass distribution carried out before starting the test. Several trials were needed to find a set of factors for the superelement stiffness matrices, but eventually this approach demonstrated to be adequate to obtain satisfactory results. The factors were all greater than one, the greatest being applied to the fuselage, and the updated stiffness matrices were obtained multiplying all their elements for the relevant factor.

Before starting with the updating procedure it was necessary to manipulate the experimental data, transforming the GRT modal shapes in perfectly symmetric and anti-symmetric modes. This step was needed since the aircraft model is a representation of half aircraft. The main problems with asymmetry in modal shapes came from modes characterised by external stores and control surfaces wide motion. For these cases the approach was to consider data coming only from the accelerometers located on the side of the aircraft which showed a better *phase index.*

The correction procedure was developed in iterative form: after having established an initial set of factors, the new model was assembled using the factored superelement matrices and modal characteristics compared with those ones measured during the GRT. From this comparison a new set of factors would be defined and the process repeated until a satisfactory comparison could be found. The modal characteristics monitored during the iterative procedure to establish when the process could be stopped were the modal frequencies, the generalised masses and the modal shapes.

Regarding the frequency, the comparison was based on the percentage difference between test and model data. Figure 10 shows the situation for some modes at the end of the procedure, pointing out to the improvement obtained for this parameter with respect to the GRT predictions.

For the comparison of the generalised masses and the modal shapes it was necessary to renormalize the theoretical modes, in order to make them homogeneous with the measured ones. In general the location of the accelerometer with the highest response level was chosen as reference point. This step was repeated for different points, depending on the modal shape and the accelerometer phase index measured during the acquisition of the mode. The aim of this repetition was to understand how the selection of the reference point could influence the calculated generalised mass. To perform these checks without problems the GRT accelerometer map was designed making the accelerometer locations coincide with model grids whenever it was possible. This approach could be easily followed for components like wings, foreplane and fin, but for the fuselage an interpolation of sensor data was necessary. For the comparison of modal shapes the following index was calculated:

$$\frac{\left(\Phi_{theory} \bullet \Phi_{GRT}\right)^2}{\left|\Phi_{theory}\right|^2 \times \left|\Phi_{GRT}\right|^2}$$

where Φ_{theory} and Φ_{GRT} are the two eigenvectors to be compared.

In the updating procedure a special attention was dedicated to the most significant modes, namely those ones that in the previous analyses had shown to have a considerable influence on flutter, SC and dynamic loads. This approach allowed to obtain a model that can be considered adequate for general dynamic analyses, the modes represented by the model with less precision being not essential for the study of aeroservoelastic criticities.

Immediately after the release the updated model was tested simulating the SCT runs carried out on ground, associating in the model to each mode the corresponding modal damping value measured during GRT. The model was quite successful, above all in the low frequency range (up to 20 Hz), which is the most critical for the NF design. At this stage a further improvement was introduced in the aeroservoelastic model, replacing the actuator transfer functions with the frequency functions measured during the preliminary phase of the test.

The results of the model were considered in good agreement with the SCT OLFRFs for all the U/W tank fuel conditions tested, and as a consequence no other upgrade was required. Figure 11 illustrates the comparison among the theoretical predictions before the updating, the OLFRFs calculated using the updated model and the SCT data in the frequency range up to the FCC sampling rate. The conclusion that can be drawn is that in the low frequency range the updated model is quite satisfactory (Figure 12), with an evident improvement with respect to the model used for the test predictions. In the high

frequency range the correspondence with test data is less satisfactory, but since this range is much less critic for the NF design this limitation can be managed using safety factors or directly measured OLFRFs, properly factored to include aerodynamics and FCS effects.

6. CONCLUSIONS

The test procedure followed for the SC identification test of a delta-canard aircraft has been described. The need for an accurate aeroservoelastic model, in order to limit the testing activity to a reduced number of external store configurations, selected on the basis of SC criticities, has been pointed out. The way followed by Alenia to update the theoretical model using Ground Resonance and SC Test results has been presented. The aeroservoelastic model, updated with test data, can be considered a reliable tool for the FCS NF design, particularly in the low frequency range where the most critical modes can be found. Above all it has been shown the noticeable improvement in the representation of the aircraft response in comparison with the situation before the update. A further updating will be possible after that flight test results are available, involving mainly the unsteady aerodynamic part of the model.

The updating procedure described in this paper is based mainly on the correction of the stiffness characteristics of the model, using data gathered during tests carried out on a small number of external store configurations. This set of configurations of course must be selected so to cover all pylons and launchers the stiffness characteristics of which can significantly influence the airframe dynamic response. Following this approach all not tested combinations of stores can be studied with the mathematical model, simulating the appropriate mass distribution, and thus limiting to a minimum very expensive test activities.

REFERENCES

1. J.Becker, V.Vaccaro, "Aeroservoelastic Design, Test Verification And Clearance Of an Advanced Flight Control System", AGARD 80th SMP Meeting on Advanced Aeroservoelastic, 5/1995
2. B.D.Caldwell, "The FCS-Structural Coupling Problem and Its Solution", AGARD FMP 4/94
3. L.R.Felt, L.J.Huttsell, T.E. Noll, D.E.Cooley, "Aeroservoelastic Encounters", Journal of Aircraft Vol16 No.7 Article 78-1289, 7/1979
4. G.Norris, "AMRAAM Block Placed On Lockheed F16s", Flight International Magazine, 20/10/93
5. M.W.Kehoe, E.J.Laurie, L.J.Bjarke, "An In-Flight Interaction of the X29 Canard And FCS", AIAA-90-1240-CP, 1990
6. MIL-F-9490D, "FCS - Design Installation and Test of Piloted Aircraft General Specification For"
7. O.Sensburg, "Interaction Between Structure and CSAS", UFE 1237 AGARD SMP
8. M.G.Allen, S.J.Pollock, "AFTI/F-16 Aeroservoelastic Analysis and Ground Test with a Digital Flight Control System", AIAA Paper No.83-0994
9. T.D.Arthurs, J.T.Gallagher, "Interaction between Control Augmentation System and Airframe Dynamics on the YF-17", AIAA Paper No.75-824
10. T.D.Smith, C.J.Yeo, R.E.W.Marshall, "Ground and Flight Testing on the Fly-By-Wire Jaguar Equipped with a Full Time Quadruplex Digital Integrated Control System", AGARD CP-321
11. MSC/NASTRAN
HANDBOOK FOR SUPERELEMENT ANALYSIS

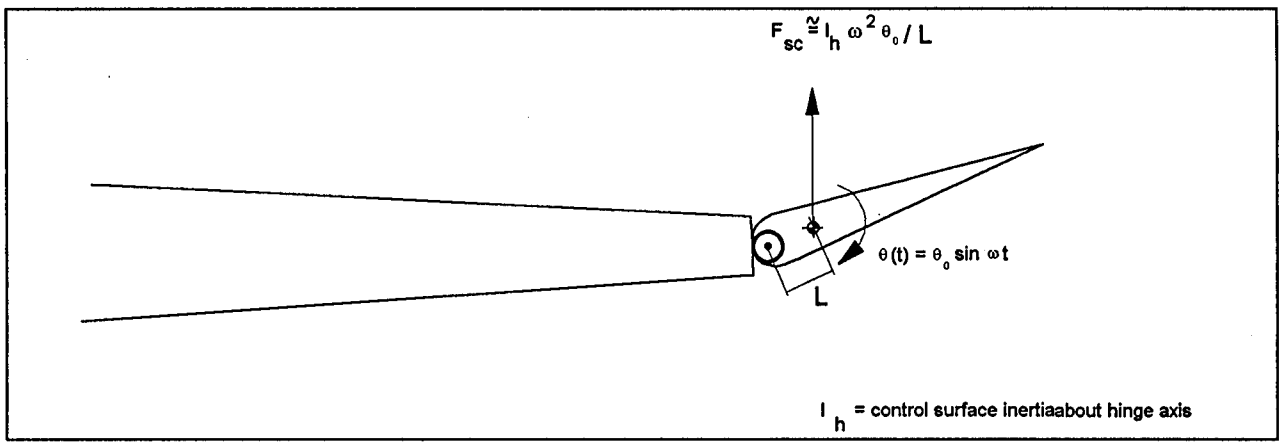

Figure 1. Simple Schematization of Structural Coupling Forces Exciting the Structure during SCT

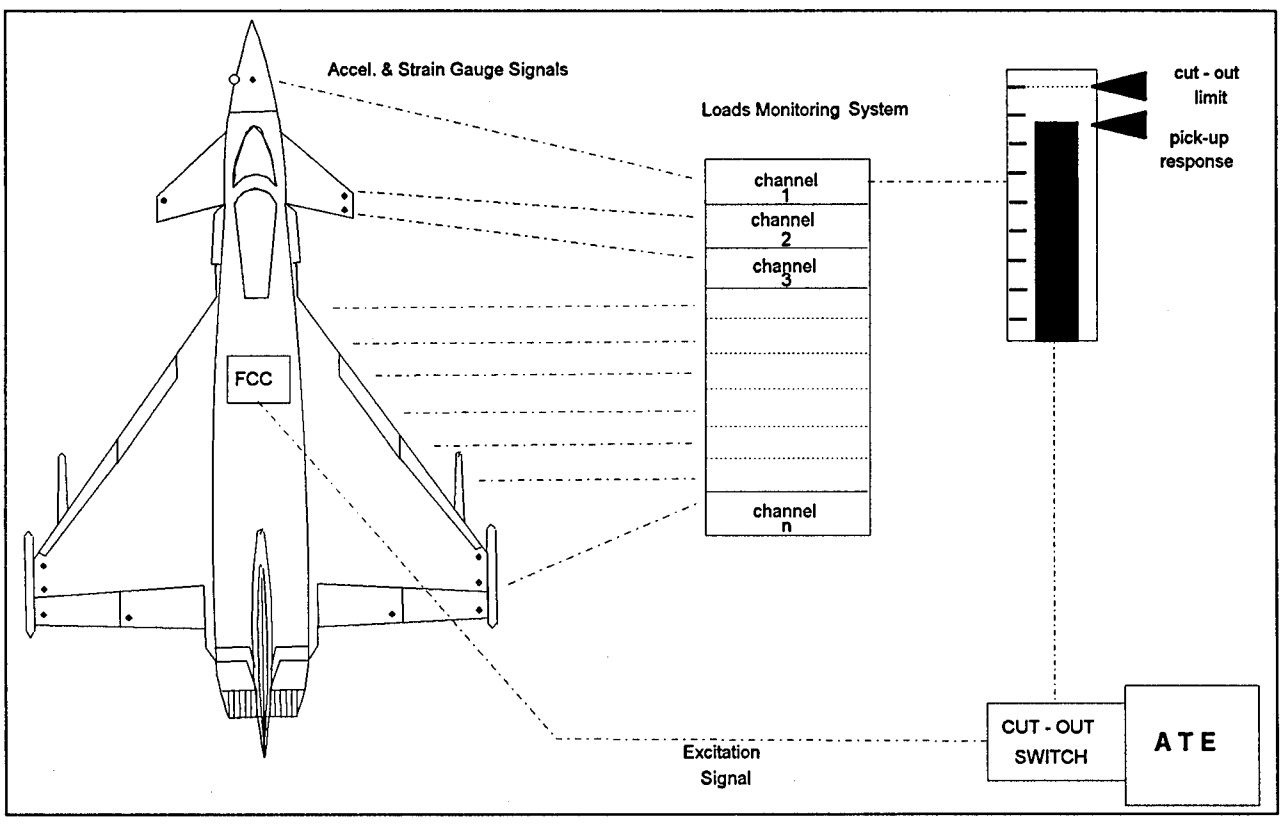

Figure 2. Load Monitoring System Lay-Out

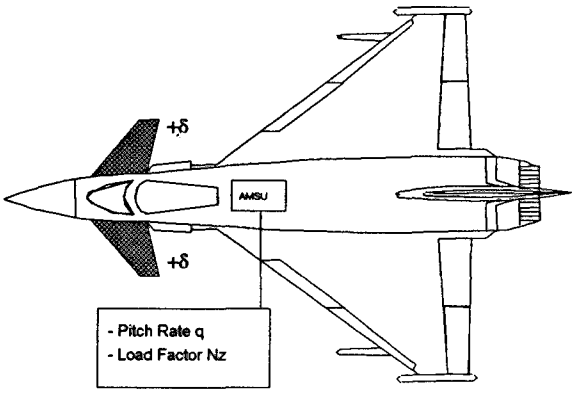

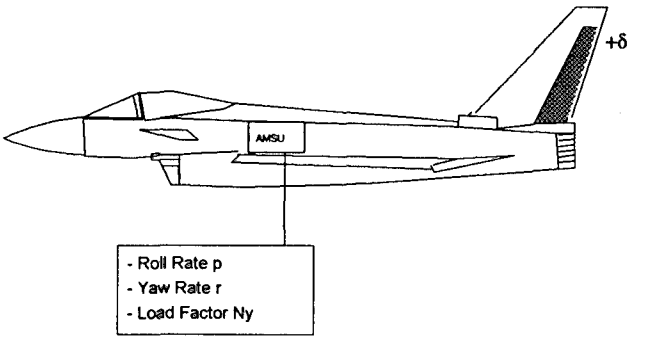

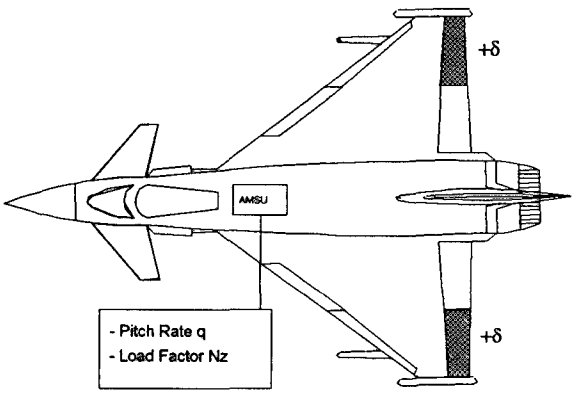

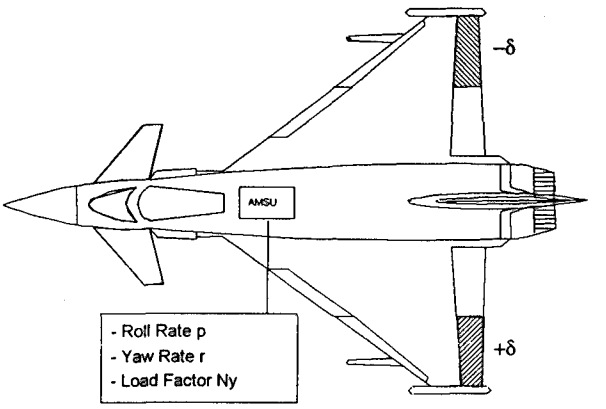

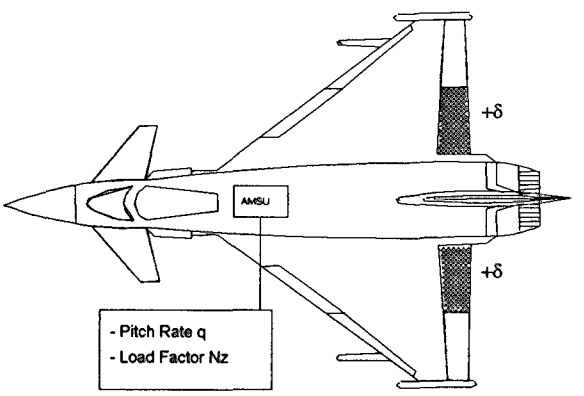

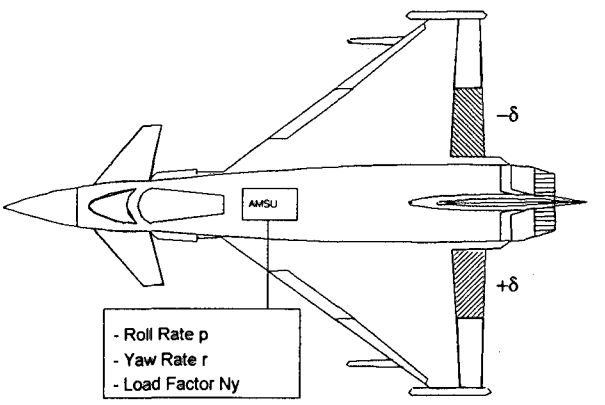

Figure 3. SCT Symmetric Excitations and Measurements

Figure 4. SCT Anti-Symmetric Excitations and Measurements

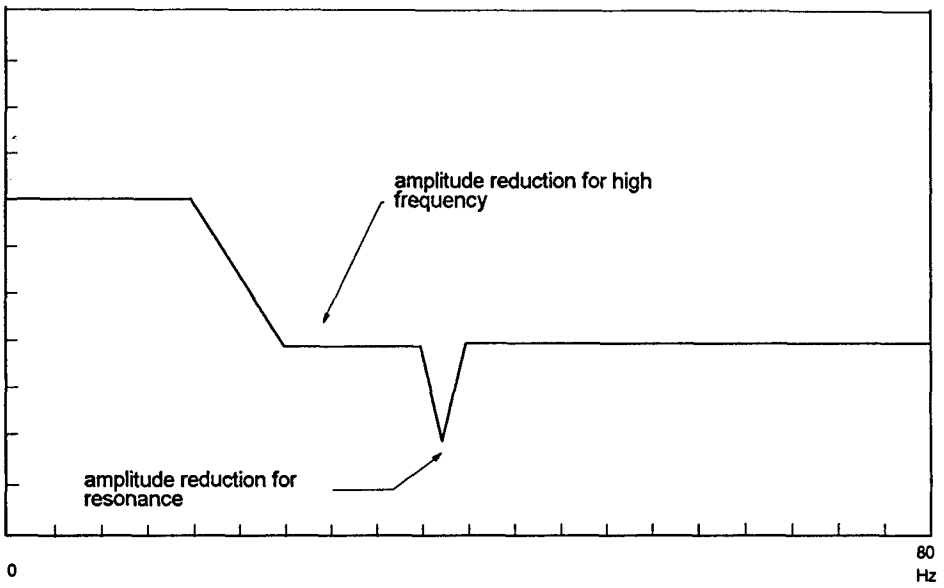

Figure 5. Example of Excitation Signal

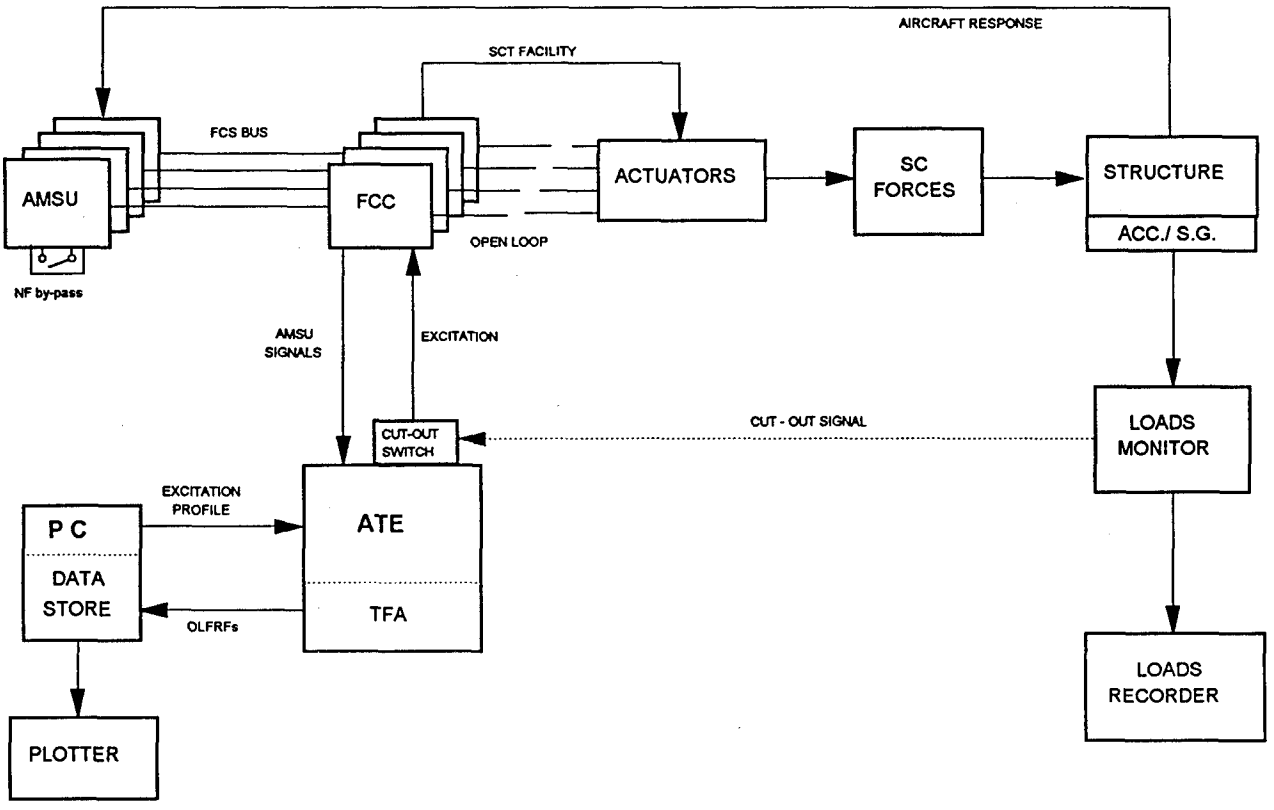

Figure 6. SCT Layout

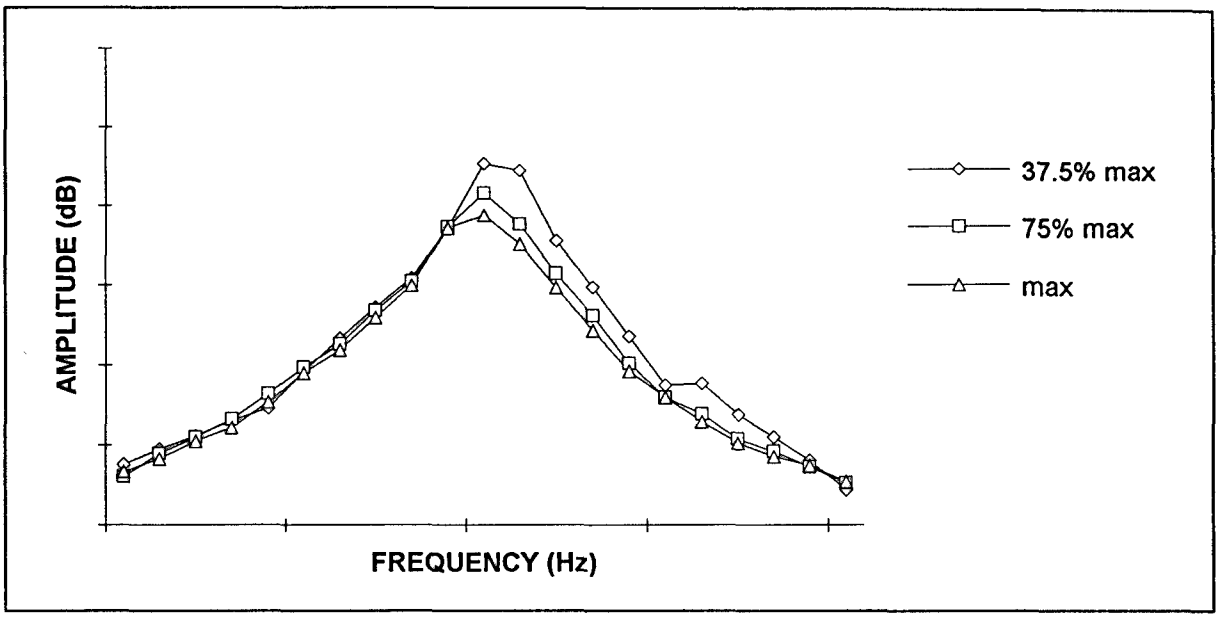

Figure 7. Influence of Excitation Amplitude on OLFRF

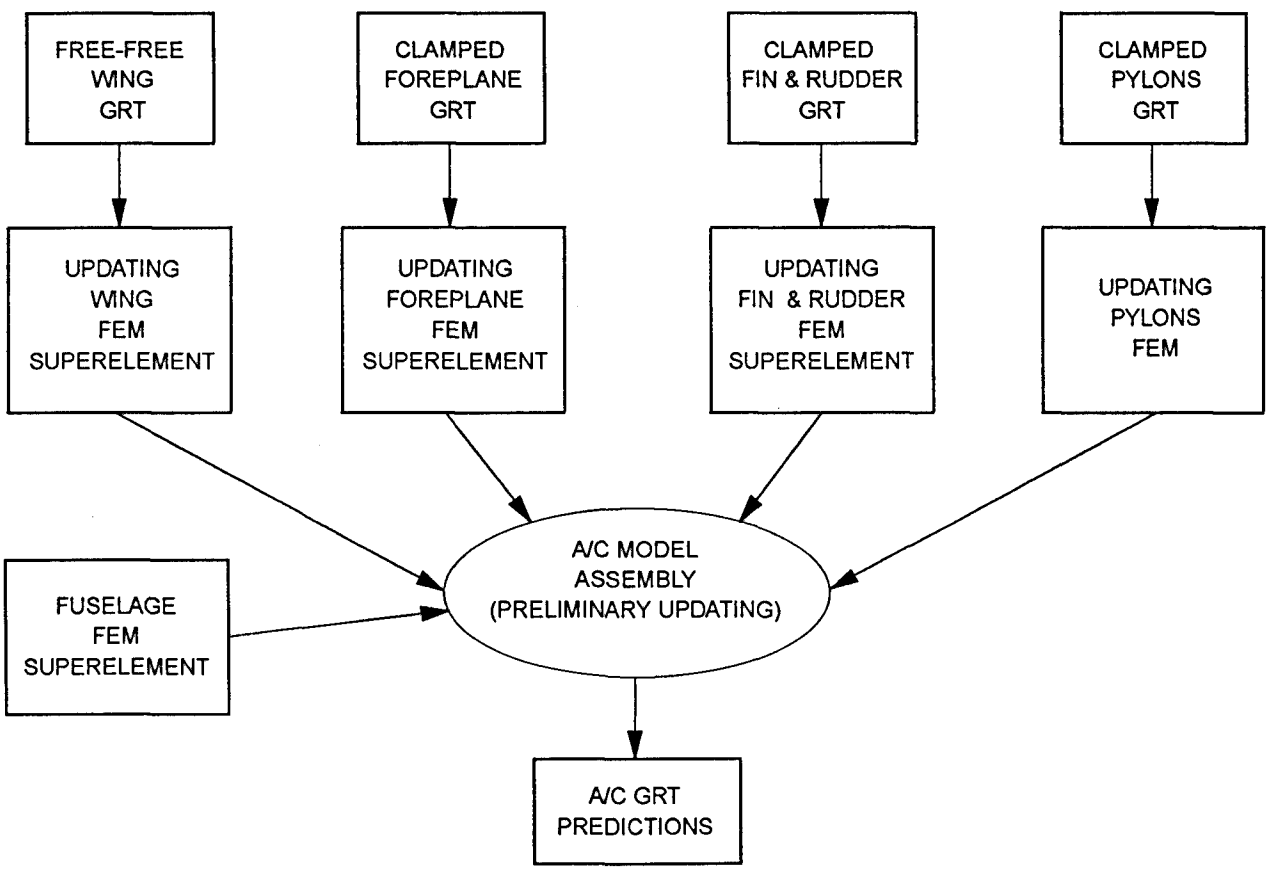

Figure 8. Model Preliminary Update Procedure (Components)

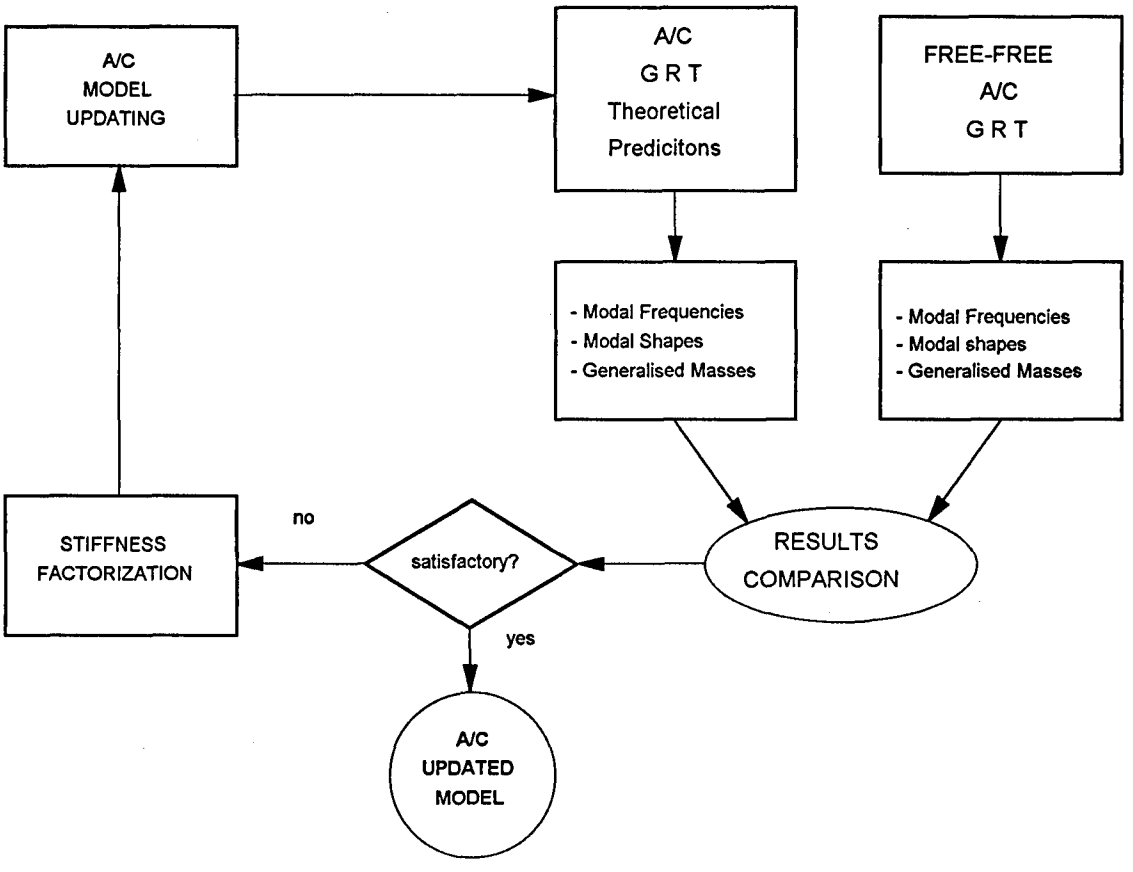

Figure 9. Aircraft Dynamic Model Update Procedure (GRT)

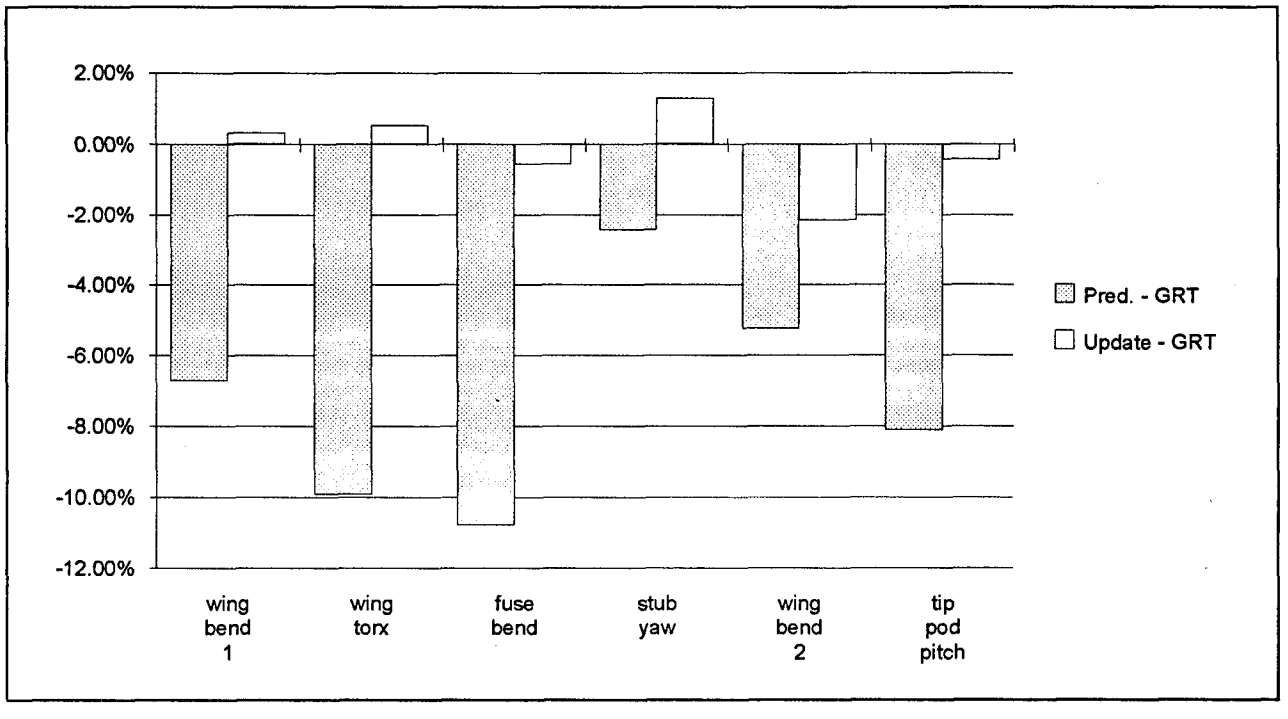

Figure 10. Modal Frequency Percentage Differences

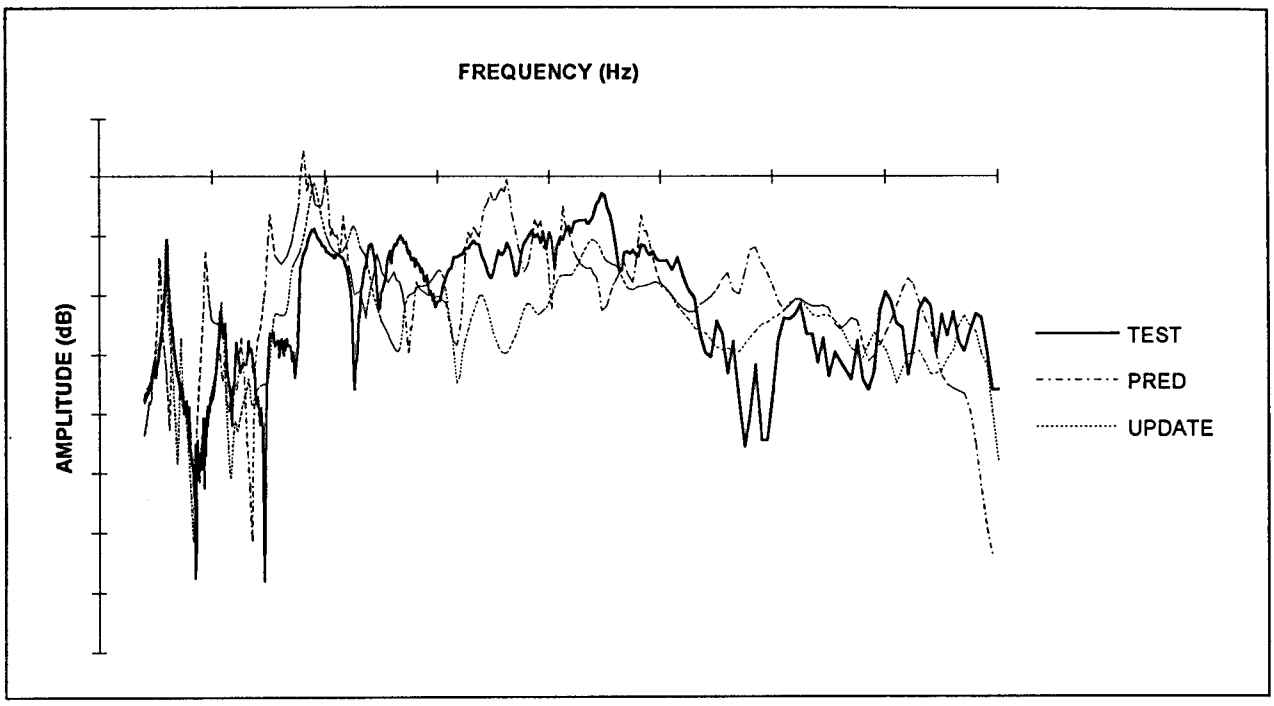

Figure 11. Comparison of Test and Prediction OLFRFs with Updated Model: Whole Frequency Range

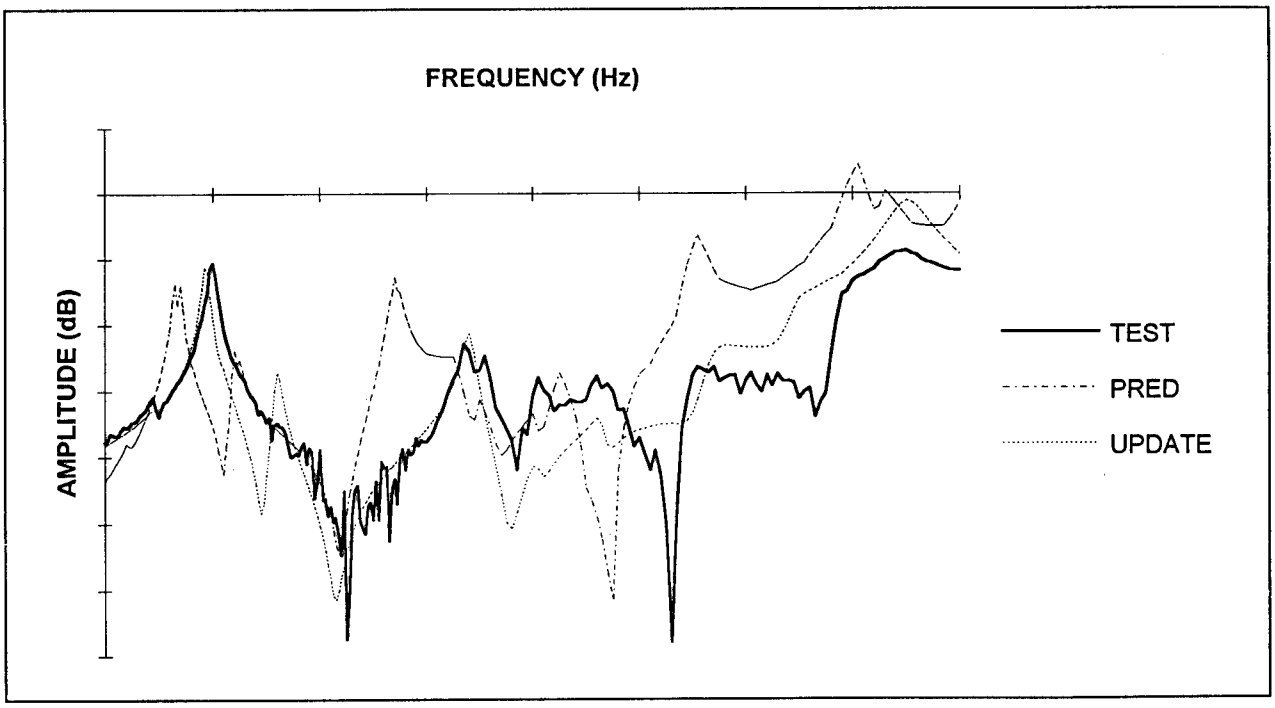

Figure 12. Comparison of Test and Prediction OLFRFs with Updated Model: Low Frequency Range

REPORT DOCUMENTATION PAGE

1. Recipient's Reference	2. Originator's Reference	3. Further Reference	4. Security Classification of Document
	AGARD-CP-566	ISBN 92-836-0017-7	UNCLASSIFIED/ UNLIMITED

5. Originator Advisory Group for Aerospace Research and Development
North Atlantic Treaty Organization
7 rue Ancelle, 92200 Neuilly-sur-Seine, France

6. Title

Advanced Aeroservoelastic Testing and Data Analysis

7. Presented at/sponsored by

The 80th Meeting of the AGARD Structures and Materials Panel, held in Rotterdam, The Netherlands, 8-10 May 1995

8. Author(s)/Editor(s)	9. Date
Multiple	November 1995
10. Author's/Editor's Address	**11. Pages**
Multiple	290

12. Distribution Statement There are no restrictions on the distribution of this document. Information about the availability of this and other AGARD unclassified publications is given on the back cover.

13. Keywords/Descriptors

Flight control	Aerodynamic stability
Flutter	Servomechanisms
Aeroelasticity	Unsteady flow
Flight tests	Dynamic response
Wind tunnel tests	Transonic flow
Aerodynamic characteristics	Aircraft

14. Abstract

Contains the papers presented at the AGARD Structures and Materials Panel's Specialists' Meeting on Aeroservoelastic Testing and Data Analysis, held in Rotterdam in May 1955.

Flutter is a potentially catastrophic aeroelastic dynamic instability. Flight flutter tests are conducted to demonstrate freedom from flutter for critical aircraft conditions and to derive data to validate the flutter analysis. Active control systems (ride control, gust load alleviation, flutter stabilization, etc.) add to the scope and complexity of these tests in that control system instability due to aeroservoelastic interactions must also be considered.

The conclusions of the meeting are that most of the tests need improvements, some tests should be better exploited, and at least one test — the in-flight measurement of unsteady air loads — should become standard practice to close a gap in the logic of flutter certification.

AGARD

NATO OTAN

7 RUE ANCELLE • 92200 NEUILLY-SUR-SEINE

FRANCE

Télécopie (1)47.38.57.99 • Télex 610 176

DIFFUSION DES PUBLICATIONS

AGARD NON CLASSIFIEES

Aucun stock de publications n'a existé à AGARD. A partir de 1993, AGARD détiendra un stock limité des publications associées aux cycles de conférences et cours spéciaux ainsi que les AGARDographies et les rapports des groupes de travail, organisés et publiés à partir de 1993 inclus. Les demandes de renseignements doivent être adressées à AGARD par lettre ou par fax à l'adresse indiquée ci-dessus. *Veuillez ne pas téléphoner.* La diffusion initiale de toutes les publications de l'AGARD est effectuée auprès des pays membres de l'OTAN par l'intermédiaire des centres de distribution nationaux indiqués ci-dessous. Des exemplaires supplémentaires peuvent parfois être obtenus auprès de ces centres (à l'exception des Etats-Unis). Si vous souhaitez recevoir toutes les publications de l'AGARD, ou simplement celles qui concernent certains Panels, vous pouvez demander à être inclu sur la liste d'envoi de l'un de ces centres. Les publications de l'AGARD sont en vente auprès des agences indiquées ci-dessous, sous forme de photocopie ou de microfiche.

CENTRES DE DIFFUSION NATIONAUX

ALLEMAGNE
Fachinformationszentrum,
Karlsruhe
D-76344 Eggenstein-Leopoldshafen 2

BELGIQUE
Coordonnateur AGARD-VSL
Etat-major de la Force aérienne
Quartier Reine Elisabeth
Rue d'Evere, 1140 Bruxelles

CANADA
Directeur, Services d'information scientifique
Ministère de la Défense nationale
Ottawa, Ontario K1A 0K2

DANEMARK
Danish Defence Research Establishment
Ryvangs Allé 1
P.O. Box 2715
DK-2100 Copenhagen Ø

ESPAGNE
INTA (AGARD Publications)
Pintor Rosales 34
28008 Madrid

ETATS-UNIS
NASA Headquarters
Code JOB-1
Washington, D.C. 20546

FRANCE
O.N.E.R.A. (Direction)
29, Avenue de la Division Leclerc
92322 Châtillon Cedex

GRECE
Hellenic Air Force
Air War College
Scientific and Technical Library
Dekelia Air Force Base
Dekelia, Athens TGA 1010

ISLANDE
Director of Aviation
c/o Flugrad
Reykjavik

ITALIE
Aeronautica Militare
Ufficio del Delegato Nazionale all'AGARD
Aeroporto Pratica di Mare
00040 Pomezia (Roma)

LUXEMBOURG
Voir Belgique

NORVEGE
Norwegian Defence Research Establishment
Attn: Biblioteket
P.O. Box 25
N-2007 Kjeller

PAYS-BAS
Netherlands Delegation to AGARD
National Aerospace Laboratory NLR
P.O. Box 90502
1006 BM Amsterdam

PORTUGAL
Força Aérea Portuguesa
Centro de Documentação e Informação
Alfragide
2700 Amadora

ROYAUME-UNI
Defence Research Information Centre
Kentigern House
65 Brown Street
Glasgow G2 8EX

TURQUIE
Millî Savunma Başkanliği (MSB)
ARGE Dairesi Başkanliği (MSB)
06650 Bakanliklar-Ankara

Le centre de distribution national des Etats-Unis ne détient PAS de stocks des publications de l'AGARD.
D'éventuelles demandes de photocopies doivent être formulées directement auprès du NASA Center for AeroSpace Information (CASI) à l'adresse ci-dessous. Toute notification de changement d'adresse doit être fait également auprès de CASI.

AGENCES DE VENTE

NASA Center for
AeroSpace Information (CASI)
800 Elkridge Landing Road
Linthicum Heights, MD 21090-2934
Etats-Unis

ESA/Information Retrieval Service
European Space Agency
10, rue Mario Nikis
75015 Paris
France

The British Library
Document Supply Division
Boston Spa, Wetherby
West Yorkshire LS23 7BQ
Royaume-Uni

Les demandes de microfiches ou de photocopies de documents AGARD (y compris les demandes faites auprès du CASI) doivent comporter la dénomination AGARD, ainsi que le numéro de série d'AGARD (par exemple AGARD-AG-315). Des informations analogues, telles que le titre et la date de publication sont souhaitables. Veuiller noter qu'il y a lieu de spécifier AGARD-R-nnn et AGARD-AR-nnn lors de la commande des rapports AGARD et des rapports consultatifs AGARD respectivement. Des références bibliographiques complètes ainsi que des résumés des publications AGARD figurent dans les journaux suivants:

Scientific and Technical Aerospace Reports (STAR)
publié par la NASA Scientific and Technical
Information Division
NASA Headquarters (JTT)
Washington D.C. 20546
Etats-Unis

Government Reports Announcements and Index (GRA&I)
publié par le National Technical Information Service
Springfield
Virginia 22161
Etats-Unis
(accessible également en mode interactif dans la base de données bibliographiques en ligne du NTIS, et sur CD-ROM)

Imprimé par le Groupe Communication Canada
45, boul. Sacré-Cœur, Hull (Québec), Canada K1A 0S7

AGARD

NATO OTAN

7 RUE ANCELLE • 92200 NEUILLY-SUR-SEINE

FRANCE

Telefax (1)47.38.57.99 • Telex 610 176

DISTRIBUTION OF UNCLASSIFIED

AGARD PUBLICATIONS

AGARD holds limited quantities of the publications that accompanied Lecture Series and Special Courses held in 1993 or later, and of AGARDographs and Working Group reports published from 1993 onward. For details, write or send a telefax to the address given above. *Please do not telephone.*

AGARD does not hold stocks of publications that accompanied earlier Lecture Series or Courses or of any other publications. Initial distribution of all AGARD publications is made to NATO nations through the National Distribution Centres listed below. Further copies are sometimes available from these centres (except in the United States). If you have a need to receive all AGARD publications, or just those relating to one or more specific AGARD Panels, they may be willing to include you (or your organisation) on their distribution list. AGARD publications may be purchased from the Sales Agencies listed below, in photocopy or microfiche form.

NATIONAL DISTRIBUTION CENTRES

BELGIUM
Coordonnateur AGARD — VSL
Etat-major de la Force aérienne
Quartier Reine Elisabeth
Rue d'Evere, 1140 Bruxelles

CANADA
Director Scientific Information Services
Dept of National Defence
Ottawa, Ontario K1A 0K2

DENMARK
Danish Defence Research Establishment
Ryvangs Allé 1
P.O. Box 2715
DK-2100 Copenhagen Ø

FRANCE
O.N.E.R.A. (Direction)
29 Avenue de la Division Leclerc
92322 Châtillon Cedex

GERMANY
Fachinformationszentrum
Karlsruhe
D-76344 Eggenstein-Leopoldshafen 2

GREECE
Hellenic Air Force
Air War College
Scientific and Technical Library
Dekelia Air Force Base
Dekelia, Athens TGA 1010

ICELAND
Director of Aviation
c/o Flugrad
Reykjavik

ITALY
Aeronautica Militare
Ufficio del Delegato Nazionale all'AGARD
Aeroporto Pratica di Mare
00040 Pomezia (Roma)

LUXEMBOURG
See Belgium

NETHERLANDS
Netherlands Delegation to AGARD
National Aerospace Laboratory, NLR
P.O. Box 90502
1006 BM Amsterdam

NORWAY
Norwegian Defence Research Establishment
Attn: Biblioteket
P.O. Box 25
N-2007 Kjeller

PORTUGAL
Força Aérea Portuguesa
Centro de Documentação e Informação
Alfragide
2700 Amadora

SPAIN
INTA (AGARD Publications)
Pintor Rosales 34
28008 Madrid

TURKEY
Millî Savunma Başkanliği (MSB)
ARGE Dairesi Başkanliği (MSB)
06650 Bakanliklar-Ankara

UNITED KINGDOM
Defence Research Information Centre
Kentigern House
65 Brown Street
Glasgow G2 8EX

UNITED STATES
NASA Headquarters
Code JOB-1
Washington, D.C. 20546

The United States National Distribution Centre does NOT hold stocks of AGARD publications.
Applications for copies should be made direct to the NASA Center for AeroSpace Information (CASI) at the address below. Change of address requests should also go to CASI.

SALES AGENCIES

NASA Center for
AeroSpace Information (CASI)
800 Elkridge Landing Road
Linthicum Heights, MD 21090-2934
United States

ESA/Information Retrieval Service
European Space Agency
10, rue Mario Nikis
75015 Paris
France

The British Library
Document Supply Centre
Boston Spa, Wetherby
West Yorkshire LS23 7BQ
United Kingdom

Requests for microfiches or photocopies of AGARD documents (including requests to CASI) should include the word 'AGARD' and the AGARD serial number (for example AGARD-AG-315). Collateral information such as title and publication date is desirable. Note that AGARD Reports and Advisory Reports should be specified as AGARD-R-nnn and AGARD-AR-nnn, respectively. Full bibliographical references and abstracts of AGARD publications are given in the following journals:

Scientific and Technical Aerospace Reports (STAR)
published by NASA Scientific and Technical
Information Division
NASA Headquarters (JTT)
Washington D.C. 20546
United States

Government Reports Announcements and Index (GRA&I)
published by the National Technical Information Service
Springfield
Virginia 22161
United States
(also available online in the NTIS Bibliographic
Database or on CD-ROM)

Printed by Canada Communication Group
45 Sacré-Cœur Blvd., Hull (Québec), Canada K1A 0S7

ISBN 92-836-0017-7